THE UNIVERSITY OF TEXAS AT AUSTIN
CENTER FOR TRANSPORTATION RESEARCH

TECHNICAL REPORT 0-6862-1
TxDOT PROJECT NUMBER 0-6862

Improved Tub Girder Details: Final Report

Stalin Armijos-Moya
Yang Wang
Todd Helwig
Patricia Clayton
Michael D. Engelhardt
Eric Williamson

December 2018; Published November 2019

http://library.ctr.utexas.edu/ctr-publications/0-6862-1.pdf

Technical Report Documentation Page

1. Report No. FHWA/TX-19/0-6862-1	2. Government Accession No.	3. Recipient's Catalog No.
4. Title and Subtitle Improved Tub Girder Details: Final Report		5. Report Date December 2018; Published November 2019
		6. Performing Organization Code
7. Author(s) Stalin Armijos-Moya, Yang Wang, Todd A. Helwig, Michael D. Engelhardt, Patricia M. Clayton, Eric B. Williamson		8. Performing Organization Report No. 0-6862-1
9. Performing Organization Name and Address Center for Transportation Research The University of Texas at Austin 3925 W. Braker Lane Austin, TX 78759		10. Work Unit No. (TRAIS) 11. Contract or Grant No. 0-6862
12. Sponsoring Agency Name and Address Texas Department of Transportation Research and Technology Implementation Division P.O. Box 5080 Austin, TX 78763-5080		13. Type of Report and Period Covered Technical Report (02/15–12/18) 14. Sponsoring Agency Code

15. Supplementary Notes
Project performed in cooperation with the Texas Department of Transportation and the Federal Highway Administration.

16. Abstract

Steel trapezoidal box girders, generally referred to as tub girders, have been widely used on a number of bridges throughout the State of Texas. The smooth profile of the girder systems provides an aesthetically appealing bridge that also possesses several structural advantages compared to other girder types. Due to the significant torsional stiffness of the closed box section, the girders are a popular choice in horizontally curved systems where the bridge geometry leads to large torsional moments. The girders have also been used on a number of straight girder systems throughout the state leading to improved bridge aesthetics.

While tub girders have primarily been used on bridges with longer spans where concrete girders are not viable, an application of relatively shallow steel tub girders was recently used in the TxDOT Waco District on a bridge with span lengths normally reserved for concrete girder systems. The resulting bridge provided an aesthetically appealing structure that satisfied a demanding vertical clearance requirement and was cost-comparable with precast concrete girders. This shallow tub girder application demonstrates that steel trapezoidal box girders offer a viable alternative that should be considered for a wider variety of bridge applications.

However, to augment the viability of tub girders, improved details need to be considered to further enhance their economic and structural advantages. Modifications in the girder geometry can provide more efficient systems. The objective of this research is to develop improved details for tub girders as well as design methodologies for the girders and bracing components.

17. Key Words Tub Girders, Trapezoidal Box Girders, Improved Details, Bracing, Curved Girders	18. Distribution Statement No restrictions. This document is available to the public through the National Technical Information Service, Springfield, Virginia 22161; www.ntis.gov.

19. Security Classif. (of report) Unclassified	20. Security Classif. (of this page) Unclassified	21. No. of pages	22. Price

Form DOT F 1700.7 (8-72) Reproduction of completed page authorized

THE UNIVERSITY OF TEXAS AT AUSTIN
CENTER FOR TRANSPORTATION RESEARCH

Improved Tub Girder Details: Final Report

Stalin Armijos-Moya
Yang Wang
Todd Helwig
Patricia Clayton
Michael D. Engelhardt
Eric Williamson

CTR Technical Report:	0-6862-1
Report Date:	December 2018; Published November 2019
Project:	0-6862
Project Title:	Improved Tub Girder Details
Sponsoring Agency:	Texas Department of Transportation
Performing Agency:	Center for Transportation Research at The University of Texas at Austin

Project performed in cooperation with the Texas Department of Transportation and the Federal Highway Administration.

Center for Transportation Research
The University of Texas at Austin
3925 W. Braker Lane
Austin, TX 78759

http://ctr.utexas.edu/

Disclaimers

Author's Disclaimer: The contents of this report reflect the views of the authors, who are responsible for the facts and the accuracy of the data presented herein. The contents do not necessarily reflect the official view or policies of the Federal Highway Administration or the Texas Department of Transportation (TxDOT). This report does not constitute a standard, specification, or regulation.

Patent Disclaimer: There was no invention or discovery conceived or first actually reduced to practice in the course of or under this contract, including any art, method, process, machine manufacture, design or composition of matter, or any new useful improvement thereof, or any variety of plant, which is or may be patentable under the patent laws of the United States of America or any foreign country.

Notice: The United States Government and the State of Texas do not endorse products or manufacturers. If trade or manufacturers' names appear herein, it is solely because they are considered essential to the object of this report.

Engineering Disclaimer

NOT INTENDED FOR CONSTRUCTION, BIDDING, OR PERMIT PURPOSES.

Project Engineer: Todd A. Helwig
Professional Engineer License State and Number: Texas No. 92480
P. E. Designation: Research Supervisor

Project Engineer: Michael D. Engelhardt
Professional Engineer License State and Number: Texas No. 88934
P. E. Designation: Research Supervisor

Project Engineer: Eric B. Williamson
Professional Engineer License State and Number: Texas No. 94410
P. E. Designation: Research Supervisor

Acknowledgments

The authors extend their appreciation to the Texas Department of Transportation for providing the funding for this research. The authors thank the Project Manager, Wade Odell, for oversight and coordination of this project. The authors also thank the entire project monitoring committee for their assistance and guidance:

- Geetha Chandar, Professional Engineering Procurement Services Division
- Jamie Farris, Bridge Division
- Dennis Johnson, Houston District
- Teresa Michalk, Materials and Tests Division
- Jason Tucker, Materials and Tests Division

Products

This report contains two products:

- **P1**–Recommended details for improved economy and efficiency in steel tub girders: See Chapter 1 and 6
- **P2**–Design methodology for top truss and internal K-frames utilizing modified details: See Chapter 6

Table of Contents

List of Figures

List of Tables

Chapter 1. Introduction and Background

1.1 Introduction

Steel tub girders are commonly used for horizontally curved bridge applications. The girders consist of a bottom flange, two top flanges, and two sloping webs and are also referred to as trapezoidal steel box girders due to the shape of the cross section. In addition to their aesthetic appeal, steel tub girder systems have distinct structural advantages over alternative I-girder systems. A major advantage of tub girders is the significant torsional stiffness of the closed box section. The large torsional stiffness makes tub girders attractive for horizontally curved bridge applications. The closed cross-section of box girders often have a torsional stiffness that is more than 1000 times the stiffness of comparable I-shaped girders (Fan and Helwig 1999).

Historically, girders with two webs and two flanges formed closed steel box girders for bridge applications in the U.S. and other countries. However, because of regulations created by the Occupational Safety and Health Administration (OSHA), the construction of enclosed steel box girders became unattainable in the U.S. This in turn promoted the study and use of open section steel girders (i.e. tub girders) with a concrete deck on top (Linzell, Hall et al. 2004). Composite box sections formed by steel tub girders and a concrete deck are currently an appealing alternative for structural systems in which the geometry produces large torsional demands (i.e. horizontally curved bridges) due to the torsional benefits. Nevertheless, the relatively low torsional stiffness of the steel tub girder before hardening of the concrete requires the addition of a top lateral truss and internal bracing of the tub in order to avoid instability issues during transportation, erection, and construction of the bridge.

Although tub girders have commonly been used on horizontally curved girders, the improved aesthetics of the girders compared to other bridge shapes have led to their use on straight bridges as well; however straight-girder applications have been limited. Economic efficiency and fabrication/handling difficulties are typical concerns that curb the use of steel tub girders compared to other structural options such as I-shaped steel girders or pre-stressed concrete girders for straight bridges. However, a relatively recent application of shallow steel tub bridge girders on I-35 in the Waco district has shown the potential to increase the usage of steel tub girders for span lengths normally reserved for concrete bridges with a comparable cost [Figure 1-1] (Chandar et al. 2010). This shallow tub girder application demonstrates that steel tub girders are a viable alternative for a wider variety of bridge applications.

Figure 1-1 -Shallow Tub Girder System – Waco (Chandar et al. 2010)

Despite the structural advantages, current design and detailing practices for steel tub girders often include a number of aspects that may lead to unnecessary fabrication costs and structural inefficiencies. To increase the viability and efficiency of steel tub girders, a TxDOT sponsored research project was carried out with a focus on the development and evaluation of improved details. The impact of these modifications on the global and local behavior of steel tub girder systems was evaluated through laboratory tests and parametric finite element analysis.

To understand the focus of the study, a basic understanding of the components that comprise steel tub girder bridges is necessary. The next section provides a brief overview of common geometrical layouts of steel tubs as well as the bracing systems that is provided. The scope of the research study is then covered.

1.2 Steel Tub Girder System Components

Steel tub girder bridges generally consist of a trapezoidal steel girder with a composite concrete deck. The trapezoidal steel girder section consists of two top flanges, two sloping webs and a single bottom flange. While the composite action between the steel girders and the cured concrete deck have a very large torsional stiffness in the finished bridge, the open section during construction is torsionally flexible. Therefore, bracing systems are provided to help maintain the geometry of the girder section as well as increasing the torsional stiffness. The primary bracing systems include top flange lateral trusses as well as internal and external cross frames or diaphragms. A tub girder with a top flange lateral truss is sometimes referred to as a "quasi-closed" box since the girder with the lateral truss simulates a closed girder. For thin-plate webs and bottom flanges, stiffeners may be utilized to prevent local plate instability issues. Additionally, shear studs are provided along the span length to connect the quasi-closed box girders with the concrete deck, achieving desired torsional rigidity by full composite action. Figure 1-2 shows the structural components of a tub girder system.

Figure 1-2 Typical Twin Tub Girder System during Construction

1.2.1 Top Flange Lateral Bracing

As noted previously, an attractive attribute of steel tub girders is the large torsional stiffness of the finished girders with the fully cured concrete deck. However, during construction, the tub girder is an open section that is relatively flexible. Therefore, a top flange lateral truss is provided

along the length of the girders as depicted in Figure 1-3. The truss creates a "quasi-closed" cross-section that significantly improves the torsional stiffness of the girder. The top flange lateral bracing systems are important during transportation, erection, and construction to maintain stability of the girder and to control deflections. The absence or poor sizing of lateral bracing can produce major issues, such as the collapse of the Marcy Pedestrian Bridge in New York State which was primarily caused by the lack of a top flange lateral truss (Helwig and Yura 2012). Additional problems have occurred in other bridges such as the girder in Figure 1-4 in which the diagonals of the truss buckled during girder erection due to improper sizing.

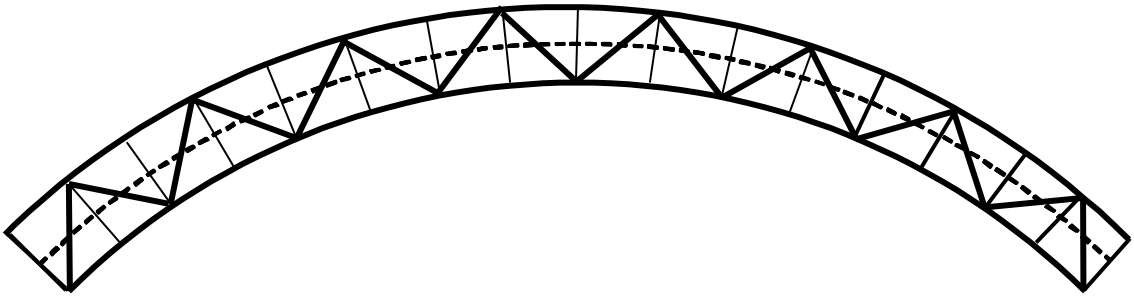

Figure 1-3 -Plan View of Tub Girder with Top Flange Truss

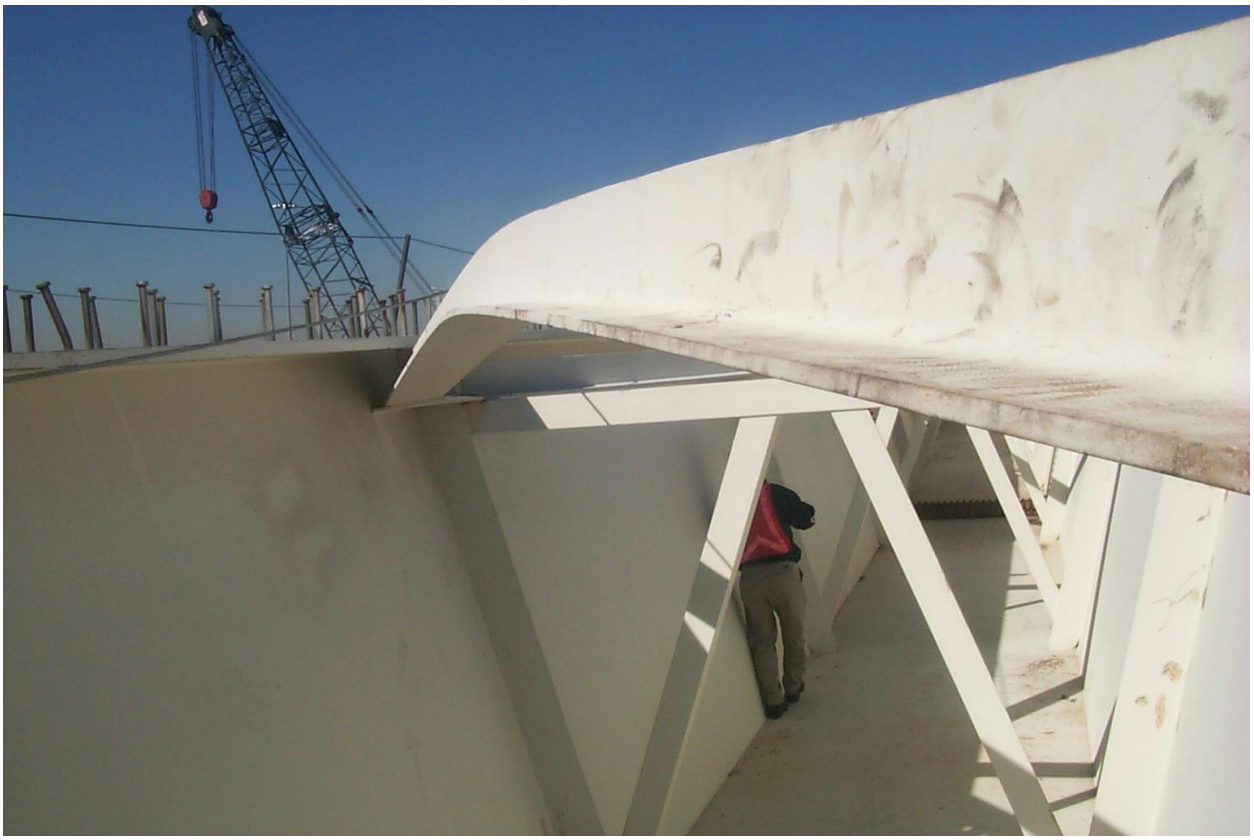

Figure 1-4 -Improperly Sized Top Lateral Truss Resulted in Buckled Diagonal

There are different configurations of the top flange lateral truss; however, the most common systems consist of either an X-Type Truss in which there are two diagonals per panel or

a Single Diagonal (SD-Type) truss. Figure 1-5 shows the most common geometries for the truss panels. With regards to the SD type truss there are generally two possibilities consisting of either a Warren Truss where the diagonal orientation varies or a Pratt Truss where the diagonals are oriented in the same direction. The selection of layout pattern depends on bracing effectiveness in resisting torsional forces with the lightest member weight and fabrication/detail cost. Ideally, the Pratt system is usually arranged such that all the diagonals are in tension, which is more suitable for simple span applications in order to obtain lighter bracing members. However, the ability for the diagonals to "only" be subjected to tension is rarely possible in continuous girder systems since the inflection point shifts depending on the applied loading in adjacent spans. For example, as the concrete deck is poured beginning at one end of the span during the construction sequence, the inflection point will shift, and compression will develop in some of the diagonals and the limit state of buckling must be considered. The Pratt system also leads to larger forces in the struts since the strut must generally transfer the entire horizontal component of the diagonal forces. However, in the Warren system, from a torsional perspective, adjacent diagonals alternate tension and compression and the strut only transfers the unbalanced force form the adjacent diagonals. In comparison, considering the case of torsion on the tub girder, a panel of the X-type system will develop compression in one diagonal and tension in the other. To achieve the same torsional rigidity, the X-type requires the lightest bracing weight. However, the fabrication requirements for the X-type bracing are generally the most costly due to the number of members and connections required. Due to the high cost, X-type systems are rarely used in practice. In the Warren system, the diagonal at the location of maximum torque is typically oriented to be in tension, but the system is controlled by maximum compression. The Warren truss is more flexible to handle the variations present during the deck pouring sequence and can be cost effective to achieve desired torsional rigidity. Thus, the Warren bracing system, or SD-truss, is still the most commonly used bracing system. There are a number of other factors that impact design requirements of the top lateral truss. A more detailed discussion of the top lateral truss behavior is outlined in Chapter 2.

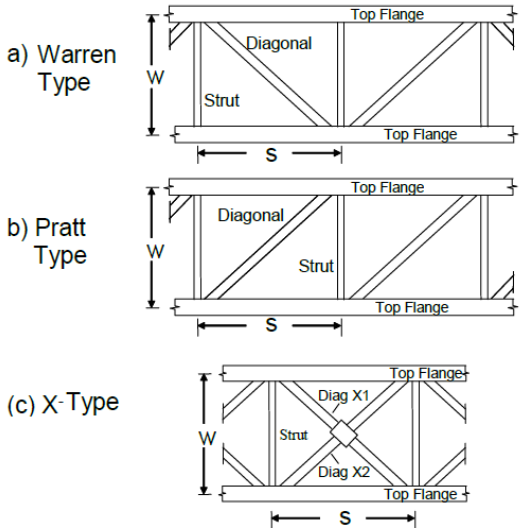

Figure 1-5 -Top Lateral Bracing Layouts (Helwig and Yura 2012)

1.2.2 Internal K-Frames

Another bracing component are the internal cross-frames or plate diaphragms that are provided along the length of steel tub girder primarily to maintain the cross-section shape against torsion-induced distortion. The most common form of internal bracing are the K-frames such as those shown in Figure 1-6. Other geometric arrangements include X-type, Z-type and solid plate diaphragms. The solid plate diaphragms are generally provided at support locations. At interior supports, an access hole is provided so that inspectors can move from one span to another. From an accessibility perspective, the most common internal cross frame is the K-frame since the geometry provides more workspace and accessibility for maintenance and inspection. In addition, the K-frame arrangement produces short diagonal lengths, which increases the efficiency of the compression diagonal sizing in the bracing system. It should be noted that the top strut of the internal K-frames also forms the strut for the top lateral truss. The most common detailing practice is to include an internal cross frame at each panel point of the top lateral truss.

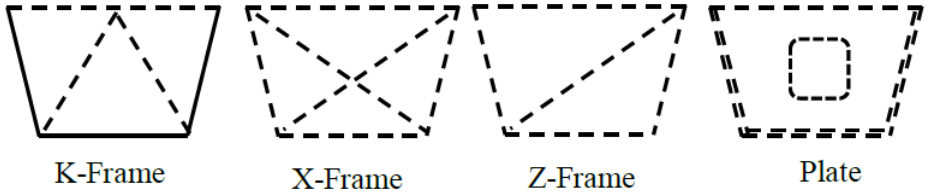

Figure 1-6 -Internal Intermediate Cross-Frame Layouts, Tub Girders (Helwig and Yura 2012)

1.2.3 External K Frame

External cross frames, such as those shown in Figure 1-7, are often provided in steel tub girders to control the relative deformations between adjacent girders during placement of the concrete deck. External cross frames or diaphragms are always provided at support regions to control twist of the tub girders and may also be provided at intermediate locations along the length. In most situations, external intermediate K-frames are removed after construction due to fatigue concerns. If not removed, the external bracing can also contribute to the load transfer between adjacent tub girders. Installing these external braces in the field can be a challenge due to the high torsional stiffness of the girder. In addition, the removal of the braces is complicated due to a lack of crane access under the girder after the concrete deck is placed. The most efficient location to place external bracing to control differential deformations between adjacent tubs is generally at mid-span. Thus, braces away from mid-span are not as effective at controlling the relative movement. External K-frames are primarily needed on horizontally curved girders. In straight girders, if diaphragms are provided at the supports and a top flange lateral truss is utilized, the girders are very stiff and intermediate external K-frames can be omitted. Diaphragms are needed for straight girder systems if a large unbalanced load is applied or if the supports have significant skew, thus most practical applications of straight girders do not require external bracing.

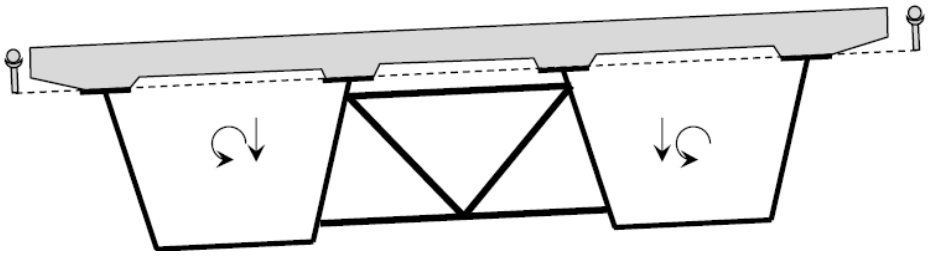

Figure 1-7 -Intermediate External Cross Frames for Tub Girder (Helwig and Yura 2012)

1.3 Proposed Improved Steel Tub Girder Details

The advantages of using steel trapezoidal box girders (tub girders) for straight and horizontally curved bridges discussed thus far have related to their structural behavior and aesthetically pleasing configuration. Although there are advantages to utilizing steel tub girders, the cost of the girder systems is usually higher than other options such as steel I-girder systems. The increase in cost is generally related to higher fabrication costs. The higher fabrication costs are exacerbated by the significant detailing requirements of the many bracing systems as well as the geometric layout of the girders themselves. The recent application of shallow steel tub girders in the Waco district demonstrated that improved economy is possible with the girders with proper detailing. Many of the detailing practices that are used for steel tub girders are based upon traditional practices that may result in structural inefficient systems and unnecessary bracing in some regions of the girders. This report highlights the results of a TxDOT sponsored study on the detailing practices for steel tub girders. The goal of the investigation is to assess the viability of improved details for steel tub girders in order to obtain not only enhanced structural response but also economic efficiency. The generally details that were studied and their possible implications in the structural system behavior are described in the following sections.

1.3.1 Cross Section Efficiency Improvements

1.3.1.1 Web Slope

Currently, AASHTO 2017 Sections 6.11.2.1 and 6.11.2.3 specify design requirements for webs on steel tub girders and specify a slope limit of 1H:4V (i.e. ratio 1 horizontal to 4 vertical) as depicted in Figure 1-8a. The usage of steel tub girders for short to moderate spans could lead to relatively shallow girders with larger tributary widths than typically used in practice. This increment in tributary width can be attained by using tub girder webs with a flatter web slope, such as 1H: 2.5V, as shown in Figure 1-8b. Furthermore, by exceeding the web slope limit specified by AASHTO, some effects can be produced into the system, such as:

- Increase of the single girder width tributary area, which may lead to a reduction in the number of girder lines across the bridge width
- Additional web shear
- Increase of the top lateral strut demands resulting from the horizontal component of the web shear
- Reduction in the spacing between intermediate internal cross-frames

- Variation in the distribution of live loads (live-load distribution factors) due to non-compliance of Section 6.11.2.3 of AASHTO.

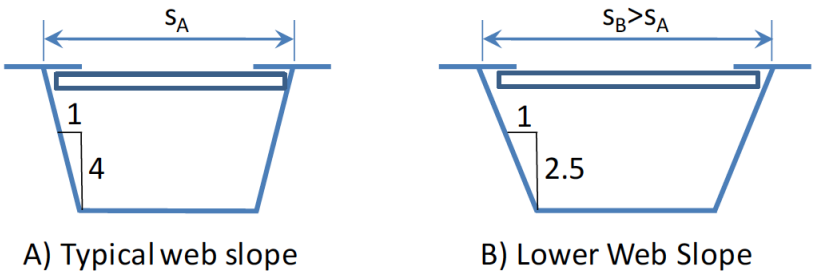

Figure 1-8 - a) Common Web Slope Limitations, b) Flatter Web Slope (proposed)

1.3.1.2 Girder Spacing

Another factor that may improve the economy of the girders is the spacing between adjacent girders. Increasing the girder spacing will potentially reduce the number of girder lines, but the impact on the proportion of the live load supported by each girder needs to be investigated by parametric study.

1.3.2 Bracing Connection Details Improvement

1.3.2.1 Top Flange Offset

Typically, top lateral trusses are detailed so that the working lines of diagonals and struts are forced to intersect (i.e. working point). Therefore, relatively large gusset plates are often required, which introduces undesired flexibility in load transferring and additional fabrication costs. A possible improvement is to connect the top lateral truss members directly to the top flange. Sufficient flange width is needed to achieve this. Sizing of the top flanges in the positive moment region is typically controlled by construction moments applied on the non-composite girders. Because large flanges are not normally needed, plate widths for the top flanges are often relatively small (i.e. b_{top} = 12 in. ~ 16 in.). AASHTO 2017 Section 6.11.2.1 specifies that the top flanges must be centered on the webs. This geometry requirement leaves only half of the top flange width ($b_{top}/2$) available for the connection, which can create geometric problems in the connection fabrication [Figure 1-9a]. A potential enhancement of the top lateral bracing connections is to offset the top flanges inwards [Figure 1-9b]. However, the impact of offsetting the top flanges on the girder bending, torsional stiffness, and ultimate strength requires further investigation. According to AASHTO 2017, the flange offset could generate additional lateral flange bending issues that should be considered. Additionally, local buckling issues of the top flanges require investigation since the offsetting of top flanges will increase the top flange slenderness ratio.

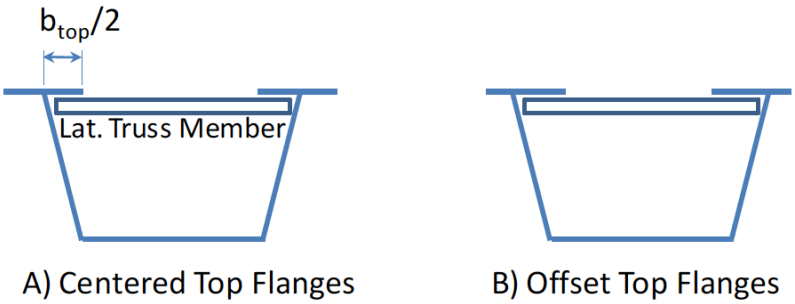

Figure 1-9 - a) Top Flanges Centered to the Web, b) Top Flanges Offset Inside the Tub Girder

1.3.2.2 Connection Eccentricity

Although offsetting the flanges could provide more efficient connections between the top lateral truss members and the top flange, in certain cases, little overlap of the truss members and the girder top flange can be attained when the working lines of truss members intersect at a single working point [Figure 1-10a]. Without enough overlap distance, the available space may not be enough to have sufficient weld length to transfer the required brace member forces to the top flanges. Larger overlap distances may be possible by slightly offsetting the working lines from the working point, as shown in Figure 1-10b. In previous studies of the stability of column bracing systems, researchers have found that offsetting the working lines of bracing members from the working joint by about 10-20% of the column length often results in very little difference in the performance of the bracing compared to cases where the working lines intersect at a point. Since the top lateral truss behaves similarly to a relative bracing system for a column, the adverse impacts on the effectiveness of the truss should not be significant. Offsetting the truss members from the working point would result in less congestion at the working point, as well as provide better force transference between the truss members and the top flanges. Additionally, the strut of the K-frame/top lateral truss can be bolted directly to the flange to avoid a vertical offset of the strut with respect to the top flange level [Figure 1-11].

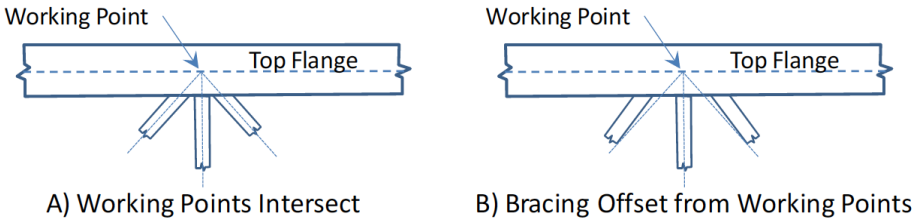

Figure 1-10- a) Concurrent Working Lines, b) Offsetting of Working Lines

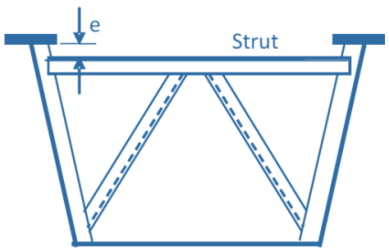

Figure 1-11- Vertical Strut Eccentricity in a Tub Girder Cross-Section (Helwig and Yura 2012)

1.3.3 Bracing Layout Optimization

1.3.3.1 Top Flange Lateral Truss Layout

As mentioned previously, significant torsional stiffness of quasi-closed box girders is mainly attained due to the inclusion of the top flange lateral truss in the open section. Its contribution in preventing stability issues, such as Lateral Torsional Buckling (LTB), has already been studied. However, the top lateral truss is primarily effective near the support ends of the girder where the shear deformations are at their maximum. In light of this fact, the truss diagonals near mid-span do not significantly contribute to the torsional stiffness or the lateral-torsional buckling resistance of the quasi-closed box. Instead of providing the top flange truss along the entire length [Figure 1-12a], a more efficient system could be to provide truss diagonals only near locations with large shear deformations (i.e. ends of the tub girder) [Figure 1-12b]. Figure 1-12b shows the un-deformed and the possible buckled shape (dashed lines) of a steel tub girder with enhanced top lateral bracing layout. The use of partial bracing will likely not be practical for girders with significant horizontal curvature; however, for straight or mildly curved girders, effective bracing may be obtained.

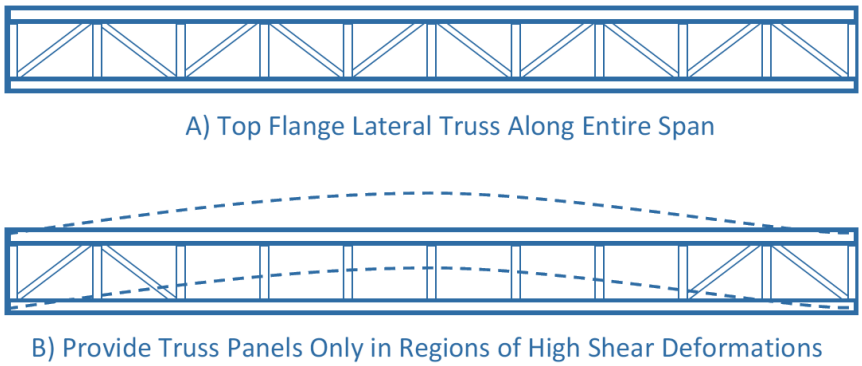

Figure 1-12 - a) Usual Top Lateral Bracing (TLB) Layout, b) Optimized TLB Layout (Proposed)

1.3.3.2 Internal K-frames Layout

Besides top lateral truss layout, another factor that requires further study is the potential for a reduction of internal K-frames. Typically, internal K-frames are placed at every panel point of the top lateral truss; however, in certain cases, a larger spacing will result in good performance of the system and will be less costly to fabricate. Since the distortion is often not significant enough to require cross frames at each panel point of the top flange lateral truss, there is no advantage to using this every panel spacing. In fact, studies have shown that systems with K-frames spaced at every single panel point led to larger forces in the top flange lateral truss. Therefore, the K-frame spacing in Figure 1-13b may be worse than the one in Figure 1-13a for both force distribution and fabrication requirements. The cross-section in Figure 1-13c corresponds to truss panel points with K-frames, while the cross-section in Figure 1-13d corresponds to panel points without the K-frames (i.e. only top strut bracing). Considering that straight tub girder systems experience very little torsion, the number of intermediate internal K-frames may be even less than the distribution shown in Figure 1-13a. The possibilities of reducing the number of internal K-frames will be

investigated considering factors such as the effects of the distribution of the cross-frames in cross-section distortion, longitudinal warping stresses, and transverse bending stresses, among others.

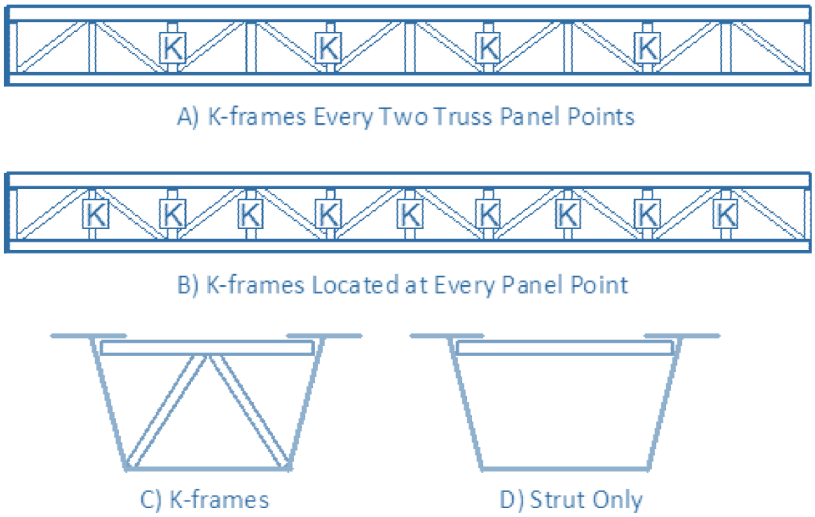

Figure 1-13 -Internal K-frame Details

1.4 Research Methods

The study of improved details for tub girders was conducted using three methods: large-scale laboratory testing, finite element modeling, and parametric studies. The laboratory experiments consisted of elastic buckling tests on three 86-foot long tub girders with different cross section characteristics. Additionally, the experimental data collected was used to validate finite element models created in the three-dimensional finite element program Abaqus/CAE. The validated models have been used to perform an extensive parametric study to extend the experimental part and to study the different proposed details.

1.5 Report Organization

This report is divided into 7 chapters. Following this introductory chapter, an overview of pertinent background information is covered in Chapter 2. The background information that is presented in Chapter 2 consists of the most important material related to the geometric configuration of the girders as well as the bracing, and a discussion of pertinent sections of the AASHTO Bridge Design Specifications. Additional information on box and tub girders from the literature is provided in Appendix A. Chapter 3 provides a discussion of the experimental program related to the elastic load tests as well as an overview of the test results. A discussion of the finite element results and the parametric FEA results are covered in Chapter 4. Chapter 5 covers the experimental results from the ultimate strength tests on the composite tub girders. Design methodology and recommendations are provided in Chapter 6. Finally, the overall project conclusions and future work are discussed in Chapter 7.

Chapter 2. Background Information

A thorough review of the literature related to previous work on steel box and tub girders was conducted as part of the study to identify related research work. A summary of this past work is provided in Appendix A. This chapter provides an overview of previous studies that provide the most relevant background information for the research outlined in this report. An overview of the specific sections of the AASHTO Bridge Design Specifications that contain provisions relevant this investigation is also provided.

2.1 General Behavior

Steel tub girders systems are an appealing alternative for horizontally curved bridges due to their aesthetic appeal and high torsional stiffness. Historically, the development of curved beam theory (Saint-Venant 1843) and thin-walled beam theory that couples bending and torsion (Vlasov 1961, Dabrowski 1968) marked the beginning of collection of studies on the analysis and design of straight and horizontally curved box-girder bridges. Based on the aforementioned work, braced tub girders behave as thin-walled beams with potentially bending, torsional, and distortional demands.

Depending on whether simple versus continuous girders are utilized, quasi-closed box girders typically have span-to-depth ratios between 25 and 35. The effects of combined bending and torsion on the girders must be considered. The flexural behavior can be analyzed with traditional beam theory to evaluate the bending and shear stresses. As depicted in Figure 2-1, the flange and web plates are subjected to in-plane normal stresses (i.e. tension or compression) due to bending moments [Figure 2-1a], and in-plane shear stresses [Figure 2-1b].

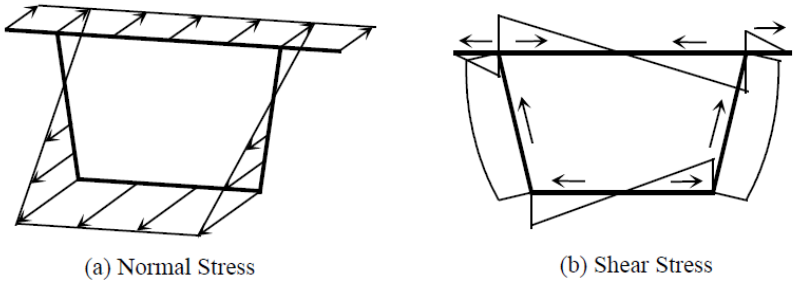

Figure 2-1 - Distribution of bending Stresses in Box Girders (Fan and Helwig 1999)

In addition to the effects of bending, the girders are also often subjected to torsional moments that are resisted on the girder cross-section through shear stresses. Normally, thin-walled members resist in-plane torsion from two torsional resistance components, 1) Saint-Venant torsion and 2) warping torsion. St. Venant torsion is associated with pure shear in-plane stresses, while warping torsion is associated with twisting of the section that leads to in-plane bending of the plate elements. Saint-Venant torsion typically dominates the torsional stiffness of box girders due to the closed cross-section such that the normal stresses produced from warping torsion can be neglected (Kollbrunner and Basler 1969). Figure 2-2 shows the typical shear flow, q, produced by the distribution of torsional shear stresses, τ, on a trapezoidal box girder.

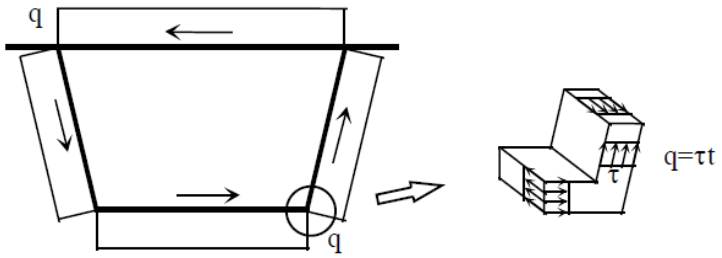

Figure 2-2 - Shear Flow in Box Girder Due to Saint-Venant Torsion (Fan and Helwig 1999)

The analysis of horizontally curved box girders can be complicated due to the combination of bending and torsional demands. Several analytical closed-form solutions [(Vlasov 1961), (Dabrowski 1968)] have been proposed to solve curved beam configurations with different span and loading arrangements. However, the solution of these analytical methods is not convenient for common practice. Instead, approximate and numerical methods have been widely used to analyze straight and horizontally curved tub girders.

An approximate method for considering the torsional behavior of horizontally curved girders is the M/R method that was developed to approximate the torsional demands produced by curved geometries of horizontally curved box girders with small to moderate curvature (Tung and Fountain 1970). As shown in Figure 2-3, the method recommends that the torsional demands can be approximately represented by two distributed lateral loads M/Rh applied on the top and bottom flanges with opposite directions, where M is the bending moment, R is the curvature of the beam, and h is the vertical distance between the top and bottom flanges [Figure 2-3]. Although modern software can allow sophisticated models to provide a direct indication of the behavior of horizontally curved bridges, the M/R method provided a method of analyzing curved structures when these resources were not available. A horizontally curved system could be modeled using straight elements with the M/Rh laterally distributed loads applied to the structure so that the design torques could be estimated.

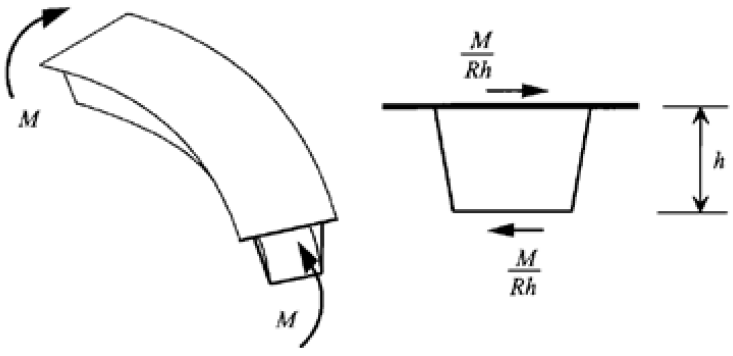

Figure 2-3- Equivalent Torsional Loads on Curved Box Girders (M/R method) (Fan and Helwig 1999)

In addition to bending and torsional effects, cross-sectional distortion can occur when the torsional shear stresses are not distributed throughout the cross section in proportion to the St. Venant shear flow. Torsional moments on box girders can come from two general sources: 1) torsional due to horizontal curvature or 2) torsion from eccentric vertical loads. The case with

horizontal curvature is depicted in Figure 2-3. Figure 2-4 shows the case of an eccentric vertical loads and the torsional can be divided into a pure bending load as well as a torsional component. Under general torsional demands, the box girder cross-section can distort from its original geometry. As a result, cross-sectional distortion produces additional longitudinal warping and transverse bending stresses in the individual plates of the box girder (Dabrowski 1968).

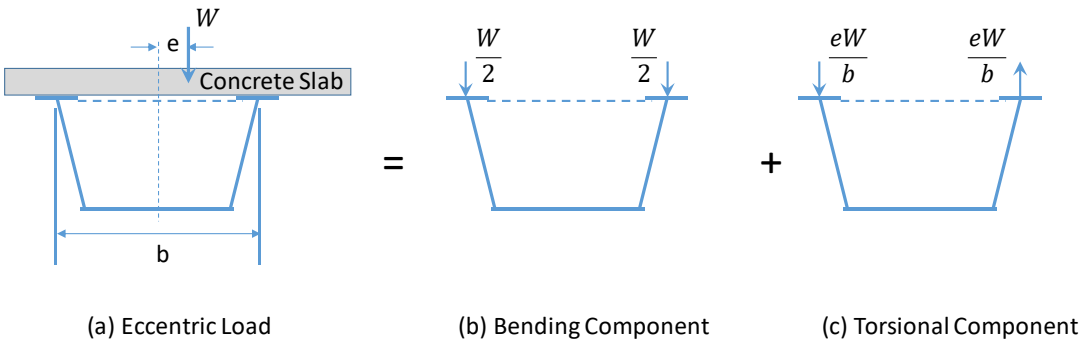

Figure 2-4- Sources of Bending and Torsion in Tub Girders (Fan and Helwig 2002)

To understand the reason the cross section distorts, the case of a torsion applied to a girder that is not distributed in proportion to the St. Venant shear flow can be considered. Figure 2-5 shows a box section that has dimensions of "b" for the width and "h" for the depth. The section has an applied torque in (a) of "T" that is represented by a force couple as shown. The torque can be idealized as a "pure torsional component" shown in (b), and the "pure distortional component" shown in (c) (Fan and Helwig, 2002).

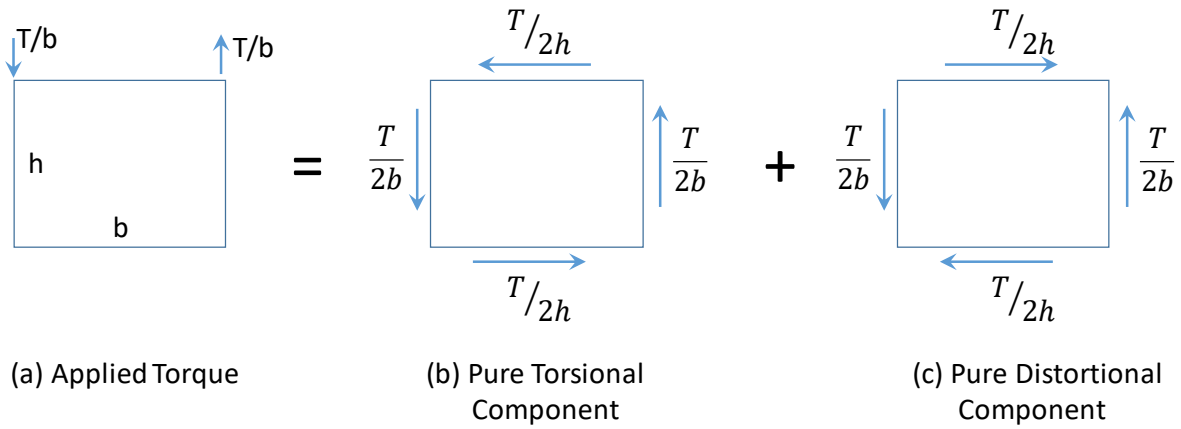

Figure 2-5 - Pure Torsional versus Pure Distortional Representation of Applied Torque

The pure distortional component does not cause any torque to the section; however, the cross-section will distort from the distortional load. Figure 2-6 shows an idealization of how the section might distort. To preserve the shape of the cross section, internal cross frames are provided that maintain the distance along the two diagonals of the box section. Internal cross frames are discussed in more detail later in the chapter.

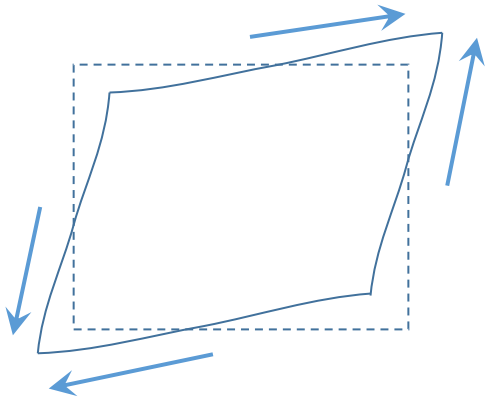

Figure 2-6 -Distortion of Box Section Due to Distortional Loads

2.2 Top Flange Lateral Bracing

As noted previously, an attractive attribute of steel tub girders is the large torsional stiffness of the finished girders with the fully cured concrete deck. However, during construction, the tub girder is an open section that is relatively flexible. Therefore, a top flange lateral truss is typically provided to create a quasi-closed cross-section, significantly enhancing the torsional stiffness. The top flange lateral bracing systems are important during transportation, erection, and construction to maintain stability of the girder and to control deflections. There have been cases in which the absence of a top lateral truss has led to major problems such as the Marcy Pedestrian Bridge that collapsed during casting of the concrete bridge deck [Figure 2-7]. Additional problems have occurred in other bridges such as the girder in Figure 2-8 in which the diagonals of the truss buckled during girder erection due to improper sizing. The problem in Figure 2-8 occurred during girder erection, which was fortunate since the erector could see the buckled diagonals as the girders were released from the crane. Had the problem occurred during placement of the concrete bridge deck, the entire bridge could have collapsed.

Figure 2-7- Collapse of Marcy Pedestrian Bridge (Structure Magazine, February 2008)

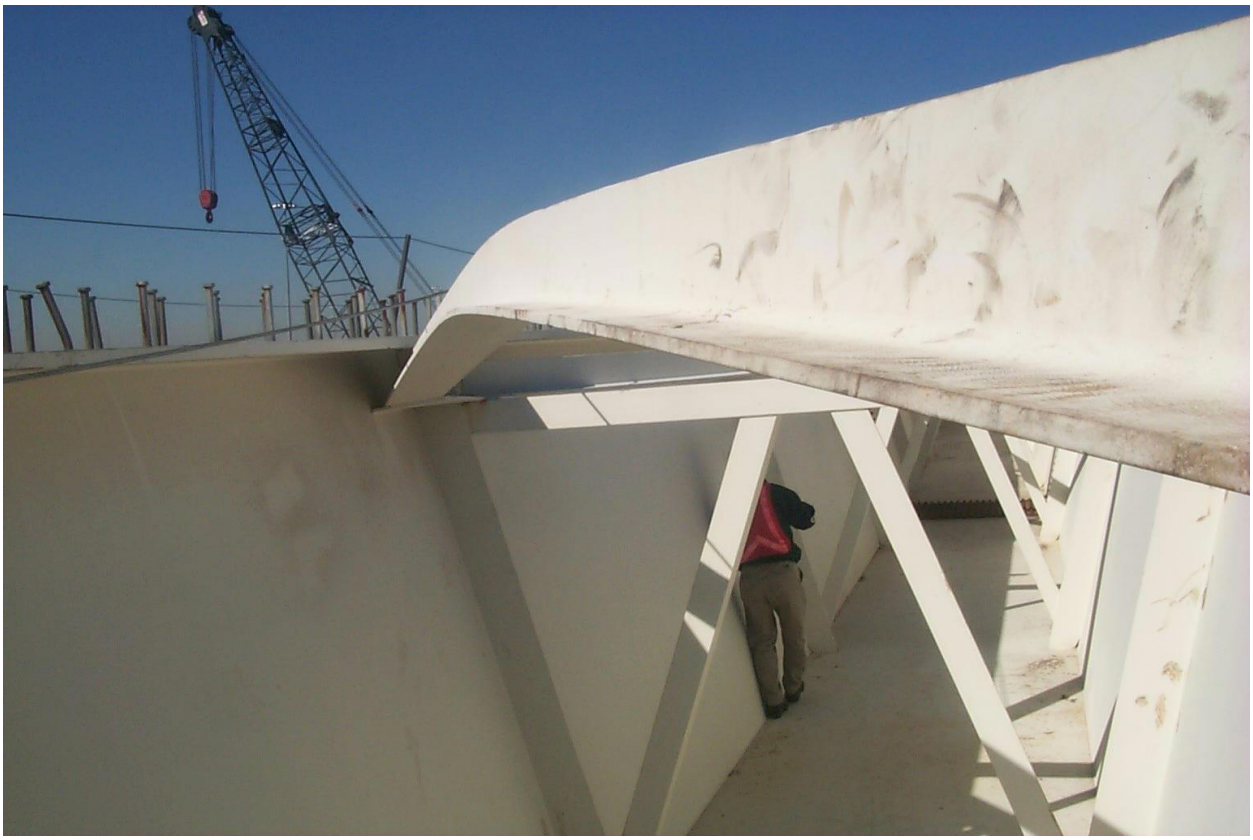

Figure 2-8 Buckling of Diagonals in Top Lateral Truss of Steel Tub Girder

The design of the top flange truss lateral bracing includes both member sizing and selecting an appropriate geometrical layout. The sizing of the top lateral bracing should meet the torsional stiffness (i.e. related to the Saint-Venant's torsion constant, J) and strength requirements. Kollbrunner and Brasler (1969) developed the Equivalent Plate Method (EPM) to analyze quasi-closed cross-sections, in which the top lateral truss is idealized as a fictitious plate to approximate the torsional properties of the section. The equivalent plate thickness is a function of the truss geometry and area of the diagonals, struts, top flanges, and webs. By providing enough cross-sectional area on the top lateral members, the Saint-Venant torsion component dominates resulting in negligible warping normal stresses and small torsional deformations. The member must also be sufficiently sized to resist the forces imposed on the system. The forces induced in the bracing members have a variety of sources: including torsional on the girders, vertical bending of the box girder, the effects of the sloping girder webs, box girder distortion, and other lateral loads on the girder.

Brace forces can be determined using several different approaches, either numerically or by approximate methods. Although numerical methods such as three-dimensional finite element analyses (FEA) of girder systems can directly provide the forces induced in the bracing members from a variety of sources, many engineers do not use these detailed models for the construction condition and as a result, approximate methods or often utilized for design. A common computational model for design is the use of a grid analyses to obtain the design forces. The grid model approximates the three-dimensional girder section geometries as line elements. However, this simplification requires alternative approaches to determine the bracing member forces. Fan

and Helwig (1999) developed a method to estimate the top lateral bracing forces including the effects of vertical bending and lateral loads. The principle of superposition can be used to add the forces from bending and lateral loads to the forces induced from torsion that can be determined using the equivalent plate method (EPM). Figure 2-9 shows the idealization of the forces in the truss induced from torsion using the EPM. Idealizations using two different types of top lateral trusses are shown: 1) a single diagonal system (SD-truss) and 2) a cross diagonal system (X-truss). Expressions to calculate approximate top lateral bracing forces induced in the truss from vertical bending of the box girder were developed by Fan and Helwig (1999). Additionally, the authors also evaluated the lateral bending stresses in the top flanges from the bending-induced truss forces. Typically, member sizes remain constant along the span to minimize cost, so regions with the largest torque often control the member sizes; however, care should be taken in regions of high torsion and bending moment such as around interior supports since the forces in the truss are additive.

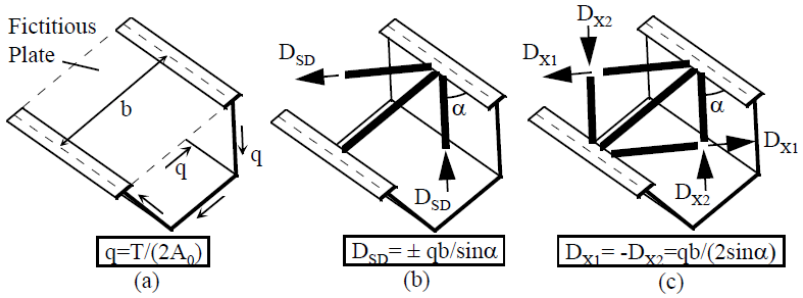

Figure 2-9 - Diagonal Brace Forces Due to Torsion According to EPM (Fan and Helwig 1999)

Kim and Yoo (2006) extended the study from Fan and Helwig (1999) by reporting modified expressions to improve the accuracy for member force calculations of single diagonal top lateral bracing systems (SD-truss). The effects of vertical and lateral bending, as well as pure torsion and distortion, were evaluated separately and considered in the formulation presented to estimate forces in diagonals and struts of SD-trusses.

In regard to bracing layout, the Warren (SD-truss), the Pratt, and the X-type trusses depicted in Figure 2-10 have been used in past applications. The selection of layout pattern depends on bracing effectiveness in resisting torsional forces with the lightest member weight and fabrication/detail cost. The Pratt system is usually arranged such that all the diagonals are in tension, which is more suitable for simple span applications in order to obtain lighter bracing members. However, if the concrete deck is poured beginning at one end of the span during the construction sequence, compression can develop in diagonals. The relatively small area of the Pratt bracing members will result in a thin equivalent plate according to the EPM, resulting in low torsional stiffness and large torsional deformations. The decreased amount of bracing in the Pratt system also leads to larger forces being developed in the strut. In comparison, the X-type system consists of one diagonal in tension and another compression. To achieve the same torsional rigidity, the X-type requires the lightest bracing weight. Additionally, fabrication requirements for the X-type bracing is costly due to the number of members and connections required. Due to the high cost, X-type systems are rarely used in practice. In the Warren system, the diagonal at the location of maximum torque is typically oriented to be in tension, but the system is controlled by maximum compression. The Warren truss is more flexible to handle the variations present during

the deck pouring sequence and can be cost effective to achieve desired torsional rigidity. Thus, the Warren bracing system, or SD-truss, is still the most commonly used bracing system.

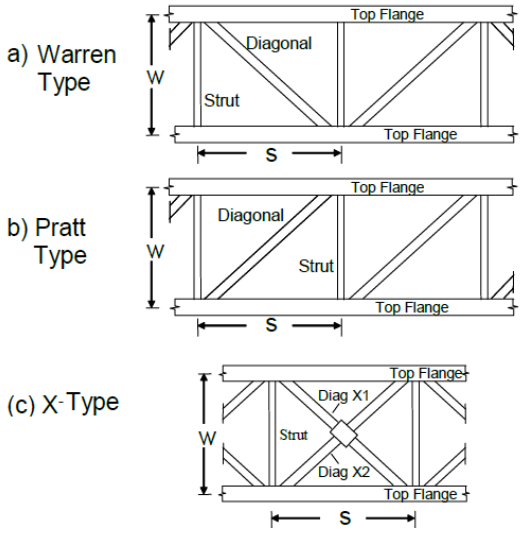

Figure 2-10 - Top Lateral Bracing Layouts (Helwig and Yura 2012)

Additional parameters to consider when defining the bracing layout are the number of panels along the span length and the angle of the diagonals. For the purposes of discussion, the angle of inclination is defined as the acute angle between the flange and the diagonal. The panel spacing is controlled by the geometry of the unbraced length of the top flange, while the angle of the diagonals should be kept between 35 and 50 degrees (Helwig and Yura 2012). The diagonals become longer with small angles and therefore buckling of diagonals in compression becomes a potential controlling design consideration. On the contrary, larger angles of inclination leads to additional panels with an increase in connections and higher fabrication costs. Properly sized top lateral trusses are important to ensure the stability of the girders during construction.

2.3 Internal K-Frames

Besides top lateral bracing, intermediate internal cross-frames are included along the length of steel tub girder primarily to maintain the cross-section shape against torsion-induced distortion. Figure 2-6 depicted the distortion of the cross section that can occur when the torsion is not distributed in proportion to the St. Venant shear flow. Internal cross frames are provided to maintain the shape of the cross section. If no top lateral truss is present, internal cross frames help provide the stability, however the internal K-frames are not necessarily a brace point for the top flanges. This was demonstrated with the Marcy Pedestrian Bridge that collapsed due to the lack of a top lateral truss, although closely spaced internal K-frames were presented (Helwig and Yura, 2012). The most common form of internal bracing are the K-frames such as those shown in Figure 2-11. Other alternative geometric arrangements include X-type, Z-type and solid plate diaphragms. Compared to X and Z-type, K-frames provide more workspace and accessibility for maintenance and inspection, while solid plate diaphragms are typically reserved for support regions. In addition, the K-frame arrangement produces short diagonal lengths, which increases the efficiency of the compression diagonal sizing in the bracing system. Over interior supports, the plate diaphragm

will usually have an access opening to allow inspectors and maintenance personnel to move from one span to the other. At exterior supports, the plate diaphragm is typically solid.

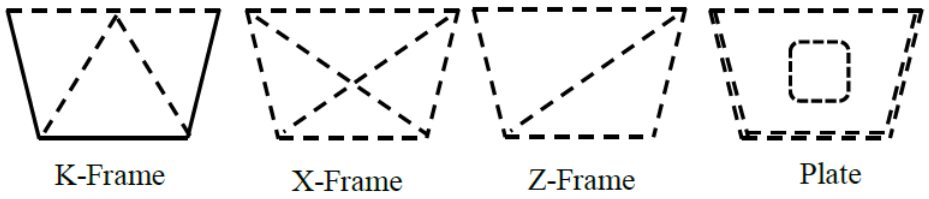

Figure 2-11- Internal Intermediate Cross-Frame Layouts-Tub Girders(Helwig and Yura 2012)

In general, torsional distortion occurs in box cross-sections when the shear in the flange and webs is not distributed through the cross section in proportion to the St. Venant shear flow. Given that most torsion occurs due to either eccentric vertical loads or gravity loads acting on a curved member, the loads are not generally distributed in proportion to the St. Venant shear flow, resulting in cross-sectional distortion. The internal K-frames minimize the distortion-induced stresses since they maintain the shape of the box section. Vlasov (1961) was the first to study torsional distortion in thin-walled beams, followed by Dabrowski (1968), who developed a more strict theory with equations to analyze box girder distortion for simple cases. Wright, Abdel-Samed et al. (1968) presented an analytical procedure based on the beam-on-elastic-foundation (BEF) analogy to analyze the distortional behavior of box girders. According to the BEF analogy, the box girder is represented by a beam on an elastic foundation whose bending stiffness represents the warping stiffness of the box girder, the stiffness of the elastic foundation simulates the out-of-plane bending resistance of the box cross-section, and discrete elastic supports simulates the stiffness of internal diaphragms. Oleinik and Heins (1975) studied the impact of internal diaphragm spacing along curved box beam bridges in order to limit the distortional effects on the cross-section. After carrying out parametric analyses, empirical expressions were formulated to estimate the number of diaphragms and their separation to avoid distortional effects. Hsu, Fu et al. (1995) presented the equivalent beam on elastic foundation (EBEF) method to perform the distortional analysis of closed or quasi-closed box girders. The EBEF is a method that takes into account the deformations of the cross-section to measure the effects of rigid or flexible internal diaphragms and the continuity over the supports. Fan and Helwig (2002) expanded upon this concept, developing a method in which the applied vertical loads could be represented by pure torsional and pure distortional components, both of which are a function of the torque at a specific point on the girder and the box section geometry. These distortional components can be transformed directly into forces induced in the internal K-frames. Because the struts of the K-frames also serve as the struts of the top lateral truss, the distortion-induced forces in the struts are superimposed on the forces in the top truss struts due to torsion and box girder bending. Kim and Yoo (2009) studied the behavior of quasi-closed trapezoidal box girders with internal X-type cross-frames under bending loading. The interaction between single diagonal top lateral bracing and X-type cross-frames was evaluated based on the panel spacing of the internal cross frames. The bracing forces in the X-type cross-frames spaced at odd numbered panels were found to be as much as 30% larger than the cross-frames spaced at even numbered panels. The authors reported an expression to calculate bracing member forces for both SD-truss top lateral bracing and X-type cross-frame bracing. Recently, Yoo, Kang et al. (2015) developed a procedure to analyze distortional stresses on horizontally curved box girders based on the analogy of beams on an elastic

foundation. Several equations were proposed to estimate longitudinal and transverse bending stresses produced by distortional warping and deformation of the cross-section, respectively. These suggested expressions are applicable to trapezoidal tub girders with overhangs and rigid or flexible cross-frames, for both simple and continuous spans. Moreover, Zhang, Hou et al. (2015) conducted an analytical study of curved rectangular tub girders to investigate the effect of internal plate diaphragm spacing in the torsional response of the girders. Based on regression analysis of data obtained by conducting parametric analyses, the authors proposed equations to calculate internal diaphragm spacing based on the radius of curvature of the bridge, span of the bridge and the target ratio of the normal warping stress and the bending normal stress.

2.4 External Cross-Frames

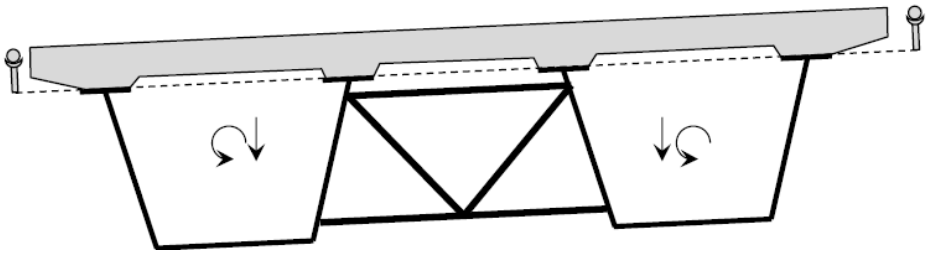

Figure 2-12- Intermediate External Cross Frames for Tub Girder(Helwig and Yura 2012)

External cross frames, such as those shown in Figure 2-12, are often provided in steel tub girders to control the relative deformations between adjacent girders during placement of the concrete deck. In most situations, external intermediate K-frames are removed after construction due to fatigue concerns. If not removed, the external bracing can also contribute to the load transfer between adjacent tub girders. Installing these external braces in the field can be a challenge due to the high torsional stiffness of the girder. In addition, the removal of the braces is complicated due to a lack of crane access under the girder. As a result, the removal is usually carried out by cutting the cross frames into smaller pieces that can be lowered in a boom lift. Due to the complexities of installation and removal, excessive external bracing is usually avoided. The most efficient location to place external bracing to control differential deformations between adjacent tubs is generally at mid-span. Thus, braces away from mid-span are not as effective at controlling the relative movement. Although the deformations often do not decrease substantially when adding braces, the forces induced in the K-frames will be smaller as more braces are added. However, the forces developed in the K-frames during the construction are often relatively small except for spans with sharp curves (i.e. R< 250 ft.) and skewed supports. A method of sizing external K-frames as well as plate diaphragms was developed by Li (2004) and outlined in Helwig et. al (2007). External K-frames are primarily needed on horizontally curved girders. In straight girders, if diaphragms are provided at the supports and a top flange lateral truss is utilized, the girders are very stiff and intermediate external K-frames can be omitted. Diaphragms are needed for straight girder systems if a large unbalanced load is applied or if the supports have significant skew, thus most practical applications of straight girders do not require external bracing. External cross frames and diaphragms are discussed in detail in Kim and Yoo (2006) and Helwig and Yura (2012).

2.5 Current Design Provisions

2.5.1 2017 AASHTO Bridge Design Provisions [AASHTO (2017)]

Section 6.11 - Box-Section Flexural Members

Section 6.11.1 – General

The 2017 AASHTO Bridge Design Code introduces design provisions for single or multiple steel tub girders in either straight steel bridges, horizontally curved steel bridges or a combination of both. These provisions are effective for simple or continuous steel beams of moderate length, defined as bridges with spans of up to 350ft.

Based on the aforementioned, steel tub girders shall be designed to satisfy the following requirements:

- Cross-section proportion limits (Article 6.11.2)
- Constructability requirements (Article 6.11.3)
- Service limit state requirements (Article 6.11.4)
- Fatigue and fracture limit state requirements (Article 6.11.5)
- Strength limit state requirements (Article 6.11.6)

Due to the nature of the current study, emphasis is given to cross-section proportion limits and constructability requirements. Additionally, tub section structural members are required to be designed including intermediate internal diaphragms and top lateral bracing systems in order to control cross-sectional deformations and to resist torsional demands. Internal cross-frames or diaphragms shall comply with the provisions of Article 6.7.4, and top flange bracing systems for tub girders shall satisfy Article 6.7.5, which are discussed later.

Flange lateral bending effects due to curvature and the effects of torsional shear must always be considered at all limit states and also during construction of horizontally curved boxes.

Section 6.11.1.1 - Stress Determinations

Live-load distribution factors, specified in Article 4.6.2.2.2b, to calculate the maximum flexural demands on bridge girders cannot be applied to the following cases:

- Single box straight or horizontally curved bridges
- Multiple box straight bridges not satisfying requirements of Article 6.11.2.3, or
- Multiple box horizontally curved bridges

For the previously mentioned cases, flexural and St. Venant torsional shear effects must be considered in the analysis and design. Moreover, transverse bending and longitudinal warping stresses must be considered and determined by rational structural analysis in conjunction with the application of strength-of-materials principles. The specifications suggest that those bridges must be analyzed using refined or approximate structural analysis methods.

Clearly, the current study involves improvement of certain cross-sectional limitations of tub girders that may eventually affect the applicability of live-load distribution factors.

Section 6.11.2 - Cross Section Proportion Limits

The specifications allow the use of inclined or vertical webs to build box-section or tub section girders. If inclined webs are considered in the section, the web plates shall not exceed an

inclination of 1H to 4V respect to a plane normal to the bottom flange. Although a limit on the inclination of the web is established, no scientific support of this limit is provided within the specifications or commentary. For all verification and design considerations, the inclined length specified for the web shall be used.

Furthermore, the top flanges are required to be connected to the webs at mid-width of the flanges. According to the commentary, top flanges of tub sections not complying with this requirement are not suggested to be used because it can originate additional unknown flange lateral bending effects that require specialized analysis. Thus, the uncertainty in the possible effects of offsetting top flanges with respect to the webs leaves to the potential to improve the efficiency of the cross-section.

Section 6.11.2.3 - Special Restrictions on Use of Live Load Distribution Factor for Multiple Box Sections

The AASHTO provisions require that straight multiple steel box sections comply with certain geometric characteristics in order to use the live-load distribution factors of Article 4.6.2.2.2b to calculate the respective flexural demands of each steel girder in the bridge. These geometric limitations of the bridge cross-section are the following:

1) At midspan, the separation from center-to-center of top flanges of adjacent box sections (*a*) must not be greater than 120% nor less than 80% of the center-to-center top flange separation of each adjacent box (*w*) [Figure 2-13].

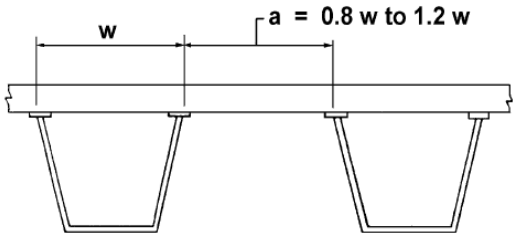

Figure 2-13- Center-to-Center Flange Separation((AASHTO) 2017)

2) In the case of non-parallel box sections, the separation from center-to-center of top flanges of adjacent box sections at supports must not be greater than 135% nor less than 65% of the center-to-center top flange separation of each box. The distance from center-to-center of flanges of each individual box shall be the same.
3) The web inclination shall not exceed 1H to 4V with respect to a plane normal to the bottom flange.
4) The cantilever overhang of the concrete deck shall not be greater than either 6 ft. or 60% of the average separation from center-to-center of top flanges of adjacent box sections (*a*).

According to the commentary, these geometric limitations are imposed because the development of the distribution factor equation of Article 4.6.2.2.2b is based on an extensive study of bridges that satisfy these limitations (Johnston and Mattock 1967). Additionally, the commentary mentions that it was found that when these restrictions are satisfied, shear due to St. Venant torsion and secondary distortional bending stress effects may be neglected if the width of the box flange does not exceed one-fifth of the effective span.

Section 6.11.3 - Constructability

Section 6.11.3.1 - General

The AASHTO specifications request the analysis of the box girders to ensure that deformations of the box section are controlled along the girder. This is done by considering different type of bracing systems, such as temporary or permanent intermediate internal diaphragms or cross-frames, external diaphragms or cross frames, and top lateral bracing.

Top flanges of tub girders must be analyzed based on the provisions in Article 6.10.3.2.1. According to the aforementioned article, a distinction between discretely and continuous braced top flanges is made in order to define the corresponding effects to consider during the analysis. Flange lateral bending effects must be considered on discretely braced top flanges (for example, tub sections with SD-truss top lateral bracing). Additionally, for horizontally curved bridges, flange lateral bending effects due to curvature must always be considered in discretely braced flanges during construction.

As recommended by the commentary, flange lateral bending effects can be reduced in discretely braced top flanges of tub sections when adding intermediate internal cross-frames, diaphragms or struts. In fact, this may apply to cases where the top flange unbraced length is longer than 30 ft., and/or where the inclination of the web plates with respect to a plane normal to the bottom flange is bigger than 1H to 4V. Clearly, the improvement of cross-sectional and bracing details might produce a better response from the tub girder system if the interaction between the cross-section geometry and the separation of intermediate cross-frames improves.

Section 6.7.4 - Diaphragms and Cross-Frames

Section 6.7.4.1 - General

In the eighth edition of the AASHTO Design Provisions, the requirement that diaphragms be separated at no more than 25.0 ft. was removed. Instead, a rational analysis is required to define the diaphragm separation along the girder.

In horizontally curved bridges, cross-frame members should be considered as primary members as they are crucial to the bracing system. The commentary mentions that adequate bracing of horizontally curved girders is fundamental in ensuring that the structural members of the system function correctly during construction. Thus, considering that they are required to provide equilibrium in the system, they are recognized as primary structural members. Certainly, the improvement of cross-framing details might contribute to a better global response of the tub girder system, which might result in economic and structural improvement of the system.

Section 6.7.4.3 - Box Section Members

The AASHTO specifications require that intermediate internal cross-frames be accommodated along the girder to avoid cross-sectional distortion. The spacing of this type of internal bracing is limited to 40.0 ft. for all single box, horizontally curved, and multiple box sections in cross-sections of bridges not complying Article 6.11.2.3 requirements or with box flanges that are not fully effective according to the provisions of Article 6.11.1.1.

Moreover, the commentary mentions that straight box girders without skew supports satisfying the Article 6.11.2.3 requirements have been reported to experience relatively small transverse bending and longitudinal warping stresses due to cross-section distortion (Johnston and Mattock 1967), and may be neglected. Furthermore, the commentary recommends that internal

cross-frames be placed at or near locations of maximum moment and near both sides of field splices. The need for additional temporary or permanent internal cross-frames for transportation, construction, and at lifting points of each shipping piece must be evaluated.

For the cases mentioned in Article 6.11.1.1, the specifications limit the stresses produced by transverse bending due to cross-section distortion to 20.0 ksi and the longitudinal warping stresses to 10% of the longitudinal stresses due to major axis bending at the strength limit state. The commentary states that these limits can be reached by introducing adequate internal cross-frames. Because the specifications consider the effect of internal and external diaphragms as critical in controlling distortional deformations of the box cross-section, especially at supports, any reliance on post-buckling resistance is not recommended.

Section 6.7.5 - Lateral Bracing

Section 6.7.5.1 - General

The specifications require that lateral bracing should be investigated for all stages of assumed construction procedures and at final condition. Indeed, in order to calculate the bracing member demands different aspects should be included such as transfer of lateral loads, deformation control of the cross-section during fabrication, and erection and placement of the deck over the steel girders. Furthermore, the provisions suggest that lateral bracing should be placed either in or near the plane of a flange.

Section 6.7.5.3 - Tub Section Members

The guidelines point out that top lateral bracing shall be provided between the top flanges of individual tub sections. The specifications suggest that full-length or partial-length lateral bracing systems can be considered for straight girders. The need for a full-length lateral bracing system should be examined in order to guarantee control of deformations and stability of the tub girders during erection and casting of the concrete deck. When partial-length lateral bracing system is considered, the local stability of top flanges and global stability of individual tub girders must be evaluated under construction sequence demands. Cross-section distortion and top-flange lateral bending stresses may need to be considered when a tub with partial-length bracing is subjected to a net torque. Meanwhile, for horizontally curved girders, a full-length lateral bracing system should be considered since the torques acting on the steel section are considered significant. For both straight and horizontally curved girders, the stability of the compression flanges between points of the lateral bracing should be investigated during concrete deck casting.

The commentary suggests that straight tub girders with spans less than 150 ft. need at least one panel on each side of a lifting point with horizontal lateral bracing. Moreover, the shear flow due to net torques on the steel section produced by uneven factored weight loads acting on the top flanges, or any kind of eccentric loads acting over the steel section during construction, must be considered during the analysis and design of the tub section. On the other hand, for straight tub girders with spans greater than 150 ft., a full-length lateral bracing system is recommended to be included along the tub. Additionally, top lateral bracing is suggested to be continuous across field splice points.

2.5.2 2015 TxDOT Preferred Practices for Steel Bridge Design, Fabrication, and Erection

Section 2.4 - Tub Girder Sections

The 2015 TxDOT Preferred Practices for Steel Bridge Design, Fabrication, and Erection Provisions allows the use of AASHTO Bridge Design Provisions and provides additional specifications for specific topics. The specifications related to this study are the following:

Section 2.4.1 - Flanges

According to the specifications, the flange width plays an important role in the tub girder stability during handling, erection, and deck placement. The provisions suggest maintaining the tub girder length (i.e. field section length) to flange width ratio below 85.

Section 2.4.4. - Top Flange Lateral Bracing

The TxDOT practices recommend using top lateral bracing in both straight and horizontally curved tub girders. The preferred top lateral bracing system is the single-diagonal truss system (SD-truss system) instead of the double-diagonal truss system (X-truss system). The specifications suggest that the angle between the top flange and the bracing member should be ideally closer to 45 degrees and not lower than 35 degrees.

The specifications require consideration of the load demands produced by erection and sequential concrete casting when defining the worst-case loading for lateral bracing. The lateral bracing members may be directly connected to the top flange through bolted connections if sufficient connection length is provided.

Section 2.4.6. Internal Diaphragms and Cross-Frames (between Piers)

Similar to AASHTO specifications, TxDOT provisions point out that internal diaphragms and cross-frames are used to control cross-section distortional deformations. They recommend the installation of an internal cross-frame or diaphragm at every other lateral bracing point within horizontally curved tub girders. This distribution should define spacing of 14 to 18 feet between cross-frames. Additionally, they suggest using horizontal struts (i.e. angle sections) between internal cross-frames to control horizontal bending of the top flange during deck casting. Similar to top lateral bracing, the struts should be connected directly to the flanges.

The TxDOT provisions permit spacing the internal cross-frame or diaphragms at every third or fourth lateral bracing point for straight tub girders.

Chapter 3. Large-Scale Laboratory Tests of Steel Tub Girders

3.1 Introduction

To investigate the impact of the proposed details on the behavior of steel tub girders, the research team conducted large-scale experiments at the Ferguson Structural Engineering Laboratory. The purpose of the tests was to measure the impact of a variety of different bracing configurations on the non-composite behavior of straight and curved steel box girders. The tests provided data for validation of three-dimensional FEA models that were then used to carry out parametric FEA studies, which are the subject of Chapter 4. Tests were later conducted on the girders with a composite deck, which is discussed in Chapter 5. Three different tub girders were fabricated for the test setup. The girders were designed to remain elastic during the non-composite tests. All intermediate bracing in the tests was fabricated with bolted connections so that the bracing of each girder could be modified in each test. The girders were subjected to both vertical and lateral loads. Although all the test girders were straight, horizontal curvature was simulated by applying eccentric loads with respect to the beam shear center through adjusting the hydraulic ram location. This chapter begins by describing the test setup that was fabricated for the studies. An overview of the specimens that were tested is then provided as well as the instrumentation that was used to measure the behavior throughout the testing. The testing procedure and data are then presented for the experiments.

3.2 Description of Test Setup

A schematic of the test setup is shown in Figure 3-1. A single tub girder was tested in each experiment. The support conditions at the ends simulated simple supports in which twist was restrained and was designed to test simply supported straight tub girders that ensured global stability but accommodated longitudinal movements while allowing in-plane rotation. The supports were spaced 84 ft. on center and consisted of three 12 ft. long W36x135 rolled beams stacked vertically to raise the elevation of the test girders above the loading system. The support located on the south side of the laboratory floor was supported laterally with two diagonal braces to stiffen the test setup and simulate “pinned conditions”. The two braces were formed by 2L4x3x3/8” LLBB connected to the steel support and to the strong floor through bolted connections. The opposing support consisted only of the stacked W36x135 sections and allowed some flexibility to simulate a “roller”. Elastomeric bearings and sole plates were used between the support system and the girders. Vertical loads over the steel tub girders were applied with two gravity load simulators (GLS) located 20 ft. from either end.

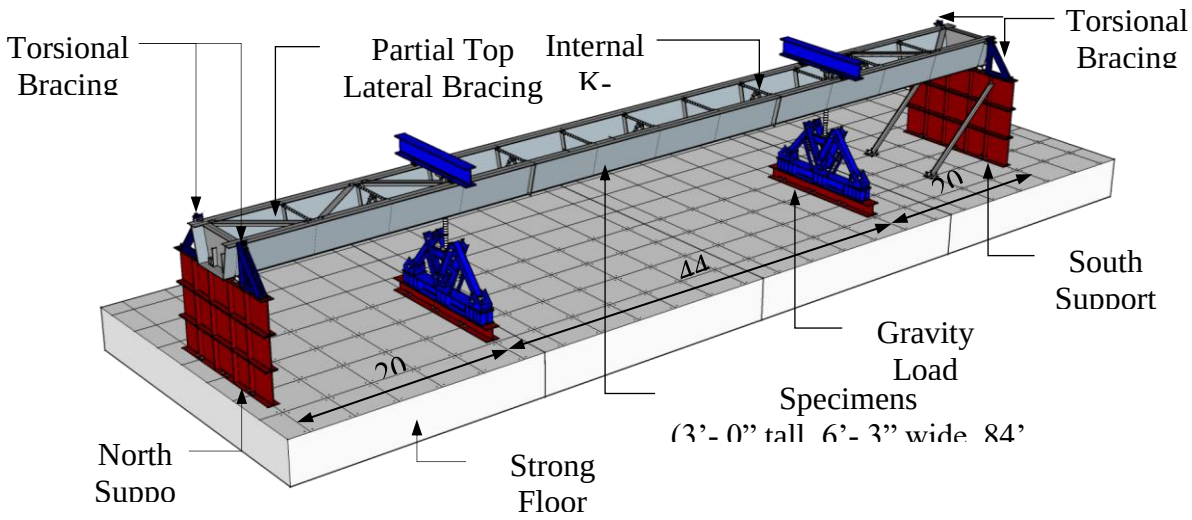

Figure 3-1 - Bending & Torsion Test Setup – Simply Supported

In addition to the vertical supports, as depicted in Figure 3-2, two L-shaped reaction frames were positioned along the length of the tub girder to apply lateral loads to the test girder. The frames were comprised of W12x65 rolled sections and braced with 2-L4x3x3/8" angles. The purpose of the lateral load tests was to obtain data on the lateral stiffness of the tub girders with various bracing conditions to provide additional data for validation of the FEA models for the parametric studies. Figure 3-3 shows a laboratory view of the test setup with all the elements previously mentioned. Additional details on the vertical and lateral load application are provided subsequently.

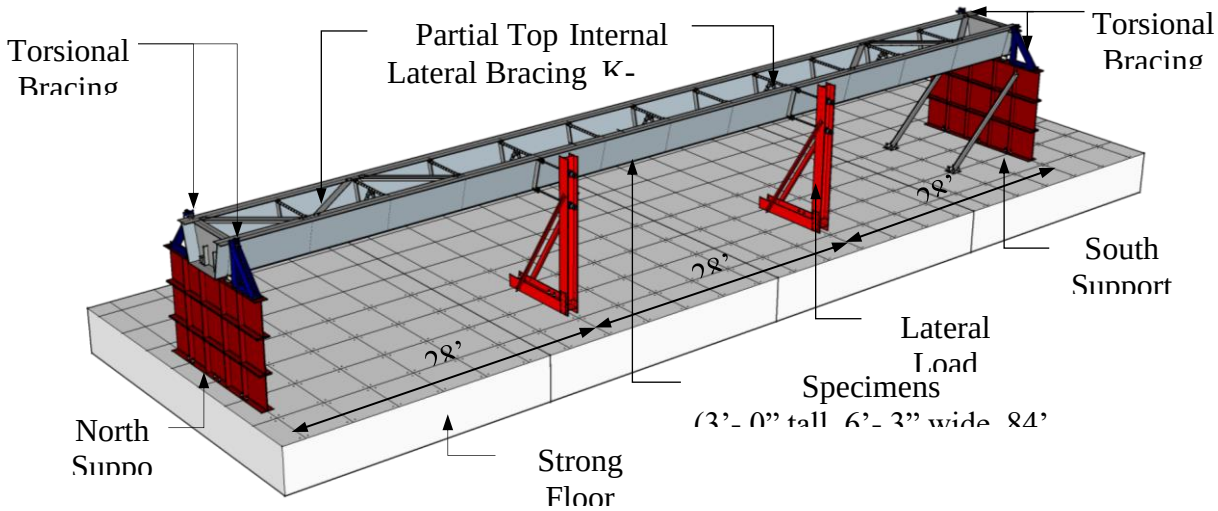

Figure 3-2 - Lateral Load Test Setup – Simply Supported

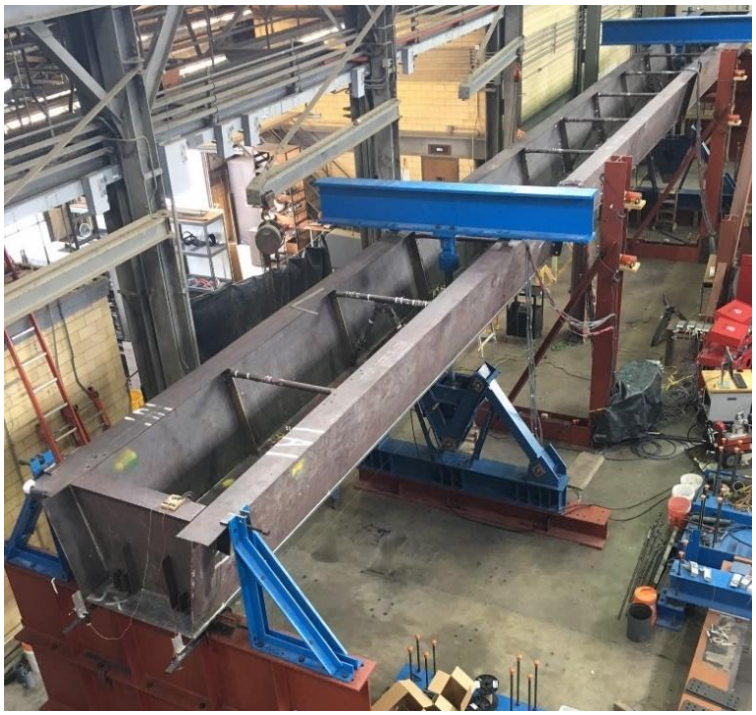

Figure 3-3 –Steel Tub Girder - Test Setup

3.2.1 Boundary Conditions

At each support of the steel specimens, efforts were made to achieve "idealized" boundary conditions such as simple supports that restrained out-of-plane twist. The support conditions for the elastic tests are presented in Figure 3-4. A 20″ long x 10″ wide x 1 ½″ sole plate was welded to each tub girder at each support location. The sole plate of each tub girder rested over an 18″ long x 9″ wide x 1 ¾″ thick elastomeric bearing pad that rested on the vertical supports. At each support, the tub girders were connected to the vertical supports with 1" diameter A325 bolts to avoid overturning of the tub girder during the elastic buckling tests. As shown in Figure 3-4, twist was restrained by laterally restraining the top flanges by 1″ diameter threaded rods connected to a triangular truss system bolted to the supports. Bearing plates were welded to the top flanges at the location of the threaded rods to prevent overturning of the girder if a threaded rod slips off the edge of the top flange. The top flanges were generally free to warp, while some warping restraint was likely present at the bottom flange due to the wide elastomeric pad. To provide lateral support of the bottom flange during the lateral load tests, a WT section was bolted to the west support [see Figure 3-4] that was removed for the GLS load cases.

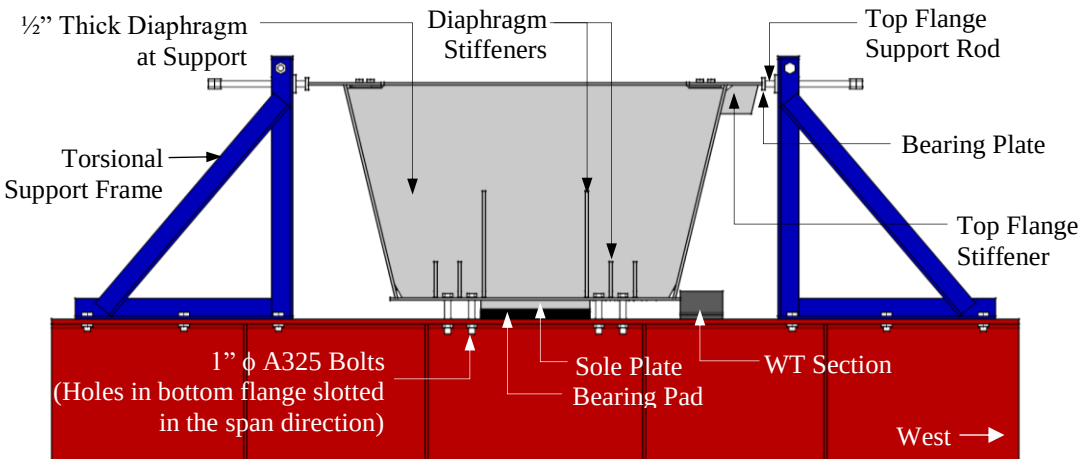

Figure 3-4 - Tub Girder Boundary Conditions at Supports

3.2.2 Load Application Setup

The tub girders were tested under two different loading conditions 1) lateral load tests and, 2) vertical load tests. Figures 3-5 and 3-6 show the details for the lateral load tests. A system of shackles, threated rods, and hydraulics rams were used to apply loads at the location of the L-shaped lateral load frames. A variety of lateral loads was applied to the top and bottom flanges. Efforts were made to apply equal loads at the two longitudinal load locations of pure lateral load (equal top and bottom flange loads). Considering that the shear center of the steel tub girder is located below the bottom flange, this loading condition also produced torsional demands over the girder. The loads were applied with hydraulic actuators connected to threaded rods reacting against the L-shape frames. A load cell was included between the hydraulic rams and the reaction frames to measure the magnitude of the applied lateral loads. As noted earlier, the purpose of these tests was to gain data to compliment the simulated gravity load data. The lateral load data provides data related to the lateral and torsional stiffness of the tub girders with various bracing configurations that was used to assist in validating the FEA models.

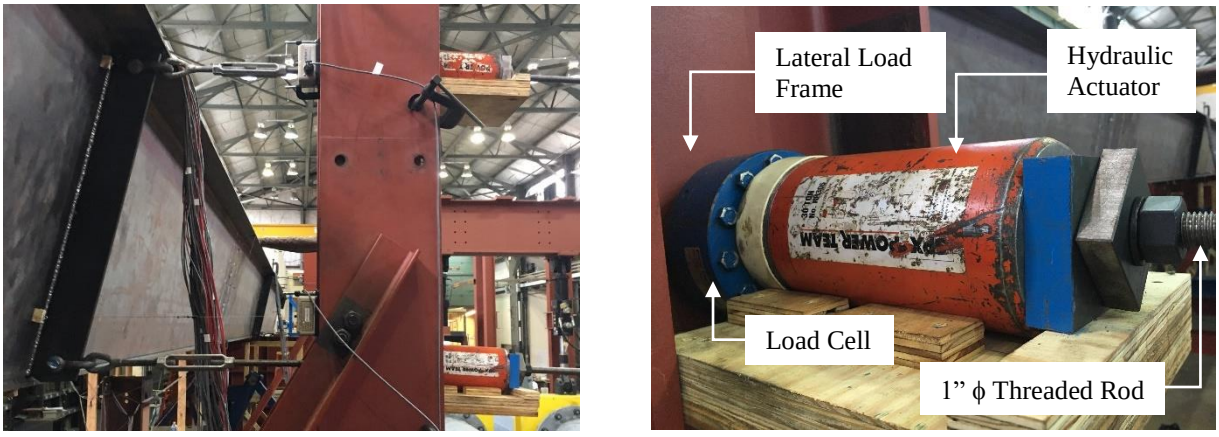

Figure 3-5 - Lateral Loading Test Setup

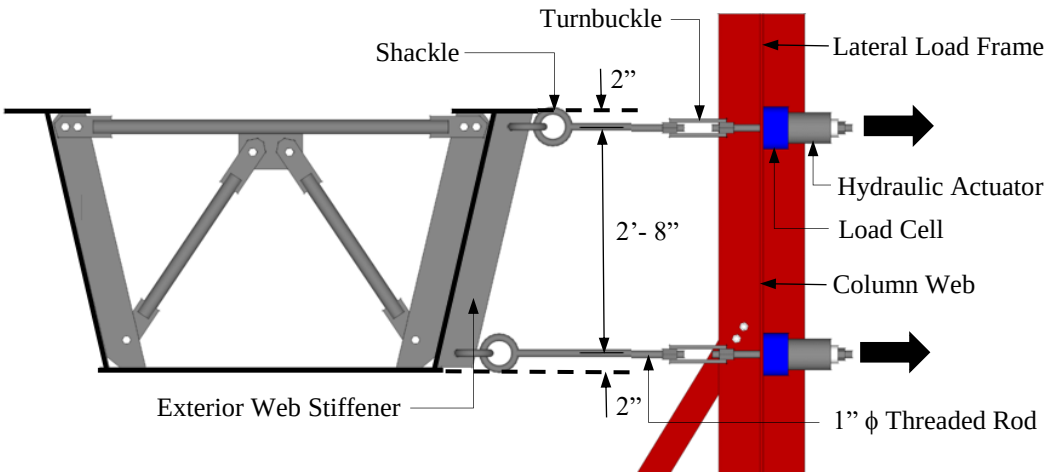

Figure 3-6 Lateral Loading - Test Setup Elements

For the vertical loading tests, the two gravity load simulators (GLS) shown in Figure 3-7 were used to apply either pure bending or bending with torsion. Each GLS is able to apply vertical loads up to 160 kips, and to keep the load vertical even if the ram moved laterally up to 6 in. Consequently, the GLS provides minimal lateral restraint and essentially “simulates gravity load”. The vertical loads were applied near the quarter points of the girder. Although the loading consisted of point loads applied near the quarter points, the resulting moment diagram is similar to that caused by a distributed load from self-weight of the girder and concrete deck, which would be the critical load during construction. This loading system provides a direct measure of the bracing effectiveness in straight girder systems and it can be used to simulate the torsional effects of horizontal curvature on the behavior of the girder and bracing systems. The vertical load from the GLS was applied with a hydraulic actuator connected to a W18x143 load transfer beam that spanned between the two top flanges of the tub girder specimens. Heat-treated knife-edges (discussed later) were used at the load points to transfer the load to the top flanges of the girders.

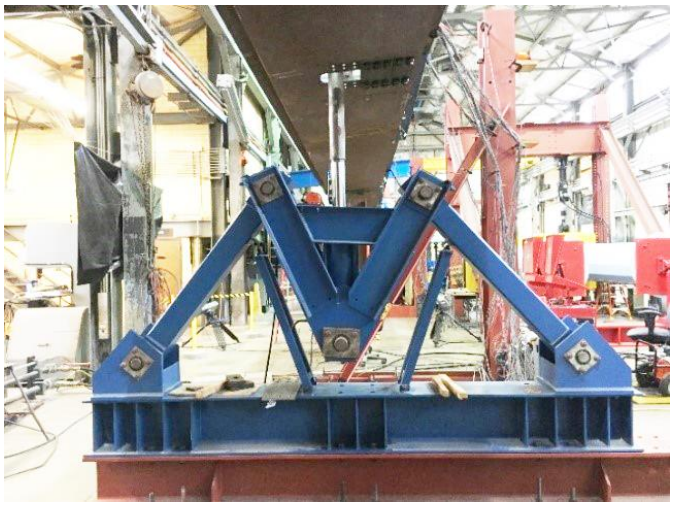

Figure 3-7 - Gravity Load Simulator (GLS) during test

The focus of this study is on both straight and horizontally curved girders. Although researchers considered fabricating horizontally curved girders, the expense of the specimens as well as the limitation of getting a single girder curvature was not desirable. Instead, the research team focused on a setup that allowed eccentric loading that could simulate the torsion from the horizontal curvature of the girder. A rectangular opening (8″x20″) was thermally cut into the bottom flange that allowed the extension rod of the GLS to pass through the bottom flange and connect to the W8x143 load spreader beam. As shown in Figure 3-8, the load could be applied at an eccentricity as large as 16 inches to simulated girder curvature. With the ability to offset the load to achieve a torque, girder geometries from straight to a simulated curvature of approximately 600 ft. was possible. Two sets of ½″ cover plates were bolted above and below the hole with 24 A490 1″ diameter slip critical bolts to minimize localize effects and provide continuity of the bottom flange across the hole.

Figure 3-8 - GLS ram location: Left) Concentric, Center) Eccentric, e=8", Right) Eccentric, e=16"

Figure 3-9 shows the loading components of the GLS as well as the load distribution from the GLS to the tub girder when the load applied was eccentric (a) and concentric (b) respective to the shear center of the specimens. Figure 3-10 presents the effects of the eccentric loading case. Figure 3-10a shows the bending and torsional components of the eccentric loading case are shown, while Figure 3-10b presents the deformed shape of the tub girder with positive twist to the west of the specimen. For the concentric loading case, the load distribution is shown in Figure 3-9b.

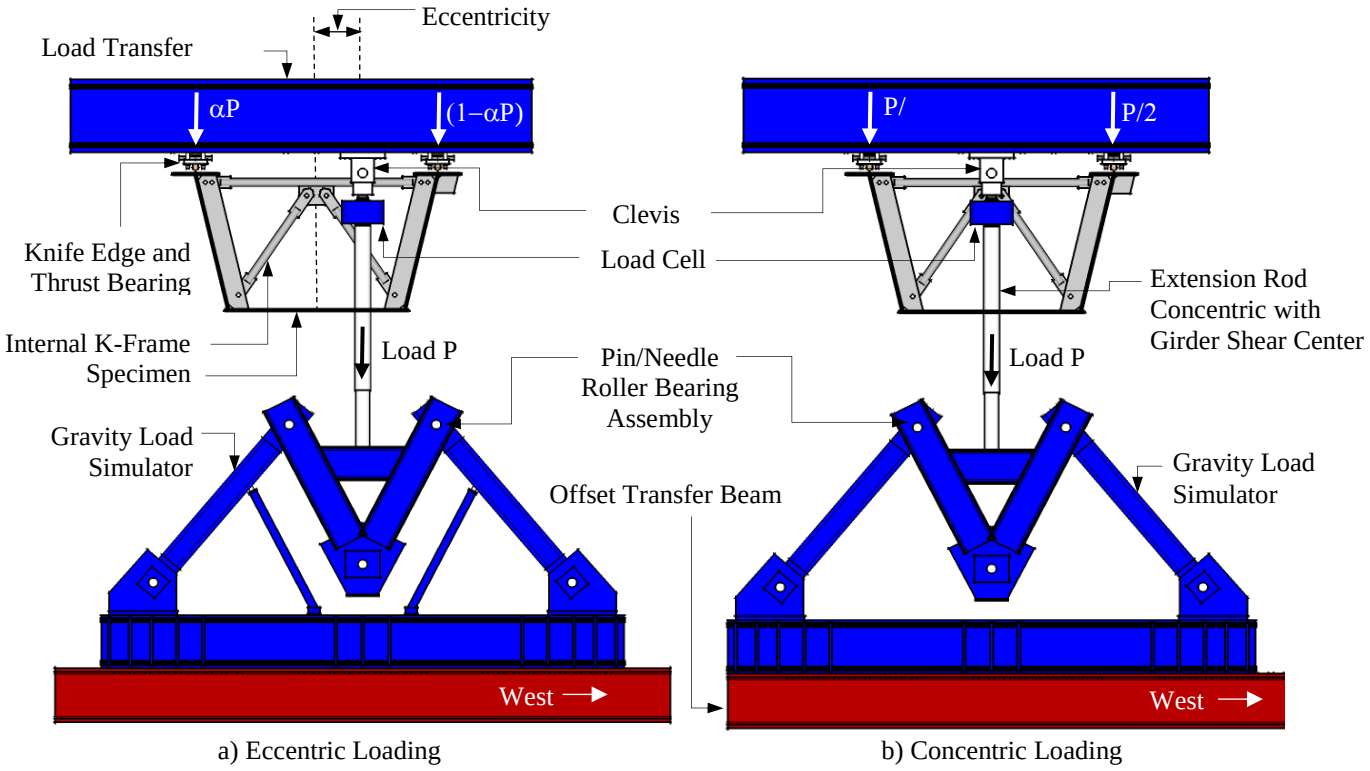

a) Eccentric Loading b) Concentric Loading

Figure 3-9 – Gravity Load Simulator Load Distribution

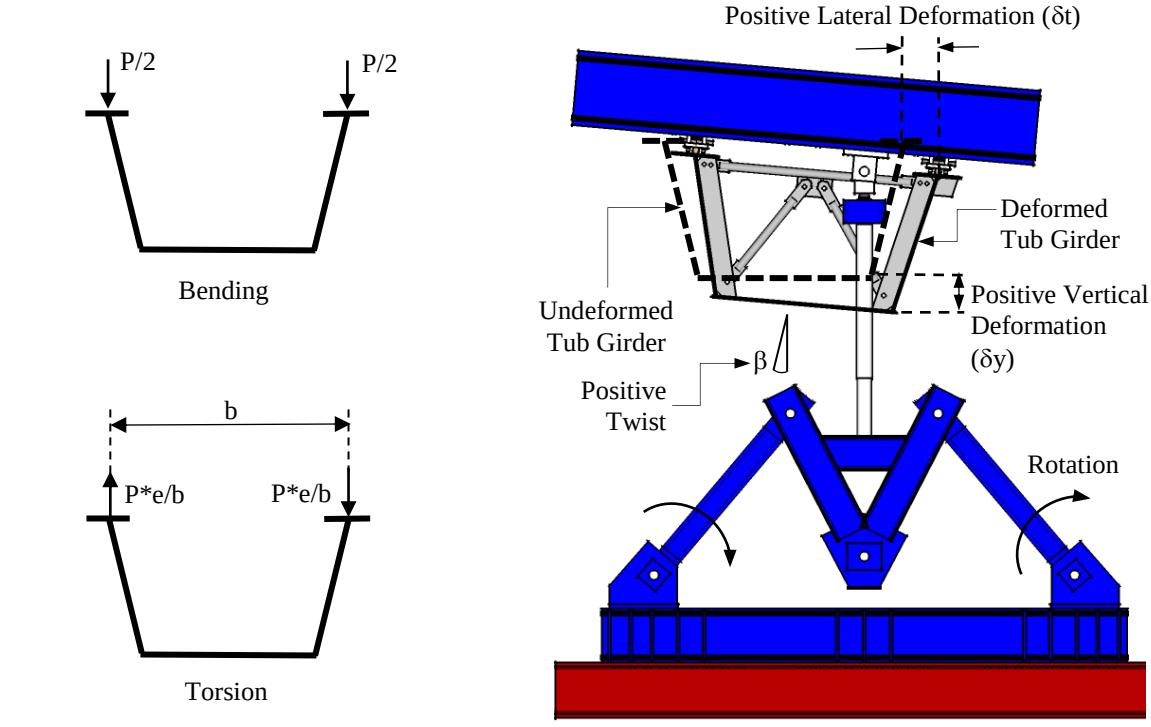

a) Bending and Torsion Applied Effects b) Deformed Shape

Figure 3-10 - Gravity Load Simulator Eccentric Loading Effects

Figure 3-11 - Knife Edge and Thrust Bearing Assembly

3.3 Bending and Torsion Diagrams for Curved and Straight Tub Girders

For the elastic buckling tests, the 86-foot-long specimens were loaded at longitudinal location 20 ft. from the supports as shown earlier in Figure 3-1. Although the beam was loaded with a point load, as shown in Figure 3-13, the resulting moment diagram was somewhat similar to the diagram resulting from self-weight of the girder during construction. The moment diagrams for horizontally curved girders can be obtained neglecting the curvature and using traditional beam theory for straight girders. Tung and Fountain (1970) showed that this approximation is reasonable for girders that are restrained to twist at the ends and that have subtended angles per span of up to 40 degrees. Helwig et al. (2007) derived closed-formed solutions for bending and torsional moments for curved steel box girders with uniform loads. These expressions assume that the box girder has enough bracing to control section distortion and torsional warping. The equations are the following:

Bending moment diagram for straight and horizontally curved girders:

$$M(x) = \frac{wx}{2}(L - x)$$

Where:
M(x) = Moment along the girder (k-ft)
L = Span length of the girder (ft)
x = Location along the girder (ft)
w = Uniform load along the girder (kip/ft)

Torsional moment diagram for horizontally curved girders:

$$T(x) = \frac{wL^2}{24R}\left(4\frac{x^3}{L^2} - 6\frac{x^2}{L} + L\right)$$

Where:
T(x) = Torsional moment along the girder (k-ft/ft)
L = Span length of the girder (ft)
R = Radius of curvature (ft)
x = Location along the girder (ft)
w = Uniform load along the girder (kip/ft)

Figure 3-12 shows the bending moment diagrams for a straight tub girder with 2 load points near the quarter points (solid line) as tested in the laboratory, and with uniform load along the

girder (dashed line) as the self-weight acts. Both moment diagrams were obtained so that the area under the curve is the same for both.

As previously mentioned, the simply supported specimens were loaded with two equal point loads located 20 ft. from each support. In order to simulate the effects of horizontal curvature in the girder, eccentric vertical loads were applied. A comparison of the torsion diagrams of the simply supported girder are provided in Figure 3-13 for the beam loaded with two eccentric loads (solid line) along with the case of self-weight on a horizontal curved girder (dotted line). The area under the two torsion diagrams is equal in order to define the relationship between curvature and eccentricity. For the 84-foot-long specimens, eccentricities of 8 and 16 in. were applied in order to replicate horizontal curvature of 630 and 1260 ft., respectively.

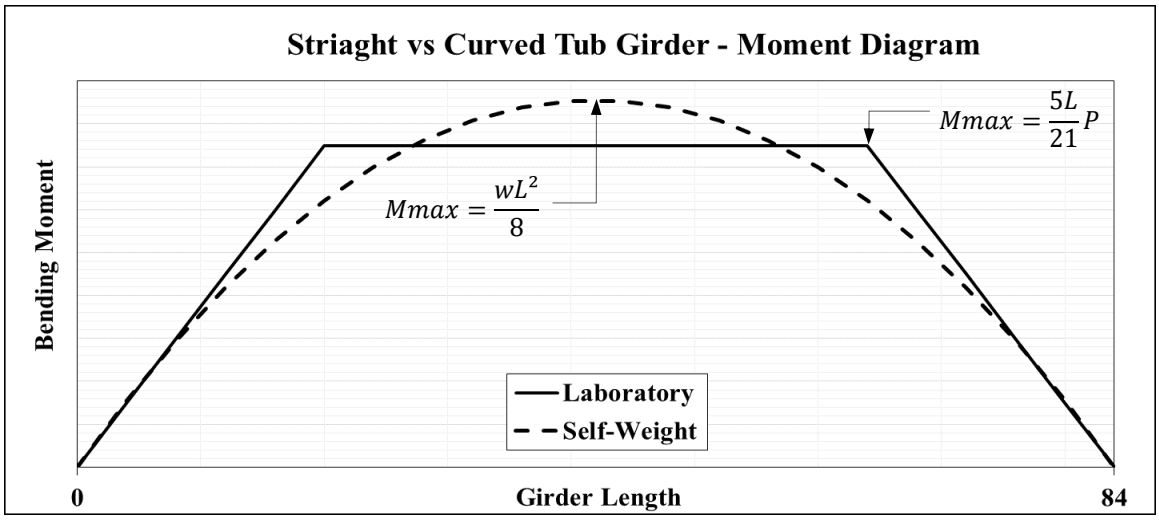

Figure 3-12 - Straight vs Curved Tub Girders – Bending Moment Diagrams

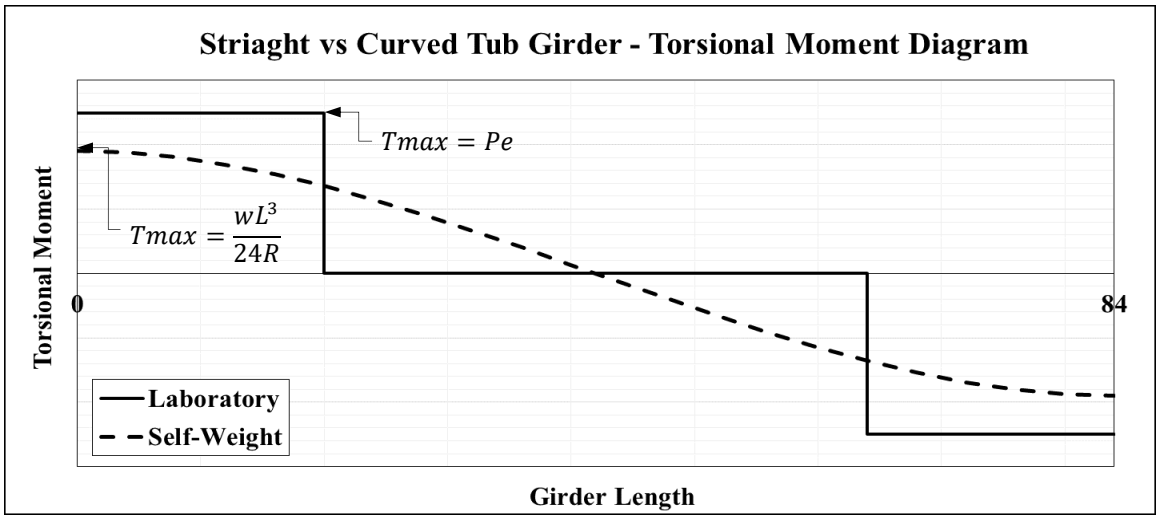

Figure 3-13 - Straight vs Curved Tub Girders - Torsional Moment Diagrams

3.4 Experimental Specimens

Three steel tub girders were designed and fabricated for the experimental program. The first girder, designated as the standard tub girder (baseline), served as the control specimen of the experiments. The baseline tub girder had a web slope of 4V:1H with the flanges centered over the webs following the current AASHTO requirements. The additional two steel tub girders were proportioned with the modified geometries that focused on the impact of offsetting the top flange and a flatter-sloped web to investigate the impact of the changes of geometry on the girder behavior. All of the specimens were designed to remain elastic for multiple testing configurations. The bracing was designed with bolted connections so that the conditions of each specimen could be varied by adding or removing select braces. There was a variety of potential instabilities within the elastic range depending on the bracing that was utilized. The instabilities may include overall lateral torsional buckling as well as local buckling. In addition to the "baseline" specimen, one specimen is referred to as the specimen with "offset flanges" while the third specimen is referred to as the specimen with the "flatter web slope". As noted earlier, the specimens were tested with concentric and eccentric loading to consider the impact of girder curvature. A description of the most important factors for the design of the specimens are discussed in the following subsections.

3.4.1 Tub Girder Geometries

The research team strived to select a geometry of the test specimens that would provide realistic results. Because the girders were to be used in multiple tests, a variety of proportions was considered so the girders would remain elastic during testing with a range of combined bending and torsional loads. The girders had clear span (L) of the specimen of 84 ft., and a girder depth (D) of 3 ft. resulting in an L/D equal to 28, which is comparable to that suggested by ASSHTO 2017 section 2.5.2.6.3 for simply supported beams (L/D=25). As shown in Figure 3-14, a distance, W, equal to 5.25 ft. was selected as the spacing of the top of the sloped webs. The resulting width-to-depth ratio (W/D) was 1.75, which is similar to values observed in current practice. The major difference between the test specimens and values used in practice is the thickness of the plates that comprise the flanges and webs. The flanges and webs of the three specimens were fabricated with AASHTO M270 (ASTM A709), grade 50W. As noted in the last section, additional variables that were selected for variation in the test girders were the position of the top flanges on the webs as well as the web slope. Three different specimen proportions were determined including a 1) Baseline Specimen (similar to current practice), 2) Specimen with Offset Flanges, and 3) Specimen with a Flatter Web Slope. The basic geometry of each of these specimens is outlined in the following subsections.

3.4.2 Baseline Tub Girder (Tub 1)

Figure 3-14 shows the cross sectional dimensions of the baseline girder, which is referred to as "Tub 1" in the discussions. Tub 1 resembles geometries in current practice. The slope of the two webs were set to match the current practice with a web slope of 4V:1H. Both the top flanges and the webs of the specimen are non-compact elements according to their slenderness ratio. The thickness of the webs and flanges was set equal to 7/16 in. The flange thickness is considerably smaller than commonly utilized in current bridge practice (flanges are usually $\geq$1 in). However, this thickness was deemed necessary to maintain the elastic response of the system based upon preliminary finite element studies. Noticeable out-of-straightness of the plates was observed in the

fabricated girder. The top flanges had a wavy profile along the length, which raised concerns about the potential for local buckling to occur before achieving elastic LTB of the system. As a result, during the tests, instrumentation was used to monitor the local buckling behavior of the plates. Tub 1was fabricated with two 12″ wide top flanges, which were centered over the sloped webs. The width-to-thickness ratio ($b_f/2t_f$) of the top flanges was equal to 13.71. Although this value exceeds the AASHTO maximum recommended flange slenderness of 12, inelasticity was not expected during any of the non-composite girder tests.

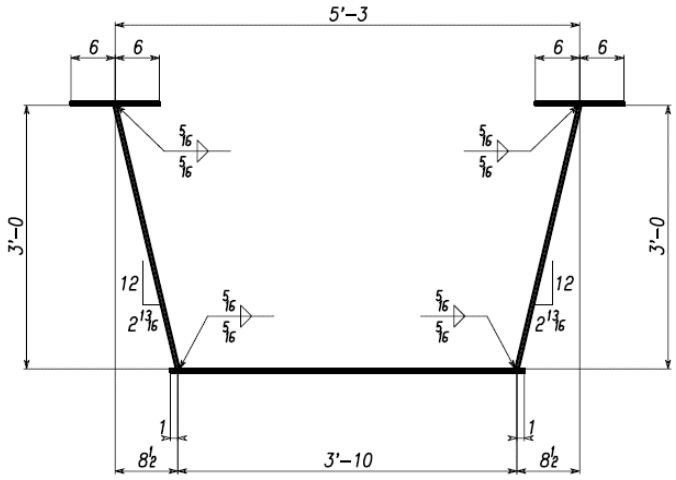

Figure 3-14 - Full-Scale Baseline Tub Girder Specimen - Cross-Section

3.4.3 Offset Top Flange Tub Girder (Tub 2)

The offset top flange girder is referred to as "Tub 2" in the discussion, and it was fabricated with two 13" wide top flanges. The flanges were offset inwards with 1″ width outside of the web to accommodate the flange-to-web weld. Therefore, 12″ of flange plate was positioned inside the edge of the web interface, as shown in Figure 3-15.

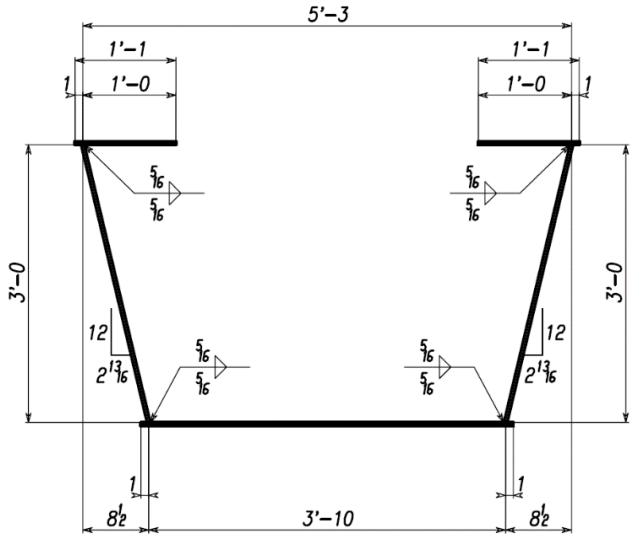

Figure 3-15 - Full-Scale Offset Top Flange Tub Girder Specimen - Cross Section

Preliminary finite element analyses were conducted to define the thickness of the top flanges for Tub 2 to ensure elastic behavior of the tub girder during the non-composite testing. The top flange thickness was set equal to 9/16″, resulting in a width-to-thickness (b/t) ratio of the top flange equal to 21.33. Clearly, this ratio is not compliant with the current code requirements of flange slenderness, but limitations in the weight of the girder (due to handling inside of the laboratory) did not allowed thicker top flanges. The bottom flange and sloped webs were sized with 7/16” thick plates, similar to the baseline tub girder.

3.4.4 Flatter Web Tub Girder (Tub 3)

The tub girder with the flatter web slope is referred to as “Tub 3” in the discussions. The slope of the two webs of Tub 3 were selected at approximately 2.5V:1H as shown in Figure 3-16, which exceeds the recommended limit according to AASHTO 2017. The top flanges were centered about the sloped webs, as depicted in Figure 3-16. Similar to Tub 1, Tub 3 was fabricated with webs and flanges that were 7/16 in. thick. Similar to the other specimens, Tub 3 was proportioned to remain elastic in the non-composite girder tests.

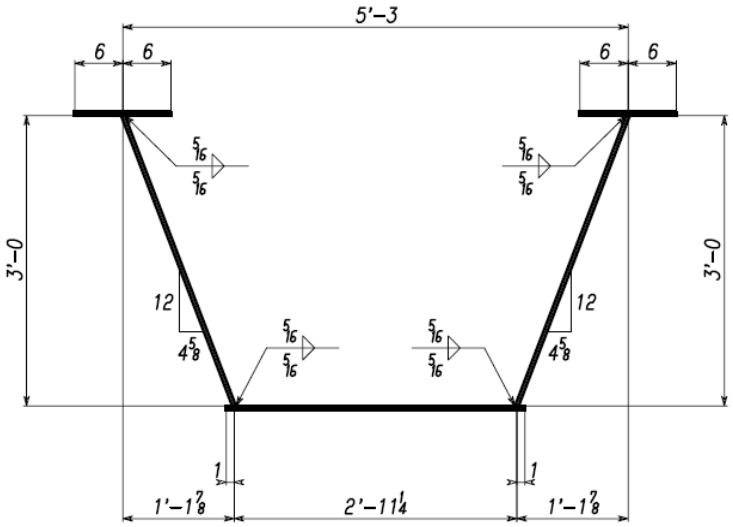

Figure 3-16 - Full-Scale Flatter Web Tub Girder Specimen - Cross Section

3.4.5 Bracing Geometry

As shown in Figure 3-17, the spacing of the top lateral truss panel points was set as 7 ft., generating 12 panels along the length of the 84 ft. clear span. As noted earlier, bolted connections were utilized on all top lateral truss members and internal K-frames so that the bracing can be added or removed for specific tests. In the cases where the internal K-frames or top lateral truss diagonals were removed, top lateral struts between the two top flanges were maintained at a 7 ft. spacing to control separation of the top flanges. As an example of a bracing configuration, Figure 3-17 shows a plan view of the at test girder, where the first two panel points denote a “strut-only” and K-frame condition. Many other configurations were tested for all three girders.

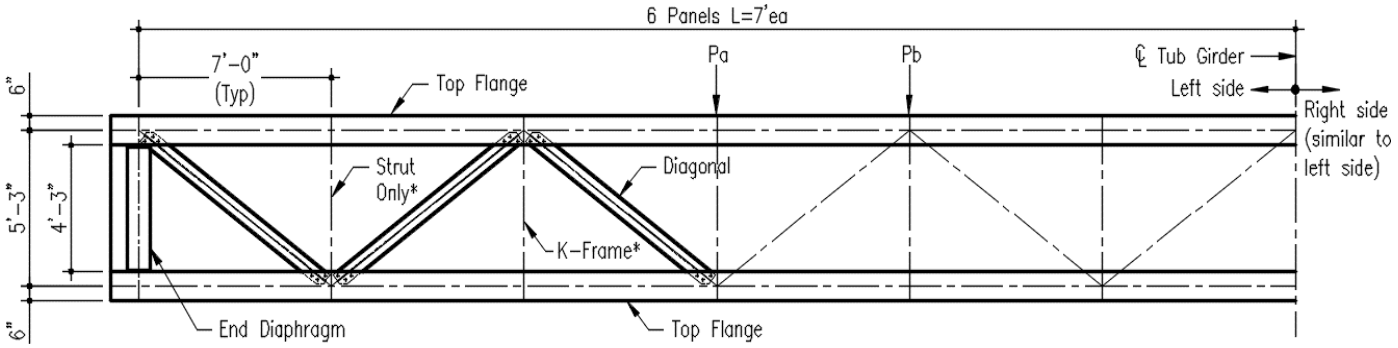

Figure 3-17 - Bracing Layout - Half of Baseline Steel Tub Girder Specimen - Plan View

3.4.6 Top Lateral Bracing

The single-diagonal type (SD-type) top truss was used because it is the most common type of lateral bracing used in current practice. The SD-type system is formed by single diagonals and struts connected to the tub girder top flanges through bolted connections in the test specimens. The diagonals were designed to be directly connected to the top flanges to avoid gusset plates as shown in Figure 3-18.

Figure 3-18 - Top Lateral Bracing System

The use of bolted connections allowed the addition or removal of the bracing elements depending on the experimental test that was conducted. The top truss diagonals were comprised of WT5x22.5 connected directly underneath the top flanges with three slip critical ¾ in. diameter A325 high strength bolts. Meanwhile, the struts were connected to a stiffener welded to the web of the tub girder through bolted connections made of 1/2 in. thick steel plates (material ASTM A-36). The vertical eccentricity between the top flange and the centerline of the strut was 3.75 in., which is an acceptable value according to Helwig and Yura (2012). The angle between the diagonal and the top flange centerline was 37 degrees. The maximum number of diagonals at each end of

the girders was set to three. Different cases of partial top lateral bracing were tested by removing diagonal members of the horizontal truss at each end (4 different arrangements of lateral bracing: 3, 2, 1, and 0 diagonals at each end).

Based upon the preliminary FEA results, the WT5x22.5 section used for the diagonals had adequate capacity in tension and compression to remain elastic during the tests. Additionally, this WT section is compliant with the slenderness ratio and minimum cross-sectional area requirements required by AASHTO 2017, which are mandatory to ensure that the quasi-closed section will undergo warping normal stresses less than 10% of the major-axis bending stresses. On the other hand, a 2 in diameter x-strong pipe (2.375 in. outside diameter and 0.218 in. wall thickness) was selected as the cross-section for the struts. Although round sections are not used in practice, the circular section was selected so that bending effects in the struts could be accounted for by averaging the readings from 2 strain gages on either side of the pipe, which is discussed in more detail later in the report. Similar to the diagonals, the strut cross-section was sized to resist the axial demands calculated during the preliminary analysis and to satisfy slenderness requirements of AASHTO 2017. The diagonals and pipes were designed and fabricated with ASTM A705 – Grade 50 and ASTM A53 – Grade B steels, respectively.

3.4.7 Internal K-Frame Bracing

Formed by one strut (which is part of the top lateral truss) and two diagonals [Figure 3-19], the K-frames were designed and fabricated accordingly to remain elastic during the experimental tests to avoid stability or overstressing issues. The section of the strut was sized for the top lateral bracing system, and the same section has been adopted for the K-frame diagonals (2 in. x-strong) for facility during fabrication. Similar to the struts outlined in the last section, round sections were used to facilitate monitoring of the axial stresses in the K-frames by simple averaging of strain gage readings. The K-frame bracing elements were fabricated with ASTM A53 – Grade B steel. Three different arrangements of internal K-frames were tested for each configuration of top lateral bracing. K-frame bracing at every two, four and six panel points were evaluated during the experimental program.

Figure 3-19 - K-frame Bracing

3.5 Instrumentation

Load cells, string potentiometers (string-pots), strain gauges and LED sensors were all utilized to collect data during the elastic tests. To monitor the loads applied in the lateral and

vertical loading tests, load cells were placed at the loading points as shown in Figure 3-5 andFigure *3-9*, respectively. Load cells with respective capacities of 25 and 100 kips were calibrated and used in the lateral and vertical buckling tests.

Horizontal and vertical deflections of the steel tub girders were measured at the third points along the tub length (28 ft. and 56 ft.) and at mid-span (42 ft.). The deflections at the third points were obtained with four string potentiometers mounted on each lateral load frame (two connected vertically to the bottom flange, and two connected horizontally to the web). The deflections at mid-span were collected with two infrared cameras that are able to monitor the signal from LED markers attached to the tub girder section. Figure 3-20 shows a picture with the cameras and section monitored with the LED sensors, which is referred to as the Vision System. Figure 3-21 and Figure 3-22 show the locations of the cameras and LED sensors. The cameras, with three lenses, are able to capture infrared signal of the LED markers and then measure three-dimensional movements. The infrared Vision System collected vertical and horizontal deflections with relatively high accuracy (error of approximately 0.01 mm). Rotations were calculated from the measured deflections. Three columns of LED markers were installed at midspan for redundancy. Each column of markers was installed around the exterior faces of the tub girders as shown in Figure 3-20. Regarding the sign convention in subsequent graphs, negative lateral displacements represent movements to the East, while positive displacements represent movements to the West.

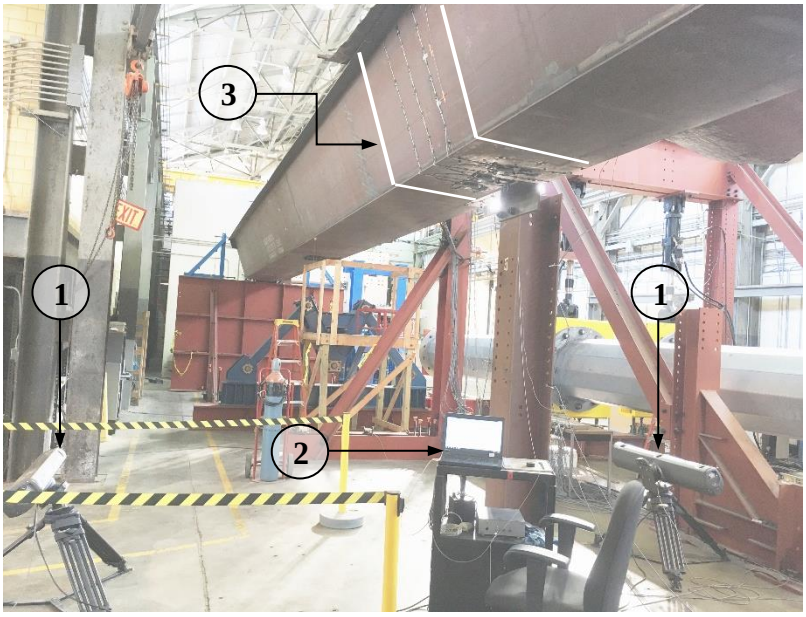

Figure 3-20 - Vision System Setup

Stresses at multiple points of the specimens were collected using conventional resistance-based foil strain gages on both faces of the web, top and bottom flange plates as shown in Figure 3-22. The strain gages provided valuable data for FEA validation studies and allowed the researchers to ensure that the girders remained elastic in the tests. Strain gages were also used on the bracing members so that the forces imposed over the bracing members could be obtained. Six strain gauges were installed at mid-length on every top lateral truss member (WT5x22.5). A linear regression method was used to calculate axial forces in the top lateral diagonals. Struts and diagonals of the K-frames were instrumented with strain gages at mid-length of the pipes, where

a pair of gages were installed on opposite sides of the pipe to allow strains due to bending of the pipe to be separated from strains due to axial forces. Axial forces in these pipes were calculated by averaging the strains of the gauges located on opposite sides of the pipes. The location of the gauges is shown in Figure 3-22. As shown in Figure 3-23, mechanical dial gauges were placed on the test setup supports (at the level of the girder bottom flange) to measure displacements of the tub girders bottom flange relative to the supports in order to capture response of the support connections.

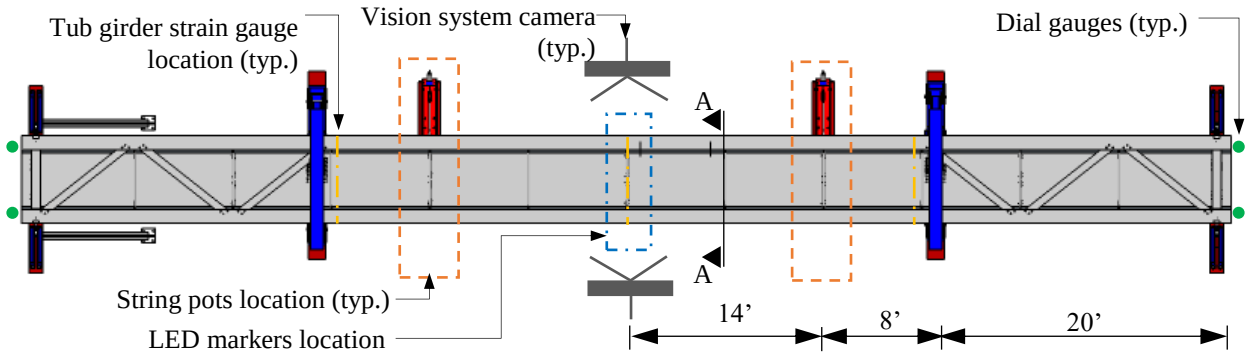

Figure 3-21 - Instrumentation Layout - Plan View

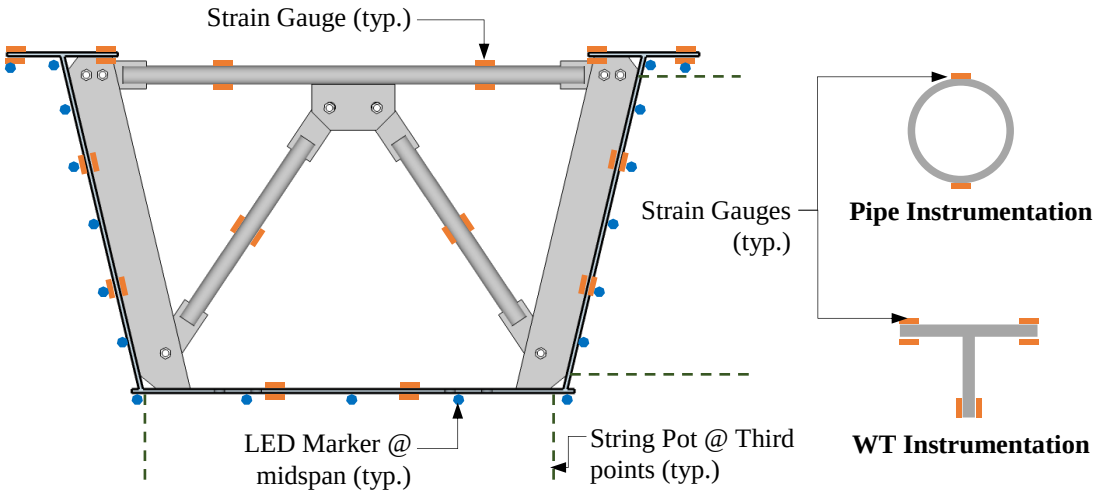

Figure 3-22 - Instrumentation Layout - Section A-A

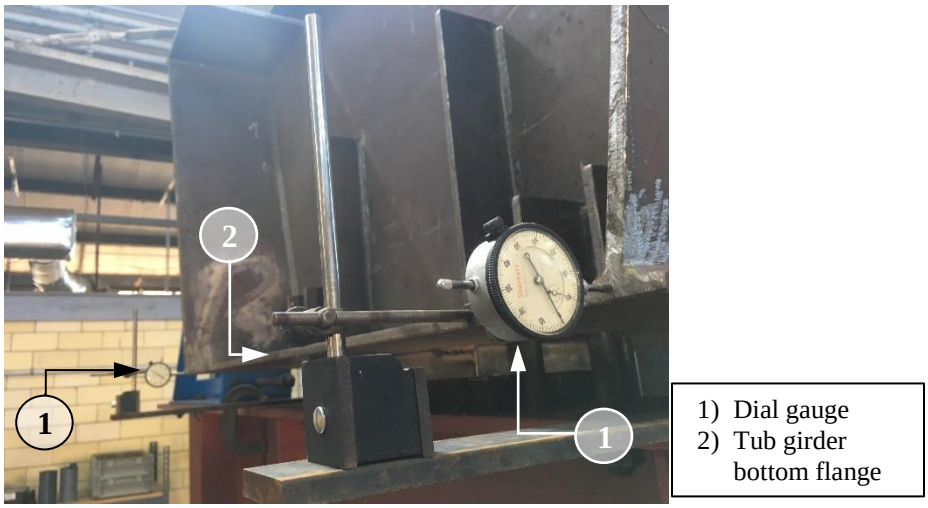

Figure 3-23 - Dial Gauges at Supports

3.6 Initial Imperfections

Prior to testing, initial imperfections of each steel tub girder were measured. Two wires (piano wire) were extended between the test setup supports located 6 in. from both edges of the bottom flange. The taut wires served as reference point to measure lateral and vertical out-of-straightness of the tub girder. The taut wires were set at the same distance from the bottom flange (d_{s_bot}) and the top flange (d_{s_top}) at each support. The deviation of the bottom (d_{bf}) and top flange (d_{tf}) along the girder were measured directly with a caliper and a plumb bob. Measurements were collected at 7 ft. interval on both sides of the girder. Each specimen was resting over the north and south test setup supports when initial imperfections were measured on the east and west sides of the girders. Figure 3-24 presents the methodology that was used to evaluate the initial lateral imperfection of the top flange (Δ_{tf}) and the bottom flange (Δ_{bf}), and the initial twist (θ).

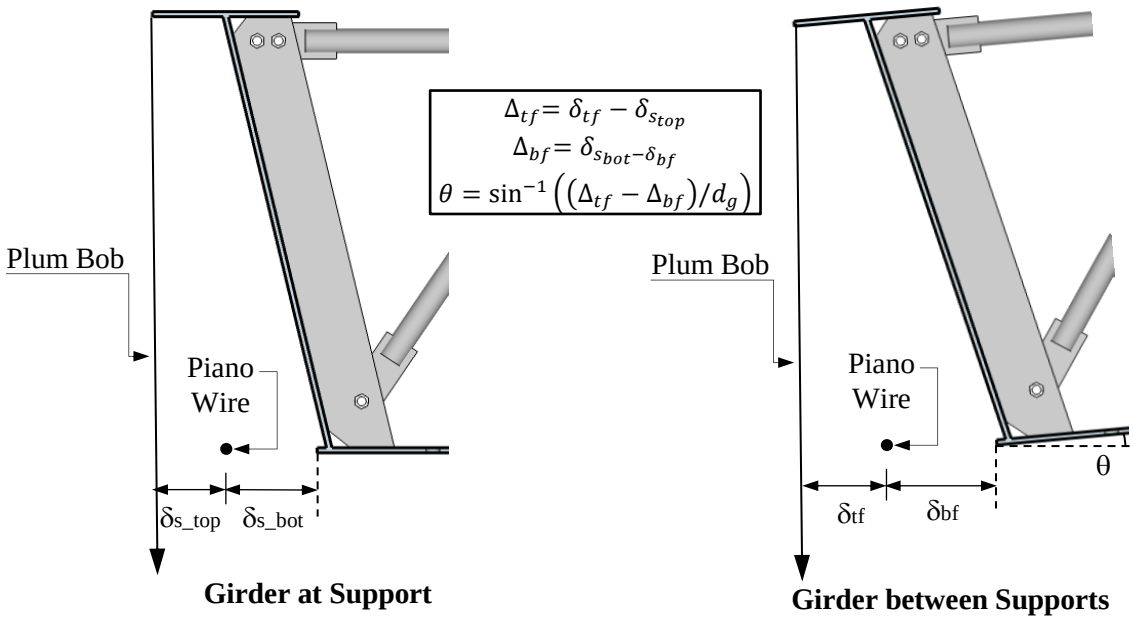

Figure 3-24 - Initial Imperfection Measurements and Calculations

Tub 1 (baseline girder) had an initial twist of 1.30 degrees (midspan) and a maximum out-of-straightness of about L/1300 (on top flange) towards the east. Tub 2 (offset flanges) had an initial twist of about 1.60 degrees (midspan) and a maximum out-of-straightness of L/750 (on top flange) towards the west. Finally, Tub 3 (flatter-sloped webs) showed an initial twist of 2.30 degrees (midspan) and a maximum out-of-straightness of about L/500 (on top flange) towards the east. Initial imperfections were measured before every elastic-buckling test; however, these imperfections did not changed significantly from test to test, with maximum variations of the order of ±0.1in.

3.7 Testing Procedure

Since the critical stages for both stability and lateral/torsional flexibility of steel tub girders generally occur during the construction phase, the range of stresses imposed over these sections are normally within the elastic range. AASHTO 2017 requires the girders during construction remain elastic. Elastic-buckling tests were carried out by limiting the maximum loads applied to the specimen to keep stresses lower than 60% of nominal yield stress (30 ksi). This maximum stress limit was set to consider the impact of residual stresses and initial imperfections in the response of the tub girder and to ensure that the girders remained elastic.

Two types of loading conditions were studied: vertical positive bending and combined bending and torsion due to vertical eccentric loads (to simulate horizontal curvature), and lateral loads (to collect data of lateral stiffness). For the lateral loading tests, four equal horizontal loads were applied, two at each reaction L-shaped frame located at the third points of the girders (location denoted as "Pb" in Figure 3-17). The maximum total lateral load applied on each test was 25 kips. For the vertical load tests, two vertical loads were applied with gravity load simulators at approximately quarter points of the specimen (location denoted as "Pa" on Figure 3-17). Henceforth, the load on each GLS will be referred to as load "P". The combined vertical bending and torsional demands were obtained by applying vertical eccentric loads at 8 in. and 16 in. from

the shear center location of the girders. Vertical loads with eccentricities of 8 in. and 16 in. were selected to simulate demand conditions produced by curvature on horizontally curved tub girders with radii of curvature equal to 1260 and 630 ft., respectively. The eccentric loads were applied so that torsional demands towards the west of the girders were imposed. The maximum total vertical load applied varied depending on the bracing configuration and the eccentricity. The maximum vertical load applied was 105 kips (2 point loads of 52.5 kips).

3.7.1 Bracing Configuration

In order to measure the impact of different details in the response of the test specimens, different bracing layouts were tested on the each tub girder under the same loading conditions.

First, four lateral loading tests were performed in each specimen. Each test was conducted with different amounts of bracing diagonals at each end of the tub so that the effectiveness of the bracing could be evaluated. The four load cases consisted of cases with zero, one, two, and three diagonals on each end of the simple supported girder. Figure 3-25 and Figure 3-26 show pictures of the girders with the different top truss bracing configurations. K-frames were positioned at every two panels for these four tests.

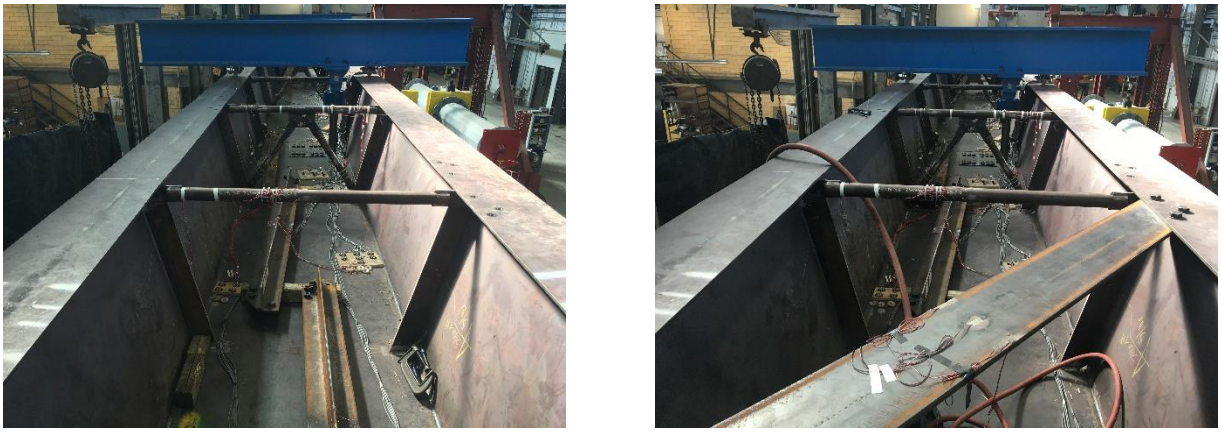

Figure 3-25 - Left) No Diagonals Case, Right) 1 Diagonals Case

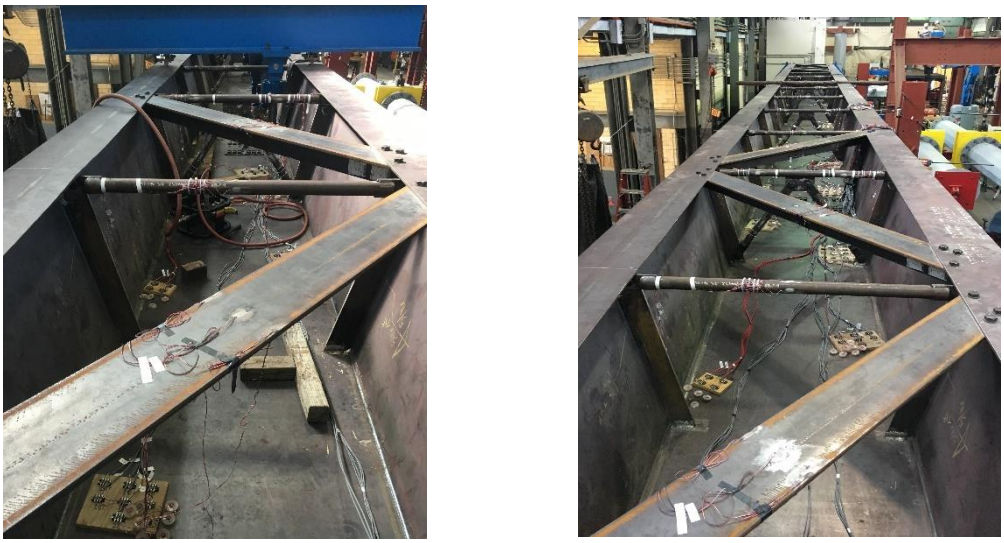

Figure 3-26 - Left) 2 Diagonals Case, Right) 3 Diagonals Case

Following the lateral load tests, 36 elastic-buckling tests were carried out. Each test was conducted with different amounts of top bracing diagonals at each end. Cases with zero, one, two, and three diagonals on each end of the simple supported girder were the four configurations of partial top lateral bracing studied. For each aforementioned top lateral bracing configuration (four bracing layouts), three different configurations of internal K-frame bracing were assessed. K-frames were located at every two, four, and six panel points for each configuration of top lateral bracing, which resulted in a total of 12 elastic buckling tests. These 12 configurations of top lateral and K-frame bracing were evaluated for the three cases of vertical loads (concentric, eccentric at 8in., and eccentric at 16in.) producing a total of 36 elastic tests performed with the GLSs. The impact of each bracing configuration in the response of the specimens is evaluated and summarized in the following sections.

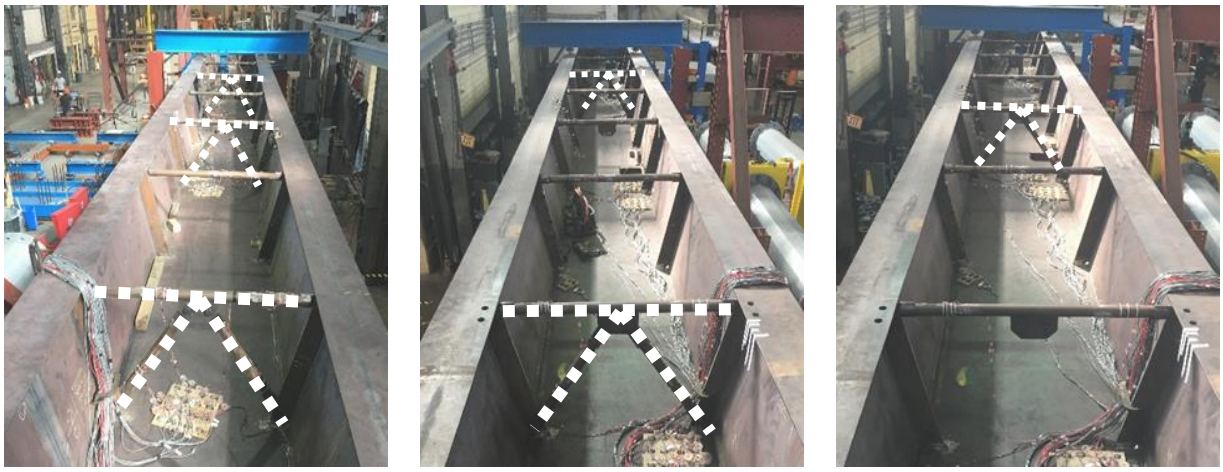

Figure 3-27 - K-Frame Layouts: Left) Every 2 Panels, Center) Every 4 Panels, Right) Every 6

3.8 Experimental Results

A total of 4 lateral load tests and 36 simulated gravity load tests were performed on each tub girder at the Ferguson Structural Engineering Laboratory. The results obtained in the tests are explained in the following sections.

3.8.1 Impact of Partial Top Lateral Bracing Distribution in Stiffness

To study the effect of partial top lateral bracing on straight and horizontally curved steel tub girders, the three specimens were loaded with combined bending and torsional loading. The response of the specimens under these two loading conditions is described in this section.

3.8.1.1 Lateral Load Experimental Results

Table 3-1 presents a summary of the four lateral load tests that were performed with Tub 1 (baseline girder) in the laboratory. The same lateral load tests were carried out with Tub 2 (offset flanges) and Tub 3 (flatter-web). Although the specimens have been referred to by both the name and brief description up to this point, henceforth, the three specimens are referred as Tub #1, Tub#2, and Tub #3, for simplicity in the discussion of the results. The nomenclature for the lateral load tests is shown in Figure 3-28.

Table 3-1 - Lateral Tests Summary –Tub #1

Test Code	Load Location	Number of Diagonals	K-Frame Location
LAT_1.1	TP	3	2-Panel
LAT_1.2	TP	2	2-Panel
LAT_1.3	TP	1	2-Panel
LAT_1.4	TP	0	2-Panel

LAT = Top & Bottom Flange Lateral Load
TP = Third Point

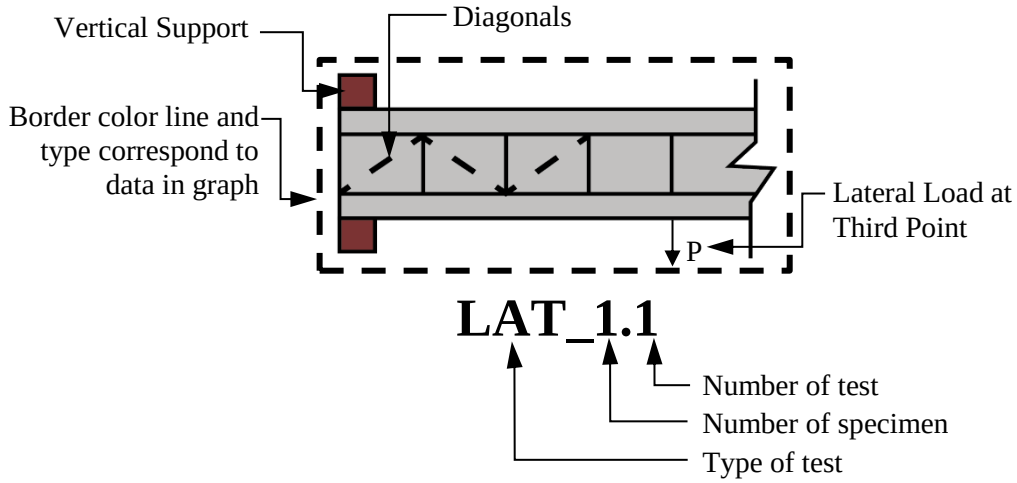

Figure 3-28 - Nomenclature for Lateral Load Experimental Tests

The lateral load tests applied lateral and torsional loads to the specimens at the two third points (28ft from each end). The torsional moments were imposed to the girder by applying equal horizontal loads "Pb" as shown in Figure 3-6 and Figure 3-17. The torsional moment T was calculated with respect to the shear center of the quasi-closed tub girder. The shear center location was 13.2, 14.3, and 10.6 in below the bottom flange of Tub #1, #2, and #3, respectively. To assess the bracing effectiveness, the lateral deflection of top flange (δt) and twist of the section (β) under the aforementioned demands were compared for different scenarios of partial top lateral bracing on each tub girder. The lateral loads were applied so that the rotations were enforced to the West of the specimen (positive twist angles according to aforementioned sign convention). Graphs for lateral deflection and twist angle at midspan are reported in this section of the report. Appendix C contains the graphs corresponding to deformations at the third points.

Figure 3-29 shows the relationship between lateral displacement at mid-span of the tub (δt) on the top flange and the total lateral load applied on the specimen (4P). As expected, the steel tub girder without any diagonals in the top lateral bracing is the most flexible system (approx. lateral stiffness of 4 kips/in) which is represented by the solid purple line. By adding a bracing diagonal on each end of the tub (dash-dot-dotted black line), the lateral stiffness improves significantly by a factor of almost three (~11 kips/in). The case with two bracing diagonals at each end (dash-dotted red line) produced a lateral stiffness enhancement of approximately six times (~23.20 kips/in) in comparison with the unbraced case. Finally, the lateral stiffness increased to approximately 31.50 kips/in (dashed green line) when the tub girder was tested with three diagonals at each end (lateral response improved by a factor of almost 8).

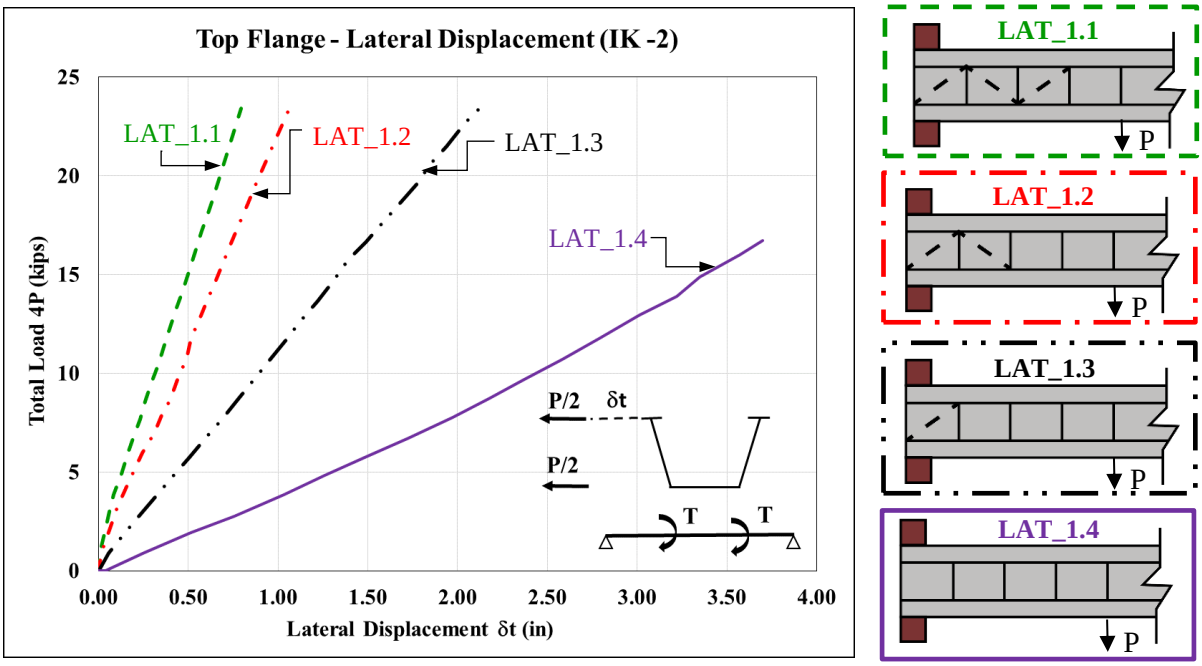

Figure 3-29 – Total Lateral Load vs Top Flange Lateral Displacement - Tub #1

As expected, in addition to improving the lateral stiffness, the diagonals also significantly improve the torsional stiffness. Figure 3-30 presents the angle of twist at mid-span (β) with respect to the applied moment T for the four different configurations of top lateral bracing. Similarly, the torsional stiffness of the specimen improves considerably with the addition of the bracing

diagonals at the supports. The torsional stiffness of the unbraced tub girder (~4.7 kips-ft./deg.) is improved in a ratio of about 3.50, 11.40 and 16.0 when adding one, two and three diagonals at the ends of the girder, respectively. This trend shows that the braces near the ends of the section are the most efficient at enhancing the lateral and torsional stiffness of the girders and the efficiency decreases with increasing distance from the ends of the section. For a given torsional/lateral stiffness demand, the amount of bracing near the ends of the section should be determined and inefficient braces near midspan may be unnecessary.

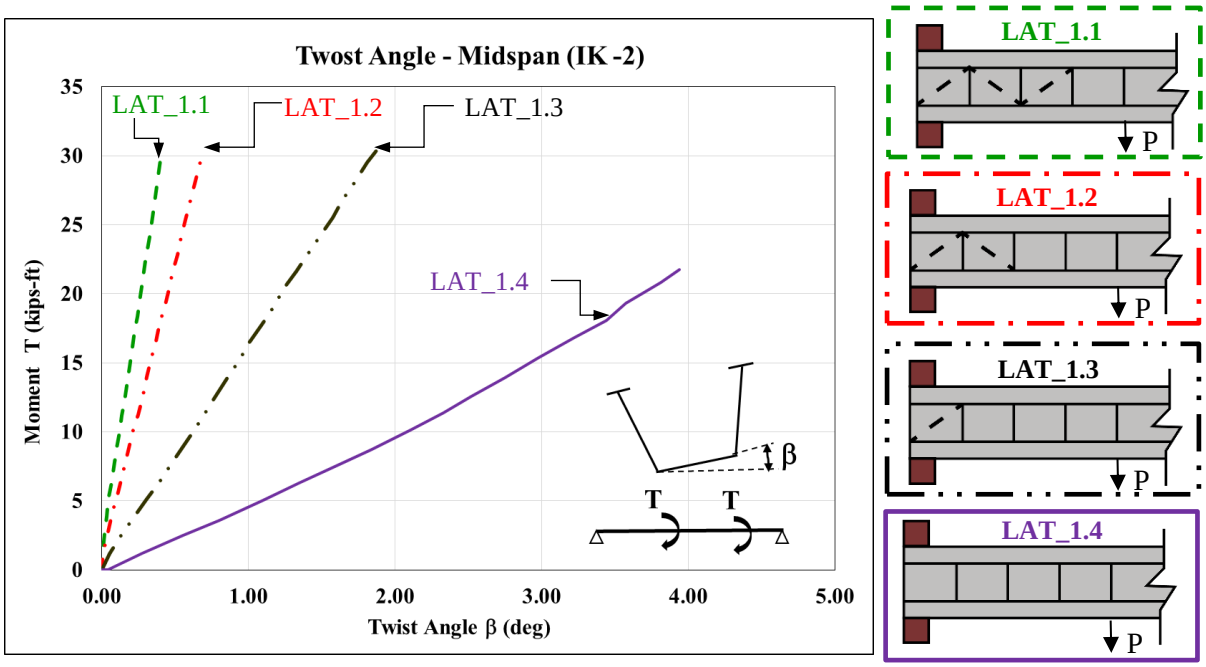

Figure 3-30 - Torsional Moment vs Twist Angle - Tub #1

Similar response was obtained during the lateral tests performed with Tub #2 and Tub #3. The unbraced cases were the most flexible; while, the lateral and torsional stiffness of the tub girders highly improved after adding partial top lateral bracing on both ends of the girder. Table 3-2 presents a summary of the results for all three specimens. A comprehensive collection of graphs for the lateral load tests is provided in Appendix C.

Table 3-2 - Summary of Lateral Load Test Results – All Specimens

	Test Code	Number of Diagonals	K-Frame Location	Max Total Load (kips)	Max Top Lat Defl. (in)	Average Lat Stiff (k-in)	Max Twist (deg)	Average Tortional Stiffness (k-ft/deg)
Tub 1	LAT_1.1	3	2-Panel	23.40	0.79	31.50	0.41	80.30
	LAT_1.2	2	2-Panel	23.40	1.06	23.20	0.70	51.30
	LAT_1.3	1	2-Panel	23.60	2.14	11.40	1.90	16.80
	LAT_1.4	0	2-Panel	21.70	3.70	4.00	3.94	4.65
Tub 2	LAT_2.1	3	2-Panel	20.23	0.56	38.50	0.24	117.40
	LAT_2.2	2	2-Panel	20.13	0.74	28.50	0.41	67.75
	LAT_2.3	1	2-Panel	20.24	1.27	16.60	0.94	30.25
	LAT_2.4	0	2-Panel	20.31	3.35	5.70	3.09	8.35
Tub 3	LAT_3.1	3	2-Panel	20.00	0.95	22.10	0.58	43.30
	LAT_3.2	2	2-Panel	20.12	1.53	13.40	1.23	20.20
	LAT_3.3	1	2-Panel	19.73	2.97	6.80	2.86	8.85
	LAT_3.4	0	2-Panel	9.04	4.62	1.68	4.95	1.90

3.8.1.2 Positive Bending Experimental Results (Straight Tub Girders)

Table 3-3 presents a summary of the 12 vertical bending load tests that were performed with Tub #1 in the laboratory. The same tests were carried out with the specimens Tub #2 and Tub #3. The nomenclature for the positive bending tests is shown in Figure 3-31.

Table 3-3 - Positive Bending Tests Summary –Tub #1

Test Code	Number of Diagonals	K-Frame Location
GLS_1.1	0	2-Panel
GLS_1.2	0	4-Panel
GLS_1.3	0	6-Panel
GLS_1.4	1	2-Panel
GLS_1.5	1	4-Panel
GLS_1.6	1	6-Panel
GLS_1.7	2	2-Panel
GLS_1.8	2	4-Panel
GLS_1.9	2	6-Panel
GLS_1.10	3	2-Panel
GLS_1.11	3	4-Panel
GLS_1.12	3	6-Panel

GLS = Gravity Load Simulator Load

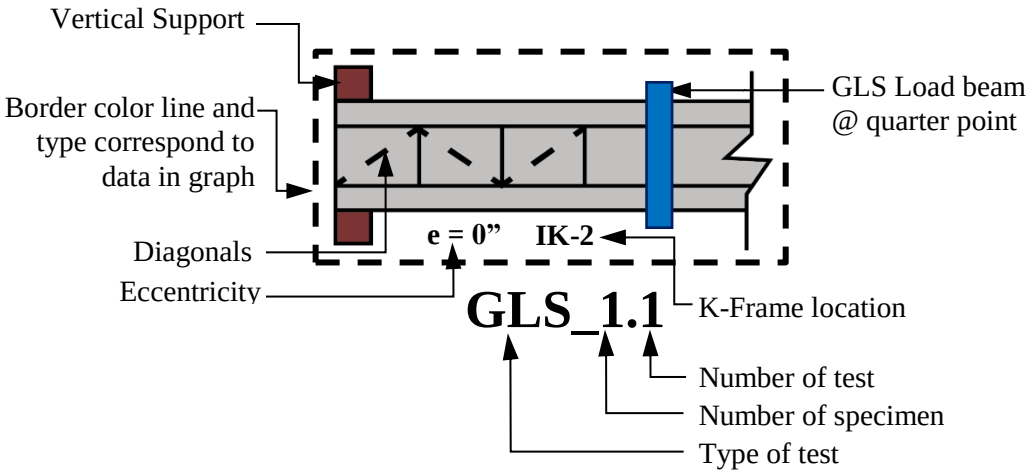

Figure 3-31 - Nomenclature for GLS Experimental Tests

Two gravity load simulators were used to apply vertical concentric loads near the quarter points of the girders to evaluate the impact of partial top lateral bracing to resist lateral torsional buckling. To assess the bracing effectiveness, lateral displacements (δt) and twist angles (β) at different load levels are compared for different layouts of partial top lateral bracing. To avoid additional variables and to obtain a more clear understanding of the effects of partial top lateral bracing, the analysis of the results in this section is focused on the tests with internal K-frames at every two panels. However, the results for other configurations are summarized in Table 3-4, while the respective graphs are presented in Appendix C.

Figure 3-132 shows the total vertical load applied (2P) versus the lateral displacement of the baseline specimen at the top flange (δt), when the specimen was tested with zero, one, two, and three bracing diagonals at each end. The tub girder without top lateral bracing presented a deformation curve that suggested the girder was approaching the elastic lateral torsional buckling limit during the test, which can be observed by the significant nonlinear response of the load versus deflection curve. The torsional stiffness of the specimen reduced significantly as the girder approached the lateral torsional buckling limit. The capacity to resist LTB is significantly improved with the addition of diagonals at the ends of the girder. The system without diagonals had a lateral displacement of 1.68 in. at 70 kips of total load; while the specimen with 1 diagonal per end had a maximum lateral displacement of 0.18 in at the same load step. This is a reduction of about 90% in the lateral displacement of the top flange and indicates that the torsional stiffness is highly improved with a single diagonal at each end. The baseline specimen with two truss diagonals per end presented a lateral displacement of 0.003 in showing a clear improvement in the torsional stiffness of the specimen. The tub girder with three diagonals per end did not show a significant improvement in torsional stiffness with respect to the previous case. Instead, the three diagonals per end produced a shift in the direction of lateral movement (shift of mode shape). Clearly, the first diagonal on each end of the specimen produced the most significant improvement in the resistance to LTB, while additional diagonals were not as effective at improving the behavior. As expected, the experimental results demonstrated that the effectiveness of the top lateral bracing is lower with increasing distance from the ends of the girders. The horizontal truss diagonals are more effective at the supports where warping deformations are higher.

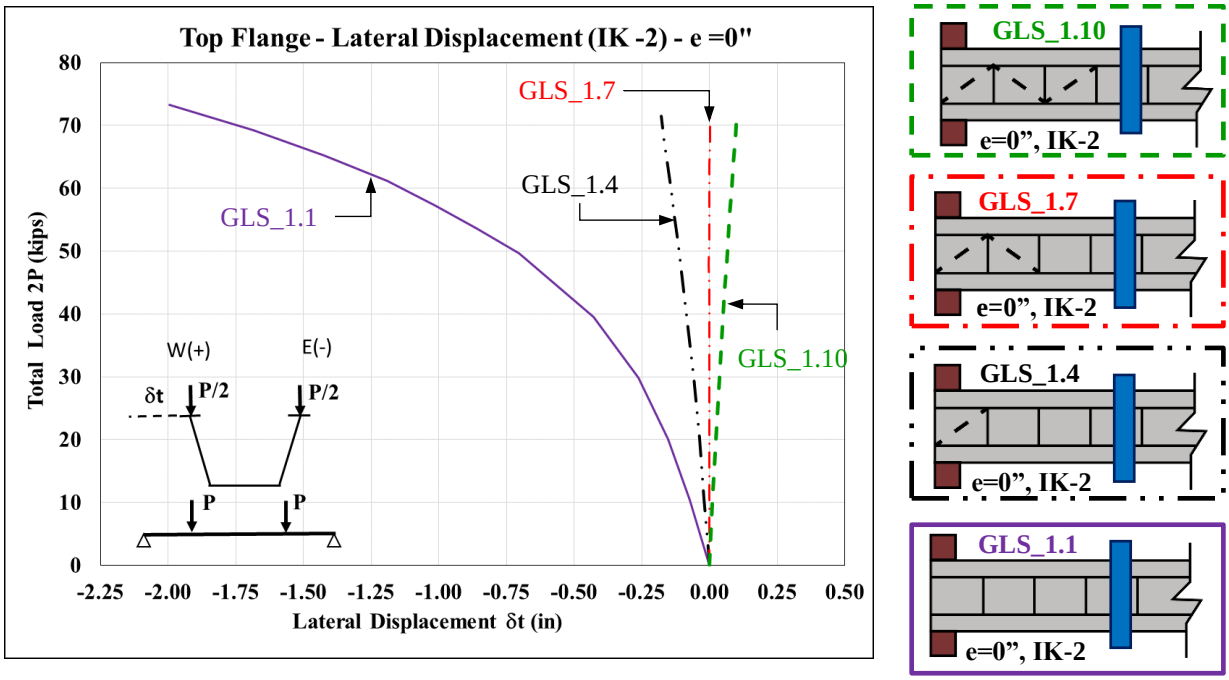

Figure 3-32 - Total GLS Load vs Top Flange Lateral Displacement - Tub #1

Figure 3-33 presents the total vertical load (2P) applied versus the twist angle at midspan (β) on the baseline tub girder for the four different arrangements of top lateral bracing. As observed in Figure 3-32, the most important improvement in the torsional stiffness of the specimen is achieved when one diagonal is added at the ends of the tub girder. The addition of extra diagonals enhances the LTB resistance, but at a much lower increment compared to the first diagonal. As depicted in Figure 3-33, when the specimen was tested with three diagonals, the rotation of the tub girder actually had a change in rotational sign, which implies a high resistance to lateral torsional buckling. While the change in rotational sign may seem counter-intuitive, it is important to note that this is just the twist that occurred at midspan. The load was applied near the quarter points and the bracing simply affected the mode shape of the girder. This shift in mode shape was also observed in Tub #3. The partial bracing tests demonstrate that "full" top lateral bracing (ie. a diagonal in every single panel) along the girder is not likely needed to control LTB; instead, partial top lateral bracing can be provided in these cases to control LTB in straight tub girders.

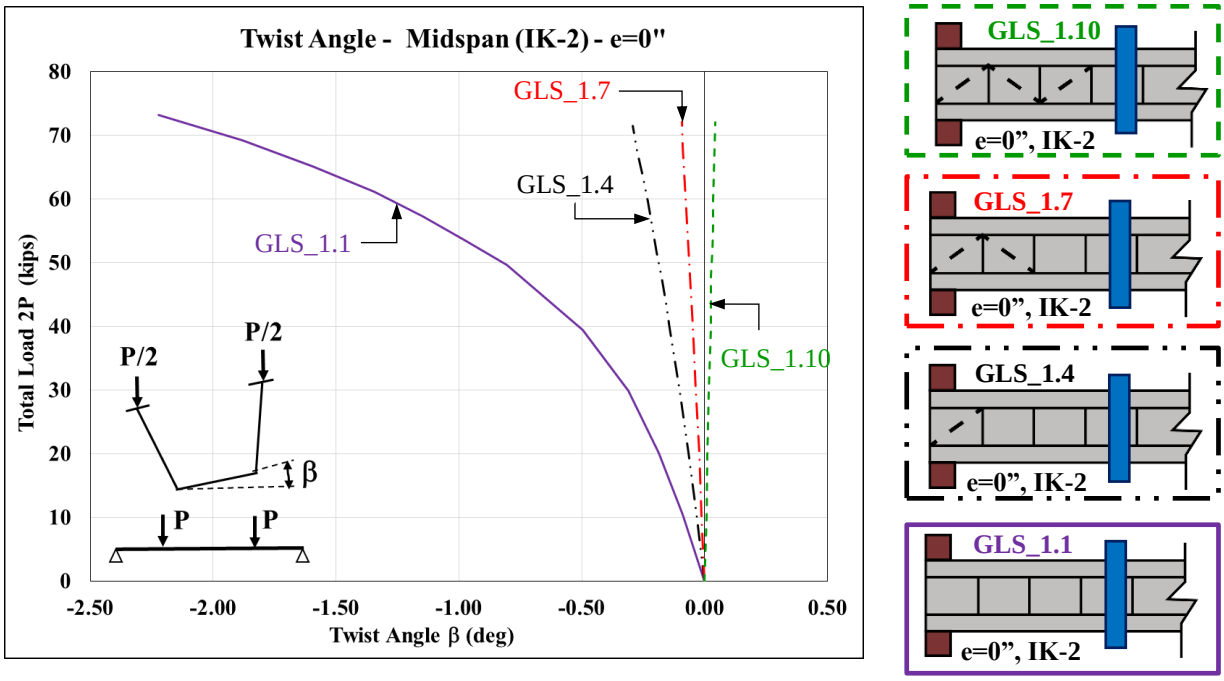

Figure 3-33 - Bending Moment vs Twist Angle - Tub #1

Similar behavior was observed in the other two specimens (Tub #2 and #3). The only difference in the response of the specimens was the direction of the lateral torsional buckling that was directly related to the initial imperfections of the girders. The baseline and the flatter web tub girders twisted towards the East, while the top flange offset tub girder deflected towards the West. The load versus deformation curve indicated that the lateral torsional buckling limit was nearing in the three specimens when the top lateral truss was not provided. In addition, the torsional stiffness of the three girders was highly improved when a single diagonal was added at each support. Adding more diagonals at each end increases the torsional stiffness of the girders but at a lower rate. Table 3-4 shows a summary of the results for all three specimens. A comprehensive collection of graphs for the positive bending tests is provided in Appendix C.

Table 3-4 - Summary of GLS Positive Bending Test Results – All Specimens

	Test Code	Number of Diagonals	K-Frame Location	Max Total Load (kips)	Max Top Lat Defl. (in)	Average Lat Stiff (k/in)	Max Twist (deg)	Average Tortional Stiffness (k/deg)
Tub 1	GLS_1.1	0	2-Panel	73.00	-2.00	-51.00	-2.24	-44.00
	GLS_1.2	0	4-Panel	59.00	-1.26	-47.00	-1.46	-41.00
	GLS_1.3	0	6-Panel	59.00	-1.32	-45.00	-1.53	-40.00
	GLS_1.4	1	2-Panel	71.00	-0.18	-390.00	-0.29	-239.00
	GLS_1.5	1	4-Panel	71.00	-0.22	-338.00	-0.34	-213.00
	GLS_1.6	1	6-Panel	71.00	-0.23	-307.00	-0.33	-216.00
	GLS_1.7	2	2-Panel	76.00	0.004	21,000	-0.10	-818.00
	GLS_1.8	2	4-Panel	76.00	-0.02	-4,050	-0.12	-663.00
	GLS_1.9	2	6-Panel	76.00	0.02	3,800	-0.12	-643.00
	GLS_1.10	3	2-Panel	80.00	0.12	670.00	0.05	1,745
	GLS_1.11	3	4-Panel	80.00	0.16	465.00	0.06	1,385
	GLS_1.12	3	6-Panel	76.00	0.14	544.00	0.05	1,690
Tub 2	GLS_2.1	0	2-Panel	100.00	1.38	70.90	1.51	65.00
	GLS_2.2	0	4-Panel	100.00	1.42	13.00	1.47	75.00
	GLS_2.3	0	6-Panel	100.00	1.38	16.00	1.52	70.00
	GLS_2.4	1	2-Panel	105.00	0.25	416.00	0.36	312.00
	GLS_2.5	1	4-Panel	105.00	0.39	274.00	0.31	343.00
	GLS_2.6	1	6-Panel	105.00	0.36	293.00	0.40	266.00
	GLS_2.7	2	2-Panel	105.00	0.06	1,830	0.14	809.00
	GLS_2.8	2	4-Panel	105.00	0.16	658.00	0.12	913.00
	GLS_2.9	2	6-Panel	105.00	0.12	854.00	0.13	784.00
	GLS_2.10	3	2-Panel	105.00	0.07	1,425	0.09	1,180
	GLS_2.11	3	4-Panel	105.00	0.12	901.00	0.09	1,300
	GLS_2.12	3	6-Panel	105.00	0.10	1,044	0.11	970.00
Tub 3	GLS_3.1	0	2-Panel	30.00	-3.37	-7.50	-3.63	-7.00
	GLS_3.2	0	4-Panel	29.00	-3.35	-8.30	-3.57	-7.70
	GLS_3.3	0	6-Panel	28.00	-3.31	-8.30	-3.56	-7.70
	GLS_3.4	1	2-Panel	75.00	-1.09	-71.00	-1.25	-61.00
	GLS_3.5	1	4-Panel	75.00	-1.61	-53.00	-1.84	-47.00
	GLS_3.6	1	6-Panel	74.00	-1.58	-58.00	-1.82	-48.00
	GLS_3.7	2	2-Panel	85.00	-0.19	-410.00	-0.36	-213.00
	GLS_3.8	2	4-Panel	85.00	-0.44	-197.00	-0.59	-175.00
	GLS_3.9	2	6-Panel	85.00	-0.41	-207.00	-0.56	-151.00
	GLS_3.10	3	2-Panel	85.00	0.13	660.00	0.04	2140
	GLS_3.11	3	4-Panel	85.00	0.18	472.00	0.02	3800
	GLS_3.12	3	6-Panel	85.00	0.17	502.00	0.04	2200

3.8.1.3 Bending plus Torsion Tests (Horizontally Curved Tub Girder)

Table 3-5 presents a summary of the 24 combined bending plus torsion load tests that were performed with Tub #1 at the laboratory. Similar tests were carried out with the specimens Tub #2 and Tub #3. The nomenclature for the bending plus torsion tests is the same as for the positive bending tests, which is shown in Figure 3-31.

Table 3-5 - Bending plus Torsion Tests Summary – Tub #1

Test Code	Eccentricity (in)	Number of Diagonals	K-Frame Location
GLS_1.13	8	0	2-Panel
GLS_1.14	8	0	4-Panel
GLS_1.15	8	0	6-Panel
GLS_1.16	8	1	2-Panel
GLS_1.17	8	1	4-Panel
GLS_1.18	8	1	6-Panel
GLS_1.19	8	2	2-Panel
GLS_1.20	8	2	4-Panel
GLS_1.21	8	2	6-Panel
GLS_1.22	8	3	2-Panel
GLS_1.23	8	3	4-Panel
GLS_1.24	8	3	6-Panel
GLS_1.25	16	0	2-Panel
GLS_1.26	16	0	4-Panel
GLS_1.27	16	0	6-Panel
GLS_1.28	16	1	2-Panel
GLS_1.29	16	1	4-Panel
GLS_1.30	16	1	6-Panel
GLS_1.31	16	2	2-Panel
GLS_1.32	16	2	4-Panel
GLS_1.33	16	2	6-Panel
GLS_1.34	16	3	2-Panel
GLS_1.35	16	3	4-Panel
GLS_1.36	16	3	6-Panel

The gravity load simulators were used to apply eccentric vertical loads near the quarter points of the girders. Eccentric loads at 8 in. and 16 in. from the shear center of the section were applied to simulate the demands on horizontally curved bridges with radii of curvature of 1260 and 630 ft., respectively.

When applying eccentric vertical loads, similar trends to the concentric cases was observed. The specimens showed poor torsional resistance when no top lateral diagonals were installed. The torsional stiffness of the girders was enhanced when bracing diagonals were installed at each end because they restricted the warping deformations on the girders.

Figure 3-34 plots the absolute values of torsional response of Tub #1 (baseline girder) with zero and three diagonals per end subjected to concentric and eccentric loads. The concentric cases are represented with black lines (dot markers); while the cases with eccentricity of 8 in. and 16 in. are illustrated with purple (line markers) and orange (triangle markers) lines, respectively. The dashed lines represent the response of the girders with no top lateral truss while the solid lines show the torsional response when three diagonals are installed on each end. As expected, in regards to the unbraced cases, the torsional stiffness of the baseline girder goes down when the torsional demands increase. The initial torsional stiffness of the unbraced concentric case is about 4 and 12 times higher than the cases with loads applied at 8 in. and 16 in. of eccentricity, respectively.

Regarding the braced cases, with three diagonals, the specimen shows lower differences in the torsional stiffness between the three loading cases. The stiffness observed during the concentric test is about 1.5 and 4 times higher than the results obtained with eccentric loading at 8 in. and 16 in., respectively. As previously discussed, the addition of top bracing diagonals produced a high increment in the torsional stiffness. The torsional stiffness increased about 10 to 30 times after installing partial top lateral bracing with three diagonals. Similar response was observed in the Tub #2 and Tub #3 tests.

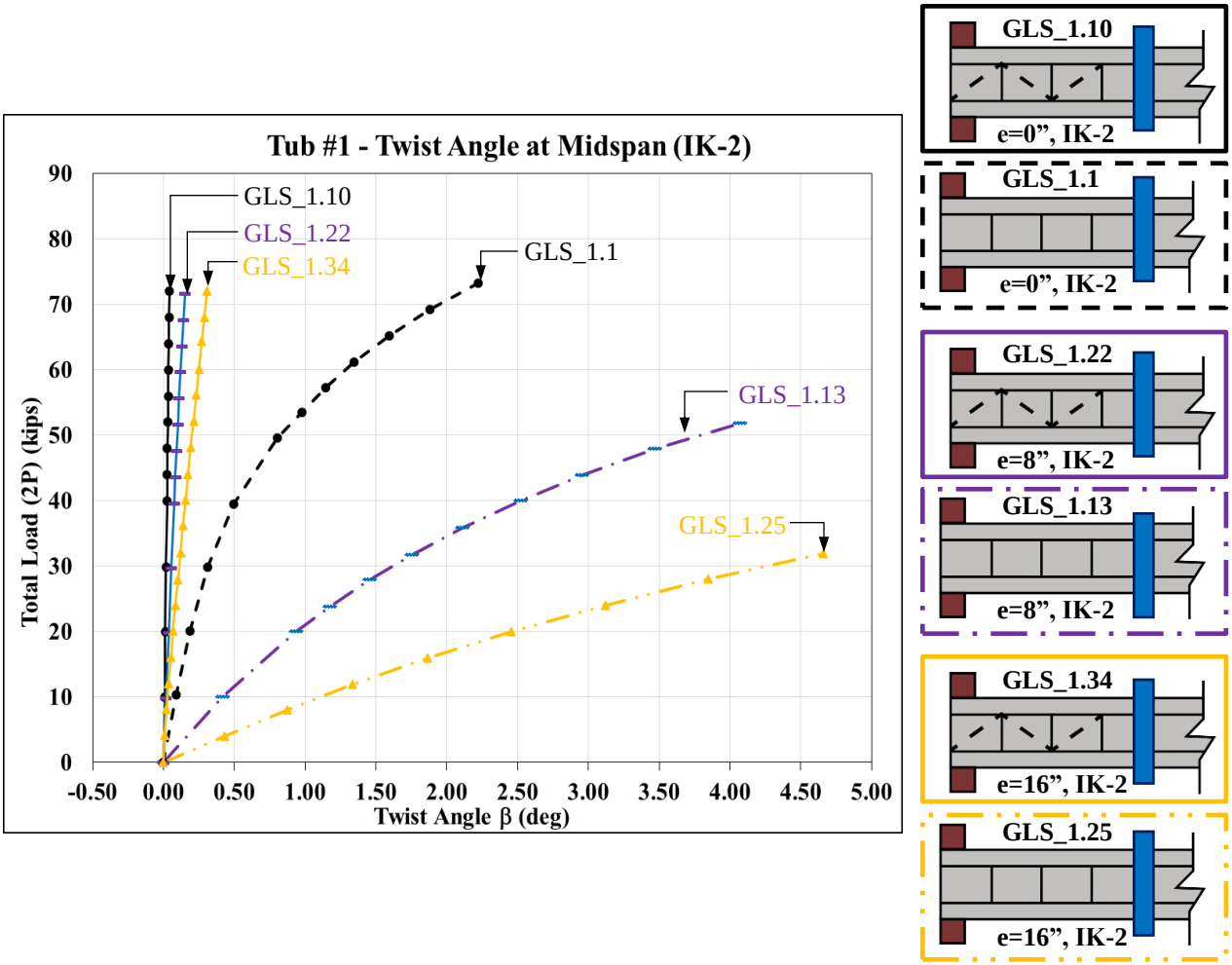

Figure 3-34 - Total Load vs Midspan Twist Angle – Tub #1 with 0 & 3 Diagonals

Similar response was observed when the absolute values of the lateral displacements of Tub #1 were compared for the same bracing and loading configurations of Figure 3-34. This comparison is presented in Figure 3-35. For the concentric case, the lateral displacement in the top flange at midspan went from 2.00in to 0.10 in when a total load of 70 kips was applied. Similarly, for the 8in and 16in eccentric cases, the lateral displacement went from 3.65in to 0.14in and 4.15in to 0.14in, when a total load of 52kips and 32kips were applied, respectively. Thus, besides improving the torsional stiffness of the tub girders, partial top lateral bracing located in the region of higher warping deformations has a tremendous impact in controlling lateral displacement of the top flanges.

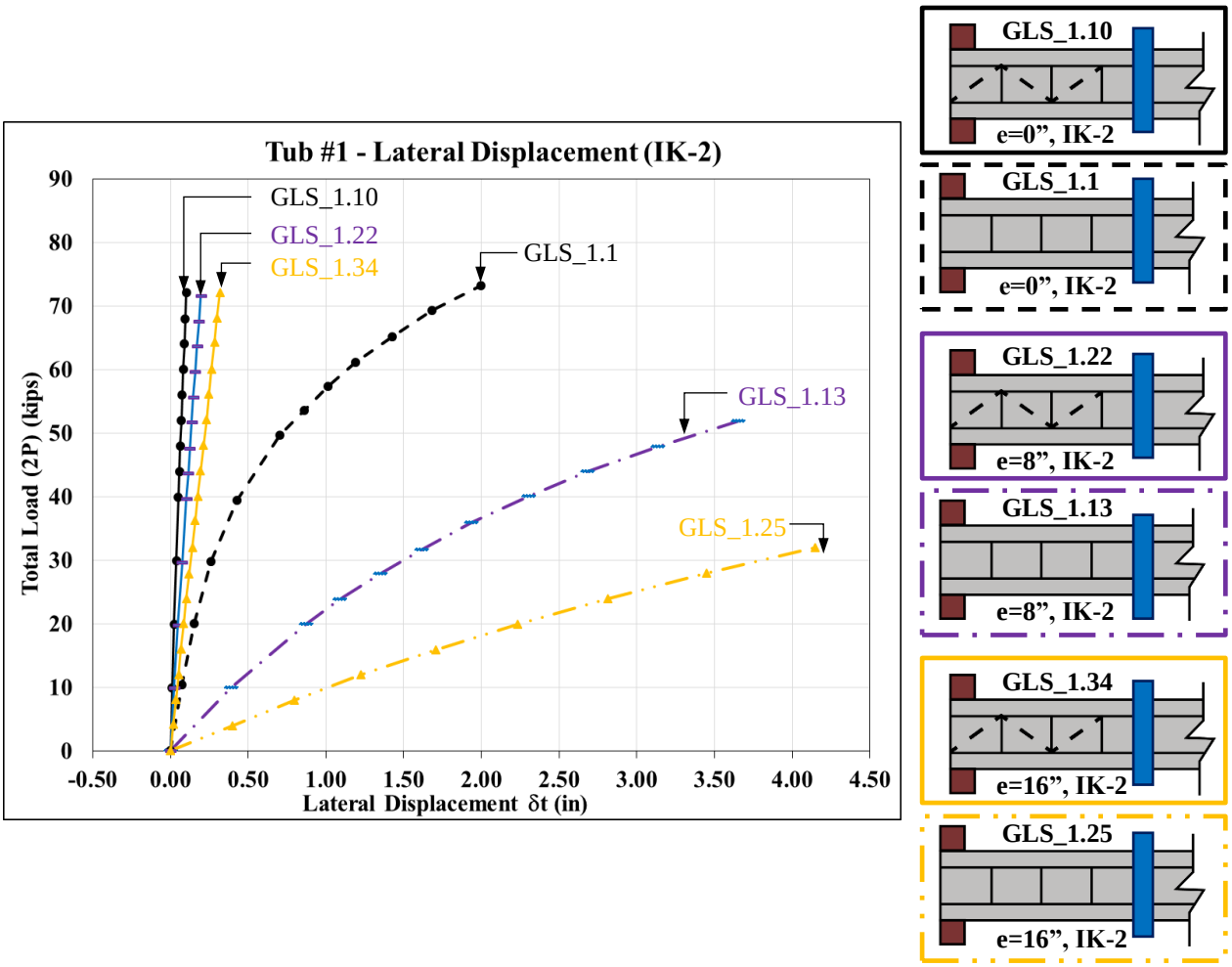

Figure 3-35 - Total Load vs Midspan Top Lateral Displacement – Tub #1 with 0 & 3 Diagonals

As previously described, one of the factors being evaluated in this study is the impact of cross-sectional details on the response of the tub girders. Tub #1 was fabricated with the maximum web slope allowed (4V:1H) by AASHTO 2017, while the Tub #3 was built with inclined webs sloped approximately 2.5V:1H, which is much larger than allowed in AASHTO. Figure 3-36 shows the absolute values of torsional response of the flatter web girder with zero and three diagonals on each end when concentric and eccentric loads were applied. Similar to the Tub #1, poor torsional stiffness was observed when no top lateral bracing was provided, while adding three diagonals on each end produced a large improvement in the stiffness. This lower torsional stiffness of the cross section can be observed in the dashed lines of Figure 3-36, which represent the unbraced case responses. However, after installing the three top diagonals on each end, the torsional stiffness increased significantly. Similar response was observed in the lateral displacements, which is consistent with the description of Figure 3-35. In fact, the stiffness values observed in the braced cases were comparable to the data obtained with the Tub #1 (baseline girder).

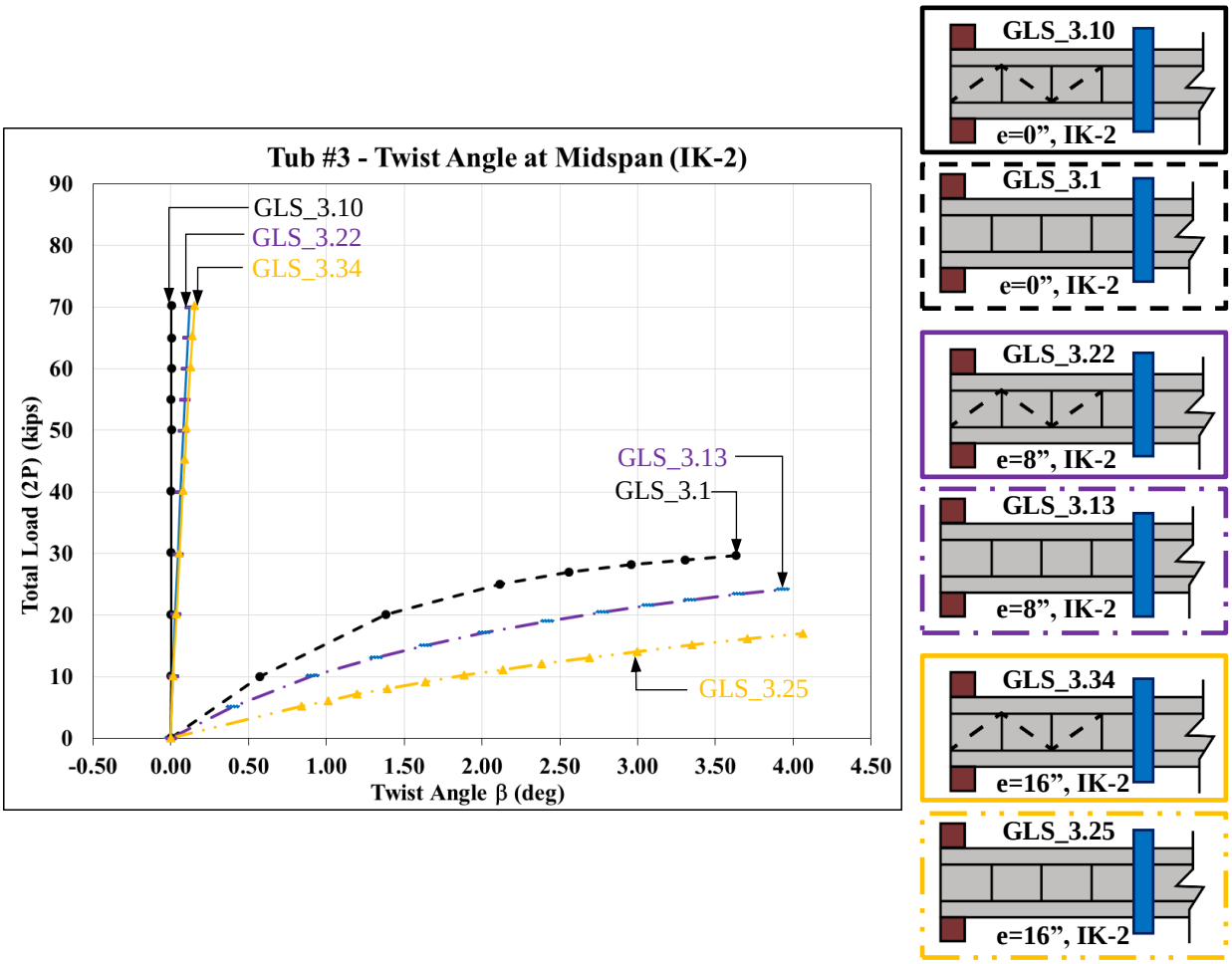

Figure 3-36 - Total Load vs Midspan Twist Angle – Tub #3 with 0 & 3 Diagonals

Figure 3-37 compares the torsional response of the Tub #1 and Tub #3 with zero and three diagonals on each end under concentric loads. In the unbraced cases, the torsional stiffness of the baseline girder is higher (about 6.5 times) than the one observed with the flatter web girder. However, the torsional response of both girders is remarkably high when partial top lateral bracing is installed in comparison to the unbraced cases. The more stiff systems showed comparable values of torsional stiffness and LTB was controlled. Clearly, the torsional response of both girders is very similar when partial top lateral bracing is provided. The only difference observed was the loads sustained by the top lateral truss. The top diagonals in the flatter web girder resisted forces as high as 4 times the ones sustained by the baseline girder under the same loading conditions. Thus, partial top lateral bracing truss has been proved effective to control LTB in straight tub girders even if the enclosed cross-section is reduced by reducing the slope of the webs. The torsional response of Tub #1 and Tub #3 with 3 diagonals on each are very similar. Due to the high stiffness of both girders, the cross-sectional rotations are small enough that the accuracy of measurements can be challenged. That may be the cause of the stiffer response of Tub #3 in comparison to Tub #1 with 3 diagonals on each end.

Partial top lateral bracing has shown to be a potential alternative to control LTB on straight and horizontally curved tub girders with mild radius of curvature. However, these results are representative of a simply supported girder which spans 84 ft.; thus, analytical studies are

necessary to extend the study of partial top lateral bracing and its applicability and to fully recommend this type of alternative bracing system. With the experimental data collected during the elastic buckling tests, finite element models were validated and subsequently, parametric finite element analyses were performed to extent the laboratory results. These results are presented in Chapter 4. Table 3-6,Table 3-7, and Table 3-8 present a summary of the bending plus torsion test results for all three specimens.

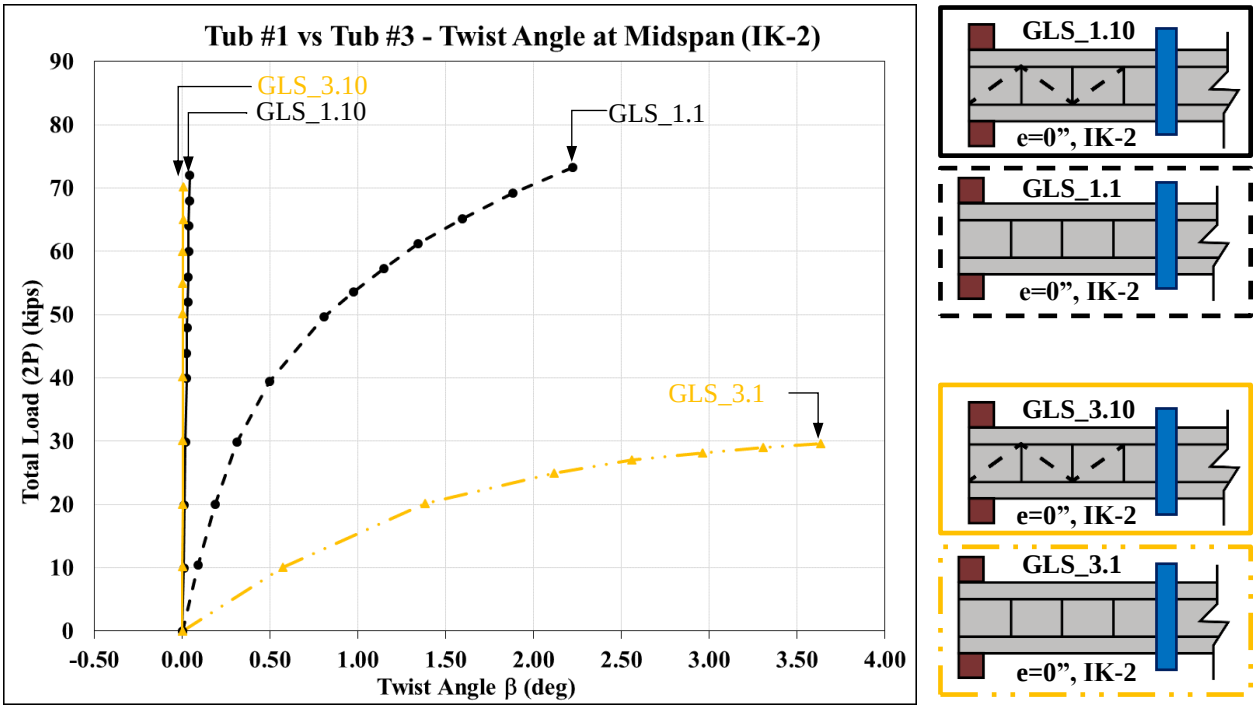

Figure 3-37 - Total Load vs Midspan Twist Angle – Tub #1 vs Tub #3

Table 3-6 - Summary of GLS Bending plus Torsion Test Results – Tub #1

	Test Code	Number of Diagonals	Eccen (in)	K-Frame Location	Max Total Load (kips)	Max Top Lat Defl. (in)	Average Lat Stiff (k/in)	Max Twist (deg)	Average Tortional Stiffness (k/deg)
Tub 1	GLS_1.13	0	8	2-Panel	52.00	3.65	14.50	4.07	13.19
	GLS_1.14	0	8	4-Panel	52.00	3.68	14.40	4.07	13.15
	GLS_1.15	0	8	6-Panel	52.00	3.76	14.20	4.19	12.96
	GLS_1.16	1	8	2-Panel	72.00	0.87	79.00	0.92	76.00
	GLS_1.17	1	8	4-Panel	72.00	1.35	51.00	1.36	51.00
	GLS_1.18	1	8	6-Panel	72.00	1.28	54.00	1.35	51.00
	GLS_1.19	2	8	2-Panel	72.00	0.22	320.00	0.17	410.00
	GLS_1.20	2	8	4-Panel	72.00	0.57	121.00	0.48	146.00
	GLS_1.21	2	8	6-Panel	72.00	0.50	139.00	0.49	142.00
	GLS_1.22	3	8	2-Panel	72.00	0.20	359.00	0.16	449.00
	GLS_1.23	3	8	4-Panel	72.00	0.32	224.00	0.19	387.00
	GLS_1.24	3	8	6-Panel	72.00	0.30	230.00	0.25	277.00
	GLS_1.25	0	16	2-Panel	32.00	4.15	8.00	4.65	7.22
	GLS_1.26	0	16	4-Panel	32.00	4.18	7.95	4.68	7.16
	GLS_1.27	0	16	6-Panel	32.00	4.18	7.92	4.71	7.11
	GLS_1.28	1	16	2-Panel	52.00	1.49	35.00	1.61	33.00
	GLS_1.29	1	16	4-Panel	52.00	2.16	25.00	2.33	23.00
	GLS_1.30	1	16	6-Panel	52.00	2.06	26.00	2.26	24.00
	GLS_1.31	2	16	2-Panel	72.00	0.51	144	0.51	146.00
	GLS_1.32	2	16	4-Panel	72.00	1.34	56	1.37	55.00
	GLS_1.33	2	16	6-Panel	72.00	1.17	63	1.26	58.00
	GLS_1.34	3	16	2-Panel	72.00	0.32	228.00	0.32	229.00
	GLS_1.35	3	16	4-Panel	72.00	0.51	143.00	0.41	178.00
	GLS_1.36	3	16	6-Panel	72.00	0.50	152.00	0.61	120.00

Table 3-7 - Summary of GLS Bending plus Torsion Test Results – Tub #2

	Test Code	Number of Diagonals	Eccen (in)	K-Frame Location	Max Total Load (kips)	Max Top Lat Defl. (in)	Average Lat Stiff (k/in)	Max Twist (deg)	Average Tortional Stiffness (k/deg)
Tub 2	GLS_2.13	0	8	2-Panel	54.00	2.40	22.00	2.57	20.40
	GLS_2.14	0	8	4-Panel	54.00	2.46	21.30	2.59	20.90
	GLS_2.15	0	8	6-Panel	52.00	2.31	21.90	2.47	20.40
	GLS_2.16	1	8	2-Panel	95.00	0.98	98.00	1.08	88.00
	GLS_2.17	1	8	4-Panel	95.00	1.36	71.00	1.32	72.00
	GLS_2.18	1	8	6-Panel	95.00	1.25	76.00	1.37	70.00
	GLS_2.19	2	8	2-Panel	105.00	0.32	329.00	0.41	255.00
	GLS_2.20	2	8	4-Panel	105.00	0.64	161.00	0.66	158.00
	GLS_2.21	2	8	6-Panel	105.00	0.57	181.00	0.64	161.00
	GLS_2.22	3	8	2-Panel	105.00	0.21	505.00	0.27	385.00
	GLS_2.23	3	8	4-Panel	105.00	0.33	319.00	0.33	321.00
	GLS_2.24	3	8	6-Panel	105.00	0.29	357.00	0.38	283.00
	GLS_2.25	0	16	2-Panel	39.00	2.80	13.70	2.99	12.90
	GLS_2.26	0	16	4-Panel	39.00	2.81	13.40	3.04	12.80
	GLS_2.27	0	16	6-Panel	39.00	2.79	13.70	3.04	12.80
	GLS_2.28	1	16	2-Panel	80.00	1.40	58.00	1.57	52.00
	GLS_2.29	1	16	4-Panel	80.00	1.92	42.00	2.02	40.00
	GLS_2.30	1	16	6-Panel	80.00	1.80	45.00	1.99	41.00
	GLS_2.31	2	16	2-Panel	95.00	0.52	180.00	0.65	145.00
	GLS_2.32	2	16	4-Panel	95.00	1.06	89.00	1.07	88.00
	GLS_2.33	2	16	6-Panel	95.00	0.92	100.00	1.09	87.00
	GLS_2.34	3	16	2-Panel	105.00	0.38	277.00	0.50	213.00
	GLS_2.35	3	16	4-Panel	105.00	0.61	173.00	0.59	181.00
	GLS_2.36	3	16	6-Panel	105.00	0.54	196.00	0.69	153.00

Table 3-8 - Summary of GLS Bending plus Torsion Test Results – Tub #3

	Test Code	Number of Diagonals	Eccen (in)	K-Frame Location	Max Total Load (kips)	Max Top Lat Defl. (in)	Average Lat Stiff (k/in)	Max Twist (deg)	Average Tortional Stiffness (k/deg)
Tub 3	GLS_3.13	0	8	2-Panel	24.00	3.57	6.30	3.93	5.80
	GLS_3.14	0	8	4-Panel	24.00	3.58	6.30	3.94	5.80
	GLS_3.15	0	8	6-Panel	24.00	3.55	6.30	3.90	5.80
	GLS_3.16	1	8	2-Panel	80.00	1.89	43.00	2.00	42.00
	GLS_3.17	1	8	4-Panel	70.00	2.28	32.00	2.32	32.00
	GLS_3.18	1	8	6-Panel	70.00	2.13	34.00	2.32	32.00
	GLS_3.19	2	8	2-Panel	85.00	0.37	224.00	0.29	285.00
	GLS_3.20	2	8	4-Panel	85.00	0.83	103.00	0.71	123.00
	GLS_3.21	2	8	6-Panel	85.00	0.73	116.00	0.72	120.00
	GLS_3.22	3	8	2-Panel	85.00	0.24	346.00	0.16	530.00
	GLS_3.23	3	8	4-Panel	85.00	0.34	242.00	0.20	424.00
	GLS_3.24	3	8	6-Panel	85.00	0.37	225.00	0.29	292.00
	GLS_3.25	0	16	2-Panel	17.00	3.62	4.60	4.05	4.10
	GLS_3.26	0	16	4-Panel	17.00	3.67	4.50	4.06	4.10
	GLS_3.27	0	16	6-Panel	17.00	3.77	4.30	4.15	3.90
	GLS_3.28	1	16	2-Panel	60.00	2.30	26.00	2.53	22.00
	GLS_3.29	1	16	4-Panel	60.00	3.06	20.00	3.28	18.70
	GLS_3.30	1	16	6-Panel	60.00	3.00	21.00	3.33	18.50
	GLS_3.31	2	16	2-Panel	80.00	0.68	116.00	0.66	120.00
	GLS_3.32	2	16	4-Panel	80.00	1.19	69.00	1.16	69.00
	GLS_3.33	2	16	6-Panel	80.00	1.05	76.00	1.06	76.00
	GLS_3.34	3	16	2-Panel	80.00	0.22	341.00	0.18	452.00
	GLS_3.35	3	16	4-Panel	80.00	0.29	277.00	0.24	346.00
	GLS_3.36	3	16	6-Panel	80.00	0.28	278.00	0.23	346.00

3.8.2 Impact of Internal K-frame distribution in Stiffness

The main function of internal K-frame bracing systems is to restrain distortion of the cross-section under torsional loads [Helwig and Yura (2012)]. The effectiveness of internal K-frame bracing in straight and horizontally curved tub girders was evaluated by conducting positive bending, and combined bending plus torsion tests on the specimen with different configurations of internal bracing. The response of the specimens with K-frames at every two, four, and six panels was evaluated in this study.

3.8.2.1 Positive Bending Tests (Straight Tub Girder)

Figure 3-38 shows the total vertical load (2P) versus the lateral displacement (δt) of Tub #1 with no top lateral bracing and three different configurations of internal K-frames subjected to concentric vertical loads. The tub girder with internal bracing at every four and six panels show the same response with no major variation in the torsional stiffness. Torsional demands in straight tub girders are small which implies that distortional effects are low. Even though the specimen with K-frames every 2 panels presents higher torsional stiffness for lower load levels, the impact on the response tended to be similar to the aforementioned two cases at higher loads. Elastic lateral torsional buckling was observed during the three tests. The relative insensitivity of girder response to the internal K-frame spacing is similar to previous observations in the case of the Marcy Pedestrian Bridge failure [Yura and Widiano (2005)], as well as the system-buckling mode of narrow I-girder systems [Yura et al. 2008].

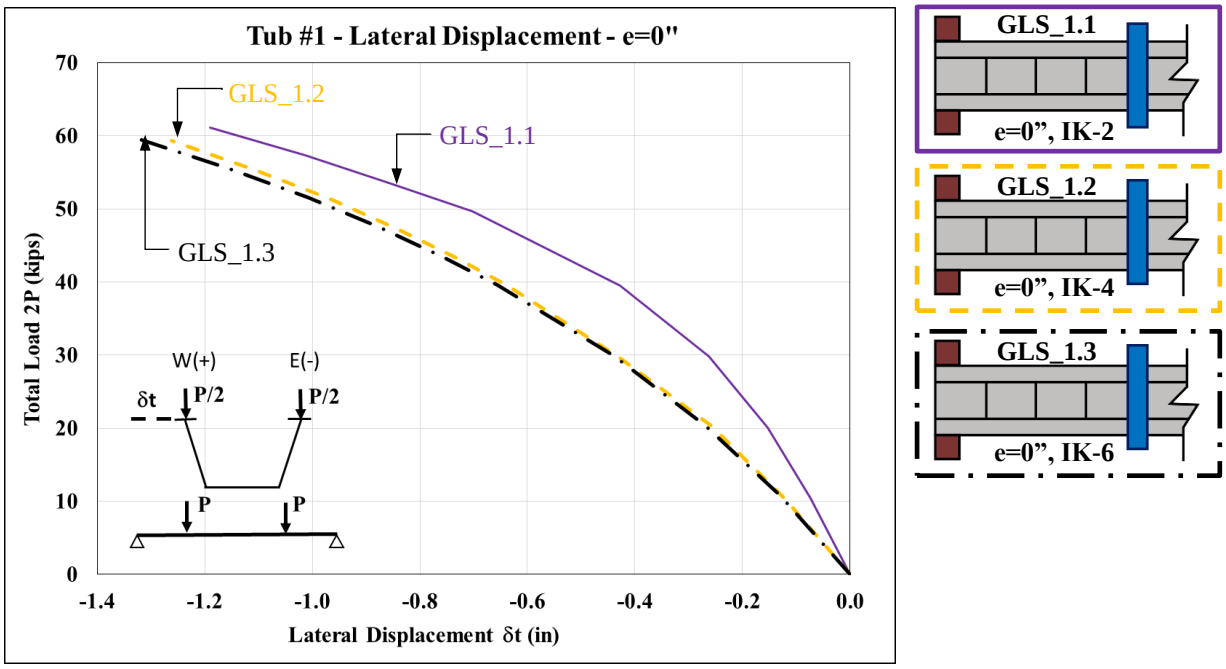

Figure 3-38 - Total Load vs Lateral Displacement - Different K-frame Layout (No TLB) – Tub #1

Figure 3-39 presents the total load (2P) versus the twist angle at midspan (β) of Tub #1 with no top lateral truss bracing and 3 different configurations of internal K-frames. Similar to Figure 3-38, the specimen with K-frames every four and six panels show very similar torsional response. The specimen with internal bracing every two panels showed higher initial torsional stiffness at lower applied loads, but similar torsional stiffness to the other two cases at higher loads. The graphs demonstrated the contribution of internal K-frames to resist LTB is minimal and their arrangement inside of the tub has relatively small impact in the global response of straight tubs.

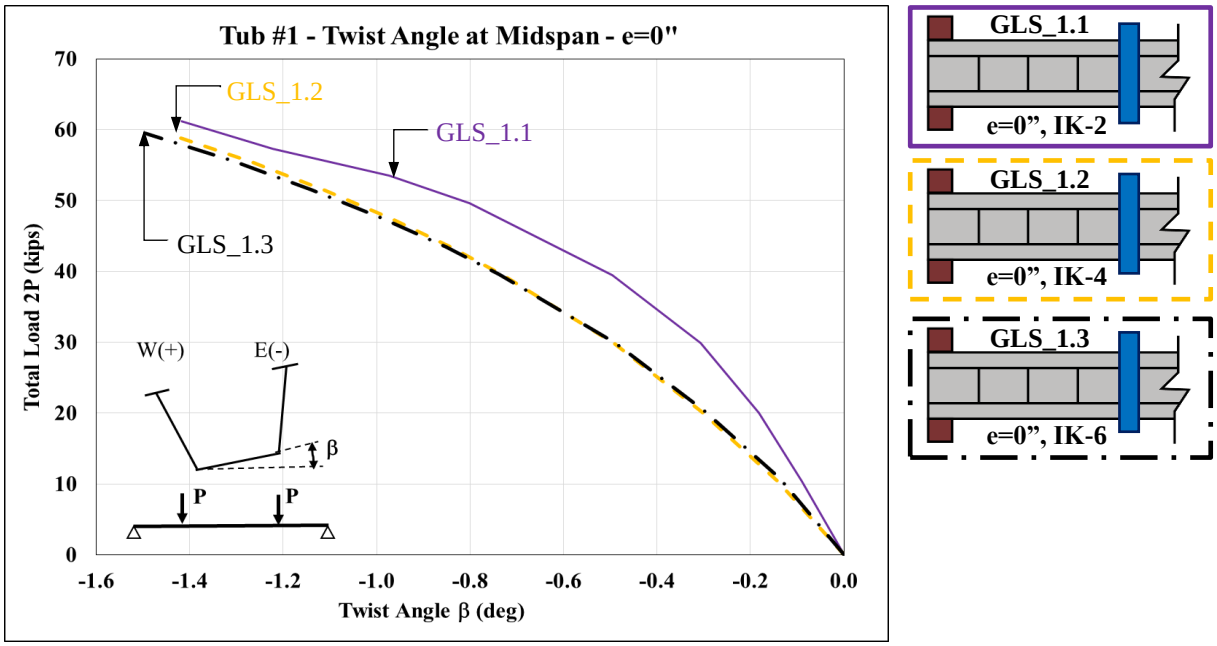

Figure 3-39 - Total Load vs Midspan Twist Angle - Different K-frame Layout (No TLB) – Tub #1

Figure 3-40 and Figure 3-41 show the respective total load (2P) versus the lateral displacement (δt) and twist angle at midspan (β) with partial top lateral bracing (1 diagonal at each end). The difference between the torsional responses of the tub girder with different K-frame arrangements is minimal when one diagonal is included at each end. In Figure 3-40, the response of the specimen with K-frames at every four and six panels is very similar with lateral displacements of 0.22 in and 0.23 in, respectively, when a total load of 71 kips was applied. While the lateral displacement of the girder with internal frames every two panels was 0.18in at the same load level. The layout with K-frames every two panels showed a response approximately 20% stiffer than the other two layouts. In Figure 3-41, the torsional response of the Tub #1 with internal frames every two panels was 10% stiffer than the other two K-frame layouts, which is relatively low in comparison to the contribution of the top lateral bracing. Although the curves are different, the magnitudes of the lateral displacements and girder twists are extremely small. Consequently, the K-frame bracing system becomes less effective in straight steel tub girders under pure positive bending, and there is no major change in its torsional behavior when the number of internal braces is reduced. Similar effect was observed in the other two specimens with partial top lateral bracing, including two and three diagonals at each end.

A summary of results of the positive bending tests with different configurations of internal K-frames is provided in Table 3-4. The corresponding graphs of the different tests are presented in Appendix C.

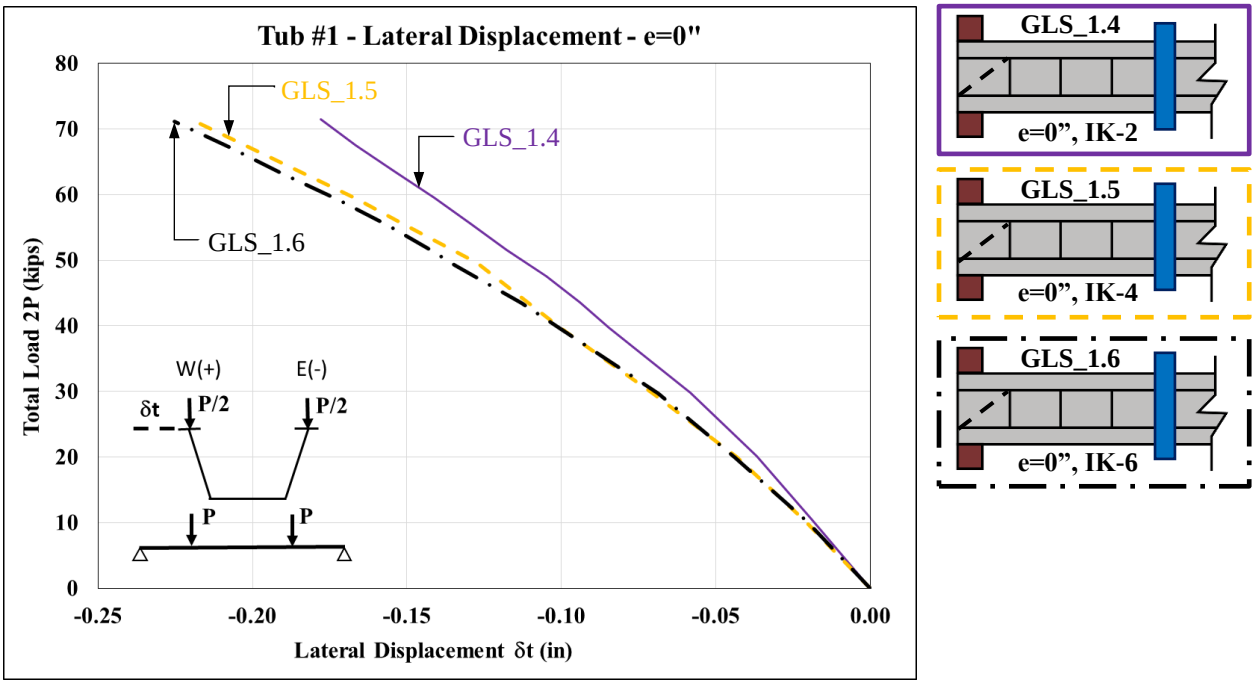

Figure 3-40 - Total Load vs Lateral Displacement – Diff. K-frame Layout (1 Diagonal) - Tub#1

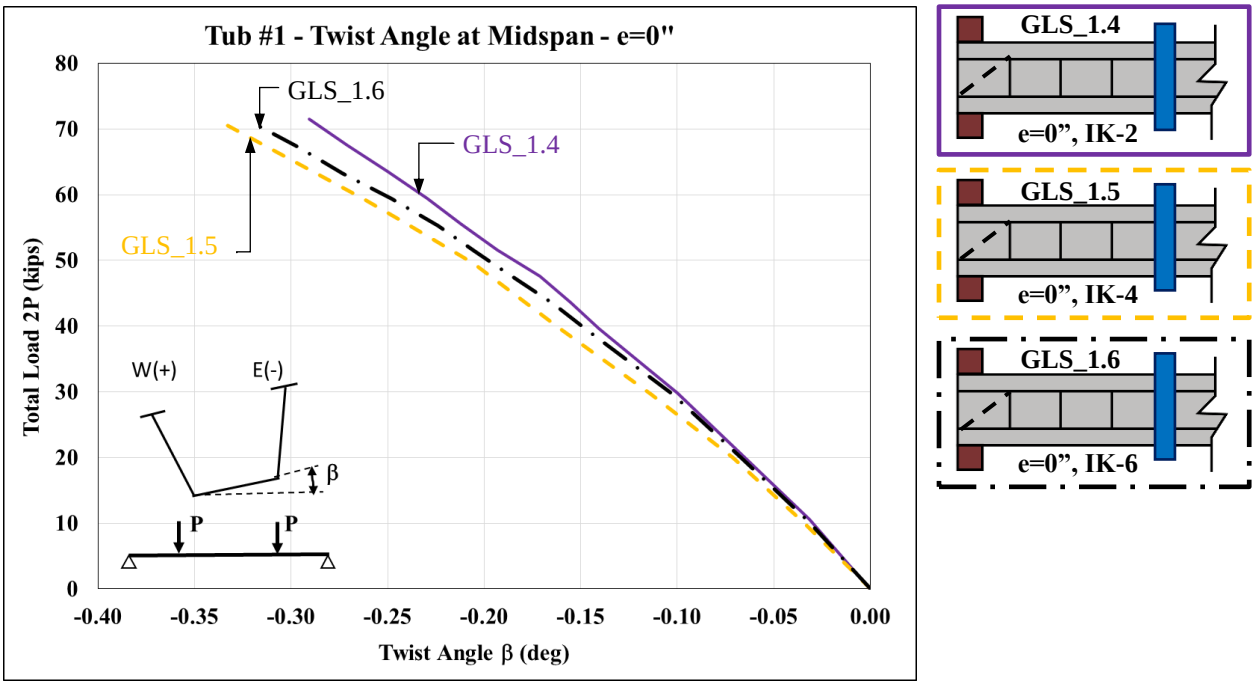

Figure 3-41 - Total Load vs Midspan Twist Angle – Diff. K-frame Layout (1 Diagonal) - Tub#1

3.8.2.2 Bending plus Torsion Tests (Horizontally Curved Tub Girder)

As previously mentioned, the purpose of the internal K-frames is to control cross-sectional distortion produced by torsional demands. Figure 3-42 shows the torsional response of Tub #1

with no top lateral bracing and three different layouts of internal K-frames when vertical loads were applied at 16in. from the shear center.

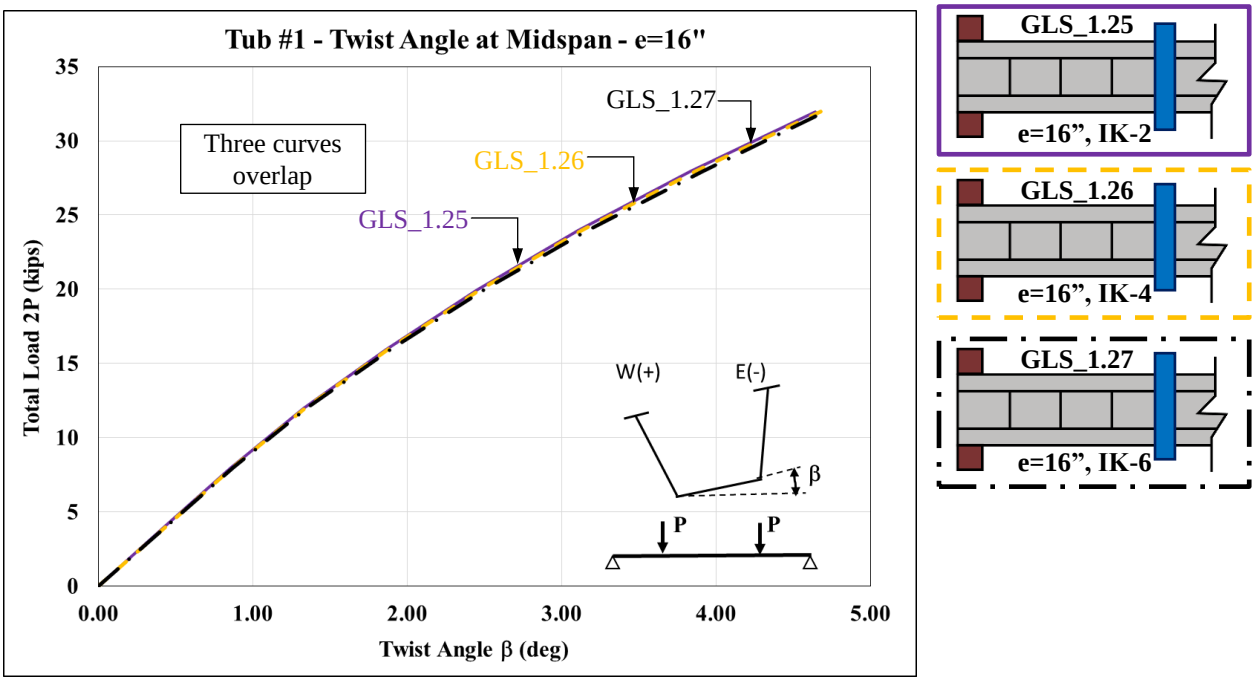

Figure 3-42 - Total Load vs Midspan Twist Angle - Different K-frame Layout (No TLB) – Tub #1

The layout of internal K-frames had no perceivable impact on improving the torsional stiffness of the baseline tub girder when the torsional demands are dominant in the system and no top lateral bracing is provided.

On the other hand, when top lateral bracing is included in the previous system, the torsional response slightly changes. Figure 3-43 shows the torsional response of the Tub #1 with 1 bracing diagonal at each end with different K-frame layouts and loaded with eccentric loading (e=16'). As in in previous graphs, the response is very similar when K-frames are every four and six panels. However, the torsional response improves around 40%, in comparison to the other two configurations, when the internal frames are placed every two panels. In a similar fashion, when two bracing diagonals are placed at each end, the torsional response of the specimen with K-frames at every two panels is around 2.5 times stiffer than the other two configurations with the same two bracing diagonals [see values in Table 3-6]. In these two last cases, K-frames were found near to a bracing diagonal. Hence, interaction between top lateral bracing and internal frames was observed when K-frames are placed in the areas of partial top lateral bracing (or near this area) under high torsional demands. As consequence of this interaction, when K-frames are near top lateral bracing the torsional response of tub girders is stiffer than when the internal frames are placed far from the bracing diagonals. This response is consistent with the findings of the parametric study. During the parametric study described in Chapter 4, it was observed that for tub girders with partial top lateral bracing, the torsional stiffness is affected when K-frames are not placed at the transition zone (or close to it) between braced to unbraced girder. During the experimental tests, a K-frame was closed to the transition zone when K-frames where placed every two panel points. On the other hand, when K-frames were placed every 4 and 6 panel points, the

K-frames were far from this transition zone. Thus, the difference in stiffness between the tests in Figure 3-43 can be attributed to the location of K-frames in the transition zones. Hence, internal K-frame distribution with more efficient layouts can be defined depending on the torsional demand without compromising the stability of the girder.

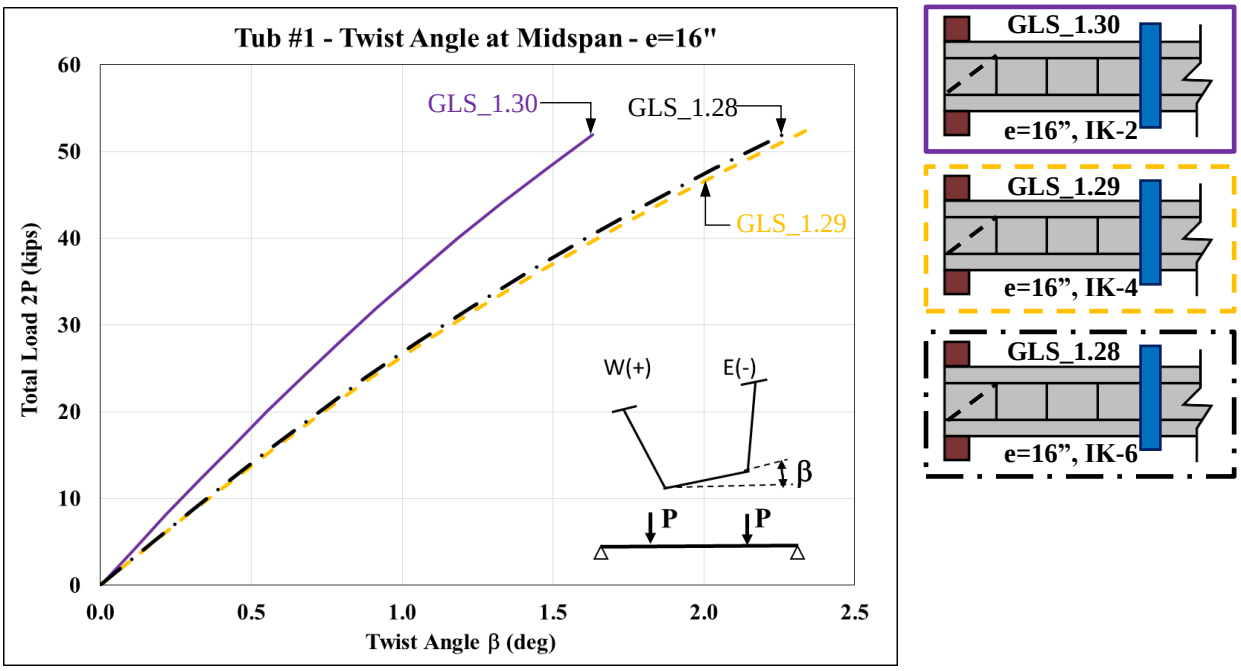

Figure 3-43 - Total Load vs Midspan Twist Angle - Diff. K-frame Layout (1 Diagonal) – Tub #1

3.8.3 Top Lateral Bracing Forces on Straight and Horizontally Curved Tub Girders

As described in the previous section, interaction between top lateral bracing and internal K-frames was observed during the elastic buckling tests. To study this interaction on straight and horizontally curved steel tub girders, the bracing forces obtained in the positive bending, and bending plus torsion tests were analyzed. This section discusses the variation of forces of partial top lateral bracing with different layouts of internal K-frames.

A total load (2P) that represents construction loads was defined to compare forces in the top lateral bracing members. Assuming 0.8 kip/ft. as a uniform construction load that represents the weight of a concrete deck, stay-in-place forms, and construction loads, a maximum moment of 706 k-ft. would be expected during construction. In order to produce the same maximum moment, a load of 35 kips on each gravity load simulator (P) is required. Thus, a total load (2P) of 70 kips is the load at which the bracing forces were compared.

To study the load distribution on partial top lateral bracing on straight and horizontally curved steel tub girders, the specimens were loaded under bending and torsional demands. The bracing force distribution observed under these two loading conditions is described in this section. Figure 3-44 shows the labels of the top lateral bracing diagonals used in the plots presented herein. Each tub girder contains 12 panels, which are defined as the area between adjacent struts. Truss diagonals S1, S2, S3, N3, N2, and N1 are located in panels 1, 2, 3, 10, 11, and 12, respectively.

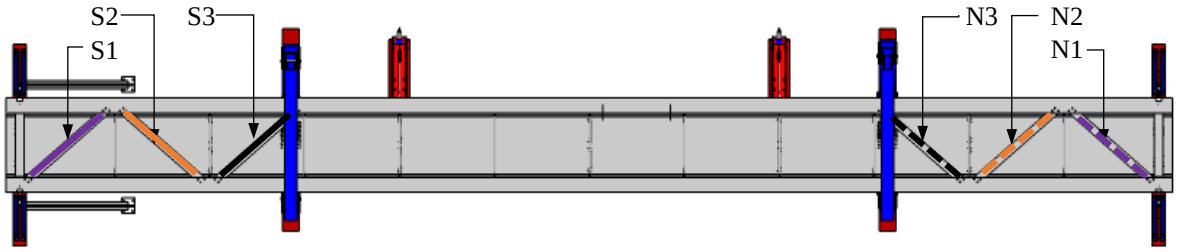

Figure 3-44 - Top Lateral Truss Labels - Plan View (N and S referring North and South supports)

3.8.3.1 Positive Bending Tests (Straight Tub Girder)

The gravity load simulators were used to apply vertical concentric loads near the quarter points of the girders to evaluate the load distribution on partial top lateral bracing under positive bending demands when different layouts of internal bracing (K-frames) were installed. Two gravity load simulators were used to apply vertical concentric loads (P) on the specimen. The forces for partial top lateral bracing were obtained for the three different configurations of partial horizontal truss (with one, two and three diagonals on each end).

Figure 3-45 shows the total vertical load applied (2P) versus the axial force on each truss diagonal when the partial lateral bracing truss is formed by 3 diagonals on each end and when K-frames are installed at every 2 panel points in Tub #1 (GLS_1.10). Additionally, the total load (2P) at which the bracing forces are compared is marked with a dashed horizontal line at 2P=70 kips on Figure 3-45. Considering the fact that the Tub #1 had an initial twist towards the East of the tub, the bracing members N1, N3, S1, and S3 sustained compression forces, while the diagonals N2 and S2 (framed in the opposite direction) experienced tensile forces. Although torsional demands were not directly imposed, axial loads were observed in the horizontal truss due to the presence of an initial imperfection in the girders as well as some vertical bending that led to compression in the top flange. The distribution of the braces forces along the length of the girder show larger bracing forces in the diagonals close to mid-span implying that vertical bending demands are dominant. The horizontal truss is connected to the top flange, which is a region of high bending stresses. Thus, the top lateral diagonals experience the same axial strains as the tub girder because of compatibility, as described by Helwig and Fan (1999). Similar general force distributions along the length of the girders was observed when the K-frame layout was modified, even though variations in the internal forces distribution were observed.

Figure 3-46 shows the top lateral bracing forces with the three different K-frame layouts under study (GLS_1.10, GLS_1.11, and GLS_1.12). As previously mentioned, the larger bracing forces were observed closer to mid-span where the bending strains are larger. When K-frames were placed every 2 panels, the bracing forces in the panels 3 and 10 were the largest. However, after changing the K-frame configuration, redistribution of forces was observed. Diagonal forces in panels 1 and 12 (next the supports) increased. The bracing forces in the diagonals of panels 2 and 11 went up about 150 to 400%; however, these forces were very small relative to the other bracing forces. On the other hand, bracing forces in panels 3 and 10 went down about 30%. When the internal bracing layout was changed from K-frames every four panels to every six panels, no significant change in top lateral bracing forces was observed. This lack of variation on bracing forces can be produced because no K-frame is located in the region of partial top lateral bracing when K-frames were placed every four and six panels. On the other hand, when the internal frames were placed every two panels, a K-frame was placed between diagonals S2 and S3, and between

N2 and N3, what created a redistribution of forces from the top lateral bracing diagonals to the internal K-frames.

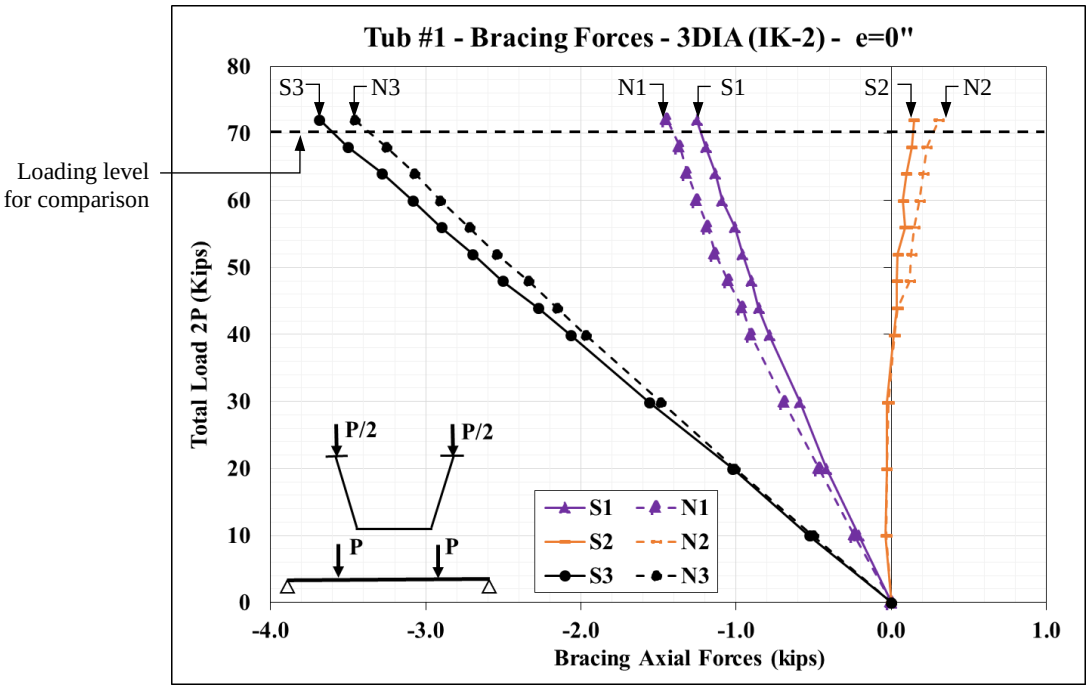

Figure 3-45 – Top Lateral Diagonal Bracing Forces due to Vertical Bending - Tub #1

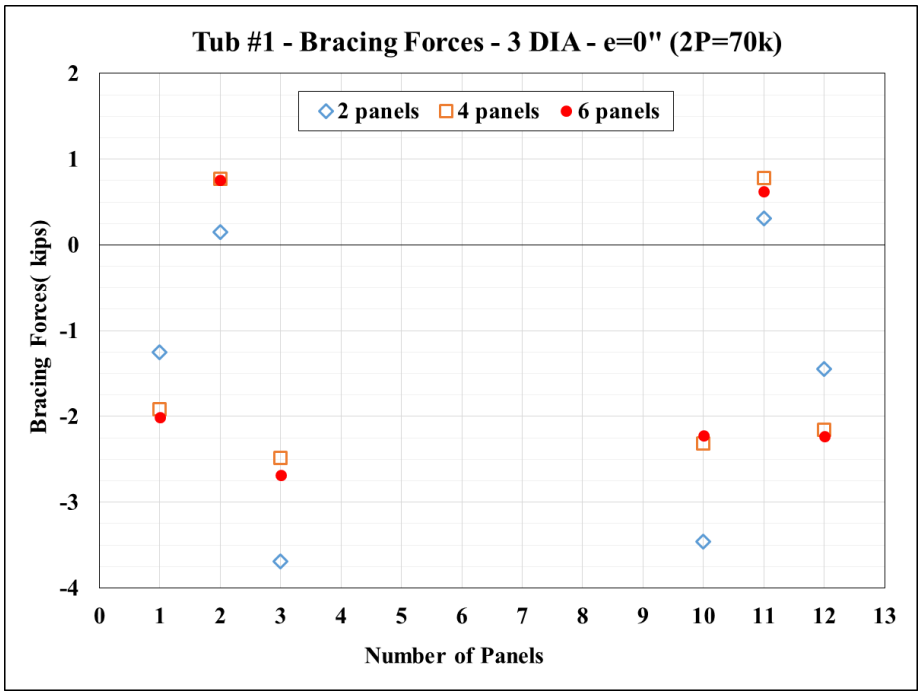

Figure 3-46 - Top Lateral Diagonal Forces for Different K-frame Layouts (3 Diagonals) - Tub #1

Figure 3-47 shows the strut forces for the Tub #1 with 3 diagonals on each end and different configuration of internal K-frames. When a panel has two equal symbols (i.e. 2 diamonds), a K-frame was located in that point and two strut forces are shown. Indeed, a strut, divided in two by the K-frame diagonals, sustains two different forces. Generally, the axial forces in the struts are small and without much variation, except in panels 2, 3, 9 and 10. The large forces in panels 3 and 9 can be attributed to localized effects produced by the loading system. The gravity load simulators were located at those panel points. The struts on panel points 2 and 10 were located between diagonals S2 and S3, and between N2 and N3, respectively. When K-frames were placed every two panels the forces the strut in panel points 2 and 10 were larger than with the other two configurations. The strut and diagonals of the K-frames between on panels 2 and 10 sustained loads of about 2.4 kips (tension) and 1.0 kip (tension and compression), respectively. When K-frames were placed every 4 and 6 panels, the previously mentioned K-frame was not present and only the horizontal strut was left (K-frame diagonals were removed). The force in that strut was about 1.15 kips (tension) which is about 50% the force that the strut sustained when K-frames were placed every 2 panels. In the absence of the K-frame diagonals, the forces are absorbed by the stiffer members (WTs) which produced an increment in the load sustained by the top lateral diagonals in panels 1, 2, 11, and 12. Hence, the K-frames located in the region of partial top lateral bracing produce interaction between the bracing forces.

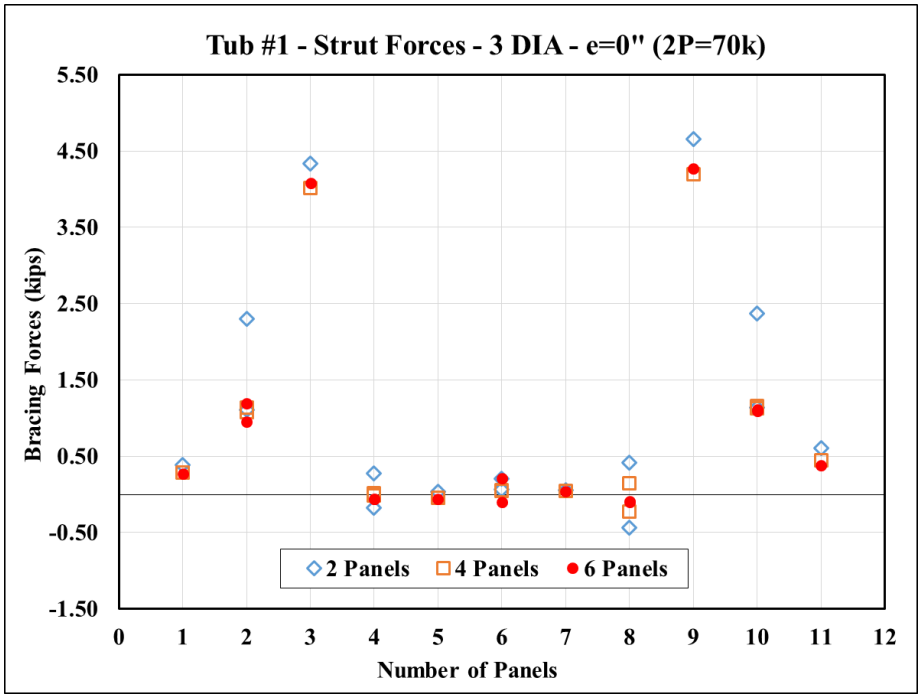

Figure 3-47 - Strut Forces for Different K-frame Layouts (3 Diagonals) - Tub #1

Although there was a redistribution of forces in the bracing systems when the K-frame layout was modified, the general response of the tub girders was relatively similar. The torsional stiffness of the girder was not highly affected when modifying the internal bracing layout. The twist angles at mid-span of the baseline girder when K-frames were placed at every 2, 4, and 6 panels were 0.05, 0.06, and 0.05 degrees, respectively.

Additionally, the change in K-frame layout from every four to every six panels did not produce significant changes in top lateral bracing forces. This effect shows that the top lateral truss can interact with the K-frames only if the internal braces are located in the regions where partial top lateral bracing is placed; specifically, between panels with top lateral diagonals.

Figure 3-48 shows the top lateral bracing forces when 2 top lateral diagonals were placed on each end with the 3 different K-frame layouts. Clearly, this arrangement of top lateral bracing members was less sensitive to force redistribution than when 3 diagonals were placed. The variation of axial forces in panels 1 and 12 were between 5 to 11%, and the forces in panels 2 and 11 varied about 6 to 18%, which is significantly less than what was observed in Figure 3-46. With no K-frame inside the region of partial top lateral bracing, the interaction between these two bracing systems is smaller. When 1 truss diagonal was placed at each end, the axial forces varied about 1 to 3%.

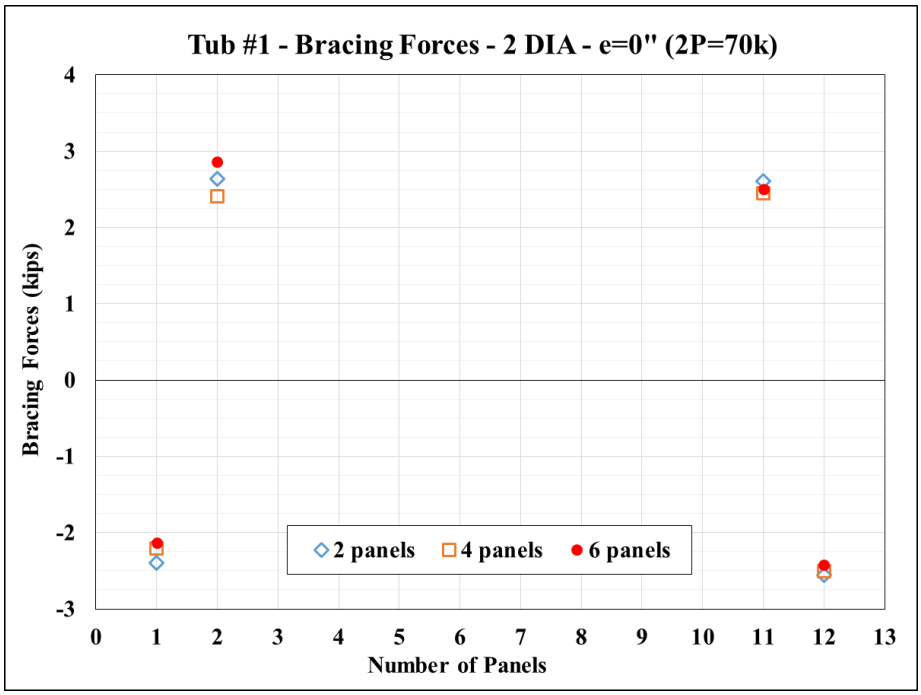

Figure 3-48 - Top Lateral Diagonal Forces for Different K-frame Layouts (2 Diagonals) - Tub #1

3.8.3.2 Bending plus Torsion Tests (Horizontally Curved Tub Girder)

Figure 3-49 shows the total vertical load applied (2P) versus the axial force on each truss diagonal when the partial lateral bracing truss is formed by 3 diagonals on each end and when K-frames are installed every 2 panel points in the Tub #1. The bracing forces were produced when eccentric vertical loads were applied at 16 in. from the shear center. The eccentric vertical loads were applied so that torsional moments towards the west of the tub were applied; in fact, opposite to the initial twist of the girder. Based on that, the bracing members N1, N3, S1, and S3 sustained tensile axial forces while the diagonals N2 and S2 (framed in the opposite direction) experienced compression axial demands. The distribution of the braces forces along the length of the girder showed larger bracing forces in the diagonals closed to the supports while the diagonals close to mid-span showed lower axial forces. This distribution of axial forces implies that the torsional

demands are dominant instead of the vertical bending. The larger torsional demands are expected to occur at the supports where the warping deformations are expected to be larger. Once the top lateral diagonals are engaged, they restrain the shear deformations associated with warping, and as a result, the truss diagonals near the girder ends experienced higher axial forces than the ones near mid-span.

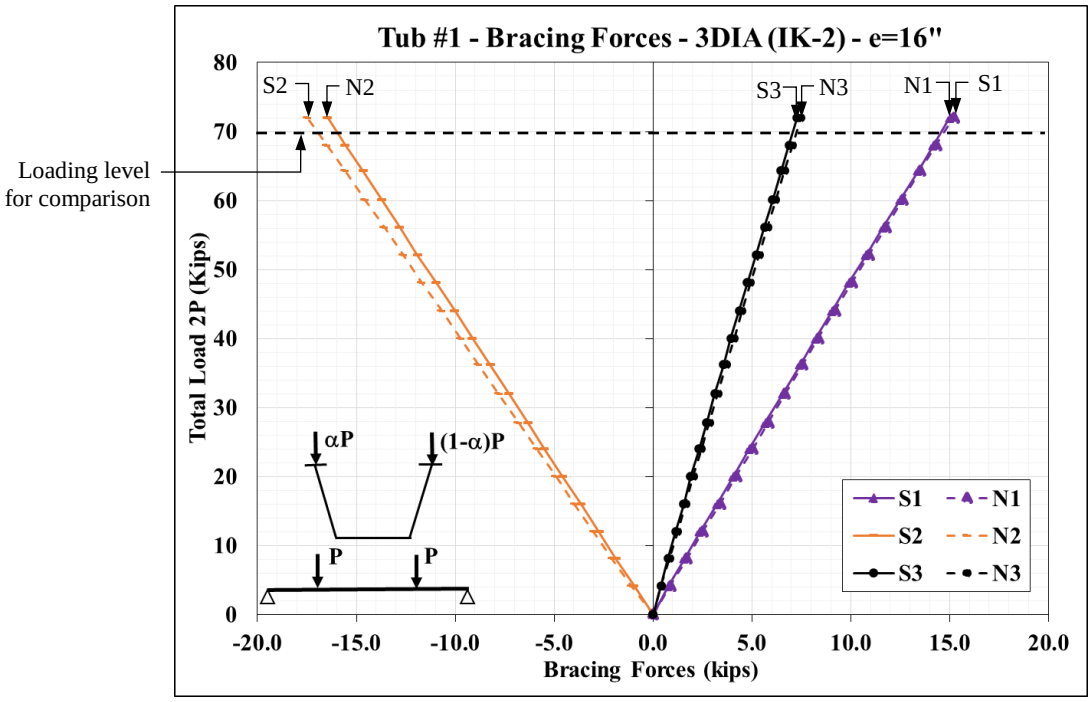

Figure 3-49 - Top Lateral Diagonal Bracing Forces due to Bending plus Torsion - Tub #1

Figure 3-50 shows the top lateral bracing forces with the three different K-frame layouts under study (GLS_1.34, GLS_1.35, and GLS_1.36). As previously, mentioned, larger bracing forces were observed close to the supports where the larger warping demands occur. When K-frames were placed every 2 panels, the bracing forces in panels 1 and 12 (tension), and 2 and 11 (compression) were very similar; while the forces in panels 3 and 10 (tension) were about 50% of the forces in panels 1 and 12. However, after changing the K-frame configuration, redistribution of forces was observed. Diagonal forces in panels 1, 2, 11 and 12 dropped about 10 to 20%. Correspondingly, bracing forces in panels 3 and 10 went up about 50%. When the internal bracing layout was changed from K-frames every four panels to every six panels a maximum variation of about 5% in the truss forces was observed.

The general response of the tub girders showed minor variations. The twist angles at mid-span of the baseline girder when K-frames were placed at every two, four, and six panels were 0.32, 0.41, and 0.62 degrees, respectively. As a result, the forces in the bracing members are comparable.

Clearly, the interaction between the top lateral bracing truss and the internal K-frames is still present when torsional demands are dominant. When K-frames were placed every two panels, the internal K-frames located between diagonals S2 and S3, and panels N2 and N3 showed higher axial forces than with the other K-frame distributions, as shown in Figure 3-51. The strut and diagonals of the aforementioned K-frame developed forces of about 6.0 kips (tension) and 4.60

kip (tension and compression), respectively. When K-frames were placed every four and six panels, the previously mentioned K-frame was not present and only the horizontal strut was left (K-frame diagonals were removed). The force in that strut was about 1.50 kips (tension) which is about 25% of the force that the strut sustained when K-frames were placed every two panels.

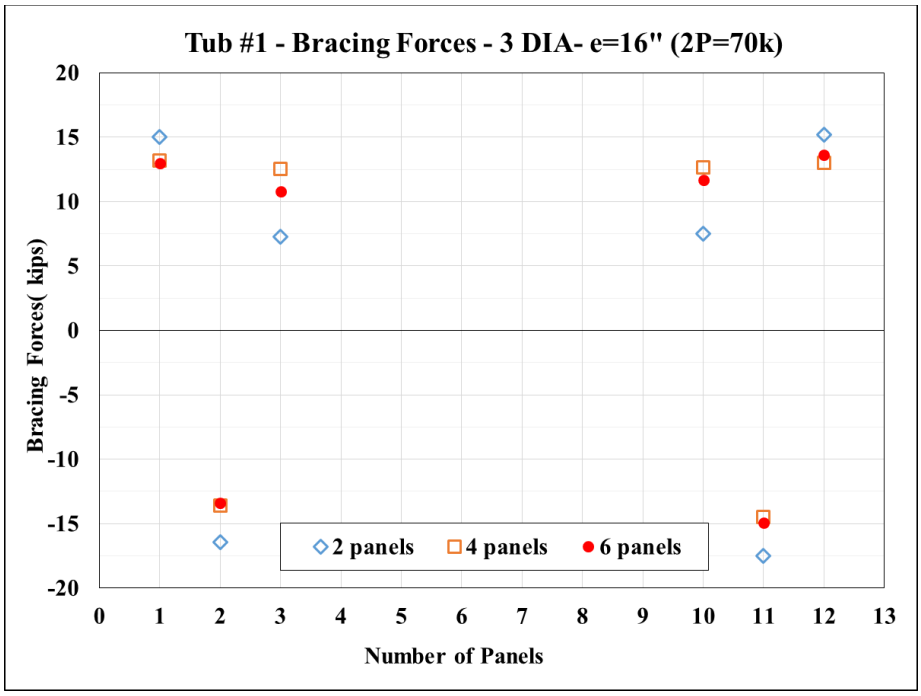

Figure 3-50 - Top Lateral Diagonal Forces for Different K-frame Layouts (3 Diagonals) - Tub #1

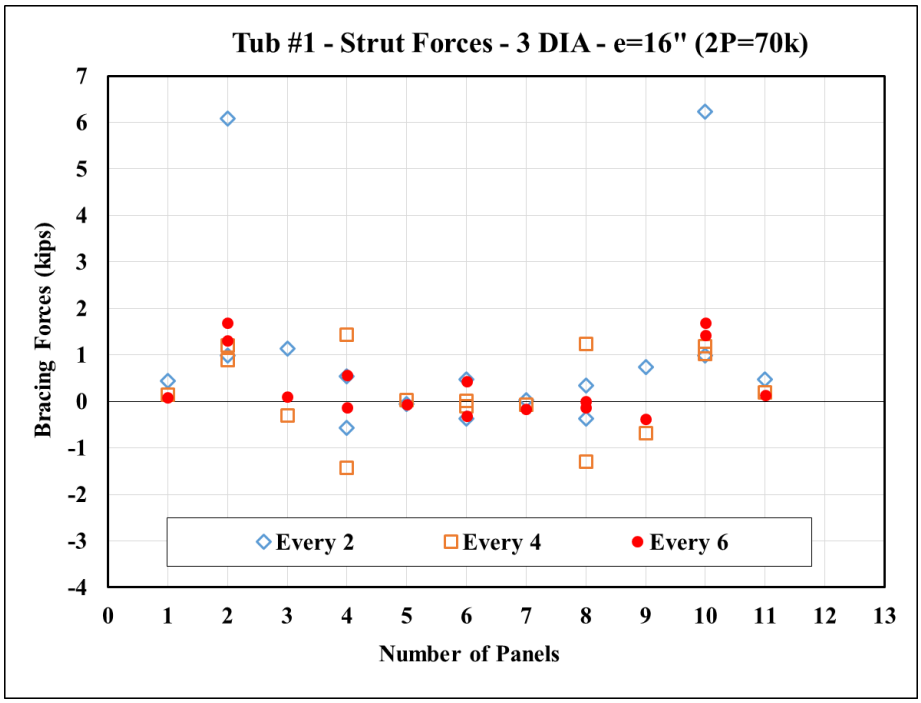

Figure 3-51 - Strut Forces for Different K-frame Layouts (3 Diagonals) - Tub #1

Figure 3-52 shows the top lateral bracing forces when 2 top lateral diagonals were placed at each girder end with the 3 different K-frame layouts for the eccentric loading case. Compared to the case where 3 diagonals were placed, this layout of top lateral bracing diagonals experienced less force redistribution. The variation of axial forces in panels 1 and 12 were about 21%, and the forces in panels 2 and 11 varied about 3 – 5%, which is significantly less than what was observed in Figure 3-51. With no K-frame inside the region of partial top lateral bracing, the interaction between these two bracing systems is smaller.

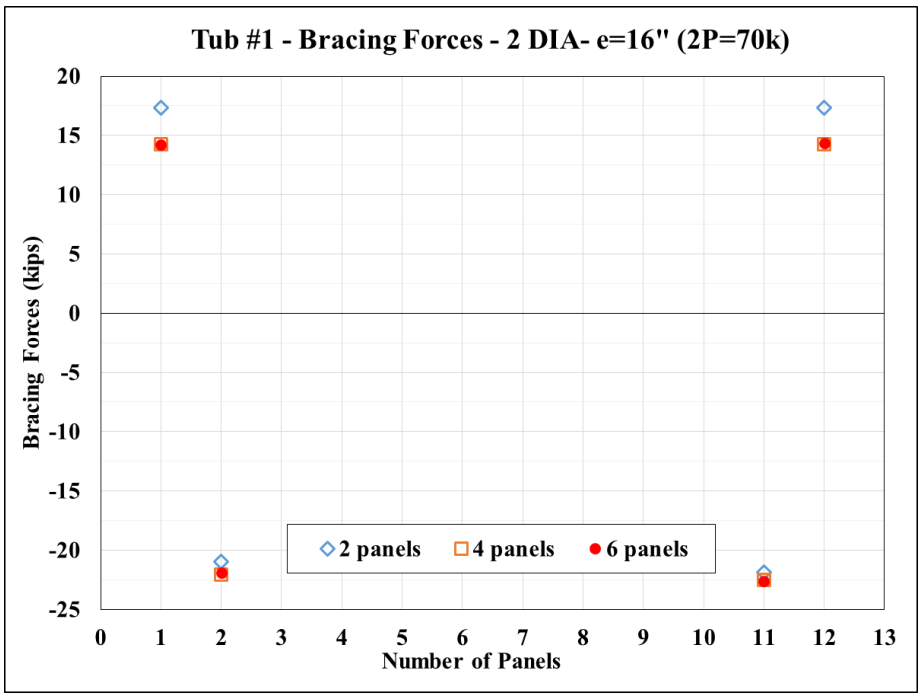

Figure 3-52 - Top Lateral Diagonal Forces for Different K-frame Layouts (2 Diagonals) - Tub #1

Although the results presented herein were for Tub #1 (baseline tub girder), similar trends in response was observed for the other two specimens under concentric and eccentric loading, and the corresponding plots are presented in Appendix C.

3.8.4 Local Effects of Offsetting Top Flange

Another aspect of the study was to understand the consequences of modifying cross-sectional details such as offseting the top flange. The main concern in offseting the top flange was to increase the stress due to lateral bending of top flanges and potential local buckling of the top flanges. In order to asses the variation of stresses in the top flanges of Tub #2, foil strain gauges were placed at the top flange tips in the middle of panel 7, as shown in Figure 3-53. The strain gauges were placed in top and bottom of the top flanges in order to obtain axial strain decoupled from bending effects.

Besides instrumanetion, local initial imperfections of the top flanges between struts were measured in order to record the initial shape of the plates. Figure 3-54 shows the local initial imperfections in panel 7, which shown a maximum out-of-straightness/flatness around b/160. The initial imperfection of the other panels is presented in Appedix B.

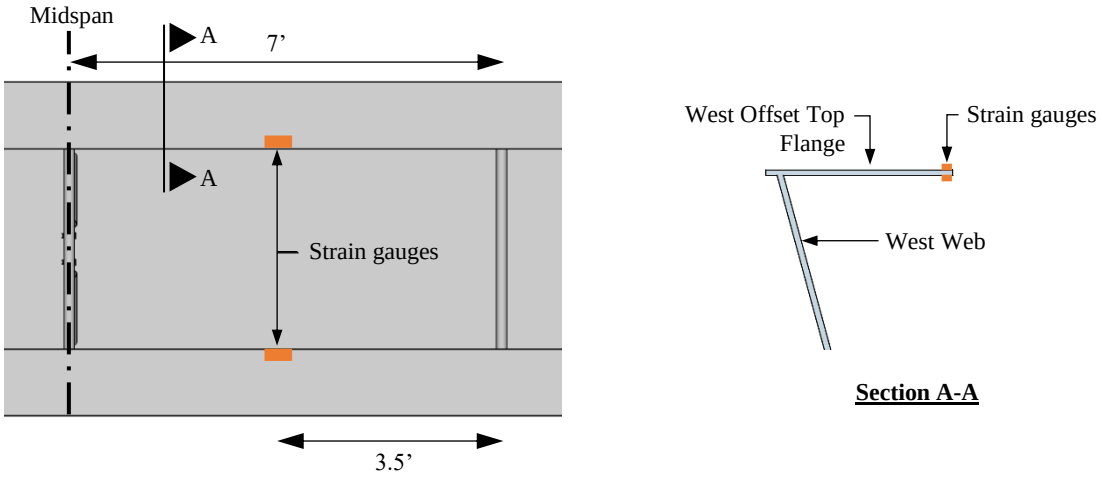

Figure 3-53 - Panel 7 - Strain Gauges Location

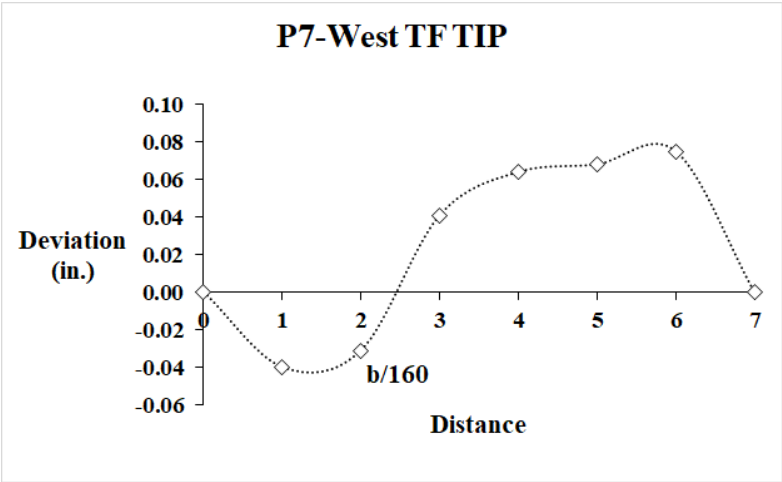

Figure 3-54 - Local Initial Imperfections of West Top Flange - Panel 7 on Tub #2

Regarding the offset top flange girder, plastic buckling of one of the 13 in-wide top flanges occurred during testing as shown in Figure 3-55 and Figure 3-56. The failure occurred after elastic LTB of the girder was observed during the tests. The girder with no top lateral bracing was loaded concentrically with the two GLS. At the instance of local buckling, the compressive stresses in the area of buckling were approximately 35 ksi (70% of yielding strength).

At the final loading step of the GLS_2.2 (no diagonals on each end with K-frames every two panels); local buckling of the west top flange was reached which induced inelastic deformations on Tub #2. Figure 3-55 and Figure 3-56 shows the inelastically deformed west top flange in panel 7.

The deformed shape was measured right after the buckling using taut wire and a caliper. The profile shape of the buckled plate is shown in Figure 3-57. The shape of the top flange panel after the buckling was very similar to the shape of the initial imperfections, what suggests that the initial imperfections had an impact in the second-order effects induced in plates.

Figure 3-55 - Local Buckling of West Top Flange of Tub #2 at Midspan – View 1

Figure 3-56 - Local Buckling of West Top Flange of Tub #2 at Midspan – View 2

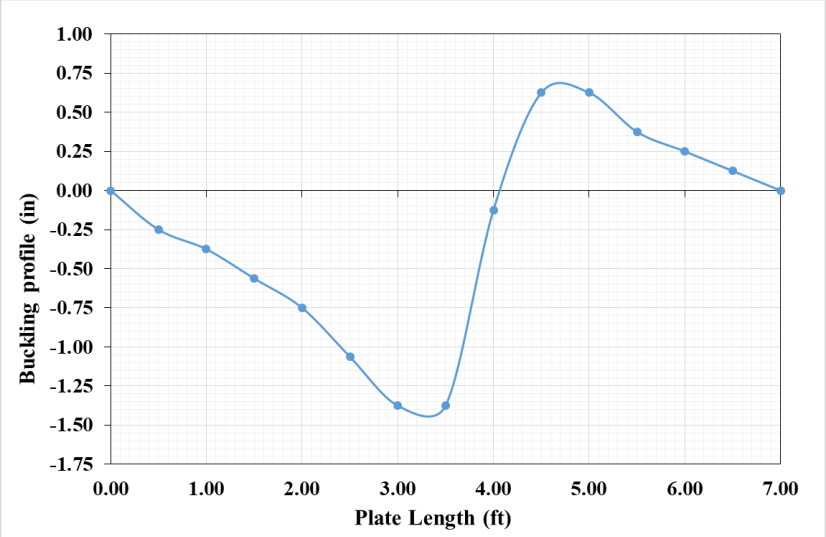

Figure 3-57 - Profile Shape of Buckled Top Flange - Tub #2

In addition to measure the profile shape of the buckled plate, the strains in the plate were analyzed to understand the response of the plate under vertical and lateral bending strains. Figure 3-58 shows the load-lateral displacement response of Tub #2 during the GLS_2.2 test. Tub #2 had

significant lateral displacement when the in elastic buckling happened, what implies that the stresses due to lateral bending of top flanges were likely significant as well.

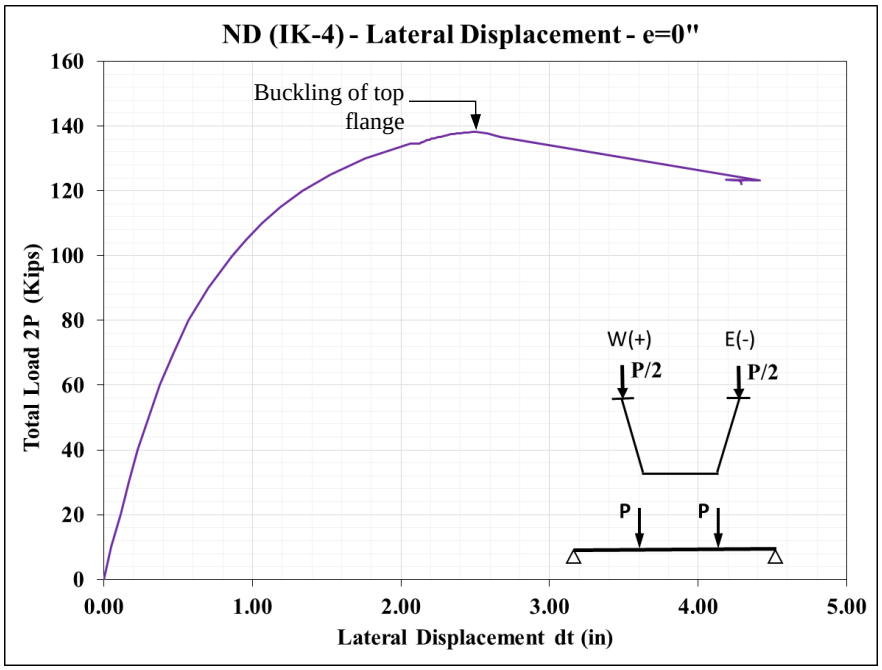

Figure 3-58 - Total Load vs Lateral Displacement - GLS_2.2 - Tub #2

Figure 3-59 shows the strain data collected on the top and bottom of the buckled plate in the location shown in Figure 3-53. The strain gauge location can be seen in Figure 3-55 as well. From the graph below, it can be seen that the strains in the top and bottom of the plate started to diverge from the very beginning, and this divergence became more noticeable after 80 kips of total loading. This behavior suggests that the lateral bending strains were significant in the top flange. Buckling occurred at about 140 kips of total load on the girder, when this divergence became very large and produced the inelastic buckling of the plate.

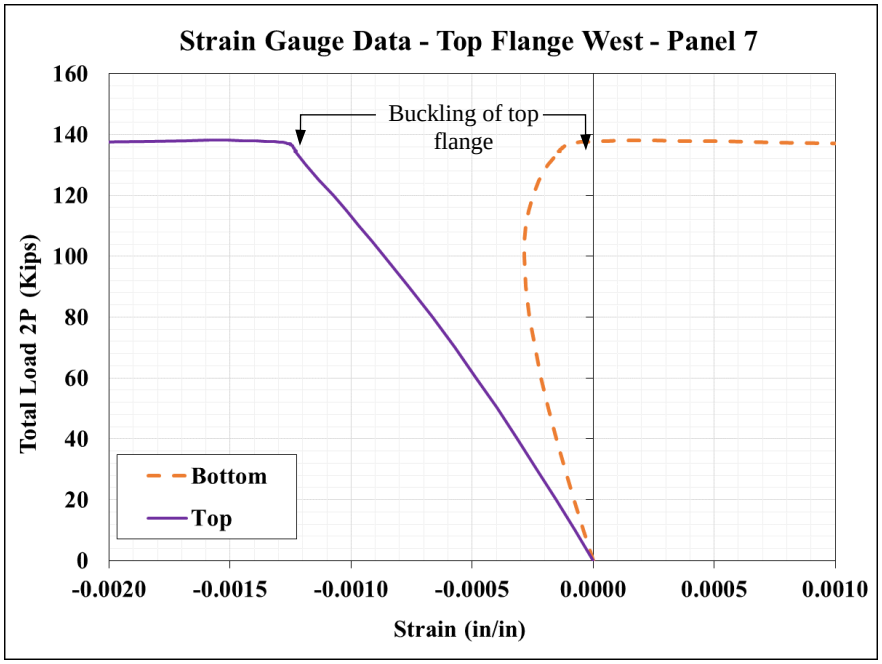

Figure 3-59 - Strain Gauge Data of West Top Flange - Panel 7 - Tub #2

Clearly, the compressive stresses in the top flange due to its lateral bending were higher than the stresses observed in the baseline tub girder. This increment of stresses might have been produced due to the high level of slenderness of the top flange as well as the plate initial imperfections. The change in the geometry of this girder made the system more susceptible to local buckling effects; however, the slenderness of the flange plate was extreme compared to what would be utilized in bridge applications. Recall that the flange slenderness was almost 21 compared to the AASHTO limit of 12. Thus, appropriate design methodologies have to be defined to control any type of weakness in the tub girders when the proposed details are going to be used

3.9 Summary of Experimental Results

This chapter focused on the experiments that were conducted in the laboratory to evaluate improved details for steel tub girders. A number of conclusions can be drawn from the experimental program:

- Experimental tests showed that the top flange lateral bracing systems are more effective in the region near to the supports of straight girders where shear deformations are at the maximum. The LTB capacity of the straight tub girders was significantly improved by adding one top truss diagonal at each support. The inclusion of subsequent diagonals resulted in significantly smaller increments in the performance as the distance to the diagonals increased. Thus, top lateral diagonals located near mid-span add little to no benefit in the LTB behavior and likely at increasing the torsional stiffness of the girder.
- Web slope does not really affect the torsional stiffness of steel tub girders. It was observed in the tests that steel tub girders with different web slopes (4H:1V and 2.5H:1V) had similar torsional response when enough partial top lateral bracing was provided (3 diagonals on each end for both).

- Internal K-frames provide minimal contribution to resist LTB in straight tub girders in comparison to top lateral bracing. Due to lower torsional demands, internal K-frames are less effective along straight tub girders. Thus, the number of K-frames, and their distribution along the straight girder, did not shown a significant impact in the torsional response of the girder.
- Experimental tests showed that the partial top lateral bracing systems interact with internal K-frames when a tub girder is subjected to either vertical bending or torsional demands. Modifications in the configuration of internal K-frames caused changes in the axial forces of the horizontal truss members. The variation in forces measured in the diagonals and struts of the truss were as high as 50% to 70%, depending on the level and the type of demand.
- When K-frames were not installed in the zones of partial top lateral bracing, rearranging the internal bracing layout did not produce significant variation in the diagonal forces of the horizontal truss.
- Offsetting the top flange makes the plate susceptible to higher lateral bending stresses and local effects. High slenderness, initial imperfections, and absence of top lateral bracing can result in high compressive stresses in the top flanges.

The results described herein are specific to the parameters tested in the laboratory. The comparison of these results with analytical finite element models are presented in Chapter 4. The purpose of analytical models was to extend the work done in the laboratory to study deeper the effect of the proposed details considering different parameters (i.e. different span, curvature, etc.).

Chapter 4. Finite Element Modeling and Parametric Studies

4.1 Introduction

This chapter describes the development and validation of finite element (FE) models of steel tub girder systems. Three-dimensional FE models were created using the finite element analysis (FEA) program Abaqus/CAE 6.14. Experimental data collected from large-scale tests are used to validate the models as a function of the various bracing layouts as well as different cross-sectional geometries. Utilizing the FE models with validated assumptions, parametric FEA studies are carried out on typical steel tub girder designs under various loading conditions. The parametric studies focused on developing an improved understanding of the impact of various design details on the fundamental behavior of tub girder systems. The studies primarily investigated non-composite girders to evaluate their behavior during construction, although some of the studies investigated the behavior of the completed bridge system under live load. Key findings from the parametric studies are summarized at the end of this chapter.

4.2 Modeling of Steel Tub Girder Systems in ABAQUS/CAE

As shown in Figure 4-1, three-dimensional FE models were developed to study steel tub girder bridges with proposed details under construction and live load conditions. Both curved and straight girders were studied. During construction, the steel tub girder section is a quasi-closed section with the top lateral truss connecting the top flanges to enhance torsional stiffness and internal K-frames maintaining the shape of the cross section. For modeling purposes, the structural components of the quasi-closed tub girder can be divided into two groups: plate components (top flanges, webs, bottom flange, stiffeners and connection plates, and solid diaphragm) and bracing components (top lateral braces and internal K-frames). The plate components are modeled with shell elements while the bracing members are modeled with beam elements.

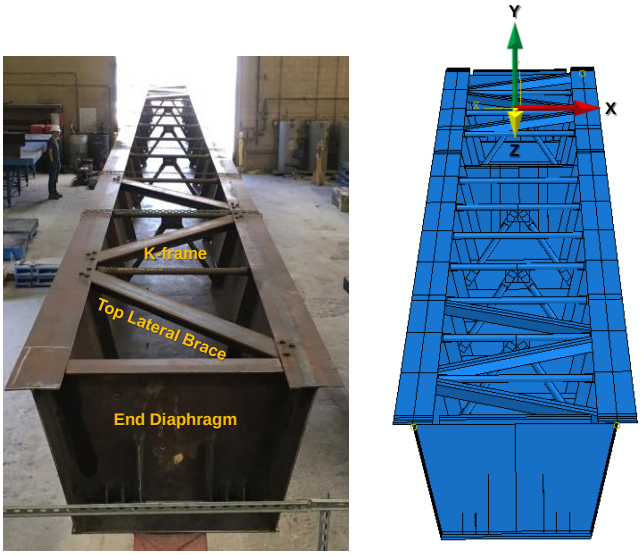

Figure 4-1 Baseline Tub Girder Specimen and 3D FE Model

The plate components of the steel tub girders were modeled with shell elements. The shell element used in this study is a 4-node quadrilateral shell element [Figure 4-2] with reduced integration scheme, designated as S4R in the ABAQUS element library. This type of shell element can model both in-plane membrane deformations and out-of-plane bending. Each node has six degrees of freedom. The S4R element is a general-purpose shell element that can provide accurate solutions for both thin shell and thick shell problems. The required input for the shell element consists of the thickness and material properties. Other important definitions for shell elements are local directions and the positive normal. Although these definitions are not required and have default settings in the program, they can affect the reporting of stress and strain as well as the direction of applied traction load.

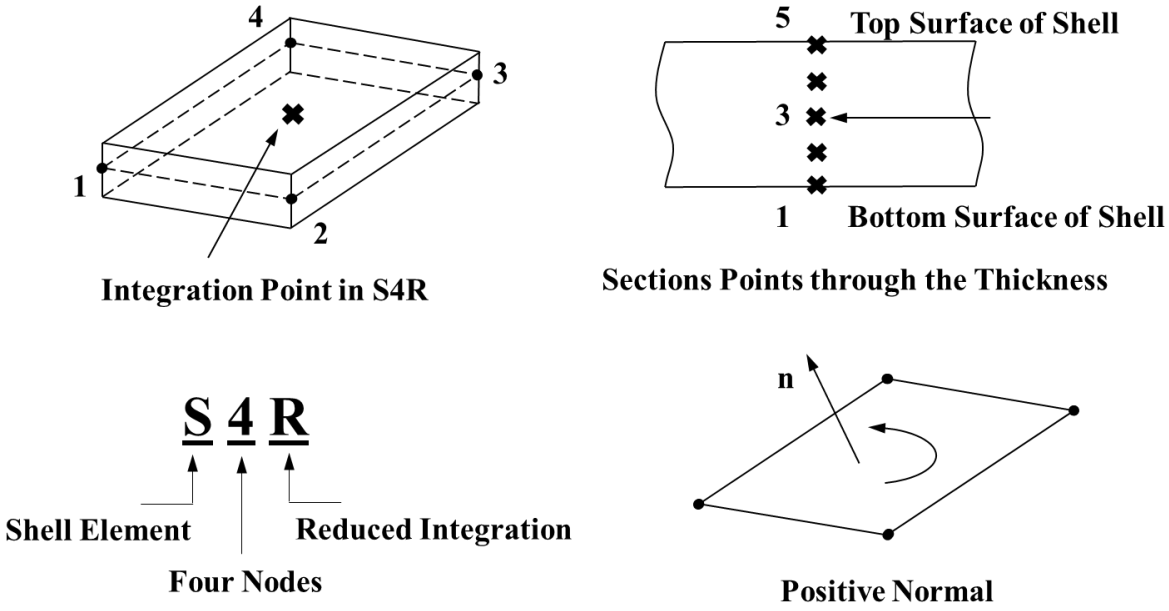

Figure 4-2 Shell Element S4R Used in FE Models

Three-dimensional beam elements were used to model the bracing members of the tub girder systems, including top lateral braces (WT Shapes) and internal K-frames (Angles in typical engineering practice or pipes in the test specimens). The beam element used in this study is a 2-node element which can model tension, compression, torsion and bending behavior as shown in Figure 4-3, designated as B31 in the ABAQUS element library. Each node of the element has six degrees of freedom. Generalized open beam section profiles were used to define the cross section of the beam elements to account for the warping effect in thin-walled beams and the secondary effect caused by connection eccentricity. The required sectional properties include moments of inertia, cross-sectional area, and torsional properties. The offset between the shear center and the center of gravity with respect to the mid surface of the shell elements are also required input for the cross-sectional definition.

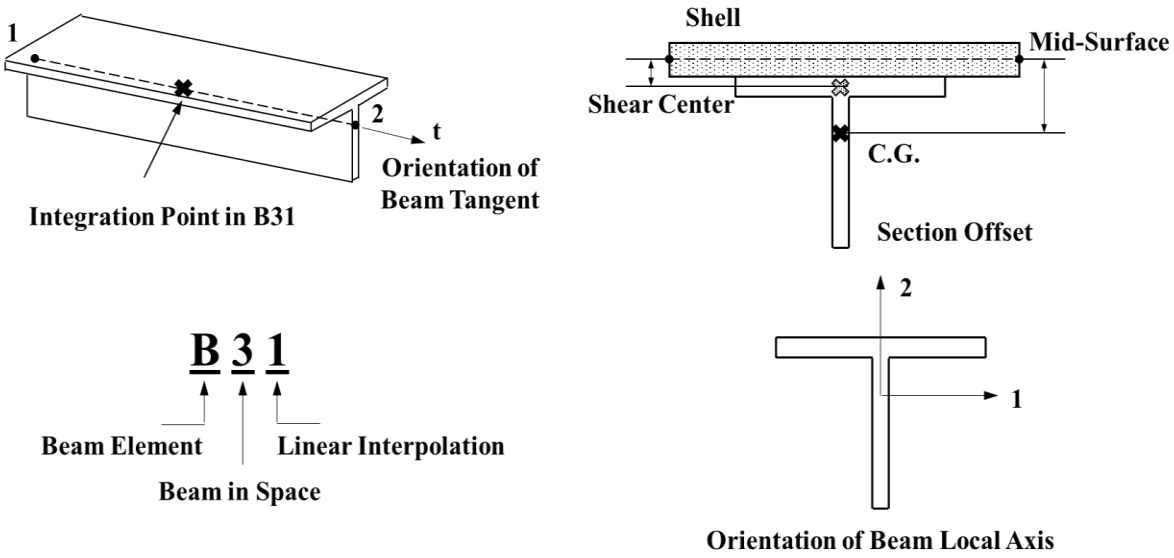

Figure 4-3 Beam Element B31 Used in FE Models

Analysis results with shell elements is sensitive to mesh distortion and element aspect ratio. A proper mesh is needed to ensure accurate results with an efficient mesh density. The aspect ratio (length-width ratio) of the shell element was controlled to be close to unity. Most of the shell elements were square or rectangular as shown in Figure 4-4. However, trapezoidal elements were used in solid end diaphragms as well as in the geometric transition regions. The mesh size was in proportion to half of the width of the top flanges.

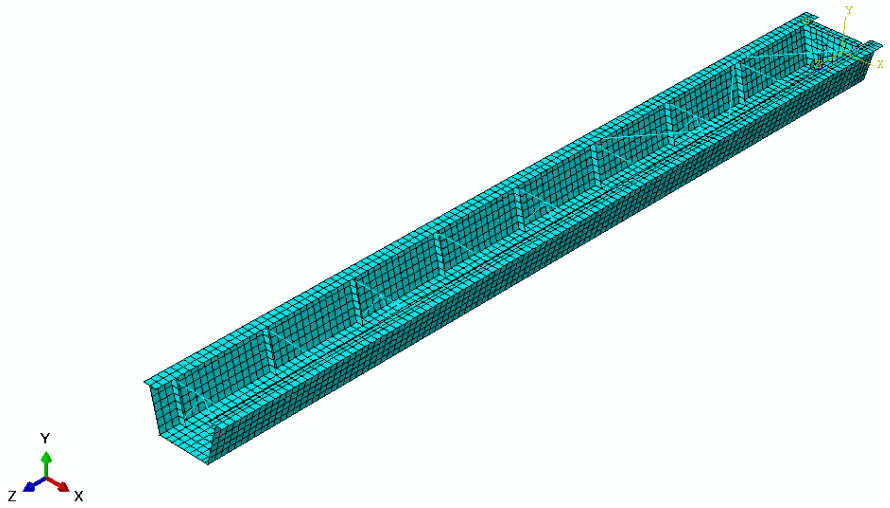

Figure 4-4 Discretized FE model of Tub Girder System

The FE models were created with the ability to vary the layout of top lateral braces, internal K-frames as well as the cross-sectional geometry. Two modeling techniques were employed to implement the geometry modifications fast and efficiently. The first technique is the feature and object suppression function in ABAQUS. This technique is suitable for varying the layout of the braces as illustrated in Figure 4-5. To study the effect of the layout of braces, the model of the

girder systems was created to include all the brace components as sets of wires. Then some of the brace features (wires) were suppressed ("temporarily removed") from the part or assembly of the model. After the features are suppressed, a new model with modified brace layout can be regenerated. The suppressed features can be placed back into the model since all the property definitions have been reserved in the model database. The drawback of this technique is that some features are not independent and have parent feature or child feature dependency. Therefore, a change in one feature might affect several related features. Moreover, the mesh can be affected since some features are connected geometrically.

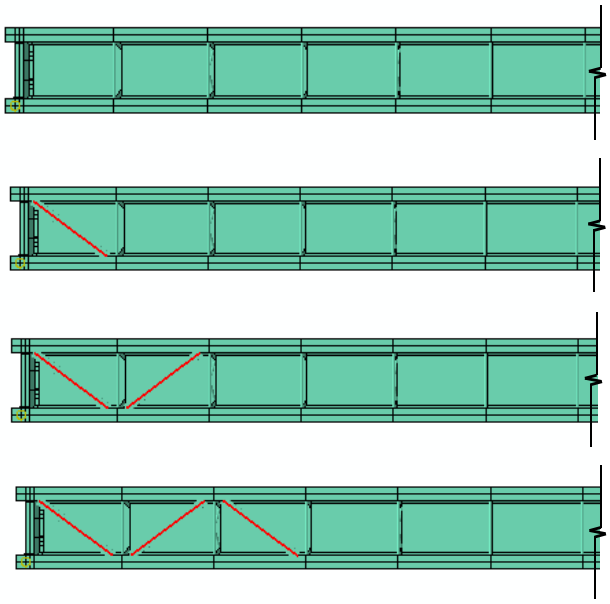

Figure 4-5 An Example of Varying the Layout of Top Lateral Braces in FE models

The other technique is a parametrized computer script integrated with a GUI (graphic user interface). The parametrized computer script for this research was created using the programming language python (www.python.org). A python script with a GUI was created to parametrize all the geometric features and generate the FE model from part to assembly with different steps, boundary conditions and mesh defined for input to Abaqus. The repetitive process of creating new models from scratch would then be reduced and simplified to entering input values for all the design parameters as shown in Figure 4-6. Interactively working with ABAQUS/CAE, the developed python scripts get user input values through type-in dialog boxes and then execute the commands based on user input information to generate the model or access the results in the output database. The required input information includes general bridge cross section (the width of deck, deck overhang, number of girder line, girder spacing), girder framing plan (span arrangement and bracing layout), girder cross section dimensions and bracing details (spacing, section information and offset). Based on the input data, the geometry features of the tub girders are created, and section properties are assigned. The defined geometry models are then sent to the assembly module. The steel girders were connected at the end diaphragm and tied together with the concrete deck. Then, analysis steps are defined based on construction staging and sequences. For each step, a corresponding construction load was defined and applied.

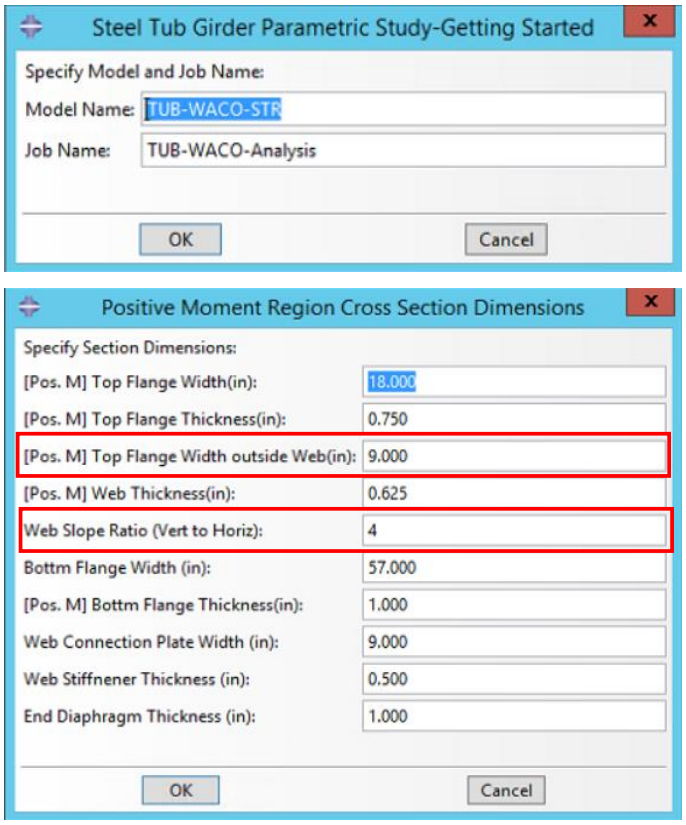

Figure 4-6 User Interface of Interactive Python Script

As a first step, models were created for the three test specimens, illustrated in Figure 4-7. Model predictions were compared with experimental results to refine various modeling procedures and assumptions and to ultimately develop a validated FE model that can be used for the subsequent parametric FE studies. The next section will present the validation process for the models based on experimental evidence.

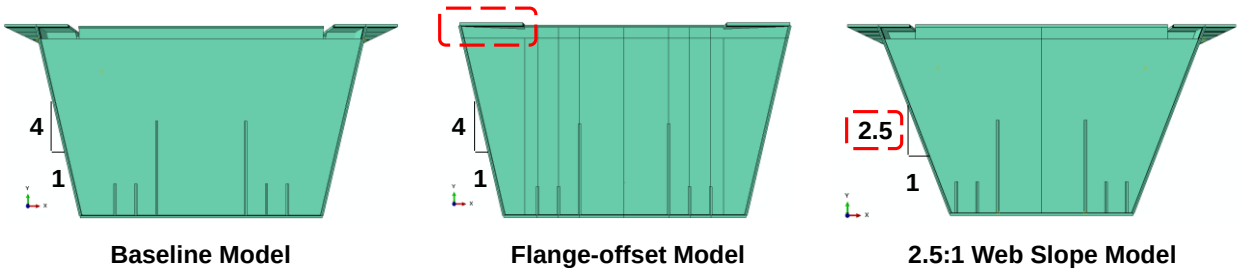

Figure 4-7 FE Models with Different Cross-Sectional Geometry

4.3 Validation of FE models of Steel Tub Girder Specimens with Experimental Data

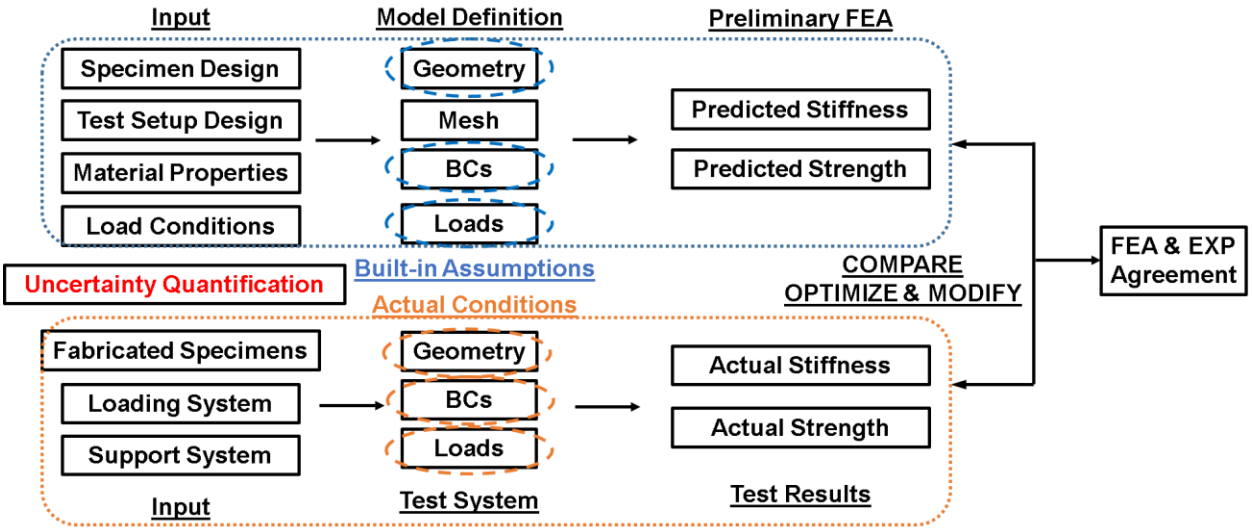

Figure 4-8 Flow Chart of the Development and Validation of Finite Element (FE) Models

Validating the finite element models using large-scale experimental results is a crucial step in this overall research project. Design recommendations for tub girders developed in this project will be based largely on the parametric FE studies. Without a thorough model validation process, little confidence can be placed on the results of the parametric FE studies, and therefore little confidence can be placed on the resulting design recommendations.

Errors in modeling assumptions can cause significant errors in the analysis results. Moreover, modeling errors can be difficult to identify without the benefit of experimental data. Although errors are inevitable in FE models and tend to accumulate as the model becomes larger and more complex, a verification and validation process can be conducted to control and minimize the modeling errors. Figure 4-8 is a flowchart that illustrates the overall validation process undertaken for this project. A more detailed list of issues involved in the validation process is as follows:

- Define the main objective of the analysis, accuracy requirements and key assumptions.
- Define model geometry based on the actual dimensions of the specimens.
- Confirm correct material properties are specified.
- Select proper element types and properties for different regions of the tub girders.
- Determine if shear deformations are significant.
- Define mesh design (shape and size) and control criteria (e.g. limits on the aspect ratio and shape distortion of the element).
- Define Boundary Conditions (applied load and support conditions) – location, magnitude and direction.
- Define proper interaction and contact between different areas of the model.
- Determine whether the model passes free thermal expansion and rigid body motion checks.
- Confirm the self-weight of the model can produce the expected reactions.
- Review and reconcile FE code errors and warning messages.

- Verify force and moment equilibrium – applied load and reactions in each direction.
- Check that the model results are consistent with the modeling assumptions and with the experimental results.
- Evaluate the effects of initial geometric imperfections on the model predictions.

Among all the factors that can have a significant impact of the model predictions, three are discussed in detail below. These three factors are:

- geometric imperfections,
- tub girder support conditions,
- eccentricity in bracing member connections.

4.3.1 Effect of Geometric Imperfections

4.3.1.1 Effect of Global Imperfections

Due to manufacturing and erection tolerances, the three steel tub girder systems tested in the laboratory are not perfectly straight and aligned on the supports. The deviations of tub girders from the "perfect" geometry is commonly referred to as geometric imperfection or initial imperfection. From a global perspective, initial sweep and twist were observed in the tub girder specimens. This section presents the measured global imperfection data and discusses its impact on the lateral torsional buckling behavior of steel tub girders during construction.

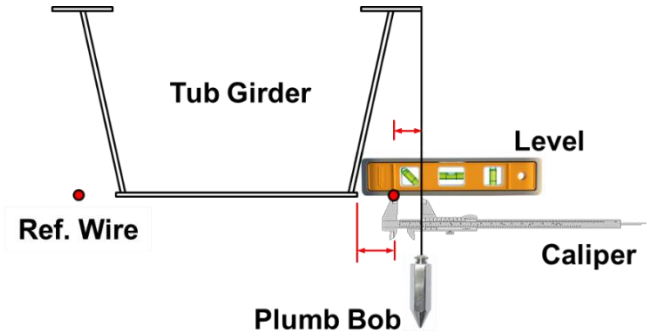

Figure 4-9 Cross-section Sketch of Global Imperfection Measurement

Little data on global geometric imperfections for steel tub girder systems are reported in the literature. To understand the impact of global imperfections and to validate the accuracy of the FE results, imperfection measurements were taken on each specimen. A global reference system was established, and measurements were made of the deviation of the edge of top and bottom flanges with respect to the reference system. These measurements are illustrated in Figure 4-9. The measurements were taken along the length of the girder at every other strut panel point. A more detailed description of this method can be found in Quadrato (2010).

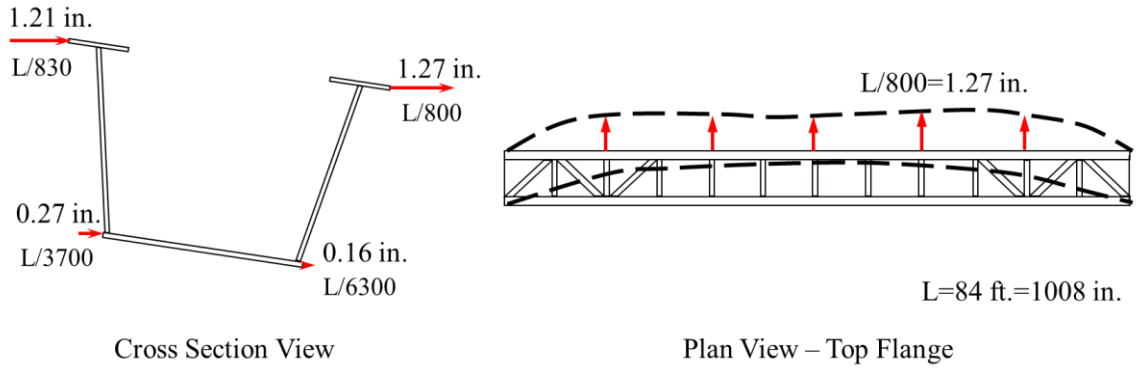

Baseline Specimen

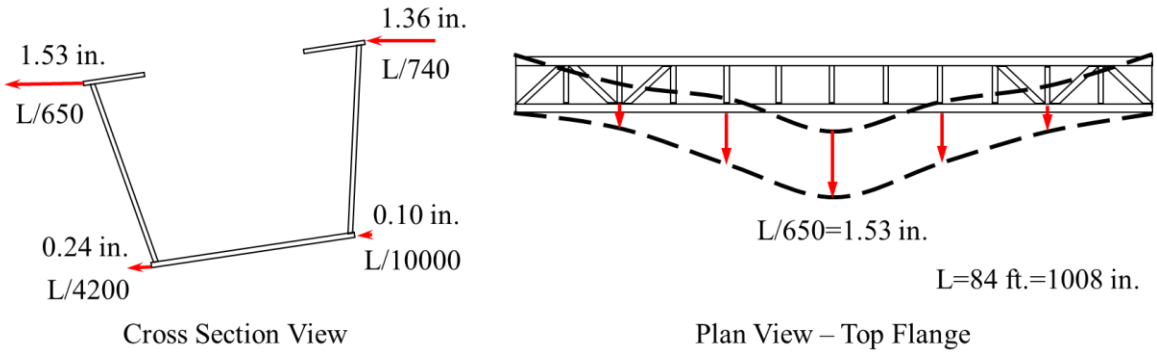

Flange-offset Specimen

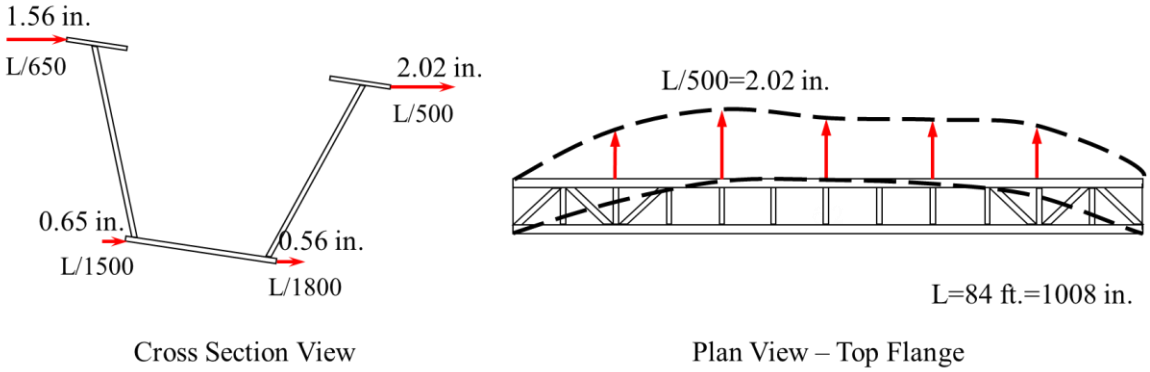

Lower-slope Specimen

Figure 4-10 Measured Global Imperfection of Steel Tub Girder Specimens

Figure 4-10 shows the measured global imperfections of three steel tub girder specimens. The cross-section views display the maximum measured lateral deviation on both top and bottom flanges. The plan views show the pattern of the global imperfection. The plan view also shows the maximum measured lateral deviation relative to the length of the girder. From the measurements,

the lateral deviations of the top flanges are greater than those of the bottom flanges. This indicates that all the girders have initial twist. For the baseline and flange-offset girders, the twist pattern dominates because the lateral displacement of the bottom flange is small compared to the top flange. The lower-slope specimen had the maximum lateral deviation on both top flanges (L/500) and bottom flange (L/1500). Compared with the other two specimens, the lower slop specimen exhibited greater initial sweep, although initial twist still dominated this specimen. Measurements also showed that the directions of initial twist differed among the girders.

To include the measured imperfections in the FE models, a separate static analysis was first carried out to obtain the deformed shape of the model. The imperfection data was introduced into the FE model by defining a lateral displacement field on the nodes at designated locations. A nodal displacement output file was requested from the analyses. This output file combined with *IMPERFECTION keyword added to the input file introduced the global imperfection into the models. Figure 4-11 illustrates the procedure described above (a scaling factor of 50 has been applied on the deformed shape of the model).

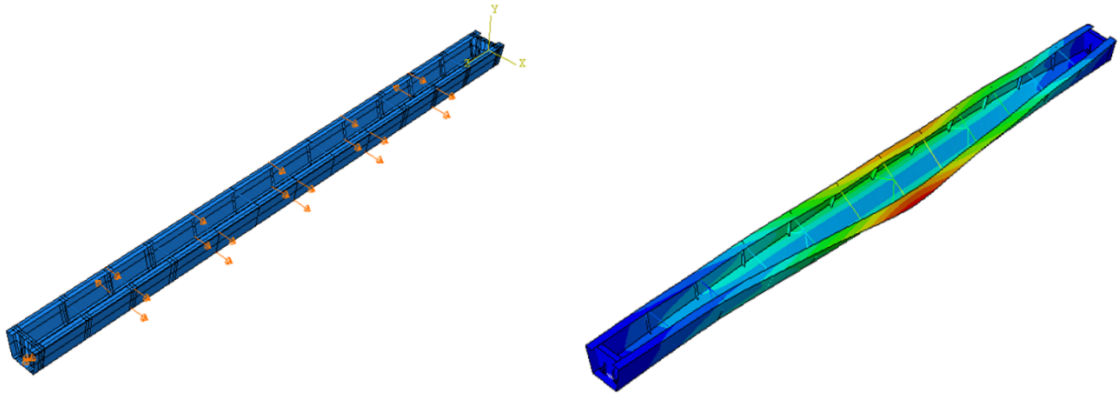

Figure 4-11 Example of Including Global Imperfection in FE Model of Flange-Offset Specimen

The moment-lateral deflection response of each specimen with open sections (no top lateral truss) under concentric loading are plotted in Figure 4-12. Experimental response is compared with the best FEA results in this plot. The term “best FEA results” refers to the results of the FEA model after modification to account for boundary conditions (discussed in Section 4.3.2). The elastic lateral torsional buckling critical moment values, determined by eigenvalue analysis, are also listed in the plot. Proper introduction of global geometric imperfections into the FE models provided good agreement between experimental response and FEA results. The magnitude, pattern and direction of imperfection all affect the FEA results. Elastic solutions without consideration of global geometric imperfections can lead to unrealistic predictions of tub girder response.

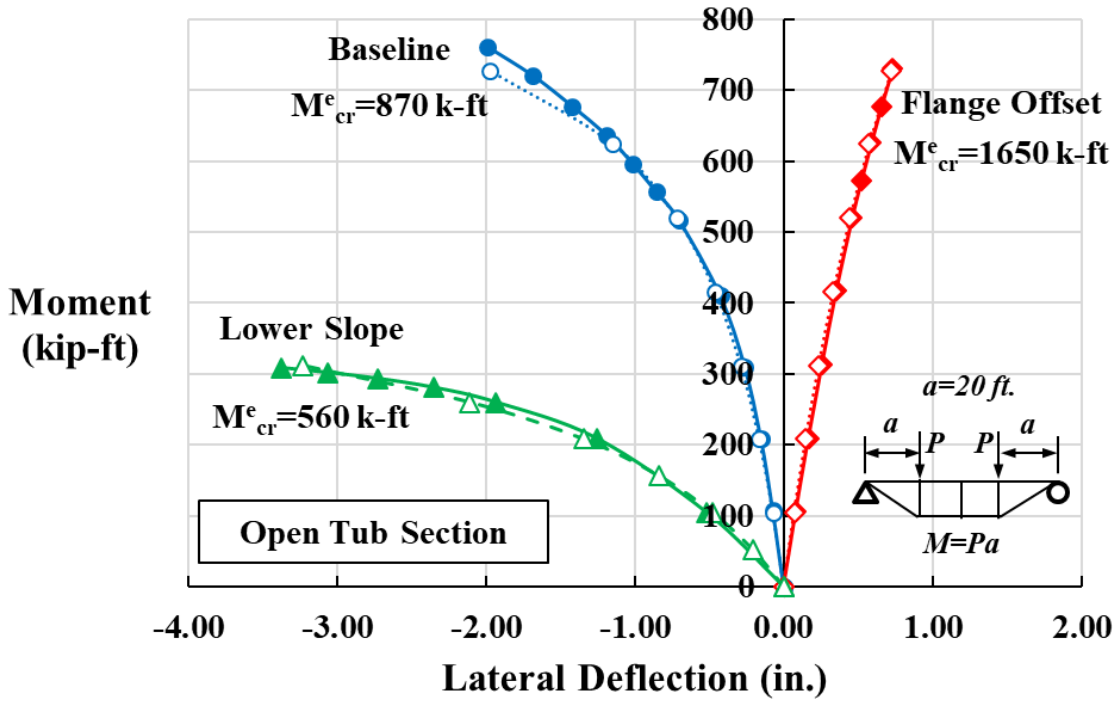

Figure 4-12 Moment-Deflection Response of Each Specimen – Experiment vs FEA (Filled Markers-Experiment; Open Markers-FEA)

4.3.1.2 Effect of Local Plate Imperfections on Local Buckling of Top Flange

Variations in the plate dimensions, and out of flatness of the plates usually exist on all plate components of steel tub girders. Some degree of initial out-of-flatness already exists in the plates during manufacturing at the steel mill. The fabrication procedures of the steel tub girder, such as heating and welding, can create out-of-plane distortion of the plates. The out-of-flatness of plates can affect the local buckling behavior of the plates. Excessive initial out-of-plane deformation of plates may also have a negative impact on the serviceability and the fatigue life of bridge girders. Therefore, plate flatness is a critical quality control factor of steel built-up sections. In the three tub girder specimens, due to the thin plates (actual thickness 0.4375 in. for baseline and lower slope specimen and 0.5625 in. for flange-offset specimen) used to ensure elastic buckling behavior, the top flanges had significant distortion after welding. An example is illustrated in Figure 4-13. The section presents measured local imperfections and discusses its impact on the local buckling behavior of the top flanges.

Figure 4-13 Baseline Specimen with Significant Plate Waviness on the Top Flanges

The initial out-of-flatness is a measurement of the geometric deviation from the ideal flat surface. Permissible out-of-flatness values are usually defined as a proportion of a characteristic dimension of the plate, commonly, the width of the plate, b. In current specifications, the tolerance on the out-of-flatness is in the range of b/200 to b/60 for different plate elements. These tolerances can be found in ASTM A6 (2001) and AWS D1.5 (1996). To properly consider local imperfections in the FE models, measurements of out-of-plane deviations of the top flanges were taken for flange-offset specimen. A simple approach was used to measure the out-of-flatness of the top flange plates and is illustrated in Figure 4-14. A more detailed description of out-of-flatness measurement of the plates can be found in Herman (2001).

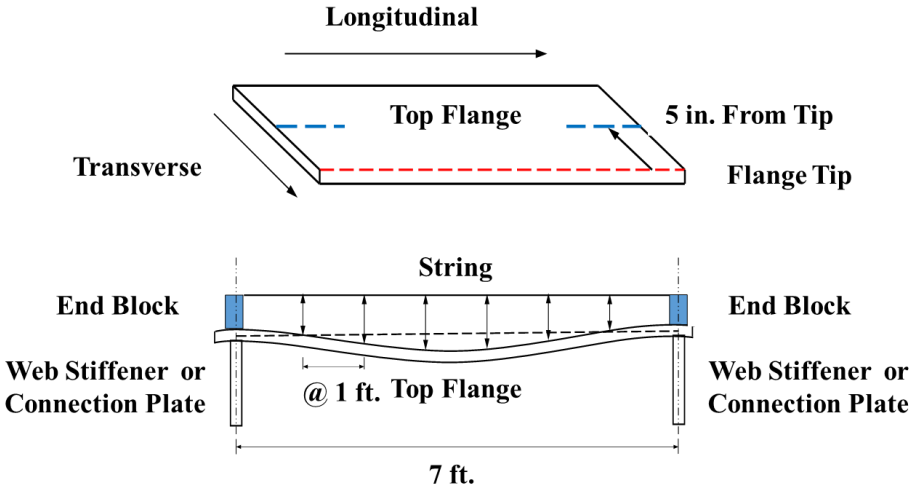

Figure 4-14 Local Plate Imperfection Measurement

Sample measurement data of local plate imperfections are shown in Figure 4-15. The maximum magnitude of the out-of-flatness ranges from b/160 to b/80.

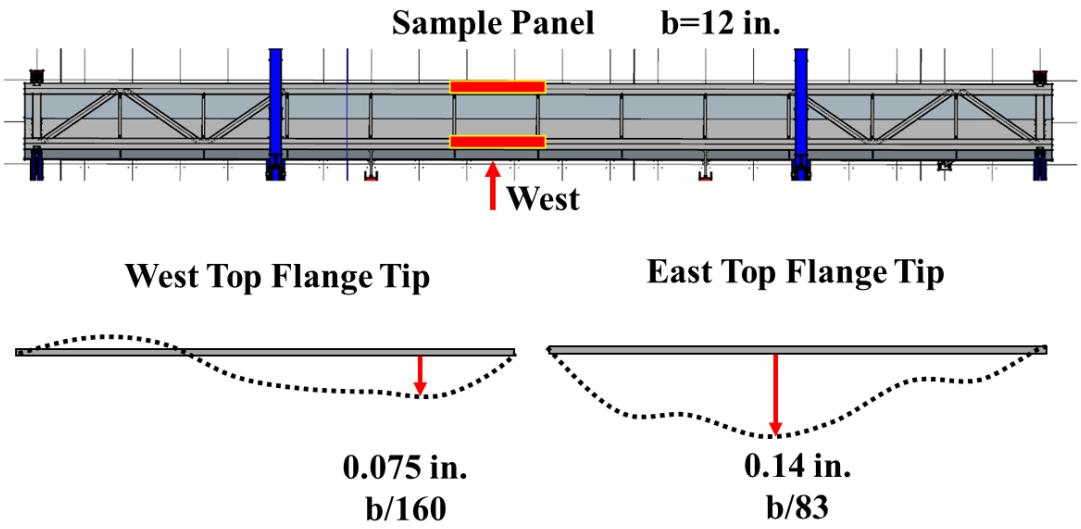

Figure 4-15 Sample Local Plate Imperfection Measurements

The importance of local initial imperfections was not given adequate attention until local flange buckling occurred during one of the elastic buckling tests on flange-offset specimen as described in Chapter 3. Key information for model validation is summarized here. The applied loading and bracing layout are shown in Figure 4-16. The buckling occurred on one of the top flange panels at mid-span in a sudden and rapid manner with a banging sound. As indicated in Figure 4-18, the applied load no longer increased and large strains were developed in the top flanges. Visual inspection after loading was stopped revealed that a wave formed on the top flange (see Figure 4-16) and the mill-scale on the critical region flaked off with notable yield lines. The buckled flange had a reverse-curved shape and the maximum deviation was around 1.38 in (b/9). The maximum deviations at the peak and valley of the distribution had a ratio of 2.0. The thickness of top flanges used was 0.5625 in. The top flanges were classified as non-compact, indicating that flange local buckling can occur before the fully plastic section capacity was reached. Preliminary FEA of this specimen did not consider local imperfections and indicted that global LTB should control the behavior and occur before flange local buckling. In the actual specimen, the presence of local imperfections clearly affected the behavior of the girder. Unfortunately, local imperfection measurements were not taken until after this local buckle occurred. To model the observed local buckling, assumptions had to be made on the shape and magnitude of the local imperfection based on data obtained afterwards. Considering the sudden and rapid nature of the incident, the hypothesis for the local buckling was that when the stress level approached the critical buckling stress, the out-of-plane deformation grows rapidly from the initially deviated position. Further, based on the observed flaking of mill scale, yielding of the flange likely occurred during the buckling process. Analyses were performed to provide some insights into the observed local buckling.

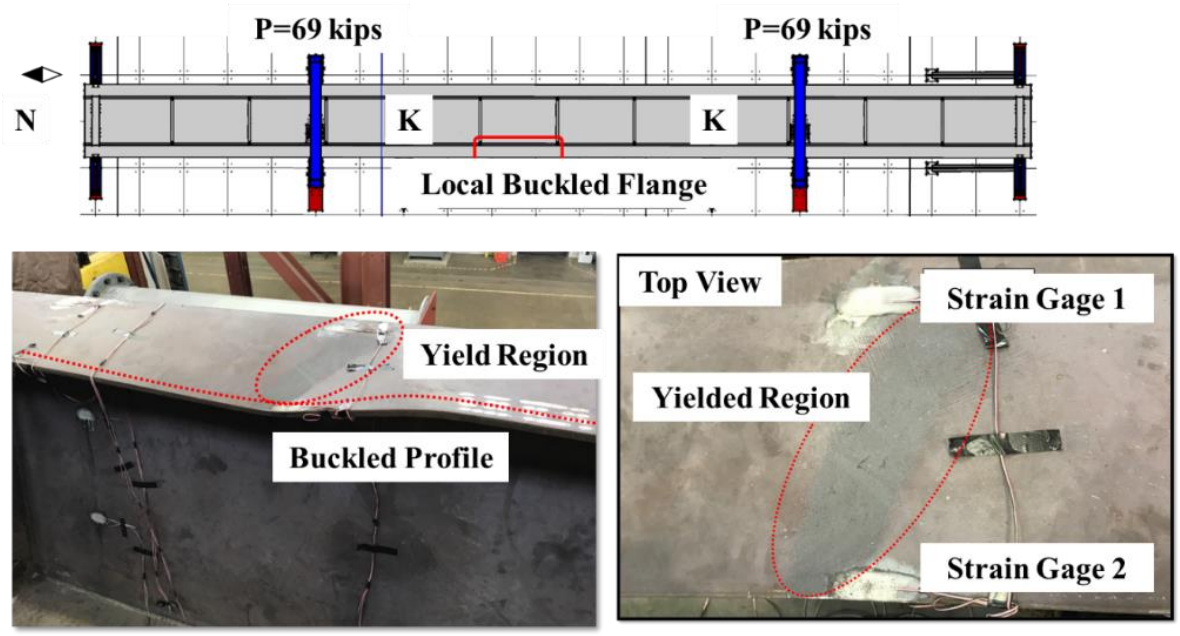

Figure 4-16 Local Flange buckling in the Experiment

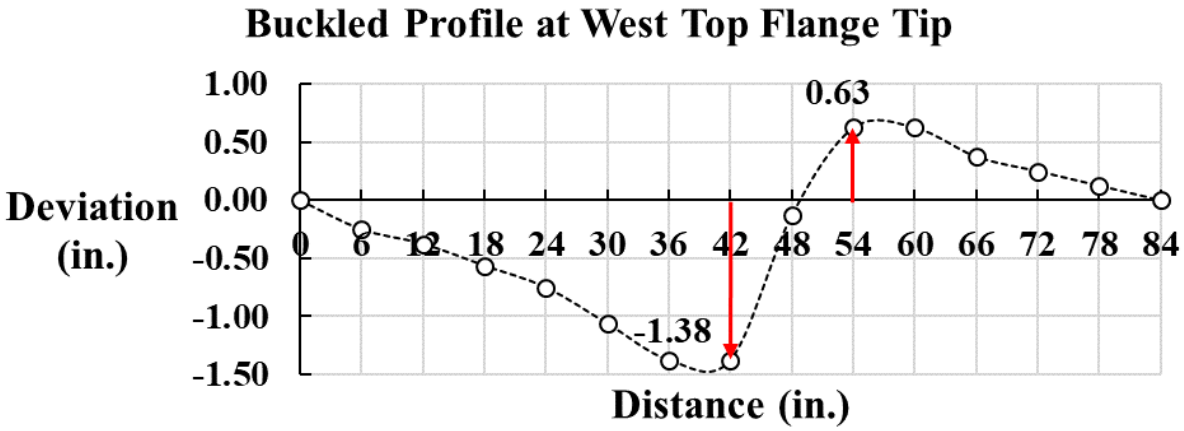

Figure 4-17 Profile of Buckled Top Flange

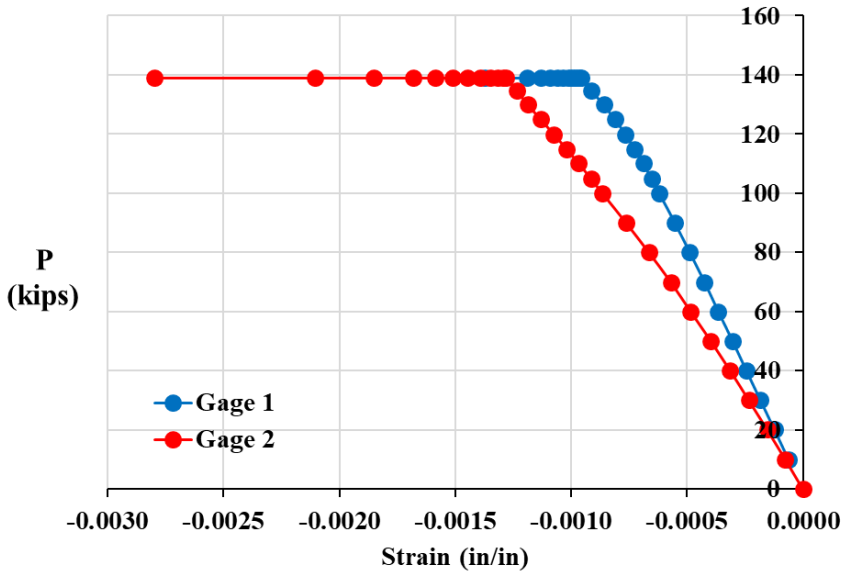

Figure 4-18 Strain Gage Readings on the Buckled Top Flange

Local plate imperfection and inelastic behavior of the steel played a critical role in the local flange buckling. Therefore, in the FE model, the inelastic material behavior and local plate imperfection were included in the model as shown in Figure 4-19 and Figure 4-20. Because the local imperfection was not measured before the test, an estimated imperfection pattern was introduced into the model based on the final buckled profile. As shown in Figure 4-19, two opposite vertical displacements with a ratio of two was applied at the two points on the tip of the top flange to generate an imperfection. The magnitude of the initial displacement was chosen according to the average maximum deviation of the measured local imperfection.

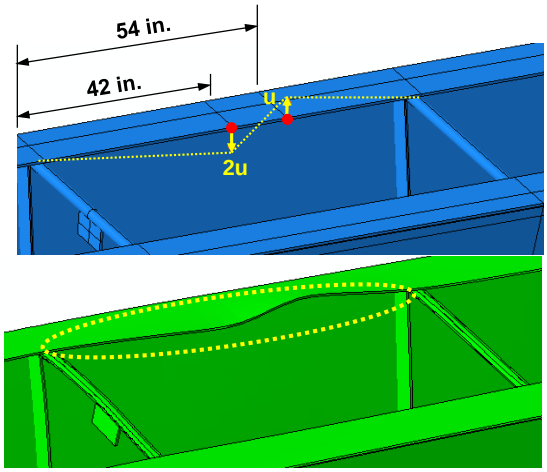

Figure 4-19 Estimating Original Local Imperfection in FE Model Based on Buckled Profile

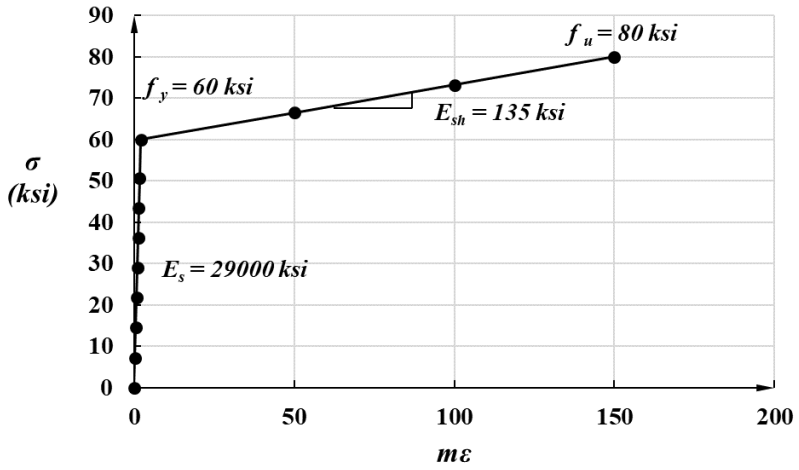

Figure 4-20 Simplified Bi-linear Stress Strain Curve for Steel in FE Model Based on Steel Coupon Test

With properly defined end warping conditions and initial local imperfection, Figure 4-21 shows that the FE model could give a reasonable estimation of the girder response under applied loads. After the initial linear stage, the girder started to experience global instability with stiffness gradually decreasing. When the stress level hit the critical stress for flange local buckling, the load deflection response reached its plateau. The girder could no longer sustain more load and developed large deformations. Numerical instability due to large deformations and material plasticity led to convergence problems, and so the FE analysis terminated at a smaller deformation than was measured in the experiment. Nonetheless, as illustrated in Figure 4-21, the FE model predicted the experimental response quite accurately.

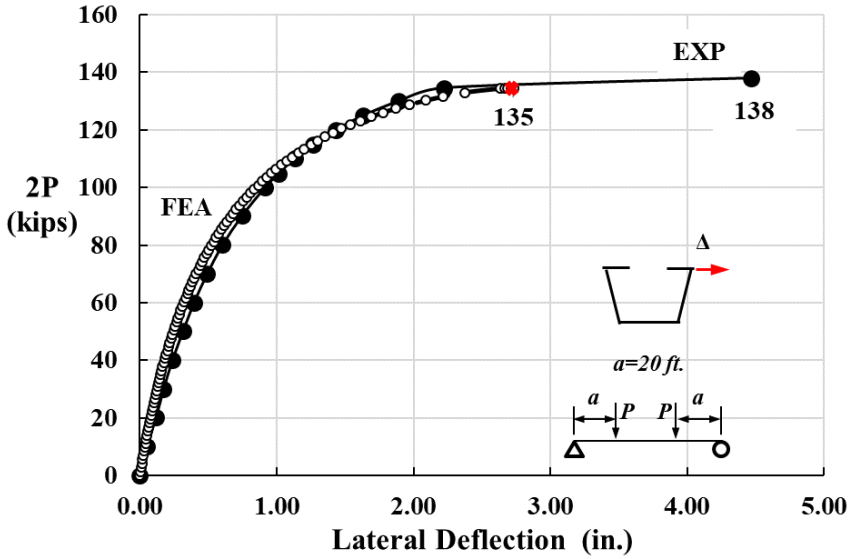

Figure 4-21 Comparison of Experimental Response and FEA Results

4.3.2 Effect of Girder Support Conditions

To reflect the support conditions in the laboratory experiment, boundary conditions must be carefully considered in the FE model. Figure 4-22 illustrates the end support fixtures used in the experiments and the corresponding boundary conditions used in the FE model. A more detailed description of the end supports used in the experiments is provided in Chapter 3.

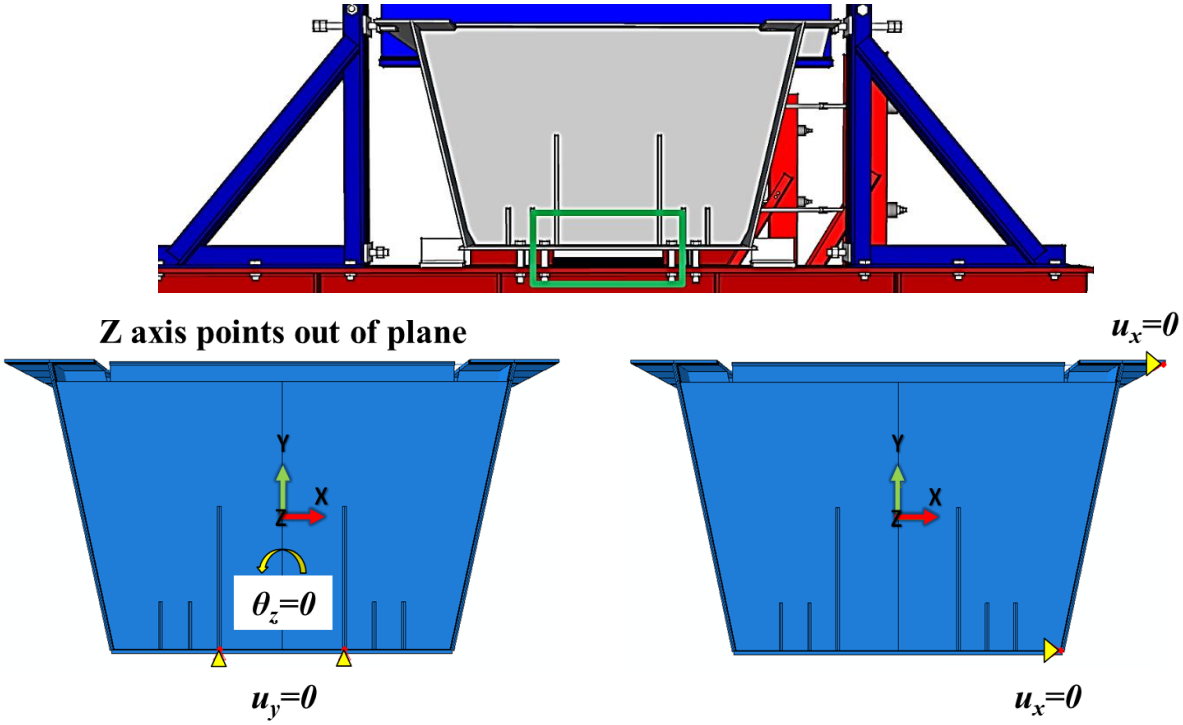

Figure 4-22 Support Conditions in the Laboratory and FE Model

In the FE model, two vertical supports were provided on the bottom flange at each end to restrain vertical movement and prevent section twist. Lateral supports were placed at the top and bottom flange to restrain out-of-plane deflection at the ends. Although the vertical and lateral boundary conditions appear straightforward, uncertainty lies in the consideration of longitudinal movement of the girder at the supports. A significant aspect of the structural response of tub girders is warping deformation. Tub girders have cross sections which tend to warp when subjected to torsion. If out-of-plane distortion is restrained at any cross section, longitudinal normal stresses and associated shear stressed will develop in the member. The warping shear stresses act together with the uniform shear stresses due to St. Venant's torsion to resist applied torque. Hence, if warping restraint is applied, the torsional stiffness may be considerably greater than that in the absence of warping restraint. End warping restraint can also have a significant influence on the stability behavior of the steel tub girder. This section discusses end warping restraint as it affects the accuracy of the FE model as well as its influence on the stability of steel tub girders.

In design for torsion, two idealized end warping conditions are commonly assumed, i.e., warping free or warping fixed as shown in Figure 4-23. However, the idealized end warping conditions are rarely attainable in practice. The degree of the end warping restraint provided by the actual supports lies somewhere between these two extremes and is difficult to quantify. This introduces significant uncertainty into the accuracy of the FE model. In the experiments, the

longitudinal movement at the support ends was monitored during the elastic buckling tests to provide evidence of support warping restraint flexibility.

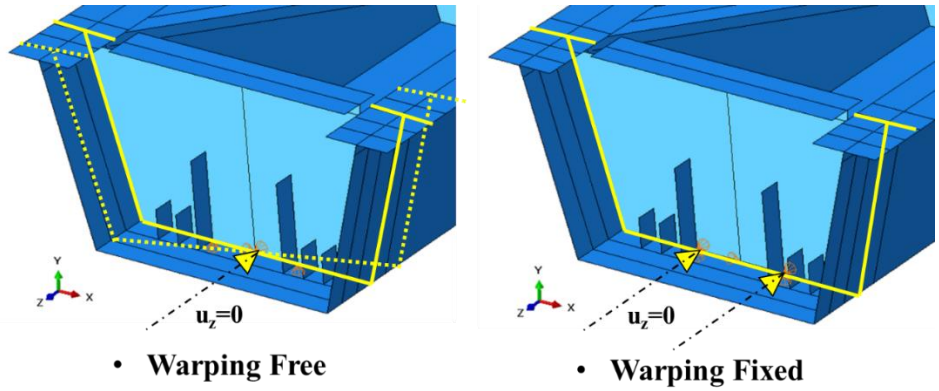

Figure 4-23 Idealized End Warping Conditions

During the experiment, linear potentiometers (for the baseline specimen) and dial gages (for the flange-offset and the lower-slope specimen) were instrumented at the support ends to capture longitudinal displacements at the support ends as shown in Figure 4-24. Four gages were installed at each end of the specimen. As indicated in Figure 4-25, the two points on the bottom flanges move in the opposite directions at different loading stages resulting in a relative rotation at the ends. The girder therefore exhibits warping deformations during the test. Warping restraint increases with the addition of top lateral diagonals at the ends as it can be seen in Figure 4-26. After two lateral diagonals are installed at each end, adding additional braces has little effect on the longitudinal movement.

For FE analysis, the influence of warping restraint caused by the girder supports becomes less significant with the addition of the top lateral truss, since the lateral truss dominates the development of warping restraint.

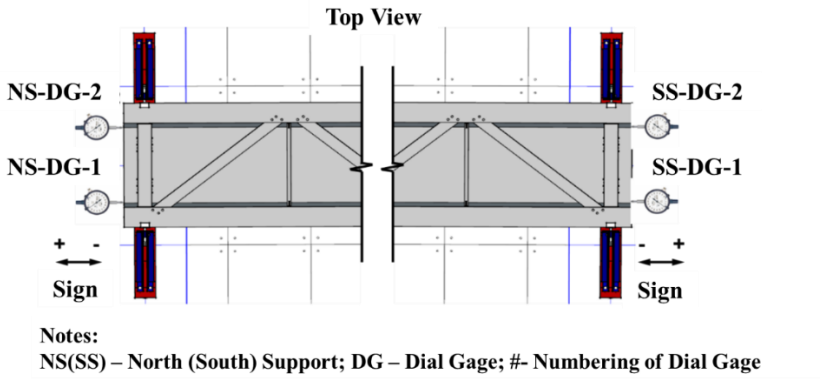

Figure 4-24 Instrumentation to Monitor Support Longitudinal Movement

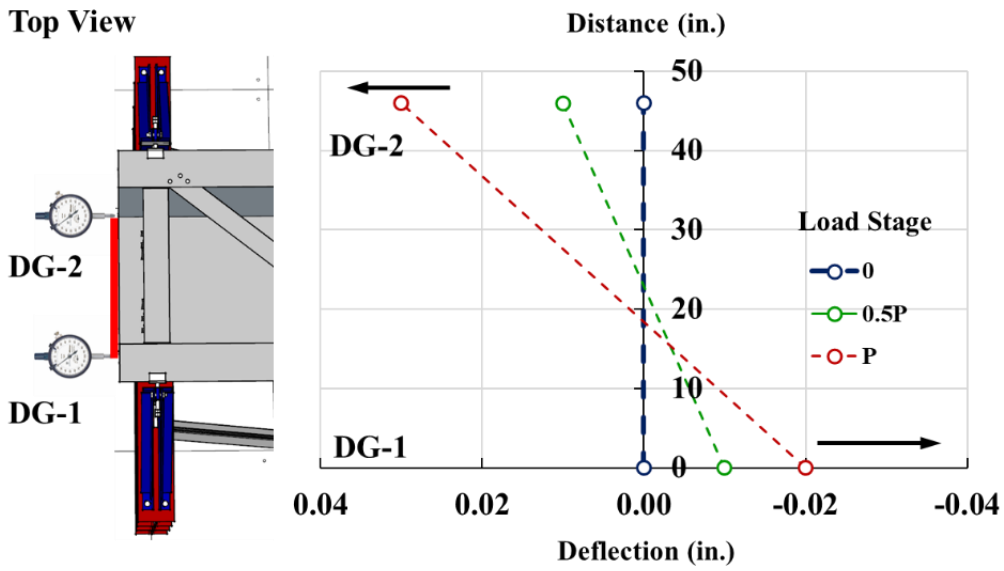

Figure 4-25 Support End Movement at Different Load Stages

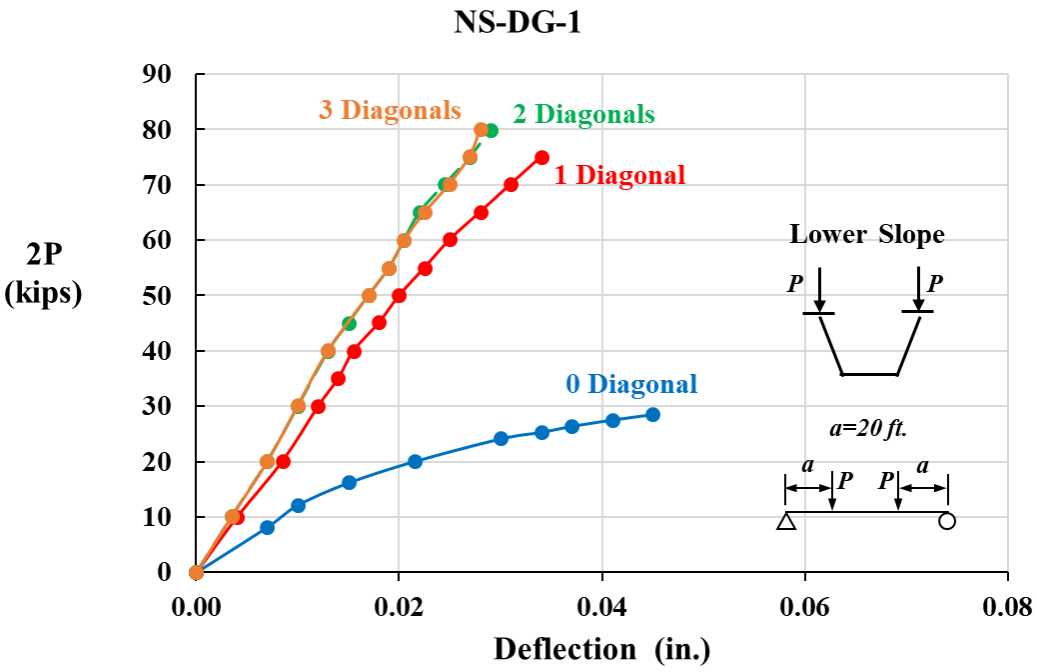

Figure 4-26 Load-Longitudinal Movement at NS-DG-1 of Lower-Slope Specimen with Different Number of Truss Diagonals at each end

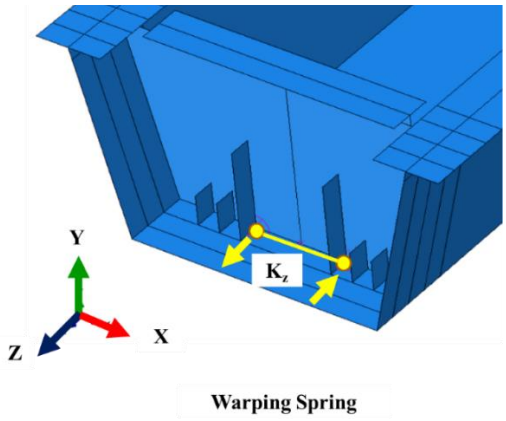

Figure 4-27 Warping Spring Defined in FE Models

To reflect the warping restraint generated by the girder end supports observed in the experiments, two spring elements at the support ends are included in the FE model, as shown in Figure 4-27. The springs are defined as translational springs that connected two points on the end diaphragm stiffeners. The determination of the stiffness of the springs to correctly represent the warping restraint is not straightforward because the forces directly associated with the longitudinal deflection was not measured during the experiment. However, based on a trial and error process, a value of spring stiffness was determined so that the FE analysis results reasonably reflected the experimental response. Figure 4-28 shows an example of the experimental load-deflection response compared with FEA predictions. The experimental response is bounded by FEA results with two idealized end warping conditions, i.e., warping fixed and warping free. This plot also shows the FEA results that includes the springs, with a spring stiffness chosen to obtain agreement between the experimental response and FEA predictions.

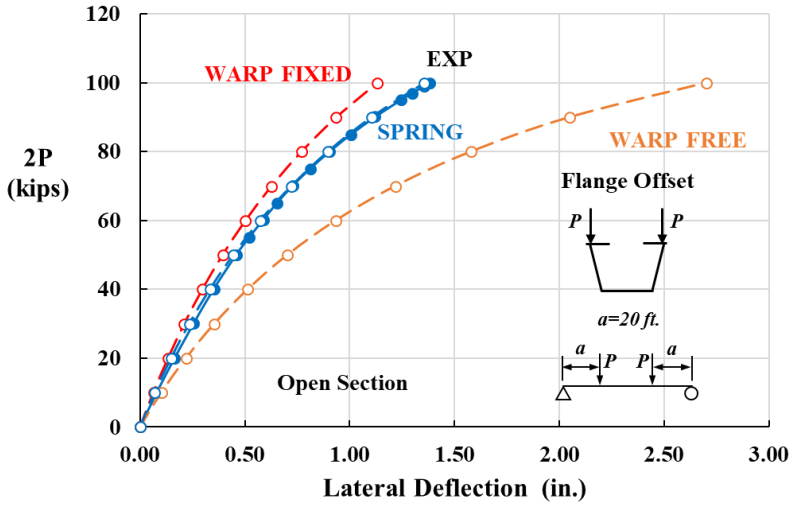

Figure 4-28 Load- Deflection Response of Top Flange at Mid-span with Different End Warping Conditions (Filled Marker – Experiment; Open Marker – FEA Results)

For analysis of tub girders where no data is available on the warping restraint generated by the girder supports, analyses with end warping-free and end warping-fixed can bound the girder response. Further, as discussed above, the influence of warping restraint generated by the girder supports on the girder response is significantly reduced when a top lateral truss is provided, which will be the case in any practical application of tub girders.

4.3.3 Effect of Bracing Connection Eccentricity

For computational efficiency, the bracing system of steel tub girders is commonly modeled in FE analysis using beam elements or truss elements. This simplification assumes that the behavior of the bracing member is dominated by axial forces. However, bending and torsion effects also exist in the bracing members due to the singly symmetric sections commonly used for the bracing members and due to eccentricities generated by commonly used connection details. In steel tub girder systems, WT shapes are commonly usually used for top lateral braces and angle shapes are commonly used for internal K-frames as shown in the photos in Figure 4-29. Both shapes are singly symmetric open sections. When these sections are connected to top flange or web connection plates, gusset plates are used to provide enough space for the connection and to ensure the working line of different members intersect at a common working point. However, the use of gusset plates creates an offset between the bracing member and the element to which it is attached (top flange or web connection plate). This, in turn, creates bending moment in the bracing member. This bending moment can affect both the stiffness and strength of the brace. Even if the gusset plate is eliminated, there will still be an eccentricity between the center of gravity of the bracing member and the connected element on the girder, as shown in Figure 4-29. If the bracing member is modeled using beam elements or truss elements, the connection eccentricity is often ignored in the FE model. In the model, the brace member is typically connected to the plate modeled by shell elements by sharing a common node. This practice may lead to errors in FEA results. This section discusses the effect of bracing connection eccentricity on the behavior of steel tub girders.

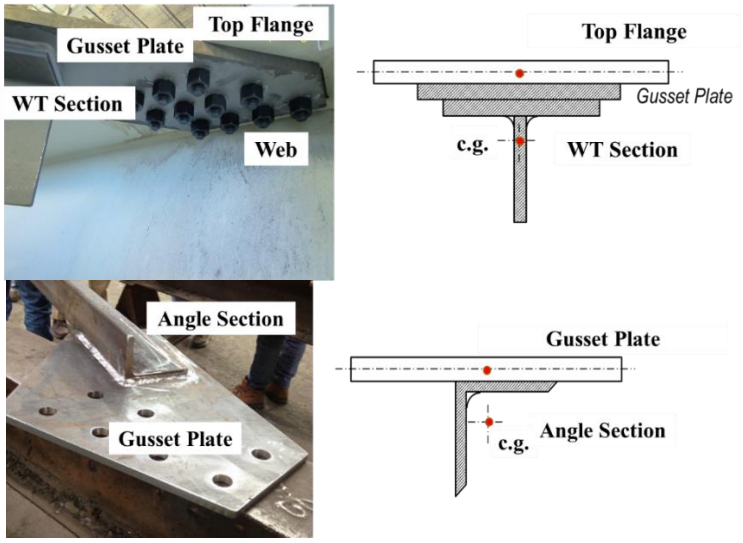

Figure 4-29 Common Bracing Members and Connection Details used in Tub Girders

Previous research has studied the effects of bracing connection eccentricity (Wang et al 2012, Battistini et al 2012, Tito 2013). These studies showed that eccentricity in bracing connections can significantly reduce the axial stiffness of a brace. Underestimating brace stiffness in an FE analysis can, in turn, result in unconservative predictions of girder stability.

An element-level FEA study was performed first to understand the effect of connection eccentricity. The studied problem was a single-diagonal member under shear to simulate a top lateral diagonal panel in a tub girder, as shown in Figure 4-30. Solid elements were used to model the WT 5x22.5 top lateral brace and the connection plates (12 in ×18 in ×Various Thickness) to simulate the top flanges with gusset plates of various thicknesses. The member size and connection details for this analysis were chosen to coincide with experiments conducted by Tito (2013).

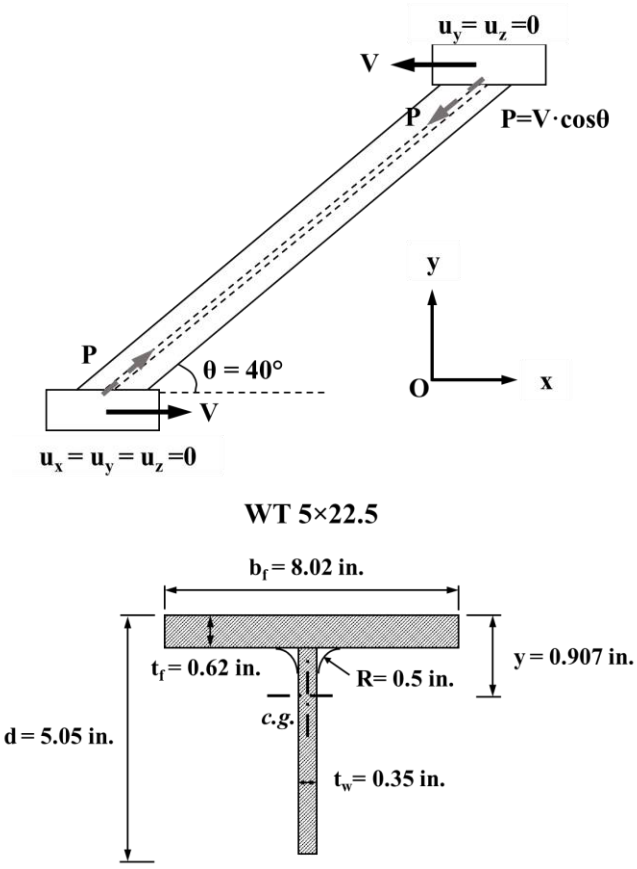

Figure 4-30 A Single-diagonal Panel under Shear and WT 5×22.5 Section in FE Model

Figure 4-31 and Figure 4-32 show the P-δ effect on the single diagonal member under axial force. As indicated by these figures, connection eccentricity generates significant bending moments in the WT bracing member. Further, the P-δ effect is nonlinear and therefore increases with the applied load. The gusset plate thickness clearly affects the response.

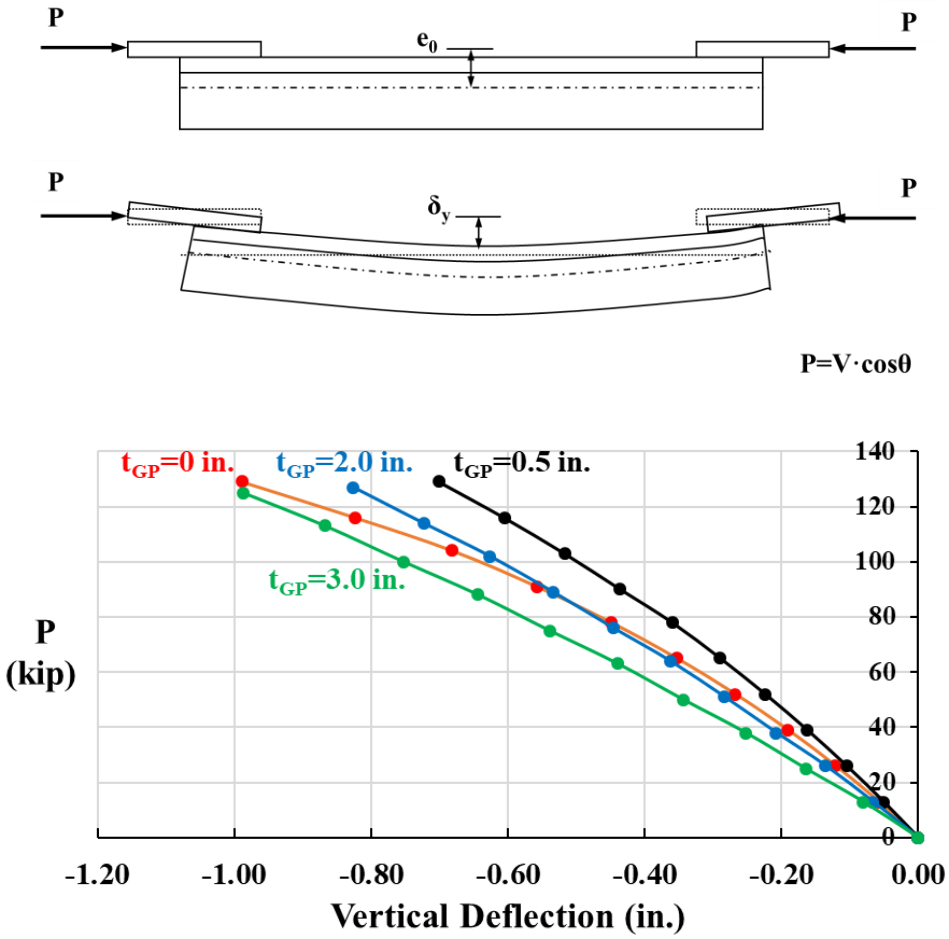

Figure 4-31 Vertical Deflection of Single-diagonal Member with Gusset Plates of Different Thicknesses (GP – Gusset Plate)

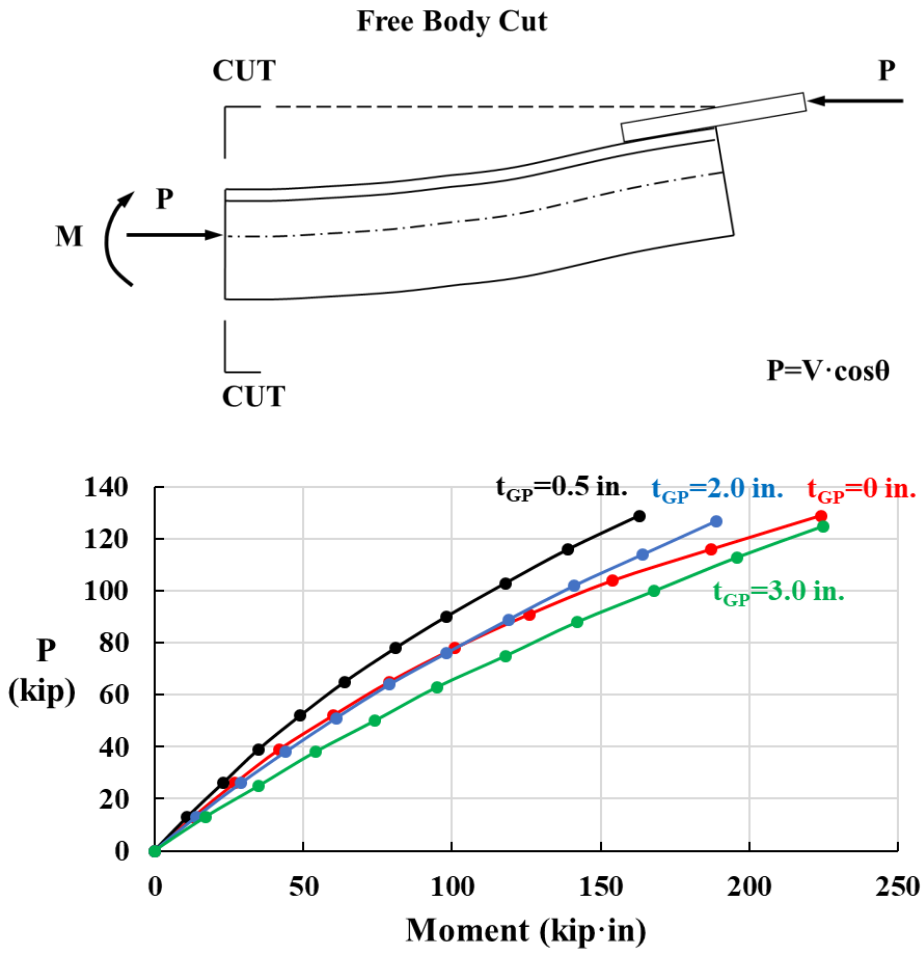

Figure 4-32 P-δ Moment of Single-diagonal Member with Gusset Plates of Different Thicknesses (GP – Gusset Plate)

Figure 4-33 shows the shear force-shear deflection response for a baring member in a top lateral truss, for a range of gusset plate thicknesses. The shear stiffness decreases rapidly with the increasing thickness of the gusset plate. Consequently, as gusset plate thickness and connection eccentricity increase, the effectiveness of the brace in providing stability decreases.

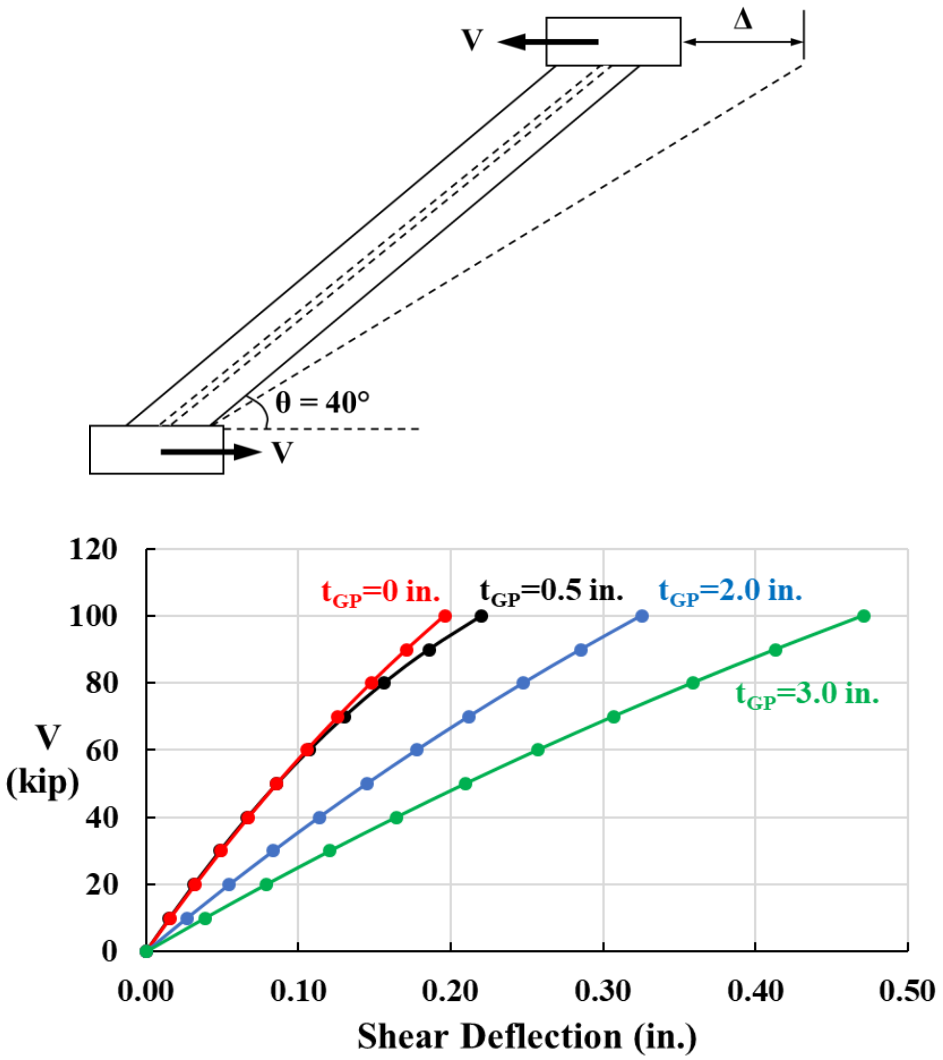

Figure 4-33 Shear Deflection Response of Lateral Brace Member with Gusset Plates of Different Thicknesses (GP – Gusset Plate)

In the experimental study, WT 5×22.5 sections were used for top lateral braces and pipe sections were used for the internal K-frames. Because of the symmetry of the pipe section, the connection eccentricity effect was minimized in the K-frames. Therefore, the connection eccentricity of WT sections was investigated further. The top lateral truss diagonal was connected with the top flange of the tub girder using a bolted connection, as shown in Figure 4-34. The centroid axis of the lateral brace is located 1.13 in. below the bottom side of the top flange.

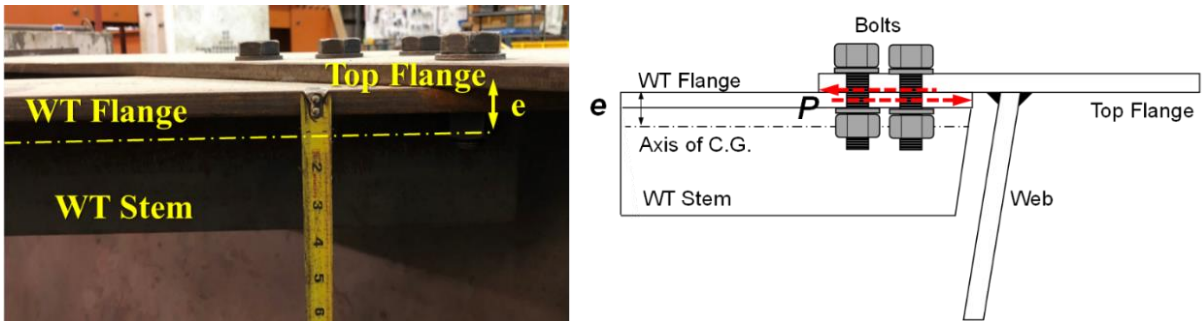

Figure 4-34 Top Lateral Brace Connection Details in the Test Specimen

From element-level analysis of a single diagonal panel under shear, shown in Figure 4-33, it is clear that connection eccentricity has a significant effect on the shear stiffness of the truss panel. However, this effect needs to be investigated on the overall response of the tub girder. To study the influence of bracing connection details, FE models with different levels of modeling details were prepared. A simplified model used beam elements to model the bracing components and a refined model used shell elements to model the bracing components. These models are shown in Figure 4-35. The beam-element brace is connected to the top flange by sharing common nodes with the shell elements. The shell element brace is connection with the top flange by defining a physical tie constraint to simulate the connection.

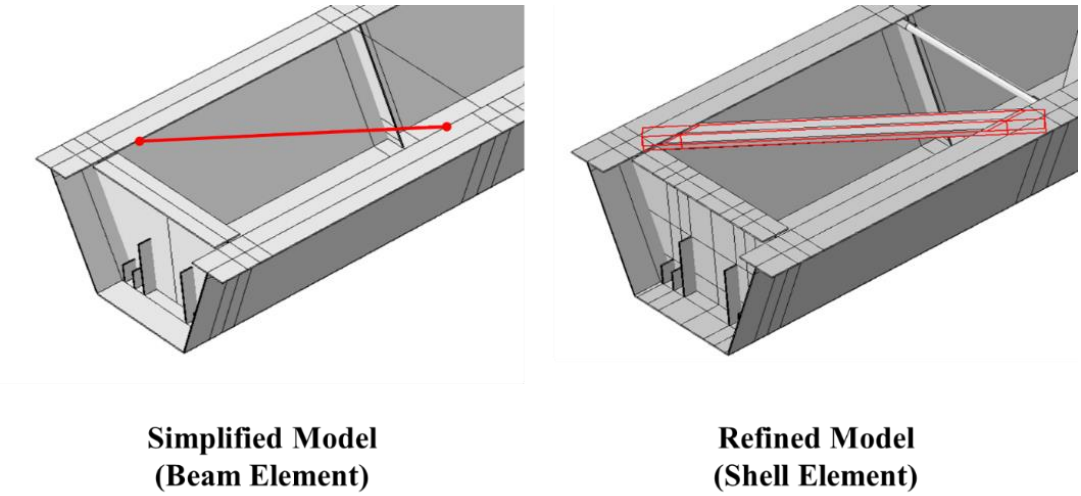

Figure 4-35 FE Models with Different Bracing Connection Details

Figure 4-36 presents the load vs. secondary moment for one of the top lateral truss panels during a lateral load test with three truss diagonals at each end for the lower-slope specimen. Both refined and simplified FEA results are compared with the experimental response. Both experimental and FEA results confirm the existence of the P-δ effect on the top lateral braces. The experimental response lies between the refined and simplified FEA results.

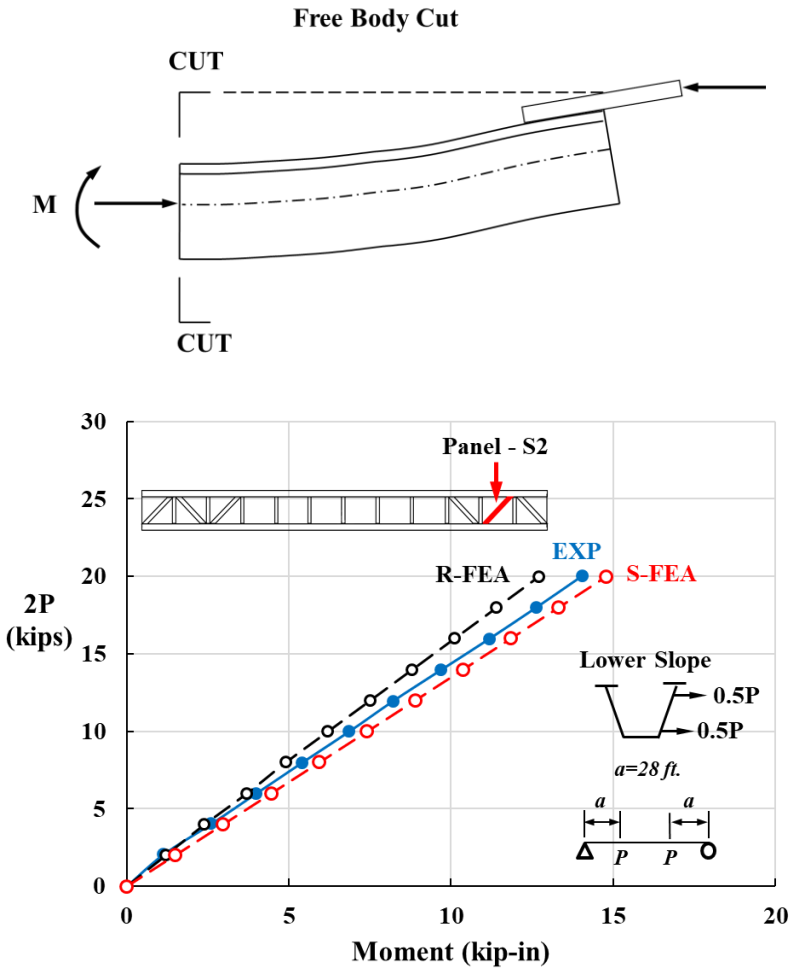

Figure 4-36 Load – Secondary Moment Response on the Lateral Brace

Figure 4-37 shows the global lateral load-deflection response at midspan. The refined FEA with shell elements used to model the braces shows an almost identical load deflection curve as the experimental data, while simplified FEA gives a more flexible response. Modeling the bracing using beam elements can lead to overestimating the system stiffness.

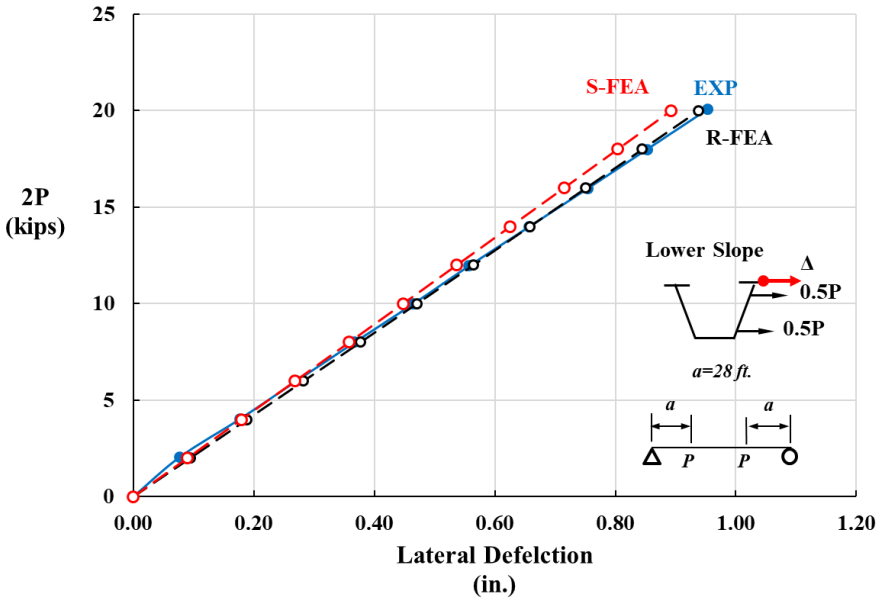

Figure 4-37 Comparison of Load-Maximum Lateral Deflection using simplified and Refined Models for the Braces

Three important factors that could significantly impact the FEA predictions have been identified through the validation of FE models. Following the same procedure of examining the three factors, FEA results has been validated based on the experimental data from various test results. A summary of comparison between measured data and FEA results can be found in Appendix D.

4.4 Parametric FEA Studies on Steel Tub Girders with Proposed Details

To further evaluate the structural response of steel tub girders with the proposed details, a series of parametric FEA studies were undertaken. Using FE modeling techniques validated by the large-scale experimental studies, the intent of the parametric FEA studies was to examine a wide range of tub girder configurations that may be used in actual field applications. This section documents the parametric FEA studies performed on tub girders with different proposed details. Results are presented to show the potential impact on the behavior of the system.
The following parameters were considered:

- Bridge configurations – span lengths, horizontal curvature, simple versus continuous spans.
- Girder Proportions – girder depth, span, web and flange plate sizes, flange offset, and web slope.
- Loading Conditions – Partial versus full placement of the concrete deck to evaluate potential controlling conditions;
- Top lateral truss layouts – working lines of braces intersecting versus offset working lines, partial panels of the top lateral truss (only for straight and mildly curved girders).
- Internal K-frame layouts.

The above parametric studies were carried out on non-composite girders simulating construction conditions. The analyses in these cases consist of a second-order elastic analysis of the girders focusing on stability and other performance criteria important during the construction phase. In addition to these analyses, the other variable that was considered is the impact of tub girder web slope and tub girder spacing on the live load distribution among girders compared with restrictions from the AASHTO empirical live load distribution equations.

4.4.1 Prototype TxDOT Steel Tub Girder Designs

Steel tub girder systems have been commonly used on highway bridges throughout the State of Texas. Two prototype TxDOT steel tub girder designs were selected for this parametric study and are shown in Figure 4-38 and Figure 4-39. The first prototype [Figure 4-38] is a shallow tub girder, similar to that used for the FM 3267 Underpass at IH35 in Waco, Texas. The second prototype [Figure 4-39] is a more typical tub girder, similar to that used at the interchange of IH45 and Beltway 8 in Houston. In this study, these two prototype sections are referred to as TUB36 and TUB90, where the 36 and 90 refer to the nominal web depth in inches. While the shallow section TUB36 may be more appropriate for straight and short span bridge girders, the typical section TUB90 are more suitable for long span and horizontally curved systems.

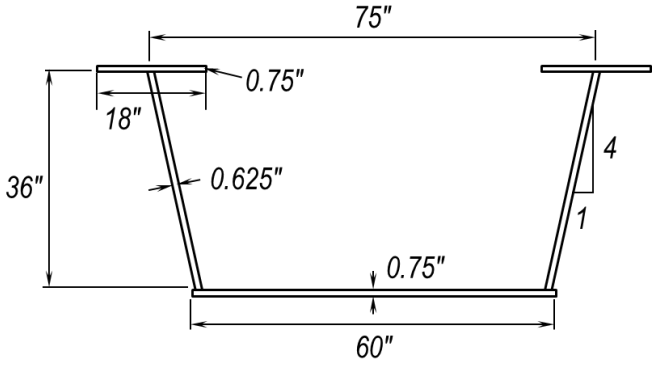

Figure 4-38 Prototype Tub Girder Cross Section - TUB36

Table 4-1 - Span and Bracing Details for TUB36

Span Arrangement	4 Simple Spans
Span Length (ft.)	45-100-100-65
Top Lateral Truss	WT 6×20
Typical Panel Length (ft.)	9 ft.
Internal K-frame	L 3×3×1/2

Following the nomenclature defined previously, the first selected prototype section is designated as TUB36 which has a nominal web depth of 36 in. The bridge is designed as a straight

4-span simply supported straight shallow tub girder system. The dimensions of the mid-span cross section of the shorter spans (45 ft. and 65 ft.) are shown in Figure 4-38. For longer spans, 1 in. thick plates are used for both top and bottom flanges. The span & bracing information are given in Table 4-1.

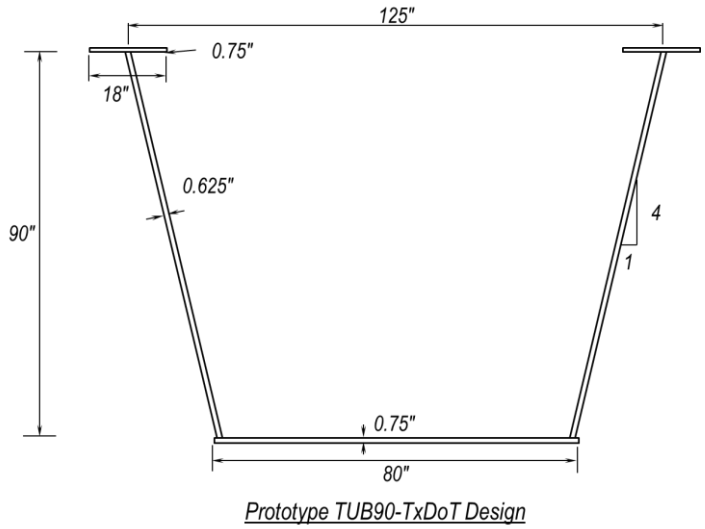

Figure 4-39 Prototype Girder Cross Section for TUB90

Table 4-2 - Span and Bracing Details for TUB90

Span Arrangement	1-Simple Span
Span Length (ft.)	160
Horizonal Radius of Curvature (ft.)	900
Top Lateral Truss	WT 8×20
Typical Panel Length (ft.)	10 ft.
Internal K-frame	L 4×4×5/16

The TUB90 section has a nominal depth of 90 inches. The girder system is a typical tub girder system used at highway interchange direct connectors. The dimensions of the mid-span cross section in the positive bending region is shown in Figure 4-39 and span & bracing information are given in Table 4-2.

4.4.2 Selected Design Parameters

The selected variables and their ranges for the parametric studies are shown in Figure 4-40 and listed in Table 4-3.

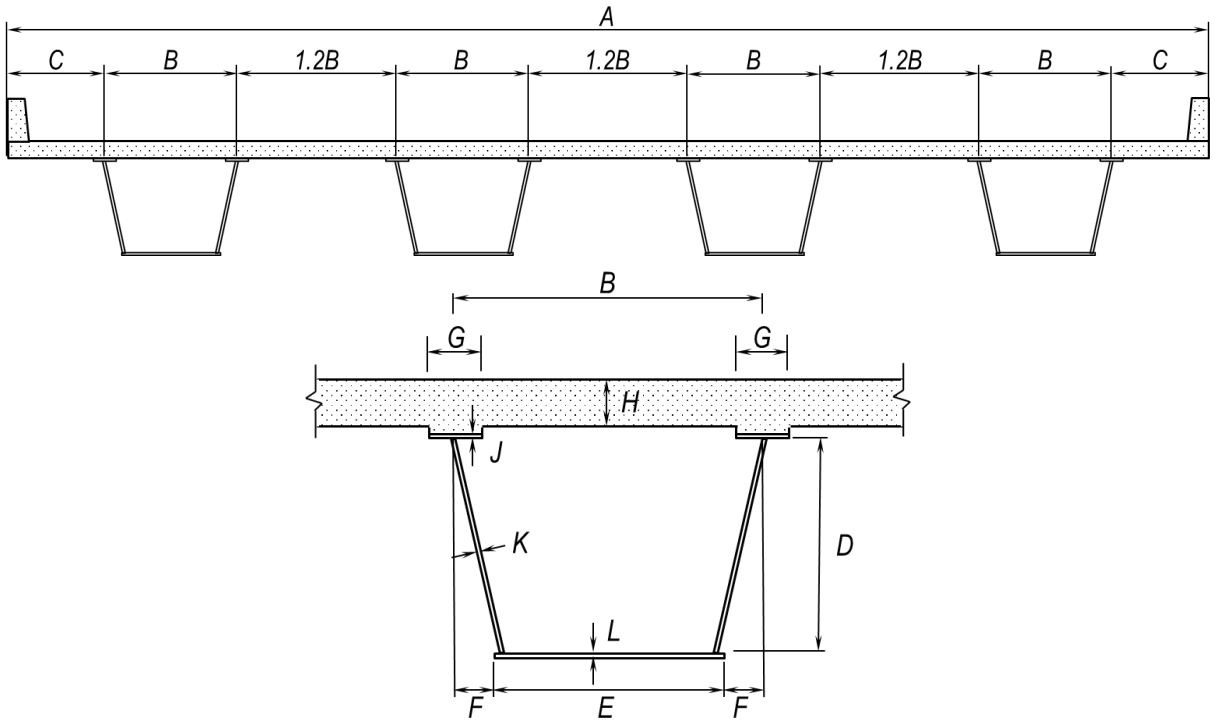

Figure 4-40 Parametric Bridge and Girder Cross Section

Table 4-3 - Design Parameters

Variables	Descriptions / Selected Values
Specification & Codes	AASHTO LRFD Specifications 2017 TxDOT Bridge Design Manual 2015
Concrete Deck Width A	Varies with number of girder lines
Concrete Deck Thickness (in.)	9.5
B-Girder Width (in.)	75 for TUB36 and 125 for TUB 90
C – Deck Overhang Width	60% of Girder Width B, less than 6 ft.
D - Girder Depth (in.)	36 and 90
Girder Spacing	120% of Girder Width, less than 10 ft.
E through L	Varies for TUB 36 and TUB90
Span to Depth Ratio (L/D)	25,30,35,40 (35,40 only considered for continuous girder systems)
Top Flange Configuration	Centered, fully offset, partially offset
Web Slope (V:H)	4:1, 3:1, 2.5:1
Horizontal Radius of Curvature (ft.)	Infinity, 2500 ft, 1800 ft., 1200 ft., 800 ft.
Span Arrangement	simple span -1 continuous span – 2 continuous span – 3
Loading Conditions	full deck placement – simple span partial deck placement – continuous span
Top truss layouts	Full-length and Partial-length
Internal K-frame layouts	Every panel, every two panels and every three panels

4.4.3 Modeling Assumptions and Considerations

4.4.3.1 Critical Geometric Imperfection

Both global and local geometric imperfection were included in the parametric FEA studies. The magnitude and pattern of imperfections used in the analyses are shown in Figure 4-41 and Figure 4-42.

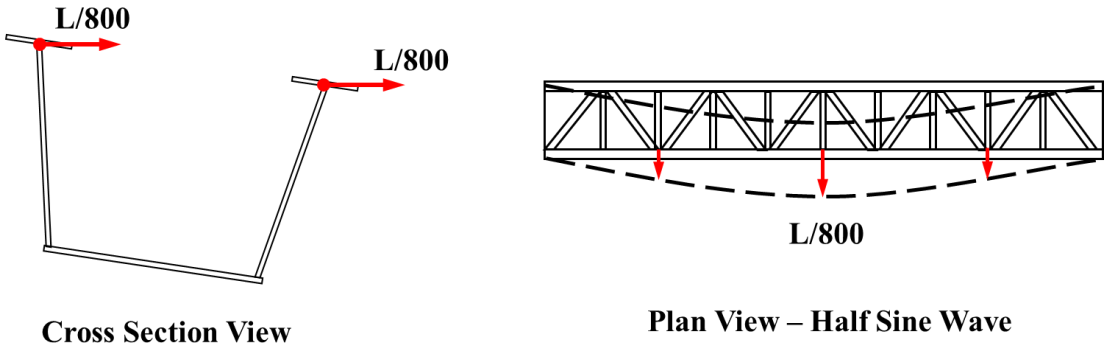

Figure 4-41 Global Geometric Imperfection Considered in Parametric Studies

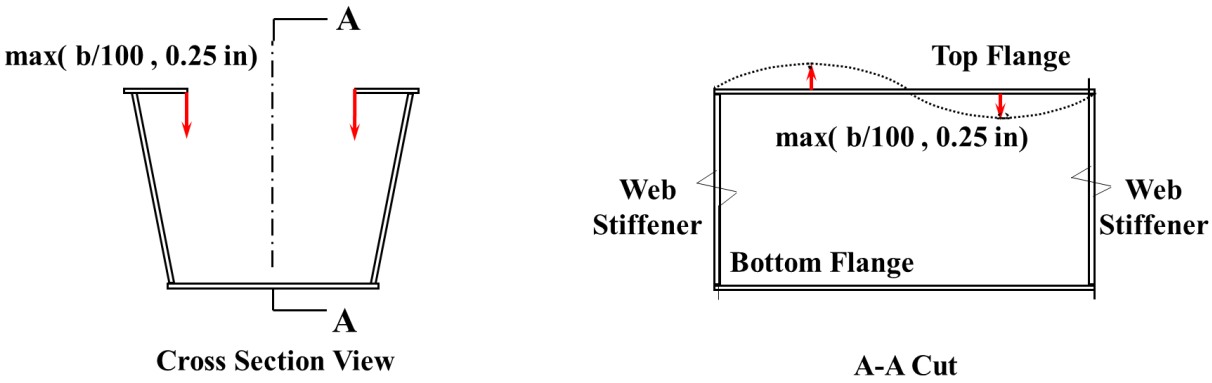

Figure 4-42 Local Geometric Imperfections Considered in Parametric Studies

4.4.3.2 Support Conditions

For FE models with a single girder, support conditions were modeled as shown in Figure 4-43 and Figure 4-44. Two lateral supports were provided on the top and bottom flange-web junction to prevent twist. For multiple girder models with end diaphragms explicitly modeled, the vertical and lateral translation restraint for each girder was applied at the mid-point of the bottom flange. The longitudinal restraint was only provided on one of the girders to reflect the fact that only one guided bearing is typically used in practice. Also, this can reflect the warping restraint provided by the plate diaphragm. Warping free conditions were assumed in the analysis to provide conservative assessment of the stiffness of the girder.

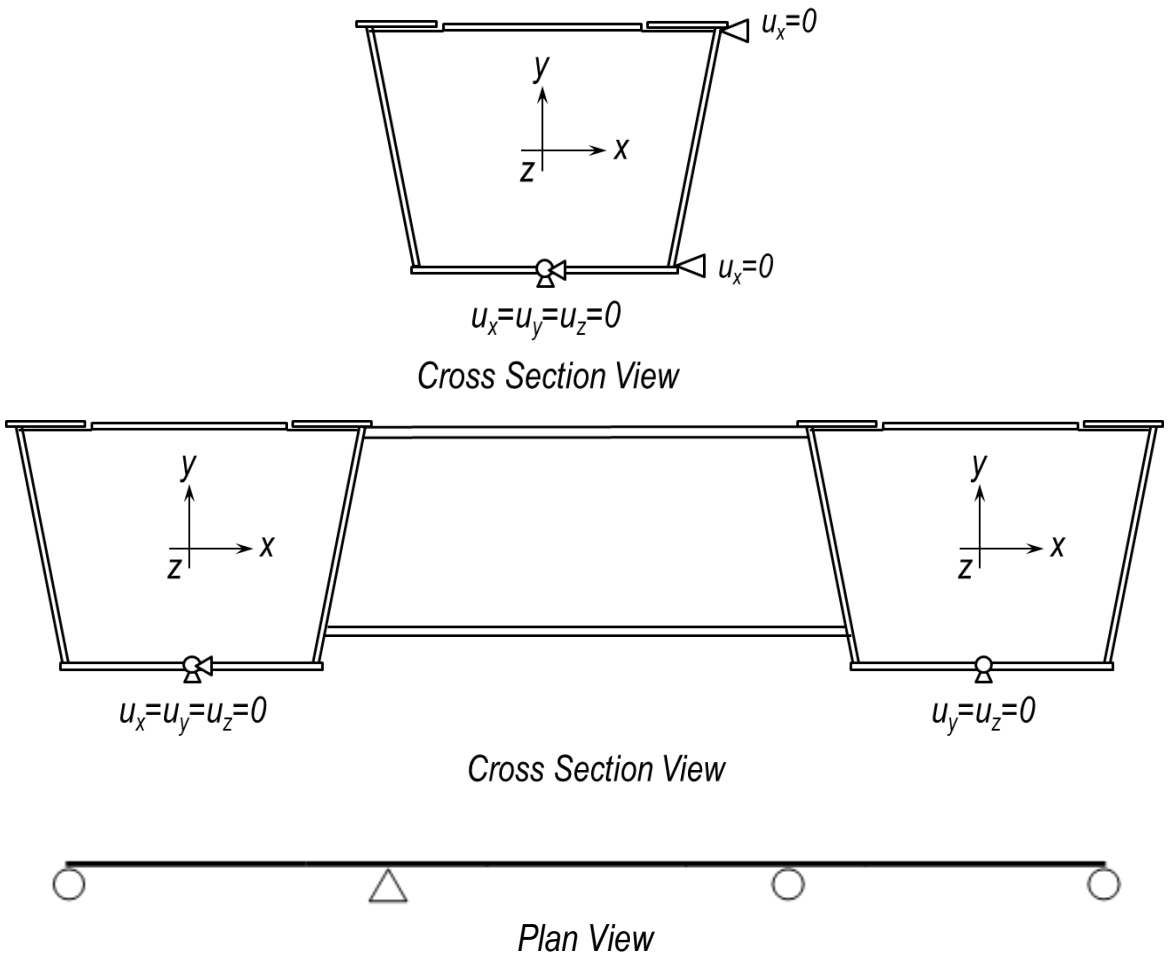

Figure 4-43 Support Conditions for Single and Multiple Tub Girder Models

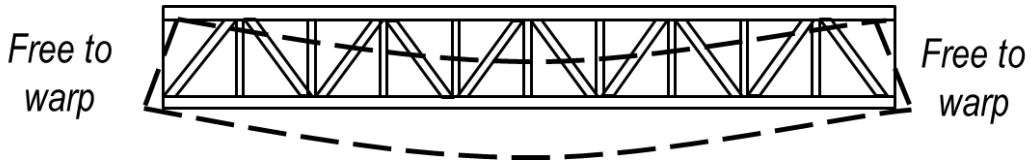

Figure 4-44 Warping Conditions for Tub Girder Models

4.4.3.3 Loading Conditions

During construction, any load applied before the concrete deck has hardened is assumed to be carried by the steel section alone. The loads on the tub girders during construction consist of the girder self-weight and the weight of the concrete slab and permanent metal deck forms. In the FE models, the weight of the concrete and other construction loads is applied to the girders in the form of distributed traction loads (kips/in^2) applied on the top flanges. The weight of the reinforced concrete is assumed to be 0.15 kips/ft^3. An additional 50 lb/ft^2 deck load is added to simulate loading from the construction workers and equipment. This load is proportioned between the top

flanges based on the layout of the concrete deck. The deck overhang is 60% of the spacing between adjacent girders as shown previously in Table 4-3.

As a result, the exterior flanges have higher loads than interior flange as shown in Figure 4-45.

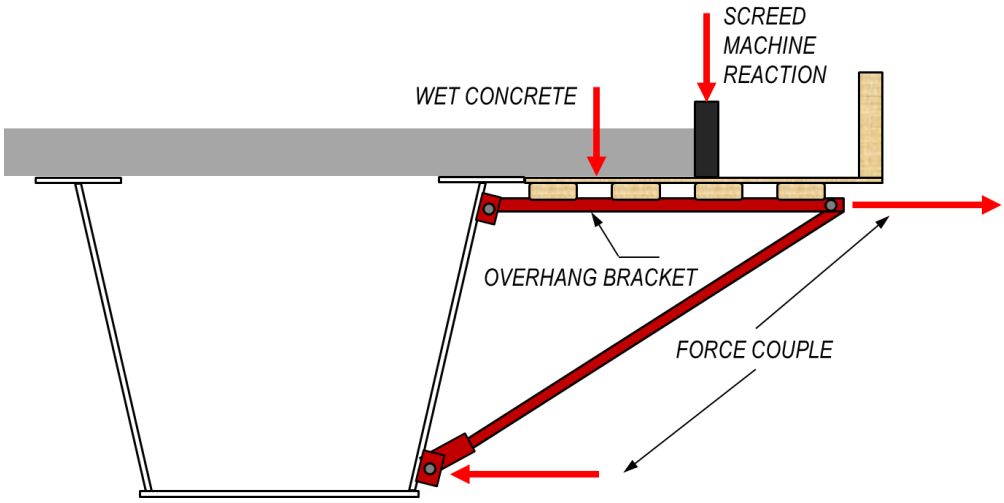

Figure 4-45 Sketch Showing Deck Overhang Bracket Loading

The construction loading was applied in two steps. The self-weight of the steel girder was applied in the first step - GRAVITY. Then, the remaining portion of the construction loading was applied in the second step – CONSTRUCTION. For simple span systems, full deck placement was assumed so that the load is applied on the girder all at once in one step. For continuous spans, staged construction load was considered. The assumed load scheme is such that positive moment regions were loaded first, followed by load applied in the negative moment regions [Figure 4-46].

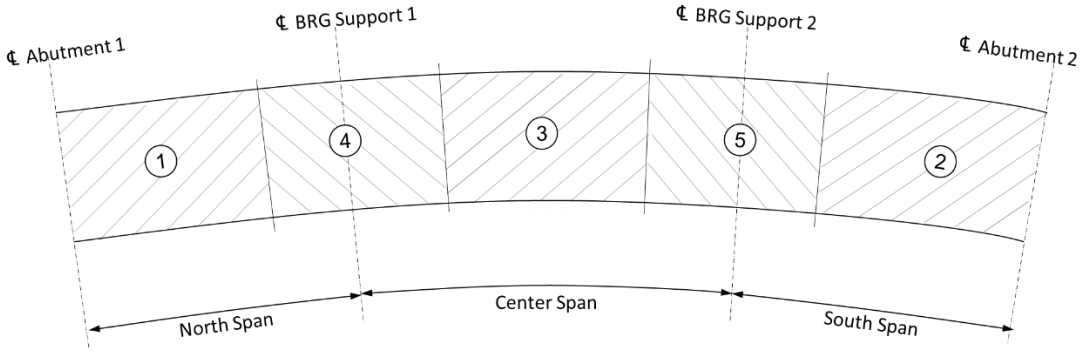

Figure 4-46 Deck Pouring Sequence for Three-span Tub Girder System

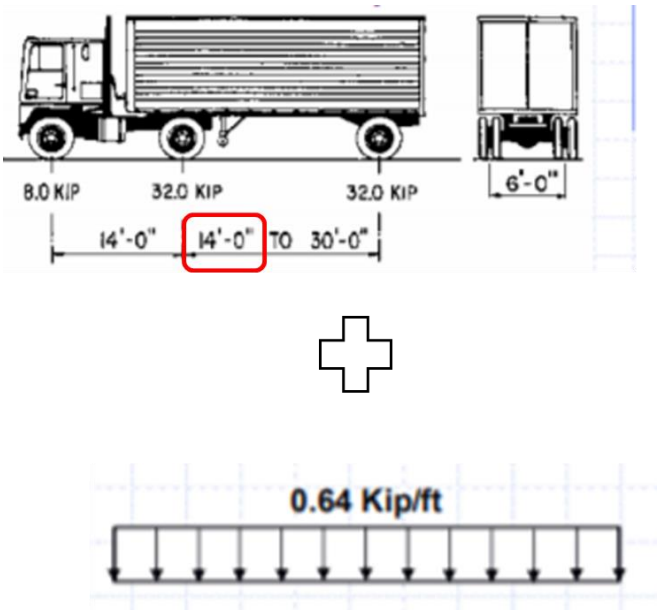

Figure 4-47 Standard Truck Loading HL-93 for LLDF analyses

For the study of the effect of web slope on live load distribution factors, the standard HL-93 load was considered [Figure 4-47]. Based on AASHTO, it was defined as the combination of either the standard truck load or design tandem with lane load. The lane width is taken as 12ft.

4.4.3.4 Bracing Details

In the parametric studies, beam elements were used to model the bracing members. The connection between the brace and top flange was modeled by making having them shares the same node. By default, shell element nodes are located at the mid-thickness of the shell, and beam element nodes are located at the center of gravity of the cross-section. Hence, if the shell and beam elements share the same nodes, the shell and the beam brace will overlap unless the beam cross-section is offset from the location of the node. However, this does not mean the connection eccentricity is not accounted for in the model. ABAQUS provides the option to specify that the section center of gravity is located at some distance from the origin of the section's local coordinate system, which is located at the element's nodes. This approach does not require the input for any specific cross-section dimensions. However, it requires definition of cross-sectional properties, including moment of inertia, total area and torsional constants.

4.5 Effect of Partial-length Top Lateral Truss on the Behavior of Steel Tub Girders during Construction

Experimental results, described in Chapter 3, suggested that partial-length top lateral bracing is a viable alternative for straight and mildly horizontally curved girders. Parametric studies were conducted to further confirm this finding and evaluate the effects of partial top lateral bracing on the stiffness of steel tub girders with different girder geometries and configurations. The TUB36 and TUB90 FE models were evaluated with different amounts of partial-length top lateral bracing. In this study, various span-to-depth (L/D) ratios and different horizontal radii of curvature were considered as listed in Table 4-3 (only R=2500 ft. was considered for curved tub

girder system). The cross-section dimensions of each prototype section were re-proportioned accordingly to satisfy the load demand. Details are provided in Appendix D. The number of top lateral truss panels for each girder was set at 16 and 10 panels per span, for TUB 36 and TUB 90, respectively. This was kept constant in the study. Following current engineering practices, K-frames were placed every panel point for all the cases presented in this section. These geometrical configurations were the starting point to analyze straight and horizontally curved girders with different amounts of partial top lateral bracing. The minimum levels of bracing for adequate performance during construction for both girder systems was then evaluated.

Two main parameters of interest were examined to evaluate the load-deflection response of the prototype steel tub girders in the analytical study. These were the lateral displacement of the top flanges (δ) and angle of twist of the cross-section (β). The results were normalized by maximum allowable displacement and section twist defined for this study. In this study, a limitation of L/1000 is defined for lateral displacement of the top flange based on the maximum out-of-straightness fabrication tolerance specified in the AISC Code of Standard Practice (2005) for straight compression members. Additionally, one degree of twist was considered acceptable in the analysis of results herein.

FEAs were first carried out on the straight girder cases with various amount of top lateral bracing to identify the minimum required top lateral bracing to satisfy the admissible requirements described above. The layout of top lateral bracing varies from non-braced to fully braced cases. Figure 4-48 shows the sample lateral displacement responses of the TUB90 (L/D=25) with three different layouts of top lateral bracing. i.e., three diagonals (0.38L) at each end, four diagonals (0.5L) at each end and a fully braced system (1.0L). The X-axis of the plot shows the lateral displacement of top flange normalized by L/1000 (δmax=2.60in), while the Y-axis shows the bending moment normalized by the estimated construction moment described in section 4.4.3. In the plot, the different cases are labelled based on the percentage of braced length with respect to the span length of the girder. In Figure 4-48, the minimum amount of bracing required not to exceed the admissible lateral displacement (1.0 in the X-axis) is 50% of bracing (0.5L) under the assumed construction demands (1.0 in the y-axis). Beyond this case, the girder starts to exhibit larger deformations. Similarly, Figure 4-49 shows the sectional twist responses of the same girder where the maximum allowable twist of 1 degree is not exceed with 50% of top lateral bracing, Similar response has been observed for straight steel tub girders with partial top lateral bracing for both simple and continuous span system with different L/D ratios.

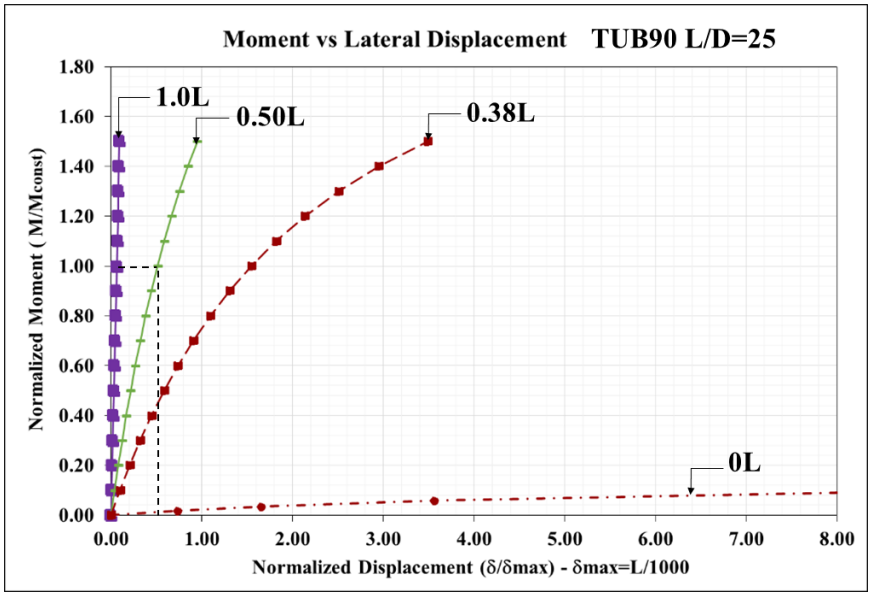

Figure 4-48 Bending Moment vs Lateral Displacement of Top Flange for TUB90 (L/D=25)

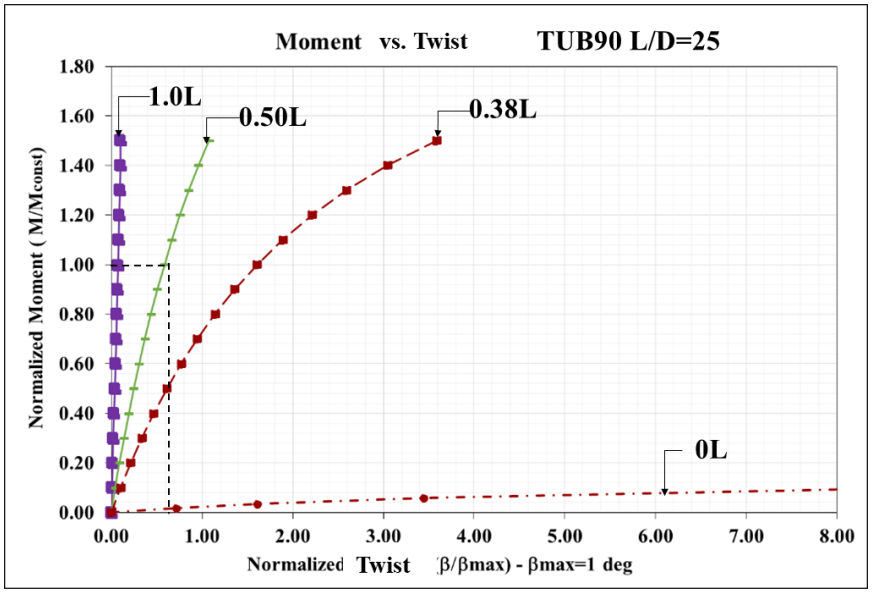

Figure 4-49 Bending Moment vs Twist Angle for TUB90 (L/D=25)

One of the effects of removing lateral truss panels is the amplified lateral bending effect of unbraced top flange. Figure 4-50 shows the normalized lateral displacement of the top flange along the length of the girder for TUB90 (L/D=30) with the same three top lateral truss layouts. Clearly, the lateral displacement of the girder increases greatly after removing more than 50% of the top lateral bracing, which results in high lateral bending of the top flanges.

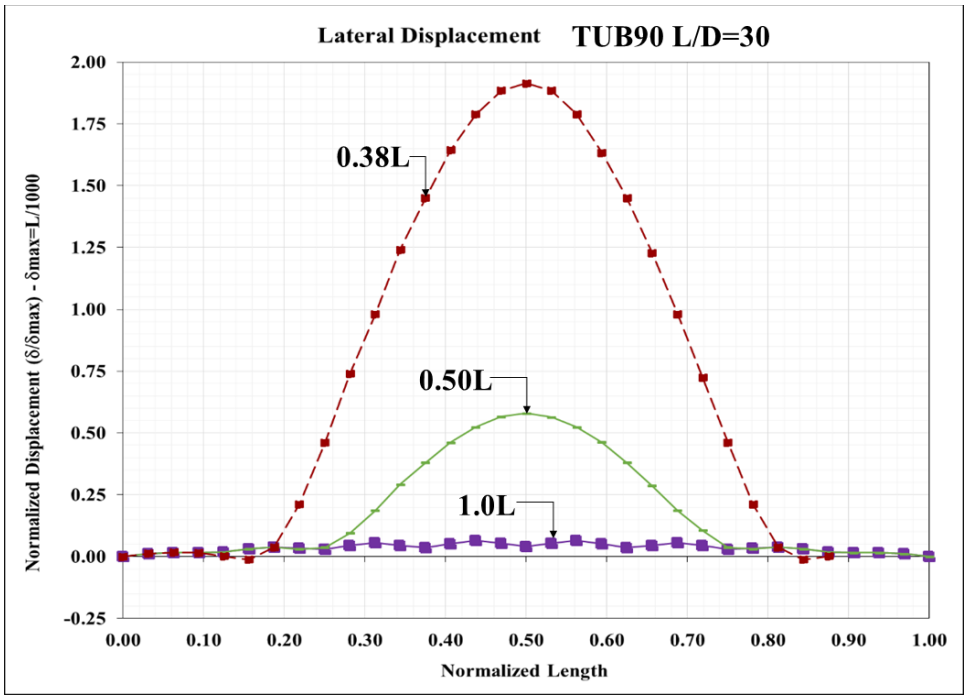

Figure 4-50 Lateral Displacement of Top Flange along the Length of TUB90 (L/D=30)

Similar FEAs were performed to examine the possibility of using partial top lateral trusses on horizontally curved tub girders. As a starting point, the curved girders were evaluated with 50% of partial top lateral bracing for different curvatures. Two initial radii of curvatures were considered in the analysis, i.e.,1800 ft. and 1200 ft. However, none of the girders was able to satisfy the admissible lateral displacements and section twist. Next, analyses were conducted with the 50% bracing held constant, while searching for an upper bound on radius of horizontal curvature that would satisfy these requirements. During preliminary analysis, it was observed that not only the clear span but also the radius of curvature of the tub girders have influence on the torsional response of the girders and in the lateral bending of the unbraced top flanges. Additionally, it was found that partial top lateral bracing permits more lateral bending of the unbraced top flanges. As result, the lateral bending stresses induced in top flanges were calculated in a different way from current design practice in order to size top flanges. Thus, when using top lateral truss bracing, the top flanges within the unbraced length had to be resized because the lateral bending stresses induced in top flanges were higher that the yielding stress.

To resize the top flanges for the unbraced length, the lateral bending stresses in the top flanges were calculated differently from current design practices. Usually, the top flange is assumed to be discretely braced along the entire length and that the highest lateral bending stresses are created at bracing points. Consequently, the calculation of stresses is carried out only considering the unbraced length L_b as shown in the top of Figure 4-51. However, when top lateral bracing diagonals are removed from the center portion of the girder, the unbraced length of the top flanges for the lateral bending check is taken as shown in the bottom of Figure 4-51, with partial lateral bracing. This change of unbraced length produced a significant increase in lateral bending stresses on the top flanges for horizontally curved girders, which was not severe in straight girders. Chapter 6 presents an outline of the procedure to follow in order to resize the top flanges when

partial lateral bending is considered in the layout. The recalculated top flange dimensions are presented in Appendix D.

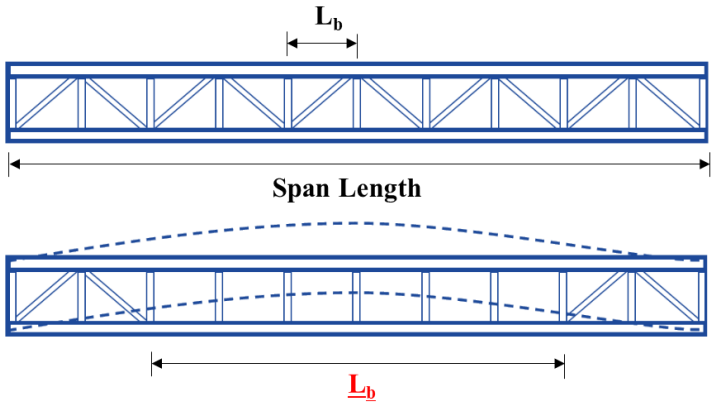

Figure 4-51 Unbraced Length for Lateral Bending Check with Partial Lateral Bracing

With top flanges sized to withstand the aforementioned lateral bending stresses, the prototype tall girder T90 was analyzed as simply supported girder with different span-to-radius of curvature ratios (L/R) in order to find and adequate L/R ratio that keeps the maximum Von Mises stresses in the top flanges below 80% of the nominal yielding stress. This analysis was performed in the T90 girder with different span-to-depth ratios (L/D= 20, 25, and 30). The higher stresses were observed at midspan and transition zones. Figure 4-52a and Figure 4-52b presents the maximum Von Mises stresses due to construction loads at midspan and at the transition zone, respectively, normalized by the nominal yield stress (Fy) versus span-to-radius of curvature ratios (L/R) for the T90 with the three previously mentioned L/D ratios. From these plots, it is observed that the girder with higher L/D ratio (L/D=30) yielded higher stresses in both regions, especially at the transition zone. At this L/D scenario, the L/R ratio equal to 0.09 yielded stresses lower than 70% and 80% of the nominal yielding at midspan and at the transition zones, respectively. This L/R ratio corresponds to a radius of curvature of about 762m (2500ft.).

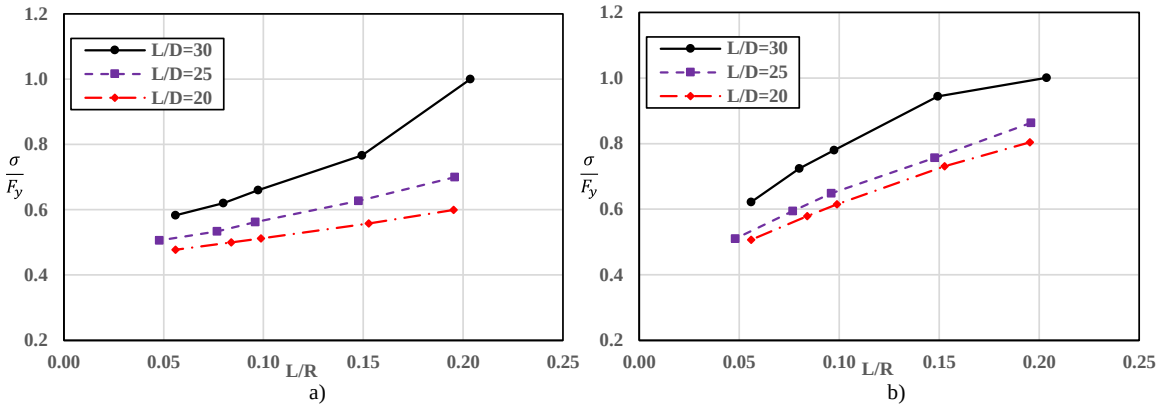

Figure 4-52 Maximum Von Mises Stress: a) Midspan, b) Transition Zone

After resizing the top flanges, the girders in this study were able to satisfy the response requirements for horizontal curvatures of 2500ft or higher. Figure 4-53 shows the bending moment

versus lateral displacement of the two span continuous TUB90 with L/D=30 and a radius of curvature equal to 2500 ft. In addition, the lateral displacement along the length of the 2-span continuous girder is presented in the Figure 4-54. Similar behavior was observed in the other curved girders except for the TUB90 with L/D=35 and 40 where the lateral displacements exceed 1.4 and 2.3 times the admissible value. However, they were able to satisfy the requirements with 60% of top lateral bracing.

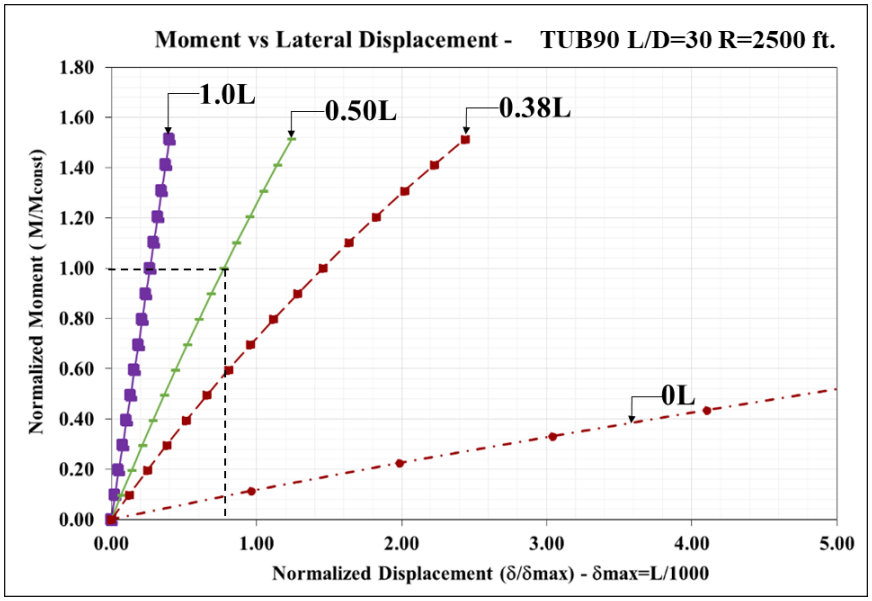

Figure 4-53 Moment vs Lateral Displacement – 2-Span Continuous T90 Girder with L/D=30

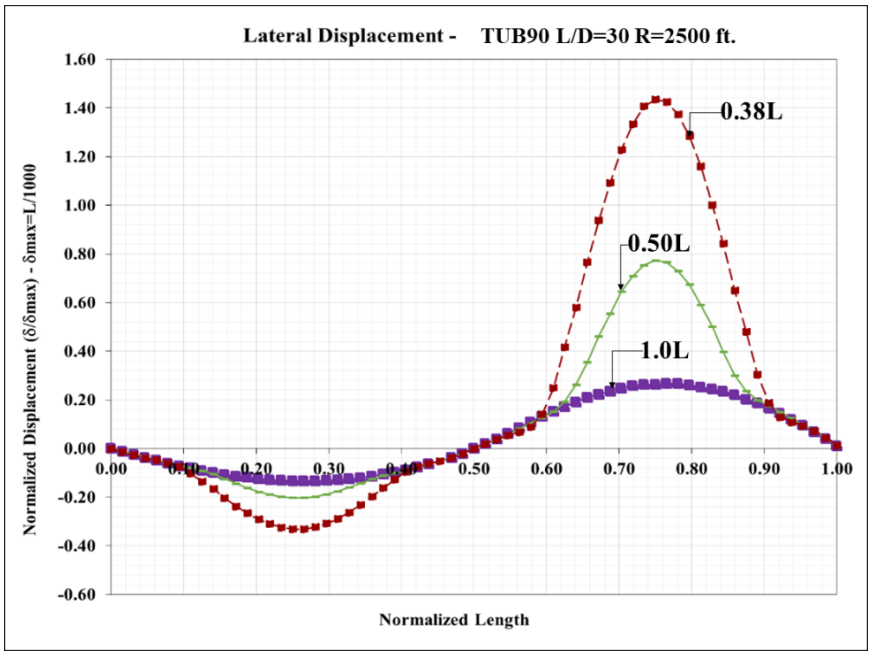

Figure 4-54 Lateral Displacement along the Length of 2-Span Continuous T90 with L/D=30

These analyses indicate that 50% partial top lateral bracing is a reasonable minimum amount of bracing to keep maintain admissible girder deformations during construction for straight and mildly horizontally curved steel tub girders with minimum radius of curvature of 2500 ft. The horizontally curved girders in this study showed acceptable response up to lengths of 216 ft. with 50% partial bracing. Longer lengths required additional top lateral bracing (60%) to maintain acceptable behavior.

Table 4-4 summarizes the normalized lateral displacements and twist angles produced due to construction loads for all the cases considered in this parametric study. For both prototype sections with single spans, the 50% top lateral bracing was effective to keep lateral displacements and twist angles under the admissible values assumed herein. Continuous systems were analyzed as well, which considered two and three span systems. It was found that the two-span system was more critical than the three-span system with larger lateral displacements and rotations. For example, the straight TUB90 with L/D=35 and 50% of top lateral bracing was analyzed with two and three spans. The 2-span system shown a maximum lateral displacement of 2.5 in, while the 3-span system had 1.9 in. Thus, the study focused on simply supported and 2-span continuous girders. For the continuous girder systems, partial deck placement was considered in order to identify the most severe loading case. For the 2-span system, the most severe scenario was when the concrete deck was placed in the positive moment region of one span while the rest of the girder had no concrete on top. Similarly, for the 3-span system, the most critical loading stage was when the concrete was placed in the positive moment region in the middle span with no concrete load on the rest of the girder. These comparisons can be found in Appendix D, which also contains all the plots corresponding to the results summarized in Table 4-4.

Table 4-4 - Summary of Results - Partial Top Lateral Bracing

						Normalized Displacement				Normalized Twist			
Section	**Radius**	**L/D**	**System**	**δmax (in)**	**βmax (deg)**	**1L**	**0.6L**	**0.5L**	**0.4L**	**1L**	**0.6L**	**0.5L**	**0.4L**
T36	Straight	20	1S	0.72	1.00	0.10	0.25	0.28	0.37	0.13	0.23	0.27	0.34
		25	1S	0.86	1.00	0.12	0.27	0.35	0.47	0.51	0.64	0.69	0.79
		30	1S	1.08	1.00	0.14	0.34	0.43	0.60	0.28	0.49	0.52	0.77
		35	1S	1.26	1.00	0.16	0.42	0.55	0.82	0.33	0.67	0.85	1.19
		25	2S	0.86	1.00	0.09	0.23	0.30	0.42	0.15	0.28	0.34	0.39
		30	2S	1.08	1.00	0.11	0.28	0.37	0.53	0.23	0.39	0.45	0.63
		35	2S	1.26	1.00	0.13	0.35	0.48	0.71	0.27	0.51	0.67	0.97
		40	2S	1.44	1.00	0.16	0.46	0.65	1.00	0.38	0.77	1.04	1.57
	2500ft	20	1S	0.72	1.00	0.13	0.26	0.32	0.42	0.13	0.23	0.27	0.35
		25	1S	0.86	1.00	0.17	0.33	0.41	0.55	0.23	0.36	0.43	0.58
		30	1S	1.08	1.00	0.24	0.46	0.60	0.83	0.32	0.57	0.71	0.96
		35	1S	1.26	1.00	0.36	0.68	0.91	1.36	0.44	0.87	1.10	1.74
		25	2S	0.86	1.00	0.14	0.29	0.37	0.50	0.18	0.30	0.36	0.50
		30	2S	1.08	1.00	0.22	0.41	0.53	0.72	0.25	0.46	0.59	0.79
		35	2S	1.26	1.00	0.19	0.39	0.53	0.77	0.29	0.54	0.71	1.00
		40	2S	1.44	1.00	0.43	0.76	1.03	1.50	0.47	0.91	1.26	1.92
T90	Straight	20	1S	2.02	1.00	0.03	-	0.40	1.06	0.06	-	0.36	0.97
		25	1S	2.30	1.00	0.06	-	0.51	1.55	0.07	-	0.59	1.61
		30	1S	2.59	1.00	0.06	-	0.58	1.98	0.10	-	0.71	2.24
		25	2S	2.30	1.00	0.04	-	0.34	0.83	0.07	-	0.42	0.95
		30	2S	2.59	1.00	0.05	-	0.44	0.99	0.08	-	0.51	1.10
		35	2S	3.17	1.00	0.07	-	0.81	2.33	0.13	-	1.10	3.08
		40	2S	3.60	1.00	0.08	-	0.88	3.35	0.17	-	1.30	4.35
		35	3S	3.17	1.00	0.05	-	0.61	1.20	0.10	-	0.85	1.64
	2500ft	20	1S	2.02	1.00	0.15	-	0.58	1.16	0.09	-	0.46	0.99
		25	1S	2.30	1.00	0.18	-	0.67	1.41	0.14	-	0.62	1.33
		30	1S	2.59	1.00	0.25	-	1.03	2.33	0.19	-	1.03	2.48
		25	2S	2.30	1.00	0.23	-	0.84	1.63	0.10	-	0.85	1.45
		30	2S	2.59	1.00	0.27	-	0.78	1.46	0.14	-	0.69	1.41
		35	2S	3.17	1.00	0.49	0.87	1.47	-	0.27	0.71	1.48	-
		40	2S	3.60	1.00	0.8	1.40	2.72	-	0.47	1.43	3.31	-

4.6 Effect of Internal K-frame Layouts on the Behavior of Steel Tub Girders during Construction

Internal K-frames are provided to control distortion of the cross section of tub girders. During the experimental study, it was found that the internal K-frames do not control lateral torsional buckling and that redistribution of forces between the internal braces and top lateral bracing is produced when the layout of K-frames is altered. Thus, a parametric study was conducted to define adequate K-frame layouts for straight and horizontally curved girders with full and partial top lateral bracing. For this part of the parametric study, not all the cases presented in Table 4-4 were analyzed because it was observed that many cases showed similar response. Instead, the most critical straight and curved girders with one and two spans were considered for this part of the study.

4.6.1 Effect of Various K-frame Layouts on the Stiffness of Steel Tub Girders During Construction

Torsional demands on straight tub girders are usually low and caused by eccentric loading during construction. Therefore, the number of K-frames can be significantly reduced in straight girders. For this analysis, K-frames were placed at every panel point, as well as every 2 and 3 panel points. The resulting systems have an alternating strut-only and internal K-frame panel along the length. Figure 4-55 shows the lateral displacement response for the straight TUB90 (L/D=30) with full top lateral bracing, and various K-frame layouts. The lateral displacement response of the tub girder is barely affected when K-frames are reduced from fully braced (K-frame every panel) to internal frames every two and three panel points. The reduction in lateral stiffness from the fully braced case to K-frames every 2 (or 3) panel points is about 4%. Similar trends can be found in the twist response of the girder, as shown in Figure 4-56. The reduction of torsional stiffness is around 7% for K-frames at every 2 and 3 panel points. The effect of removing K-frames does not have significant impact on the global lateral stiffness of the girder.

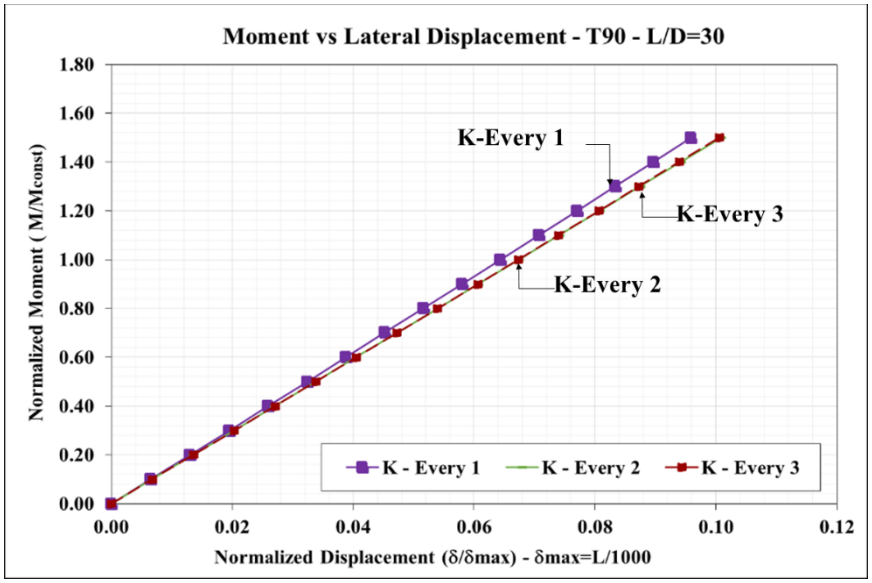

Figure 4-55 Moment vs Lateral Displacement – 1-Span TUB90 with L/D=30 – Various K-Frame Layouts

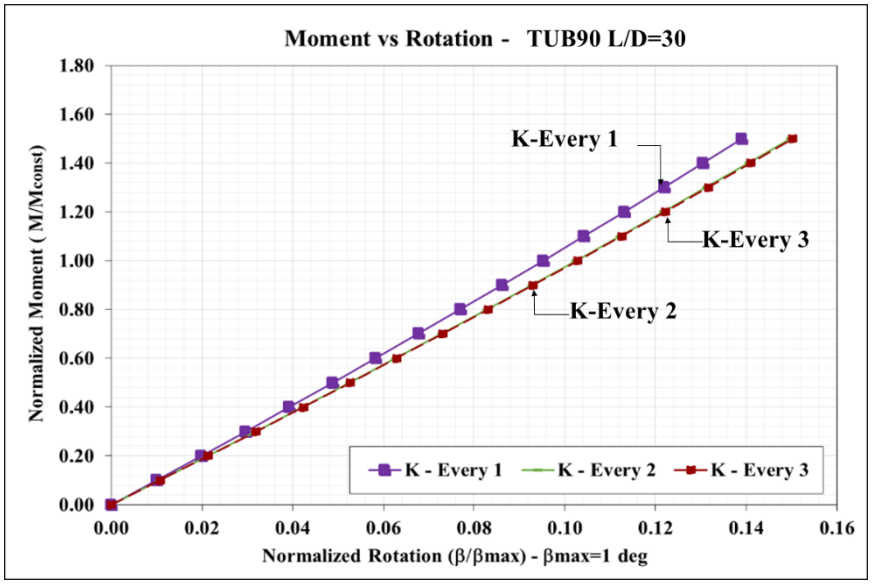

Figure 4-56 - Moment vs Twist - 1-Span Girder TUB90 with L/D=30 – Various K-Frame Layouts

This observation was further confirmed by FEAs performed on horizontally curved girders. In curved systems, higher torsional demands are induced by the horizontally curved geometry. TUB90 (L/D=30) with R= 800 ft was analyzed to evaluate the impact of different K-frame layouts. Full-length top lateral bracing was assumed. Figure 4-57 shows the torsional response of this girder with three different configurations of K-frames (every 1, 2 and 3 panel points). No change in torsional behavior was observed when the K-frame configuration was altered.

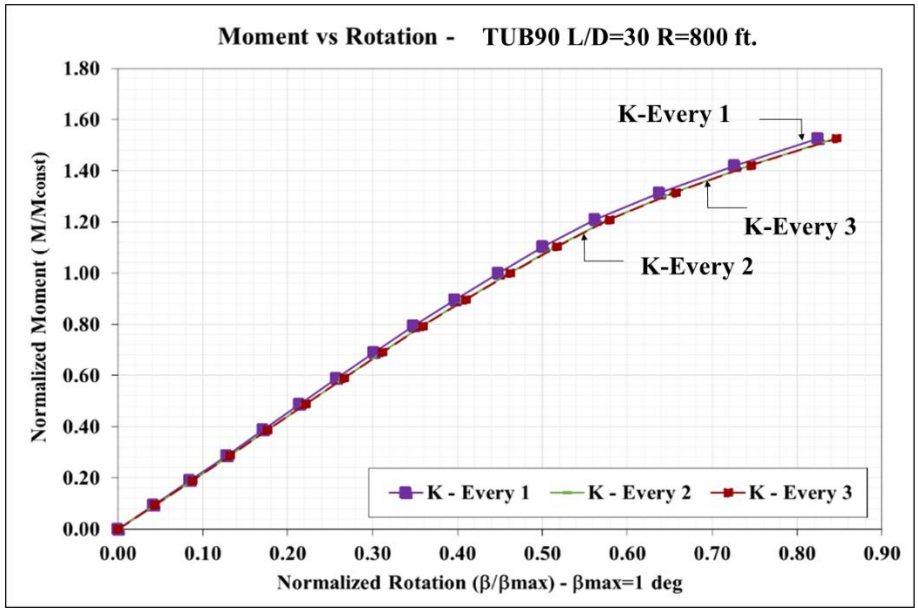

Figure 4-57 Moment vs Twist - 1-Span Girder T90 - L/D=25 – Various K-Frame Layouts

4.6.2 Effect of Various K-frame Layouts on the Brace Force Distribution in the Top Lateral Truss of Steel Tub Girders During Constructions

Based on the experimental results, the modification of the internal K-frame layout in straight tub girders affects the distribution of forces in the top lateral truss. The FEA results showed similar results. Figure 4-58 presents the force distribution in the diagonals of the top lateral bracing system. Higher loads are induced in these braces when K-frames are placed at every panel point. When reducing the number of K-frame diagonals to every two and three panel points, the loads drop up to 26% in the diagonals sustaining higher loads.

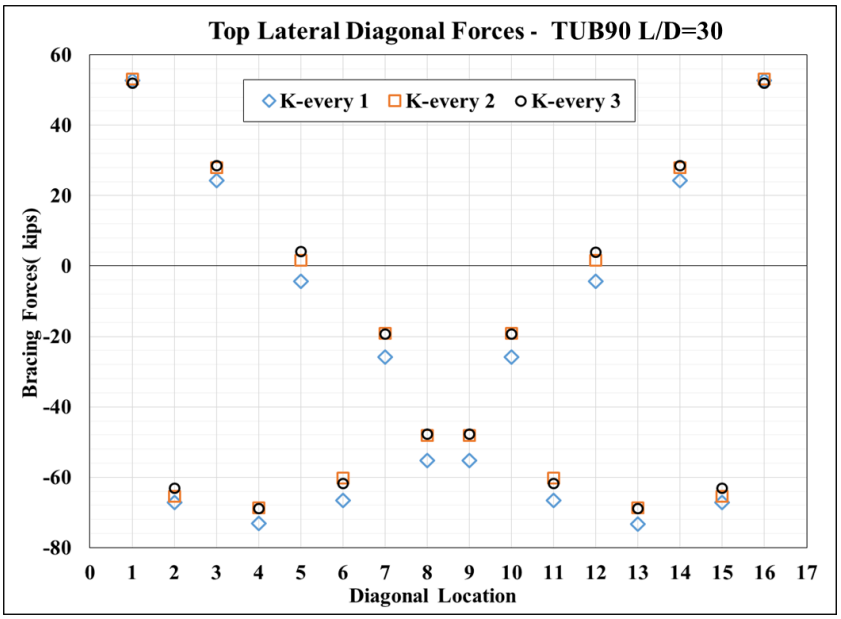

Figure 4-58 - Top Lateral Bracing Forces –1-Span TUB90 L/D=30- Various K-Frame Layouts

Similar variations in forces were observed in the K-frame struts (shared with the top lateral bracing), and the K-frame diagonals. Figure 4-59 shows the forces in one of the struts, for struts along the entire length of the girder. When K-frames were placed every two-panel points, the forces in the struts reduced up to 27% in comparison to the strut forces of the girder with K-frames at every panel point. In addition, when the the internal bracing layout was changed from two to three panel points, most of strut forces reduced up to 16%. Although only the force results for one strut were presented here, similar force distributions were found in the other strut.

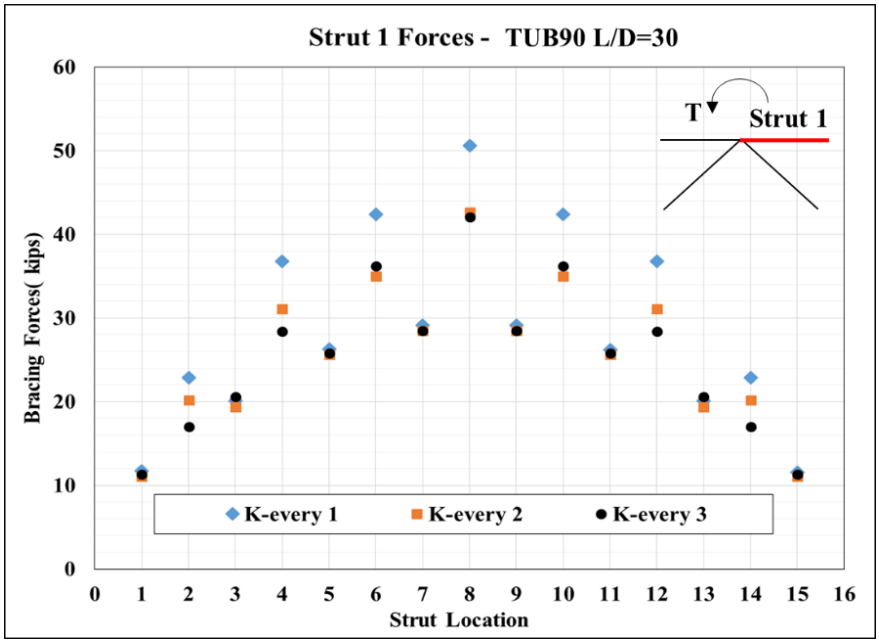

Figure 4-59 Strut 1 Forces – 1-Span TUB90 with L/D=30 - Various K-Frame Layouts

The reduction in strut forces also affected the forces induced in the K-frame diagonals. Figure 4-60 presents the forces for both diagonals of the K-frames. The most significant reduction in forces was observed when the internal frames were reduced from every panel to every two-panel points with a maximum reduction of around 90% of the forces. After changing the K-frame layout from every two to every three-panel point, the diagonal forces increased up to 40%. Despite this increase in forces, the diagonal forces of the latest configuration are still considerably lower than the configuration full of K-frames. In addition, for the configuration with K-frames every three-panel points, the diagonals in the panel points number 3 and 13 are carrying almost no load and the K-frames at and near midspan are the ones effectively working. This response implies that these non-effective diagonals may be removed, and the behavior will not be significantly affected. Even though those diagonals seem to be not effective in the torsional behavior of the girder, they may be important for construction process and it may not be practical to remove them.

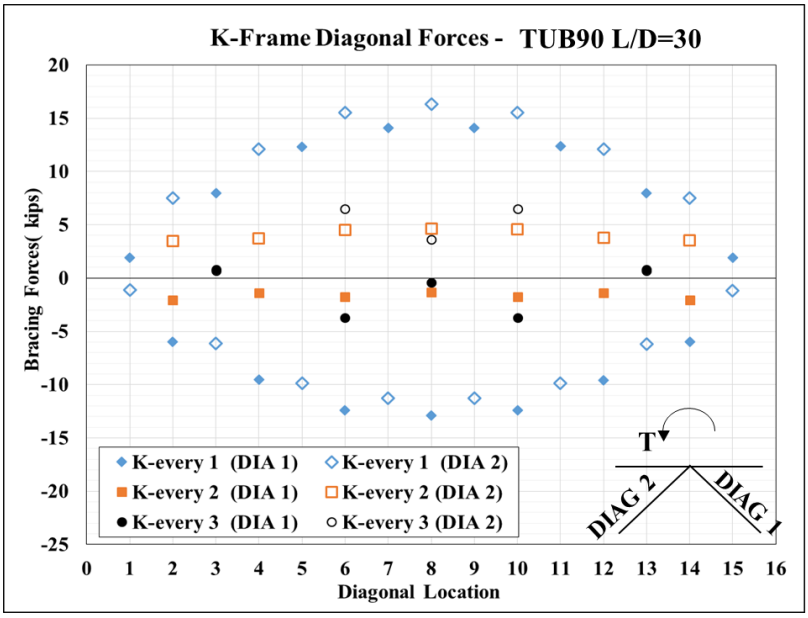

Figure 4-60 K-Frame Diagonal Forces – 1-Span TUB90 Girder L/D=30 - Various K-Frame Layouts

The parametric FEA studies confirm the experimental finding that internal K-frames are not effective in controlling lateral torsional buckling in straight tub girders since a reduction of these internal frames did not significantly affect the torsional response of the prototype tub girders in this study. In a 1-span tub girder, when the number of K-frames was reduced about 66% from 15 (every panel) to 5 (every 3 panels), the reduction in torsional stiffness was about 7%, the reduction in top lateral bracing forces was up to 25%, the reduction in strut forces was up to 27%, and the reduction in K-frame diagonal forces was up to 90%. Similar behavior was observed in a 2-span straight tub girder. For a 2-span TUB90 girder with L/D=40 and full top lateral bracing system, the reduction of K-frames from being placed every panel to every three-panel points showed a similar response than the one observed for the simply supported girder. The analyses showed the reduction in torsional stiffness was about 7%, the reduction in top lateral bracing forces was up to 28%, the reduction in strut forces was up to 21%, and the reduction in K-frame diagonal forces was up to 95%. Detailed results for this 2-span girder system are presented in Appendix D. Based on the parametric FEA studies, K-frames are not required to be placed every panel point for straight girders. Placing K-frames every 2 and every 3 panel points provides adequate torsional response and at the same time, reduces force levels in the top lateral truss members as well as in the K-frame members.

For curved girder systems, no significant change in top lateral forces was observed as the layout of internal K-frames was varied. Figure 4-61 and Figure 4-62 show the strut forces for the three K-frame configurations considered in the analysis. The maximum axial force in Strut 1 (Figure 4-61) drops about 40% at midspan when the K-frame configurations changes from every panel to every 2-panel points. When the configuration is changed from K-frames every 1 to every 3-panel points, the maximum strut force is found in panel points 4 and 12 and is about 80% of the maximum axial force in the first configuration.

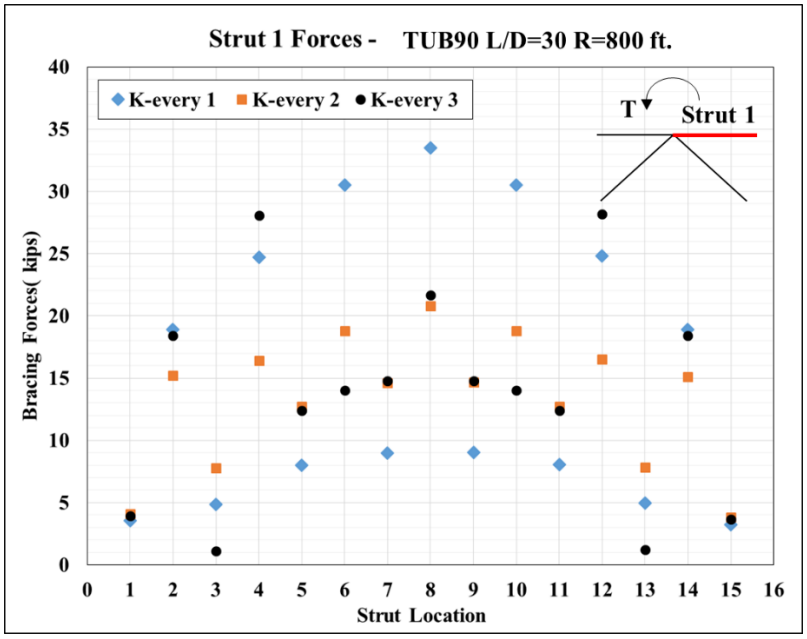

Figure 4-61 - Strut 1 Forces – 1-Span TUB90 Girder, L/D=30, R=800ft - Various K-Frame Layouts

Regarding the axial forces in Strut 2, the maximum forces are found at midspan. This force increases about 15% when the configuration of K-frames changes from fully braced to internal braces every two and 3 panel points. In addition to this increment in forces, the axial forces in almost half of the Strut 2 braces drop up to 50%.

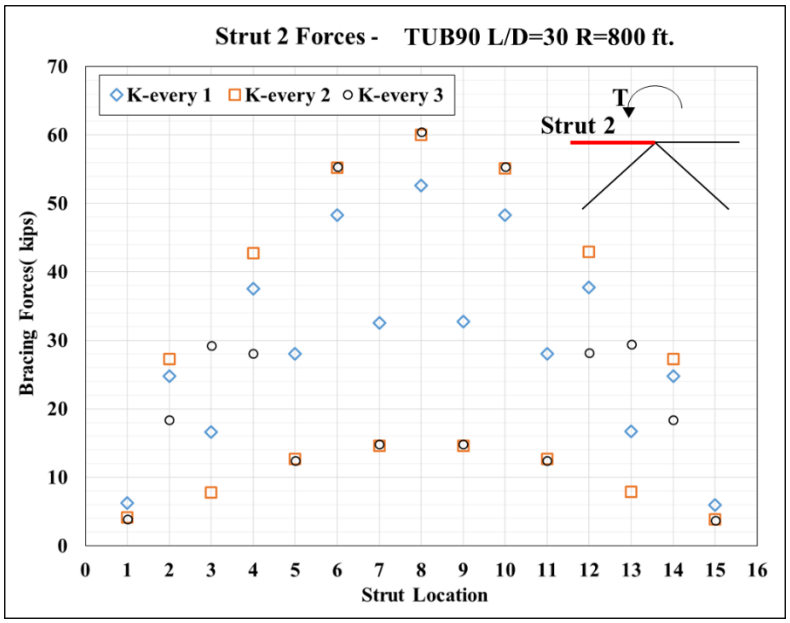

Figure 4-62 Strut 2 Forces – 1-Span TUB90 Girder, L/D=30, R=800ft - Various K-Frame Layouts

The most significant variation in axial forces due to the change in K-frame layout in curved tub girders was produced in the K-frame diagonals. Figure 4-63 presents the axial forces of the K-frame diagonals for the three layouts. The axial forces in these diagonals increased up to 120% and 145%, when the configuration of K-frames changed from fully braced to every two and three panel points.

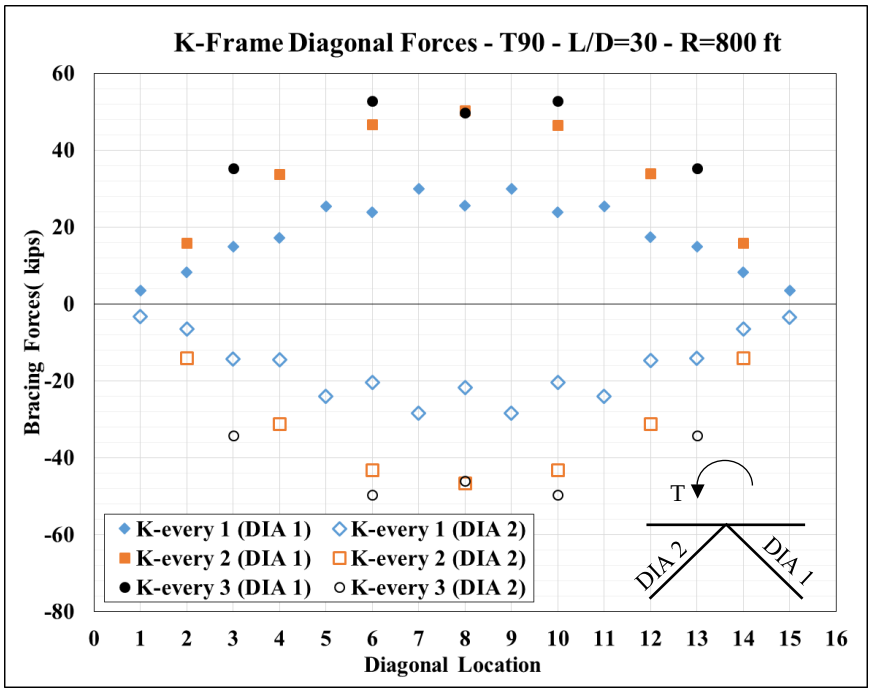

Figure 4-63 – K-Frame Diagonal Forces – 1-Span T90, L/D=30, R=800ft – 2 K-Frame Layouts

Horizontally curved girders with full top lateral bracing can use different configurations of K-frame bracing systems without affecting the global response of the girder. Placing K-frames every panel point will result in the smallest loads in the struts and diagonals. The number of internal K-frames can be reduced so that they can be placed every 2 or 3 panel points, but the K-frames should be sized to accommodate the increased loading demands.

4.6.3 Effect of Various K-frame Layouts on the Behavior of Steel Tub Girders Combined with Partial-length Lateral Bracing

Parametric FEA studies were also performed to evaluate the impact of the K-frame configuration in combination with partial top lateral bracing. The results for a straight 1-span TUB90 girder with L/D=25 and 50% of partial top lateral bracing are presented first. Figure 4-64 shows the torsional response of the girder with three different configurations of K-frames. The girder with K-frames every two panel points showed a reduction in the average torsional stiffness of about 13%; while the torsional response became highly nonlinear and dropped around 50% when the internal K-frames were placed every three panel points. With partial-length lateral bracing, internal K-frames contribute significantly to the torsional stiffness of the girder.

Figure 4-65 shows the layout of internal K-frames at one of the ends of the girder, as used in the analyses. The location of K-frames every two and every three panel points are represented by the number 2 and 3, respectively in this figure. As illustrated in this figure, a K-frame is located

at the end of the region of top lateral bracing when the K-frames are distributed every 2 panel points. On the other hand, a K-frame is not located at the end of the region of top lateral bracing when the K-frames are distributed every 3 panel points. This bracing detail had a significant impact on the torsional response of the girder.

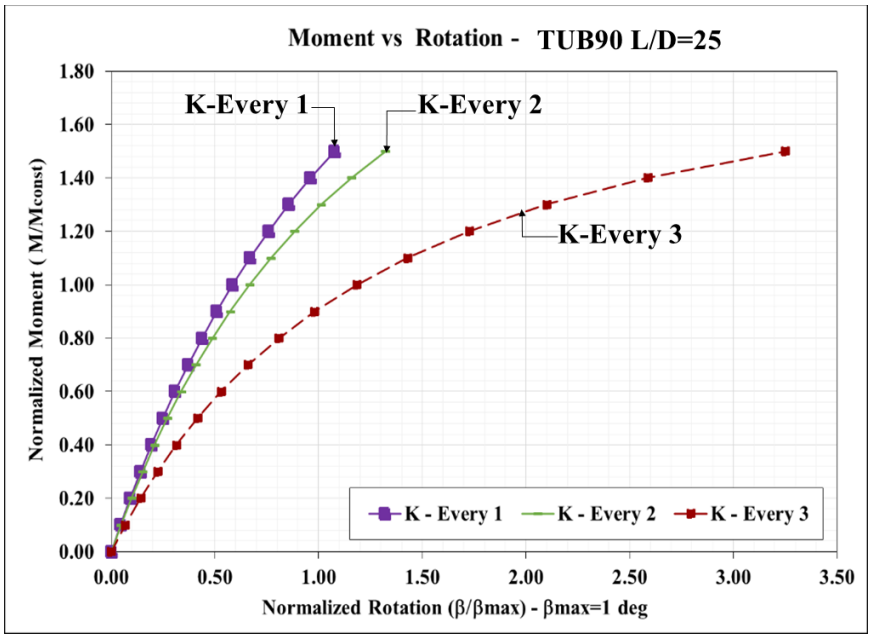

Figure 4-64 - Moment vs Twist - 1-Span Girder TUB90 - L/D=25 – Various K-Frame Layouts

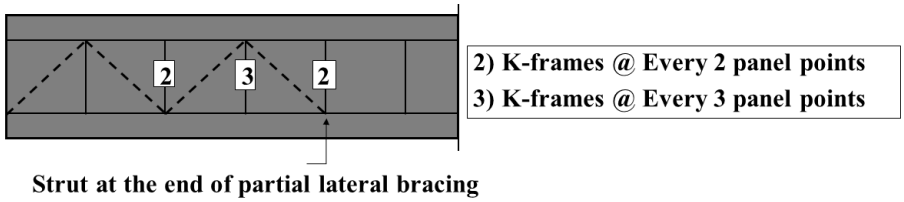

Figure 4-65 - Scheme of K-frame Location - 1-Span TUB90 Girder with L/D=25

The strut located at the end of the top lateral truss diagonals sustains large axial forces because of the partial top lateral bracing. This is a critical point where the tub girder transitions from a fully to a partially braced system, and the transfer of loads should be smooth to ensure adequate performance of the system. This is achieved when a K-frame is placed at the end of the partial top lateral bracing. To further explore this concept, two more K-frame configurations were evaluated. First, a K-frame was placed at the end of each zone with partial top lateral bracing, and K-frames were distributed at every two-panel points in the zone without top lateral bracing (K-Every 4-2 in Figure 4-65). Second, a K-frame was placed at the end of each zone with partial top lateral bracing and one K-frame at midspan (K- Every 4-4 in Figure 4-65). Figure 4-66 shows the torsional response of these two new K-frame configurations as well as the response of the girder with internal K-frames every two-panel points. The new K-frame layouts resulted in adequate torsional response of the girder even though they have equal or a smaller number of K-frames. Thus, when partial top lateral bracing is provided, the most critical locations to place K-frames are the end of the regions with partial truss diagonals and at midspan.

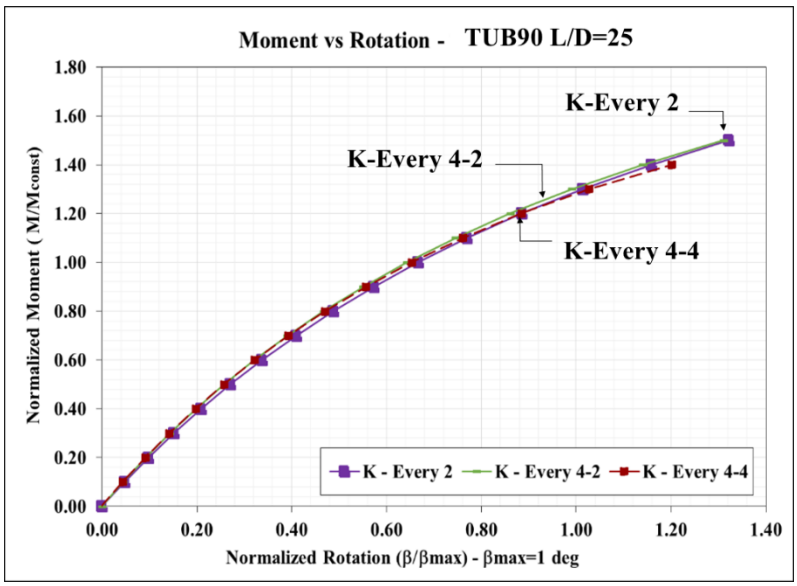

Figure 4-66 - Moment vs Twist - 1-Span Girder TUB90 - L/D=25 – Various K-Frame Layouts

The change in K-frame layouts in tub girders with partial top lateral bracing also affects the distribution of forces between the top lateral bracing and internal K-frame braces. Figure 4-67 shows axial forces in the diagonals of the prototype girder with K-frames every 1 and 2 panel points. For the latter case, the axial forces in the truss diagonals in compression decreased about 8% while the axial forces in the truss diagonals in tension increased up to 19%. Similar redistribution of loads was observed for the other two K-frame configurations (K-every 4-2 and K-every 4-4). For these two cases, the axial forces in the compression diagonals decreased up to 13%, while the axial forces in the tension diagonals increased up to 16%. The load is being transferred from the diagonals with more force to the ones with less force. This, a more balanced distribution of forces in the top lateral truss diagonals is attained. This was also observed in the experimental results.

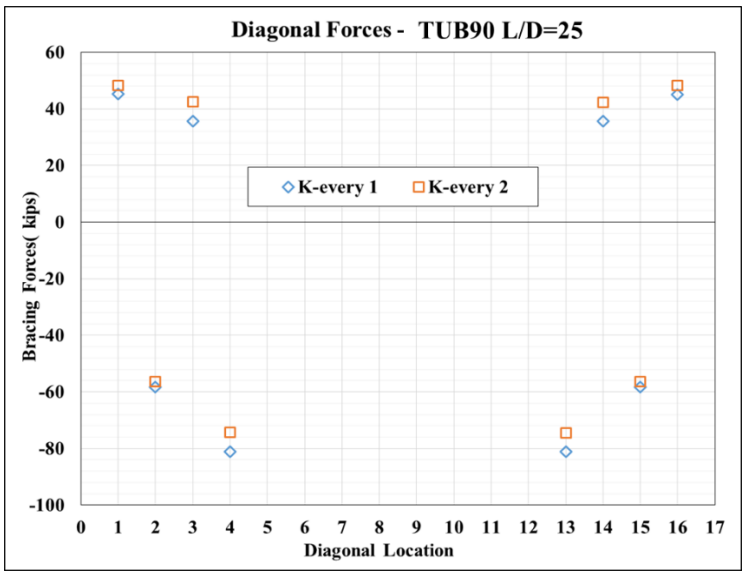

Figure 4-67 Top Lateral Bracing Forces –1-Span TUB90 Girder L/D=25- Two K-Frame Layouts

When a tub girder has partial top lateral bracing, the distribution of axial forces in the struts changes significantly from the fully braced case. Strut forces for a tub girder with partial top lateral bracing and with two different layouts of internal K-frames are shown in Figure 4-68 and Figure 4-69. The highest strut forces are found at the end of the partial top lateral bracing. The forces in the other struts are less than the 35% of the maximum forces found in the strut locations 4 and 12. When the K-frame configuration changes from braces at every panel to every two-panel points, most of the strut forces drop up to 40% except the highest strut forces at the end of the zones with partial top lateral bracing and at midspan. The other two K-frame configurations (K-every 4-2 and K-every 4-4) showed similar trends. Results are presented in Appendix B.

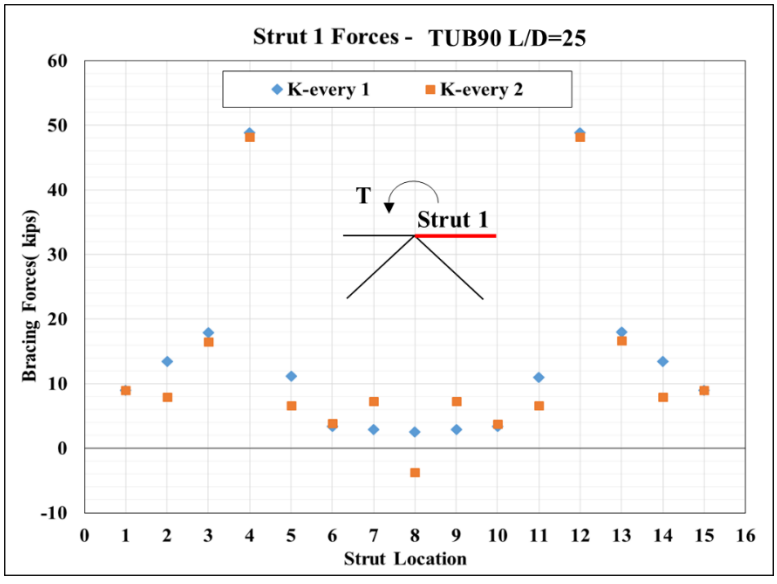

Figure 4-68 - Strut 1 Forces – 1-Span TUB90 Girder with L/D=25 - Two K-Frame Layouts

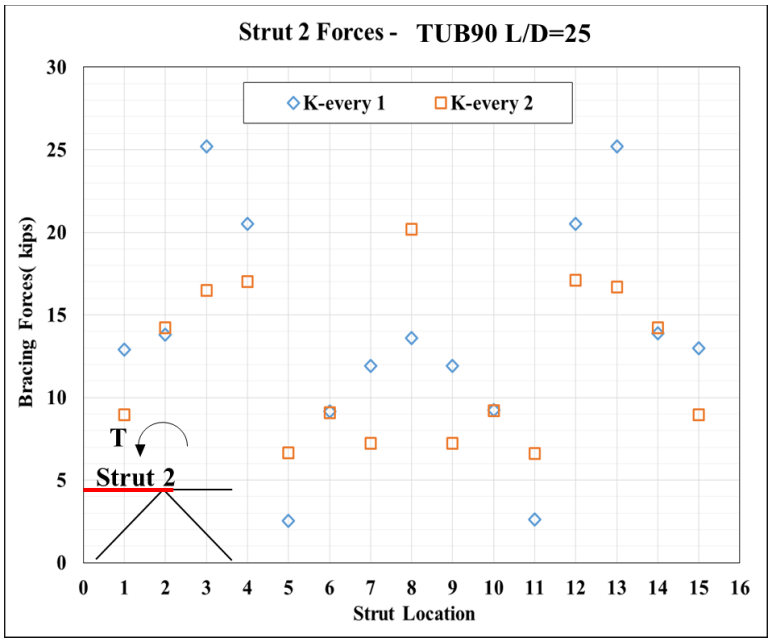

Figure 4-69 - Strut 2 Forces – 1-Span TUB90 Girder with L/D=25 - Two K-Frame Layouts

Figure 4-70 shows the axial forces of the K-frame diagonals for the configurations with internal braces every one and two panel points, for a girder with partial top lateral bracing. Like the strut axial forces, the distribution of the axial forces in the K-frame diagonals is considerably different from the those for a fully braced girder, presented in Figure 4-63. Likewise, the largest axial forces appear to be in the location at the end of the partial top lateral bracing. When the K-frame layout is modified from every panel to every two panel points, the largest changes in axial forces occurs in the K-frame diagonals at the end of the horizontal truss diagonals (4 and 12) and at midspan (8), where the axial forces increase around 10% and 120%, respectively. Similar trends in the axial forces in the K-frame diagonals were observed in the other two K-frame configurations (K-every 4-2 and K-every 4-4). In addition to the simply supported girder system, a 2-span continuous system was evaluated in this analytical study. The results of this analysis showed similar trends in the results obtained with the 1-span system. Details are provided in Appendix B.

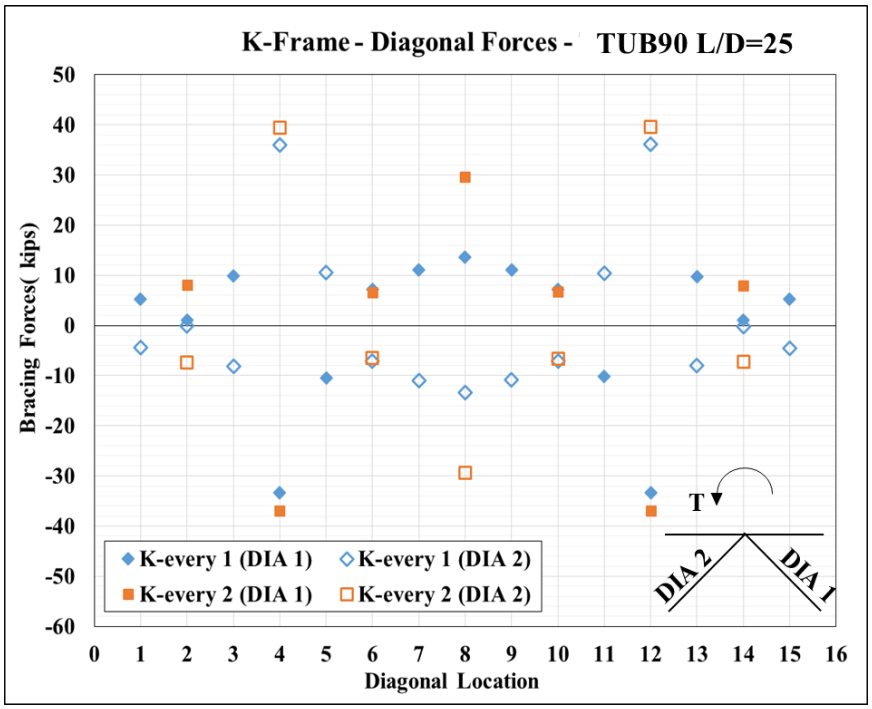

Figure 4-70 - K-Frame Diagonal Forces – 1-Span TUB90 Girder L/D=30 - Various K-Frame Layouts

Based on the parametric FAE studies, alternative distributions of internal K-frames can be used in straight tub girders with partial top lateral bracing. As a minimum, K-frames should be placed at the end of the zones with top lateral bracing and at midspan. Any configuration of K-frames that satisfies this distribution will result in adequate torsional response. Additionally, the K-frames placed at the end of the horizontal truss diagonals must be properly sized in order to sustain the high axial forces produced in this region.

The impact of different K-frame configurations was also evaluated in horizontally curved girders with partial top lateral bracing. As described earlier, 50% of partial top lateral was found to be a minimum amount of bracing for curved girders with a radius of curvature of at least 2500 ft. A 1-span and a 2-span TUB90 girder with L/D=30 and 35, respectively, and a radius of curvature equal to 2500 ft. were evaluated. Figure 4-71 shows the torsional response of the simply supported TUB90 with K-frames located at every one, two and four panel points (one K-frame at each end of the horizontal truss and another one at midspan). Clearly, the configuration of internal K-frames did not have a significant impact on the torsional response of the girder. The axial forces in the top lateral bracing diagonals were very similar between these two cases with a variation less than 5%.

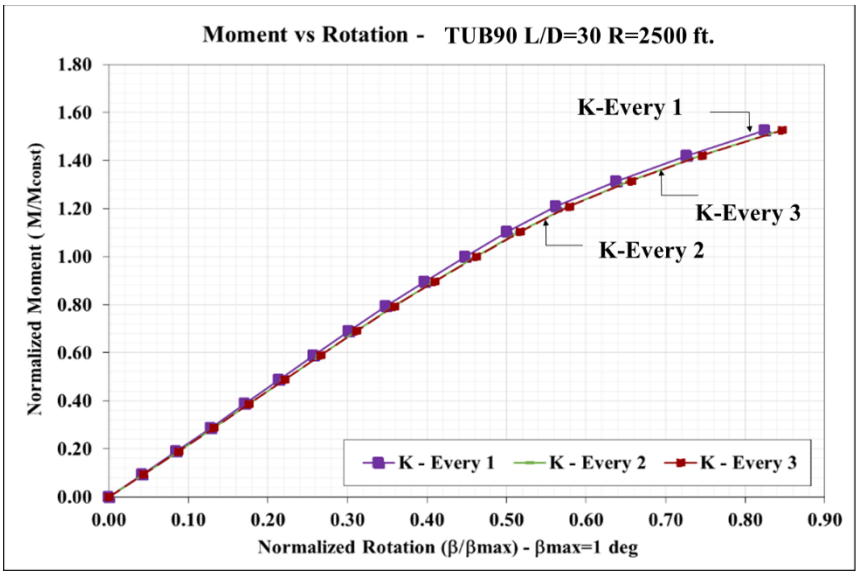

Figure 4-71 - Moment vs Twist - 1-Span TUB90 - L/D=30, R=2500' - Various K-Frame Layouts

Similar distributions of axial forces in the struts and K-frame diagonals were observed in the curved girder as in the straight girder, although the magnitude of these forces was larger in the curved girder. The largest axial loads were observed in the struts at the end of the zones with top lateral bracing. When the number of K-frames was reduced from every panel to every two and four panel points, the forces in the struts (Strut 2) close to areas at the end of the horizontal trusses tended to decrease, while the strut (Strut 2) forces at midspan increased. Additionally, the forces in thet K-frame diagonals at midspan increased more than twice and they became even larger than the forces in the K-frame diagonal placed at the end of the horizontal truss. Plots showing the axial forces in the top lateral bracing and internal K-frame bracing systems are presented in Appendix D. The configuration of K-frames at every panel point showed stiffer torsional response for the curved girder, but most of the K-frames were ineffective and attracted more load than the other two configurations. The layout with K-frames every four-panel points resulted in a slightly more flexible torsional response, and the K-frames at midspan and at the end of the horizontal truss sustained higher loads. The configuration with K-frames at every two-panel points appears to be a good option for this system since it produces a reasonable torsional response (Figure 4-57), the axial forces in the K-frames located in the critical zones are lower than the other two layouts, and this layout facilitates the fabrication of the tub girder.

4.7 Effect of Flange Offset Details on the Behavior of Steel Tub Girders during Construction

4.7.1 Effect of Flange Offset on the Local Stability of Steel Tub Girders During Constructions

Offsetting the top flanges of tub girders can eliminate the gusset plates and improve the effectiveness and economy of the bracing system. However, the impact of top flange offset on local instability of tub girder during construction requires further investigation in FEA parametric studies. The first series of analyses were performed to understand the impact of flange offset on

the local buckling capacity on FE models with offset flange layout considering local imperfection. The sample case presented the analysis of a simple span TUB36 during construction. The flange layout represented the most extreme offset configuration which only has one inch of flange width extended outside the web. In the model, top lateral truss was provided along the entire span length and K-frame was located at every strut panel point. Therefore, global instability and section distortion was prevented. TUB36 was chosen for this case since it has a relatively compact web and bottom flange. As a result, local instability mode on top flange predominated over local modes on other plate element. Elastic eigenvalue analyses were conducted first to obtain the elastic critical stress under notional distributed traction load. Then, the critical load was applied on girder to perform large displacement analysis considering both material inelasticity and local imperfection. The analyses were terminated by numerical instability. Global and local imperfection were included as discussed in the Section 4.4.3., i.e. half sine wave for global pattern with a maximum magnitude of L/800 and full sine wave for local pattern with a maximum magnitude of 0.25 in (greater than b/100). This assumed critical local plate imperfection used in the analyses was based on an investigation discussed later in this section. Since no residual stress data was collected during the experiment, the effect of residual stress was not considered. The material inelasticity model was a simplified bi-linear curve with (F_y=50 ksi and F_u=65 ksi @ 15% strain with a modulus of strain hardening of 100 ksi).

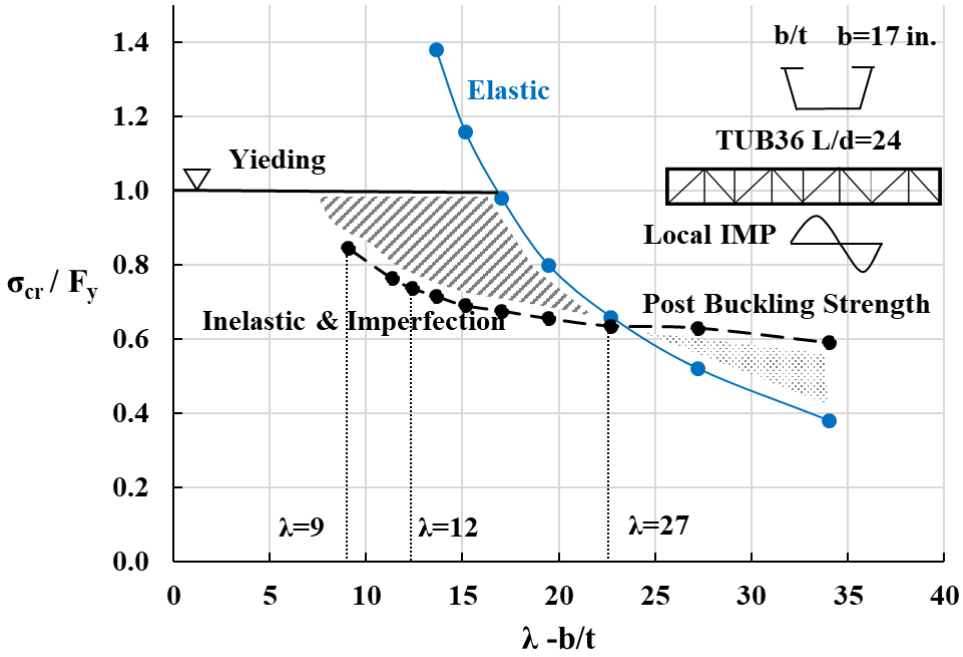

Figure 4-72 Critical Buckling Stress vs. Plate Slenderness Ratio

The critical buckling stress of the flange plate depends on the slenderness ratio of the plate (λ=b/t, b is the unsupported edge of the plate to the first row of welds or bolts, t is the thickness of the plate) and can also depend on the rotational stiffness provided to the flange by the web. The FE model of a tub girder system has already taken web rotational restraint into consideration. Critical buckling stress is plotted against the slenderness ratio of the top flange in Figure 4-72. The

elastic critical stress curve is based on eigenvalue analyses and inelastic critical stress with imperfection was based on the stress results of final converged step. The unsupported flange width b was 17 in. in this case. From the plot, the elastic buckling stress was in proportion to $1/\lambda^2$. The inclusion of material inelasticity and local plate imperfection increases the local buckling capacity of the top flanges if λ is greater than 27 (which corresponds to a plate thickness of 0.625 in). This indicated that top flanges have post buckling strength. As λ decreases (less than 27), the effect from material and geometric non-linearity decreases the critical buckling strength. Therefore, for very slender plates, post buckling strength exists after the plates experience local instability. For thicker plates, the presence of local imperfection reduces the critical buckling stress. In the graph, λ=12 corresponds to a critical stress value of 37 ksi, which is specified as the proportion limit of top flanges in current AASHTO LRFD Specification (2017).

The analyses above assumed a critical local imperfection pattern of full sine wave (AWS, 1996). However, the measured imperfection on the flange-offset and lower-slope specimen shows that the pattern of local plate imperfection on many panels deviates from this assumption. Three different patterns of local imperfection were identified from the measured results: half sine wave with a peak, half sine wave with a valley, and a full sine wave. To determine the most critical shape for flange local buckling, a large displacement analyses was carried out on the same model using arc length method. The moment versus vertical defection responses are plotted in Figure 4-73. From the non-composite moment capacity of FE models with different assumed imperfection patterns, the full sine wave is the most critical shape for flange buckling.

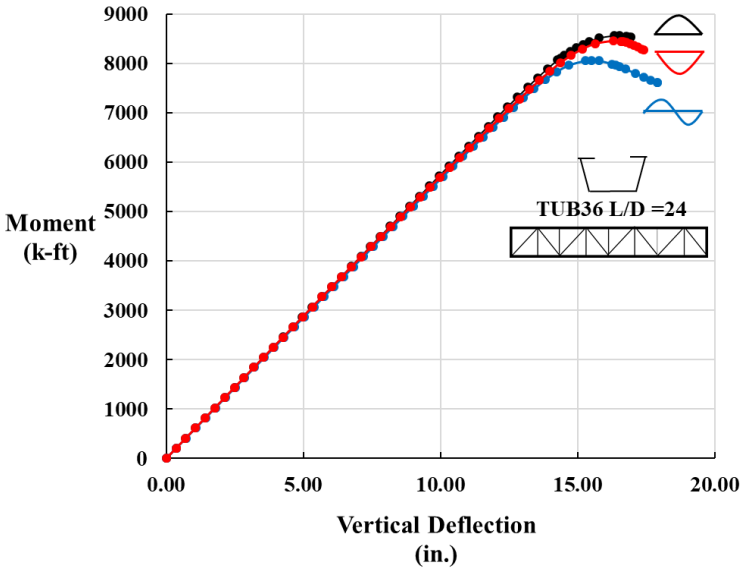

Figure 4-73 Moment vs. Lateral Deflection with Different Local Imperfection

4.7.2 Effect of Flange Offset on the Global Instability of Steel Tub Girders

The impact of flange offset details on the global stability of steel tub girders was also investigated in the parametric FEA studies. With the slenderness ratio of top flanges was properly controlled (compact top flanges), the analyses considered unbraced models (without any top lateral truss) to study the impact of offset flange on the global buckling behavior due to the geometry change of the girder. Sample resutls from analyses perfomred on a straight 180 ft TUB90 girder was presented. Three different flange offset configurations were analyzed as shown in Figure 4-

74. The percentage of the top flange width inside the box is shown for reference in the figure. Internal K frames are provided at every strut panel points. Both global and local imperfection have been included in the models as before. In this section, the three different top flange configurations are designated as ‘Centered’, ‘Offset-4’ and ‘Offset-E’. Figure 4-75 presents the moment vs. lateral reponse of the TUB90 model with various amounts of top flange offfset. The elastic critical moments for lateral torsional buckling for each case were also listed in the graph. Offsetting the top flange towards the inside makes the section less prone to global instability. A similar observation was made in the experiemnts.

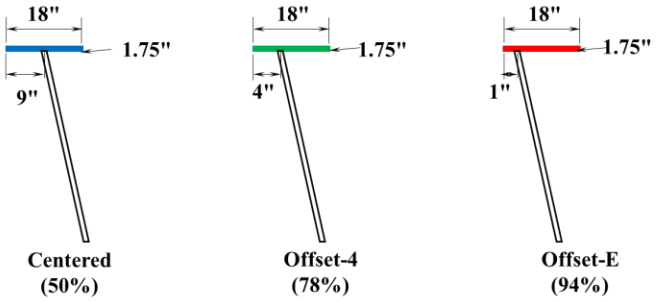

Figure 4-74 Different Flange Offset Configurations

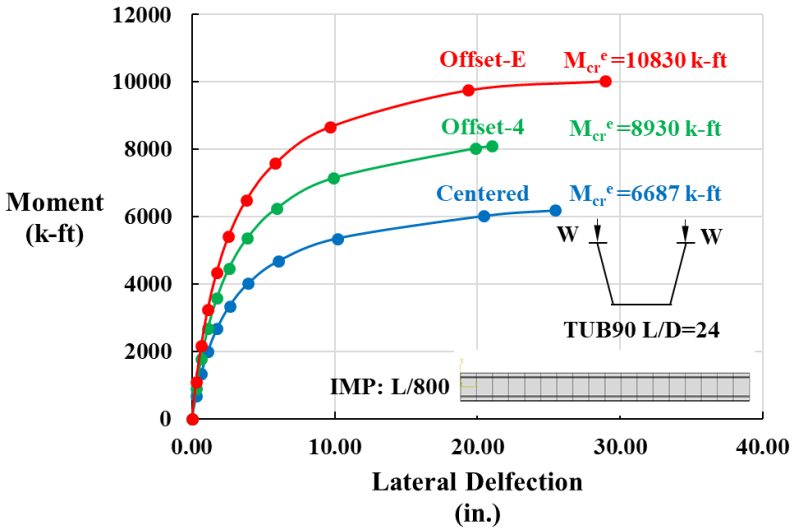

Figure 4-75 Moment vs. Lateral Deflection for Different Flange Offset Configurations (Unbraced)

Another comparison study was performed on FE models with full-length and partial-length (55%) top lateral trusses as shown in Figure 4-76. The moment vs. lateral reponse of the TUB90 model with various amounts of top flange offfset coincide with each other for the full-length top lateral truss. For the partial-length lateral truss, the model with the most extreme flange offset case shows the stiffest response. The resutls indicated that with full length top lateral truss, the impact of flange offset on the stiffness of the girder is almost negligible.

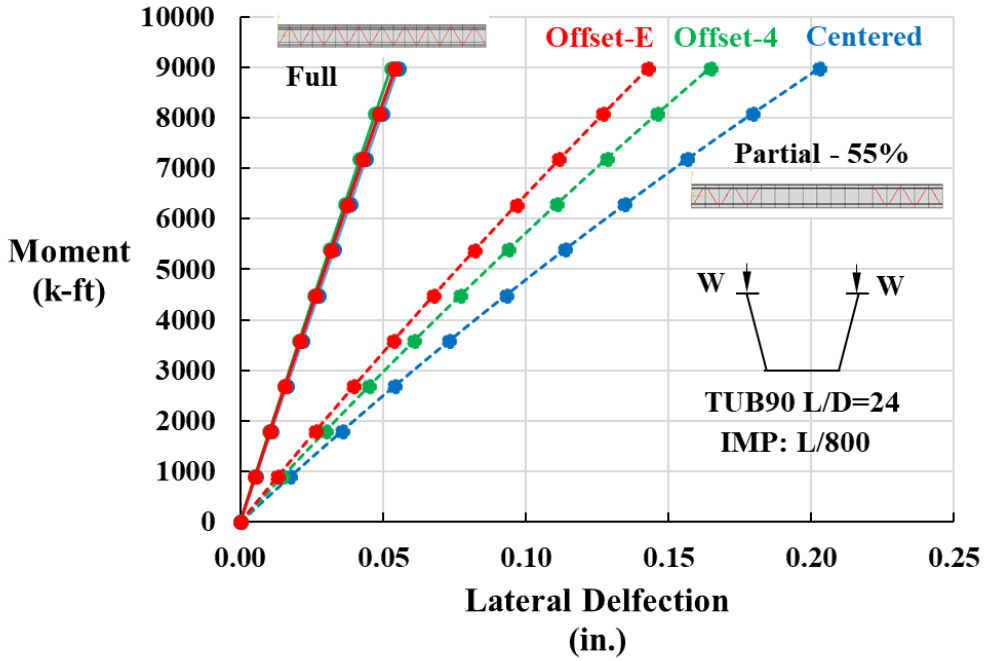

Figure 4-76 Moment vs. Lateral Deflection for Different Flange Offset Configurations (Full and partial top lateral trusses)

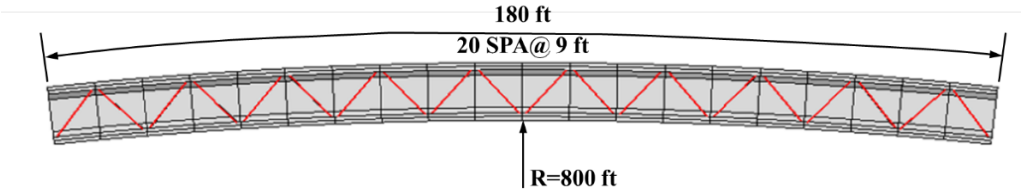

Figure 4-77 Plan View of Curved Tub Girder TUB90 Model R=800ft

Results from analyses performed on a curved TUB90 with a horizontal radius of curvature R=800 ft. are shown in Figure 7-7. The graph plots the bending moment vs. maximum lateral deflection of the outer edge of the top flange as indicated with a red dot in the figure. The framing plan of the FE models considered in the analyses were sketched in Figure 4-77. Like the response of the straight TUB90 models, with full-length top lateral bracing, the load deflection plots are almost identical for different amount of flange offsets up until 70% of the estimated construction moment level. Thereafter, offsetting the top flange can limit the lateral movement of the outer edge of the top flange. The extreme offset case has the smallest lateral deflection compared with the other two cases. Offsetting the flange does not affect the global stiffness of the girder up until 70% load level and is beneficial to control lateral deflection at higher load levels for the curved system. Similar trend was observed for the angle of twist of the girder.

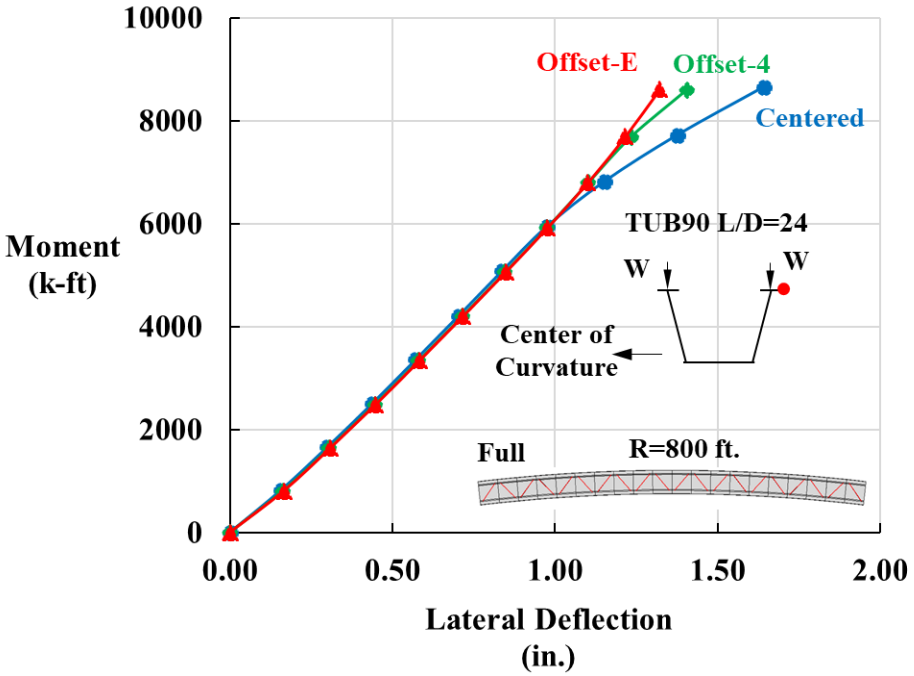

Figure 4-78 Bending Moment vs. Maximum Lateral Deflection for Different Top Flange Offsets

Local buckling of offset flanges is a major concern during construction. Inelastic behavior and local plate imperfections can affect the critical buckling strength of the unstiffened top flanges. With more unsupported flange width, local bucking checks are critical. However, limiting the slenderness ratio of the top flange is an effective way to prevent premature local flange buckling. Once the top flanges are properly proportioned, offsetting the top flanges is beneficial in terms of providing global stability. The tub girder systems will still experience large deflections if top lateral bracing is not adequately designed regardless of the different top flange layouts. In curved tub girders, the use of flange offset detail is advantageous to limit lateral movement of the top flange.

4.7.3 Effect of Flange Offset on the Flange Lateral Bending and Brace Force Distribution of Steel Tub Girders

The rationale behind the current requirement for a centered flange-web intersection is related to the concern of additional lateral bending of the top flanges. Parametric study results from the curved TUB90 FEAs were used to investigate the lateral bending effect of the top flange. The distribution of maximum lateral deflection of the critical outer edge of the top flange is presented in Figure 4-79. The FE model with the extreme flange offset has the minimum lateral deflection along the length. Thus, offsetting the top flange reduces the lateral movement of the top flange.

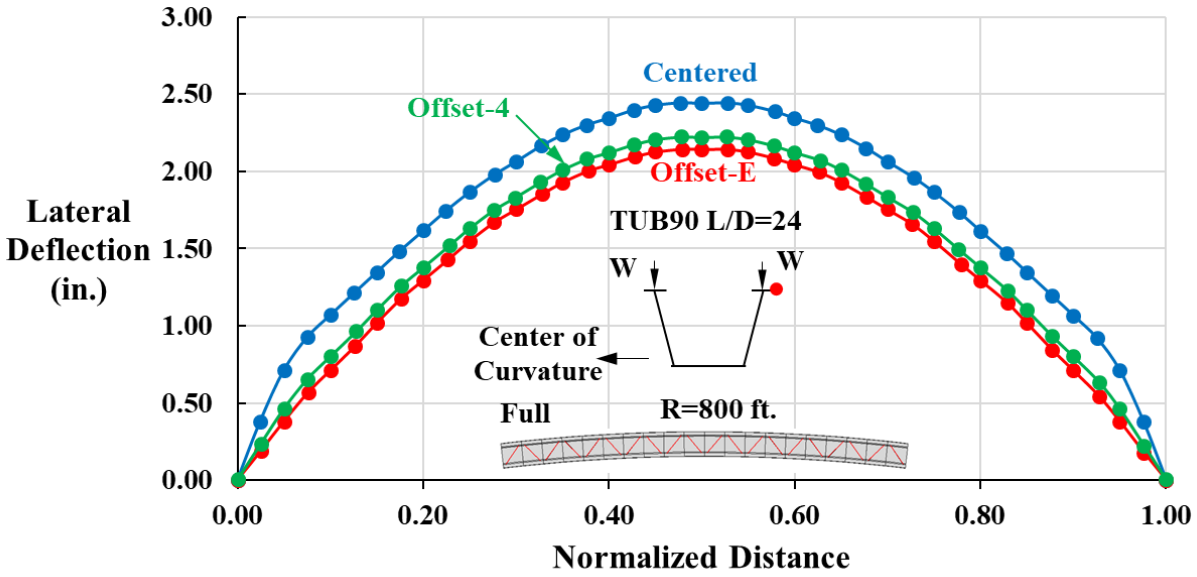

*Figure 4-79 Maximum Lateral Deflection on the **Outer** Edge of the Top Flange*

The maximum Von Mises stress on the critical inner edge of the top flange along the length of the girder is plotted in Figure 4-80. As the amount of flange offset increases, the maximum stress in the flange increases somewhat compared to the case of the centered flange, although the stress is somewhat more uniform along the length of the girder for the offset flange cases.

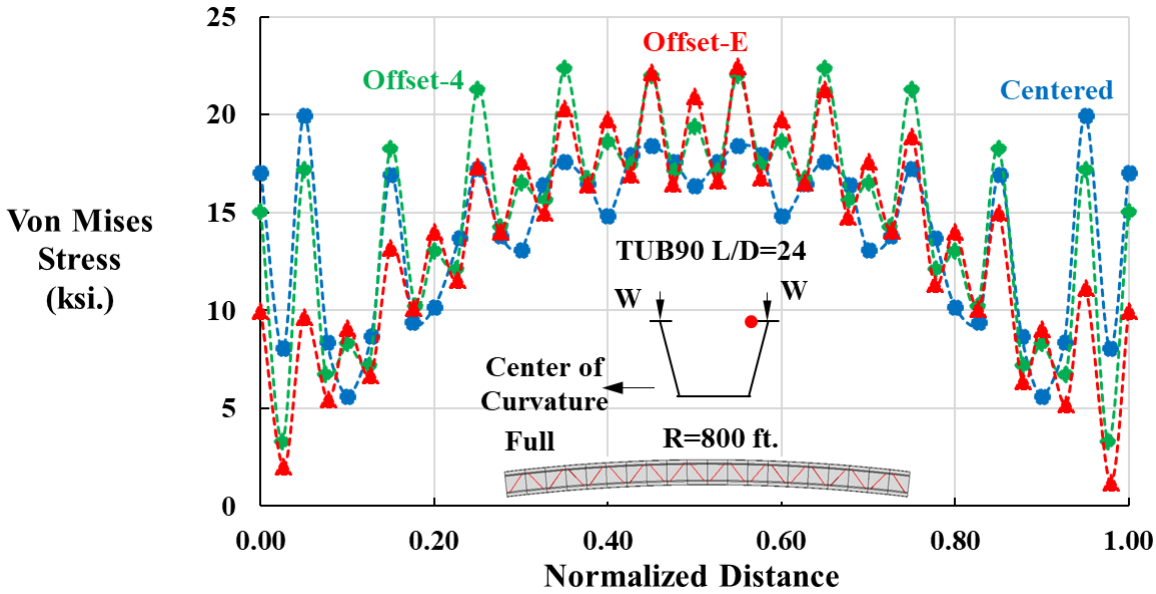

*Figure 4-80 Von Mises Distribution on the **Inner** Edge of the Top Flange*

Offsetting the flange can potentially alter the force distribution on the top lateral truss. The distribution of top lateral truss force for different amounts of flange offset are plotted in Figure 4-81. For all cases, the forces in the end panels are greater than panels close to the mid-span region.

Offsetting the flange increases the tension force in the very end panels. The tension forces in the other panels are reduced by a small amount for the offset flanges. In the compression diagonals, flange offset results in a small reduction of force in the end panels.

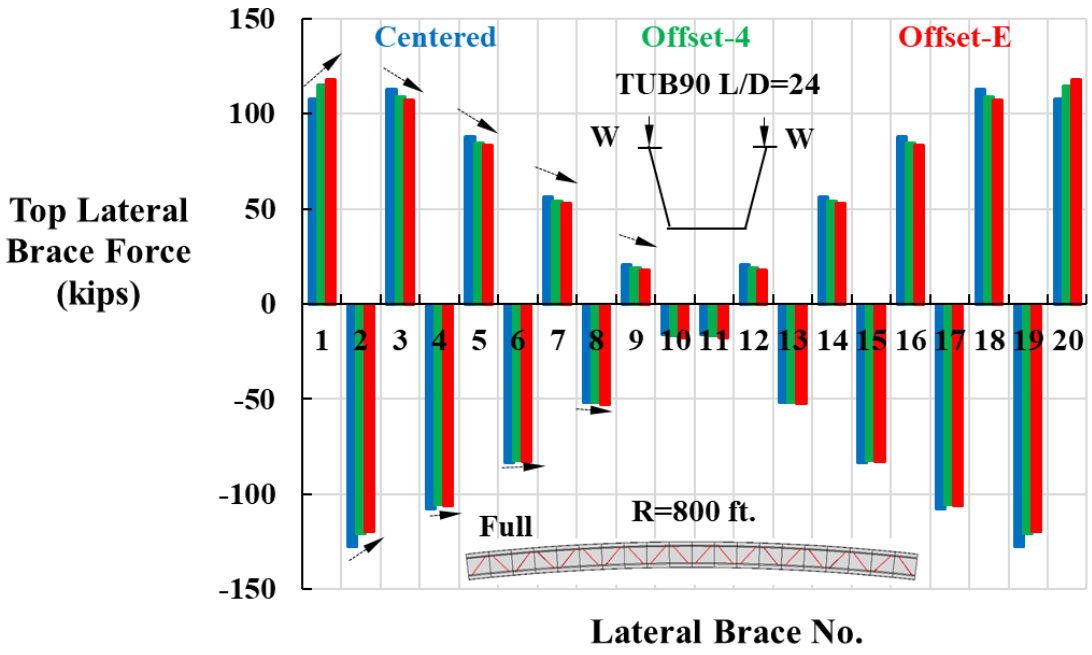

Figure 4-81 Top Lateral Brace Force Distribution with Different Flange Offsets

The distribution of top strut forces is plotted in Figure 4-82 and Figure 4-83 with different flange offsets. The resultant of strut forces has been decomposed into two components: the bending/torsion component and the distortional component. For the bending/torsion component, offsetting the flange decreases the force magnitude with a maximum reduction of 60% at the panels next to the end panels. For the distortional component, the flange-offset increases the demand in the end panels and decreases the force component on other panels.

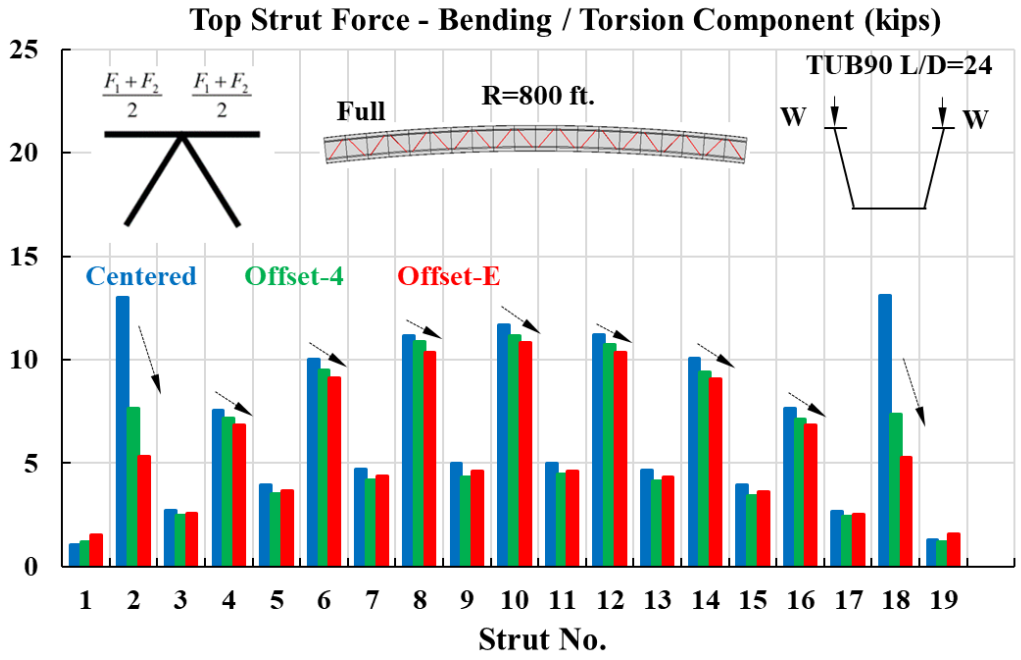

Figure 4-82 Bending / Torsion Component of Top Strut Force with Different Flange Offsets

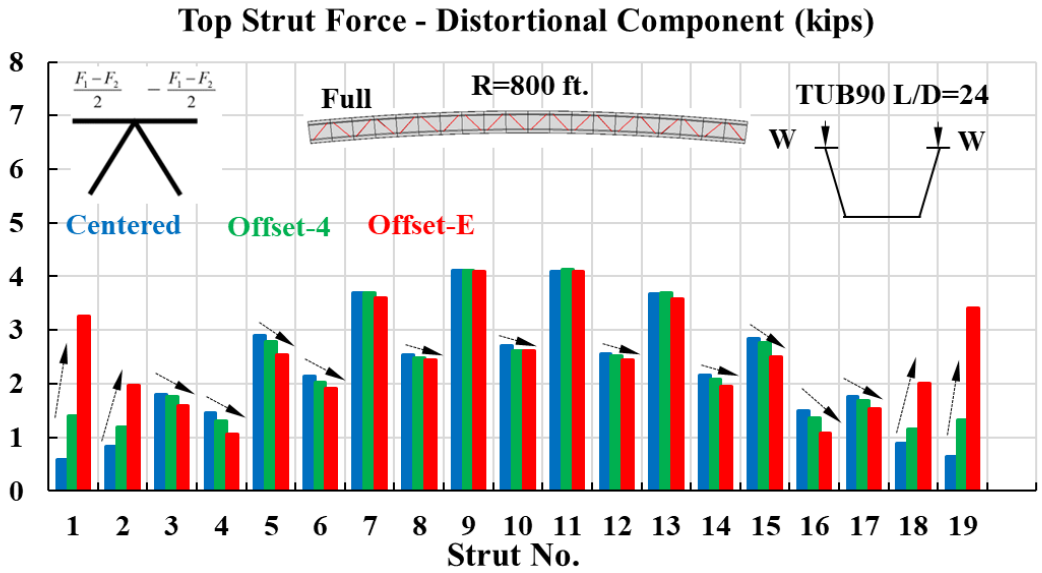

Figure 4-83 Distortional Component of Top Strut Force with Different Flange Offsets

4.7.4 Summary of Flange Offset Studies

The effect of offsetting the top flange on the girder behavior has been examined in this section. Local buckling of the top flange can be prevented by limiting the slenderness ratio of the plate element. Offsetting the top flange is beneficial for global instability. Offsetting the flange causes mode changes in the top flange stresses as well in the forces in the members of the top lateral truss. These changes should be considered in the design of the tub girder.

4.8 Effect of Various Web Slopes on the Behavior of Steel Tub Girders

4.8.1 Effect of Global Web Slope on the Stability of Steel Tub Girders During Construction

The use of lower web slopes can increase the tributary width of each individual girder while keeping the bottom flange width constant. However, reducing the web slope may affect the global stability of the girder. To better understand the effect of web slope on the stability of steel tub girders during construction, parametric studies were first performed on unbraced FE models with different web slopes. The 160-ft Straight TUB90 (L/D=21) FE models were considered in this study. The separation between the top flanges varied with the various web slopes as shown in Figure 4-84. From a web slope of 4 to 2.5, the cover width of the tub girder increases by 27 inches. FEAs were performed to study the behavior of the system with three different web slopes, designated as 'WS-4', 'WS-3' and 'WS-2.5'. For this first series of analyses, the girders were analyzed without a top lateral truss. Internal K-frames were provided at every strut point with a typical spacing of 10 ft.

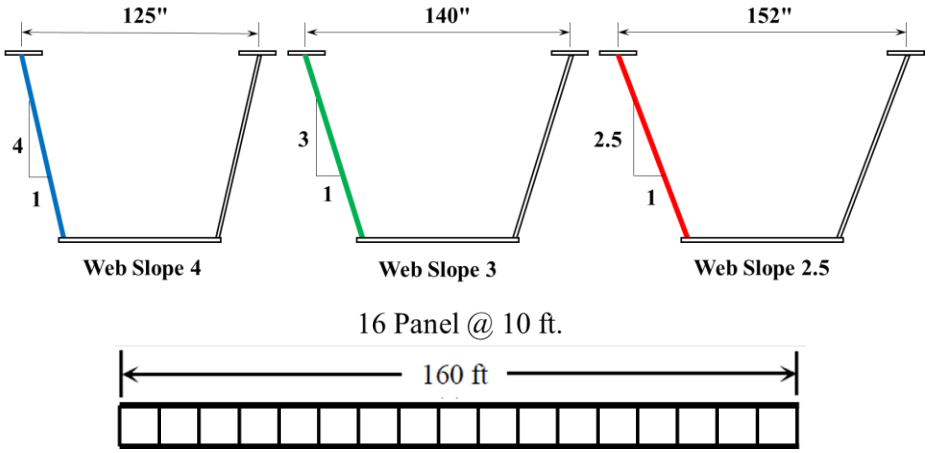

Figure 4-84 Simply-supported Straight TUB90 with Various Web Slopes (Unbraced)

The lateral torsional buckling (LTB) capacity (critical moment M_{cr}) was determined from three-dimensional FEAs using elastic eigenvalue analyses. Two different loading cases were considered, i.e., uniform moment and uniformly distributed load applied at the level of the top flanges. Results are listed in Table 4-5. As the web slopes decreases, the critical moments decrease for both loading conditions. The tub girders with open section tends to buckle with lower web slopes.

Table 4-5 - Critical Moment of Open Straight TUB90 with Various Web Slopes

Web Slope	Uniform Moment $M_{cr}{}^{M}$ (kip-ft)	Distributed Load $M_{cr}{}^{DL}$ (kip-ft)	Moment Gradient factor $C_b = M_{cr}{}^{DL} / M_{cr}{}^{M}$
4	12307	12261	1.00
3	10543	10746	1.02
2.5	9360	9732	1.04

Second-order large displacement analyses were then performed considering global imperfections. The imperfection is introduced into the model by scaling the buckled shape from eigenvalue analyses. Figure 4-85 shows the estimated construction moment vs. maximum lateral deflection of the top flange. With the deceasing web slope, the load deflection curve approaches the plateau at a lower moment level. These results confirm that without any top lateral truss, the tub girders with lower web slopes are more prone to global instability.

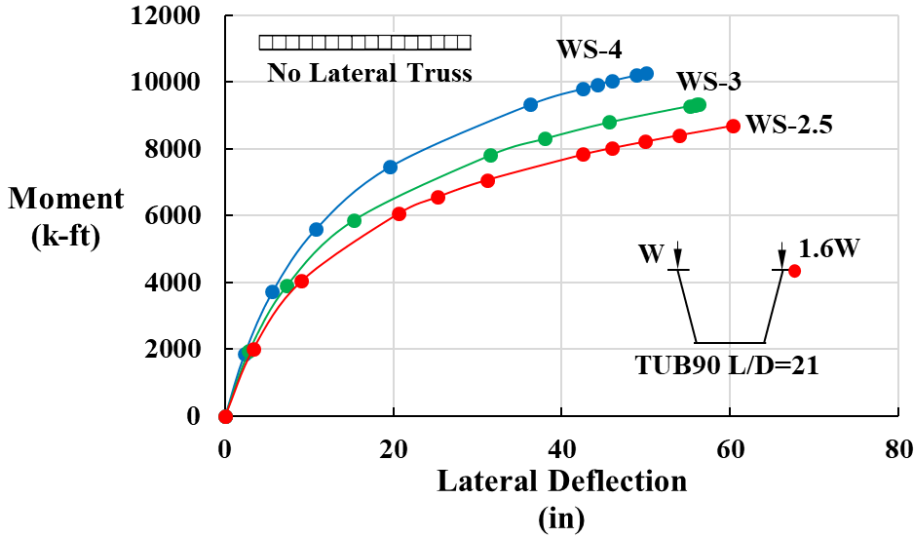

Figure 4-85 Moment vs. Lateral Deflection Response with Various Web Slopes

Additional analyses were performed on the same FE models with full and partial top lateral bracing. The moment vs. lateral deflection responses are plotted in Figure 4-86. The lateral deflection is significantly reduced with both full and partial length lateral truss. The web slope 4 exhibited stiffer behavior in comparison with web slopes 3 and 2.5.

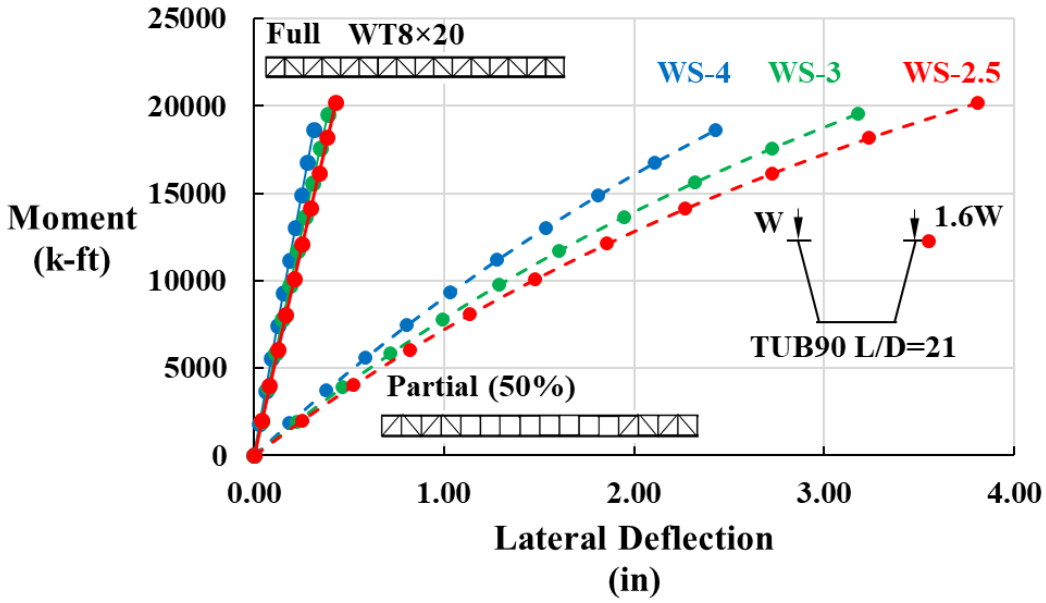

Figure 4-86 Moment – Deflection Response of Straight TUB90 with Various Web Slopes (Fully-braced -solid line; Partially braced -dashed line)

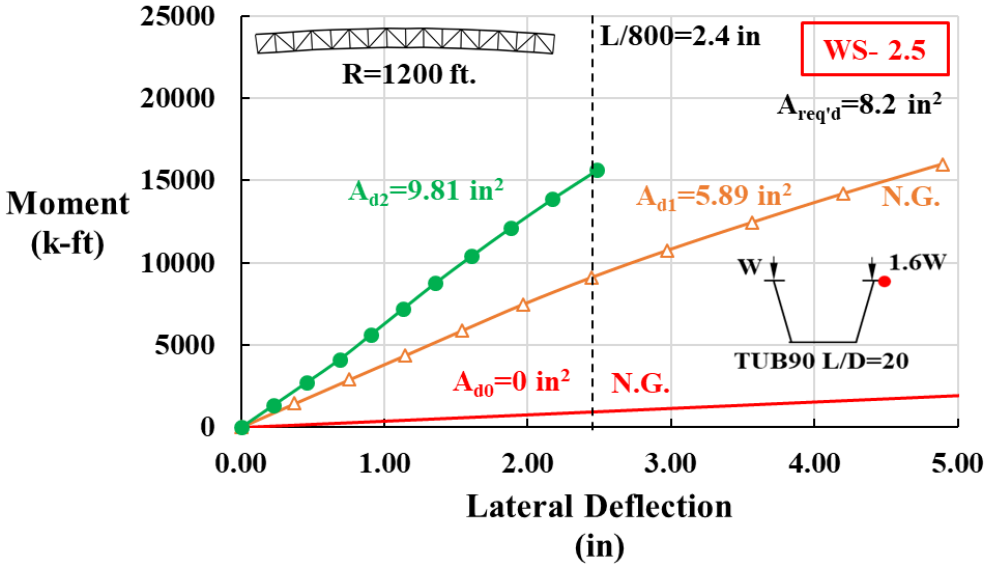

Figure 4-87 Moment vs. Lateral Deflection for Web Slope 2.5

In the current AASHTO LRFD specification, for curved tub girder systems, the minimum required area for lateral truss members for X-type trusses is directly related to the separation of top flanges (0.03*w*, where *w* is the separation between top flanges). Although this minimum requirement is intended to control warping normal stresses, a similar requirement applied to warren truss type bracing would result in a minimum required area of 0.054*w*. As the web slope decreases, the minimum required area of lateral truss members increases. An example is presented in Figure 4-87 for a curved TUB90 (L/D=20 and R=1200 ft.). For WS-2.5, the calculated minimum area is

8.2 in^2. Once the area of the diagonal member exceeds this minimum requirement, the lateral deflection can be limited within L/800.

4.8.2 Effect of Various Web Slopes on the Distribution of Brace Forces

As the web slope decreases, each top lateral truss panel becomes wider. The forces in the top lateral truss members increase as indicated in Figure 4-88 and Figure 4-89. Similar trends can be found in both curved and straight tub girder models with different section geometries.

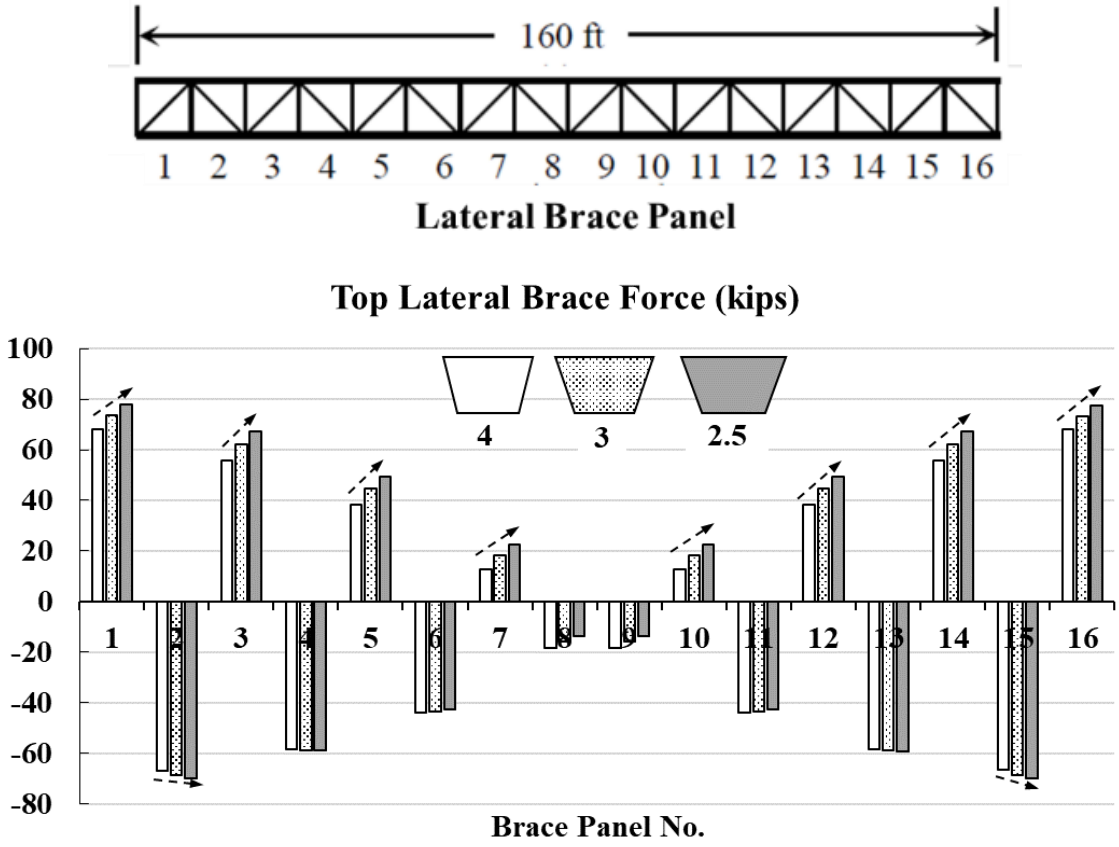

Figure 4-88 Top Lateral Truss Force for Various Web Slopes for Straight TUB90

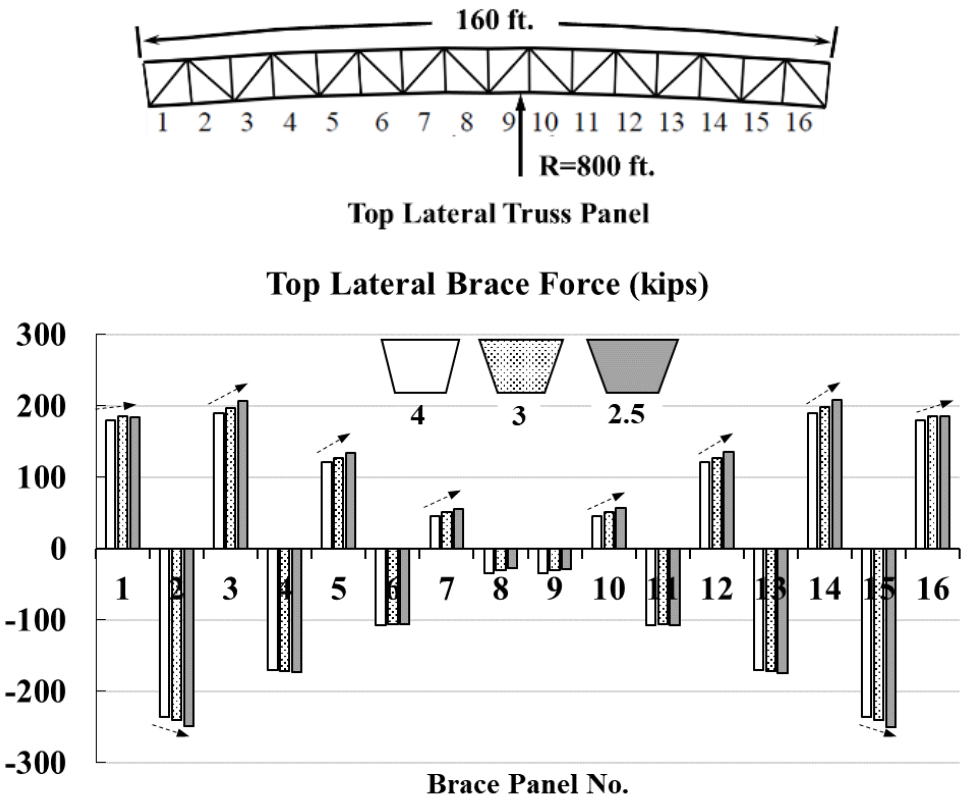

Figure 4-89 Top Lateral Truss Force for Various Web Slopes for Curved TUB90 with R=800 ft.

The sloping webs of the tub girders induce a lateral load component on the top flange (Fan and Helwig 2000). This lateral load component causes additional lateral bending stress as well as axial forces in the lateral struts of the top flange truss. The struts of the top flange truss are typically designed to carry the horizontal component due to the sloping webs. As demonstrated by a free body diagram of the top flange, with a distributed load of W/2 applied to each flange, the horizontal component, p (force per unit length) is in proportion to tan(θ). The use of a lower slope will increase the axial load in the top struts.

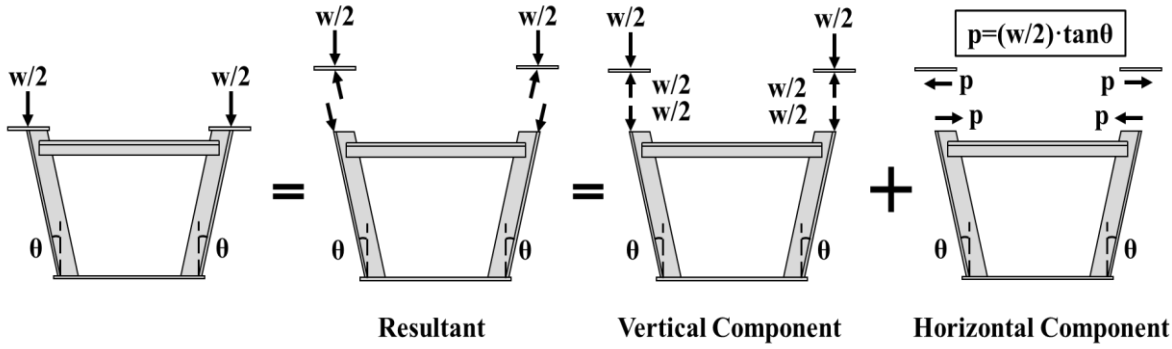

Figure 4-90 Horizontal Component of Applied Loads on the Top Flanges (Fan and Helwig 2000)

The struts of the top lateral truss are also part of internal K-frames. The force components in the struts are due to both distortion and tub girder bending and torsion (Helwig, Herman and Li 2004). Since the component due to the sloping web is tensile in nature, the effect is superimposed on the bending and torsion component. In the discussion of the effect of web slope on top strut force, distortion and the bending/torsion components in the top struts are separated using equations shown in Figure 4-91. The effect of the sloping webs is included in the bending/torsion component.

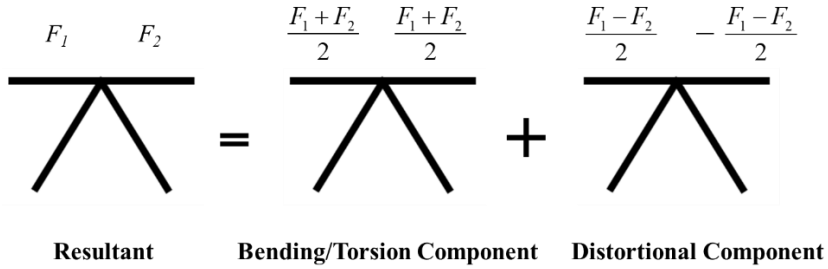

Figure 4-91 Example of Strut Forces Component

To study the effect of various web slopes on the top strut force distributions, FEAs were performed on both straight and curved TUB90 models. Twist of the girders was prevented at the ends and uniformly distributed loads during construction were considered. A single-diagonal top lateral truss was provided along the entire length and internal K-frames were located at every strut panel point. Figure 4-92 shows the bending/torsion component of the top strut forces for the straight TUB90 with different web slopes. The use of a lower web slope increases the horizontal component on the top struts. This effect was most significant at the girder ends and mid span region with a 60% increase in the axial forces. Similar analyses on a simply-supported curved TUB90 (R=800 ft.) are shown in Figure 4-93. The distribution of strut forces was different from that of straight girders with the panels close to the end (Panel 2 and 14) developing the largest forces. On those panels, the force demand on the top struts increased significantly. The panels also have the most force increase due to the use of lower slopes. The forces in other panels also increase but not as notable as in panels 2 and 14.

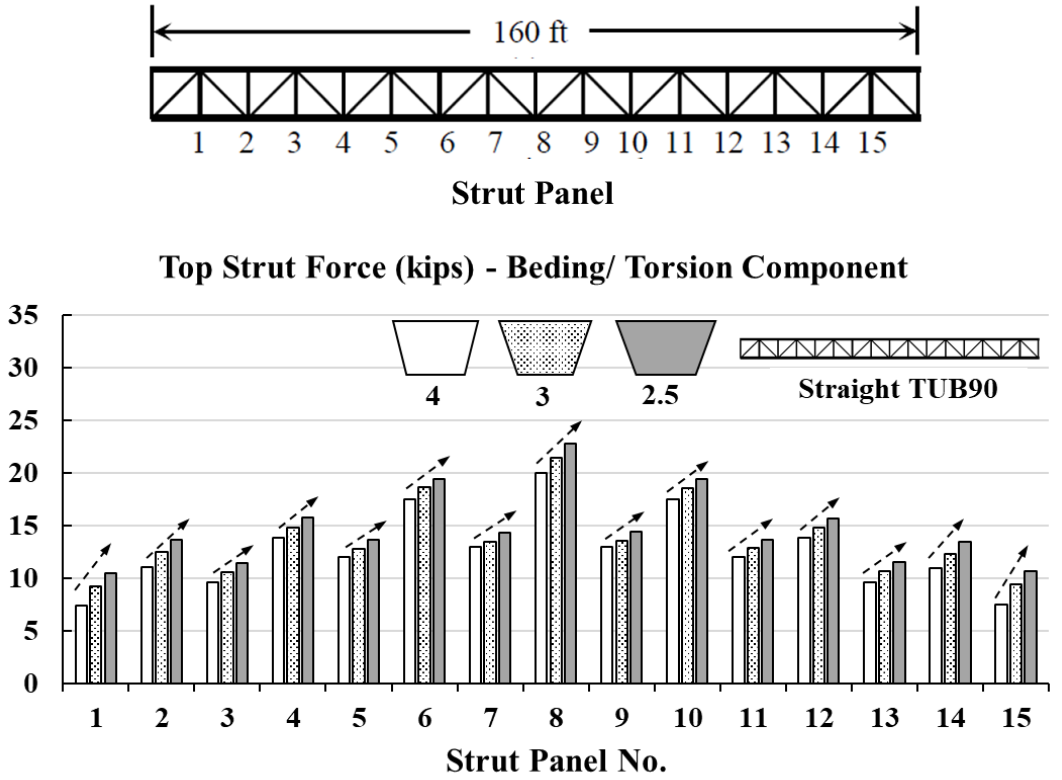

Figure 4-92 Forces in Top Struts Due to Bending/Torsion -Straight TUB90

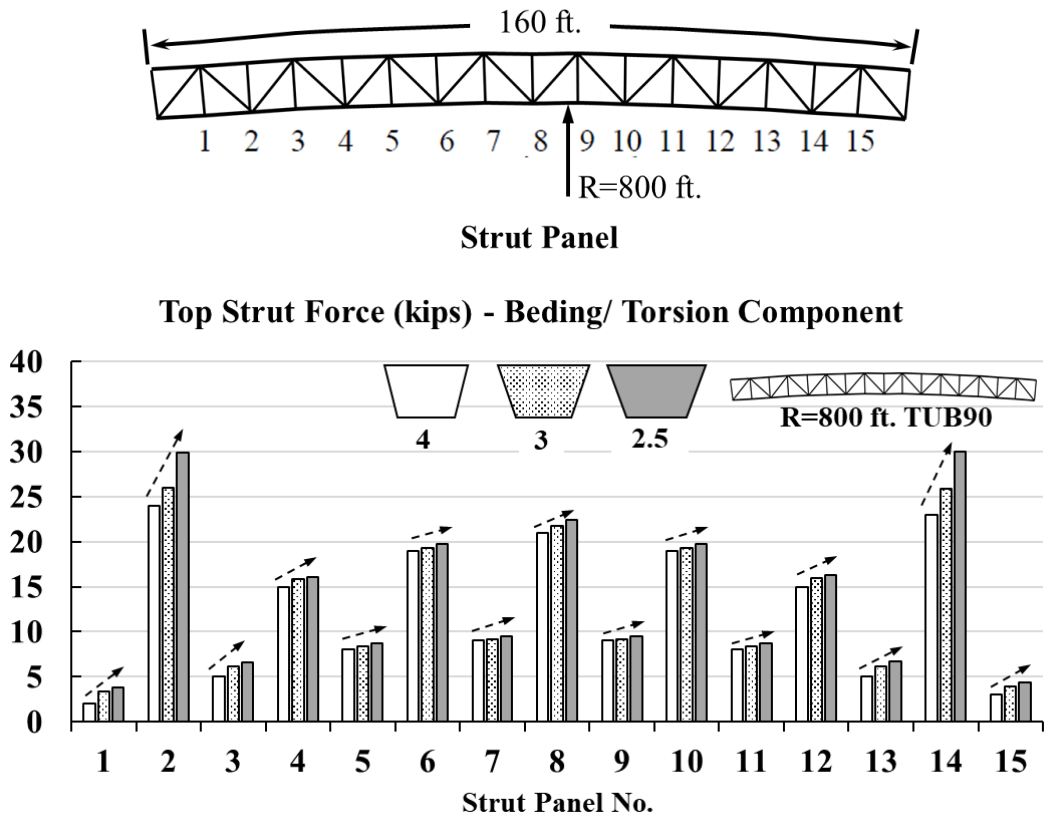

Figure 4-93 Forces in Top Struts Due to Bending/Torsion -Curved TUB90 R=800ft.

4.8.3 Effect of Various Web Slopes on the Distribution of Live Load

AASHTO Sections 6.11.2.1.1 and 6.11.2.3 address the web slope and specify a limit of 4:1 (4 vertical to 1 horizontal). The use of lower web slopes is restricted mainly because of the empirical equation for live load distribution factor listed in Table 4.6.2.2.2.b-1 in the AASHTO LRFD Specification. This equation, which is independent of the number of loaded lanes, is as follows:

$$LLDF = 0.05 + 0.85\frac{N_L}{N_b} + \frac{0.425}{N_L}$$

in which,
LLDF = Live load distribution factor,
$N_L = W_C/12$, reduced to the nearest whole number,
W_C = roadway width, ft, between curbs,
N_b = number of box girders, and $0.5 \le \frac{N_L}{N_b} \le 1.5$

This equation is based on work conducted by Johnston and Mattock (1967) on simply supported straight bridges. In the original experimental and analytical study, web slopes lower than 5V:1H were not considered. Therefore, three-dimensional parametric FEAs were performed to examine the effect of various web slopes on the live load distribution considering composite action and the interaction between girders. The live load distribution factor (LLDF) represents the lateral

distribution of live load between girders. Based on this concept, an individual girder is analyzed so that the moment due to the standard truck load HL-93 is obtained. The design moment of the girder is equal to this standard moment multiplied by the LLDF. The LLDF is a parameter reflecting the maximum amount of load that would be transmitted to a girder, i.e.:

$$LLDF = \frac{M_{\max}}{M_0}$$

in which M_{max} is the maximum bending moment developed in a girder in the composite tub girder bridge, and M_0 is the bending moment in the individual girder due to a standard truck load (Fan and Helwig 2000). In this study, M_{max} is determined based on three-dimensional FEA. A standard procedure has been documented in the FHWA report by Sotelino and Liu (2004). An influence surface study was performed first on three-dimensional FE models to determine the critical truck position that produces the maximum moment. The maximum moment on one composite girder with s specified effective width was then obtained through a free body section cut. Then 1D line element analysis was carried out on a beam element with the same span length with one line of truck wheel loads positioned at the same critical location. The procedure of determining the live load distribution factor is illustrated in Figure 4-94.

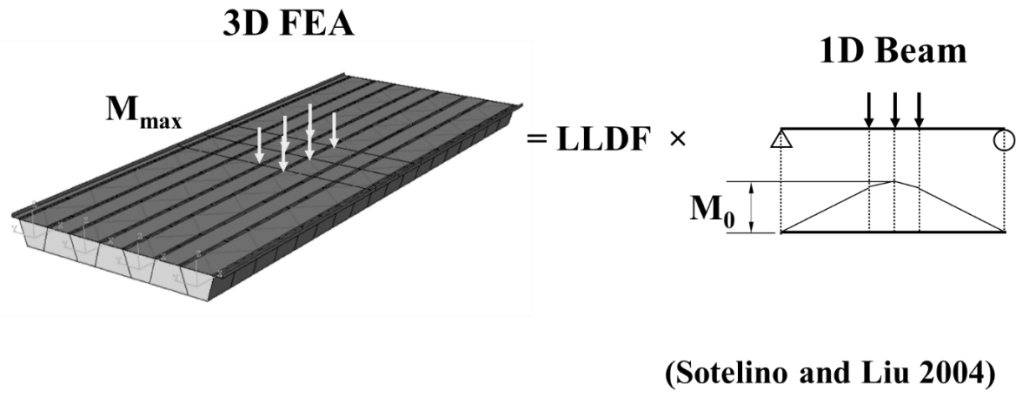

Figure 4-94 Determination of Live Load Distribution Factor

The behavior of composite tub girder bridges under live loads is quite different from quasi-closed girders during construction. The deck fully closes the tub girder section and greatly enhances the torsional and bending stiffness of the girder. Therefore, proper modeling assumptions must be made to account for the composite action. In this study, tie constraints were used to model the interaction between the deck and the girder. Uncracked concrete properties were assumed.

Following the procedure described above, sample analyses results are presented for a four-girder simply supported TUB36 system. Three different web slopes were considered in the FEAs. The bridge cross section used in the analyses is shown in Figure 4-95. The girder spacing was selected as the maximum spacing allowed in the current AASHTO LRFD Specification, i.e., 1.2 times of the distance center-to-center of top flanges of each girder (girder width). The deck width was designed to allow for maximum four traffic lanes. The maximum moment results were extracted from the analysis results for the composite tub girder section. The effective width of the section was determined according to the current AASHTO LRFD Specification.

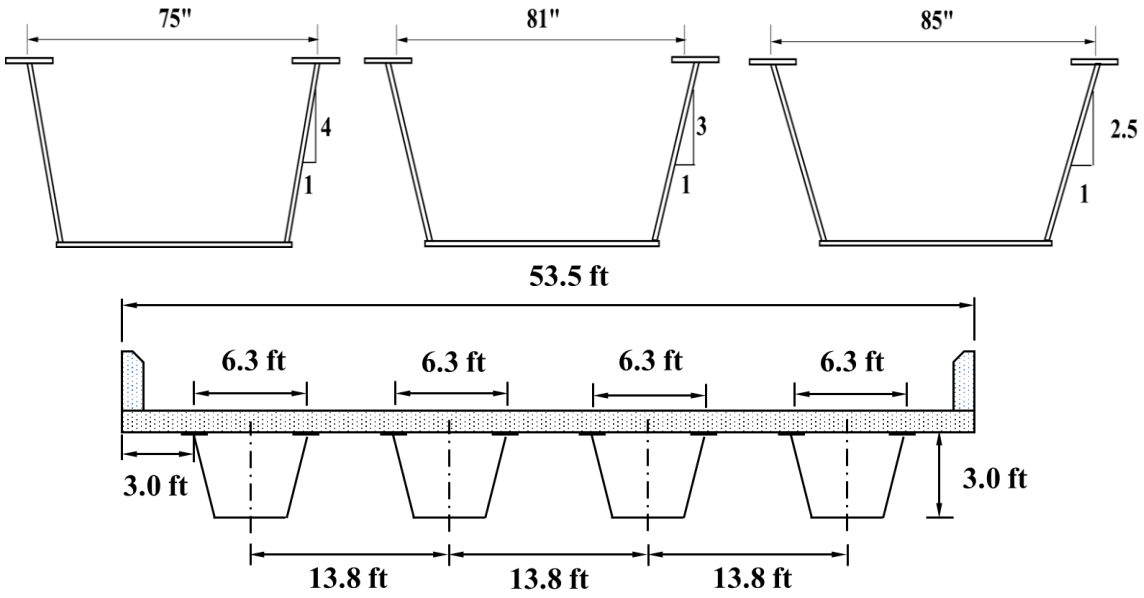

Figure 4-95 Four Girder Simply Supported Straight TUB36 with Various Web Slopes

Table 4-6 - Live Load Distribution Factor Based on 3D FEA

Live Load Distribution Factor LLDF based on 3D FEA					
Web Slope 4		**Web Slope 3**		**Web Slope 2.5**	
Ext	Int	Ext	Int	Ext	Int
1.02	0.83	1.02	0.82	1.01	0.81

Table 4-7 - Live Load Distribution Factor Based on Current Design Method

Current AASHTO EQN		Lever Rule	
Ext	Int	Ext	Int
1.01	1.01	1.02	0.83

The live load distribution factors determined from three-dimensional FEAs are summarized in Table 4-6. For different web slopes, the LLDF values are almost identical for both exterior and interior girders. The factor for interior girder is less than that for exterior girder. In typical design practice, empirical equations and the lever rule are commonly used to calculate the LLDF. The results from three-dimensional FEAs are compared with values calculated based on these methods. The equation in AASHTO does not distinguish exterior from interior girders. The values from the equation are very close to the results from 3-D FEA. The lever rule method can distinguish exterior and interior girders. This method gives the same results as 3-D FEA. Similar analyses have been performed on other FE models to further confirm the conclusions. The change in the web slope does not affect the live load distribution significantly. The use of the empirical

equation in the current AASHTO LRFD Specification is not be affected by adopting a web slope greater than 1H:4V. The level rule can still be used to calculate LLDF if the assumptions for the empirical equation are violated.

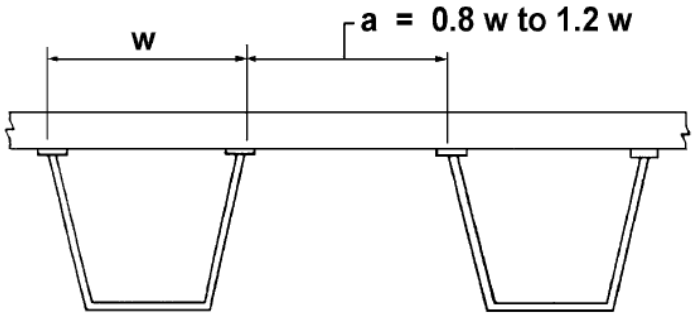

Figure 4-96 AASHTO Restriction on Girder Spacing

Another parameter investigated in this study was the possibility of increasing the girder spacing in combination with using a lower slope to reduce the number of girder lines. Simply supported straight TUB90 models were considered in the analyses. The bridge deck dimensions used are shown in Figure 4-97. Different girder spacings were considered, i.e., 1.0 and 1.4 times of the center-to-center distance between top flanges of each girder (girder width), resulting in a four-girder and three-girder system respectively. The deck overhang was kept at the same width.

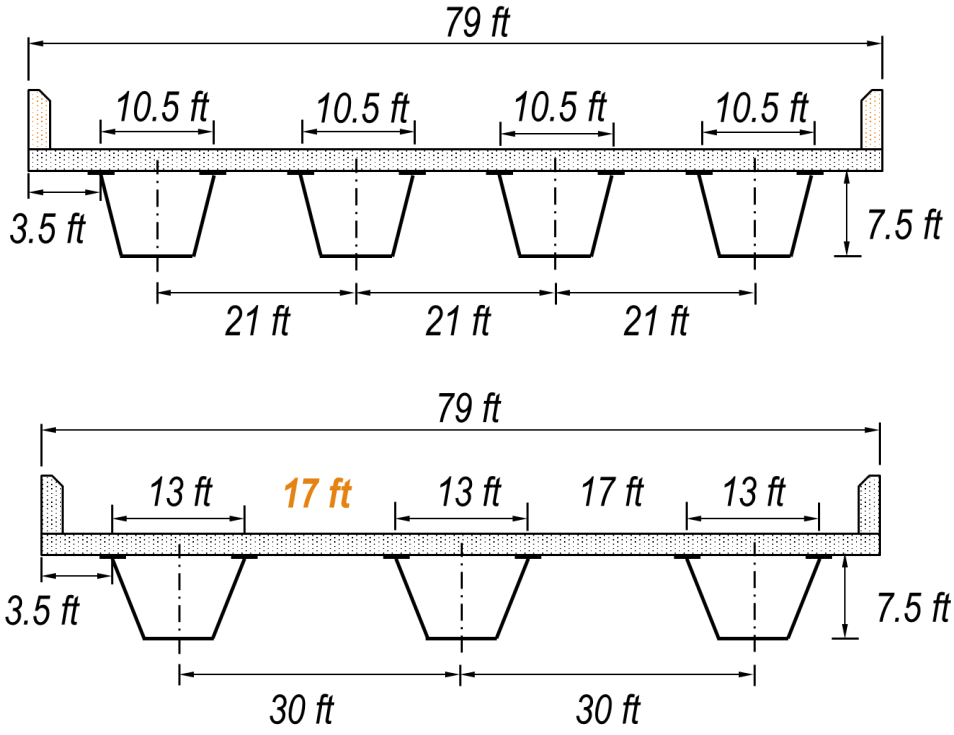

Figure 4-97 Sketch Showing the Bridge Cross Section with Increased Girder Spacing

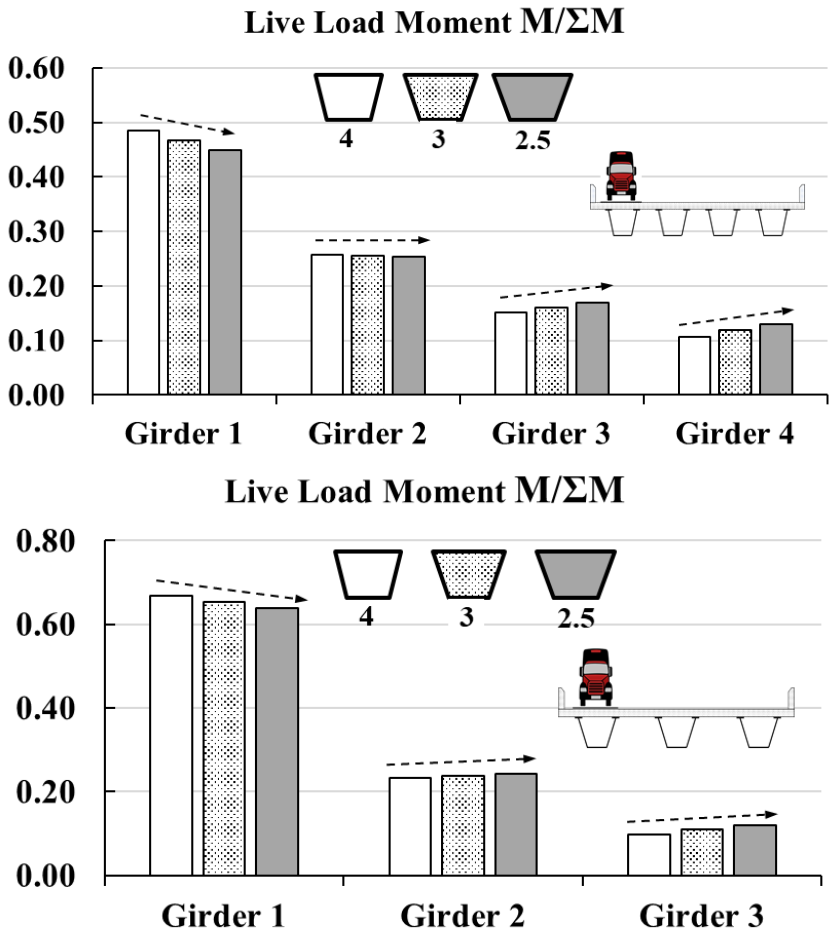

Figure 4-98 Distribution of Moment due to Live Load with Different Web Slopes

The distribution of bending moment due to live load among the girders for 4-girder and 3-girder system are shown in Figure 4-98. The use of the wider girder spacing increases the demand on the loaded Girder 1 (girder directly under truck) by approximately 10% to 15%. On the other hand, changing in the web slope has little effect on the moment distribution.

4.8.4 Summary of Web Slope Studies

The effect of various web slopes on the girder behavior has been studied in this section. Reducing the web slope increases the forces in the top lateral truss members. Changes in web slopes do not alter the live load distribution significantly. Increasing the girder spacing can cause one girder carrying significantly larger load.

4.9 Effect of Working Point Offset Details on the Behavior of Steel Tub Girders during Construction

Another parameter that was investigated as part of this research project was the offset of the working point of top lateral brace from a single working point. The current practice of detailing

working lines to intersect at a single work point results in relatively little overlap of the truss members and the girder flange and consequently can lead to the need for large gusset plates. Larger overlap distances are possible if the working lines can be offset slightly as illustrated in Figure 4-99. In previous research on stability bracing systems for columns, analytical studies showed that offsetting the working line of the bracing from the joint by 10-20% of the column length often results in very little difference in the performance of the bracing compared to cases where the working lines intersect at a point. Since the top lateral truss behaves like a relative bracing system for a column, the adverse impacts on the effectiveness of the truss may not be significant. Offsetting the truss members from the joint results in less congestion at the joint and provides for better force transfer between the truss members and the flange. In addition, the strut of the K-frame/top truss can be fastened directly to the flange.

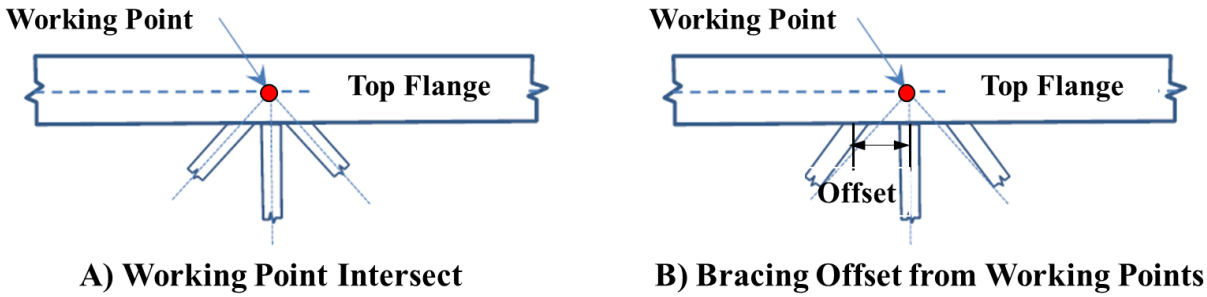

Figure 4-99 Alignment of Bracing Relative to Working Points

FEAs were performed to examined how offsetting braces from a single working point affects the behavior of the tub girders during construction. Lateral displacement, the Von Mises stresses in the top flanges, and the axial load on top lateral braces were chosen as parameters of interest. Figure 4-100 illustrates the top lateral truss of a 72-ft long straight TUB36, which consists of ten panels with a typical panel length of 7.2 ft. The baseline model has concentric braces as shown in Figure 4-101(a). Three other model with various amounts of offset were considered. The offset was set at 1% (0.9 in), 3% (2.6 in) and 5% (4.3 in) of the length of the panels (L_b) respectively [see Figure 4-101(b)]. The offset used in the test specimen is 5 in.

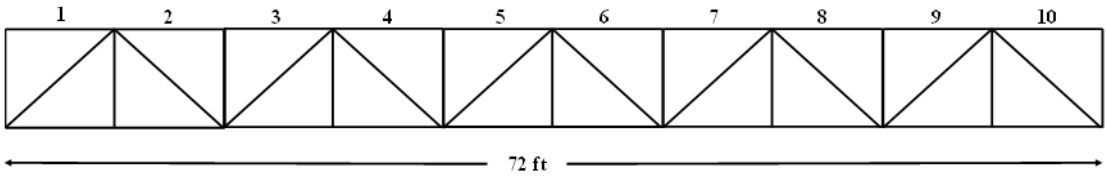

Figure 4-100 Straight Tub 36, 72 ft. long with ten panels

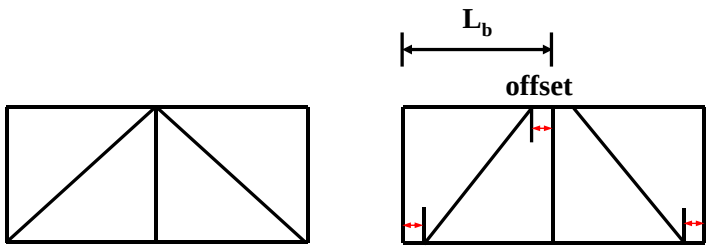

Figure 4-101 Tub girder panels with braces. (a) Working point does not have offset, and (b) Working point has offset

The lateral displacement of the top flange along the tub girder is shown in Figure 4-102 with various amounts of offset. The maximum lateral displacement of the TUB36 was increased by 8% and 16% for offsets of 3% of the panel length and 5% of the panel length respectively. However, the absoltue change is relavely small and less than 0.1 in. When the brace working point was offset by 1% of panel length (L_b), the lateral displacement was essentially the same as the case of the concentric brace connection.

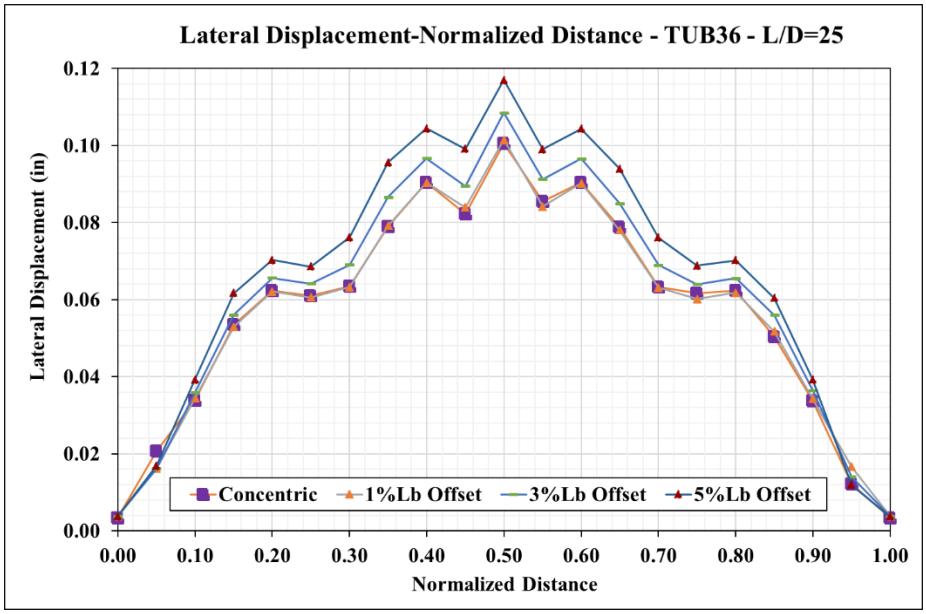

Figure 4-102 Lateral displacement for concentric brace connections, and for brace connections whose working point has an offset equal to 1%, 3% and 5% of the panel length.

Figure 4-103 shows the Von Mises stress distribution of the girder's flanges with different alignments of bracing and working point offsets. All the cases show very similar stresses. Thus, the flange stresses of the TUB36 were not sensitive to the brace offset.

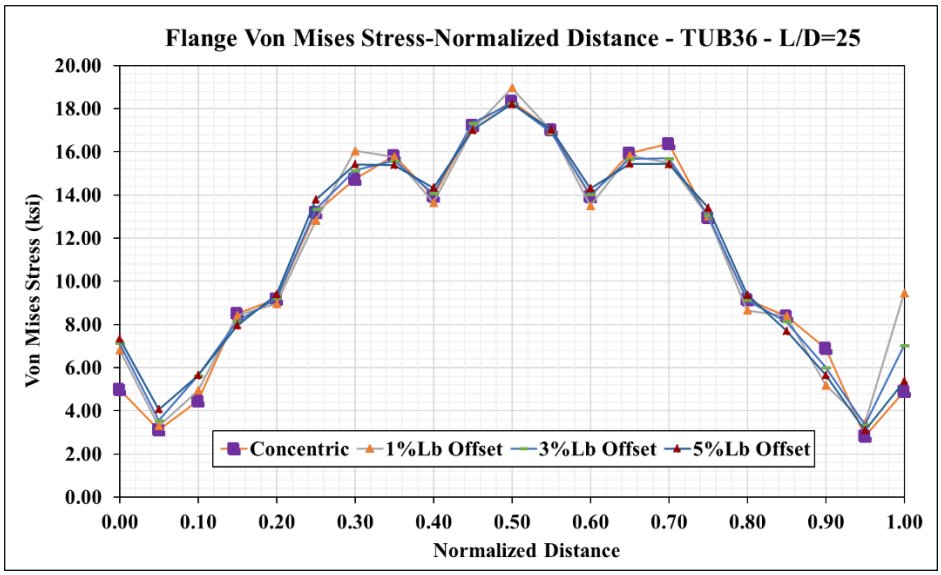

Figure 4-103 Top flange Von Misses stresses for concentric brace connections, and for brace connections whose working point has an offset equal to 1%, 3% and 5% of the panel length.

The effect of the working point offset on the axial force of the top lateral braces is shown in Figure 4-104. The maximum axial forces in the braces of the TUB36 were increased by 61%, 88% and 115% for the cases where the braces working point was offset by 1% of the panel length, 3% of the panel length and 5% of the panel length, respectively. The panels with the maximum increase were Panel 4 and Panel 7 as shown in Figure 4-100.

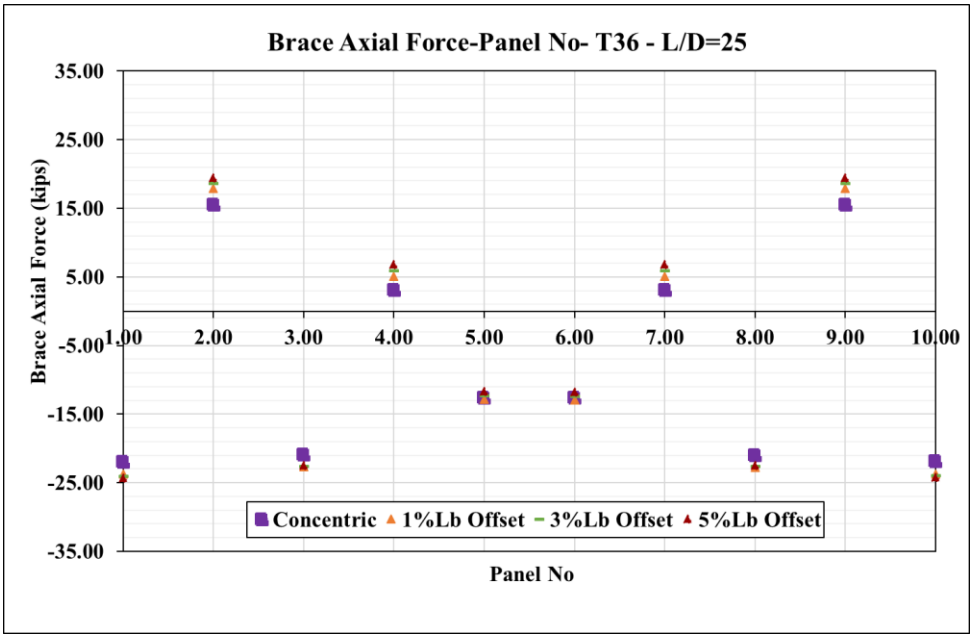

Figure 4-104 Change of the brace axial load for concentric brace connections, and for brace connections whose working point has an offset equal to 1%, 3% and 5% of the panel length.

4.10 Summary

This chapter documented finite element modeling techniques and parametric FEA studies performed on steel tub girder systems with proposed details. The FE models were validated using experimental data. With validated assumptions, parametric studies were performed. Key findings are summarized as the follows:

- A partial length top lateral truss can be used on straight or mildly curved tub girder (radius greater than 2500 ft.) systems with a minimum of 50% braced length of the entire span. For curved systems, additional lateral bending on the unbraced top flange should be properly accounted for to limit stress and lateral deflection. A partial length top lateral truss affects the force distribution among the lateral braces and internal K-frames.

- The layout of internal K-frames does not affect the global stiffness of the girder. Internal K-frames located at every two or three panel points is beneficial in terms of brace force distribution in the struts and K-diagonals. When combined with a partial length top lateral truss, the interaction between the top lateral truss and K-frames can be amplified. Analysis is required to determine an optimal layout.
- Top flange offsets make the flange more prone to local instability but can be controlled by limiting the flange slenderness ratio. Top flange offsets contribute to girder global stability. Offsetting the top flanges does not cause additional lateral bending of the flanges but will affect the force distribution in the top lateral braces.

- The use of lower web slopes increases the forces in the diagonals and struts of the top lateral truss. The use of lower web slopes does not affect the live load distribution significantly.

- Offsetting the braces from a single working point does not affect the global behavior of the girder significantly but increases the axial forces in the top lateral truss members.

The findings will used for the development of design recommendations in Chapter 6.

Chapter 5. Ultimate Strength Experimental Tests

5.1 Introduction

The primary focus of the experimental portion of this research project was the behavior of steel tub girders during construction, and these experiments were conducted on bare-steel (i.e. non-composite) tub girder specimens, as described in Chapter 3. These experiments were conducted primarily in the elastic range of behavior, and so the tub girder specimens were largely undamaged at the completion of the test program. As a final step in the experimental program, a composite concrete slab was added to the tub girder test specimens. The resulting composite tub girder test specimens were then tested to destruction to determine their ultimate strength. The purpose of these tests were to investigate the impact of the proposed improved details on the ultimate capacity of composite steel tub girders. This chapter provides details on the configuration of the test setup, the description of the three specimens, testing program and results of the ultimate capacity tests.

5.2 Description of Specimens

This section describes the composite Baseline Tub Girder (with a 4V:1H web slope and the top flanges centered over the webs), the composite tub girder with Offset Top Flanges, and the composite girder with Flatter Web (with a 2.5V:1H web slope). All three specimens were designed as fully composite. That is, sufficient shear studs were welded on the top flanges so that the flexural strength of the girders was governed by the steel tub girder and the concrete deck rather than by the shear studs.

The composite specimens were tested up to failure in continuous and simply supported configurations to evaluate the ultimate strength behavior of the tub girders under negative and positive moment demands, respectively. First, each composite specimen was tested as a two-span continuous girder with 28-foot and 56-foot spans, as shown in Figure 5-1. These span lengths were selected so that the cross-section under negative moment was able to reach the inelastic range without exceeding the maximum allowed loads in the test setup, which was limited by the capacity of the anchor bolts in the strong floor. After testing the continuous girder configuration, the intermediate support was removed and the girders were tested as simple supported with a span of 84 ft., as shown in Figure 5-2.

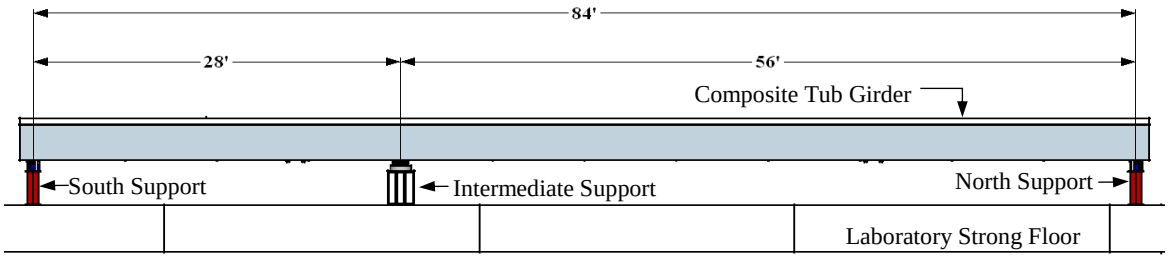

Figure 5-1 - Continuous Girder Configuration

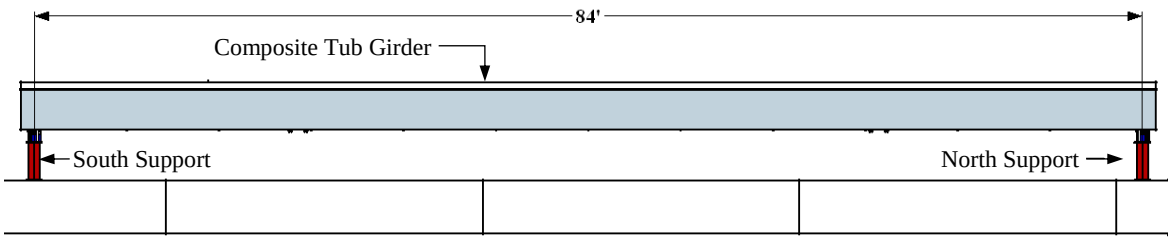

Figure 5-2 - Simply Supported Girder Configuration

Three composite tub girder specimens were tested, as follows:

- Tub # 1: Standard Tub Girder (4V:1H web, top flanges centered over the web)
- Tub #2: Offset Top Flange Tub Girder (4V:1H web, top flanges offset inward from the web)
- Tub #3: Flatter Slope Web (2.6V:1H web, top flanges centered over web).

Cross-sections of the three composite specimens are shown in Figure 5-3 for Tub #1, in Figure 5-4 for Tub #2, and in Figure 5-5 for Tub #3.

The steel tub girders were built with ASTM A709-50 steel, and the design compressive strength for the concrete was 4 ksi. Reinforcing bars with a nominal yield stress of 60 ksi were used in the concrete deck. Material tests were conducted to characterize the actual strength of the concrete and steel of the specimens. Concrete cylinders were tested at 7, 14 and 28 days after the casting of the concrete deck, and on the first day of testing for each specimen. Results of the material tests are reported in Section 5.4.

The design geometry of the concrete deck was 111 inches wide and 6.5 inches thick along the entire length of the girders. The concrete deck was constructed with two 2-foot-long overhangs. The length of the overhang is about 0.76 times the distance “w” between the centerline of the top of the webs (w=63 inches for the specimens). Section 6.11.2.3 of AASHTO 2017 requires that the distance between adjacent tub girders (between centerlines on the top of the adjacent webs) to be between 0.80 and 1.20 times the distance “w” in order to use the distribution load factors listed in AASHTO 2017. Assuming the overhang is half of the distance between adjacent girders, the 2-foot-long overhangs provide a reasonable effective width of concrete slab for the girder. The thickness of the concrete deck is less than typical concrete decks built in Texas. However, the 6.5 inch thickness was selected to reflect the reduced scale of the test specimens.

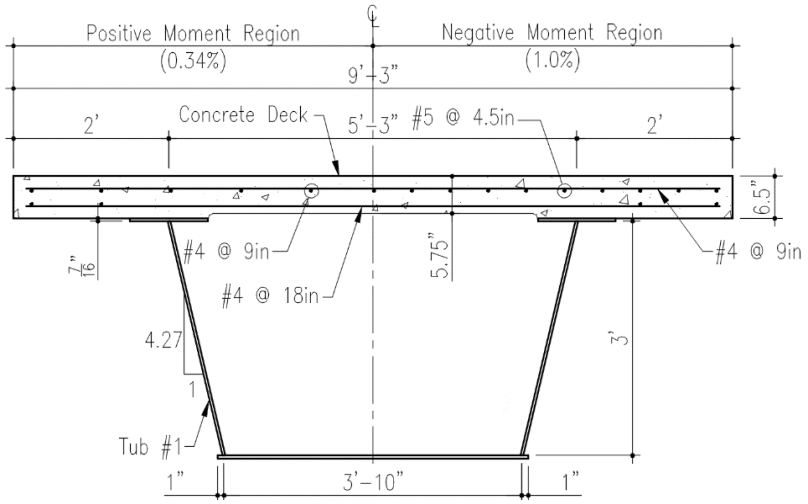

Figure 5-3 - Composite Tub #1

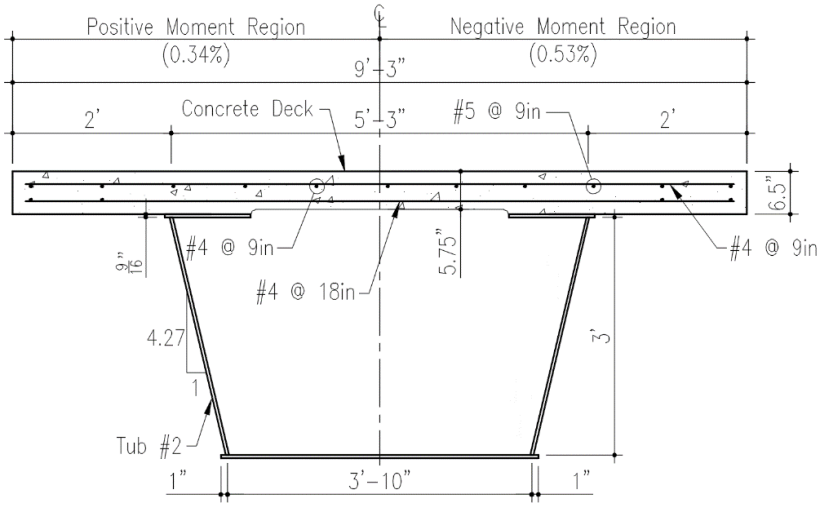

Figure 5-4 - Composite Tub #2

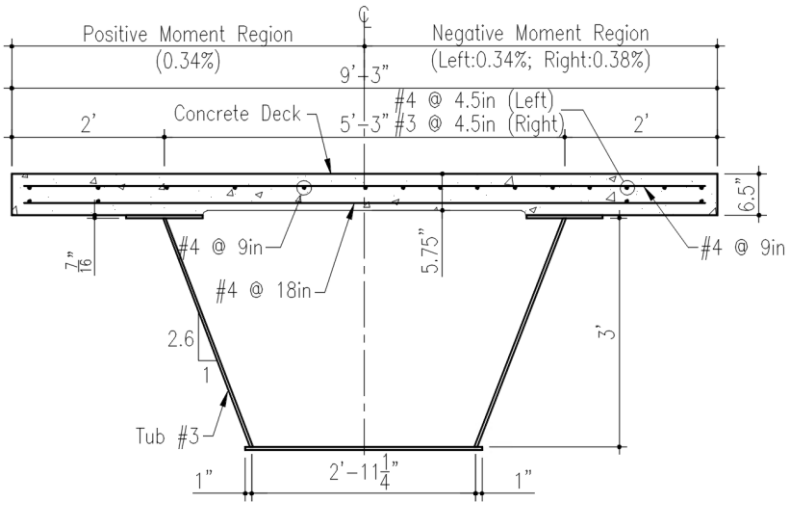

Figure 5-5 - Composite Tub #3

Initially, the three steel tub girders were designed so that they can behave elastically during the experimental buckling tests with a simple supported configuration, which were reported in Chapter 3. Thus, the specimens were sized only for positive bending demands and not for negative bending. As a consequence, the bottom flange of the specimens was reinforced to avoid local buckling in the region subjected to negative bending (over intermediate support) during the ultimate strength tests. In addition, a solid steel diaphragm was added in the tub girders at the location of the intermediate support in order to withstand the reaction forces at that location.
The solid diaphragm of Tub #1 was built from a W30x90 wide flange section. Considering that the web of this wide flange (t_w=0.47") was not enough to withstand the large reaction force over the support, a half-inch thick doubler plate was welded to the web and half-inch thick vertical stiffeners were added on both sides of the diaphragm. Additionally, the bottom flange of Tub #1 was reinforced with a longitudinal stiffener consisting of a 7-foot long L5"x5"x1/2" on each side of the solid diaphragm, as depicted in Figure 5-6.

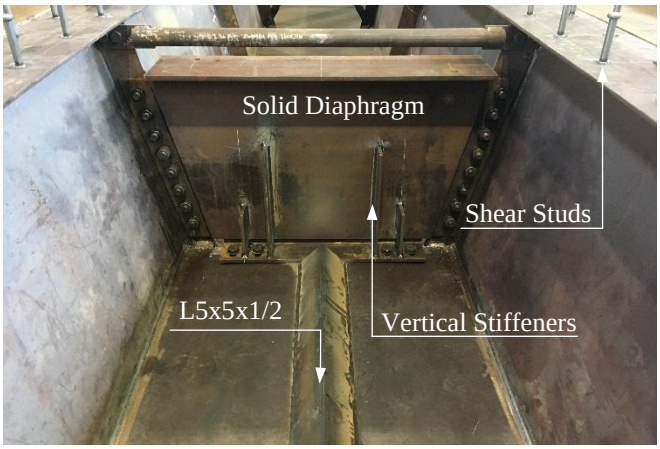

Figure 5-6 - Solid Diaphragm and Bottom Flange Reinforcement – Tub #1

The solid diaphragm of the Tub #2 was fabricated from a W24x250 wide flange section. A doubler plate was not required for this cross section because the web of this wide flange (t_w=1.04")

was thick enough to withstand the large reaction force over the support. However, half-inch thick full vertical stiffeners were added on both sides of the diaphragm. Different from Tub #1, the bottom flange of Tub #2 was reinforced by casting a 6.5-inch thick concrete slab along the bottom flange in the negative moment region (14-foot long concrete slab over the intermediate support). Enough shear studs were welded to the bottom flange to provide fully composite action between the bottom flange and the concrete slab. In addition, shrinkage reinforcement was added to the concrete slab.

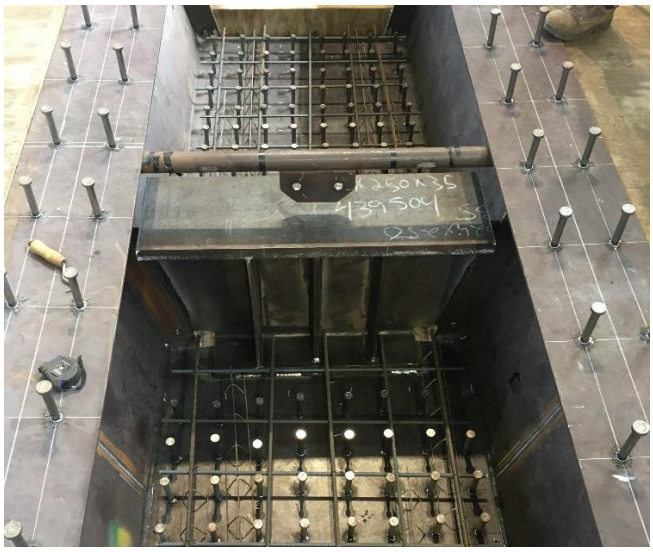

Figure 5-7 - Solid Diaphragm and Bottom Flange Reinforcement (before Casting) - Tub #2

The solid diaphragm of the Tub #3 was fabricated with a 1 ½ in-thick plate. Full vertical stiffeners were not required due to the thickness of the plate. Similar to Tub #2, the bottom flange of Tub #3 was reinforced by casting a 6.5-inch thick concrete slab along the bottom flange in the negative moment region (14-foot long concrete slab over the intermediate support). Again, enough shear studs were welded to the bottom flange to attain fully composite action between the bottom flange and the concrete slab. Also, shrinkage reinforcement was added to the concrete slab.

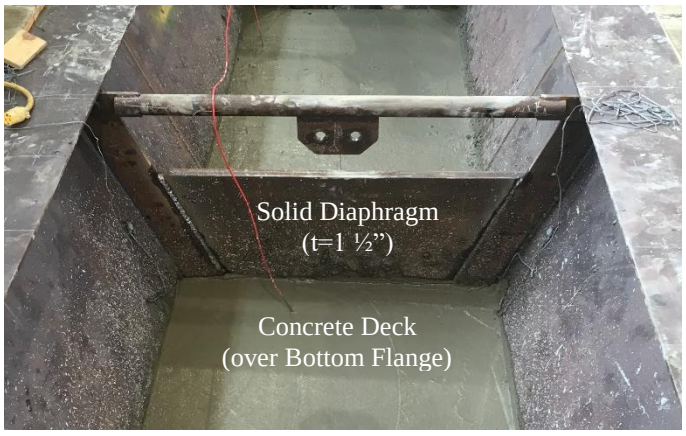

Figure 5-8 - Solid Diaphragm and Bottom Flange Reinforcement (after Casting) - Tub #3

The concrete deck of Tub #1 was provided with steel reinforcement in the positive and negative moment regions. The deck in the positive moment region was reinforced for shrinkage (0.34%) according to the Section 5.10.8 of AASTHO 2017. The maximum spacing of reinforcing bars for shrinkage is less than 1.5 times the thickness of the slab to satisfy Section 5.10.3.2 of AASHTO 2017. In the negative moment region, the steel reinforcement represented 1% of the concrete deck cross-sectional area, to satisfy Section 6.10.1.7 of AASHTO 2017. Similarly, the concrete deck on Tub #2 and Tub #3 was provided with shrinkage reinforcement in the positive moment region. The negative moment region was reinforced with a steel ratio of about 0.53% in Tub #2. For Tub #3, the steel reinforcement in the negative moment region was split in two parts: left and right side respect to girder centerline). The steel ratios of 0.34% and 0.38% were used for the left and right sides, respectively. The variations in negative moment reinforcing among the specimens was done to provide data on deck cracking in negative moment regions for a different research project. Although the deck reinforcing influenced the cracking pattern of the concrete, the steel did not have significant impact on the ultimate capacity of the girders. The layout of steel reinforcing rebar of the concrete deck on Tub #1 is shown in Figure 5-9. The reinforcing rebar layout of Tub #2 and #3 was similar except for the rebar distribution on the negative moment region. Figures 5-10 and 5-11 show photos of the deck for Tub #1 before and casting of the concrete.

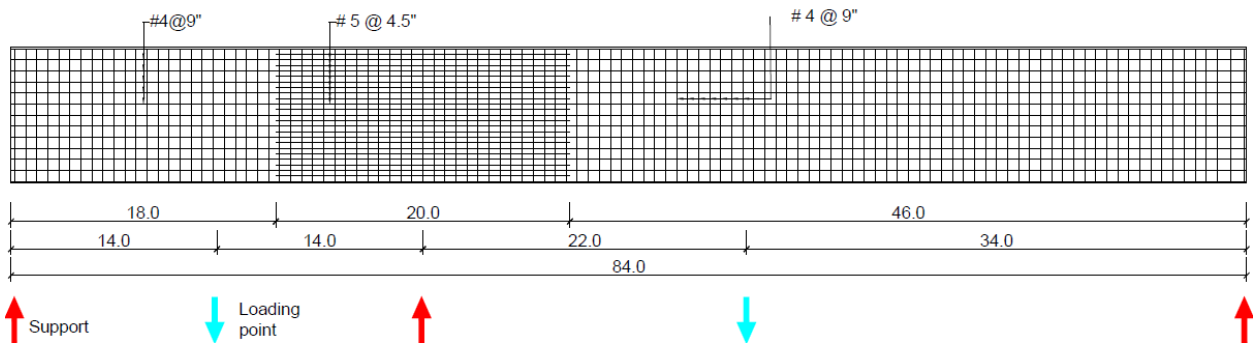

Figure 5-9 - Steel Reinforcement Rebar Layout – Tub #1

Figure 5-10 - Steel Reinforcement of Concrete Deck –Tub #1

Figure 5-11 - Concrete Deck Casting - Tub #1

5.3 Description of Test Setup

A test setup was designed and built in the Ferguson Structural Engineering Laboratory to test the three composite specimens up to failure in continuous and simple supported configurations. The setup consisted of three supports and two loading frames (three loading frames for the Tub #2 and #3) that were placed on and connected to the strong floor in the laboratory, as shown in Figure 5-12. The intermediate support was designed to work as a pin support by allowing rotation and restricting translation. The north and south supports allow some rotational and lateral flexibility due to the web flexibility of the W36x135 wide flange sections that served as supports. Each specimen was seated over two tilt saddles on the north and south supports and a larger single tilt saddle over the intermediate support, which allow rotations of the specimen on each support. Two 200-kip load cells were placed under the two tilt saddles on each end support. A 1000-kip load cell supported the larger tilt saddle on the intermediate support as shown in Figure 5-13. Hydraulic rams with capacities of 1000 kips were mounted on the loading frames.

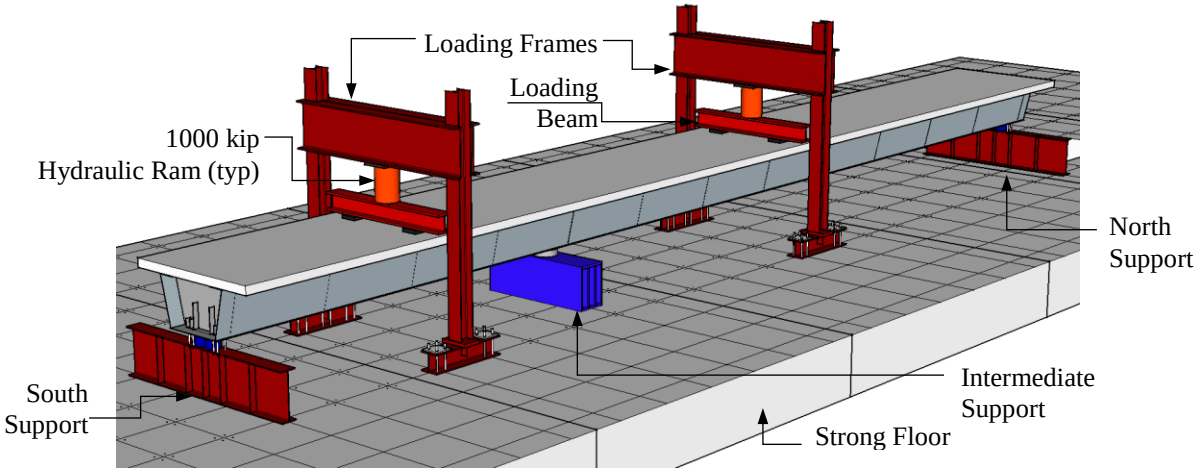

Figure 5-12 - 3D Rendering of Test Setup - Tub #1

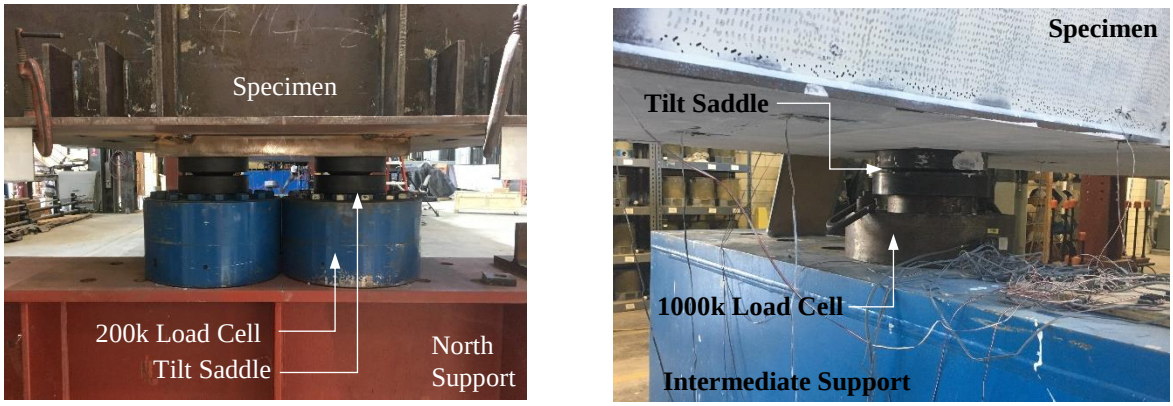

Figure 5-13 - Tilt Saddles and Load Cells at End Supports (left), at Intermediate Support (right)

The test setup was fabricated and constructed to permit two individual tests to be carried out on each girder. The first test consisted of a two-span continuous girder, while the second test consisted of a single span girder with simple supports. An elevation of the test setup for the continuous girder test for the Tub #1 is shown in Figure 5-14. Two equal loads were applied simultaneously at both loading frames during the test. The test setup that was used for Tub #2 for the continuous girder configuration had three loading frames. Because of the thicker top flanges and the concrete deck in the bottom flange in the negative moment region, the ultimate capacity of Tub #2 was higher than Tub #1. Thus, the third loading frame (10ft. from the intermediate loading frame, Figure 5-15) was necessary to reach the load levels to yield the second tub girder at the intermediate support location. This third loading frame was anchored directly to the laboratory strong floor with each column connected to one anchor bolt group, different from the other two loading frames that were connected to a spreader beam anchored to the strong floor by two anchor bolt groups. Because of the difference in the connection to the laboratory strong floor, the two original loading frames had more load capacity than the third one. For this new configuration, the loading protocol was to load the two original frames up to their maximum capacity. Then, while holding the load in the two frames, the third loading frame was activated to add more load. This protocol was found cumbersome not only for testing, but also to post-process data. Thus, the test setup configuration was altered for the third specimen. For the Tub #3 test setup, shown in Figure 5-16, the third loading frame was anchored to the laboratory strong floor (8ft from the intermediate loading frame) in a similar way that the other two loading frames so that all the loading frames had the same loading capacity. Three equal loads were applied simultaneously at the three loading frames during the test. Photos of the continuous girder test setups for all three specimens are shown in Figures 5-18, 5-19 and 5-20.

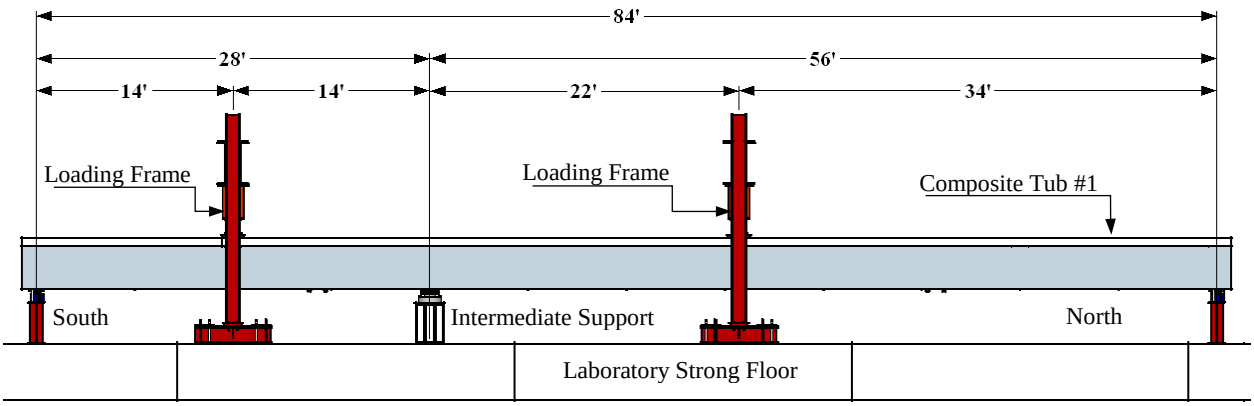

Figure 5-14 - Continuous Girder Test Setup - Tub #1

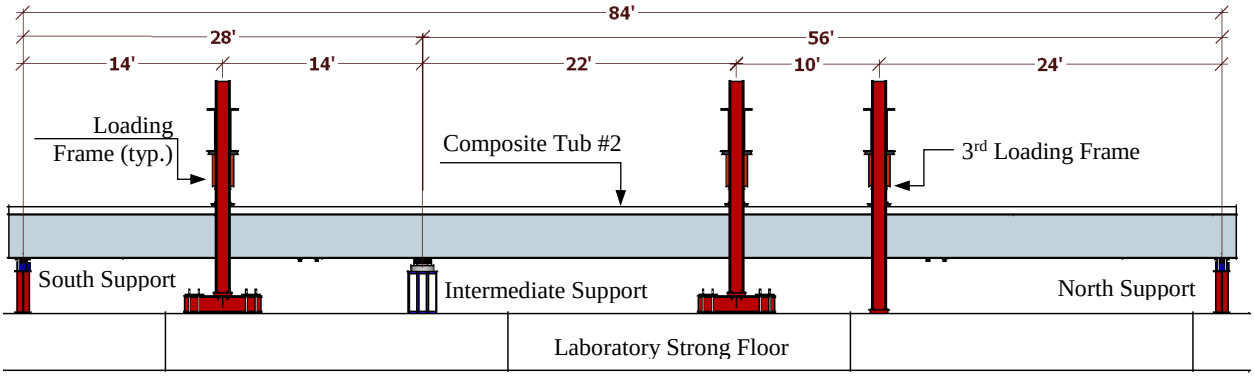

Figure 5-15 - Continuous Girder Test Setup - Tub #2

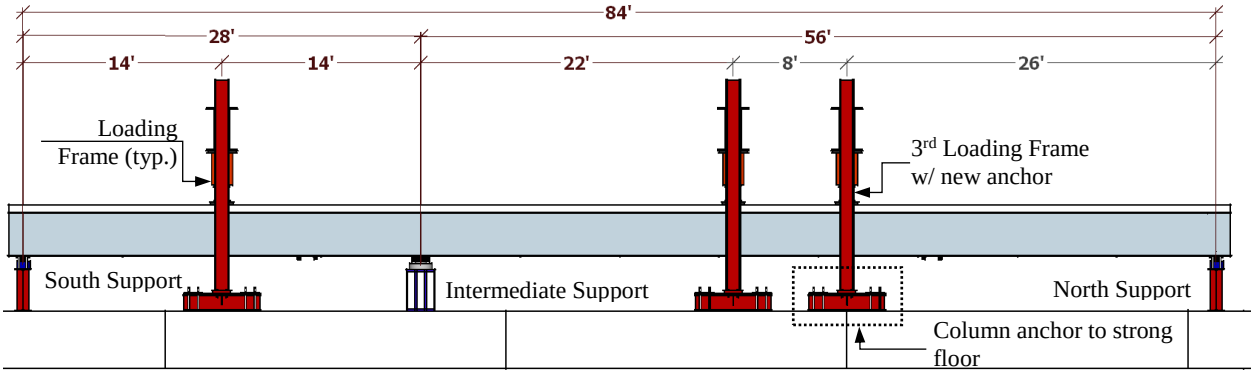

Figure 5-16 - Continuous Girder Test Setup - Tub #3

The testing sequence consisted of first testing the continuous girder configuration followed by the simply supported girder configuration. To obtain the simply supported configuration, the intermediate support was removed. In this configuration, the load was applied in the loading frame located 34ft. from the north support, as shown in Figure 5-17. The three specimens were tested with the same simply supported test setup configuration.

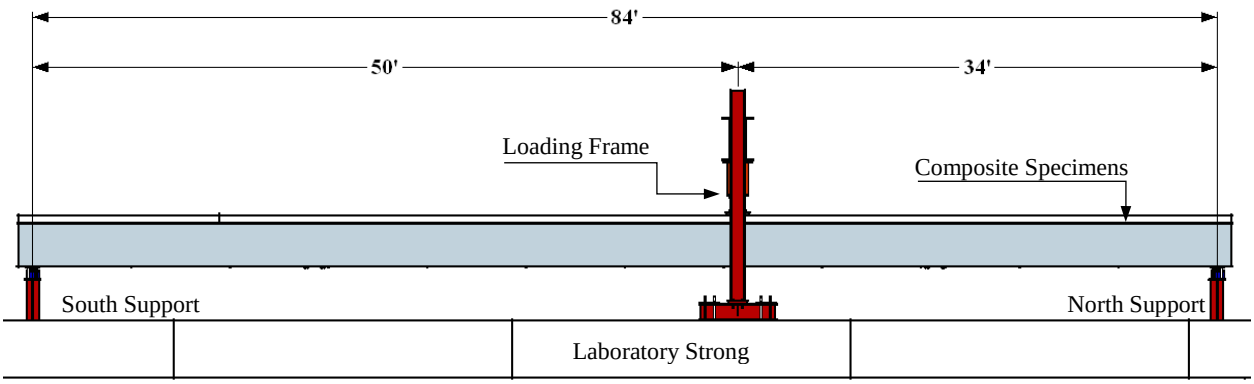

Figure 5-17 - Simply Supported Girder Test Setup

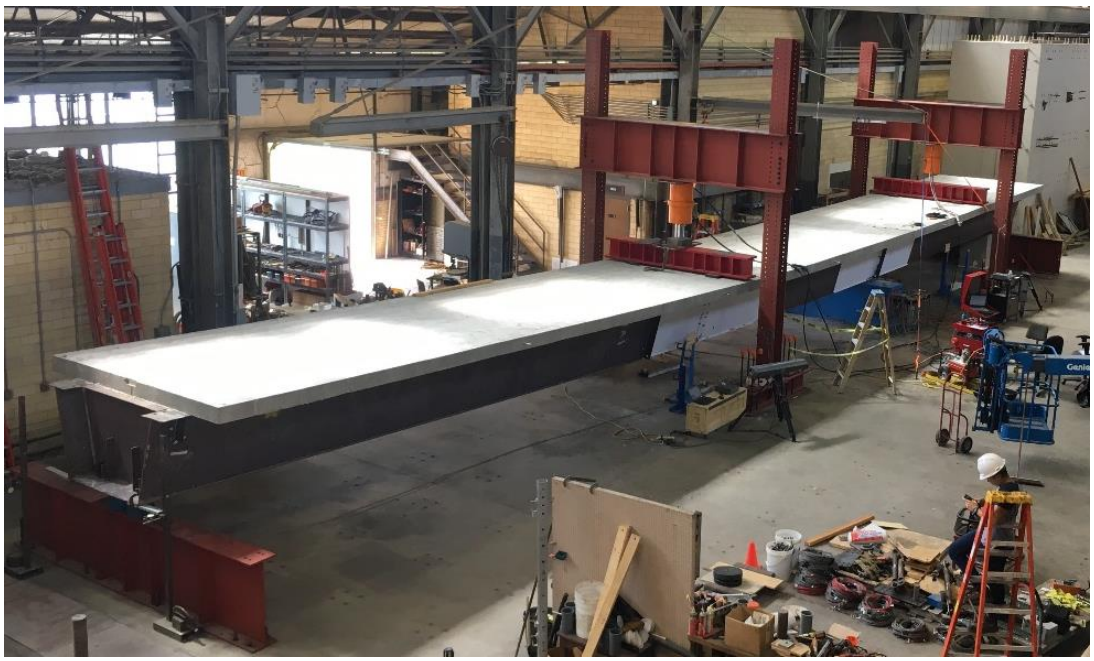

Figure 5-18 - Continuous Girder Test Setup - Tub #1

Figure 5-19 - Continuous Girder Test Setup - Tub #2

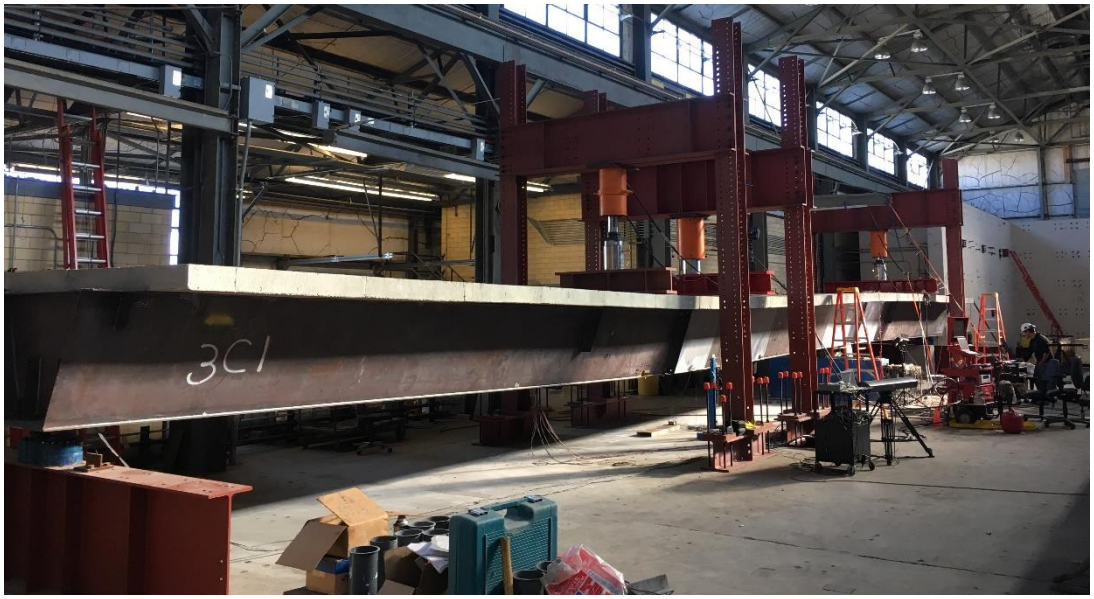

Figure 5-20 - Continuous Girder Test Setup - Tub #3 (During Test)

In order to apply the loads, a hydraulic ram with 1000 kips capacity was mounted on each loading frame. The load was transferred to the composite girders through steel loading beams placed over two 18" long x 9" wide x 1 ¾" thick bearing elastomeric pads, which were located over the steel tub girder top flanges (63in apart). Under the hydraulic ram, a tilt saddle on top of a load cell was located over the loading beam. The purpose of the saddle and the load cell was to accommodate rotations in the specimen and to record the applied loads during the test, respectively. Figure 5-21 shows the loading setup on each loading frame. When three frames were loaded, load cells were provided at the location of two loading frames. For simply supported configurations, no load cell was placed at the loading point.

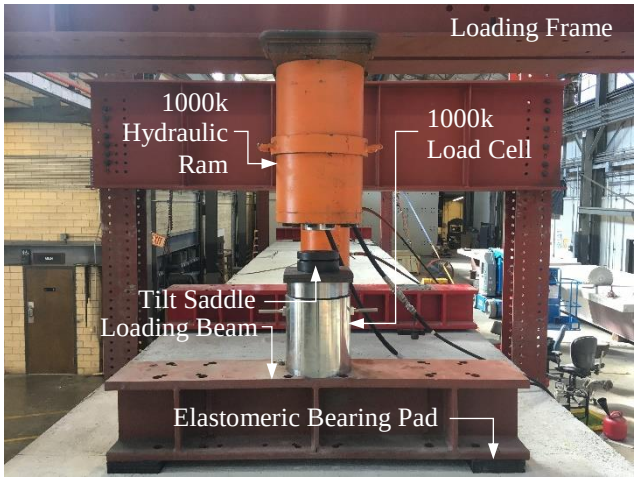

Figure 5-21 - Loading Setup

5.4 Material Testing

To characterize the material strengths of the different components of the composite girders, material tests were performed on the deck concrete, the reinforcing steel, and the steel plates of the tub girders. The concrete material properties were determined before conducting the ultimate strength tests on both girders. The compression strength was determined by compression testing of 4-inch diameter cylinders, while modulus of elasticity tests were performed in the same type of cylinders. The casting of the concrete decks took two trucks for each specimen due to the volume of concrete. The concrete on the negative and positive moment regions were poured from the first and second trucks, respectively. Cylinders were made during the casting from both trucks. The two ultimate strength tests were performed before 28 days after the casting; however, no significant variation in the strength of the concrete was observed between the test day and at 28 days. The material properties of the concrete for the three specimens are shown in Table 5-1.

Table 5-1 - Concrete Material Properties

	Positive Moment		Negative Moment		Bottom Flange		Test Time
	f'c (ksi)	MOE (ksi)	f'c (ksi)	MOE (ksi)	f'c (ksi)	MOE (ksi)	(days)
Tub #1	5.84	5180	5.85	5700	N/A	N/A	21
Tub #2	5.40	6050	4.08	4175	5.70	4450	14
Tub #3	4.85	5025	5.10	4675	5.90	5550	28

f'c: Compressive Strenght
MOE: Modulus of Elasticity

The material properties of the steel plates of the tub girders were obtained by conducting tension tests on coupons that were cut from the top flanges, from the bottom flange, and from the webs. All the plates that form each tub girder specimen were fabricated by splicing two plates along the length of the girder. Coupons from both spliced plates were produced and tested. Table 5-2, Table *5-3*, and Table *5-4* report the properties of the stress-strain curve corresponding to the plates on each tub girder. The static yield stress, as it is comparable to the slow load rate used to test the specimens in the laboratory, were used to calculate the ultimate strength of the girders.

Two steel coupons were produced and tested from each plate, and they were averaged to estimate the ultimate strength of the specimens.

Table 5-2 - Steel Plate Properties - Tub #1

Location	Plate Element	Coupon	Upper Yield Point (ksi)	Dynamic Yield Stress (ksi)	Static Yield Stress (ksi)	Strain at Onset of Hardening (ksi)	Initial Strain Hardening Modulus (ksi)	Dynamic Tensile Strength (ksi)	Strain at Development of Tensile Strength	Elongation (strain at fracture)
	Top Flange	1N_1	63.1	60.9	57.5	1.7%	360	83.3	14.8%	34.40%
	Top Flange	1N_2	62.3	60.7	57.3	1.6%	290	83.7	14.7%	33.60%
North End	Bottom Flange	1N_3	65.6	61.7	58.3	1.80%	340	83.9	15.50%	32.20%
	West Web	1N_4	64.1	61.7	58	1.90%	375	82.7	16.10%	32.30%
	East Web	1N_5	61.8	61.3	58.2	1.6%	405	84	14.90%	29.40%
	Top Flange	1S_1	63.8	61.5	58.6	1.70%	480	84	14.70%	34.60%
	Top Flange	1S_2	63.9	61.5	58.7	1.6%	590	83.8	14.80%	34.70%
South End	Bottom Flange	1S_3	64.8	61.4	58.3	1.70%	430	84.1	16.10%	31.30%
	West Web	1S_4	64.6	62.95	59.5	2.20%	400	77.2	16%	36.50%
	East Web	1S_5	65.5	61.97	58.4	2.40%	450	76	14.90%	35.20%

Table 5-3 - Steel Plate Properties - Tub #2

Location	Plate Element	Coupon	Upper Yield Point (ksi)	Dynamic Yield Stress (ksi)	Static Yield Stress (ksi)	Strain at Onset of Hardening (ksi)	Initial Strain Hardening Modulus (ksi)	Dynamic Tensile Strength (ksi)	Strain at Development of Tensile Strength	Elongation (strain at fracture)
	Top Flange	2N-1	62.2	61.5	59.1	1.7%	505	83.8	20.1%	36.1%
	Top Flange	2N-2	61.4	60.4	58.0	1.6%	310	82.7	20.0%	33.4%
North End	Bottom Flange	2N-3	65.9	60.6	58.0	1.6%	425	84.4	15.5%	33.6%
	West Web	2N-4	64.4	59.8	58.1	2.0%	365	83.1	15.0%	31.2%
	East Web	2N-5	63.1	59.8	58.1	1.7%	405	83.3	16.5%	31.2%
	Top Flange	2S-1	62.5	60.8	58.0	1.6%	370	82.6	20.0%	35.0%
	Top Flange	2S-2	63.4	62.6	60.1	1.7%	375	84.0	20.0%	35.3%
South End	Bottom Flange	2S-3	64.9	61.6	59.4	1.6%	450	85.1	17.5%	32.6%
	West Web	2S-4	64.0	61.5	58.9	2.4%	330	76.6	15.5%	34.4%
	East Web	2S-5	64.9	60.6	58.5	2.4%	260	76.7	16.4%	33.7%

Table 5-4 - Steel Plate Properties - Tub #3

Location	Plate Element	Coupon	Upper Yield Point (ksi)	Dynamic Yield Stress (ksi)	Static Yield Stress (ksi)	Strain at Onset of Hardening (ksi)	Initial Strain Hardening Modulus (ksi)	Dynamic Tensile Stress (ksi)	Strain at Development of Tensile Strength	Elongation (strain at fracture)
	Top Flange	3N-1	62.9	58.4	56.4	1.6%	420	83.0	16.5%	33.3%
	Top Flange	3N-2	61.0	60.0	58.0	1.0%	410	82.9	10.8%	29.5%
North End	Bottom Flange	3N-3	64.8	59.8	57.7	1.7%	460	83.5	15.1%	32.30%
	West Web	3N-4	65.5	61.4	59.7	2.0%	410	83.4	15.5%	32.0%
	East Web	3N-5	64.4	62.0	59.7	2.0%	425	83.9	14.9%	29.4%
	Top Flange	3S-1	60.7	59.8	57.0	1.5%	590	84.2	15.1%	29.0%
	Top Flange	3S-2	66.3	61.9	60.1	1.5%	520	84.7	15.3%	33.5%
South End	Bottom Flange	3S-3	65.7	60.7	58.5	1.7%	520	83.8	16.2%	31.1%
	West Web	3S-4	60.2	57.9	56.0	1.9%	480	80.8	17.9%	32.0%
	East Web	3S-5	60.0	56.0	54.6	1.6%	530	81.8	15.8%	33.2%

Similar to the steel coupons, uniaxial tension testing of the deck reinforcement was conducted on short samples of reinforcing bars that were used in the deck of each specimen. Table 5-5 presents the measured yield stress and tensile strength values.

Table 5-5 - Reinforcing Rebar Material Properties

Rebar Number	Dynamic Yield Stress (ksi)	Static Yield Stress (ksi)	Dynamic Tensile Strenght (ksi)	Specimen
#3	71.4	70.3	117.4	Tub3
#3	72.4	72.2	117.7	Tub3
#4	61.3	59.3	99.4	Tub1
#4	64	61.7	104.3	Tub2
#4	59.2	57	93.5	Tub3
#5	63.5	61	102.9	Tub1
#5	63.7	61.1	103.3	Tub2

5.5 Instrumentation

The behavior of the tub girders during testing was recorded by instruments installed along the girder, which measured the reaction forces, longitudinal strains, vertical deflections and support movements. Four 200-kip and 1000-kip load cells were calibrated to record reaction loads. Two 1000-kip load cells were calibrated to record loads applied at loading points. The experimental data was collected from the instruments using an Agilent data acquisition system and LabVIEW software. A photo of the data acquisition system is shown in the left portion of Figure 5-22. Deflections of the tub girder cross-section in three-dimensions were measured at loading points using an optical motion tracking system known as the Optotrak Certus, shown in the right portion of Figure 5-22. The cameras of this system, with three lenses, are able to capture infrared signals of the LED markers mounted on the test specimen and then measure three-dimensional movements. This infrared vision system collected vertical and horizontal deflections with relatively high accuracy (error of about 0.01 mm). In addition, vertical deflections were measured with string potentiometers connected to opposite sides of bottom flange at loading point locations.

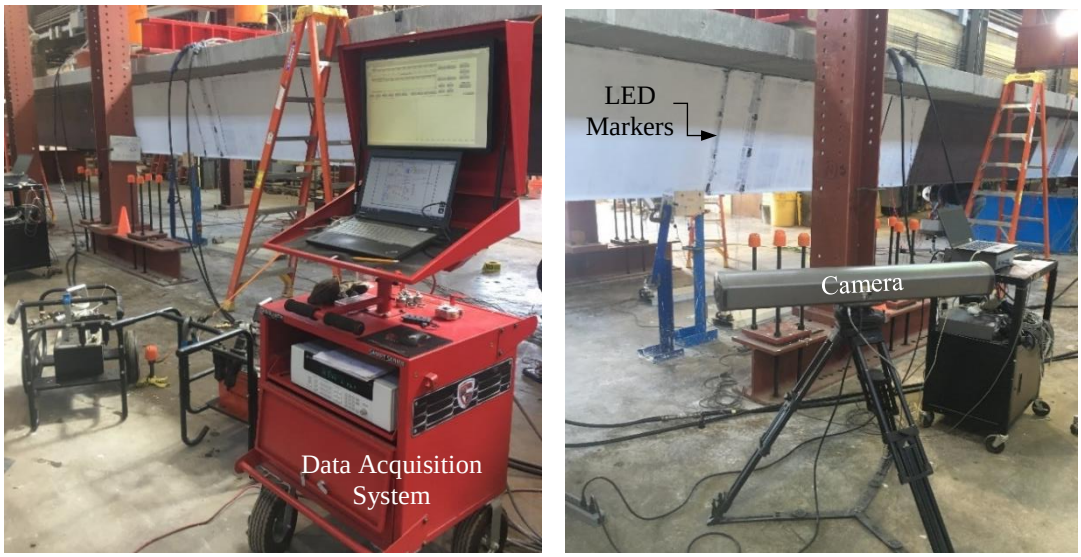

Figure 5-22 – Data Acquisition System (left), and Optical Motion Tracking System (right)

Longitudinal strains were measured with linear foil gauges installed in the steel tub girder and in the concrete deck. Figure 5-23 shows a plan view of a typical specimen location of

instrumentation. Figure 5-24 shows additional details of the instrumentation layout in the steel girder at the intermediate loading frame location.

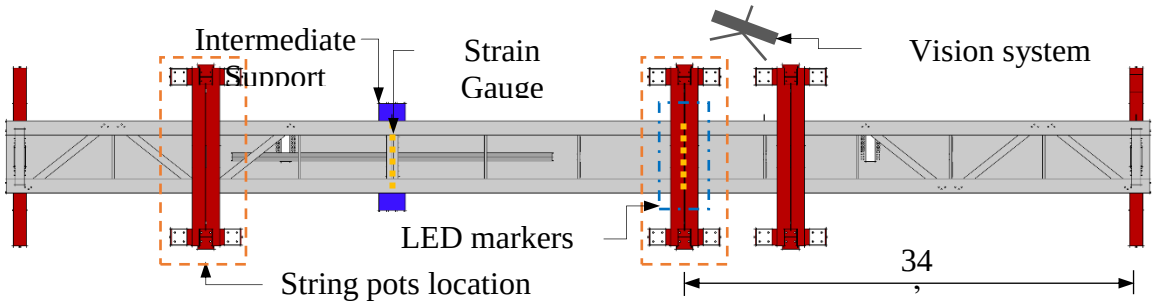

Figure 5-23 – Instrumentation Layout on Steel Girders - Plan View

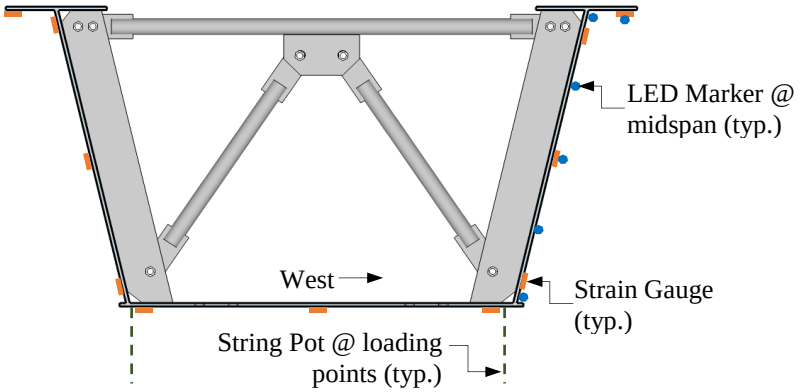

Figure 5-24 - Instrumentation Layout at Intermediate Loading Point – Section

Besides longitudinal strain gauges, a digital image correlation (DIC) system was used to measure longitudinal strains more accurately, as shown in Figure 5-25. The DIC calculates strains by comparing digital photographs of the specimen at different stages of the test.

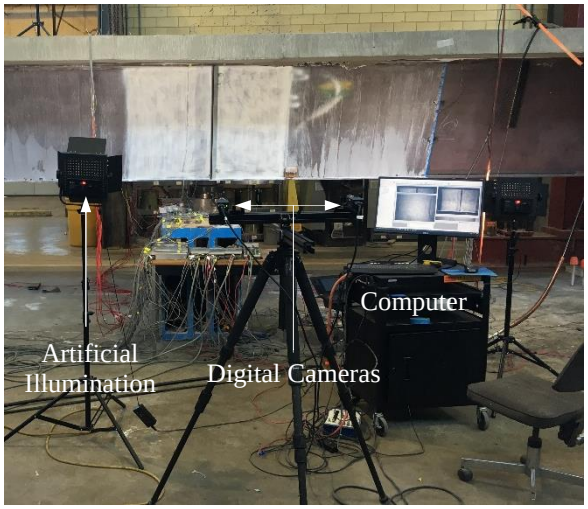

Figure 5-25 - Digital Image Correlation (DIC) Setup

5.6 Test Program

Each specimen was tested as a continuous and as a simply supported system. The continuous girder configurations were monotonically loaded until significant yielding was observed in the cross-section over the intermediate support. The simply supported configurations were subjected to monotonic loading up to failure to determine the ultimate flexural strength of the composite tub girders under positive moment.

The first test for all three specimens was as a continuous system. Tub #1 was loaded with two loading frames (one on each span, Figure 5-14) simultaneously with equal loads. Tub #2 was first loaded with the two initial loading frames with 525 kips on each frame, and then the third frame was loaded while maintaining a constant load in the other two loading frames. Tub #3 was loaded with three loading frames (Figure 5-16) simultaneously with equal loads when tested as continuous girder. For the simply supported configuration, all girders were monotonically loaded with the loading frame located 34' from the north support (Figure 5-17). Control of the applied loads was manual, using a pneumatically driven hydraulic pump. Data was constantly recorded during the entire tests at one-second intervals. Visual evaluation was performed at every 25-kip increment in total load in the elastic range, and every ½-inch increment in deflection beyond that.

5.7 Test Results

As previously mentioned, two phases of ultimate strength testing each specimen conducted on each specimen: a continuous configuration and a simply supported configuration. A description of the tests followed by an analysis of the results is presented in the following sections.

5.7.1 Standard Tub Girder (Tub #1)

Figure 5-26 presents the load-deflection behavior of Tub #1 during the ultimate strength test in the continuous girder configuration. Two load deflection plots are presented in Figure 5-26 which correspond to the vertical deflections at the loading frame locations versus the total load applied on the girder. The total load is the sum of the loads at the two loading frames. Since the loads were equal at each loading frame, the load at each individual loading frame was half the total load. The north span showed higher deflections as it is the longest span of the continuous system. At around 700 kips of total load, a loud noise came from the test specimen, and the load dropped about 75 kips. Loading was then continued on the girder. The test was stopped at a total load of 1090 kips when the load deflection curve started to flatten significantly. No further load was applied to avoid significant plastic deformations in the girder that might hinder the simply supported configuration test. After completion of testing on the simply supported configuration, the girder was cut apart, revealing that the internal diaphragm over the intermediate support had buckled, as shown in Figure 5-27. The buckling of the diaphragm was the apparent cause for the load drop observed during the continuous configuration test.

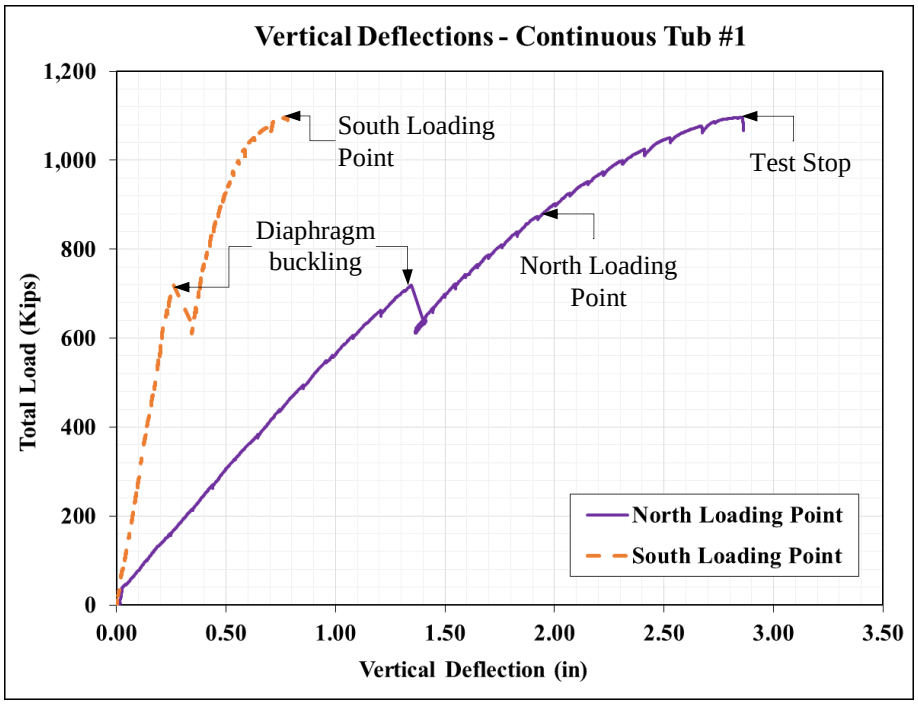

Figure 5-26 - Load-Deflection Curves - Continuous Tub #1

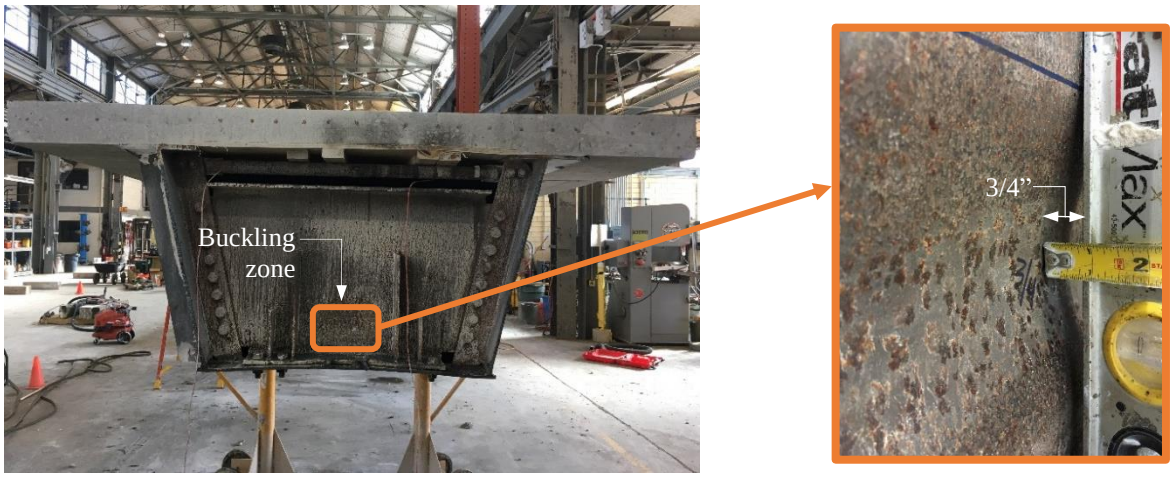

Figure 5-27 - Section Cut at Diaphragm Location - Tub #1

Figure 5-28 shows the load-deflection behavior of Tub #1 tested in the simply supported configuration. The limitation of 9 inches in the stroke of the hydraulic ram required that the test be completed in three loading stages. When the limit of the stroke in the actuator was reached, the actuator was unloaded and shim plates were installed before the girder was reloaded. In Figure 5-28, the graph shows the loading and unloading as shim plates were added. At a load of around 260 kips, and a deflection of 5 inches, the response of the systems started to become inelastic with a gradual change of stiffness in the system. Extensive plastic deformations where observed at deflection of about 13.5 inches, when the response started to flatten significantly at a load of 353 kips. The test was stopped at this point to avoid any damage to the test setup. The white wash

flaking shown in Figure 5-29 indicates the significant amount yielding produced in the web and bottom flange during the test.

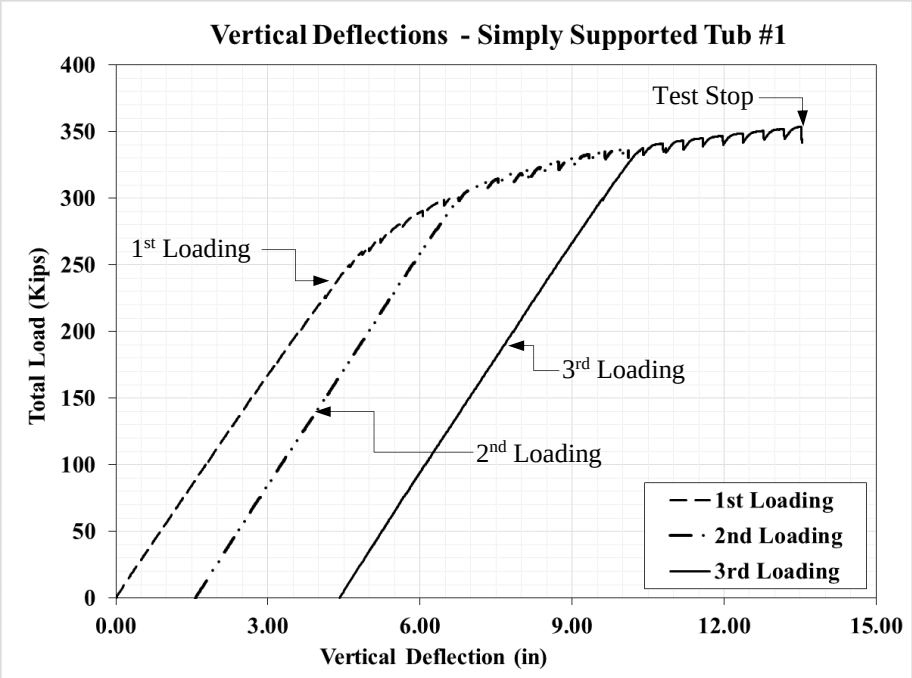

Figure 5-28 - Load-Deflection Curve - Simply Supported Tub #1

Figure 5-29 - White Wash Showing Yielding: West Web (left), and Bottom Flange (right)

5.7.2 Offset Top Flange Tub Girder (Tub #2)

Figure 5-30 presents the load-deflection response of Tub #2 tested in the continuous configuration. Two load-deflection curves are presented which represent the deflections at the initial two loading frames versus the total load applied. The experimental test was stopped at a total load of 1320 kips when the load deflection started to flatten significantly. As described previously, the load on this tub girder configuration was applied with three loading frames, as shown in Figure 5-15. First, the initial two loading frames applied a total load of 1050 kips. The total load of 1050 represented the maximum load that could be applied with these two loading

frames. After the limiting load in these two frames was reached, the force in the two actuators was held constant while the third load was incremented. The third load was applied to the system through a test frame located 24 ft. from the North support (10 ft. from the other load in the north span). This change in load produced the change in slope in the load-deflection curves in Figure 5-30 because the deflection measurements are taken in a different location than where the third load is applied. As the third load was applied, a slight degradation in the stiffness was noticed with increasing load. This change in slope was due to yielding in the top flanges and top of the webs in the tub girder at the intermediate support location, and at the bottom flange at the location of the north loading point. The yielding of the steel plates in both cross-sections was determined from strain gauge readings. To obtain more data about the source of inelasticity, the Digital Image Correlation (DIC) system described earlier was used to measure the deformations, and strains at one of the webs at the intermediate support. Figure 5-31shows the strain contour of the west web captured with the DIC system. The top flange and the top of the web experienced significant yielding, based on the DIC measured strains.

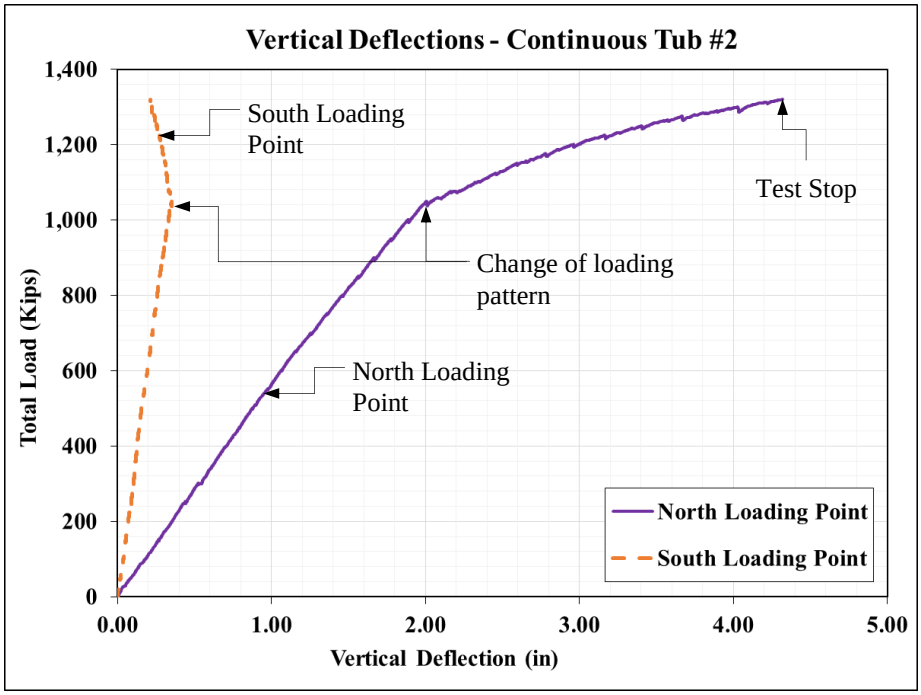

Figure 5-30 - Load-Deflection Curve - Continuous Tub #2

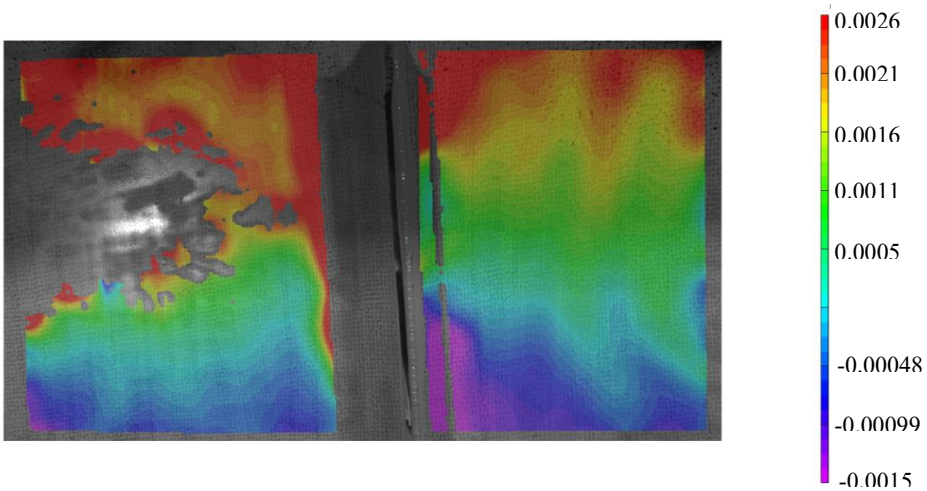

Figure 5-31 - Strain Contour on West Web at Intermediate Support Location – Tub #2

Figure 5-32 shows the load-deflection behavior of the Tub #2 tested in the simply supported configuration. As was the case for Tub #1, several loading stages were required due to stroke limitations of the hydraulic ram. At a load of around 266 kips, and a deflection of 5.3 inches, the response of the systems started to become inelastic with a gradual change of stiffness in the system. The load-deflection response became almost flat after application of the third stage of loading. Extensive plastic deformations were observed with a maximum deflection of about 16.6 inches, when the concrete in the deck crushed, the top of the webs buckled, and the tub girder unloaded suddenly unloaded, indicating ultimate failure of the girder. Figure 5-33 to Figure 5-35 show the girder after failure. To remove the failed Tub #2 from the test setup, the girder was cut in several pieces and removed from the setup. Those multiple cuts in the girder facilitated the inspection of the failed area from inside. It was found that both top flanges suffered plastic bending in the zones of crushing of the concrete deck, as shown in Figure 5-36. Separation of the top flanges and the concrete deck was observed, and a gap between the plywood formwork and top of the top flange was about ¾". Thus, the failure mechanism was crushing of the concrete with a subsequent buckling of the top flanges and the top of the webs. The whitewash flaking seen in Figure 5-33 shows the significant amount yielding that occurred in the web.

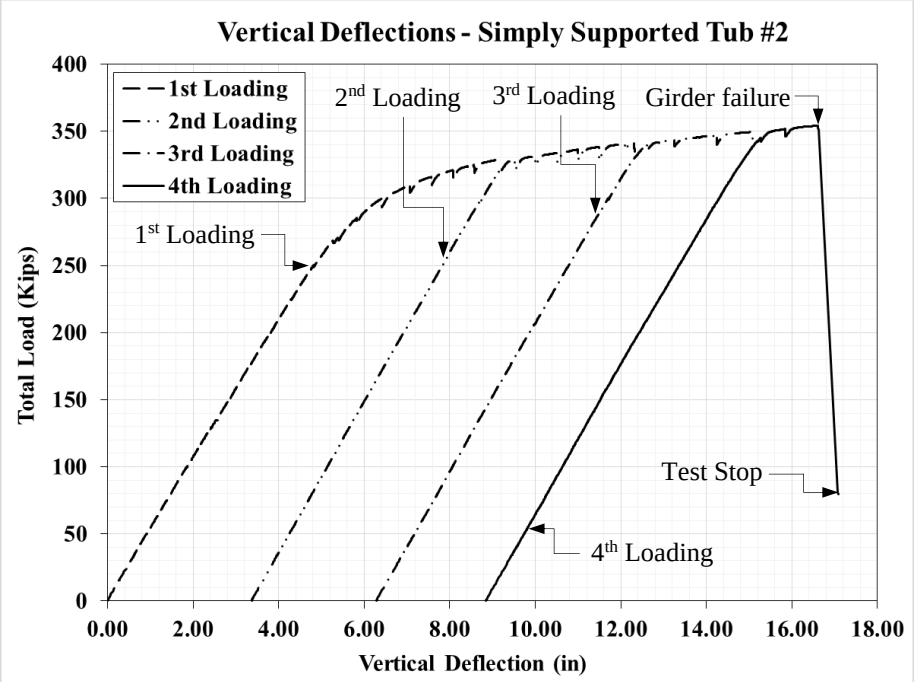

Figure 5-32 - Load-Deflection Curve - Simply Supported Tub #2

Figure 5-33 - Concrete Deck Crushed and Top Web Buckled – Tub #2

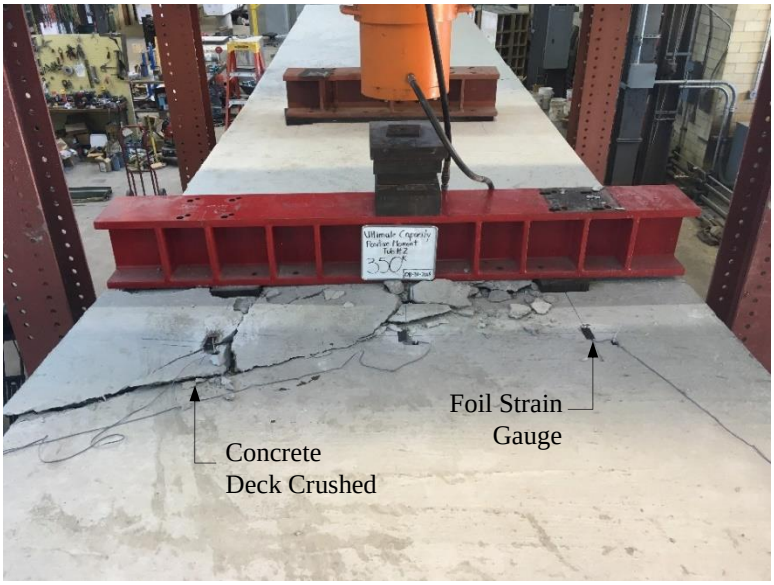

Figure 5-34 - Concrete Deck Crushed at Loading Point – Tub #2

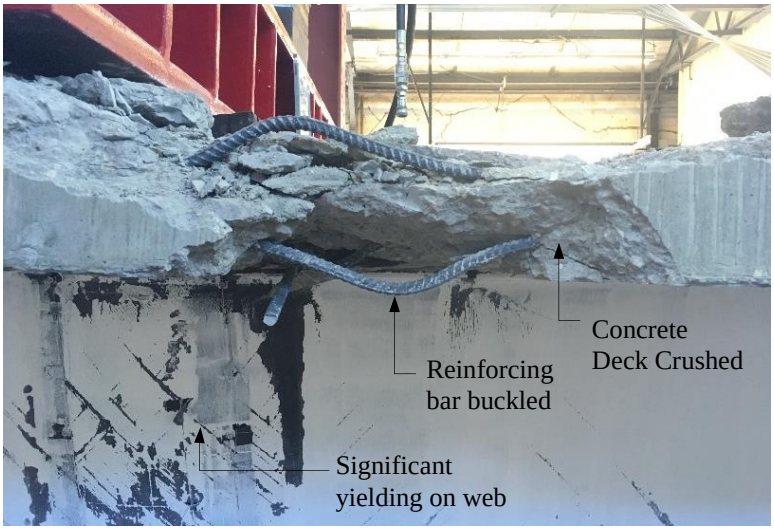

Figure 5-35 - Concrete Deck Reinforcement Buckled – Tub #2

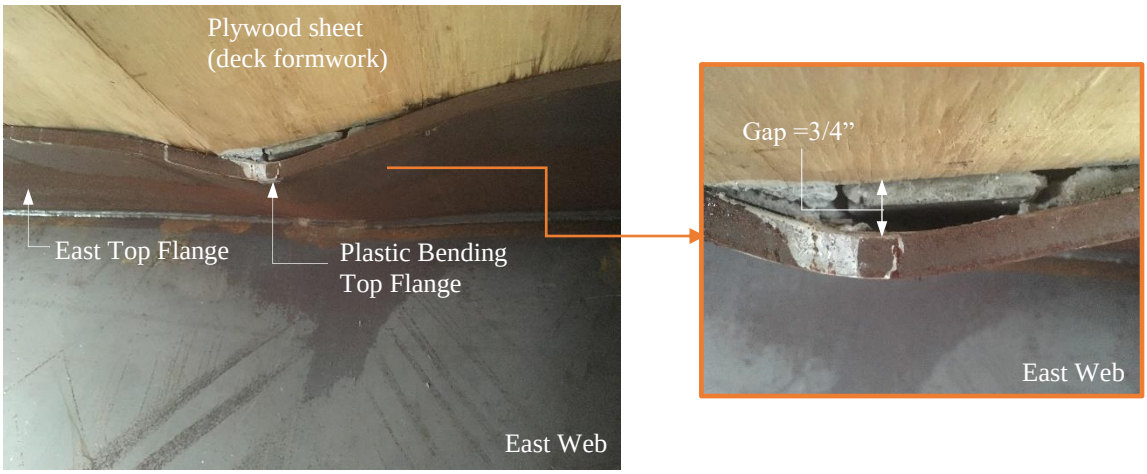

Figure 5-36 - Top Flange Plastically Bending – East of Tub #2

5.7.3 Flatter Web Tub Girder (Tub #3)

Figure 5-37 presents the load-deflection response of Tub #3 tested in the continuous configuration. The load-deflection curve represents the deflections at the intermediate loading frame located 34ft. from the north support (see Figure 5-16), versus the total load applied. The load on this tub girder configuration was applied by loading the three frames simultaneously with equal loads. At a total load of around 630 kips, and a deflection of 2.30 inches, the response of the systems started to show a slight reduction in the stiffness with increasing load. Eventually, the response became increasingly inelastic with a gradual reduction in stiffness of the system. This change in slope was due to yielding in the top flanges and top of the webs in the girder at the intermediate support location, and at the bottom flange at the location of the intermediate loading point. Both, longitudinal strain gauges and the DIC system showed that top flanges and the top of the webs had experienced significant yielding. The test was stopped at a total load of 1011kips to avoid large plastic deformations that could have hindered the simply supported configuration test.

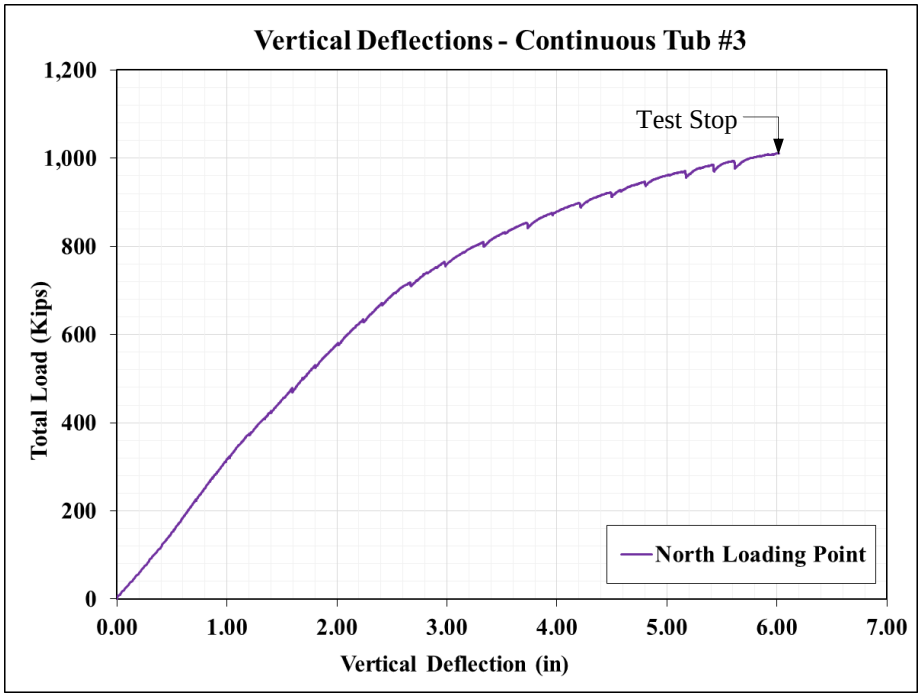

Figure 5-37 - Load-Deflection Curve - Continuous Tub #3

Figure 5-38 shows the load-deflection behavior of Tub #3 tested in the simply supported configuration. Two loading stages had to be completed before failure of the girder due to stroke limitations in the hydraulic ram. At a load of around 225 kips, and a deflection of 5.26 inches, the response of the systems started to become inelastic with a gradual reduction in stiffness of the system. Significant plastic deformations where observed with a maximum deflection of about 13.40 inches, when the concrete in the deck crushed, the top of the webs buckled, and the tub girder suddenly unloaded, indicating ultimate failure of the girder. Figure 5-39 shows the girder at the load application point after failure. The concrete deck had a compression type of failure with concrete crushed and buckled rebar, as seen in Figure 5-40 and Figure 5-41, similar to Tub #2. The top flange sides outside of the girder shown slight plastic bending between the location of shear studs, where very small separation (approximately 3/8") between the top flanges and the concrete deck was observed, as seen in Figure 5-42. The buckling in the top of the webs was not as severe as for Tub #2. Similar to Tub #2, the failure mechanism was crushing of the concrete and buckling of the top flanges and the top of the webs. The whitewash applied on the evaluated areas was not as good as for Tubs #1 and #2. Thus, in Figure 5-39 the whitewash does not clearly show the significant yielding that the webs experienced.

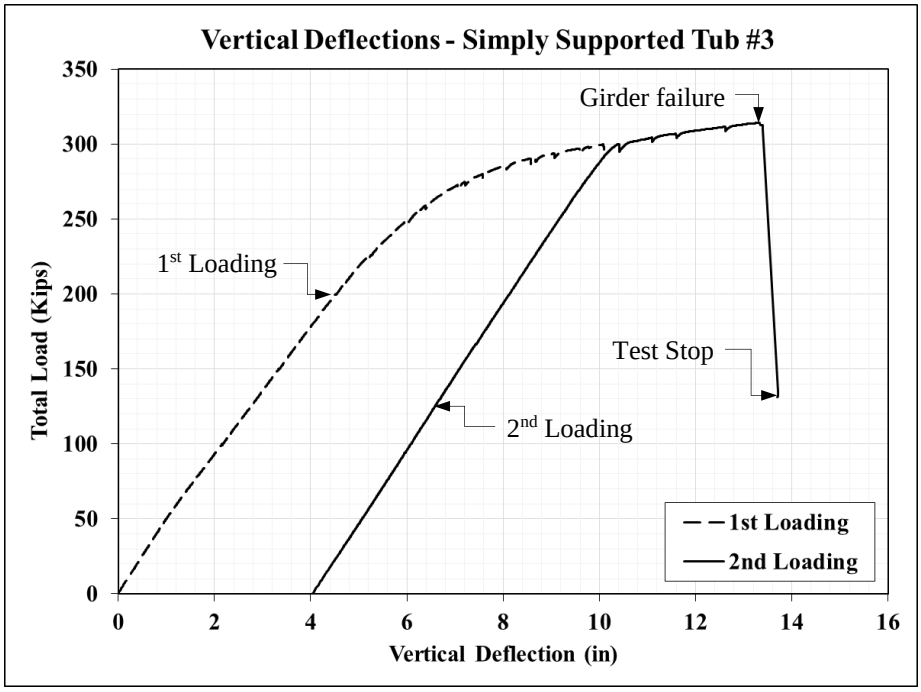

Figure 5-38 - Load-Deflection Curve - Simply Supported Tub #3

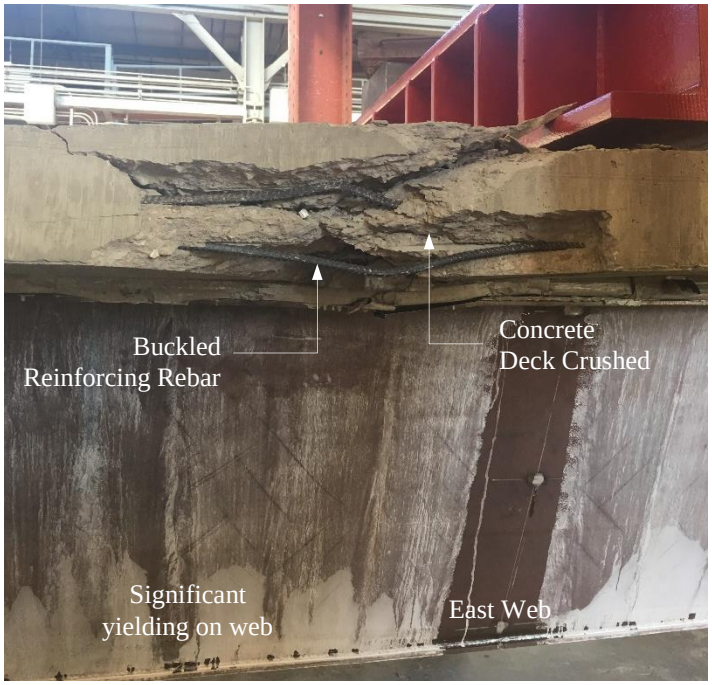

Figure 5-39 - Concrete Deck Crushed and Top Web Buckled – Tub #3

Figure 5-40 - Concrete Deck Crushed at Loading Point – Tub #3

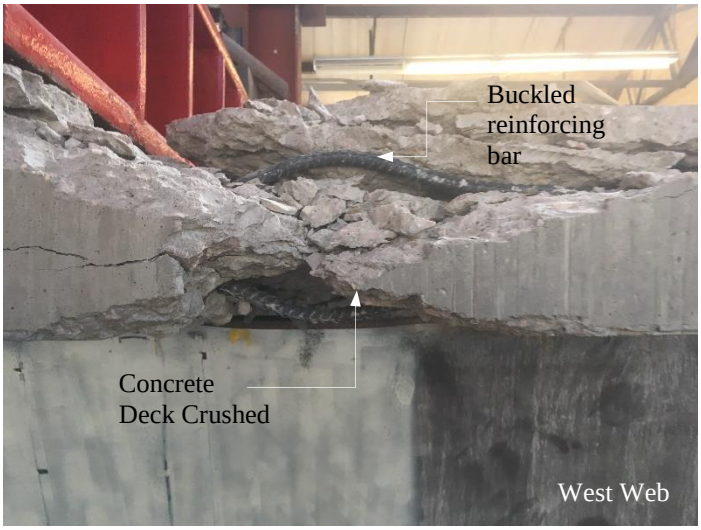

Figure 5-41 - - Concrete Deck Reinforcement Buckled – Tub #3

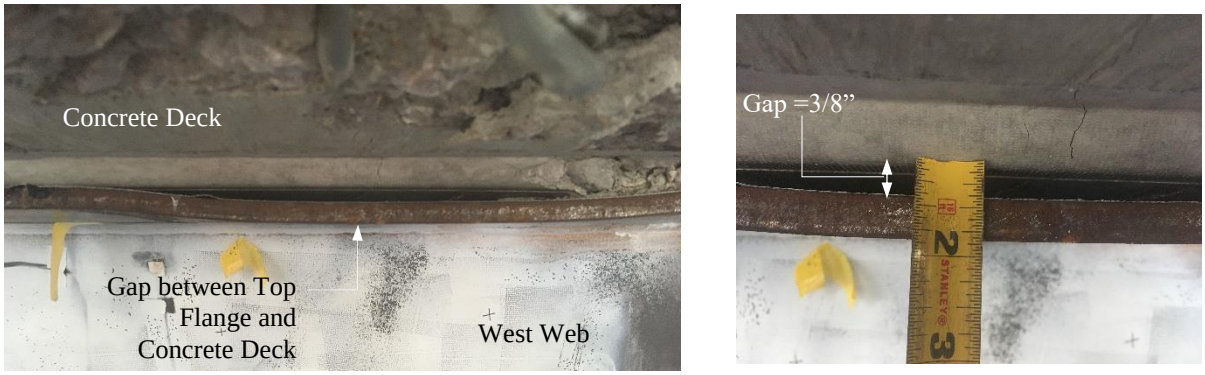

Figure 5-42 - Gap between Top Flange and Concrete Deck - Tub #3

5.7.4 Comparison of Results

To evaluate the impact of the proposed details on the ultimate capacity of the steel tub girders, the response of the specimens in the ultimate strength tests is compared. First, the flexural response of the three girders under negative moments is compared. Then, the flexural behavior of the specimens under positive moment demands are compared.

The three composite tub girders were tested as continuous girders in order to collect data on their behavior under negative moment, over the intermediate support. However, the load pattern used to applied loads was different for all three specimens. Thus, the load-deflection response of the girders are not easily comparable. As result, the moment-curvature response of the cross-section over the intermediate support was calculated for all the composite specimens. Moments were calculated with the load cell readings from the supports and loading points. Curvatures were computed with the data collected from the strain gauges installed on the tub girder at the intermediate support. Figure 5-43 shows the moment versus curvature calculated for the three composite specimens in the negative moment region. The absolute value of the moments have been plotted in the Y-axis, while negative curvatures are plotted on the X-axis. In addition, analysis of the cross-section of each composite girder was performed to compute their estimated values of elastic moment of inertia and plastic moment capacity, and are reported in Table 5-6. Absolute values of the plastic negative moment capacity are presented in Table 5-6. The steel girder, the reinforcing rebar, and the concrete in compression on the bottom flange were considered to compute the estimated moment of inertia (the concrete in tension was not included). The experimental moment of inertia was calculated by dividing the linear slope of the moment vs curvature curve (after cracking of the concrete) over the steel modulus of elasticity (E=29000 ksi). The experimental plastic moment is the maximum moment measured during the tests.

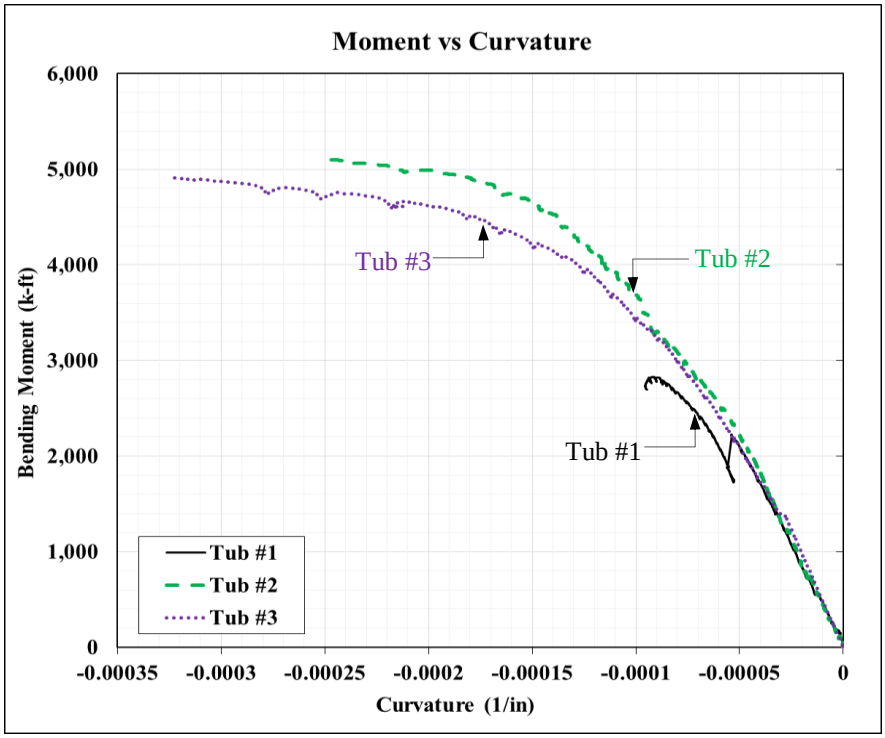

Figure 5-43 – Negative Moment vs Curvature - Composite Specimens

Table 5-6 - Computed vs Experimental Moment of Inertia and Plastic Moment Capacity - Negative Moment

	Moment of Inertia "Ie" (in^4)			Plastic Moment "Mp" (k-ft)		
	Calculated	Experimental	Diff (%)	Calculated	Experimental	Diff (%)
Tub #1	17,204	17,581	-2.1	4,080	2,826	-30.7
Tub #2	21,767	22,222	-2.0	5,251	5,102	2.9
Tub #3	19,244	18,876	1.9	4,776	4,915	-2.8

As previously mentioned, Tub #1 was not able to reach its plastic moment capacity due to buckling of the internal diaphragm, and its final load was 70% of its computed capacity. For all other values listed in Table 5-6, there is good agreement between the computed and experimental values, with a maximum difference of 3%. Tub #1 had the lowest moment of inertia because it is only specimen without a concrete slab over the bottom flange. Tub #3 had the second highest moment of inertia after Tub #2. By casting a 6.5" thick concrete slab over the bottom flange of Tub #3, its moment of inertia was the same as if a 1 ¼" thick steel plate was welded to the bottom flange. Likewise, Tub #2 had a 6.5" thick concrete slab cast on top of the bottom flange, which adds stiffness that is comparable to welding a 1" thick steel plate to the bottom flange. Tub #2 had the highest moment of inertia due to the thicker top flanges and the inclusion of the bottom concrete slab. Another effect of including the concrete slab on top of the bottom flange is a shift of the plastic neutral axis (PNA). For Tub #1, the PNA was located in the web approximately 14in above the top of the bottom flange. On the other hand, Tub #2 and Tub #3 had the PNA located in the bottom concrete slab at 4.8in and 6.3in above the top of the bottom flange, respectively. Due to these cross-sectional differences, similar trends were observed in the plastic moment capacities. Tub #2 and Tub #1 shown the highest and the lowest plastic moment capacities. As consequence, the proposed improved details did not produce any unexpected effect in the flexural behavior of the composite tub girder. The cross-sectional properties and ultimate capacity can be calculated using traditional section analysis when bending demands govern.

Similar to the negative moment region, the moment-curvature response of the cross-section of the three composite specimens was calculated at the location of the load application point for the simply supported configuration tests. Moments and curvatures were calculated as previously described. Figure 5-44 presents the moment-curvatures plots calculated for the three specimens at the location of maximum moment during the ultimate strength tests. Additionally, section analysis was carried out in order to estimate the moment of inertia and plastic moment capacity of the composite girders in positive moment. To calculate these values, all the cross-sectional components were considered (steel girder, concrete deck and reinforcing rebar). The experimental moment of inertia and the plastic moment capacity were obtained similar to the ones calculated for the negative moment region. Results are listed in Table 5-7. There is good agreement between the computed and the experimental values with a maximum difference of about 4%. The moment-curvature plots for Tubs #1 and #2 are very similar, both in the elastic and inelastic ranges of behavior. The elastic moment of inertia of Tubs #1 and #2 are very similar with a 3% difference. The ultimate capacity of Tub #1 is slightly higher than Tub #2, which can be attributed to higher concrete strength for Tub #1, as indicated in Table 5-1. The moment of inertia of Tub #3 was 15% lower and the plastic moment capacity was 12% lower than the other 2 composite specimens. Additionally, Tubs #1 and #2 exhibited a more ductile response than Tub #3 because of wider bottom flange in Tubs #1 and #2. In all three composite specimens, the PNA was located in the top flange. Consequently, the proposed improved details do not affect the ultimate positive

moment capacity of composite tub girders. The thickness and offset of the top flanges of Tub #2 had minor effects in its moment of inertia and ultimate strength.

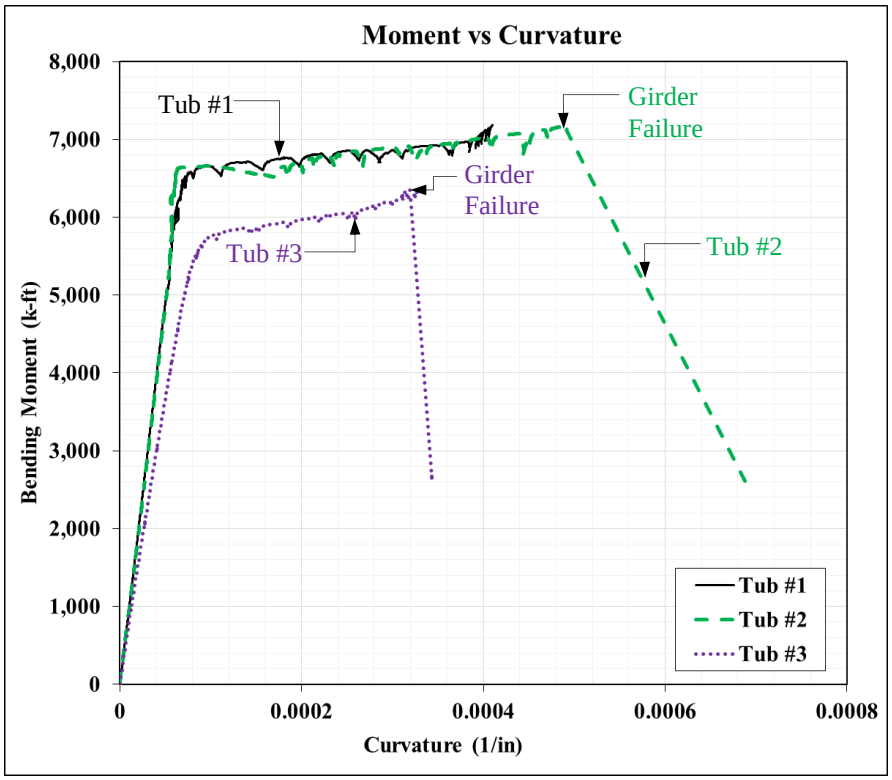

Figure 5-44 – Positive Moment vs Curvature - Composite Specimens

Table 5-7 - Computed vs Experimental Moment of Inertia and Plastic Moment Capacity - Positive Moment

	Moment of Inertia "Ie" (in^4)			Plastic Moment "Mp" (k-ft)		
	Calculated	Experimental	Diff (%)	Calculated	Experimental	Diff (%)
Tub #1	38,225	38,338	-0.3	7,147	7,184	0.5
Tub #2	39,613	39,353	0.7	7,055	7,175	-1.7
Tub #3	33,431	32,027	4.4	6,399	6,349	0.8

Lastly, as the three composite specimens were loaded with the same load pattern in the simply supported configuration, their load-deflection response curves can be compared. Figure 5-45 presents a comparison of the load-deflection curves of the simply supported tests of the three composite specimens. For clarity in the plot, the elastic reloading of the tests were removed and the inelastic parts were kept for better comparison. It is clear that the general behavior of Tub #1 and Tub #2 is quite similar, in terms of stiffness and strength. The small difference in strength may be attributed to the difference in strength of the concrete, as previously mentioned. According to Table 5-1, the difference in concrete compressive strength is of about 0.44 ksi, which represents 8% of the strength of the concrete of the Tub #2. Tub #3 showed lower stiffness in the elastic range; however, its inelastic stiffness was similar to the other two girders. Its ultimate moment capacity was about 88% of the other two specimens, what can be attributed to the narrower bottom flange. Thus, offsetting the top flanges inwards did not affect the ultimate capacity and failure

mode of steel tub girders. Additionally, the flatter webs did not affect their ultimate moment capacity since the bottom flange and the concrete deck are the key components in the flexural response of composite tub girders.

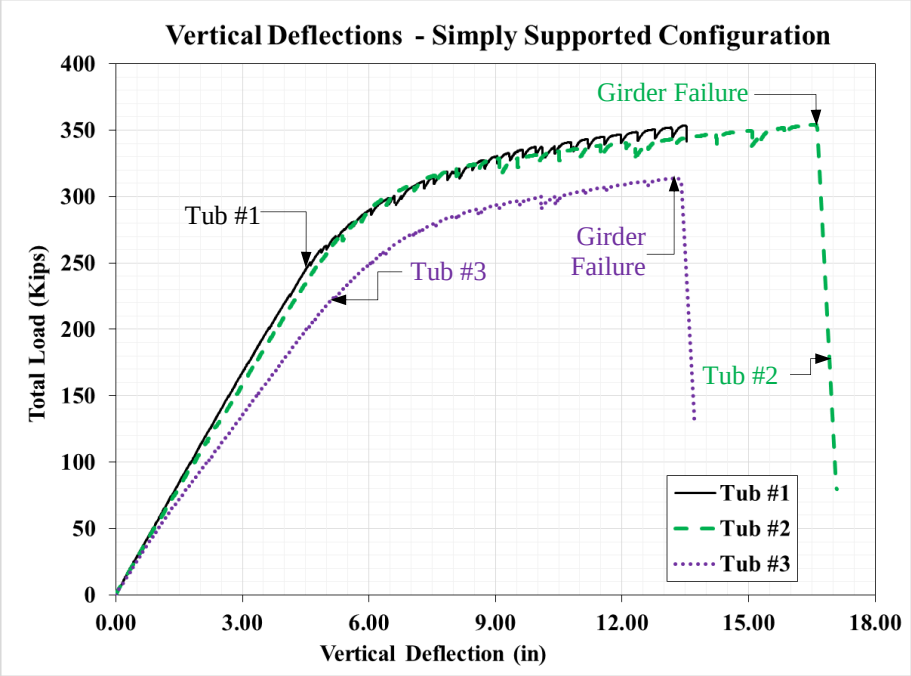

Figure 5-45 - Comparison of Load-Deflection Behavior - Simply Supported Configuration

5.8 Summary of Ultimate Strength Experimental Results

This chapter focused on the experimental ultimate capacity tests that were conducted in the laboratory on the composite steel tub girders. A number of observation can be made from the experimental program:

- By casting a concrete slab on the bottom flange of two of the composite tub girders, a significant increase was observed in stiffness (30% for Tub #2, 40% for Tub #3) and in plastic moment capacity (16% for Tub #2, 6% for Tub #3) under negative moment demands. For these double composite sections, the PNA was located in the bottom concrete slab according to section analysis, what implies that the top of the concrete deck was sustaining tensile strains. However, not all the strain gauges installed on top of the bottom concrete deck registered tensile strains. In fact, few strain gauges registered compressive strains during the entire negative moment test. Further research is suggested to understand the behavior of concrete slabs over bottom flanges.

- Under negative moment, no impact on the flexural stiffness nor on the negative moment capacity of composite tub girders with offset top flanges and flatter webs was observed.

- The flexural response of composite tub girders under positive moment demands was not affected by offsetting top flanges. Tub #1 and Tub #2 had very similar flexural response in the elastic and inelastic ranges of behavior.

- The flexural stiffness and positive moment capacity of Tub #3 were lower than that observed in the other two specimens due to a narrower bottom flange. The flatter webs had no significant impact in the ultimate positive moment capacity of the specimen.
- The composite steel tub girders exhibited ductile response.
- Similar failure modes were observed in the specimens with improved details as compared with the baseline specimen. Under positive bending, after significant yielding of the bottom flange and webs, the failure mode of the composite tub girders was produced by crushing of the concrete followed by buckling of the top flanges and the top of the webs
- For both negative and positive moment, conventional cross-section analysis accurately predicted measured values of stiffness and strength.

Chapter 6. Design Recommendations for Improved Details

This chapter outlines design recommendations towards improved cross-sectional and bracing details in the design of steel tub girders. The suggestions presented herein are based on the experimental and parametric FEA results presented in Chapters 3-5. The guidelines outlined in this chapter are suggestions from the authors, and designers should consider the feasibility and impact on the behavior of the girders in their design applications.

6.1 Design Recommendations for Improved Bracing Details

Recommendations to design steel tub girders with partial top lateral bracing and different configurations of internal K-frames were developed based on the experimental and analytical studies described in Chapters 3 and 4. These recommendations and a general design procedure are summarized and presented in this chapter.

6.1.1 Design of Steel Tub Girders with Partial Top Lateral Bracing

The design methodology recommended herein follows the standard procedure to design steel tub girders applied in common engineering practice with few changes. Since the top lateral bracing and internal K-frames are important during the construction phase, the proposed methodology covers only constructability checks. The author recommends that before considering partial top lateral bracing in the design, a good practice would be to first design the tub girders considering a full bracing system and then evaluate the girder capacity with partial top lateral bracing. Upon the completion of the design with full top lateral bracing, the steps to follow in order to apply partial top lateral bracing in the design are to define the amount of truss diagonals necessary based upon the force and deformation limitations. In addition, the lateral bending stresses in the top flanges without lateral bracing should be evaluated

6.1.1.1 Define Amount of Partial Top Lateral Bracing

After completing the design of the steel tub girder with top lateral bracing along the entire length, the first step is to define the amount of partial top lateral bracing to be considered in the design. From the parametric finite element analysis carried out in this project, it was observed that keeping 50% (even 40% depending on the span length) of the truss diagonals could guarantee an adequate torsional behavior during construction of straight tub girders in simply supported or continuous girder configurations. Similarly, horizontally curved girders with radius of curvature greater than approximately 2500ft and span lengths up to 215 ft. showed adequate torsional response with at least 50% of the diagonals in place. Partial top lateral bracing should be placed at the support locations where they are effective to control warping deformations. The amount of partial top lateral bracing suggested herein is based on assumed adequate levels of torsional performance. It is up to the designer to define if those levels are adequate for their applications, or to set new minimum levels of torsional response.

6.1.1.2 Lateral Bending Stresses in Top Flange

Based upon the number of truss diagonals included within a given span, the next step is to check the lateral bending stresses induced in the unbraced top flanges. Top flange lateral bending

is caused by the horizontal component of the web shear, temporary overhang bracket supports for the deck overhangs (exterior girders), horizontal curvature, and wind loads. Commonly, the top flanges in tub girders are discretely braced by the horizontal truss along the entire length of the girder, and the highest lateral bending stresses are created at bracing points. Consequently, the calculation of lateral bending moments is carried out considering the unbraced length Lb as shown in the top of Figure 6-1. However, when top lateral bracing diagonals are removed from the center of the girder, the unbraced length of the top flanges changes to the one that is shown in the bottom of Figure 6-1, because now the tub girder has partial relative bracing. This change of unbraced length produces increments in lateral bending stresses induced on the top flanges. It was observed in the parametric study that this increase of lateral bending moments was significant for horizontally curved girders due to the curvature, while it was not severe in straight girders.

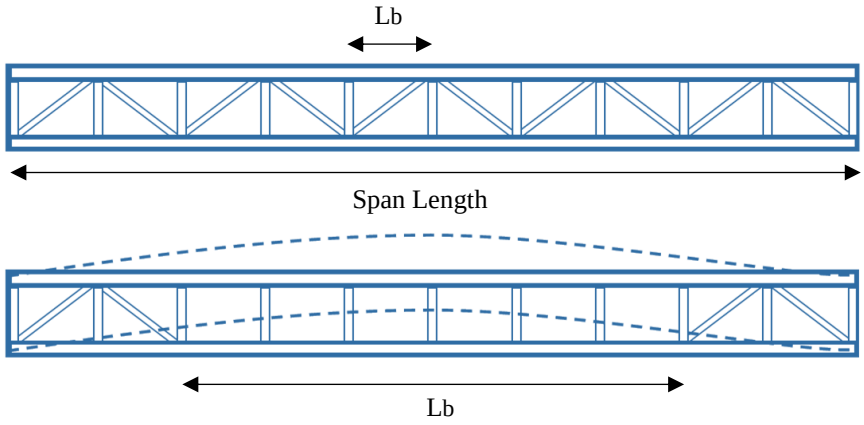

Figure 6-1 - Change in Unbraced Length with Partial Lateral Bracing

The formulation required to calculate the lateral bending moments in top flanges is the same used in common engineering practice. Three main sources produce lateral bending on one top flange as shown in Equation 6-1. Assuming that the top flange is continuous, this horizontal component can be approximated as an equivalent uniformly distributed lateral load. AASHTO 2017 suggests in its commentary C6.10.3.4.1 that Equation 6-2 can be used to calculate lateral bending moment (M_{l_1}) in flanges loaded with statically equivalent uniformly distributed lateral loads (F_l). First, the horizontal component of vertical loads due to inclined webs create lateral stresses on top flanges. The uniform lateral component (F_{lat}) of the vertical applied load along L_b can be calculated with Equation 6-3, where ΔV_v is the change in shear along L_b, and θ_{web} is the angle of inclination of the web.

$$F_l = F_{lat} + \frac{1}{2}F_{h\_bracket} + \frac{1}{2}F_{curv} \qquad \text{Equation 6-1}$$

$$M_{l_{\_1}} = \frac{F_l {L_b}^2}{12} \qquad \text{Equation 6-2}$$

$$F_{lat} = \frac{1}{2}\Delta V_v \tan\theta_{web} \qquad \text{Equation 6-3}$$

Second, temporary brackets installed in exterior girders to support the deck overhang loads produce lateral bending stresses on top flanges. Deck overhang brackets that rest on the webs near the bottom flanges and that are anchored by hangers connected to the top flange create force couples on the tub girders. Loads to be considered on the overhang bracket include the weight of the deck overhang, formwork, and any other suitable construction loads. Figure 6-2 shows an overhang bracket with different loads acting on the plywood form. The tributary area of the overhang bracket is assumed to be the spacing between the brackets that can be taken as a few feet or a much larger value. The assumed spacing does not matter since that spacing will be removed when the load is converted to an equivalent distributed load by dividing by the spacing. The vertical component on the bracket ($F_{vbracket}$) can be found by summing moments with the applied loads about the edge of the girder top flange. The horizontal component ($F_{h\ bracket}$) can then be found with Equation 6-4:

$$F_{h\ bracket} = \frac{F_{v\ bracket}}{tan\theta} \qquad \text{Equation 6-4}$$

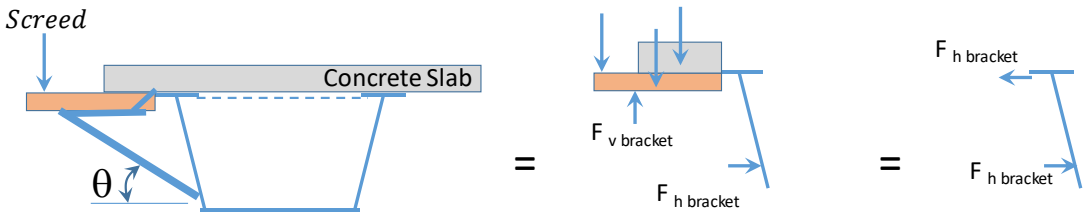

Figure 6-2 - Overhang Bracket Loads

The horizontal component of the overhang load ($F_{overhang}$) can be converted into a distributed load acting on the flange by simple dividing by the assumed spacing between the brackets. Equation 6-2 can be used to calculate the lateral bending moments produced by the uniformly distributed lateral force produced by these loads.

Additionally, horizontal curvature of the girder is another source of lateral bending in the top flanges. The effect of horizontal curvature can be approximated using the M/R method. This method considers that the torsional demands can be approximately represented by two distributed lateral loads *M/Rh* applied on the top and bottom flanges with opposite directions. Where *M* is the bending moment, *R* is the curvature, and *h* is the vertical distance between top and bottom flanges. Thus, the distributed lateral load F_{curv} in Equation 6.1-5 produces lateral bending of top flanges. Half of this lateral load is resisted by each top flange. Since the bending moment varies along the length of the girder with unbraced top flanges, it is conservative to choose the maximum bending moment.

$$F_{curv} = \frac{M}{Rh} \qquad \text{Equation 6.1-5}$$

As previously mentioned, after removing the truss diagonals from the girder mid-span, the top flange unbraced length (L_b) becomes the one shown in the bottom of Figure 6-1. Additionally, it was observed that the transition zones work as warping restrains of the top flanges. As the two unbraced top flanges are linked by the struts, they bend laterally with fixed boundary conditions

at the transition zones. Additionally, the top flanges are connected to the bottom flange by the K-frames, what contributes to lessen lateral bending on top flanges. The following recommendations are intended to calculate moments in the top flanges due to lateral bending.

Figure 6-3a shows a tub girder at the location of an internal K-frame subjected to a lateral load 2F shared between the two top flanges. The internal K-frames connect the top flanges with the bottom flange. Due to this connection, the lateral stiffness of the top flanges depend also on the lateral bending stiffness of the bottom flange and the axial stiffness of the K-frame members. The interaction of these elements can be modeled like a spring array, as shown in Figure 6.3b. Equation 6.1-6 and Equation 6.1-7 show the lateral bending stiffness of the top flange (β_{top}) and bottom flange (β_{bottom}) as beams with both ends fixed subjected to a lateral load, where E is the elastic modulus; I_{top} and I_{bottom} are the lateral moment of inertia of the top and bottom flanges, respectively; L_b is the unbraced length of the top flanges; and L is the clear span. Additionally, the expressions to calculate the axial stiffness of the one K-frame diagonal (β_{dia}) and a strut (β_{strut}) subjected to a lateral load are shown in Equation 6.1-8 and Equation 6.1-9, respectively, where A_{dia} and A_{strut} represent the area of K-frame diagonals and struts, L_{dia} and L_{strut} are the K-frame diagonal and strut length, and γ is the inclination of K-frame diagonals. Since one K-frame connects two top flanges to one bottom flange, it is assumed that the lateral bending stiffness of one top flange gets contribution from half the stiffness of the bottom flange, from the axial stiffness of half strut, and axial stiffness of one K-frame diagonal. Based on Figure 6.3b, the lateral stiffness of the bottom flange and the axial stiffness of the K-frame members can be idealized as springs in series, while the bending stiffness of the top flange works in parallel. As result, an effective stiffness (β_{effe}) can be calculated with Equation 6.1-10. Consequently, the formulation to estimate the maximum lateral displacement of the top flanges without truss diagonals is shown in Equation 6.1-11.

$$\beta_{top} = \frac{384EI_{top}}{{L_b}^3} \qquad \text{Equation 6.1-6}$$

$$\beta_{bottom} = \frac{384EI_{bottom}}{L^3} \qquad \text{Equation 6.1-7}$$

$$\beta_{dia} = \frac{EA_{dia}}{L_{dia}}(\cos\gamma)^2 \qquad \text{Equation 6.1-8}$$

$$\beta_{strut} = \frac{EA_{strut}}{L_{strut}} \qquad \text{Equation 6.1-9}$$

$$\beta_{effe} = \beta_{top} + \left(\frac{1}{{}^1\!/_{0.5\beta_{bottom}} + {}^1\!/_{\beta_{dia}} + {}^1\!/_{\beta_{strut}}}\right) \qquad \text{Equation 6.1-10}$$

$$\delta_{lat} = \frac{F_l L_b}{\beta_{effe}} \qquad \text{Equation 6.1-11}$$

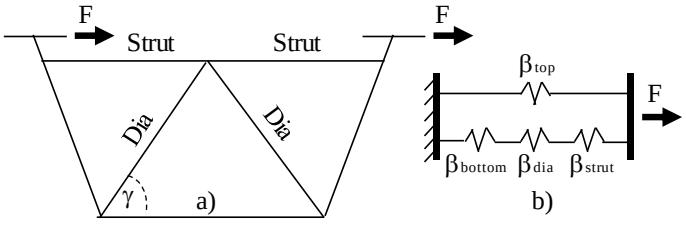

Figure 6-3- a) Tub Girder under Lateral Loading, b) Top Flange Stiffness Idealization with Spring Array

This estimated lateral displacement is then used to calculate an equivalent distributed lateral load w_{equi} that will produce a lateral displacement δ_{lat} in a top flange without the contribution of other bracing. Recall, each unbraced top flange alone is assumed to work as a beam fixed at both ends. Thus, the equivalent lateral load F_{l_equi} can be calculated with Equation 6.1-12.

$$F_{l\_equi} = \frac{384EI_{top}}{L_b{}^4}\delta_{lat} \qquad \text{Equation 6.1-12}$$

Once the equivalent uniformly distributed lateral load F_{l_equi} was calculated, the maximum moment due to lateral bending can be estimated. AASHTO 2017 suggests in its commentary C6.10.3.4.1 that Equation 6-2 can be used to calculate lateral bending moment (M_{l_1}) in flanges loaded with statically equivalent uniformly distributed lateral loads. The number 12 in the denominator can be reduced up to 10 to account for flexibility in the system, depending on how conservative the designer wants to be.

In addition to the uniform load acting on the flange, the critical position of the screed load will usually be at $L_b/2$. Since the screed load is resisted by the overhang brackets in the vicinity of the point of load application, a lateral point load can be determined from simple statics of the overhang similar to the method outlined above. Equation 6-13 can be used to calculate the lateral bending moments in top flanges when concentrated lateral forces are applied (P_l).

$$M_{l\_2} = \frac{P_l L_b}{8} \qquad \text{Equation 6-13}$$

When evaluating lateral bending for sections with full top flange bracing, the overhang load acts on the flange between the brace points and therefore the outside flange experiences the full overhang force. However, with partial top lateral bracing, since the struts will link the two top flanges together, each flange can be assumed to take half of the overhang load when evaluating lateral bending with partial top lateral bracing.

6.1.1.3 Top Lateral Bracing Forces

The diagonals in cases with partial top lateral bracing experience larger forces compared to cases with a full braced system. When bracing diagonals are removed in the regions away from the ends of the section the forces in the unbraced length are redistributed to the areas with top lateral bracing, specifically to the transition zones. The transition zones are the first panel with a

top flange diagonal truss member (closest to midspan region), as shown in Equation 6-3. During the experimental and analytical study, it was observed that the K-frame and top lateral diagonal in the transition between braced to un-braced system sustained higher loads than the fully braced configuration. Thus, special attention should be taken when designing those bracing members.

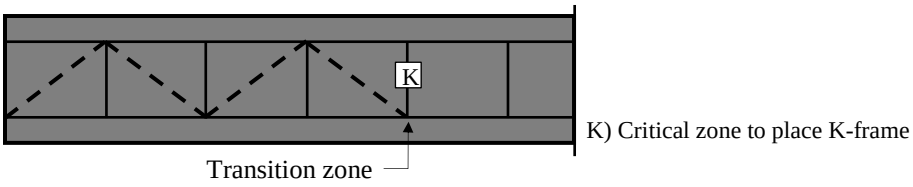

Figure 6-4 - Transition Zone between Braced and Unbraced Tub Girder

Brace forces can be determined by several approaches, either numerical or approximated. 3D-finite element analysis programs can be used to obtain results with the highest accuracy. For example, the UT Bridge program can provide good estimates of the forces induced in the top lateral truss and internal K-frame members during construction. An approximate method is described herein for single diagonal type of horizontal truss. Fan and Helwig (1999) developed a method to estimate top lateral bracing forces including the effects of vertical bending, the lateral component of vertically applied loads, and torsional moments. The method is still applicable to calculate brace forces in the regions with top lateral bracing, except in the transition zones were the distribution of forces changes. The formulation to estimate bracing forces in the braced and transition zones are presented in this section.

To estimate the brace forces resulting from torsional moments, the Equivalent Plate Method (EPM) can be applied. Kollbrunner and Brasler (1969) developed the EPM to analyze quasi-closed cross-sections, in which the top lateral truss is idealized as a fictitious plate to approximate the torsional properties of the section. The equivalent plate thickness is a function of the truss geometry and area of the diagonals, struts, top flanges, and webs. The fictitious plate allows the shear flow to be transformed in diagonal member forces in the horizontal truss as shown in Figure 6-5.

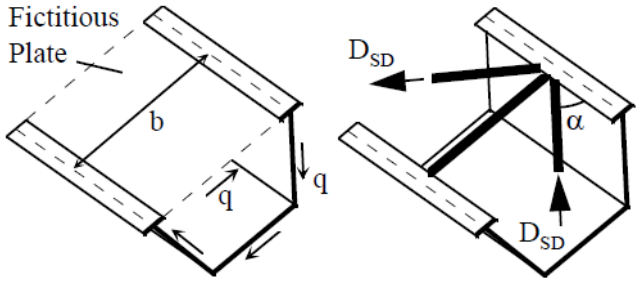

$$q = \frac{T}{2A_o} \qquad \text{Equation 6-14}$$

$$D_{EPM} = D_{SD} = \pm\frac{qb}{\sin\alpha} \qquad \text{Equation 6-15}$$

Figure 6-5 Diagonal Brace Forces Due to Torsion According to EPM (Fan and Helwig 1999)

Where:

$D_{EPM} = D_{SD}$ = Diagonal force due to torsional moments

q = Shear flow

T = Torsional moment

Ao = Enclosed area of the quasi-closed tub girder

b = Separation between top of the webs (panel width)

α = Angle between top flange and truss diagonal

The formulation above still applies for the horizontal truss with partial top lateral bracing, except in the transition zone where the force distribution changes. For a continuous truss, the EPM method assumes that the diagonal forces (D_{SD}) in Figure 6-5 are similar and that the horizontal strut does not sustains load. However, for partial top lateral bracing this not true since in the transition zone there is only one diagonal and one strut framing into the joint. To keep equilibrium in the joint, the strut must resist a force with opposite sign than the diagonal force equal to the shear flow times the panel width [Equation 6-16].

$$S_{EPM} = \pm qb \qquad \text{Equation 6-16}$$

To analyze the torsional behavior of horizontally curved girders, the M/R method can be applied to approximate the torsional demands produced by curvature of the alignment on horizontally curved box girders with small to moderate curvature (Tung and Fountain 1970). This method considers that the torsional demands can be approximately represented by two distributed lateral loads M/Rh applied on the top and bottom flanges with opposite directions, where M is the bending moment, R is the curvature of the beam, and h is the vertical distance between the top and bottom flanges [Figure 6-6]. Additionally, Memberg et al. (2002) presents formulation to calculate torsional demands in simply supported curved beams under concentrated and uniformly distributed loads.

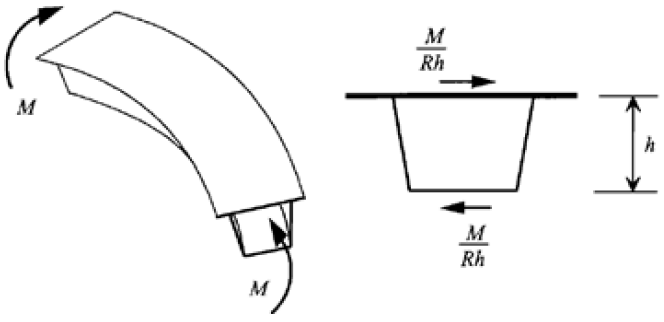

Figure 6-6 - Equivalent Torsional Loads on Curved Box Girders (Fan and Helwig 1999)

According to Fan and Helwig (1999), the vertical bending component of the horizontal truss forces depends on the geometry of the horizontal truss, the cross-section of the braces, dimensions of top flange, and the bending stresses on the top flange. The interaction of brace forces due to bending at joint locations is shown in Figure 6-7.

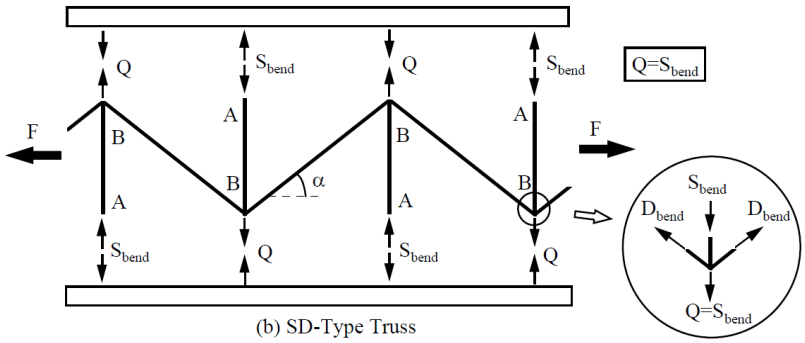

Figure 6-7 - Interactive Bracing Forces due to Bending at Joints (Fan and Helwig 1999)

The formulation to calculate the forces due to vertical bending in the top lateral bracing members is presented below by Equation 6-17 and Equation 6-19:

$$D_{BEND} = \frac{f_{xtop}\, s\, \cos\alpha}{K_1} \qquad \text{Equation 6-17}$$

$$K_1 = \frac{d}{A_d} + \left(\frac{b}{A_s} + \frac{s^3}{2{b_f}^3 t_f}\right)\sin^2\alpha \qquad \text{Equation 6-18}$$

$$S_{BEND} = -D_{BEND}\sin\alpha \qquad \text{Equation 6-19}$$

Where:

D_{BEND} = Diagonal force due to vertical bending

S_{BEND} = Strut force due to vertical bending

f_{xtop} = Longitudinal stress in the girder at the truss connection

A_d, A_s = Area of the truss diagonal and strut, respectively

s, b = Panel length and width, respectively

d = Length of the truss diagonal

b_f, t_f = Width and thickness of the top flange

This formulation and distribution holds adequate for partial top lateral bracing except at the transition zones. Derivation of Equation 6-17 is based on axial deformations of the bracing diagonals and struts due to lateral displacement of top flanges due to strut forces assuming that the top flange has fixed ends at the ends of braced two panels, as in Figure 6-8.

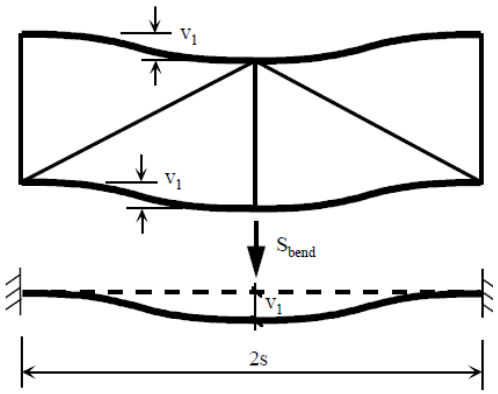

Figure 6-8 - Lateral Displacement of Top Flanges due to Strut Force (Fan and Helwig 1999)

In the transition zones, this assumption is not valid due to the absence of a truss diagonal in one of the side of the strut. The lateral displacement of the top flange should be higher at the transition zone. For the continuous brace case, the top flange in one panel can be assumed as a beam (of length s) fixed at one end and free to deflect vertically (but not rotate) at the location of lateral displacement of the top flange (v_1). At this point, the displacement v_1 is equal to $S_{bend} * s^3/12EI$. However, for the last panel of a partial top lateral bracing configuration this assumption changes. The top flange can be assumed as a cantilever beam (of length s) with the free end at the top flange lateral displacement location (v_{1p}). For this configuration, the displacement v_{1p} is equal to $S_{bend} * s^3/3EI$. Thus, the new lateral displacement is higher than the continuous bracing system due to the flexibility of the system ($v_{1p} = 4v_1$). As result, this new displacement induces larger axial deformations in the bracing diagonals. In order to consider this augment of axial deformation in the force of the diagonal in the transition zone, the diagonal force D_{BEND} in Equation 6-17 can be multiplied by 4 conservatively. This increment of four conservative when comparing against FEA results during the parametric study. Additionally, the force of the last strut of the partial truss has to be half of the one calculated with Equation 6-19 in order to keep equilibrium in the joint.

In addition to torsional and vertical bending components, the horizontal truss forces are produced by the lateral component of the web shear produced by vertical loads. The formulation considers that the top flanges resist the full horizontal component of the vertical loads (p). Additionally, their method assumes that this horizontal component is transferred only to the strut, while there is no contribution to the diagonal forces. According to the author, no modification may be needed to apply these equations for partial top lateral bracing. Thus, the formulation for the lateral component is the following:

$$D_{LAT} = 0 \qquad \text{Equation 6-20}$$

$$S_{LAT} = ps \qquad \text{Equation 6-21}$$

Where:

D_{LAT} = Diagonal force due to lateral component of web shear

S_{LAT} = Strut force due lateral component of web shear

s = Unbraced length

The force components due to vertical bending, torsional moments, and lateral component of the web shear can be superimposed to obtain the final bracing forces. The total strut and diagonal forces can be calculated with Equation 6-22 and Equation 6-23 , respectively.

$$S_{TOTAL} = S_{EPM} + S_{BEND} + S_{LAT} \quad \text{Equation 6-22}$$

$$D_{TOTAL} = D_{EPM} + D_{BEND} \quad \text{Equation 6-23}$$

From the parametric study of partial top lateral bracing, it was observed that the force in the truss diagonal in the transition zone as much as 1.8 times higher than the force of the same diagonal in a fully braced configuration. Thus, another rule of thumb to calculate the total force of the diagonal in the transition zone is to double the force of the same diagonal in a fully braced configuration.

The forces in the diagonals and struts calculated with the expression above are a function of the brace size so that stiffer brace members will attract more force. Thus, this method needs some iterations until getting a final load for designing.

Besides satisfying axial force demands, the diagonal bracing members must satisfy slenderness requirements for primary members specified in Article 6.9.3 in AASHTO 2017 since must of the time the compression forces will govern the design of the diagonal.

$$\frac{kL}{r} \leq 120 \quad \text{Equation 6-24}$$

Article C6.7.5.3 in AASHTO 2017, recommends a minimum required cross-sectional area for top lateral bracing diagonals in order to limit the warping normal stresses to 10% of the maximum bending stresses when X-type of braces are used. The recommendation requires that the diagonal cross-sectional area (A_d) be less than 0.03 times the separation of the top flanges (w, all units in inches). However, for a single diagonal truss system, which is commonly used in Texas, Helwig and Yura (2012) suggests that this value should be the one presented in Equation 6-25. The research team recommends using this requirement as well for partial top lateral bracing.

$$A_d \geq 0.054w \quad \text{Equation 6-25}$$

6.1.1.4 Internal K-Frame Bracing Forces

Internal K-frames are intended to avoid distortion of the cross-section produced by non-uniform shear stresses due to torsional demands. To estimate axial loads in K-frame bracing members, the method developed by Fan and Helwig (2002) can be applied. Equations can be used to calculate the axial loads in diagonals and struts of K-frames due to distortional loads. The +/- sign represents that the struts and diagonals will have the same magnitude of distortional load, but with opposite sign.

$$D_{KF} = \pm \frac{s_K L_{DK}}{2A_o}\left(\frac{M}{R} - \frac{a}{b}ew\right) \quad \text{Equation 6-26}$$

$$S_{KF} = \pm \frac{s_K a}{4A_o}\left(\frac{a}{b} ew - \frac{M}{R}\right)$$ Equation 6-27

Where:
D_{KF} = K-Frame diagonal force due to distortional loads
S_{KF} = K-Frame strut force due to distortional loads
s_K = K-frame spacing
L_{DK} = Diagonal length of internal K-Frame
a = Tub girder bottom flange width
b = Panel width
e = Vertical load eccentricity
w = uniformly distributed vertical load
M = Bending moment
R = Horizontal radius of curvature
A_o = Tub girder enclosed area

The strut forces produced due to distortional loads should be superimposed with the strut forces produced due to vertical bending, torsional moments, and lateral loads (Equation 6-16, Equation 6-19, and Equation 6-21). To obtain the final loads in the K-frame diagonals, equilibrium in the intersection between K-diagonals and strut should be satisfied.

As observed during the numerical study, when partial top lateral bracing is used, the critical locations for internal K-frames are at the transition zones and at midspan with any arrangement of internal K-frames. To calculate the axial forces of struts and diagonals of the K-frame at midspan, conservatively, it can be assumed that there is not K-frames between the midspan and the K-frame at the transition zone.

The current section outlined the most important aspects to consider when calculating the forces in partial top lateral bracing. Numerical or approximated methods can be used to calculate the horizontal truss forces when the tub girder is not fully braced. 3D-FEA programs such as UT can be used to analyze straight and curved steel tub girders during erection and construction for more accurate results. The method developed by Fan and Helwig (1999) to calculate the diagonal forces of the horizontal truss is suggested to be applied in the absence of more exact FEA numerical methods. The original method can be used to calculate the forces in the diagonals of the partial truss except the diagonal and K-frame in the transition zone. The forces in the aforementioned braces should be calculated with the recommendations described in this section. Special attention should be placed in calculating the forces in the transition zone due to the larger bracing forces concentrated in the region. Additionally, the method proposed by Fan and Helwig (2002) to calculate the axial forces in K-frames due to distortional loads can be applied when partial top lateral bracing is used. The strut forces caused due to distortion should be superimposed to the forces produced due to vertical bending, torsional moments, and lateral component of the web shear. Equilibrium in the K-frame should be satisfied to obtain K-frame diagonal forces. Internal K-frames should be placed at end of the transition zones and at midspan where they are critical.

K-frame layouts for tub girders with partial top lateral bracing are discussed in the following section.

6.1.2 Improved Layouts for Internal K-Frames

The main purpose of internal K-frames is to control distortion of the cross section of steel tub girders under torsional loads. Additionally, they are fundamental during the fabrication of the tub girders since fabricators use them to assemble the girder. Hence, the improved K-frame layouts suggested herein are intended to reduce fabrication costs without hindering the structural stability and to keep the facilities for fabricators to connect the plates to form a tub girder. Additionally, the distribution of forces in K-frames when full top lateral bracing is used is different from when partial top lateral bracing is used. Thus, K-frame layout suggestions for both cases are described.

6.1.2.1 K-frames in Tub Girders with Full Top Lateral Bracing

The spacing between K-frames in straight and horizontally curved girders are recommended to be at least every 2 panel points. The following paragraphs summarize the general observations.

Regarding straight tub girders, it was observed in the parametric study that the distribution of internal K-frames had little impact in the torsional response of the girders. Placing K-frames, every panel point produced the largest forces in the K-frame struts and diagonals. Placing K-frames very 2 or 3 panel points had a negligible impact on the torsional response of the girders, and the forces in the K-frame struts and diagonals were lower compared to the case with K-frames placed every panel point. Thus, K-frames can be placed every 2 to 3 panel points in straight steel tub girders.

In regards to horizontally curved tub girders, K-frames can be placed every 1, 2, and 3 panel points without affecting the torsional behavior of horizontally curved tub girders with a radius of curvature greater than approximately 800 ft. The K-frame layout with braces every panel point produced the lowest forces in struts and K-frame diagonals, while a distribution of K-frames every 2 and 3-panel point shown higher forces. The axial forces of internal frames placed every two and three panel point shown little difference. Hence, K-frames placed every 2 and 3 panel points are applicable to horizontally curved tub girders.

6.1.2.2 K-frames in Tub Girders with Partial Top Lateral Bracing

As previously mentioned, K-frames are required to be placed at the critical zones. First, internal frames must be placed at the transition point between the braced and un-braced sections of the tub girder so that the torsional stiffness of the girder is not affected. Additionally, a K-frame should be placed at midspan to control distortion of the cross section.

Similar to the fully braced system, the distribution of internal K-frames for straight tub girders had little-to-no impact in the torsional response of the girders provided K-frames were placed at the critical zones. In the parametric study, K-frames were placed every 1, 2 and 4 panel points with K-frames at the critical points. No major variation in the torsional stiffness was observed when reducing K-frames from every panel point to every 2 and 4 panel points. Layouts with internal braces every 2 and every 4 panel points produced slightly higher forces at midspan, while no major variation of K-frame brace forces was observed at the transition zones. Thus, K-frames can be placed every 1 and 2 panel point without compromising the torsional stiffness of the girder. Any other layout can be considered provided the K-frames are placed at the critical points, but keeping K-frames every other panel point is highly recommended.

K-frames can be placed every 1, 2, and 4 panel points without affecting the torsional behavior of horizontally curved tub girders with radius of curvature at least of 2500ft. Placing K-frames every 1 panel point produced the lower axial forces in the struts and diagonals at midspan. The forces at the transition zone did not change with different internal brace layouts. Similar to straight tub girders, any layout of K-frames can be considered only if K-frames are placed at critical points. The configuration with K-frames every 2 panel point is suggested.

6.2 Design Recommendations for Steel Tub Girders with Flange-Offset Details

6.2.1 Flange Proportion with Flange-Offset Details

To use the flange-offset detail on steel tub girder system, top flange proportions should be modified to accommodate to this change in the geometry. Current and proposed flange alignments are shown in Figure 6-9. Since the top flanges are no longer centered on the webs, the amount of flange offset needs to be established first. As the unsupported flange width ($b_f{}^i$ in the figure) increases, design parameters used in the slenderness ratio evaluation must be changed accordingly.

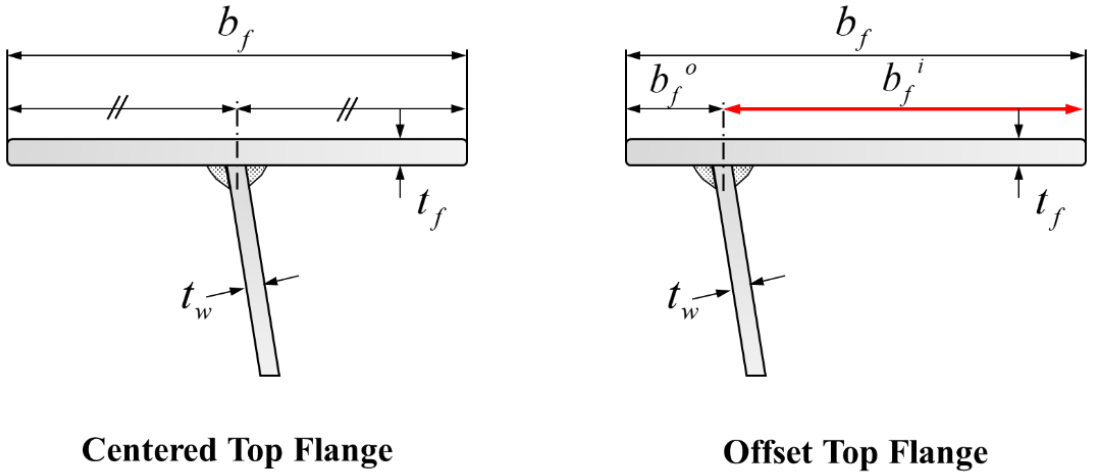

Figure 6-9 - Alignment of Top Flange

The amount of flange offset can be affected by many practical limits. In Commentary C 6.11.2.2 (AASHTO 2017), it requires that the bottom flanges of box girders should extend at least one inch beyond the outside of each web to allow for welding of the webs to the flange, therefore:

$$(b_f{}^o)_{\min} \geq 1in. \qquad \textit{Equation 6-28}$$

During girder lifting and handling, beam clamps are commonly used to pick up the girders as shown in Figure 6-10.

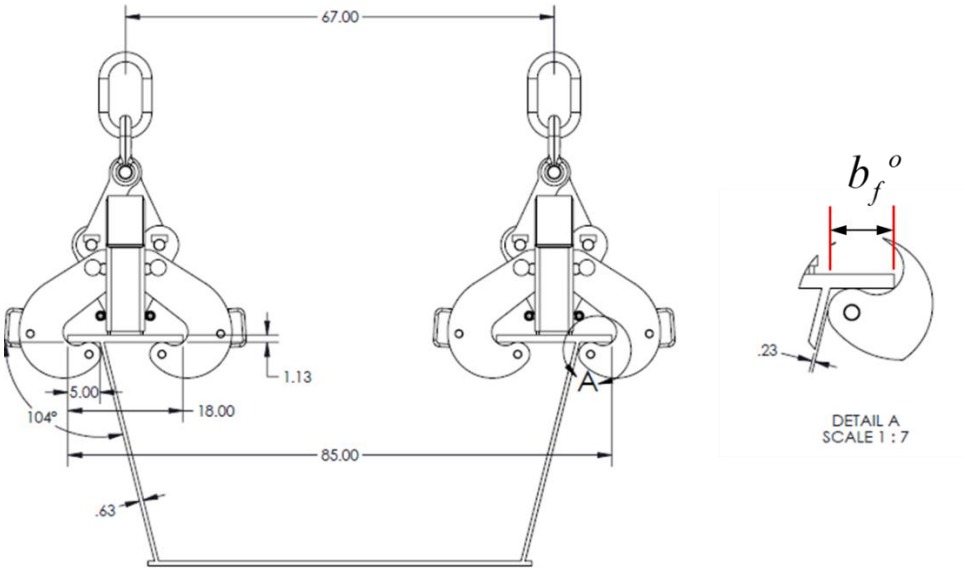

(Courtesy of Caldwell Group Beam Grab Model in the sketch F-25)

Figure 6-10 - Beam Grab and Required Flange Overhang Width

Flange offset detail should consider this. A small survey was sent out to the industry to investigate the desired flange overhang width $b_f{}^o$. Based on the response, to fit a claw of a typical beam clamp, a minimum required flange overhang width should be:

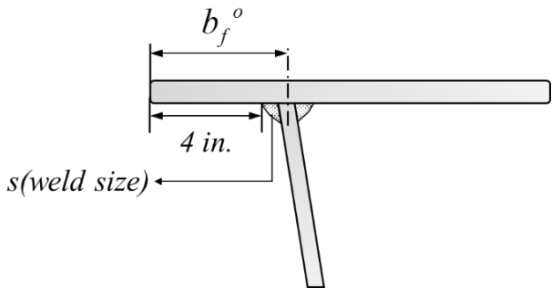

Figure 6-11 - Minimum Required Flange Overhang

$$(b_f{}^o)_{\min} \geq 4in. + s \qquad \textit{Equation 6-29}$$

where *s* is the weld size at flange-web conjuncture. For a full bite of the beam clamp, the flange overhang would be at least 5~6.5 in (Hirschfeld and Caldwell Group). This limit gives a lower bound for flange offset. The final selected offset should also be able to fit all the bolts in a simple bolted connection between the top flange and the top lateral truss.

In the preliminary stage of steel tub girder design, a typical section geometry is usually developed first based on the cross-section proportion limits specified in Article 6.11.2 AASHTO LRFD Specification. This section design is used as an initial minimum section for the iterative design process. Section 6.11.2.2 specifies that the top flanges of tub girders subject to compression or tension shall be proportioned such that:

$$\frac{b_f}{2t_f} \leq 12 \qquad \textit{Equation 6-30}$$

This equation is a practical limit to ensure the flange will not distort excessively when welded to the web and also limits the likelihood of flange local buckling. The form of this equation assumes that the top flanges are centered on the webs. Therefore, half of the flange width is considered unsupported flange width. For offset top flanges, this limit must be addressed because both experiment and FEAs have proven that without enforcing this limit distorted plates are prone to local instability. However, the form of the current equation needs to be altered. The top flanges of tub girders can be classified as unstiffened elements since they are only supported along one edge parallel to the direction of the compression force. As specified in the AISC Manual (AISC 2011),for unstiffened element, the unsupported flange width is the distance from the free edge to the first row of fasteners or the line of welds. For flange-offset layout, the critical width used in the equation should be b_f^i, the flange width inside the box section. Therefore, the modified equation is:

$$\frac{b_f^{\,i}}{t_f} \le 12 \qquad \textit{Equation 6-31}$$

6.2.2 Design Checks with Flange-offset Detail

Once an initial flange proportion is defined, the constructability of the top flanges of tub girders should be checked according to the provisions of Articles 6.10.3.2.1 through 6.10.3.2.3. These design checks of the top flanges during construction include three different force effects, i.e., flange lateral bending, flange flexure as well as flange lateral torsional buckling. With offset top flanges, some of the design parameters used in the equations should be changed.

The rationale behind current restrictions on centered flange-web intersection is the concern of additional lateral bending effect. Therefore, this effect needs to be carefully considered. The lateral bending effect on the top flanges during construction comes from three different sources: the deck overhang, bracket load, horizontal component of web shear as well as horizontal curvature. The design calculations combine all the three different sources and calculate the stress on the top flanges:

$$f_l = \frac{M_{tot\_lateral}}{S_l} \qquad \textit{Equation 6-32}$$

where f_l is the flange stress due to lateral bending; $M_{tot\_latreal}$ is the combined lateral bending moment; and S_l is the elastic section modulus of one of the top flanges in the lateral direction. When calculating this stress, the proper section modulus should be used for flange-offset layout since the axis of bending has shifted away for the center as depicted in Figure 6-12.

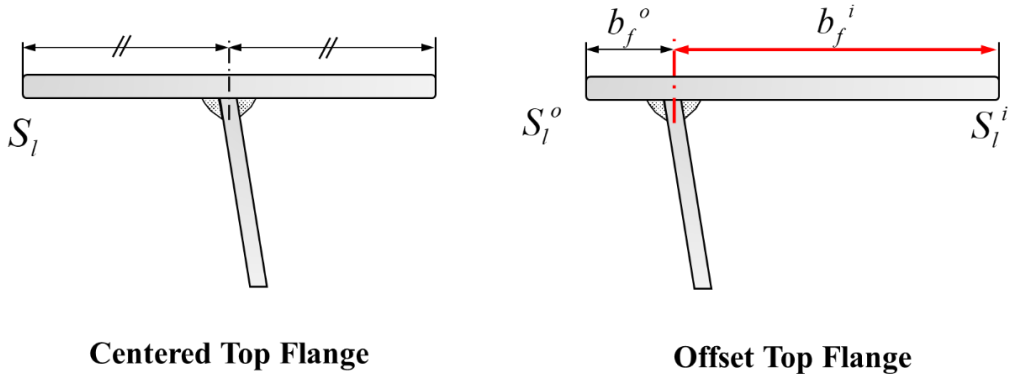

Figure 6-12 - Section Modulus for Flange Lateral Bending Check

When examining the flexural resistance of top flanges, the local buckling resistance of the top flanges is a critical limit state for tub girders with flange-offset detail. The local buckling is controlled by limiting the slenderness ratio of the top flange. The critical slenderness ratio that should be used for the offset flange is $\frac{b_f{}^i}{t_f}$, in which the flange width inside the box section is used. This slenderness ratio will then be compared with two limiting ratios λ_{pf} and λ_{rf}:

$$\lambda_{pf} = 0.38\sqrt{\frac{E}{F_{yc}}} \text{ and } \lambda_{rf} = 0.56\sqrt{\frac{E}{F_{yr}}} \qquad \textit{Equation 6-33}$$

where λ_{pf} is the limiting slenderness ratio for a compact flange; λ_{rf} is the limiting slenderness ratio for non-compact flange; F_{yc} is the yield stress of compression flange; F_{yr} is the compression-flange stress at the onset of nominal yielding within the cross-section, including residual stress effects, but not including compression-flange lateral bending, taken as the smaller of $0.7F_{yc}$ and F_{yw}, but not less than $0.5F_{yc}$.

6.2.3 Top Flange Field Splice with Flange-offset Detail

In current bridge engineering practices, long span and continuous girder systems are usually assembled segment by segment through bolted splice connections in the field. A Schematic of a typical top flange field spice is shown in Figure 6-13. The flange-offset detail complicates the splice design since some provisions in Section 6.13 are difficult to achieve with off-center top flanges. Article 6.13.1 states that in general, splice connection should be made symmetrical about the axis of the members. Article 6.13.6.1.4a requires at least two rows of bolts on each side of the connection. With offset top flanges, the limited flange on one side of the web may not be able to fit in two rows of bolts and the splice connection will not be symmetrical about the axis of the girder if directly spliced together. With an asymmetric splice connection, the force and moment transferred to the bolts will not be evenly distributed which leads to premature failure of bolts with larger load demand. Some modification at the splice location can be made on the offset flange to satisfy these requirements mentioned before.

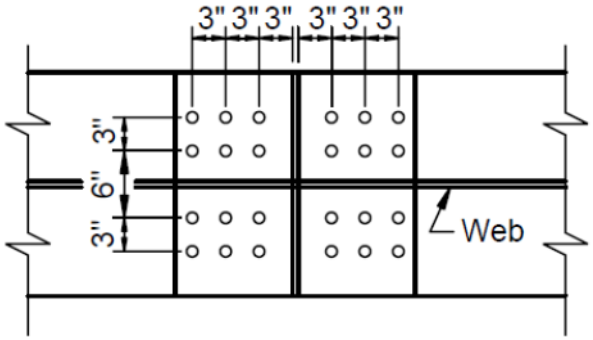

Figure 6-13 - Typical Bolt Pattern - Top Flange Field Splice (Steel Bridge Design Handbook)

For continuous tub girder systems, the most commonly used practice is to keep the girder depth constant and use different widths for top flanges in positive and negative bending regions. In current designs, increasing top flange width is generally more effective for resisting the lateral bending stresses than increasing the top flange thickness (Coletti 2005). Therefore, the flange width for negative bending regions is usually around 24~30 in. compared to 12~ 18 in. for positive bending regions. A potential splice details for a tub girder with flange width transition would be to keep the top flange in negative bending regions centered while only offsetting the top flange in the positive region. A flange overhang of 5~6 in will be kept outside the webs for handling (Figure 6-14). Because splice connections should be symmetrical, shop welded splice plates could be attached at the end of offset flange in the positive region. Additional research could be done to investigate the importance of having a symmetric splice connection since the moment demands in this region are relatively low.

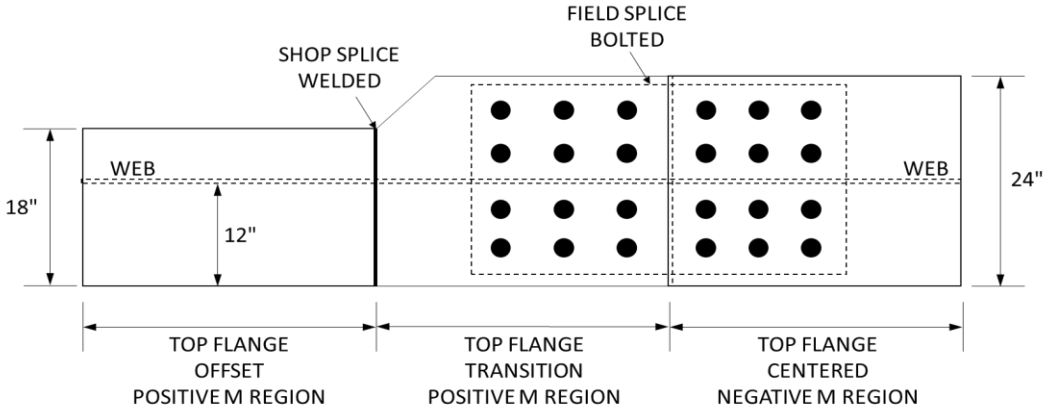

Figure 6-14 - Splice Detail for Tub Girder with Flange Width Transition (Top View)

Another commonly used practice is to vary the depth of the girder while use top flanges of the same width but different thicknesses for positive and negative bending regions. Therefore, a potential flange offset detail for tub girders with this configuration would be to offset the top flange in both the positive and negative bending region with two splice plates welded at the end of the offset flange to ensure symmetry at the splice location as shown in Figure 6-15. However, providing two full penetration welded connections on either side of the splice is likely to be uneconomical to fabricate. Additional research on the splice demands are recommended since

significant savings can be made. The research team feels that having a single line of bolts on the outside of the girder at the splice region would like have acceptable behavior during the construction condition. Since top lateral truss panels will likely be provided on either side of the splice, the two top flanges and the top truss behave in a similar manner as the bottom flange, which is only spliced on the inside of the girder.

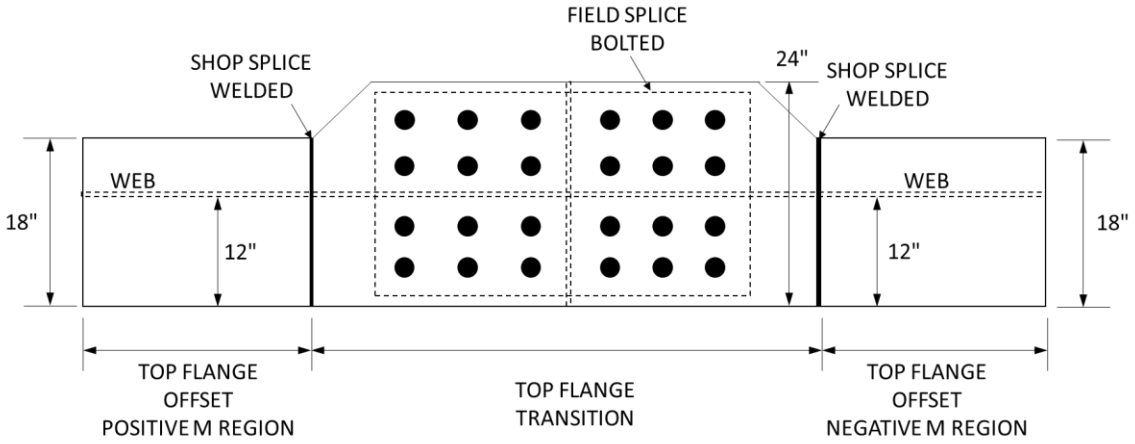

Figure 6-15 - Splice Detail for Tub Girder with Flange Thickness Transition (Top View)

6.2.4 Alternative Detail for Girder Handling with Flange-offset Detail

With a sufficient flange overhang width, the beam grab will have enough room for an effective pickup. However, feedback from the fabrication industry indicates that with the off-center flange configuration, eccentric loading would be expected on the hook of the beam grab. This eccentricity is not generally considered in design. Another alternative detail is provided for girder handling. In the experimental study of this research project, the test specimen with extreme flange offset configuration was fabricated and tested in Ferguson Laboratory. To solve the girder handling issue, bolted extension plates were added on the top flanges to provide more width for the beam clamp to pick up as shown in Figure 6-16. These extension plates were provided at multiple location along the length with simple bolted connections.

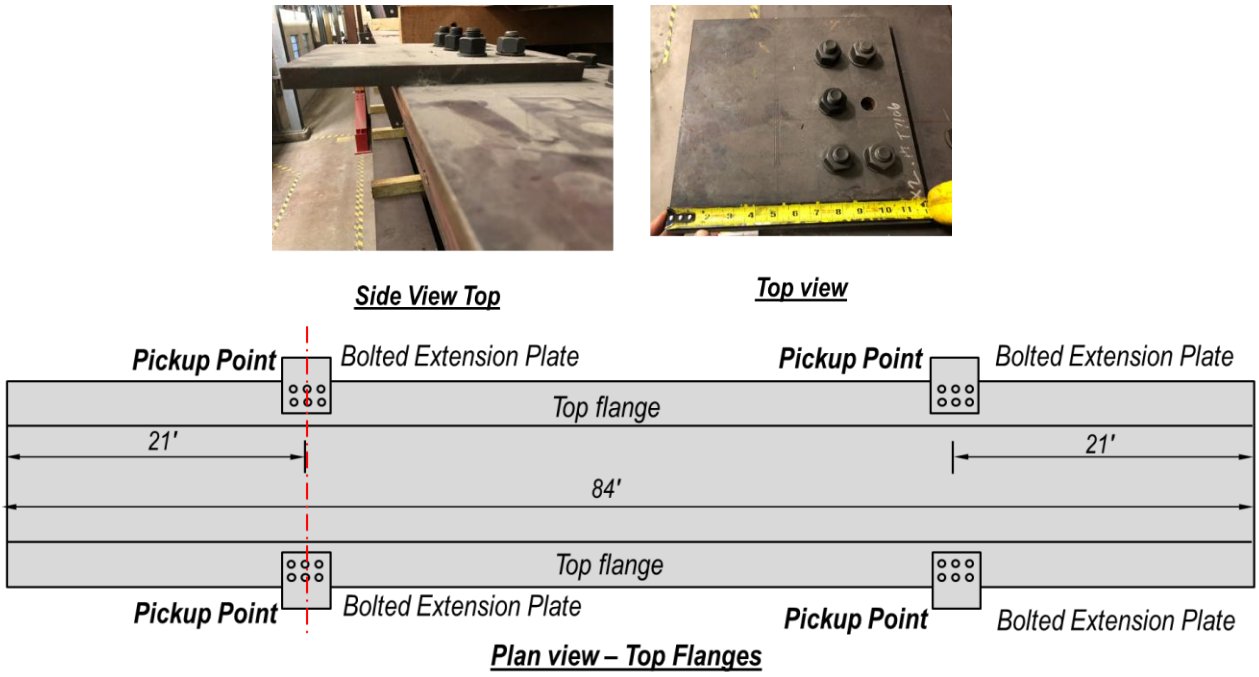

Figure 6-16 - Bolted Extension Plates on the Girder Top Flange

6.3 Design Recommendations for Steel Tub Girders with Lower Web Slopes

6.3.1 Bridge Cross Section and Girder Spacing with Lower Web Slope

The use of lower web slope (less than 4 Vertical to 1 Horizontal) is intended to reduce the number of girder lines with an efficient deck design and girder spacing. When developing the bridge cross section, the designer will typically evaluate the number of girder lines required, relative to the overall cost (Steel Bridge Design Handbook 2012). The economy of bridge cross section design depends on girder spacing and deck overhang dimensions. These key design parameters have been identified in Figure 6-17. Flexibility in the specification of the web slope can lead to potential reduction in the number of girder lines as well as minimizing the bottom flange width. A conceptual design process will be presented in this section to give an example of how to optimize the number girder lines.

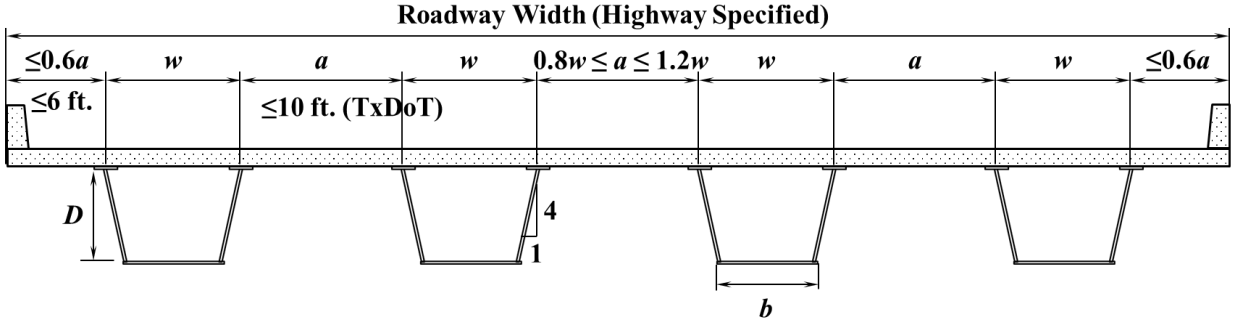

Figure 6-17 - Typical Cross Section of Tub Girder Bridge

The current AASHTO LRFD Specification and TxDOT Bridge Design Manual contain requirements and limitations for the composite tub girder bridge section as indicated in Figure 6-15. Most of limitations are due to the use of empirical equations for the live load distribution factor. The girder spacing, which is defined as the center-to-center distance of top flanges of adjacent girders, is restricted within 80% ~120% of the girder width *w* as specified in AASHTO Article 6.11.2.3. The TxDoT Bridge Design Manual (TxDOT 2015) further limits this spacing to be less than 10 ft. Article 6.11.2.3 also requires that the cantilever overhang of the deck shall not be greater than 60% of girder spacing *a* or 6.0 ft. In addition, the web slope ratio is restricted to be no less than 4V: 1H (or no greater than 1H:4V in the specification). All these restrictions are consistent with the geometry used in the original research study on box girder (Mattock 1967). However, in this research project, both experimental and FEA studies have suggested that lower web slope can be used on tub girders without significant impact on the behavior. To reflect the correlation with this study, lower slope in this design guide refers to slope ratio greater than or equal to 2.5 V:1 H.

In the bridge cross section design, the total roadway width is directly determined and dictated by the bridge owner. With this given geometry, the roadway width can be simply expressed as:

$$Road\ Width = 2 \times Overhang\ \ Width + N \times w + (N-1) \times a \qquad \textit{Equation 6-34}$$

where *N* is the number of girder lines. To minimize the number of girder lines, the overhang width and girder spacing should be maximized. Therefore, the clear spacing between adjacent girders, *a,* is set to *1.2w* and the overhang width is set to *0.6a*. The equation can then be rewritten as:

$$Road\ Width = 2 \times 0.6 \times 1.2 \cdot w + N \times w + (N-1) \times 1.2 \cdot w \qquad \textit{Equation 6-35}$$

$$Road\ Width = (2.2N + 0.24) \cdot w \qquad \textit{Equation 6-36}$$

To minimize the number of girder lines, a relatively large girder width needs to be selected with a given roadway width. The maximum value of *w* can be determined by many practical factors. Girder width *w* can be selected based on the transportation limit on the width of a girder or the minimized bottom flange width with a lower slope. Consider the tub girder design for a roadway with a width of 78 ft and span length L=100 ft. The girder is 4 ft deep based on a L/d ratio of 25. A minimum recommended bottom flange width of 4 ft is assumed in the design. Designs with a web slope of 4 and 2.5 is compared:

- For web slope ratio of **4V: 1H**:
  Girder Width – *w* =6 ft.
  Required Number of Girder Line N=5.8 so increase to **6 Girders**
- For web slope ratio of **2.5V: 1H**:
  Girder Width – *w* =7.2 ft.
  Required Number of Girder Line N=4.8 so increase to **5 Girders**
- The original design (FM3267 – IH 35):
  used a bottom flange width of 5 ft with web slope of 4.0.
  The resulting system has a total of **6 Girders**

From this numerical example above, one girder line can be reduced if the lower slope is properly used with efficient deck dimensions for multiple girder system (more than 4).

In this example, the girder spacing, and the deck overhang width still satisfy current AASHTO restrictions. The use of larger girder a spacing, and deck overhang requires further investigation on current deck details for transverse bending/ cantilever bending effects. Increasing the deck span between the girders requires new deck details which may not be economical compared with current practices. Wider deck span is in general difficult to form and construction. Current specification for permanent metal deck form may not be suitable for this purpose. Wider deck span also creates limitations for future deck placement and partial deck removal. For deck overhangs, a large overhang will result in large forces on the exterior web of tub girders and additional bending moment caused by cantilever effects, which needs to be considered.

6.3.2 Web Proportion with Lower Web Slopes

Proportion limits for webs of tub girders are specified in AASHTO Article 6.11.2.1. For inclined webs, the distance along the web shall be used for checking all design requirements. As depicted in Figure 6-18, the distance used in the design check is:

$$D' = \frac{D}{\cos\theta} \qquad \textit{Equation 6-37}$$

where D is the vertical depth of the web in inches; θ is the angle of inclination of the web plate to the vertical (degrees).

Web Slope (V:H)	θ (Deg)
4:1	14.0
3:1	18.4
2.5:1	21.8

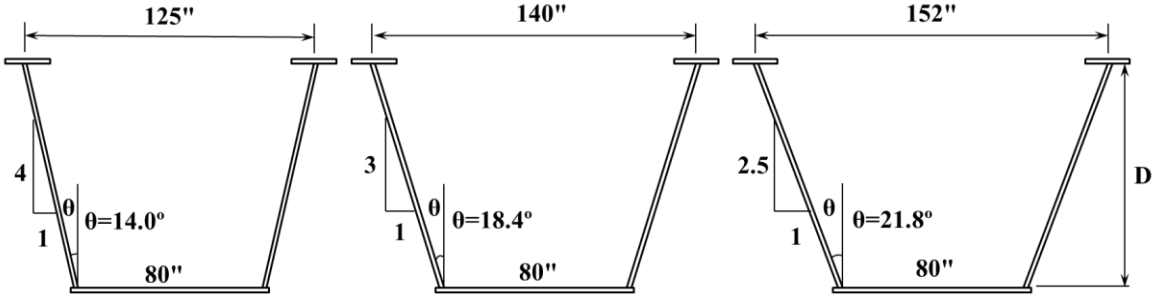

Figure 6-18 - Section Design with Various Web Slopes

For webs without longitudinal stiffeners, the web plate shall be proportioned such that:

$$\frac{D}{t_w} \le 150 \qquad \textit{Equation 6-38}$$

6.3.3 Shear Checks with Lower Web Slopes

As stated in the commentary C 6.11.9, for tub girders with inclined webs, the web must be designed for the component of the vertical shear in the plane of the web due to the factored loads (see Figure 6-19), taken as:

$$V_{ui} = \frac{V_u}{\cos\theta} \qquad \textit{Equation 6-39}$$

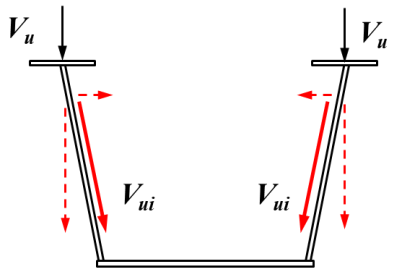

Cross Section View

Figure 6-19 - Factored Shear Load Demand on Inclined Webs

As the web slopes decrease, the angle of inclination θ increases. The shear demand on each sloping web will increase with a lower web slope. However, with two webs in a tub girder, providing adequate shear strength should not be a major concern. To calculate the shear resistance of a single web, the provisions of Article 6.10.9 shall be applied for determining the factored shear resistance of a single web. In all the equations, *D* shall be taken as the depth of the web plate measured along the slope for web shear buckling and bending buckling checks.

6.3.4 Increased Strut Forces with Lower Web Slopes

Another impact of decreasing the web slope is a corresponding increase in the demand on the struts that connect the top flanges since the strut handles the horizontal component of the shear in the web as depicted in Figure 6-20.

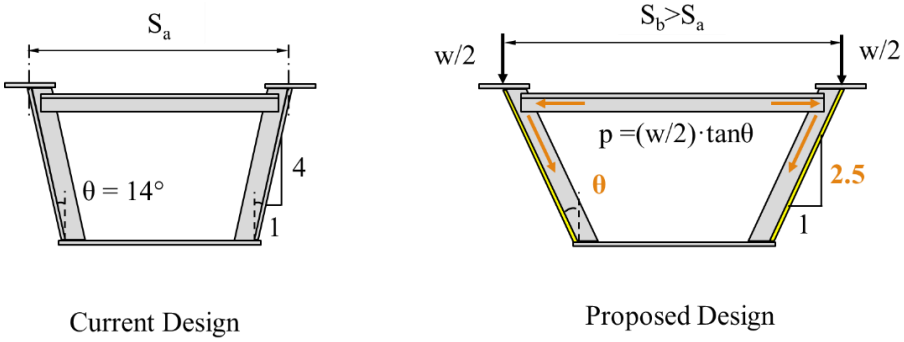

Figure 6-20 - Increased Force Demand in Top Struts

As this force component is tensile in nature, the effect of sloping webs on the top struts will be included when calculating the force effect due to bending and torsion. The design equation should be able to account for the increase in the force demand on the struts.

6.3.5 Live Load Distribution Factor with Lower Web Slopes

The current AASHTO specification restricts the use of lower web slope mainly due to the empirical equation for live load distribution factor. Example parametric FEA results showed that even with a lower slope, the live load distribution will not be affected significantly. Therefore, for tub girders with lower web slopes, the empirical equation can still be utilized. However, lever rule

can still be used to evaluate the behavior. Current TxDOT design practice uses both methods to determine the live load distribution factor.

The empirical equation used in the current AASHTO Specification to calculate live load distribution factor regardless of number of loaded lanes is given in the following expression:

$$LLDF = 0.05 + 0.85\frac{N_L}{N_b} + \frac{0.425}{N_L} \qquad \textit{Equation 6-40}$$

The use of this equation needs to abide by the restrictions specified in Article 6.11.2.3 except for the web slope limitation.

Another commonly used method to determine the live load distribution factor is the lever rule method. In this method, for exterior and interior girders, an assumed 'hinge' is placed on the deck and the wheel loads are placed to generate the maximum moment and shear effect as shown in Figure 6-21.

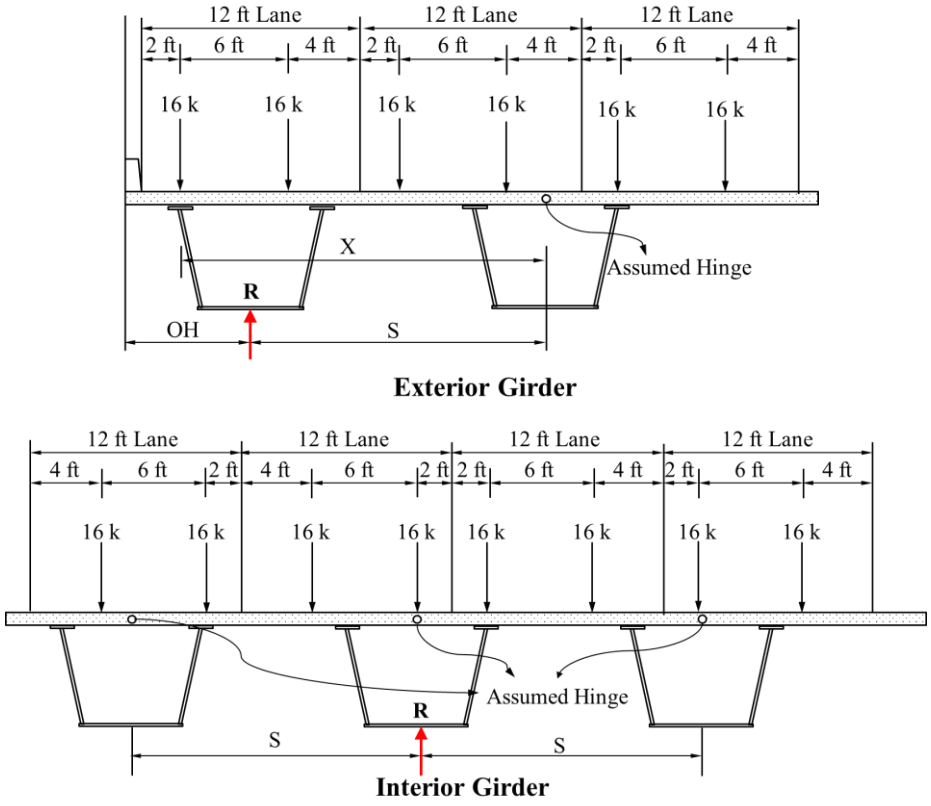

Figure 6-21 - Lever Rule for Exterior or Interior Girder in Tub Girder System

Chapter 7. Summary and Conclusions

Current practices for design and fabrication of steel tub girders sometimes employ inefficient cross-sectional geometries and inefficient bracing details that can be improved to obtain more cost-effective tub girders for straight and horizontally curved bridge applications. The purpose of this project was to investigate alternative details that can simplify fabrication, improve the structural efficiency, and thereby enhance the economy of steel tub girders. Research conducted in this study was divided in two main areas of focus: 1) improved bracing, and 2) improved cross-sectional geometry. The primary emphasis of these studies was to examine the behavior of steel tub girders during construction, before they become composite with the concrete bridge deck. Thus, much of the experimental and finite element studies were on bare steel tub girders. A brief summary of these studies and the primary findings related to improved bracing details and improved cross-sectional geometry are provided in Sections 7.1 and 7.2 below. As a final aspect of this research, three steel tub girders with composite concrete deck were tested to failure, to evaluate the effects of modified bracing details and cross-sectional geometry on the ultimate strength of the girders. The tests are summarized in Section 7.3.

7.1 Improved Bracing Details

Improved bracing details for steel tub girders were investigated in this project. Different top lateral bracing and internal K-frame layouts were studied to determine more cost-effective bracing configurations for straight and horizontally curved steel tub girders. The project also considered the influence of allowing the line of action of the diagonals of the top flange lateral truss and that of the strut to not intersect at a single working point. To study these new details, large-scale laboratory testing and parametric finite element modeling were conducted. The laboratory experiments consisted of elastic load tests on three non-composite 86-foot long tub girders with different cross section characteristics. The experimental data collected was used to validate finite element models created in the three-dimensional finite element program Abaqus/CAE. The validated models were used to perform parametric studies to extend the knowledge gained in the experiments to consider a wider range of variables.

7.1.1 Experimental Studies

Experimental tests were conducted on non-composite steel tub girders to investigate the effects of partial top lateral bracing and the configuration of internal K-frames on the structural behavior. The experimental program consisted of testing three 86-foot-long tub girders with different cross-sectional geometries with a variety of loading and bracing configurations. Top flange lateral braces and internal K-frames were designed and fabricated with bolted connections so that different configurations of bracing could be evaluated in the experiments. Each tub girder had 12 panels along the girder. Panels with diagonal bracing were varied from zero to three panels at each end. The spacing between internal K-frames was varied from every 2, 4, and 6 panel points. A total of 12 different bracing configurations were tested on each girder. Additionally, elastic load tests were conducted using gravity load simulators. Both concentric and eccentric vertical loads were applied to the girders. The eccentric loads were applied to simulate the combined bending and torsion that a horizontally curved girder would experience. The eccentric loading cases simulated girders with radii of curvature of 1260 ft. and 630 ft. For each loading case (concentric

plus two eccentric cases), the 12 bracing configurations were tested to perform 36 elastic load tests on each girder. During the tests, it was observed that providing partial top lateral bracing in the regions of high cross-sectional warping substantially improved the torsional and lateral stiffness of the steel tub girders. The results were consistent in the three girders with different cross-sections. Additionally, it was observed that the distribution of K-frames has little impact on the torsional stiffness of straight and curved steel tub girders. The diagonals of the top lateral bracing in the specimens were fabricated so that the working point of the diagonal was located 6% of the panel length away from the working point of the struts. No significant impact was observed in the local or global stability of the girders.

7.1.2 Finite Element Studies

An extensive series of finite element studies were conducted to extend the findings from the experimental program to a broader range of tub girder configurations found in typical bridge applications. Finite element modeling techniques and assumptions were first refined based on the experimental data to establish a validated approach to model steel tub girders. Using the validated finite element models, a parametric study was conducted to extend the analysis of partial top lateral bracing, internal K-frame distribution, and offsets in the line of action of the truss diagonal relative to the working point.

Two-prototype tub girders were selected for the parametric finite element studies: a 3 ft. tall and a 7.5 ft. tall girder. For each prototype girder, different parameters were considered such as the span length/depth ratio (L/D), span configuration, radius of curvature, amount of partial top lateral bracing and internal K-frame layouts. L/D ratios from 20 to 45 were evaluated in simple span and continuous 2 and 3 span girder configurations. Radii of curvature down to 800 ft. were evaluated as well. From this study, it was observed that in straight girders, adequate torsional stiffness can be achieved while providing a top lateral truss over only 50% of the length of the girder. In these cases, 25% of the bracing was positioned near the two supports at the ends of the span, with the central portion of the span remaining unbraced. Horizontally curved girders with a radius of curvature of 2500 ft. or greater and span lengths up to 216 ft. also showed adequate torsional stiffness with 50% top lateral bracing. Longer spans require more diagonals for adequate stiffness. However, in the unbraced portions of horizontally curved tub girders, lateral bending stresses increase in the top flanges. Consequently, the top flanges must be sized to accommodate these higher lateral bending stresses.

Regarding internal K-frame configurations, it was observed that the distribution of K-frames along the length of the girder did not affect the torsional behavior of the girder. In straight tub girders, reducing the number K-frames from every panel to every 2 or 3 panels reduced the axial loads on the K-frame members. For horizontally curved girders, the torsional response was not affected when reducing the number of K-frames. However, the axial forces in the K-frame members increased when the number of K-frames was reduced. For tub girders with partial top lateral bracing configurations, it is important to locate K-frames at the transition point between braced and unbraced girder, i.e., at the end of partial top lateral bracing, as well as at midspan. When placing K-frames at these critical locations, other configurations of K-frames did not affect the torsional response of the girder. Overall, the results of this study indicate that the spacing between internal K-frames can be increased to every 2 panels in both straight and horizontally curved girders, and in some cases, can be increased even further.

The finite element studies also investigated the effects of offsetting the top lateral truss diagonal working point up to 5% of the panel length from the strut working point. Not requiring a

common working point for intersection of the truss diagonal and the strut can simplify the fabrication of the top lateral truss connections. Offsetting the braces from a single working point did not affect the global behavior of the girder significantly but increased the axial forces in the top lateral truss members.

Based on the experimental and parametric finite element studies, design recommendations were developed for improved bracing details for steel tub girders. These design recommendations are provided in Chapter 6 of this report.

7.2 Improved Cross-sectional Geometry

This research project examined two possible modifications to current practice in establishing the cross-section geometry of steel tub girders: 1) offsetting top flanges, and 2) using a shallower web slope.

The first modification considered was the use of offset top flanges. In current practice, the top flanges are typically centered on the webs. By offsetting the top flanges towards the inside of the tub girder, connections between the top lateral truss and the top flanges can be simplified. The second modification considered was the use of shallower webs. In current practice, the slope of the tub girder webs is 4:1 (4 vertical to 1 horizontal). The use of a lower slope, such as 2.5:1, can increase the tributary area of the girder and may eliminate a girder line across the width of a bridge.

The effect of these two cross-section geometry modifications on the steel tub girders during construction was examined both in experimental studies and in parametric finite element studies. These are briefly summarized below.

7.2.1 Experimental Studies

Experimental tests were conducted on three different non-composite steel tub girders. The first specimen, designated as a baseline specimen, had a cross-sectional geometry that followed current practices, with centered top flanges and a 4:1 web slope. The second specimen, designated as an *offset top flange* specimen, had flanges offset towards the inside of the tub, but maintained the 4:1 web slope. The third specimen, designated as a *lower web slope* specimen, had a web slope of 2.6:1, and had top flanges centered on the webs. The bottom flange width of the flatter web slope specimen was the same as for the other two specimens. Note that these were the same three specimens used for the bracing studies described above. Elastic tests were conducted to evaluate the behavior of these specimens, considering both variations in bracing combined with variations in cross-section geometry.

Experiment results showed that offsetting the top flange made the girder less prone to global instability. However, offsetting the top flange resulted in somewhat larger forces in the top lateral truss members. During one of the tests, local buckling occurred in one of the top flanges. Subsequent analysis showed that the stress in the top flange had reached the critical buckling stress, which could be predicted by finite element analysis and by simple hand calculations. Overall, the experiments showed no significant disadvantages of using offset top flanges but emphasized the need to check local buckling of the top flange in the tub girder design process.

Experimental results on the lower web slope specimen showed that the lower web slope made the girder with no top lateral truss more prone to global instability. Once the top lateral truss was provided, global instability could be prevented. The top lateral truss had similar force distribution to that of baseline specimen under the same loading since these two specimens had the same truss panel size. The lower web slope, however, lead to increased forces on the top struts.

7.2.2 Finite Element Studies

Similar to the bracing studies, parametric finite element studies were conducted to more closely examine the effects of offset top flanges and lower web slopes on the behavior of steel tub girders during construction.

For tub girders with offset top flanges, the finite element studies confirmed the experimental observations that the offset top flanges enhance the global stability of the girder. Offsetting the top flanges also causes modest changes in the top flange stresses as well as in the forces in the top lateral truss, that should be considered in design.

For tub girders with lower web slopes, the finite element studies confirmed the experimental observations that the lower web slope makes a tub girder without a top lateral truss significantly more prone to global instability. However, when a top lateral truss is provided, global stability can be maintained. The lower web slope, however, causes an increase in the forces in the members of the top lateral truss, and most significantly, in the struts. The finite elements studies also showed that changes in web slope did not significantly change the live load distribution of the completed bridge.

7.3 Ultimate Strength Tests on Composite Tub Girders

After all of the elastic tests on the non-composite tub girder specimens were completed, the three tub girder specimens were provided with a composite concrete slab and tested to failure. The elastic tests on non-composite girders and companion parametric finite element studies described above focused on the behavior of tub girders during construction. These final ultimate strength tests on composite tub girder specimens were conducted to determine if changes to girder bracing and girder cross-section geometry had an unexpected adverse effect on the ultimate strength of the girders.

All three tub girder specimens were provided with a reinforced concrete slab, and a sufficient number of shear connectors on the top flanges to develop the fully composite strength of the girders. The three girder cross-section geometries were the baseline specimen, the girder with offset flanges, and the girder with the flatter sloped webs. All three girders were tested with internal K-frames located at every other panel point and with the three top flange truss diagonals located at each end of the span.

The girders were tested with two different configurations: 1) a two span configuration to investigate negative moment behavior, and 2) a simply supported configuration to investigate positive moment behavior. A longitudinal stiffener was added to the bottom flange of the first girder (baseline section) in the negative moment region to prevent bottom flange buckling. For the other two specimens, shear studs were welded to the bottom flange in the negative moment region and a concrete slab was cast on top of the bottom flange, inside of the tub.

The tests showed no unexpected results in the behavior of the three specimens, Further, the experimentally determined flexural stiffness and strength of the girders under negative and positive moment agreed well with the predictions from conventional cross-section analysis. Finally, the tests showed that the composite concrete slab cast on the bottom flange in the negative moment region for two of the specimens was effective in preventing bottom flange buckling.

7.4 Conclusions

The results of this study have shown there are significant opportunities to improve bracing details and the cross-section sectional geometry of steel tub girders, to enhance the economy of steel tub girders. For straight and mildly horizontally curved tub girders, the top lateral truss can be eliminated over a significant length of the girder. Further, the number of internal K-frames for both straight and horizontally curved tub girder can be reduced. The research also showed that it is possible to use top flanges that are offset towards the inside of the tub, as well as using tubs with lower web slopes. These changes to bracing layouts and cross-section geometry can simply fabrication and reduce the cost of tub girders, while maintaining good structural performance, both during construction and in the finished bridge. However, incorporating changes to bracing layouts and cross-sectional geometry requires additional analysis and design checks. Detailed recommendations for improved bracing layouts and cross-sectional geometry, and associated design checks, are provided in this report.

References

ABAQUS. (2016). Abaqus Analysis User's Manual.

AISC. (2011). Steel Constrction Manual (14th ed.). American Institute of Steel Construction.

(AASHTO) (2017). AASHTO LRFD Bridge Design Specifications, 6th Ed. Washington, DC, American Association of State Highway and Transportation Officials.

ASTM. (2001). Standard Specification for General Requirements for Rolled Structural Steel Bars, Plates, Shapes, and Sheet Piling. *A6-01*. West Conshohocken, PA: ASTM International.

Asadnia, Mahdi (2018). Out-of-Flatness Plate Tolerance for Steel I-Shaped and Tub Highway Bridge Plate Girders, PhD Dissertation, George Washington University, Washington, D.C.

AWS. (1996). Bridge Welding Code. *AWS D1.5*. Miami, FL: American Welding Society.

Barnard, T. J. (2006). "Constructing a Full-Scale Horizontally-Curved Twin Steel Trapezoidal Box Girder Bridge Segment to Determine Redundancies in Fracture Critical Bridges". Department of Civil Engineering, The University of Texas at Austin: 121.

Battistini, A., Wang, W., Helwig, T., Engelhardt, M., and Frank, K. (2012). Comparison of the Stiffness Properties for Various Cross Frame Members and Connections. Proceedings, Annual Stability Conference, Structural Stability Research Council, Dallas, April 18-20, 2012.

Branco, F. A. and R. Green (1985). "COMPOSITE BOX GIRDER BRIDGE BEHAVIOR DURING CONSTRUCTION." Journal of Structural Engineering 111(3): 577-593.

Brennan, P. J. and J. A. Mandel (1979). "Multiple Configuration Curved Bridge Model Studies." Journal of the Structural Division 105(ST5): 875-890.

Chandar, G., et al. (2010). "Rapid, Economical, Bridge Replacement". Modern Steel Construction, National Steel Bridge Alliance

Chen, B. S. (2002). "Top-Lateral Bracing Systems for Trapezoidal Steel Box-Girder Bridges". Department of Civil Engineering. Austin, Texas, The University of Texas at Austin. Ph.D.

Chen, B. S., et al. (1999). "Top Lateral Bracing of Steel U-Shape Girders", The University of Texas at Austin: 1-104.

Chen, B. S., et al. (2005). "Top-Lateral Bracing Systems for Trapezoidal Steel Box-Girder Bridges", Center for Transportation Research, The University of Texas at Austin: 1-116.

Cheplak, B. A. (2001). "Field Measurements of Intermediate External Diaphragms on a Trapezoidal Steel Box Girder Bridge". Department of Civil Engineering. Austin, Texas, The University of Texas at Austin.

Choi, B. H., et al. (2008). "Experimental study on the ultimate bending resistance of steel tub girders with top lateral bracing." Engineering Structures 30(11): 3095-3104.

Chu, K. and S. G. Pinjarkar (1971). "Analysis of Horizontally Curved Box-Girder Bridges." Journal of Structural Division, ASCE 97(10): 2481-2501.

Coletti, D. F. (2005). Practical Steel Tub Girder Design. National Steel Bridge Alliance (NSBA).

Culver, C. G. and I. Mozer (1971). "Horizontally Curved Highway Bridges, Stability of Box Girders". Department of Civil Engineering, Carnegie Mellon University, Carnegie Institute of Technology: 1-91.

Culver, C. G. and J. Mozer (1970). "Horizontally Curved Highway Birdges, Stability of Curved Box Girders". Department of Civil Engineering, Carnegie Mellon University, Carnegie Institute of Technology: 1-118.

Dabrowski, R. (1968). "Curved thin-walled girders: Theory and Analysis." Cement and Concrete Association, U.K.

Daniels, J. H. (1985). "Ultimate Strength Test of Horizontally Curved Composite Box Girder". Fritz Engineering Laboratory, Lehigh University.

Daniels, J. H., et al. (1978). "Fatigue of Curved Steel Bridge Elements - Ultimate Strength Test of Horizontally Curved Composite Box Girder". Fritz Engineering Laboratory, Lehigh University: 1-81.

Daniels, J. H. and W. C. Herbein (1977). "Fatigue of Curved Steel Bridge Elements - Fatigue Tests of Curved Plate Girder Assemblies". Fritz Engineering Laboratory, Lehigh University: 1-150.

Daniels, J. H., et al. (1976). "Fatigue of Curved Steel Bridge Elements - Analysis and Design of Plate Girder and Box Girder Test Assemblies". Fritz Engineering Laboratory, Lehigh University: 1-109.

Davidson, J., et al. (2004). "Design and Construction of Modern Curved Bridges". Department of Civil & Environmental Engineering, The University of Alabama at Birmingham.

Dezi, L. (1985). "Aspects of the deformation of the cross-section in curved single cell box beams." Industria Italiana Del Cemento 55(7-8): 500-808.

Dogaki, M., et al. (1979). "Further Test of The Curved Girder With Orthotropic Steel Plate Deck." Technology Reports of Kansai University 20: 123-132.

Dowling, P. J., et al. (1973). "Experimental and prodicted collapse behavior of Rectangular Steel Box Girders " Steel Box Girder Bridges, Intitution of Civil Engineers: 77-94.

Dowling, P. J., et al. (1977). "The Effect of Shear Lag on the Ultimate Strength of Box Girders." Steel Plated Structures, ed. By P.J. Dowling, J.E. Harding and P.A. Frieze, Crosby Lockwood Staples: 108-141.

Dowswell, B. and Brice A. (2010) Horizontal Bracing-an Overview of Lateral Load Resisting System and How to Implement them. Modern Steel Construction, 06-2010.

Espinoza, O. R. (2007). "Measurements of Deformations and Stresses Due to Plate Out-of-Flatness in a Steel Twin Box Girder Bridge System". Department of Civil Engineering, The University of Texas at Austin: 179.

Fam, A. R. and C. J. Turkstra (1975). "A finite element scheme for box bridge analysis." Computers and Structures 5: 179-186.

Fan, Z. and T. Helwig (1999). "Behavior of steel box girders with top flange bracing." Journal of structural engineering New York, N.Y. 125(8): 829-837.

Fan, Z. and T. Helwig (1999). Field and computational studies of steel trapezoidal box girder bridges. Ann Arbor, University of Houston. 3025709: 300-300 p.

Fan, Z. and T. Helwig (2002). "Distortional Loads and Brace Forces in Steel Box Girders." Journal of Structural Engineering 128(6): 710-718.

Gilchrist, C. L., et al. (1997). "Buckling Behavior of U-Shaped Girders". Center for Transportation Research, The University ofTexas at Austin: 1-69.

Hall, D. H., et al. (1999). "NCHRP Report 424: Improved Design Specifications for Horizontally Curved Steel Girder Highway Bridges". Washington,DC., Transportation Research Board.

Heins, C. P. and R. S. Humphreys (1979). "Bending and Torsion Interaction of Box Girders." Journal of the Structural Division 108(ST5): 891-904.

Helwig, T. (2015). "Background and Significance of Work (Improved Tub Girder Details)". 2015.

Helwig, T. and J. Yura (2012). "Steel Bridge Design Handbook: Bracing System Design", U.S. Department of Transportation Federal Highway Administration. 13.

Helwig, T., Yura, J., Herman, R, Williamson, E., and Li, D. (2007), "Design Guidelines for Steel Trapezoidal Box Girder Systems", TxDOT Report 0-4307-1, April 2007.

Herman, R. S. (2001). "Behavior of stiffened compression flanges of trapezoidal box girder bridges". Department of Civil Engineering. Austin, Texas, The University of Texas at Austin. Ph.D.

Hovell, C. G. (2007). "Evaluation of redundancy in trapezoidal box-girder bridges using finite element analysis". Department of Civil Engineering. Austin, Texas, The University of Texas at Austin.

Hsu, Y., et al. (1995). "EBEF Method for Distortional Analysis of Steel Box Girder Bridges." Journal of Structural Engineering 121(3): 557-566.

Johnston, S. B. and A. H. Mattock (1967). "Lateral distribution of load in composite box girder bridges." National Research Council -- Highway Research Board -- Highway Research Record(167): 25-33.

Kim, J. (2010). "Finite Element Modeling of Twin Steel Box-Girder Bridges for Redundancy Evaluation". Department of Civil Engineering. Austin, Texas, The University of Texas at Austin.

Kim, J. and E. B. Williamson (2014). "Finite-element modeling of twin steel box-girder bridges for redundancy evaluation." Journal of Bridge Engineering 4014106.

Kim, K. and C. Yoo (2006). "Brace Forces in Steel Box Girders with Single Diagonal Lateral Bracing Systems." Journal of Structural Engineering 132(8): 1212-1222.

Kim, K. and C. Yoo (2006). "Effects of external bracing on horizontally curved box girder bridges during construction." Engineering Structures 28(12): 1650-1657.

Kim, K. and C. Yoo (2006). "Interaction of Top Lateral and Internal Bracing Systems in Tub Girders." Journal of Structural Engineering 132(10): 1611-1620.

Kim, K. and C. Yoo (2008). "Ultimate strengths of steel rectangular box beams subjected to combined action of bending and torsion." Engineering Structures 30(6): 1677-1687.

Kim, K. and C. Yoo (2009). "Bending behaviors of quasi-closed trapezoidal box girders with X-type internal cross-frames." Journal of Constructional Steel Research 65(8): 1827-1835.

Kollbrunner, C. F. and K. Brasler (1969). "Torsion in Structures - An Engineering Approach". Berlin, New York, Springer-Verlag.

Korol, R. M., et al. (1988). "Experimental investigation of the effects of imperfections on the strength of steel box girders." Canadian Journal of Civil Engineering 15(3): 443-449.

Li, D., "Behavior of Trapezoidal Box Girder with Skewed Supports," (2004) PhD Dissertation, Civil and Environmental Engineering Department, University of houston, August 2004.

Linzell, D., et al. (2004). "Historical Perspective on Horizontally Curved I Girder Bridge Design in the United States." Journal of Bridge Engineering 9(3): 218-229.

Lopez, M. G. (1999). Thermally-Induced Deformations and Stresses in a Steel Trapezoidal Twin-Box Girder Bridge. Department of Civil Engineering. Austin, Texas, The University of Texas at Austin.

Manko, Z. (1984). "Model Investigation of Steel Box Spans." Proceedings of the Institution of Civil Engineers, London 77(2): 491-500.

Mattock, A. H. and S. B. Johnston (1968). Behavior under load of composite box-girder bridges. American Society of Civil Engineers Proceedings. New York, NY, United States, American Society of Civil Engineers (ASCE). 94: 2351-2370.

Memberg et al. (2002). “A Design Procedure for Intermediate External Diaphragms on Curved Steel Trapezoidal Box Girder Bridges”, FHWA/TX-03/1898-1, Texas Department of Transportation, 119

McDonald, R. E. and Y. S. Chen (1976). "Open Steel Box Sections with Top Lateral Bracing." Journal of the Structural Division 102(ST1): 35-49.

Mikami, I., et al. (1987). "ULTIMATE STRENGTH TESTS ON STEEL BOX GIRDERS UNDER BENDING." Technology Reports of Kansai University(29): 175-192.

Mikami, I. and K. Niwa (1993). Ultimate strength test of steel box girders with unsymmetrical cross-section: 159-184.

Moore, D. B. and Currie, D. M (1988). Warping Restraint, Member Stability and Standards. 9th International Specialty Conference on Cold-Formed Steel Structures 1988.

Nakai, H., et al. (1992). "On Ultimate Strength of Horizontally Curved Box Girder Bridges." Proceedings of the First World Conference on Constructional Steel Design: 108-117.

Nakai, H., et al. (1990). "An Experimental Study on Ultimate Strength of Thin-Walled Box Beam Subjected to Bending and Torsion." Journal of Structural Engineering, JSCE 36A: 63-70.

Oleinik, J. and C. Heins (1975). "Diaphragms for Curved Box Beam Bridges." Journal of Structural Engineering, ASCE 10: 2161-2178.

Popp, D. R. (2004). Thermally-Induced Deformations and Stresses in a Steel Trapezoidal Twin-Box Girder Bridge. Department of Civil Engineering. Austin, Texas, The University of Texas at Austin.

Quadrato, C. G. (2010). Stability of Skewed I-Shaped Girder Bridges Using Bent Plate Connections, PhD Dissertation, The University of Texas at Austin, TX

Rageh, A., et al. (2012). Eccentricity effect of flange bracing on the performance of box girders. IABSE 2012 Spring Conference on Global Thinking in Structural Engineering: Recent Achievements, May 7, 2012 - May 9, 2012, Sharm El Sheikh, Egypt, International Association for Bridge and Structural Engineering (IABSE).

Saint-Venant, B. (1843). "Memoire sur le calcul de la resistance et de la flexion des pieces solides a simple ou a double courbure, en prenant simultanement en consideration les divers efforts auxquels elles peuvent entre soumises dans touts les sens." Compts-Rendus, l'Acadenic des Sciences de Paris 27: 1020-1031.

Samaan, S. (2004). Dynamic and static analyses of continuous curved composite multiple-box girder bridges. Ann Arbor, University of Windsor (Canada). NQ92551: 454-454 p.

Samaras, V. A. (2009). Simplified Methods of Evaluating the Redundancy of Twin Trapezoidal Box Girder Bridges. Department of Civil Engineering, The University of Texas at Austin. Masters.

Seible, F. (1982). Nonlinear analysis and ultimate strength of multi-cell reinforced concrete box girder bridge. Dept. of Civil Engineering. California, University of California, Berkeley. Ph.D.

Sennah, K. and J. B. Kennedy (1998). "Shear distribution in simply-supported curved composite cellular bridges." Journal of Bridge Engineering 3(2): 47-55.

Sennah, K. and J. B. Kennedy (1999). "Simply supported curved cellular bridges: Simplified design method." Journal of Bridge Engineering 4(2): 85-94.

Sivaganesh Selvaraj and Mahendrakumar Madhavan (2018).Geometric Imperfection Measurements and Validations on Cold-Formed Steel Channels Using 3D Noncontact Laser Scanner. Journal of Structural Engineering 144(3).

Solelino, E. D. and Liu, J. (2004). Simplified Load Distribution Factor for Use in LRFD Design

Tito, J. (2013) Eccentric Compression Test of WT shape Steel Braces. 11th LACEEI Latin American and Caribbean Conference for Engineering and Technology (LACCEI' 2013). Cancun, Mexico.

Topkaya, C. (2002). Behavior of curved steel trapezoidal box girders during construction. Department of Civil Engineering. Austin, Texas, The University of Texas at Austin. Ph.D.

Tung, D. H. and R. S. Fountain (1970). "Approximate Torsional Analysis of Curved Box Girders by the M/R Method,." Engineering Journal, AISC 7(3): 65-74.

Turkstra, C. J. and A. R. Fam (1978). "Behaviour study of curved box bridges." Journal of Structural Division 104(ST3): 453-462.

TxDOT. (2015). Bridge Design Manual. Texas Department of Transportation.

Van Dalen, K. and S. Narasimham (1980). "ELASTIC BEHAVIOUR OF COMPOSITE BOX GIRDER BRIDGES." Canadian Journal of Civil Engineering 7(3): 492-501.

Veikos, N. Verifying Your Finite Element Analysis Results (2016). Http://www.engineering.com/DesignSoftware/DesignSoftwareArticles/ArticleID/11356/Verifying-Your-Finite-Element-Analysis-Results.aspx

Vlasov, V. Z. (1961). Thin-walled elastic beams. Jerusalem, Published for the National Science Foundation, Washington, D.C., by the Israel Program for Scientific Translations.

Wang, W., Battistini, A., Helwig, T., Engelhardt, M., and Frank, K. (2012). Cross Frame Stiffness Study by Using Full Size Laboratory Tests and Computer Models Proceedings, Annual Stability Conference, Structural Stability Research Council, Dallas, April 18-20, 2012.

William, K. J. (1969). Finite element analysis of cellular structures. Dept. of Civil Engineering. California, University of California, Berkeley. Ph.D.

William, K. J. and A. C. Scordelis (1972). "Cellular structures of arbitrary plan geometry." Journal of Structural Division 98(7): 1377-1394.

Wright, R. N., et al. (1968). "BEF analogy for analysis of box girders." Journal of Structural Engineering, ASCE 94(7).

Yabuki, T. and Y. Arizumi (1989). "Provision on intermediate diaphragm spacing in curved steel-plated box-bridge-girders." Doboku Gakkai Rombun-Hokokushu/Proceedings of the Japan Society of Civil Engineers(410 pt 1-12): 37-46.

Yen, B. T. and Y. S. Chen (1982). Strength of Rectangular Composite Box Girders: testing of large size composite box girders. Fritz Engineering Laboratory, Lehigh University.

Yen, B. T., et al. (1986). Composite Compression Bottom Flange For Steel Box Girders. Fritz Engineering Laboratory, Lehigh University: 1-178.

Yilmaz, C. (1975). "Ultimate strength of box girders by finite element method [Ph.D. Thesis]." 134P-134P.

Yonezawa, H., et al. (1978). "Test of a Curved Girder with Orthotropic Steel Plate Deck." Technology Reports of Kansai University 19: 115-125.

Yoo, C., et al. (2015). "Stresses due to distortion on horizontally curved tub-girders." Engineering Structures 87: 70-85.

Zhang, Y., et al. (2015). "Torsional behaviour of curved composite beams in construction stage and diaphragm effects." Journal of Constructional Steel Research 108: 1-10.

Appendix A. Literature Review

A.1 Previous Finite Element Analysis Studies

Up through the 1960s, computers were not yet properly developed to adequately analyze large structural systems. Though the finite element method is capable of analyzing a wide array of complex structural systems, the limited technology required engineers to put a lot of effort towards developing efficient finite element schemes to balance the economical computational cost and desired accuracy. Based on specific bridge geometry, loading demands, and applications, special elements with a certain number of degrees of freedom were chosen. However, near the end of the decade, more advanced FEA studies applicable to steel tub girders became more prevalent. These studies were thoroughly reviewed and are discussed below.

William (1969) developed a special element for straight and skewed steel box bridges analysis. William and Scordelis (1972) later analyzed cellular structures of constant depth with arbitrary geometry in plan using quadrilateral elements. Another study conducted by Chu and Pinjarkar (1971) evaluated curved box girder bridges by specifying horizontal sector plates for flanges and vertical cylindrical shell elements for webs. This approach considered both membrane and bending actions for the plate, as well as independent shell elements. However, this method can only be applied to simply supported bridges without intermediate diaphragms.

Fam and Turkstra (1975) developed a finite element scheme for static and free vibration analysis of steel box bridges with orthogonal boundaries and arbitrary combinations of straight and horizontally curved sections. For top and bottom flanges, four-node in-plane bending rectangular and annular elements with two radial boundaries were used. Meanwhile, rectangular and conical elements were used for inclined webs. The scheme was verified to reliably predict deflections and stresses for a variety of analytical and experimental tests. A follow-up study by Turkstra and Fam (1978) established the importance of warping and distortional stresses in single-box curved bridges with respect to longitudinal normal bending stresses.

Yilmaz (1975) studied the ultimate strength and load-deflection behavior of straight steel rectangular box girders under point loads with both simply supported and cantilevered boundary conditions. Two types of formulations were developed for both elastic and inelastic analysis. Load-deflection curves were well predicted and closely matched experimental data when geometric nonlinearity was very small. The estimated ultimate strength was higher than actual capacity, but this overestimation can be reduced using a finer mesh and small incremental load for the incremental tangent stiffness method. However, this FEA made assumptions to ignore plate shearing effect, out-of-plane bending and plate instability issues, all of which play very important roles in steel box girder behavior.

Numerous other publications in the 1970s also focused on the analysis of box girder bridges from which very useful outcomes were obtained, such as the distortional effects produced by curved geometries and sloped web. However, several proposed finite element approaches seemed to be impractical at that time since they required very fine mesh and unique element shapes valid only for specific application scenarios. Therefore, further study was needed to find a more general finite element scheme to do all-purpose structural analysis with the unified elements and reasonable computation time.

During the 1980s and early 1990s, a certain period of inactivity in the area of steel box girder research was observed. Most of the finite element models developed during this period of time were focused on reinforced or pre-stressed concrete box girders. Seible (1982) analyzed the nonlinear behavior and ultimate strength of multi-cell reinforced concrete box girders. Dezi (1985) studied the effect of parameters including external loads locations, span-to-radius ratio, width-to-depth of the cell, and number of cross diaphragms on the deformation of the cross section in curved single-cell box beams and compared the results with those of straight single-cell box beams.

Following that inactive period, the development of personal computers and the emerging of commercial finite element packages revitalized the research of steel tub girder analysis. Researchers began using more detailed finite element models to develop a fully clear understanding of steel tub girders with the goal of improving design efficiency and reliability.

Gilchrist, Yura et al. (1997) studied the elastic buckling behavior of straight rectangular and trapezoidal box girders under uniform moment using the finite element method and experimental tests. Throughout this study, two analytical models were used. First, a simplified model of half of a box girder with continuous torsional lateral restraint was created to find factors affecting the buckling behavior of steel box girders and to properly proportion laboratory test specimens. Second, a complete model of a box girder was analyzed in ABAQUS to verify the simplified half girder model and to study the difference between rectangular and trapezoidal cross-section shapes. Some conclusions obtained from the study are that the stiffness of the torsional bracing depends on the width and thickness of the bottom flange, and that the buckling strength of steel box girder is limited by web distortion. It was also observed that the trapezoidal section produced a buckling load lower than the rectangular section due to additional shearing effect in the sloped web.

Lopez (1999) modeled a three-span simply-supported curved twin girder system with an overlying concrete slab and support diaphragms in SAP 2000 to study thermal effects on girder stresses and deformations. The intention of the study was to compare measured thermally induced displacements and rotations with theoretical values. Four-node shell elements with specified thickness were used to model the girder cross-section. The study results showed that thermal deformations from the FEA are similar to the ones calculated by using a potential energy method.

Fan and Helwig (1999) developed three dimensional finite element models for both straight and curved steel tub girders with ANSYS, studying the girder behavior under various loading conditions. The steel box girder, bracing members, and concrete deck were modeled using shell, beam or truss and brick elements, respectively. The study also utilized a moderate mesh density with controlled aspect ratio. To reduce computational cost, the substructure method was implemented to simplify the twin-girder system into single girder models with lateral support. Some assumptions and considerations were made to simplify the analysis procedure such as the loading conditions at different construction sequences, composite action, and metal deck form effect. Based on these assumptions, the stresses and forces obtained from the FEA agreed well with data from field tests in terms of magnitude and distribution with some exception during certain construction stages. Additionally, the parametric studies also showed that design equations often underestimated bracing member forces. Based on these findings, the authors developed a new design equation for internal bracing member forces calculation.

Chen (2002) studied top lateral bracing systems for steel tub girders with a three-dimensional finite-element model built in ABAQUS, verifying his results with experimental measurements.

The metal deck form was included in this model by using an equivalent plate simulating the shearing stiffness. Analysis showed that the bracing force distribution was partially affected by the stiffness of external diaphragms connected to them. It also showed that the presence of deck forms resulted in significant decreases in measured top-lateral brace forces by contributing to the section's torsional stiffness. Finite-element analysis using the equivalent-plate approximation and the Steel Deck Institute (SDI) shear stiffness of the deck panels reasonably predicted the brace force response of the decked bridge.

Herman (2001) used the finite element method to study the behavior of stiffened compression flanges of steel tub girder systems. In order to do this, models of unstiffened plates with various size were developed. An appropriate level of mesh refinement was then selected for both eigenvalue buckling and load-displacement study. The buckling loads predicted by ABAQUS agreed well with solutions determined using recommendations from Timoshenko and Gere. When compared with AASHTO formulas, ABAQUS tended to overestimate the capacity. This discrepancy between the FEA and AASHTO results was discussed, and it was determined that the AASHTO formula contained an error.

Cheplak (2001) conducted a research study of intermediate external diaphragms by modeling a Z-type segment of a highway bridge and comparing linear analytical results with measured field data. The structural components were modeled with shell, beam and brick elements in a similar way as conducted by Fan and Helwig (1999) however the focus of this study was shifted to the behavior of the external diaphragm. It was found that the FEA overestimated the force distributed from one box girder to the other. The author explained that the discrepancy in the measured and predicted results might come from several sources, such as the connection detail between the diaphragm and each box girder, the full depth connection in the diaphragm and the girder, and the omitted metal deck form in this model.

Topkaya (2002) studied the early composite action of tub girders with overlying concrete slab by developing a specific finite element package UTrAp. This software package was developed to be easy to employ by users with limited FEA knowledge, and is capable of analyzing single or twin girder during the construction stage. The meshing was defined to be completed automatically within the program and the post processor was developed so that the user can interpret all necessary information in a very a straightforward and graphical way. Special load schemes were applied to simulate the construction sequence. In general, analytical predictions were found to be higher than field test results. Some effects not included during the modeling, such as super elevation, deck thickness profile, support movements, permanent deck forms and simplified support conditions, could have produced this. Sensitivity studies of these factors were also carried out in ABAQUS. Overall, the results from the program were acceptable when compared with results from ABAQUS.

Additionally, the stability of steel tub girder systems during the construction stage has been of particular concern. To understand and predict the buckling behavior of steel trapezoidal girders**,** Popp (2004) modified the original version of UTrAp to include buckling analysis capacity. The new version, UTrAp 2.0, was developed to perform a linear buckling analysis including geometric nonlinearities, but no material nonlinearities. Visualized deflections and rotations results were provided for user reference. The linearized buckling load from UTrAp was validated by the general finite element software ABAQUS.

Kim and Yoo (2008) studied the behavior of horizontally curved steel rectangular box girders under the combination of bending and torsional demands. The strength of these structural systems was examined by using detailed finite element models in ABAQUS. The models were loaded up to collapse through nonlinear incremental analyses considering the influence of residual stresses and initial imperfections. Based on parametric results, the authors proposed ultimate interaction expressions for bending-torsion and bending-shear-torsion.

Recently, Rageh, Salem et al. (2012) studied the effects of eccentric top lateral bracing systems in the behavior of trapezoidal tub girders under bending loading. Several finite element models with different eccentricities of the struts and diagonals with respect to the top flange were evaluated. It was concluded that, by moving the top lateral truss downwards, the forces produced in the bracing members decrease. This results in lower forces developing in the struts, as well as lower lateral bending stresses on the top flange.

Hovell (2007), Kim (2010), and Kim and Williamson (2014) used detailed finite element models to evaluate the redundancy of twin steel box-girder bridges. Material inelasticity was included in the models to represent cracking and crushing of concrete, as well as steel yielding. Shear stud connection failure mechanisms were also introduced into the model to capture deck haunch separation. This model was intended to simulate potential local and global failures of critical bridge components. The accuracy of the model was verified with experimental results obtained from a full-scale bridge fracture test. The results showed that typical twin steel box girder bridges have greater redundancy levels than the ones indicated in current AASHTO provisions and that stud connection failures could significantly affect the redundancy of steel box girder bridges.

A.2 Previous Experimental Studies on Steel Tub Girders

Numerous experimental projects to study the behavior of straight and horizontally curved steel box girders have been carried out during the last 50 years. In simple terms, box girders are longitudinal structural members that can be divided in two major categories: enclosed box girders, and tub or “trough” girders (Hall, Grubb et al. 1999). Enclosed box girder are structural members whose cross section is constituted by two webs connected by two flanges [Figure A1a], while tub girders are open steel box sections formed by a single bottom full-width flange plate connecting two webs with narrow top flanges braced by a top flange bracing system[Figure A1b]. Commonly, open steel box girders are accompanied with bracing systems (i.e. top lateral bracing and internal cross-frames) to guarantee torsional rigidity and avoid distortion of the cross-section. The top lateral bracing system is typically installed at the top flange level of the tub girder forming a quasi-closed box section with improved torsional stiffness, while internal diaphragms are included to control distortion of the cross-section. Due to work regulations established by the Occupational Safety and Health Administration (OSHA), building enclosed box girders started to be unattainable in the United States, which in turn promoted the use and study of tub girders (Linzell, Hall et al. 2004). Thus, the earliest studies investigated girders with enclosed box sections, while the most recent ones focused on the behavior of steel tub girders with top lateral and distortional bracing.

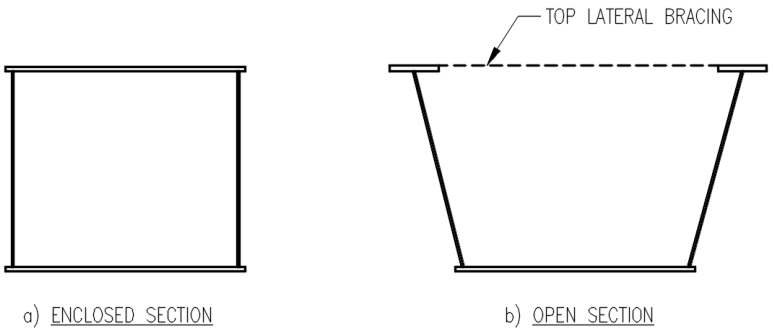

Figure A1 – Steel Box Girder Types

The experimental tests mentioned herein were conducted on both scaled and full-size specimens for composite and non-composite box girder systems. In general, different configurations of steel box girders have been experimentally studied until now. Box girder specimens with either vertical or inclined webs (rectangular or trapezoidal cross-section, respectively) haven been tested for both enclosed and open box girders. Simple, continuous, and overhanging span beams have been examined under different demands, such as pure bending, pure torsion, or combined bending and torsion. The experimental programs consisted of different types of tests, such as static, dynamic, elastic or up-to-collapse experiments. Experimental elastic studies of box girders have mainly been performed to compare and validate analytical solutions and computer software developed, while most ultimate capacity tests were used to assess or define design specifications. As opposed to elastic tests, up-to-collapse experiments are less common for both straight and horizontally curved box girder bridges. The following section describes the principal findings reported in previous experimental research projects.

Mattock and Johnston (1968) performed an experimental study to investigate the lateral distribution of live loads in straight composite box girders with the purpose of developing expressions to estimate life load lateral-distribution factors. As the second part of a comprehensive project, the experimental program consisted of building and testing two scaled simple span composite specimens with trapezoidal cross-section. The first of these specimens was a 1/4 scaled model of a 2-lane bridge spanning 80 ft. supported by three box girders, and the other a 1/5 scaled model of a 2-lane bridge spanning 100 ft. supported by two box-girders. Only rigid diaphragms were built on the supports while no stiffeners or internal diaphragms were included along the beam. Experimental results were used to validate computer software output based on folded plate theory, and to study the elastic behavior of box girder bridges with loads eccentrically applied. Expressions to calculate life-load distribution factors on interior and exterior girders were reported.

An extensive research program to study curved girders named CURT (Consortium of University Research Team) started in the 1960s and was completed by early 1970s under the sponsorship of the Federal Highway Administration (FHWA) (Hall, Grubb et al. 1999). The main objective of the program was to study the behavior and to develop simplified methodologies of analysis and design of horizontally curved girder bridges based on analytical and experimental studies. As part of the CURT project, Culver and Mozer (1970) and Culver and Mozer (1971) performed experimental tests on six small and two large scale horizontally curved box girder specimens at Carnegie Mellon University. The specimens tested consisted of simple span rectangular and trapezoidal (i.e. 1H: 3.8V and 1H: 4.5V web slope) enclosed box girders with transverse and longitudinal stiffeners. The small-scale specimens were built with thick plate internal diaphragms, while the two large

ones had K-frames as internal diaphragms. The experimental program consisted of testing elastically the six small and the two large specimens under eight and thirteen different static loading cases of bending and torsion, respectively. Only the large specimens were tested up to failure. Based on their findings, the ultimate strength of box girder sections was found to depend on: torsional shear stress, compression flange buckling resistance and cross-section distortion. Little post-buckling strength was observed in the response of the compression flanges. Close space between internal cross-frames contributed in reducing section distortion, vertical deflections and box rotations.

At Syracuse University, Brennan and Mandel (1979) conducted an experimental research project to study the elastic response of curved I and box girder bridges by testing scaled bridge models with multiple configurations. Within the project, two composite and two non-composite box girders extending over three spans without skewed end supports were statically tested under different loading cases to obtain stresses, moments, deflections and reactions of the girders. Through variation in the configuration of internal bracing and other bridge elements, different effects on the response of the models were observed such as the influence of internal bracing in the moment capacity and deflections of the girders. A three-dimensional analysis program developed at Syracuse University was verified with the experimental data obtained during the different cases studied in the project.

At the University of Maryland, College Park, Heins and Humphreys (1979) studied the interaction between bending and torsion of horizontally curved steel box girders as part of a comprehensive research project of "Curved Box and I-Girder Bridges". Through an experimental and analytical investigation, the authors proposed an interaction equation for a pseudo-ultimate strength design. Four rectangular box girder models with internal cross diaphragms and top lateral bracing were tested. Non-composite sections were tested under static combination of bending and torsion within the elastic range by applying concentric and eccentric loads at mid span. Finally, a concrete slab was cast on top of the models, which were tested until ultimate strength capacity to study the failure response of curved box girders.

Additionally, numerous experimental studies about the behavior of horizontally curved steel box girders were conducted at Lehigh University. McDonald and Chen (1976) performed an experimental and analytical research project to study the behavior of steel tub girders and to assess the stresses in top lateral bracing members under eccentric vertical loads. Two scaled straight open box sections with top lateral bracing (X-type truss) were tested in the elastic range. The tub girders with rectangular cross-section were tested as simple span beams with a cantilever span including plate diaphragms at the supports, mid span, and at the cantilever tip. Static tests were conducted in the elastic range to obtain beam deflections and bracing strains to compute stresses. The experimental results were used to compare analytical calculations. Subsequently, a multi-phase investigation ("Fatigue of Curved Steel Bridge Elements") to study the fatigue performance of horizontally curved steel bridges was conducted at Lehigh University. The project encompassed five tasks which included among others the analysis and design of full scale plate and box girder specimens (Daniels, Zettlemoyer et al. 1976), fatigue tests of the specimens (Daniels and Herbein 1977), and ultimate strength test of the experimental specimens (Daniels, Fisher et al. 1978). During this multi-phase project, three enclosed box girder specimens were designed and tested during the experimental phase. Each single-cell box girder with rectangular cross-section was built with differing interior diaphragms (i.e. X-type, V-type and plate diaphragms). A top lateral bracing

system (Warren-truss) was used to connect the two top flanges to avoid stability issues during their transportation; however, a thick steel plate replaced the top lateral truss before testing. The test setup used to impose concentric and eccentric vertical loads is presented in Figure A2a and Figure A2b, respectively. The fatigue capacity of different welded connections were experimentally tested by imposing dynamic cyclic loads on the specimens. After the fatigue tests, two out of the three specimens were repaired and a composite reinforced concrete slab was cast on top of each beam. Different shear stud and reinforcement arrangements were used for each specimen. The composite beams were tested to study the load-deflection behavior until ultimate strength capacity, and the experimental results were compared with analytical results obtained in available software.

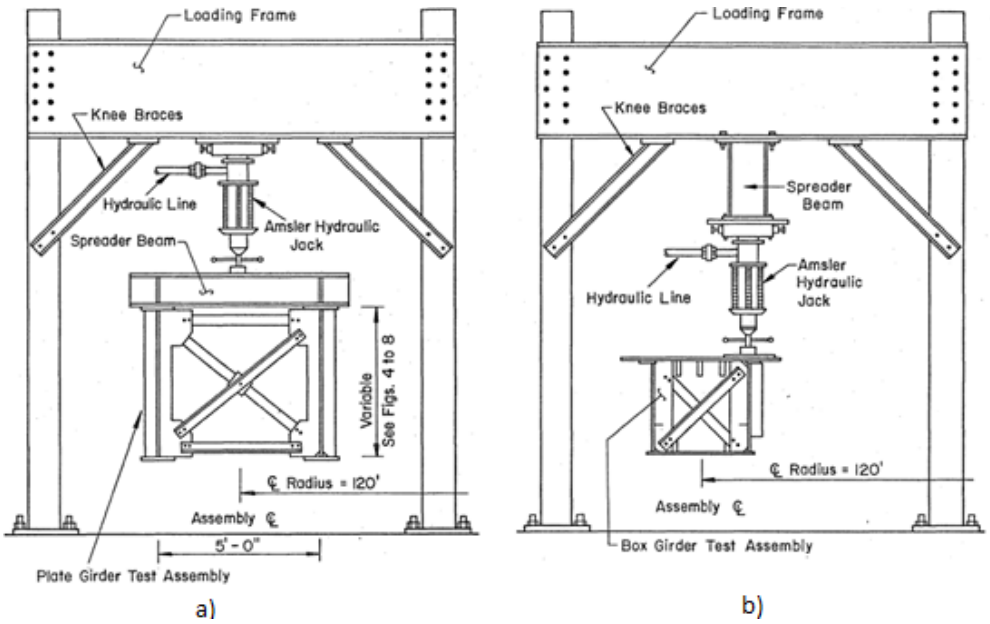

Figure A2 – Test Assemblies, Concentric & Eccentric Loading (Daniels, Zettlemoyer et al. 1976)

In an ensuing study, Yen and Chen (1982) tested two relatively large straight composite box girders up to failure under combined bending and torsion. Initially, the experimental program consisted of testing two simply supported non-composite open box steel girders with an overhang span with and without top lateral bracing system (X-type truss) under elastic static loads. Subsequently, after casting a reinforced concrete slab on top of each beam, the girders were tested under positive and negative bending, both of them combined with torsional demands, up to collapse. The two non-composite steel girders with rectangular cross-section contained internal plate diaphragms in addition to transverse and longitudinal stiffeners along the length. The results obtained in this study contributed as an experimental basis to develop methodologies for evaluating the ultimate strength of composite box girders. Following these findings, Daniels (1985) carried out an experimental study to obtain the elastic and ultimate strength load-deflection response of one of the beams used for fatigue tests during the "Fatigue of Curved Steel Bridge Elements" project (Daniels and Herbein 1977). The box girder was retrofitted so that cracks produced during the fatigue tests would not affect the ultimate strength of the girder. Before casting the concrete slab, elastic tests were carried out on the retrofitted girder for both cases, the open box girder (without top lateral bracing) and the box girder with metal bridge forms serving as lateral bracing. The girder was subjected to elastic static loading on one of the webs in order to simulate bending and torsional demands. After concluding the elastic tests, a concrete slab was cast and the composite girder was

tested up to ultimate load. The composite girder presented unpredicted premature failure between the slab and the steel girder what invalidated the results. Yen, Huang et al. (1986) carried out an experimental study of the behavior of continuous box girders with composite compression in the bottom flange. The experimental program consisted of testing five full-scale enclosed box girders with rectangular cross-section under pure bending and pure torsion. The continuous box girder included transverse and longitudinal stiffeners, K-frames as internal diaphragms, and a layer of plain concrete in the regions of negative moment between diaphragms. At the conclusion of the study, design guidelines to guarantee the full yield strength of the steel plate and full composite action when using composite compression flanges in negative moment regions were shown.

A substantial amount of experimental research related to the behavior of enclosed box girders was developed in the United Kingdom as well during the 1970s and 1980s. In London, Dowling, Chatterjee et al. (1973) and Dowling, Moolani et al. (1977) performed experimental tests on ten large scale box girder models to study the behavior up to failure of multi-stiffened box girders subjected to pure bending and combined bending and shear. Similarly, Manko (1984) conducted an experimental study to investigate the ultimate load capacity of straight box girders subjected to four different loading conditions. The experimental study consisted of monitoring the stability of twelve enclosed steel box girder models built with varying configurations and number of stiffeners along the beams. The results served to conclude that the ultimate load capacity of these structural members depends on both the stiffness and type of loading applied (Davidson, Abdalla et al. 2004).

Similarly, Japan has contributed with meaningful experimental studies about the behavior of horizontally curved box girders. Yonezawa, Mikami et al. (1978) and Dogaki, Mikami et al. (1979) performed experimental tests on curved enclosed box girders under pure bending demands. The small-scale specimens with an enclosed rectangular cross-section reinforced with longitudinal and transverse stiffeners were tested under two concentrated loads. The elastic behavior and ultimate load capacity of the box girders produced by inelastic buckling of the top flanges were registered and compared against theoretical results at the experiment's conclusion. Mikami, Morisawa et al. (1987) studied the behavior of straight open box girders without top lateral bracing under pure bending loading. The experimental program consisted of testing three small steel box girders with rectangular cross section reinforced with longitudinal stiffeners. The bending behavior of the girder components after local buckling was monitored until failure. The experimental results displayed the abrupt failure of the girders after local buckling of one element. Afterwards, Yabuki and Arizumi (1989) tested two simple span steel models of horizontally curved enclosed box girders (with a rectangular cross-section) as part of a comprehensive research project to suggest design provisions related to internal diaphragm spacing on such girders. Plate diaphragms were constructed on each girder with different spacing in addition to rigid diaphragms at the ends. The test setup employed to conduct the experimental study is presented in Figure A3. Upon completion of the experimental setup, the steel models were subjected to static loading at midspan in order to obtain bending and distortional stresses produced in the cross-section in the elastic range. The experimental results of bending and torsional warping stresses were then compared with the thin-walled beam theory developed by Vlasov (1961), while the distortional warping stresses were checked with analytical values calculated with the BEF theory (Wright, Abdel-Samed et al. 1968). In later studies, Nakai, Murayama et al. (1990) and Nakai, Kitada et al. (1992) performed experiments to understand the behavior of thin-walled curved box girders up to failure with and without longitudinal stiffeners. The experimental project consisted on testing four trapezoidal enclosed box-girders. The first two girders were subjected to pure bending and pure torsion,

respectively, while the other two girders were tested under combined bending and torsion. Based on experimental results, an interaction equation was developed to approximately calculate the ultimate bending and torsional moment capacity of this type of structural member. Immediately after, Mikami and Niwa (1993) conducted an experimental study to investigate the behavior and strength at ultimate load of steel box girders with unsymmetrical cross-sections subjected to different loading demands. The experimental program consisted of testing two open steel box girders subjected to pure bending and combined bending and shear, respectively. In addition, an enclosed steel box girder with rectangular cross-section was tested under combined bending, shear and torsional demands. The post-buckling response of the girders until failure was observed and recorded, where it was apparent that the bottom flanges endured local buckling of the plate due to the compressive forces in the negative moment regions.

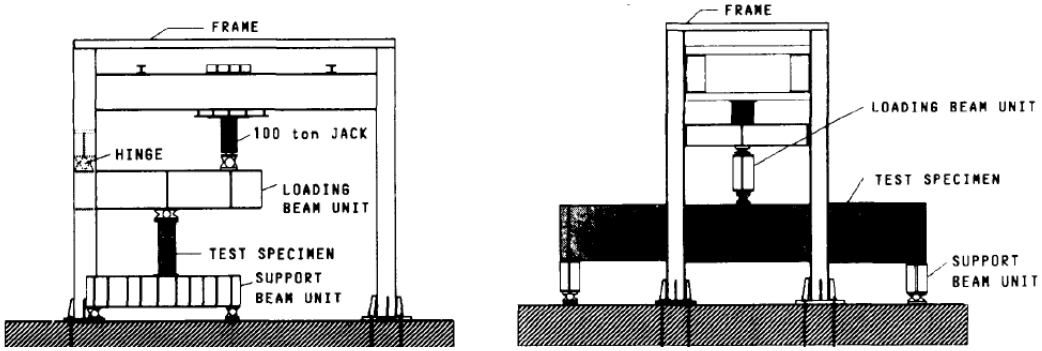

Figure A3 – Test Setup (Yabuki and Arizumi 1989)

Additionally, some experimental research associated with the study of curved and straight steel box girders has been reported in Canada since 1980. Van Dalen and Narasimham (1980) conducted an experimental and analytical study to examine the elastic behavior of composite box girders for bridges. The experimental component of the project consisted of five small-scale models of composite steel-concrete box girders. These models were then tested by applying 16 equal point loads to simulate distributed loading demands. Four out of the five specimens were enclosed steel box girders while the last specimen was an open steel box girder, all of which were connected by shear studs to a reinforced concrete slab on top of the girders. The experimental results obtained were compared with theoretical results obtained by folded plate analysis. In a separate study, Branco and Green (1985) investigated the effect of transverse stiffeners, distortional bracing, and top lateral bracing on the behavior of open box bridge girders during construction. A 1/4 scale model of a simple span open box girder with inclined webs (such as for a trapezoidal cross-section) was tested by applying concentric and eccentric distributed loads along the top flanges. Static tests in the elastic range were performed on the beam with different types of bracing systems. The resulting data values were later used to check the outcome of an analytical study based on finite strip method and torsional-bending analysis. Through this study, the importance of internal diaphragms and top chord bracing in the stability of open box sections was highlighted. Korol, Thimmhardy et al. (1988) conducted an experimental investigation to examine the influence of plate imperfections on the strength of steel box girders. A large-scale simple span box girder with two overhanging spans and a varying level of imperfections produced by welding processes was used for the tests. The rectangular open box girder was built with internal cross-frames (i.e. K-frame bracing) along the girder, and transverse and longitudinal stiffeners along the full-width

bottom flange. Testing of the beam was accomplished by applying static punctual loads on the cantilever beam tips until failure. Comparison of the experimental results with values obtained from an analytical model suggested that member imperfections could greatly affect load strength capacity of open box girder systems. At another time, Sennah and Kennedy (1998) and Sennah and Kennedy (1999) studied the distribution of forces produced by live and dead loads on composite curved box girder bridges through analytical and experimental methods. Four 1/12 scale curved simple span composite box girders were tested in the elastic range by imposing load through a system replicating truck loads. Thick plates were implemented as rigid diaphragms on the supports and evenly spaced internal cross-frames were built radially inside three of the specimens. During the elastic tests, loads were concentrically and eccentrically applied with respect to the box webs. Free vibration tests were then conducted on the girders, proceeded by static loads imposed over the beam until collapse. Based on experimental results and parametric analyses, Sennah and Kennedy (1998) suggested empirical expressions to estimate shear distribution factors for straight and horizontally curved bridges under live and dead loads. Sennah and Kennedy (1999) also proposed empirical equations to calculate moment and deflection distribution factors, as well as an expression to estimate the maximum axial forces on the bracing members of simply supported composite box girders. In the mid-2000s, Samaan (2004) performed an experimental and analytical study of the static and dynamic response in the elastic range of continuous curve box girders for bridges. This was accomplished by conducting static and dynamic tests on two 1/8 scale composite box girder models in the laboratory. The first specimen was straight while the second was horizontally curved with a span-to-radius of curvature ratio equal to one, both of which included internal cross bracing equally distributed along the beams. The results of this experiment were then applied in order to validate finite element models used for the parametric study of load distribution factors of continuous composite box girders.

Representative experimental studies were carried out at The University of Texas at Austin during the end of the 1990s and early 2000s. Gilchrist, Yura et al. (1997) conducted an analytical and experimental study to investigate the buckling behavior of unstiffened and transversely stiffened open box girders with internal diaphragms. The final purpose of this experiment was to develop a procedure to design lateral bracing of open box girders. The experimental phase consisted of laboratory tests of two simple span 1/4 scale open box girder models with two overhang spans designed to buckle elastically when unbraced. The two models, one with rectangular and the other with trapezoidal cross-section, were tested with a variety of bracing layouts under static uniform moment loading. Upon completion of the investigation, the authors concluded that the buckling capacity of the open box girder is highly depend on the distortion of the webs. Thereafter, Chen, Yura et al. (1999) performed a research project to study the bending, torsional and buckling behavior of open box girders with top flange lateral bracing (tub-girders). The experimental program consisted of testing two tub-girders with rectangular and trapezoidal cross-sections built with an X-type truss and metal deck panels as the top lateral bracing system, respectively. Multiple elastic bending and torsional tests were performed considering different top lateral bracing configurations. The authors emphasized that top-flange lateral bracing is important to increase the buckling capacity of tub-girders and that appropriate detailing in the connections is required to guarantee stability. Additionally, the torsional benefits and limitations of using permanent metal deck forms as lateral bracing were discussed. Chen, Yura et al. (2005) proposed guidelines for designing top lateral bracing systems on steel box bridge girders based on laboratory tests and field experiments. The experimental program consisted of a full-scale trapezoidal box girder with multiple configurations of top chord lateral bracing (i.e. Pratt-type truss) and stay-in-place metal

decking forms elastically tested under pure tension and pure torsion. The loading system used to conduct the experimental study is illustrated in Figure A4. A simple span box girder with an overhang span and plate diaphragms at the supports was used as a test specimen. According to the study, by increasing the bracing member size or brace inclination, the forces within the brace will increase as well. Furthermore, even though the metal deck forms performed well to increase the torsional stiffness of the open box girder, its use as a stand-alone bracing system is not recommended due to its insufficient shear strength. In 2006, a full-size twin trapezoidal box girder bridge was constructed at the Ferguson Structural Engineering Laboratory at the University of Texas in order to collect important amounts of experimental data in different research topics. The twin steel box girders used in this study were removed from the I-10 highway in Houston and repaired for their usage in the experimental study (Barnard 2006). Barnard (2006) studied the behavior of the aforementioned bridge during the construction phase and under different configurations of live loads. Different bridge components were monitored by observed measurements and strain gage data gathered during the two loading phases. Exploring a similar topic, Espinoza (2007) investigated the effect of plate imperfections (i.e. out-of-flatness of plates) on the behavior during construction and live load testing. As part of the same project, Samaras (2009) conducted a series of experimental tests to examine the structural response of the composite twin box bridge in the event of failure of a fracture critical member (i.e. tension flange fracture). The experimental study consisted of gathering data related to the structural redundancy of the bridge by fracturing the tension flange of one of the girders using a shape charge. Several paths to redistribute the loads were discovered after a full-depth fracture occurred in one of the girders. As a result, a high level of redundancy was observed due to the capacity of the fractured bridge to sustain high loads.

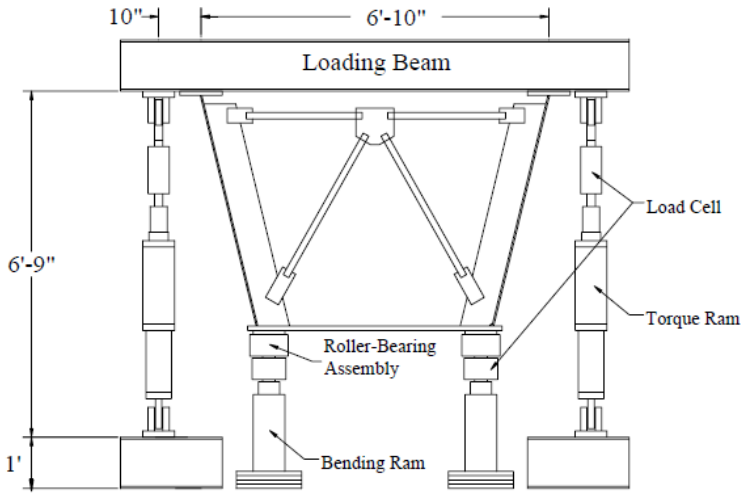

Figure A4 – Schematic of Loading System (Chen, Yura et al. 2005)

In a recent endeavor, (Choi, Park et al. 2008) performed an experimental and analytical study to investigate the ultimate strength in the bending of steel tub girders with top lateral bracing. Three 1/2 scale tub girder models were tested under uniform bending loading with a variety of top lateral truss configurations (i.e. Warren-type truss). The objective of this study was to examine the inelastic buckling behavior of non-composite tub girders, to evaluate the ultimate bending capacity during positive bending, and to confirm that top lateral bracing points define the unbraced length of tub girder top flanges.

Appendix B. Initial Imperfection Measurement

The load-bearing capacity of steel bridge girder is highly sensitive to initial imperfection. Both global imperfection and local out-of-flatness of the plate were measured in the experimental study. This appendix documents the measured imperfection data. Section B.1 presents the global imperfection on the three test specimens. Section B.2 presents the local imperfection measured on flange-offset and lower-slope specimen.

B.1 Global Imperfection Results

B.1.1 Baseline Specimen

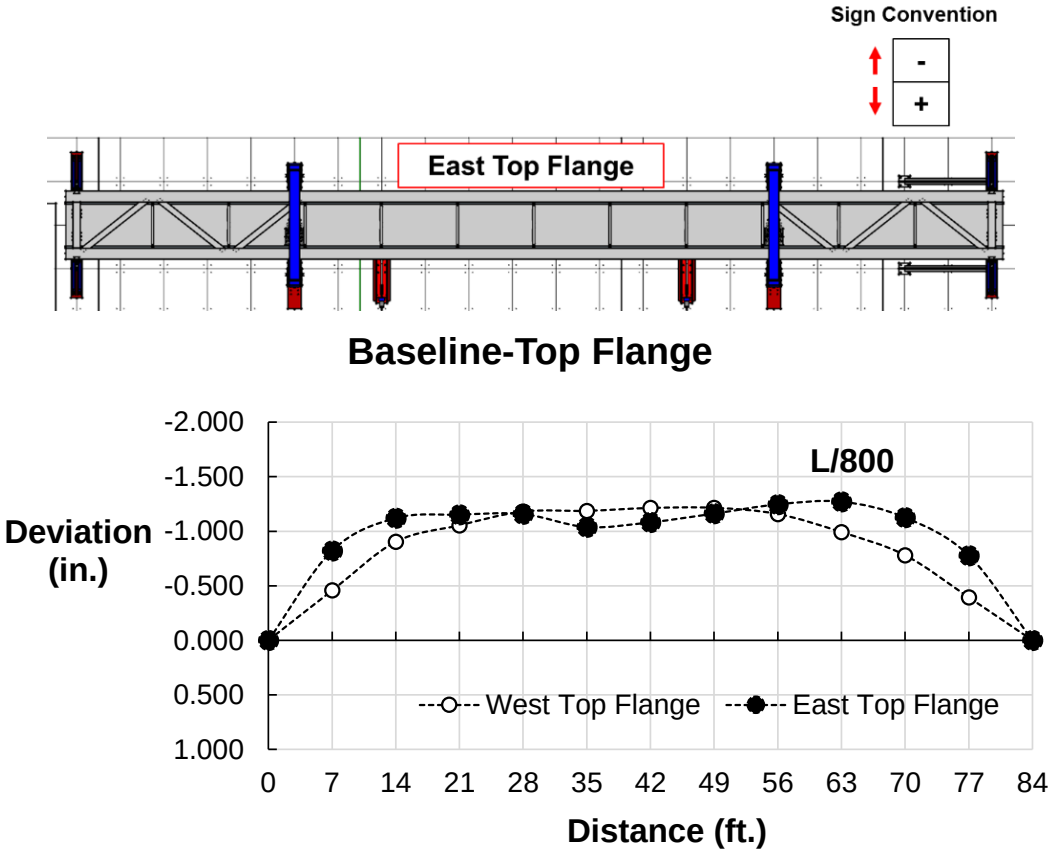

Figure B-1 – Global Imperfection of Top Flanges in Baseline Specimen

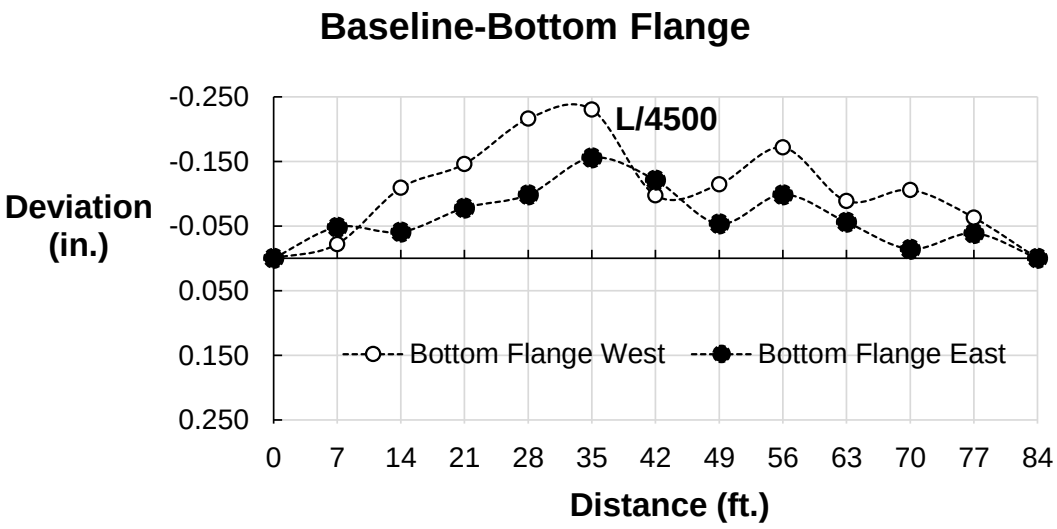

Figure B-2 – Global Imperfection of Bottom Flanges in Baseline Specimen

B.1.2 Flange Offset Specimen Before Local Flange Buckling

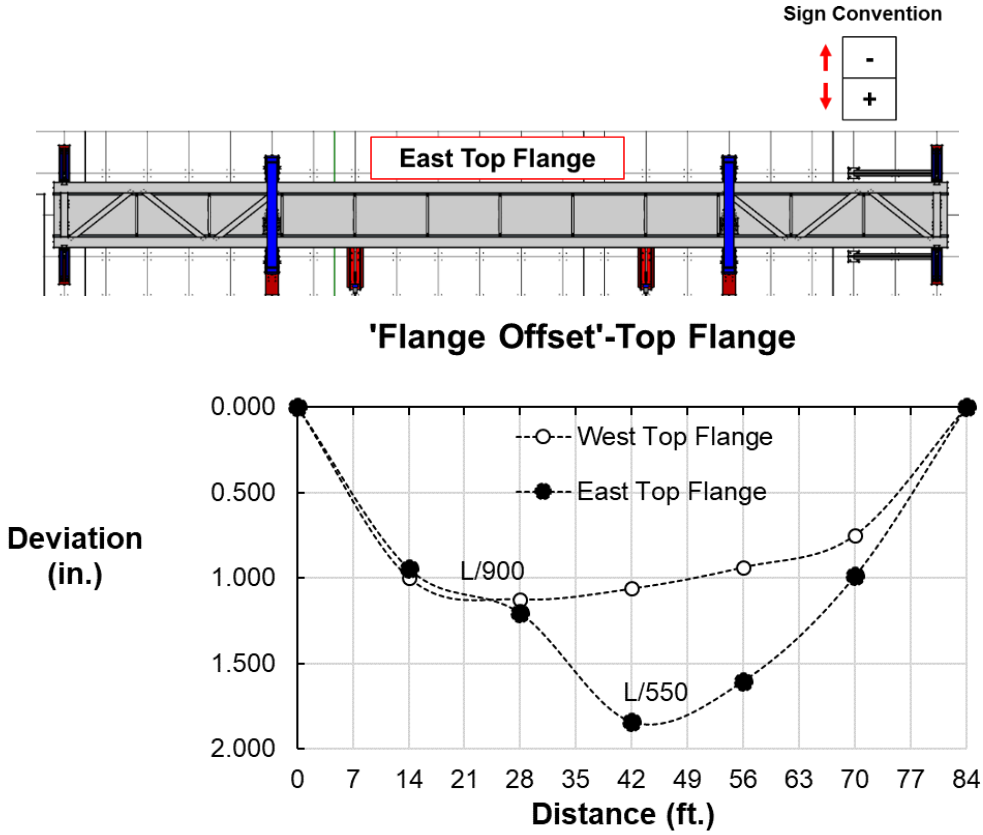

Figure B-3 – Global Imperfection of Top Flanges in Flange-offset Specimen

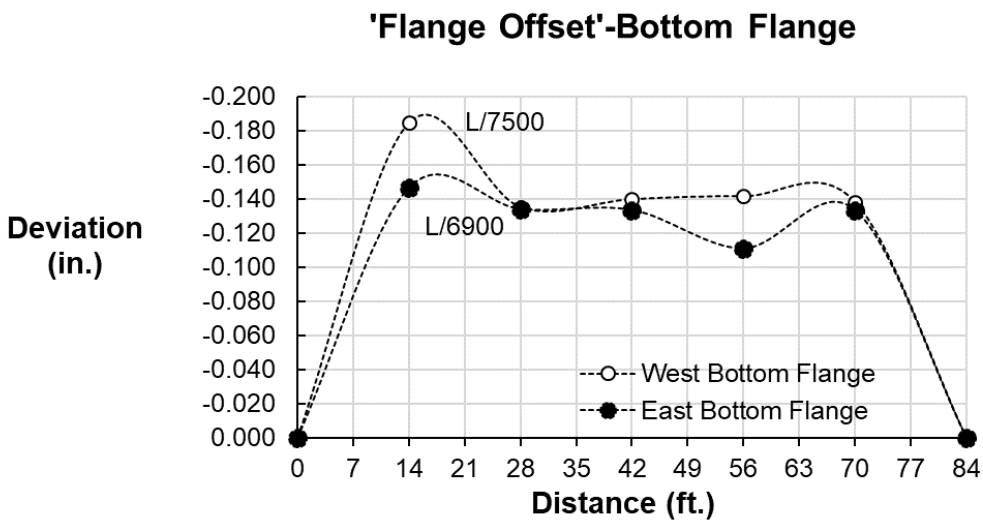

Figure B-4 – Global Imperfection of Bottom Flanges in Flange-offset Specimen

B.1.3 Flange Offset Specimen after Rehabilitation of Local Buckled flange

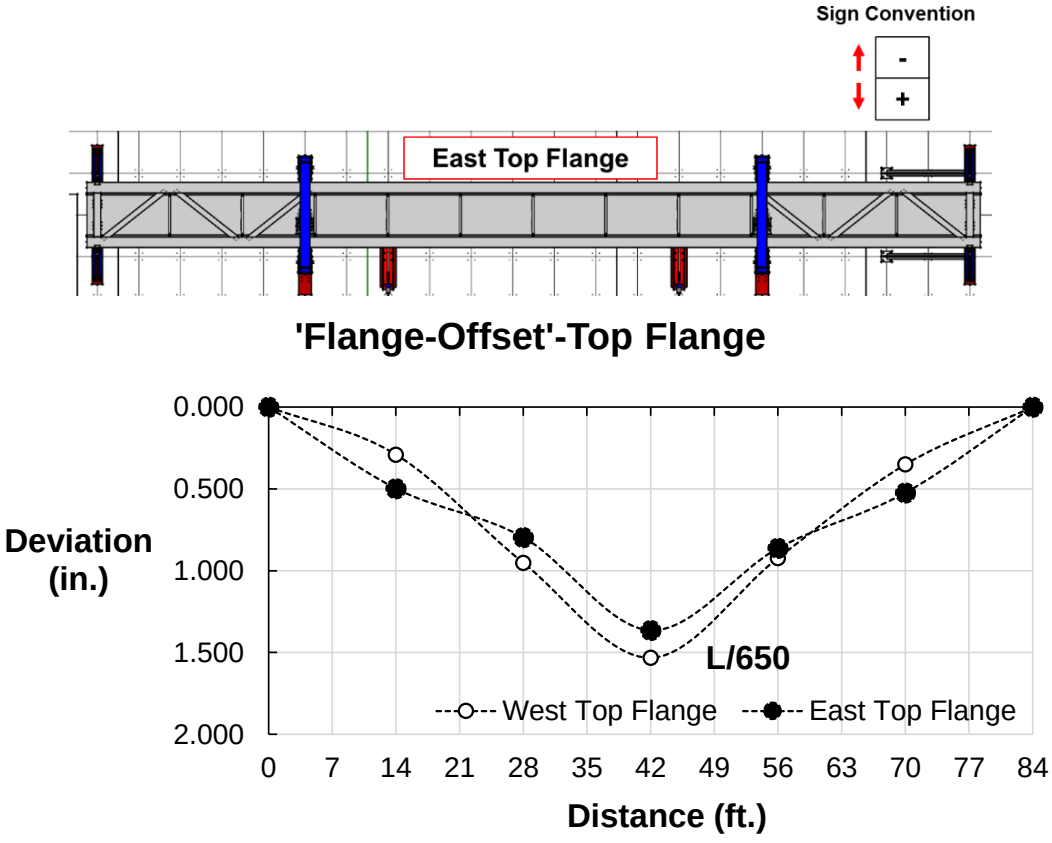

Figure B-5 – Global Imperfection of Top Flanges in Flange-offset Specimen

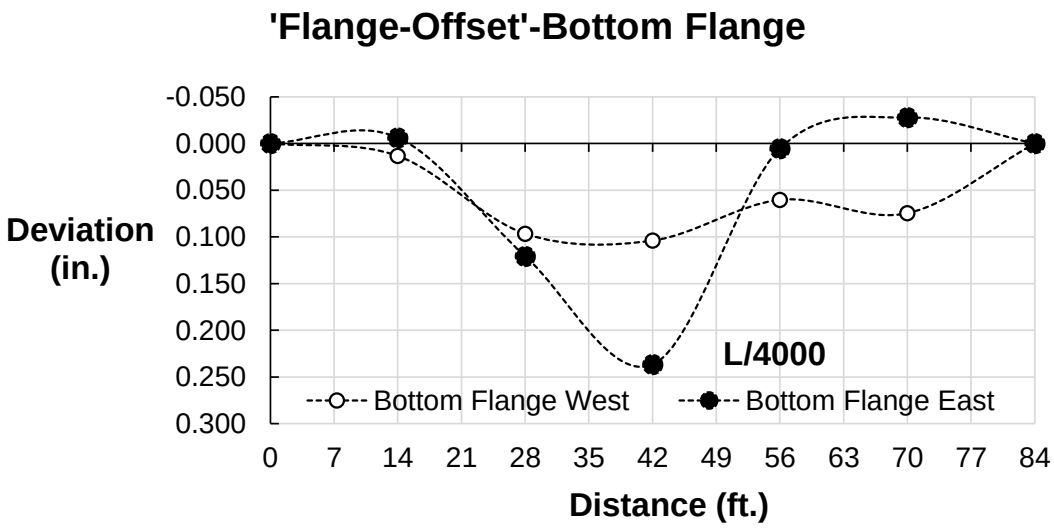

Figure B-6 – Global Imperfection of Bottom Flanges in Flange-offset Specimen

B.1.4 Flatter Slope Specimen

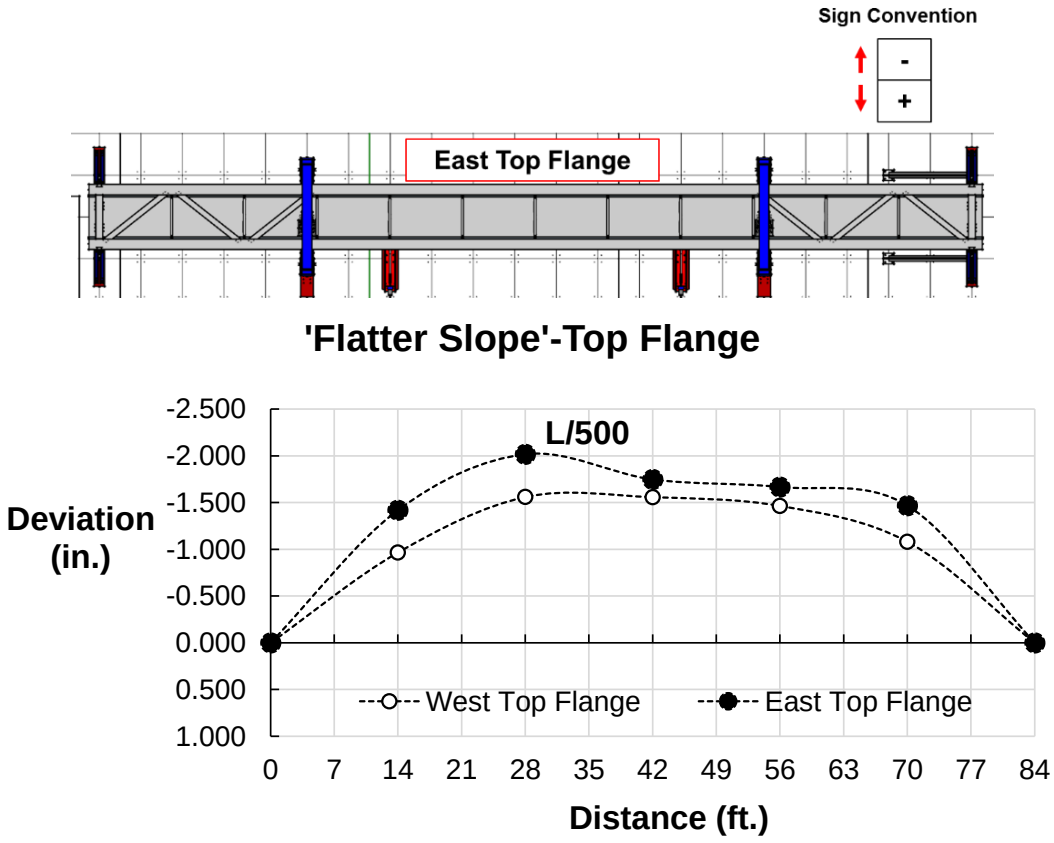

Figure B-7 – Global Imperfection of Top Flanges in Flatter Slope Specimen

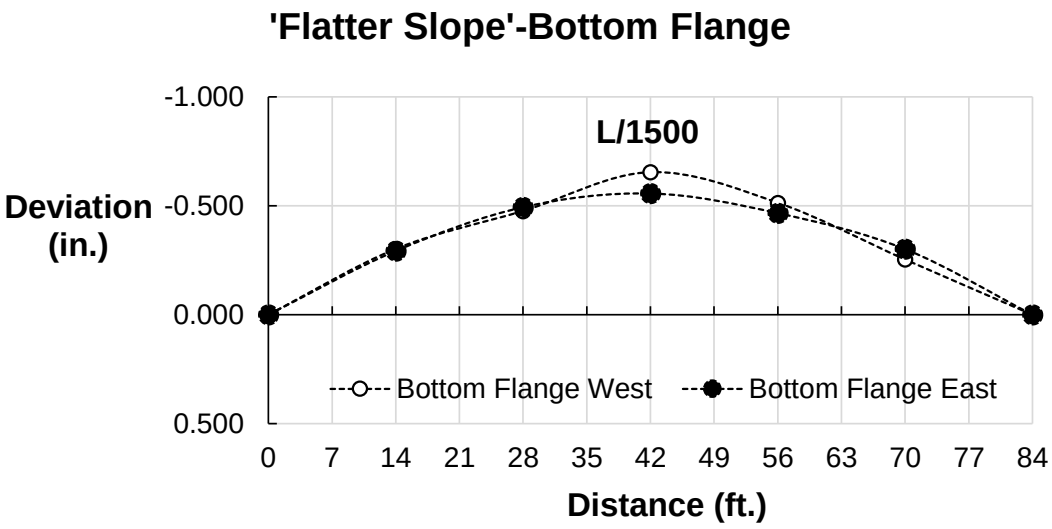

Figure B-8 – Global Imperfection of Bottom Flanges in Flatter Slope Specimen

B.2 Local Out-of-Flatness of Top Flanges

B.2.1 Top Flanges of Flange Offset after Rehabilitation of Local Buckled Flange

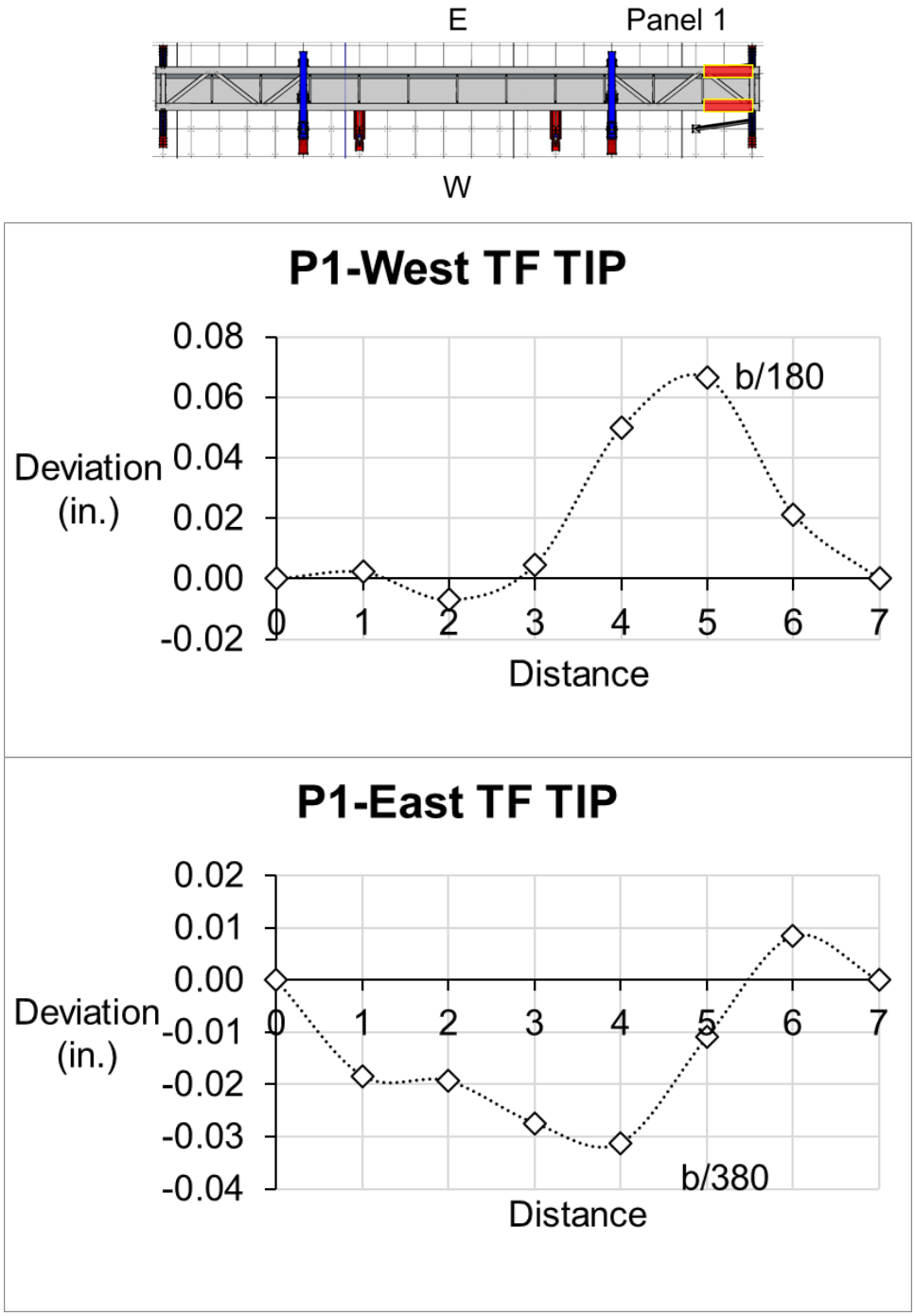

Figure B-9 – Local Out-of-Flatness of Flange Tip in Flange Offset Specimen (Panel 1)

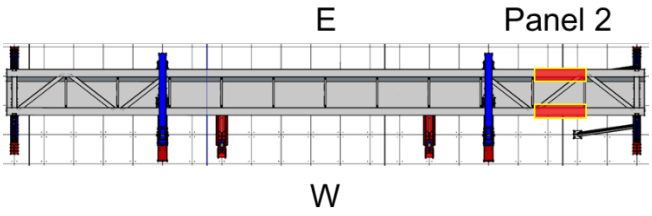

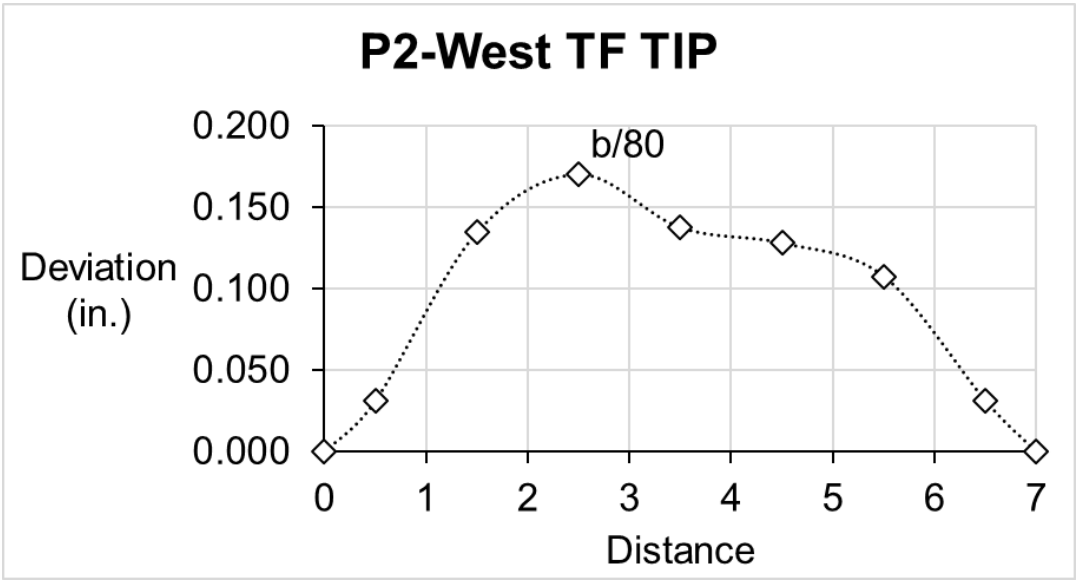

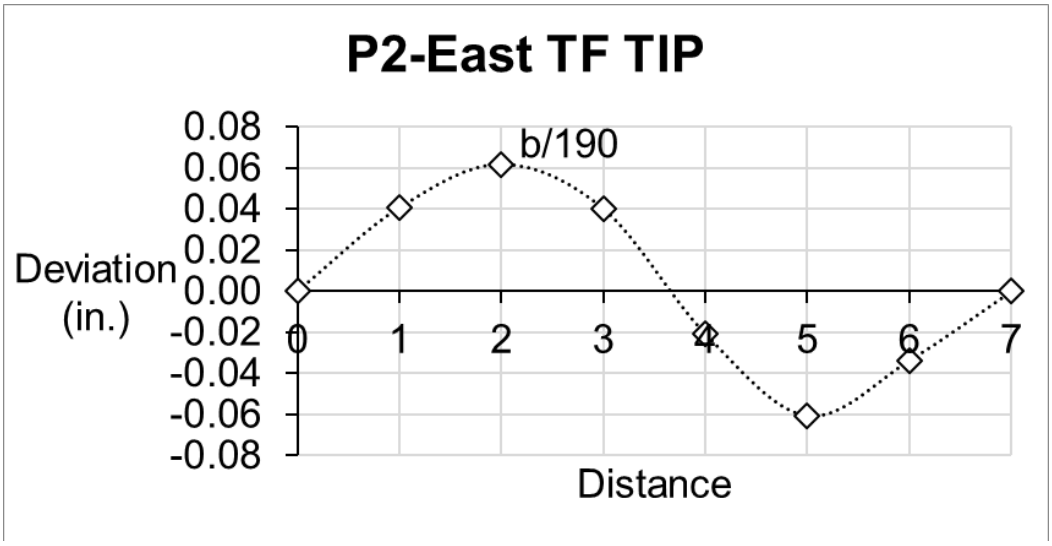

Figure B-10 – Local Out-of-Flatness of Flange Tip in Flange Offset Specimen (Panel 2)

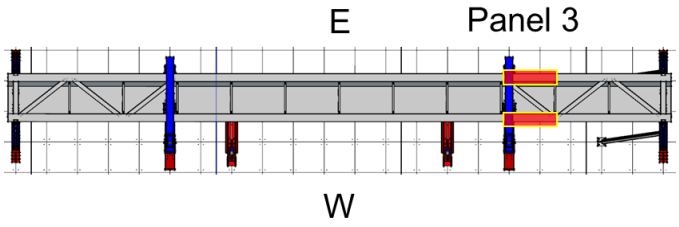

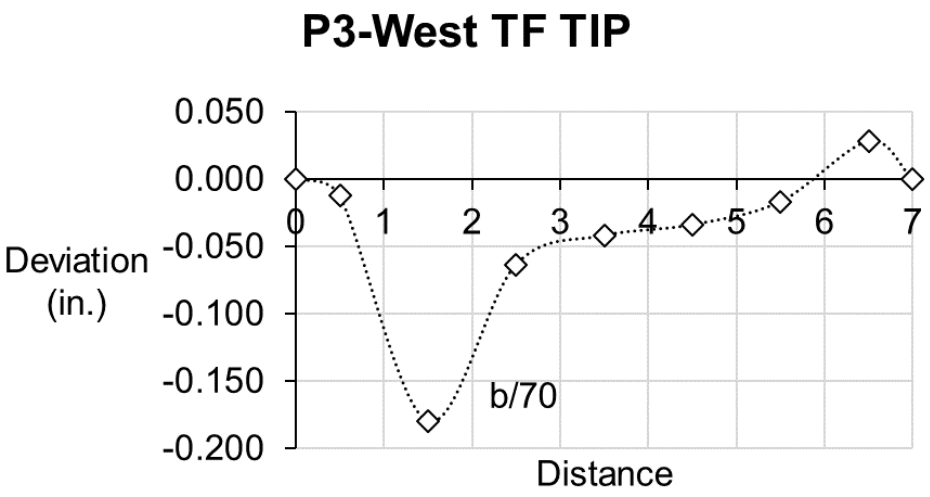

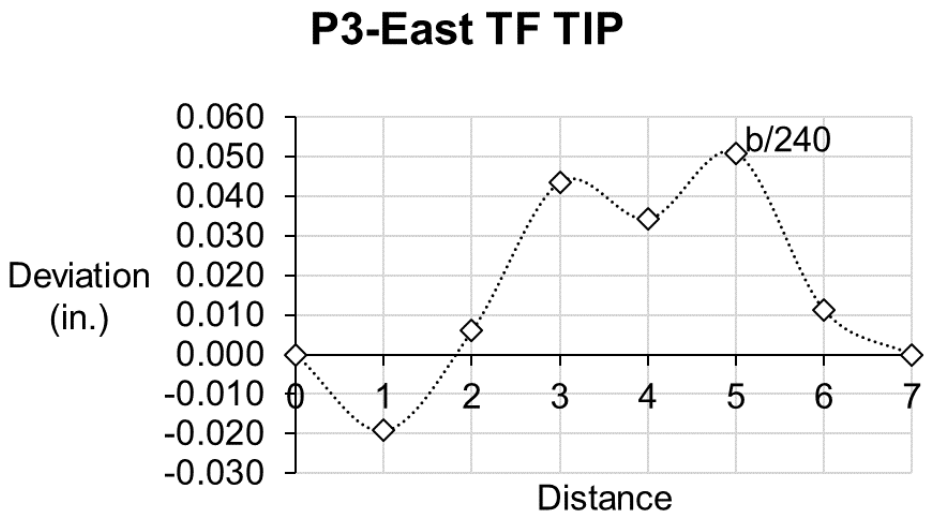

Figure B-11 – Local Out-of-Flatness of Flange Tip in Flange Offset Specimen (Panel 3)

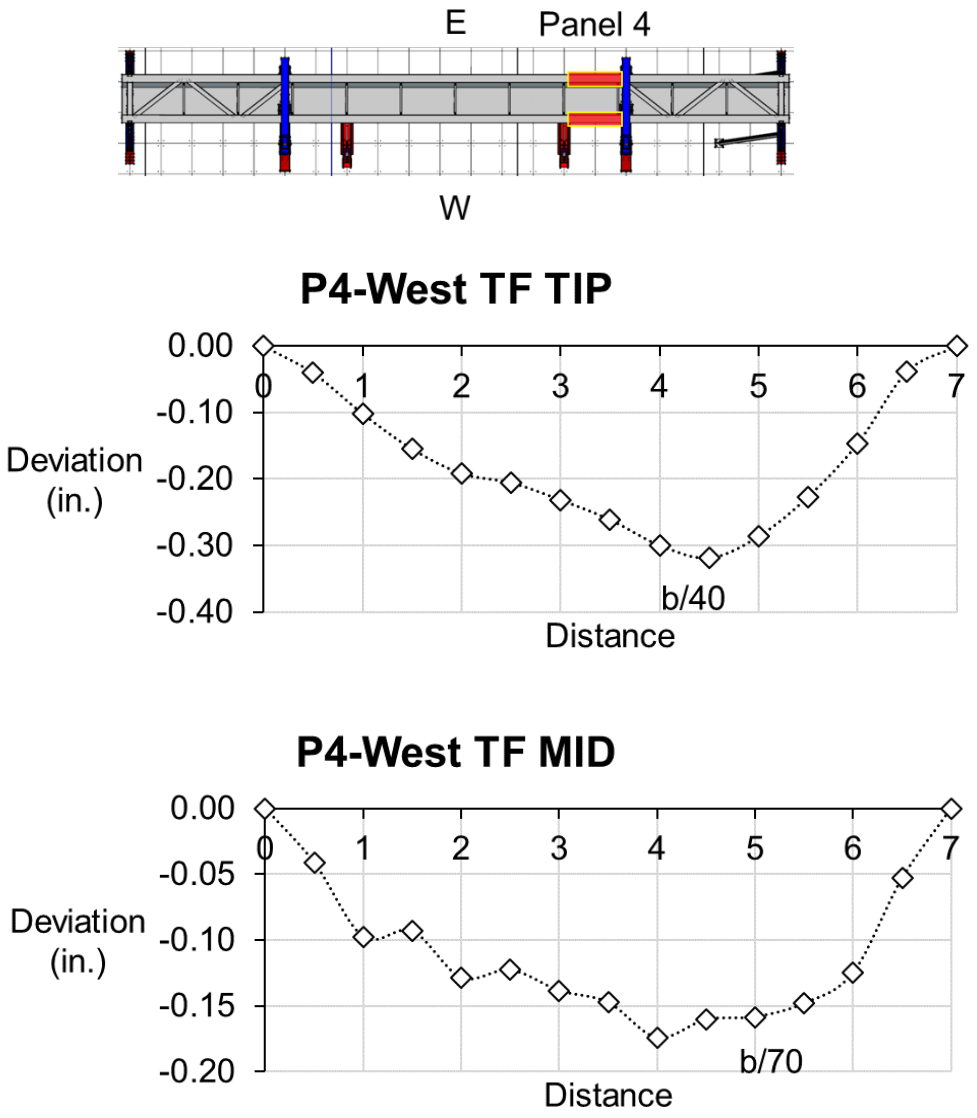

Figure B-12 – Local Out-of-Flatness of Flange Tip in Flange Offset Specimen (Panel 4)

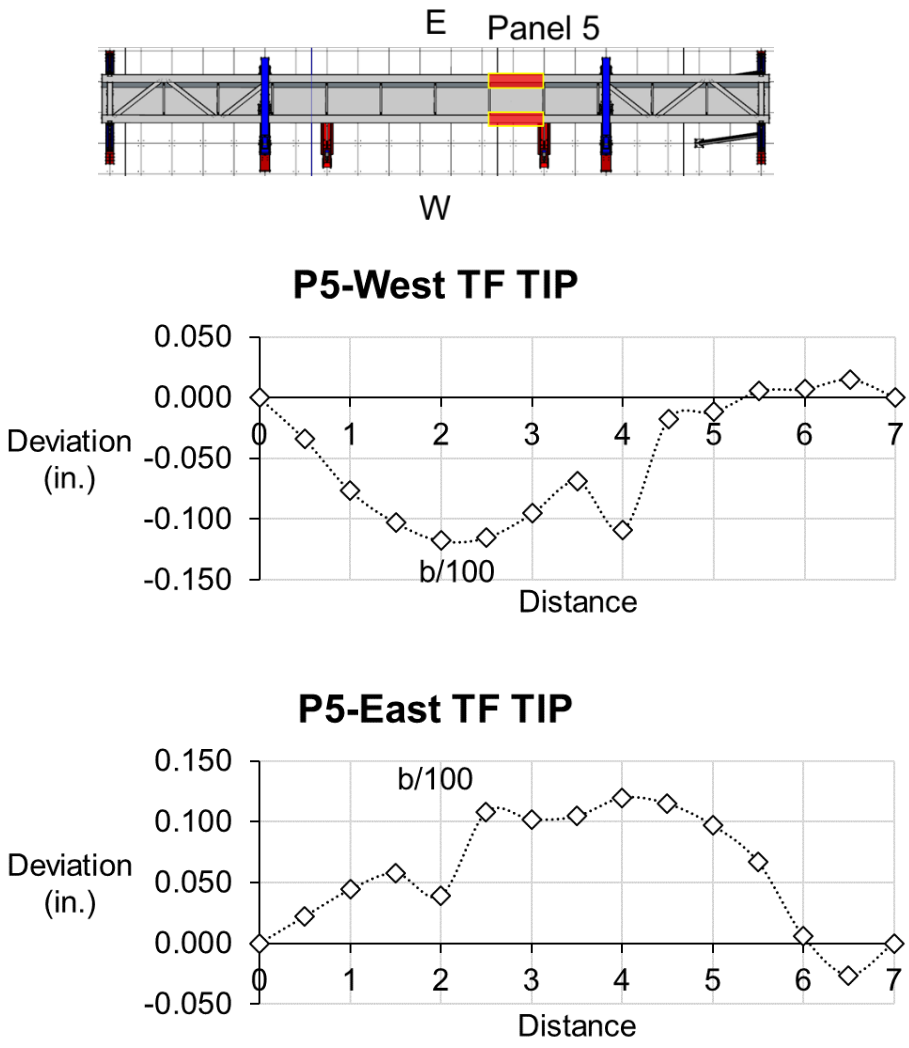

Figure B-13 – Local Out-of-Flatness of Flange Tip in Flange Offset Specimen (Panel 5)

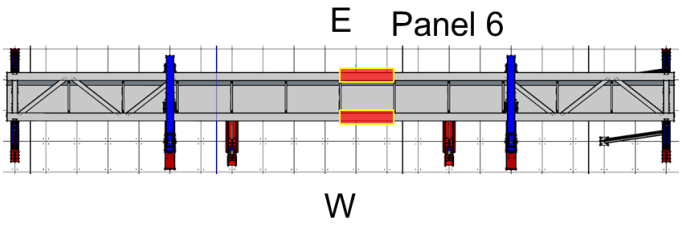

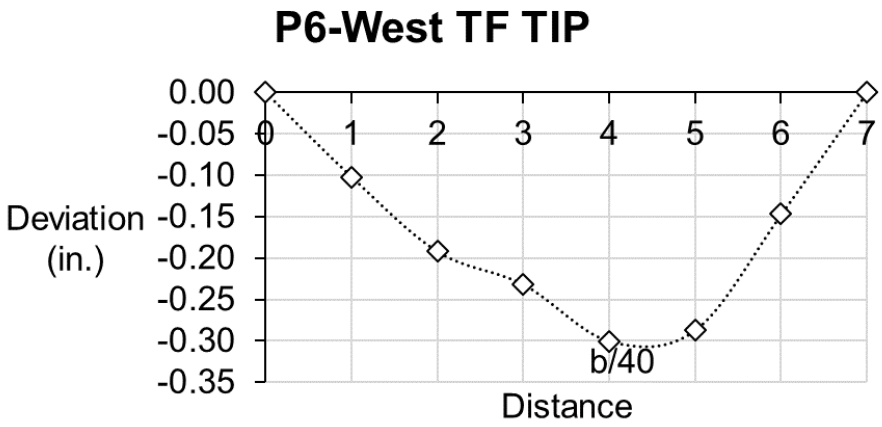

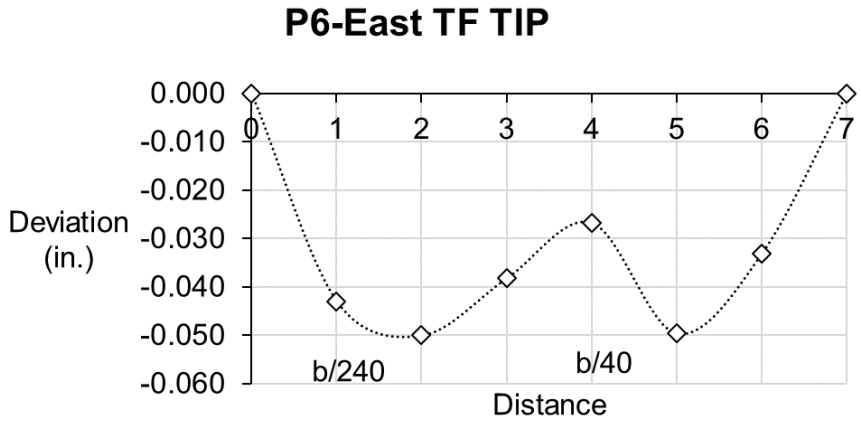

Figure B-14 – Local Out-of-Flatness of Flange Tip in Flange Offset Specimen (Panel 6)

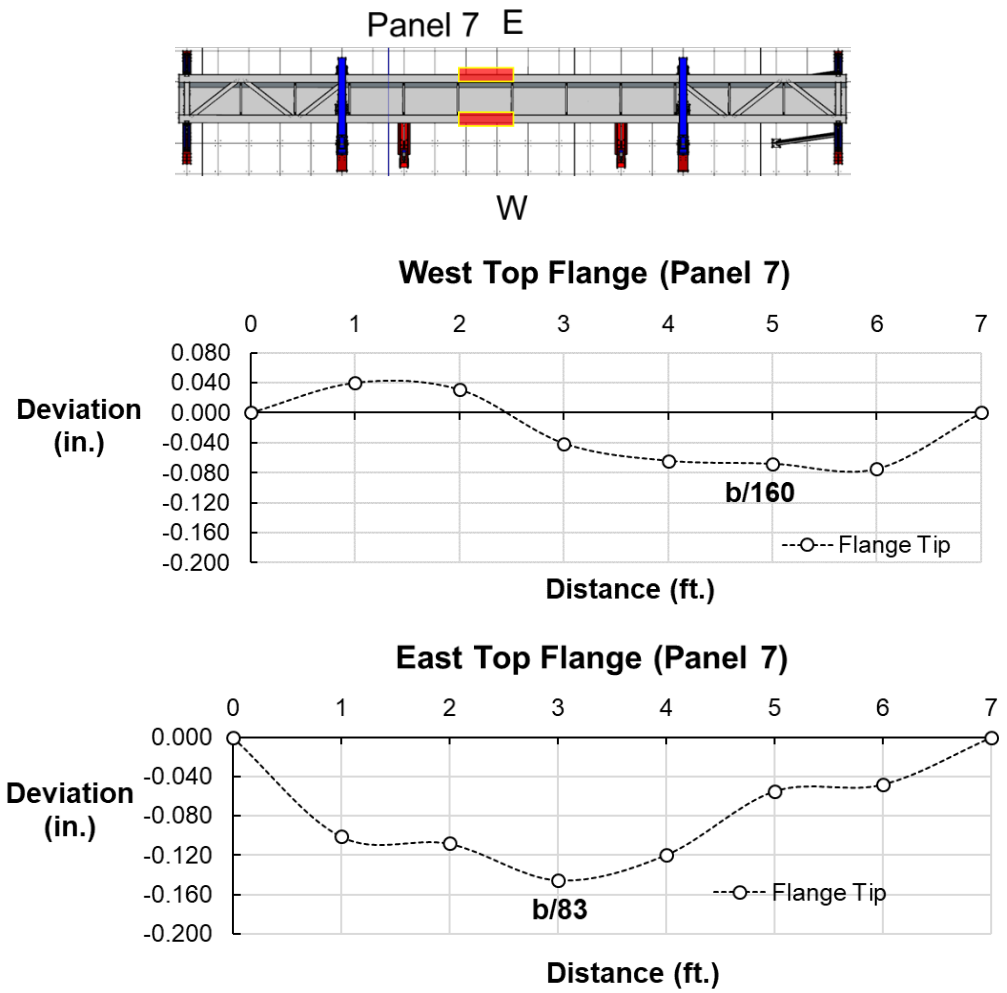

Figure B-15 – Local Out-of-Flatness of Flange Tip in Flange Offset Specimen (Panel 7)

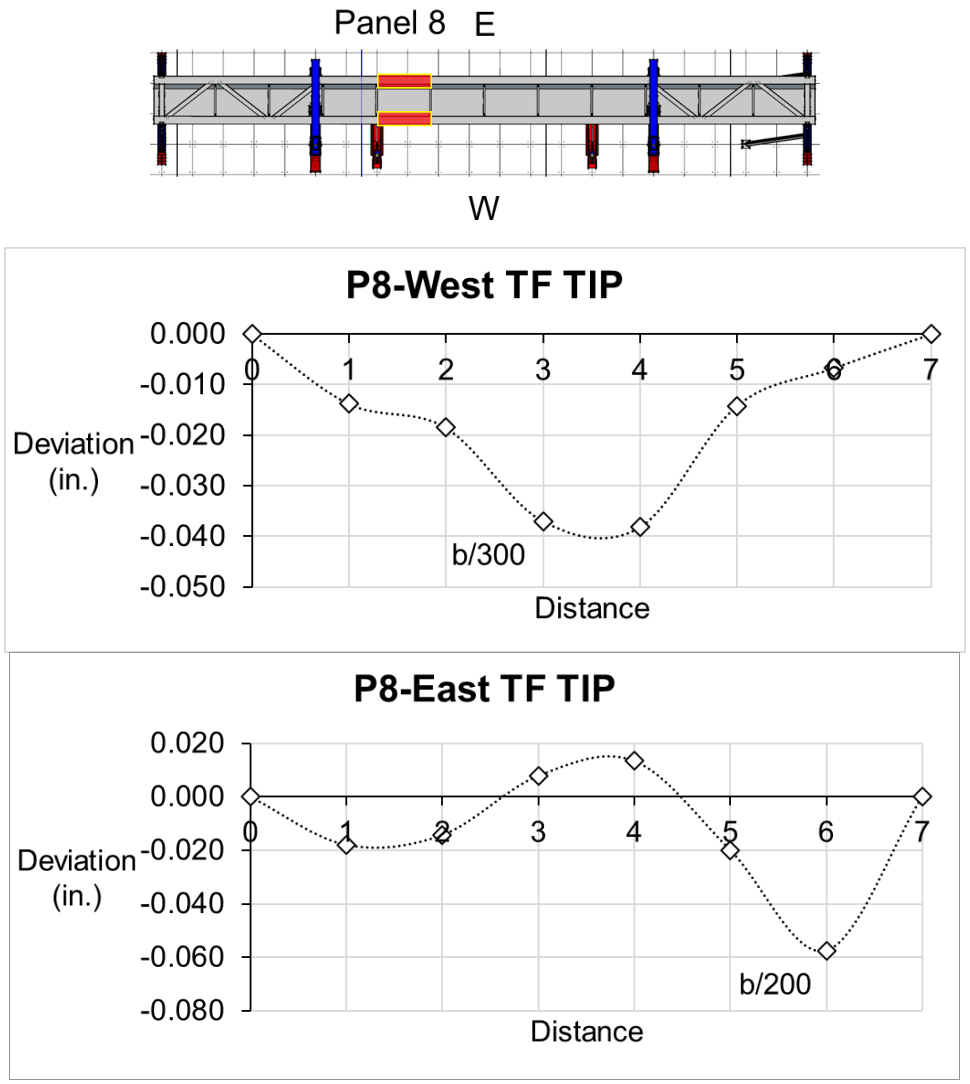

Figure B-16 – Local Out-of-Flatness of Flange Tip in Flange Offset Specimen (Panel 8)

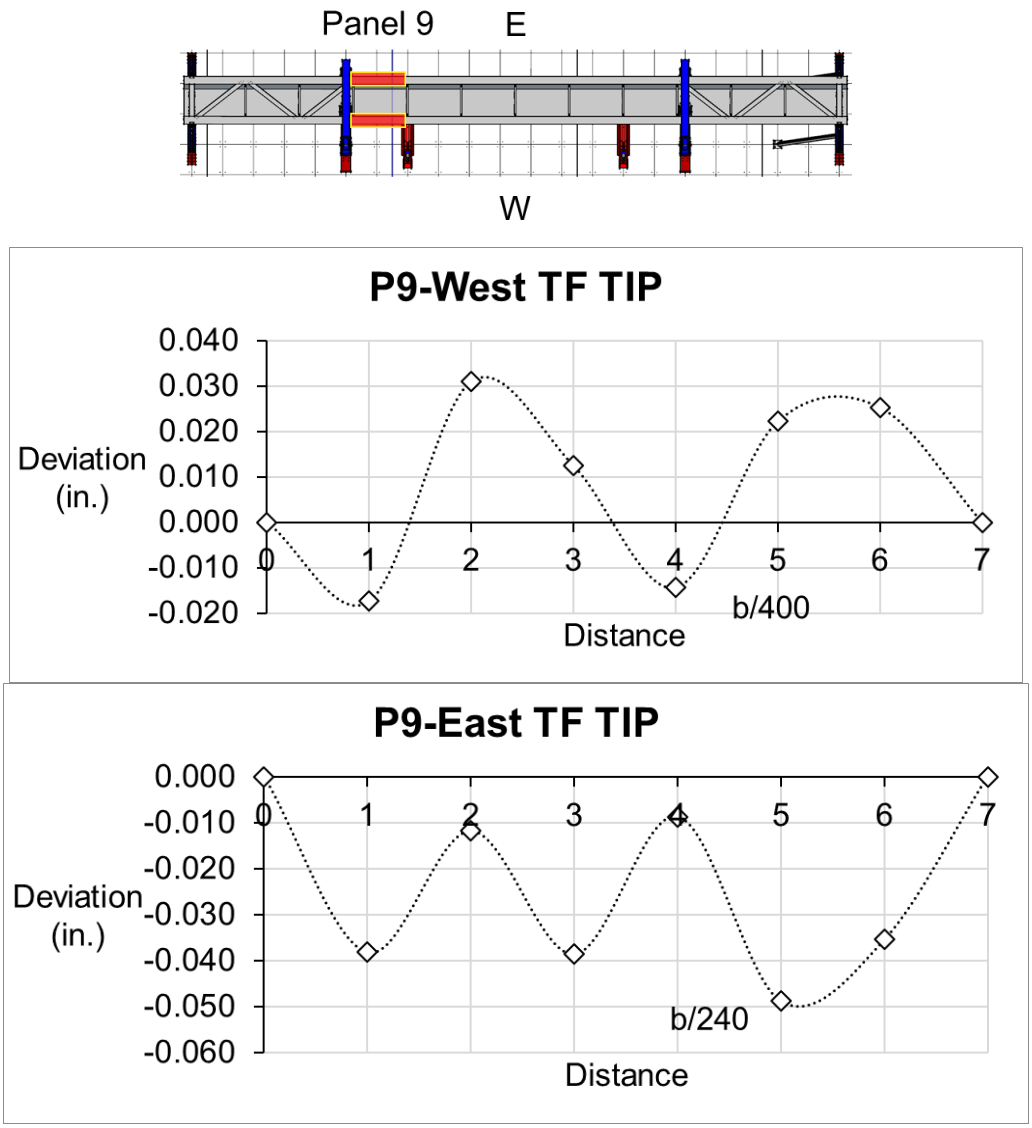

Figure B-17 – Local Out-of-Flatness of Flange Tip in Flange Offset Specimen (Panel 9)

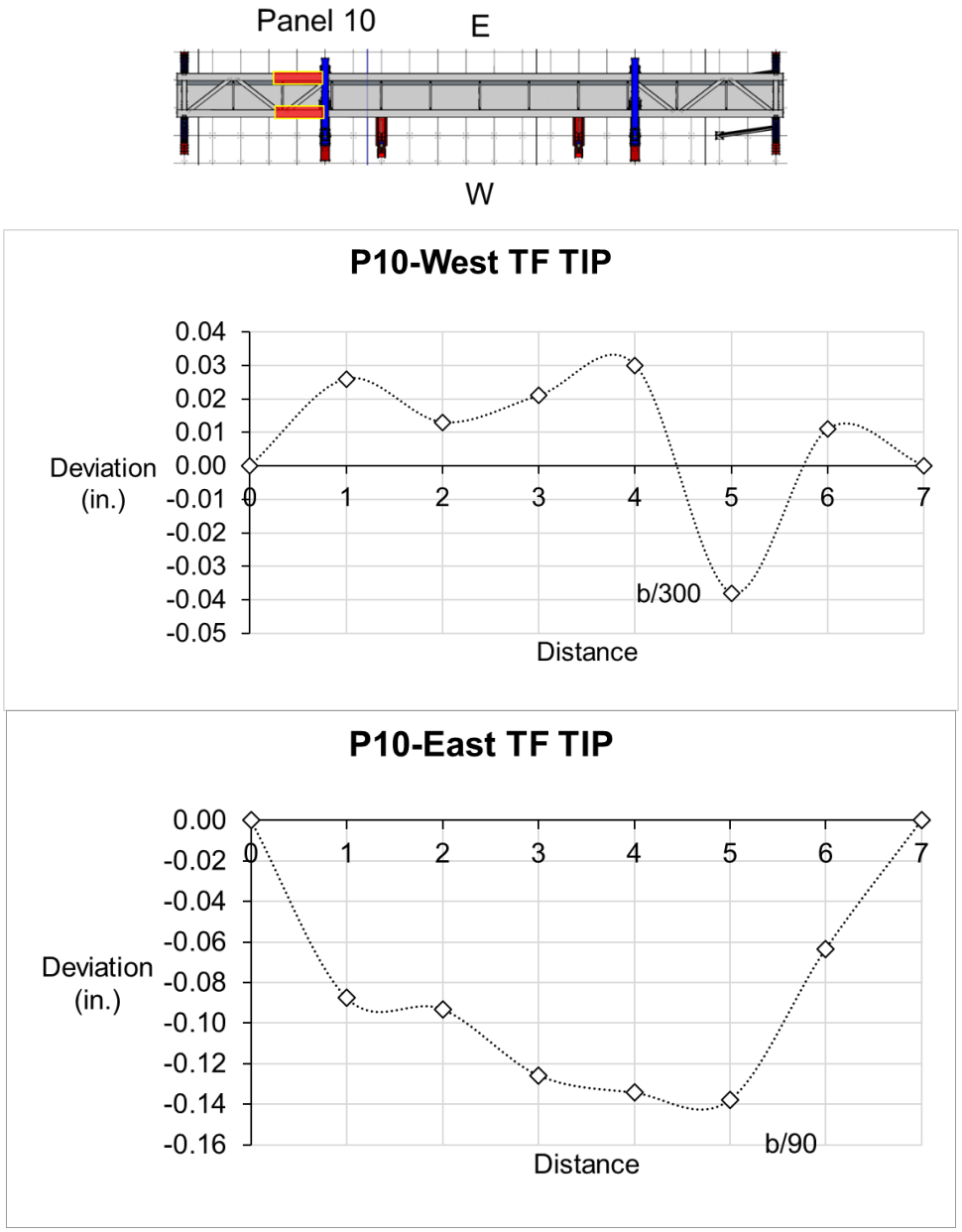

Figure B-18 – Local Out-of-Flatness of Flange Tip in Flange Offset Specimen (Panel 10)

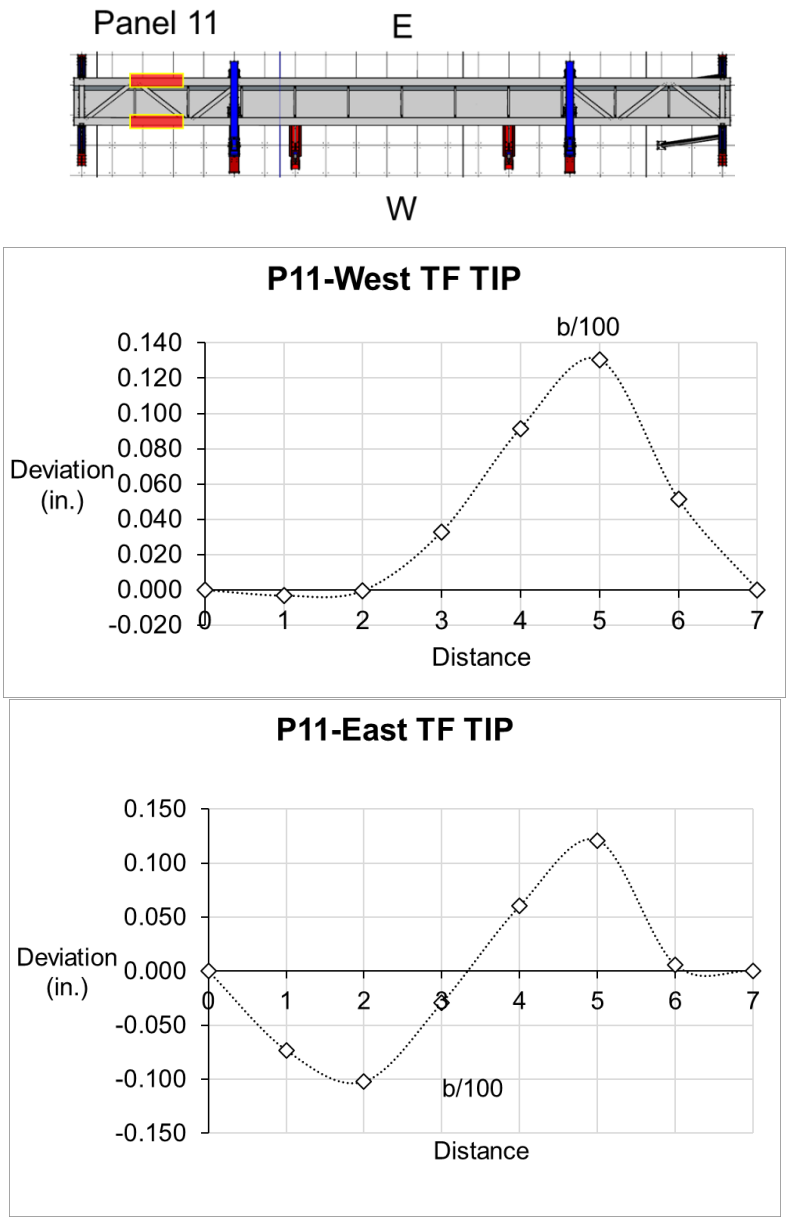

Figure B-19 – Local Out-of-Flatness of Flange Tip in Flange Offset Specimen (Panel 11)

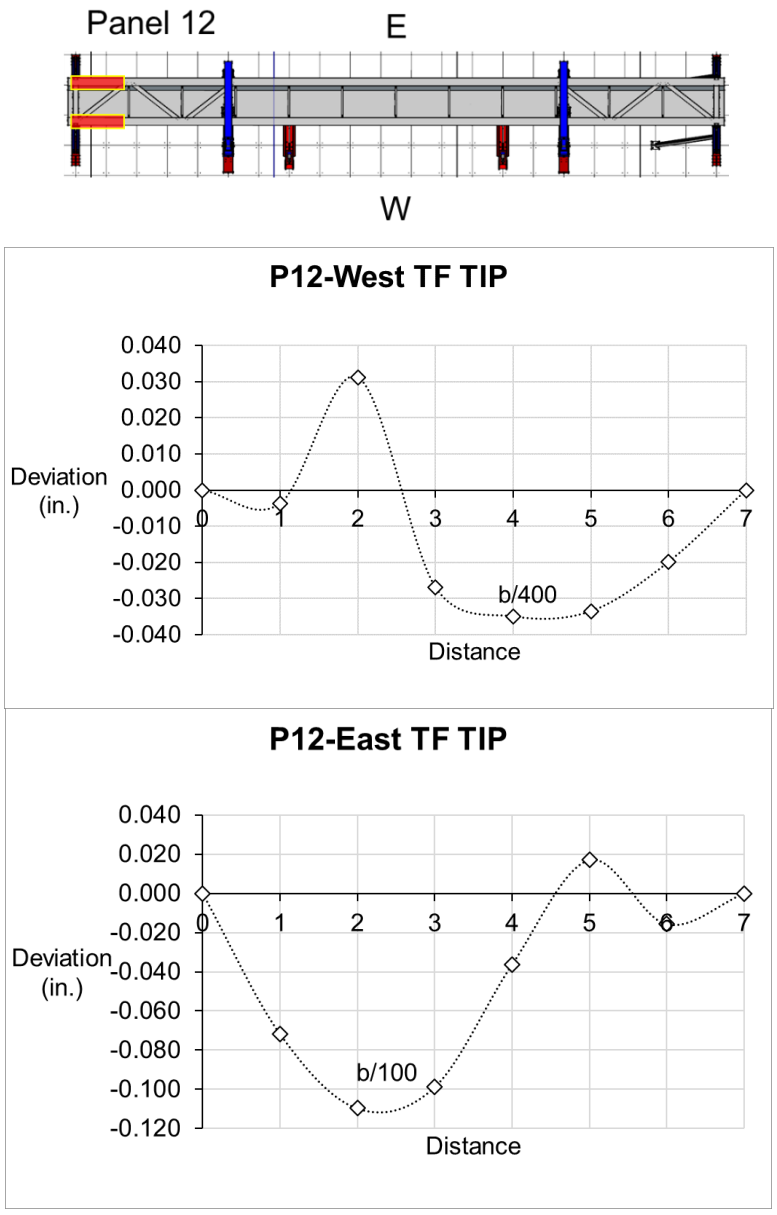

Figure B-20 - Local Out-of-Flatness of Flange Tip in Flange Offset Specimen (Panel 12)

B.2.2 Flatter Slope Specimen

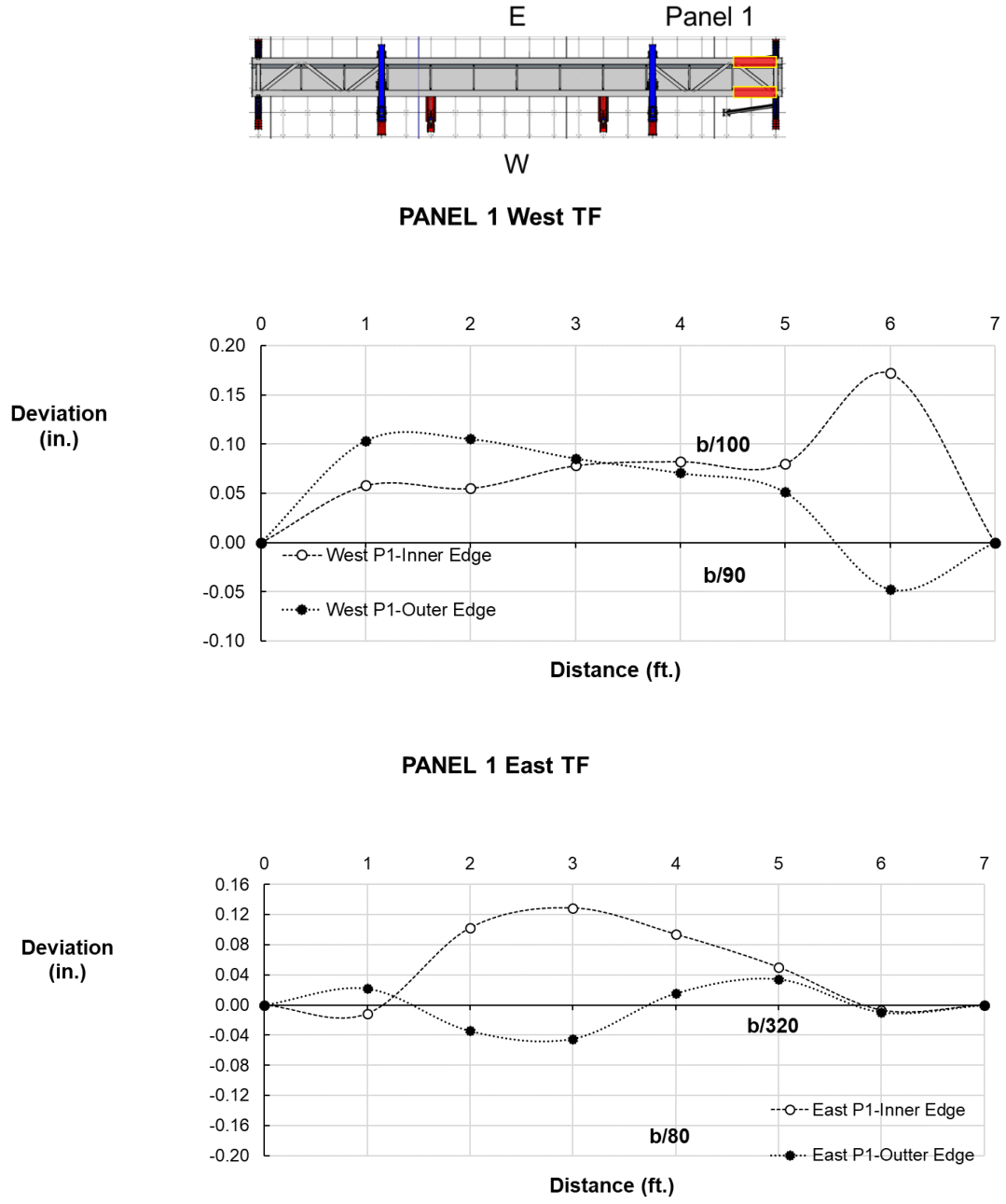

Figure B-21 – Local Out-of-Flatness of Flange Tip in Flatter Slope Specimen (Panel 1)

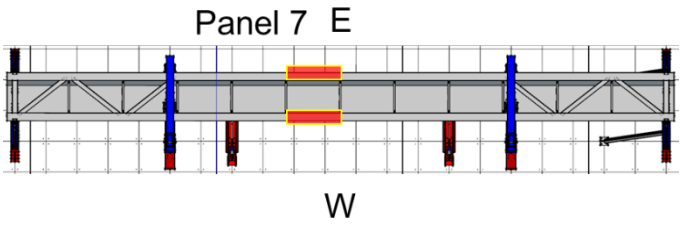

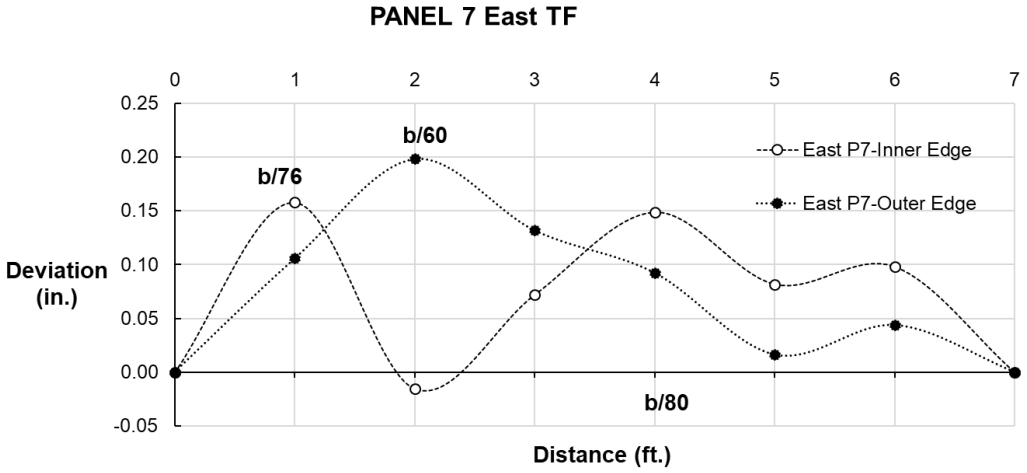

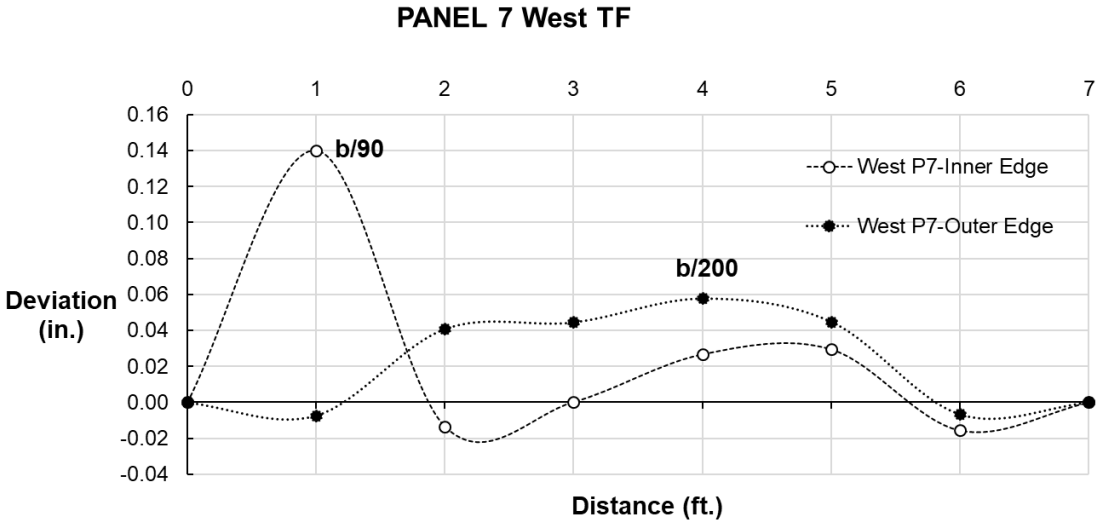

Figure B-22 – Local Out-of-Flatness of Flange Tip in Flatter Slope Specimen (Panel 7)

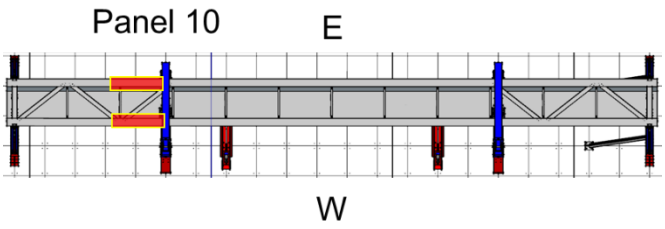

PANEL 10 East TF

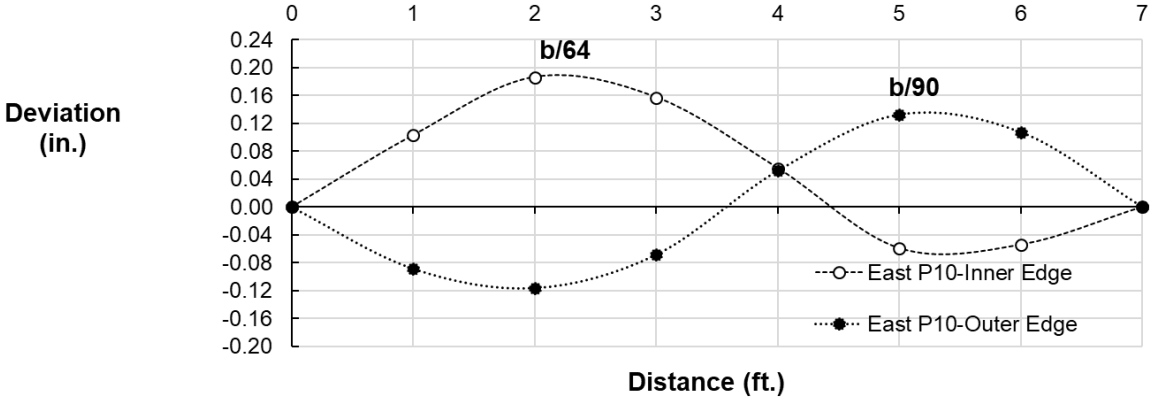

PANEL 10 West TF

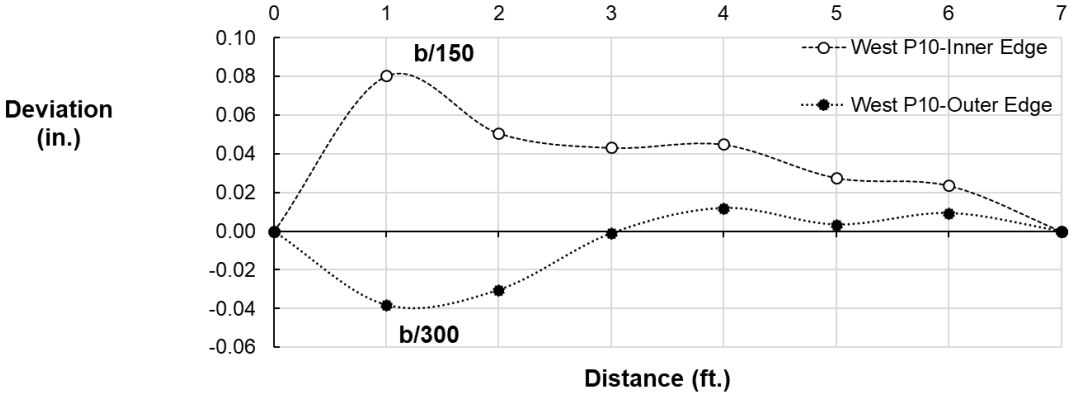

Figure B-23 – Local Out-of-Flatness of Flange Tip in Flatter Slope Specimen (Panel 10)

Appendix C. Experimental Results – Elastic Tests

C.1 Lateral Load Experimental Results

Table C-1 – Lateral Tests Summary

Test Code	Load Location	Number of Diagonals	K-Frame Location
LAT_1.1	TP	3	2-Panel
LAT_1.2	TP	2	2-Panel
LAT_1.3	TP	1	2-Panel
LAT_1.4	TP	0	2-Panel
LAT_2.1	TP	3	2-Panel
LAT_2.2	TP	2	2-Panel
LAT_2.3	TP	1	2-Panel
LAT_2.4	TP	0	2-Panel
LAT_3.1	TP	3	2-Panel
LAT_3.2	TP	2	2-Panel
LAT_3.3	TP	1	2-Panel
LAT_3.4	TP	0	2-Panel

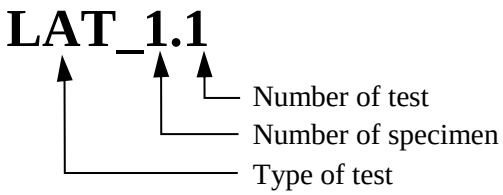

C.1.1 Tub #1 (Baseline Tub Girder) – Load-Deflection Response

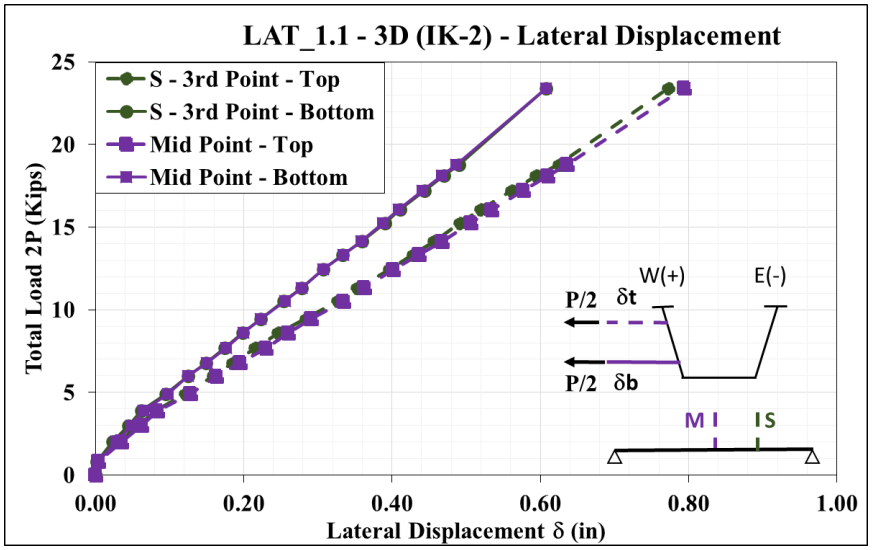

Figure C-1 – Total Load - Lateral Displacement - LAT_1.1

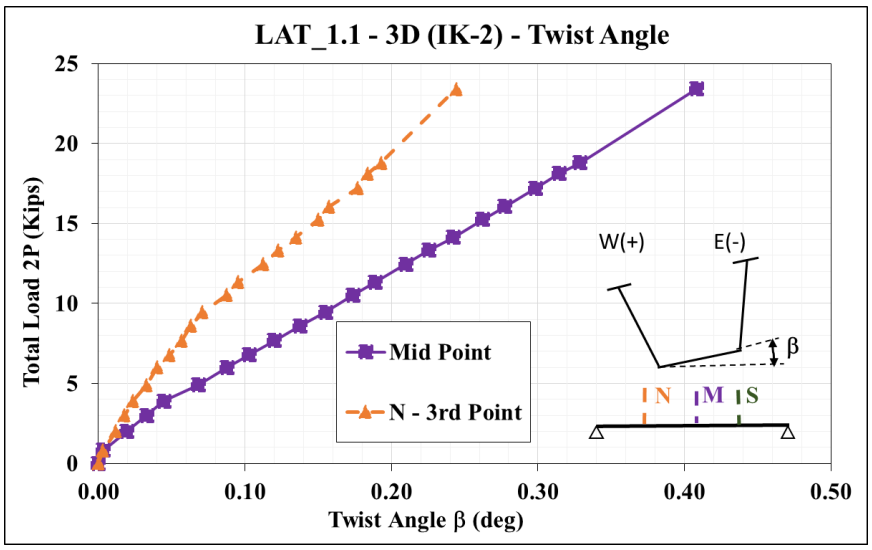

Figure C-2 – Total Load - Twist Angle - LAT_1.1

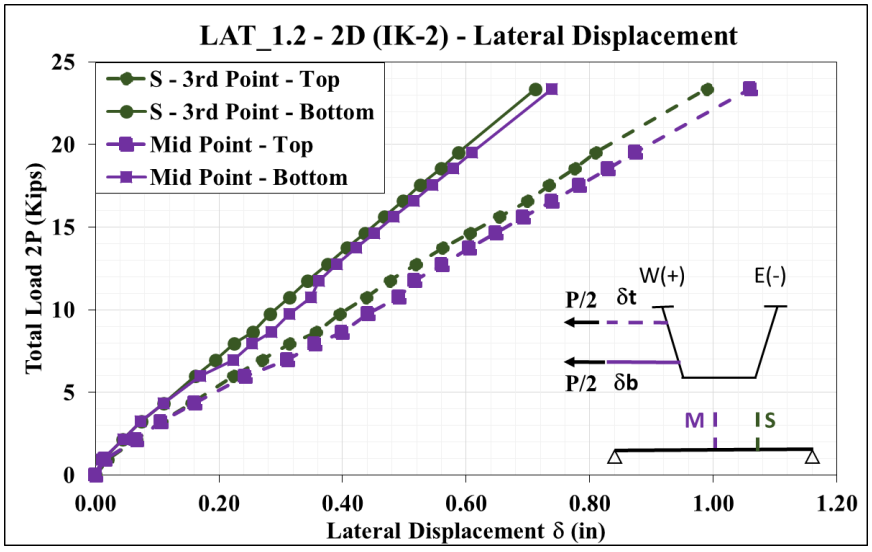

Figure C-3 – Total Load - Lateral Displacement - LAT_1.2

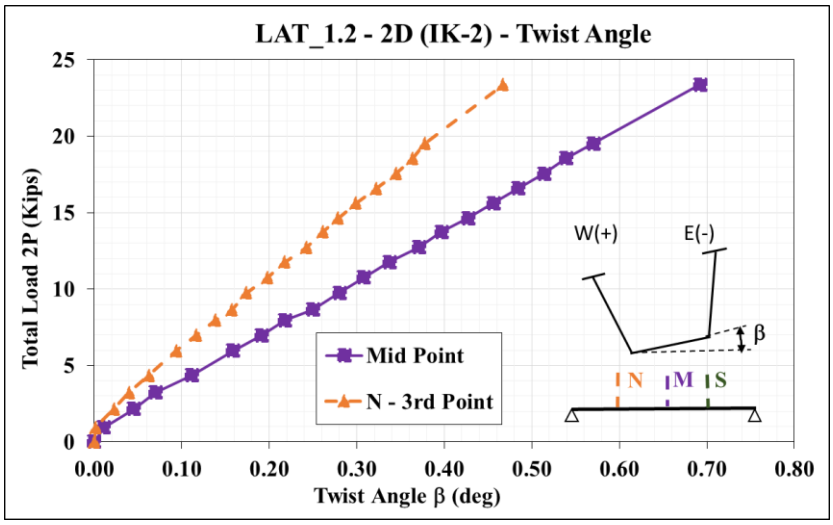

Figure C-4 – Total Load - Twist Angle - LAT_1.2

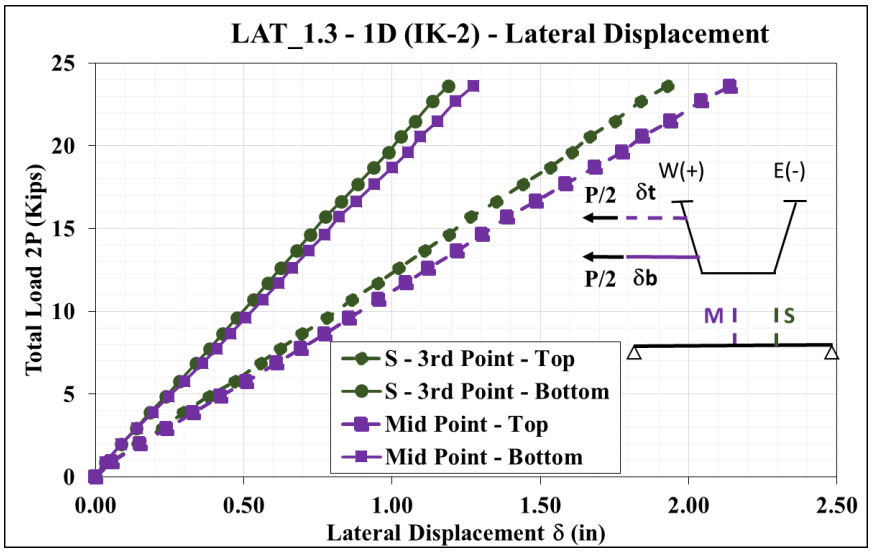

Figure C-5 – Total Load - Lateral Displacement - LAT_1.3

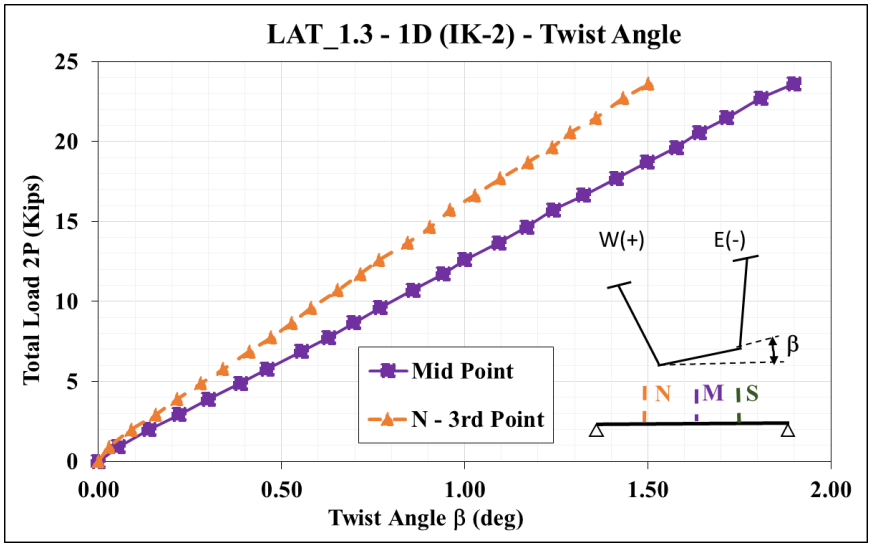

Figure C-6 – Total Load - Twist Angle - LAT_1.3

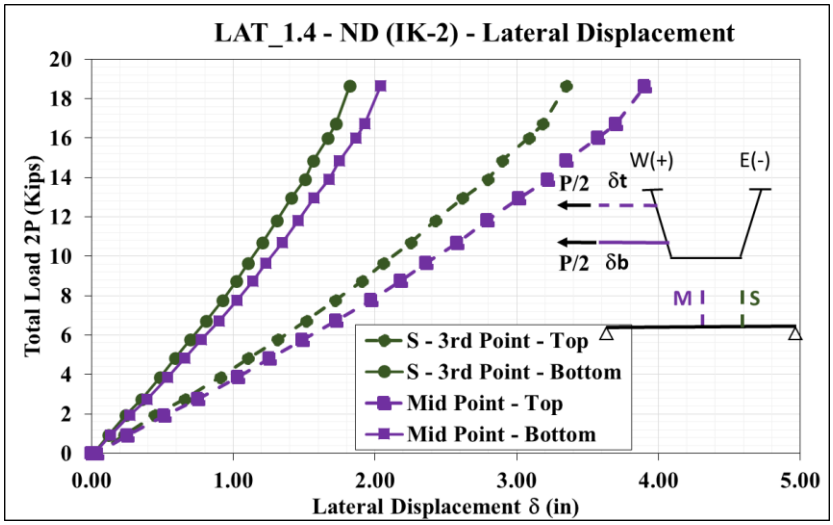

Figure C-7 – Total Load - Lateral Displacement - LAT_1.4

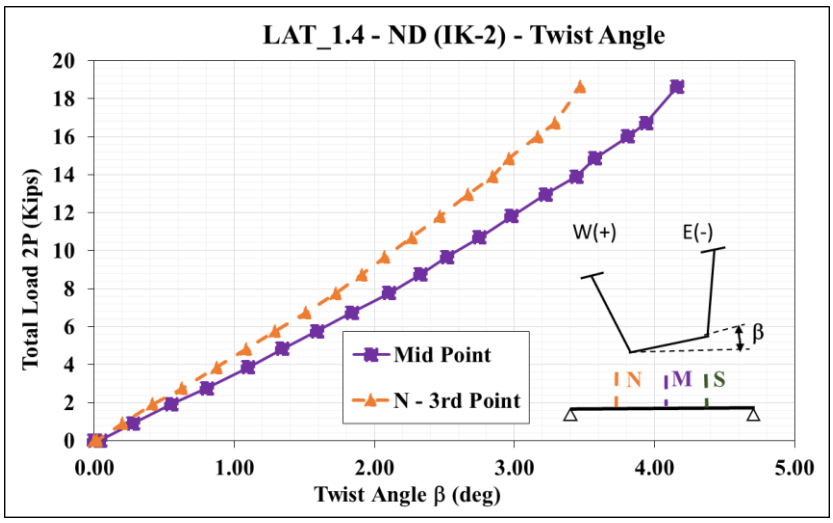

Figure C-8 – Total Load - Twist Angle - LAT_1.4

C.1.2 Tub #1 (Baseline Tub Girder) – Bracing Forces

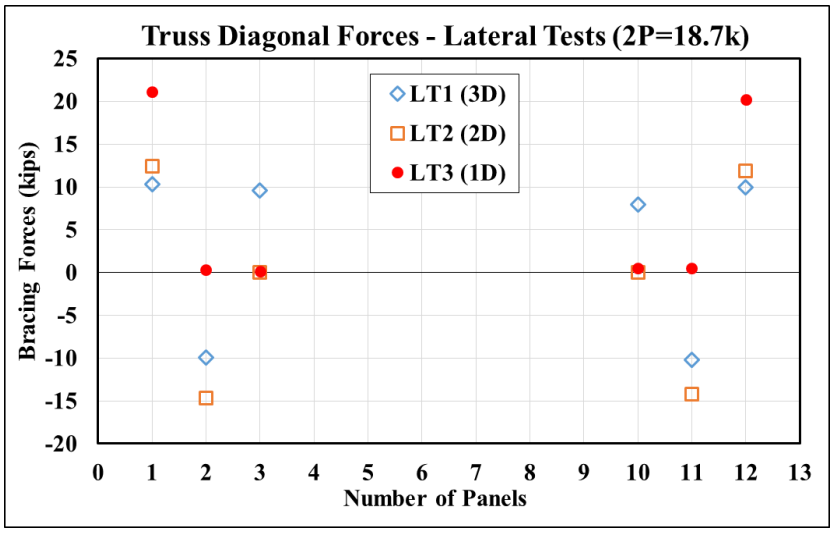

Figure C-9 – Top Lateral Bracing Diagonal Forces

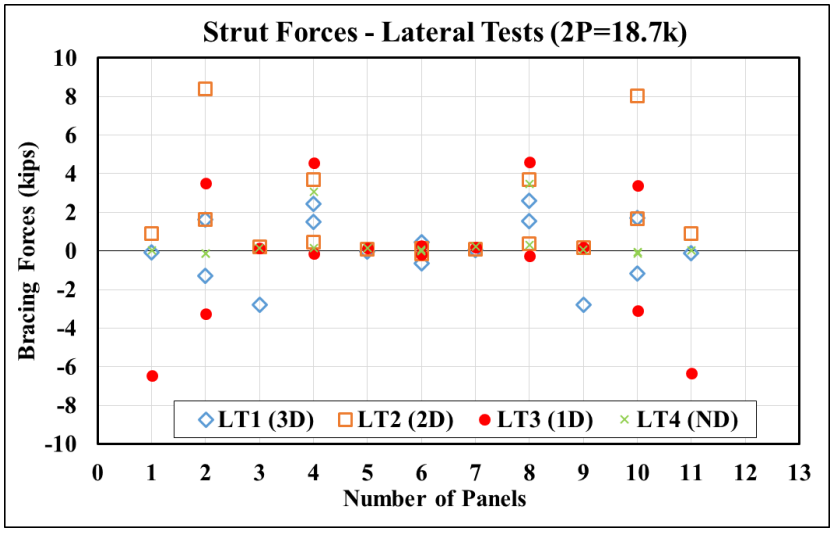

Figure C-10- Strut Forces

C.1.3 Tub #2 (Flange Offset Tub Girder) – Load-Deflection Response

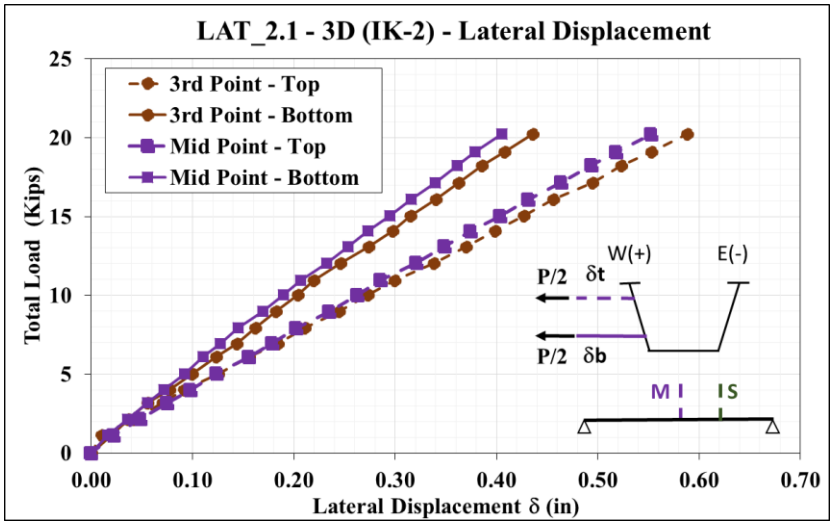

Figure C-11 – Total Load - Lateral Displacement - LAT_2.1

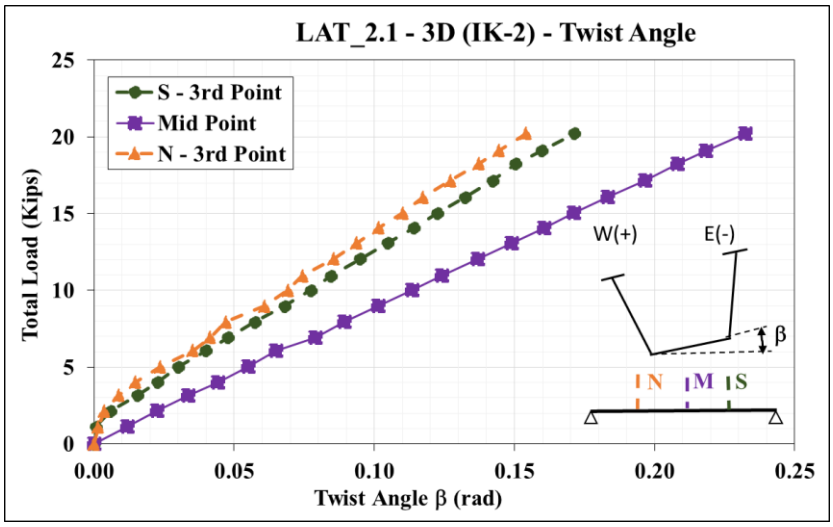

Figure C-12 – Total Load - Twist Angle - LAT_2.1

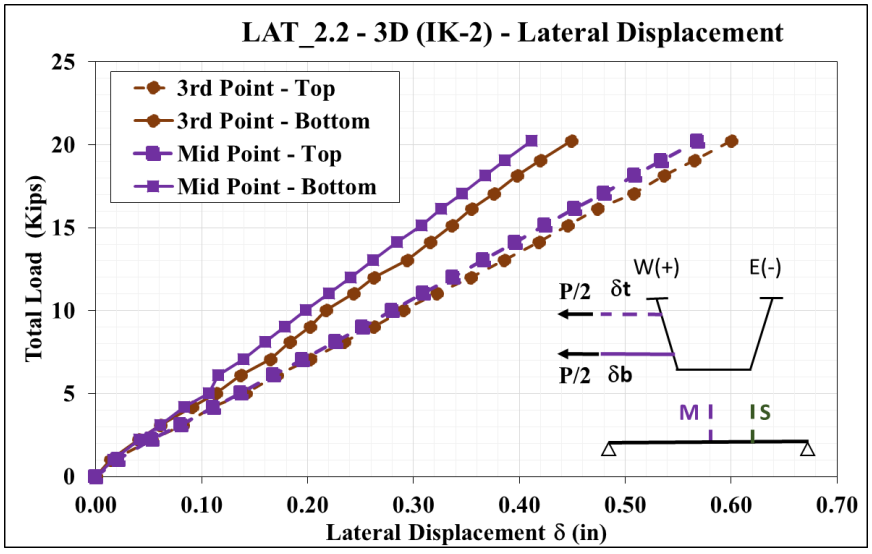

Figure C-13 – Total Load - Lateral Displacement - LAT_2.2

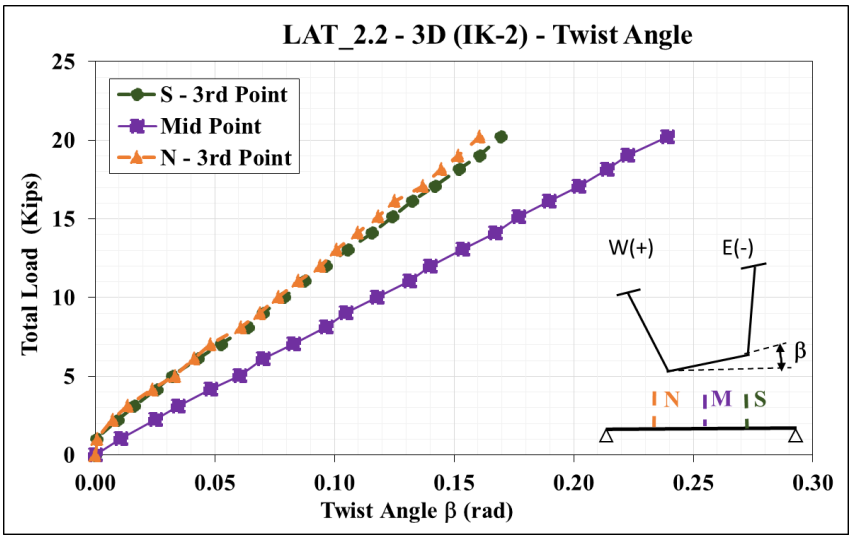

Figure C-14 – Total Load - Twist Angle - LAT_2.2

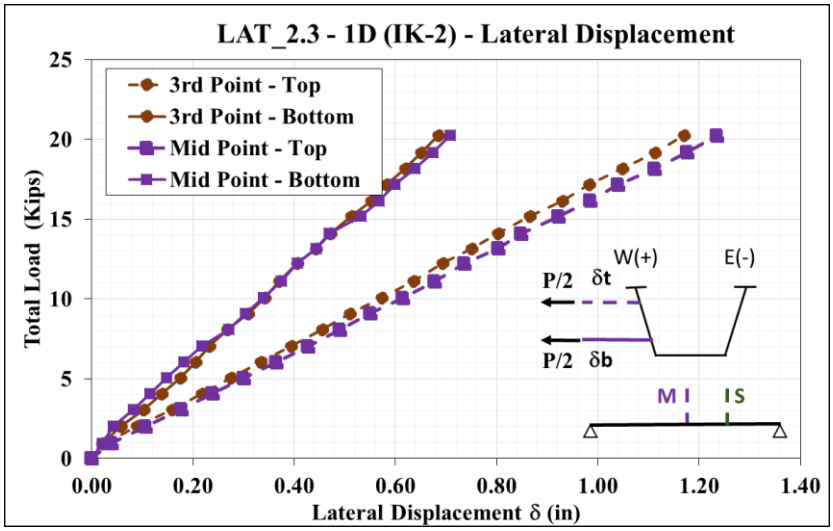

Figure C-15 – Total Load - Lateral Displacement - LAT_2.3

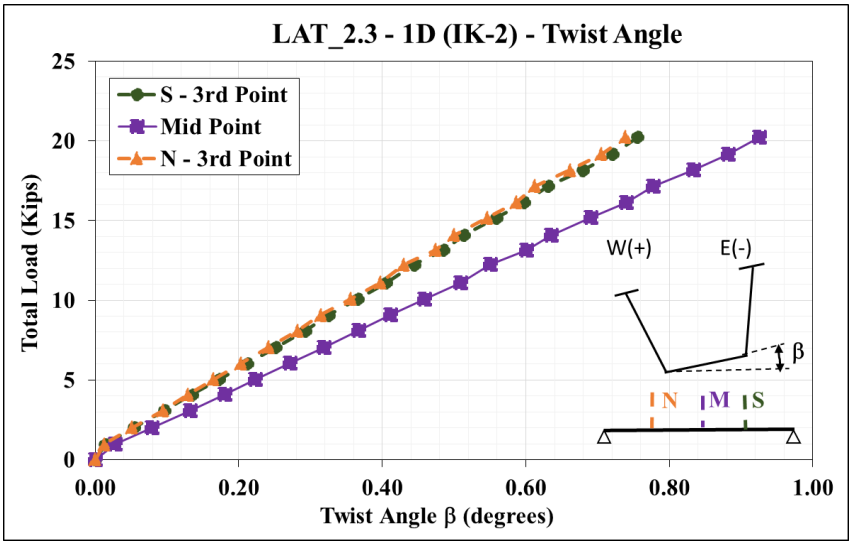

Figure C-16 – Total Load - Twist Angle - LAT_2.3

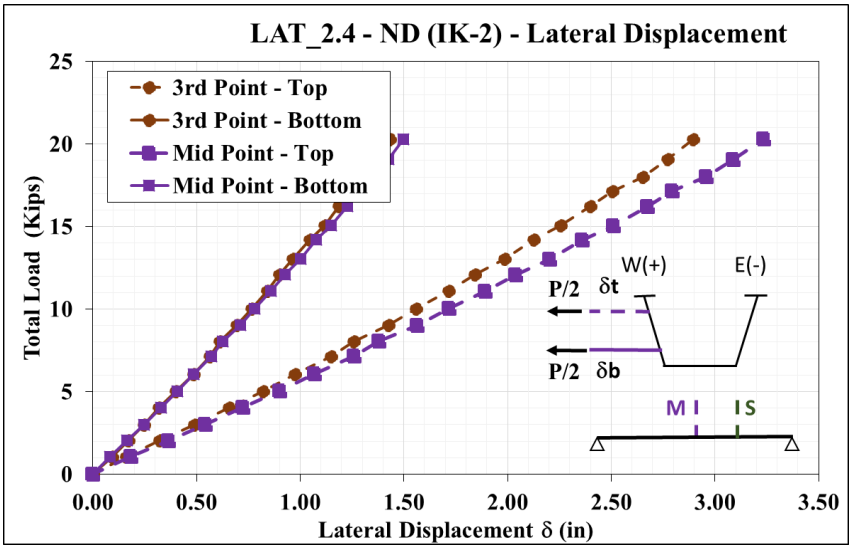

Figure C-17 – Total Load - Lateral Displacement - LAT_2.4

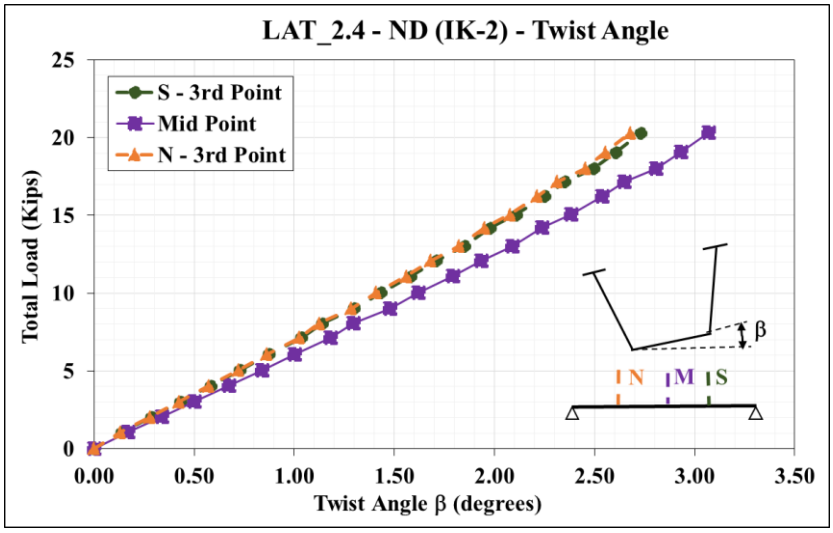

Figure C-18 – Total Load - Twist Angle - LAT_2.4

C.1.4 Tub #2 (Flange Offset Tub Girder) – Bracing Forces

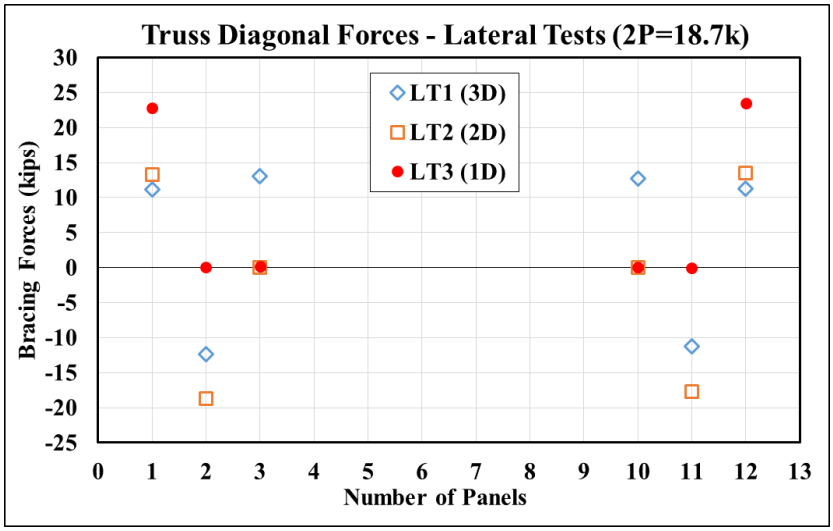

Figure C-19 – Top Lateral Bracing Forces

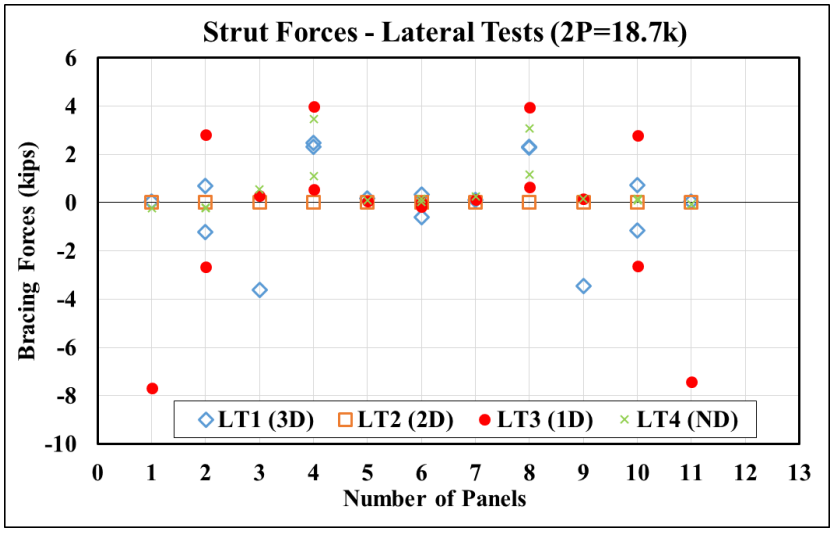

Figure C-20 – Strut Forces

C.1.5 Tub #3 (Flatter Web Tub Girder) – Load-Deflection Response

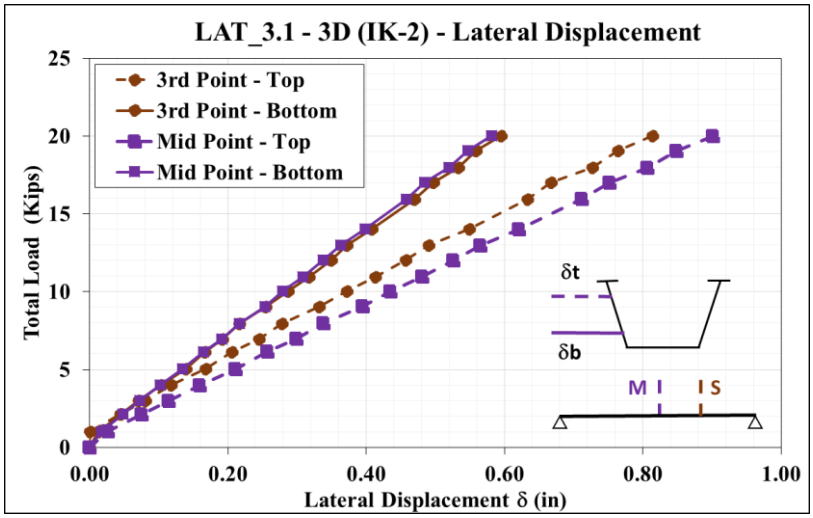

Figure C-21 – Total Load - Lateral Displacement - LAT_3.1

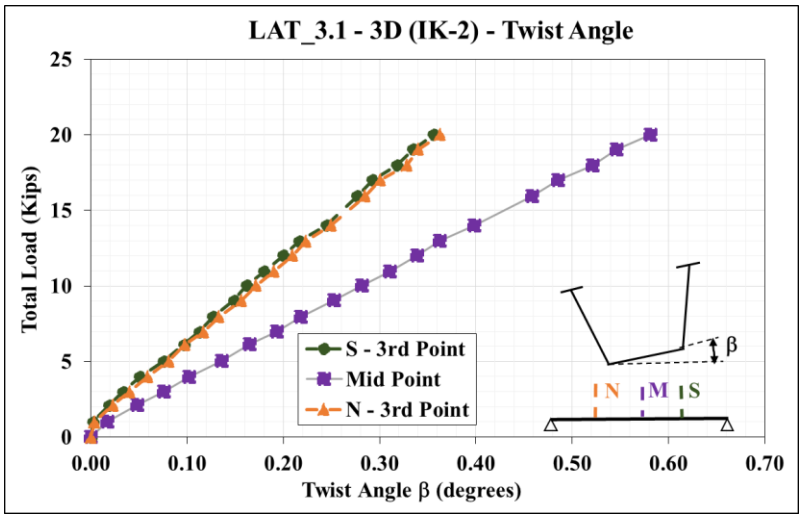

Figure C-22 – Total Load - Twist Angle - LAT_3.1

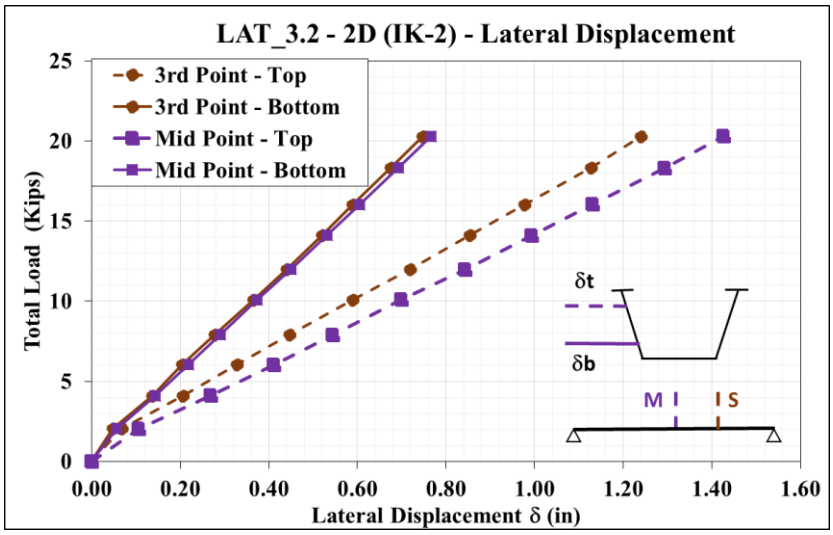

Figure C-23 – Total Load - Lateral Displacement - LAT_3.2

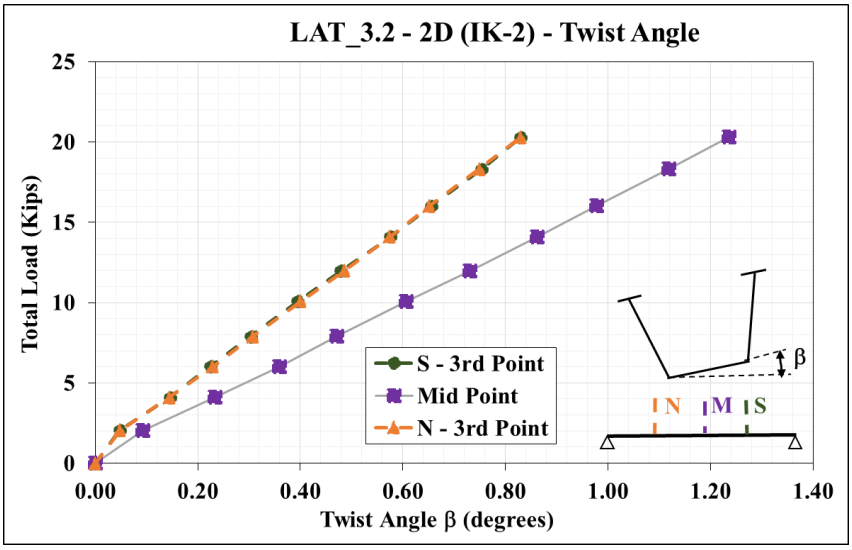

Figure C-24 – Total Load - Twist Angle - LAT_3.2

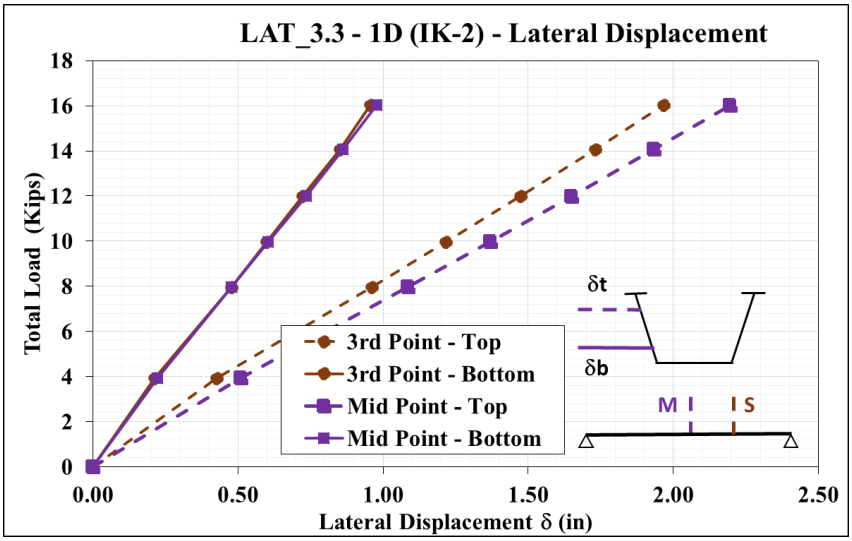

Figure C-25 – Total Load - Lateral Displacement - LAT_3.3

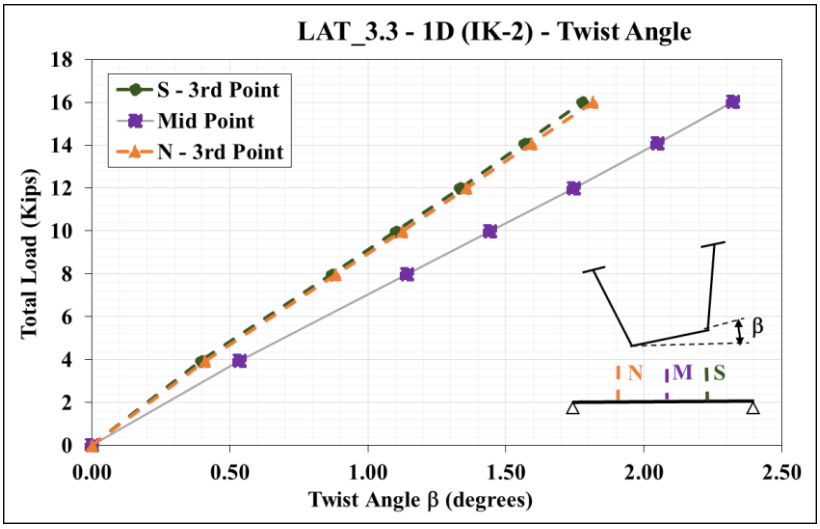

Figure C-26 – Total Load - Twist Angle - LAT_3.3

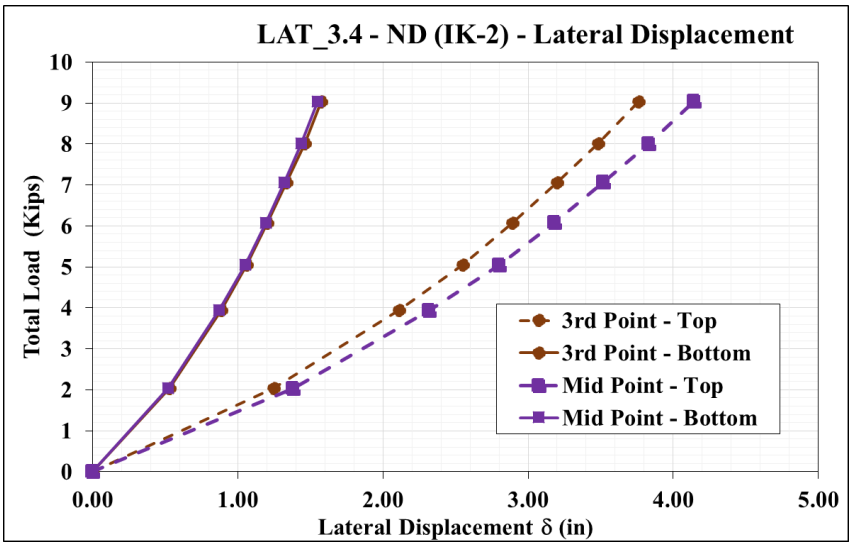

Figure C-27 – Total Load - Lateral Displacement - LAT_3.4

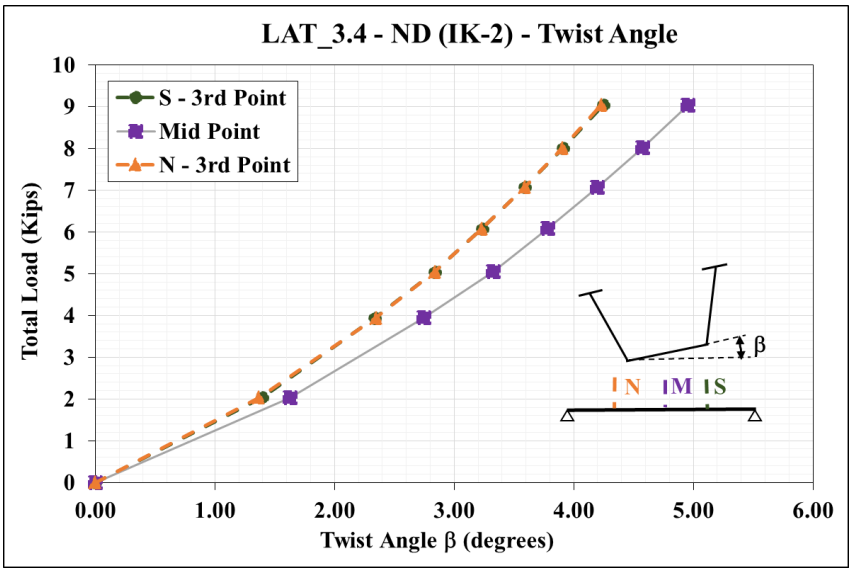

Figure C-28 – Total Load - Twist Angle - LAT_3.4

C.2 Positive Bending Experimental Results

Table C-2 – Positive Bending Test Results

Test Code	Number of Diagonals	K-Frame Location
GLS_1.1	0	2-Panel
GLS_1.2	0	4-Panel
GLS_1.3	0	6-Panel
GLS_1.4	1	2-Panel
GLS_1.5	1	4-Panel
GLS_1.6	1	6-Panel
GLS_1.7	2	2-Panel
GLS_1.8	2	4-Panel
GLS_1.9	2	6-Panel
GLS_1.10	3	2-Panel
GLS_1.11	3	4-Panel
GLS_1.12	3	6-Panel
GLS_2.1	0	2-Panel
GLS_2.2	0	4-Panel
GLS_2.3	0	6-Panel
GLS_2.4	1	2-Panel
GLS_2.5	1	4-Panel
GLS_2.6	1	6-Panel
GLS_2.7	2	2-Panel
GLS_2.8	2	4-Panel
GLS_2.9	2	6-Panel
GLS_2.10	3	2-Panel
GLS_2.11	3	4-Panel
GLS_2.12	3	6-Panel
GLS_3.1	0	2-Panel
GLS_3.2	0	4-Panel
GLS_3.3	0	6-Panel
GLS_3.4	1	2-Panel
GLS_3.5	1	4-Panel
GLS_3.6	1	6-Panel
GLS_3.7	2	2-Panel
GLS_3.8	2	4-Panel
GLS_3.9	2	6-Panel
GLS_3.10	3	2-Panel
GLS_3.11	3	4-Panel
GLS_3.12	3	6-Panel

C.2.1 Tub #1 (Baseline Tub Girder) – Load-Deflection Response

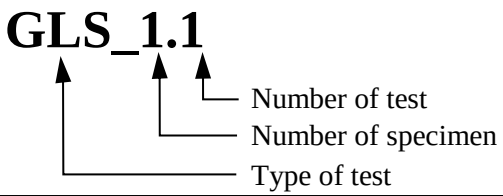

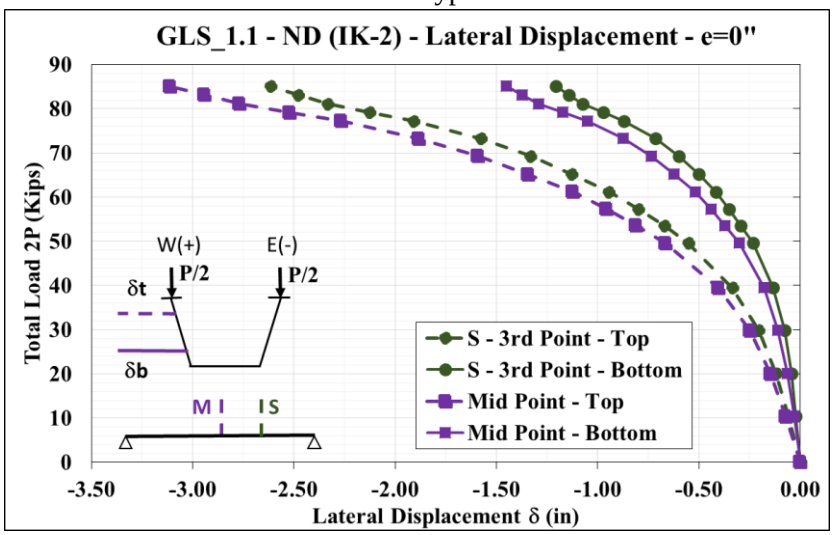

Figure C-29 – Total Load - Lateral Displacement - GLS_1.1

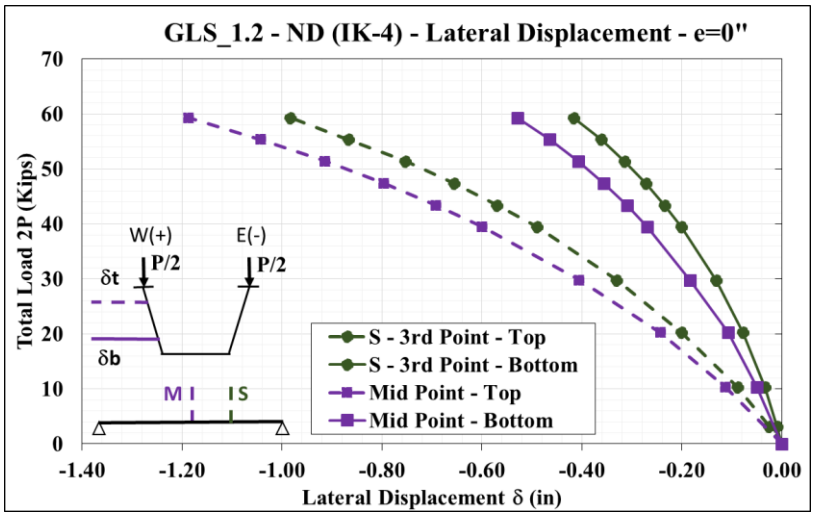

Figure C-30 – Total Load - Lateral Displacement - GLS_1.2

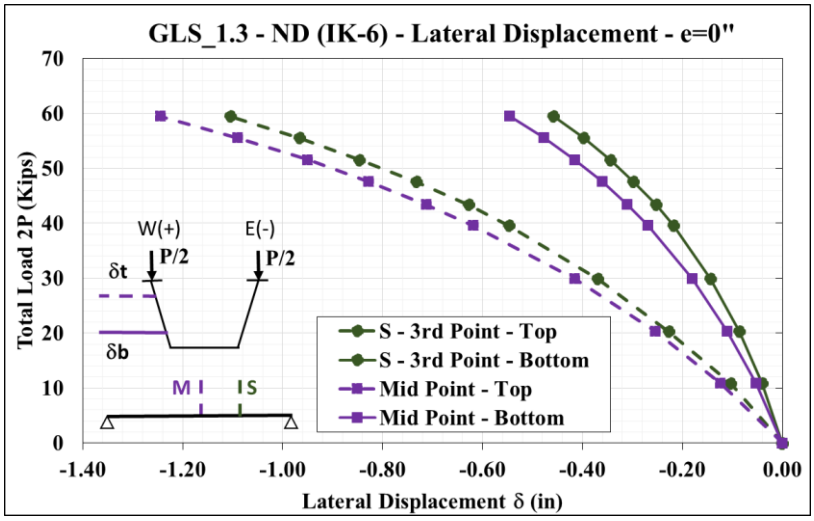

Figure C-31 – Total Load - Lateral Displacement - GLS_1.3

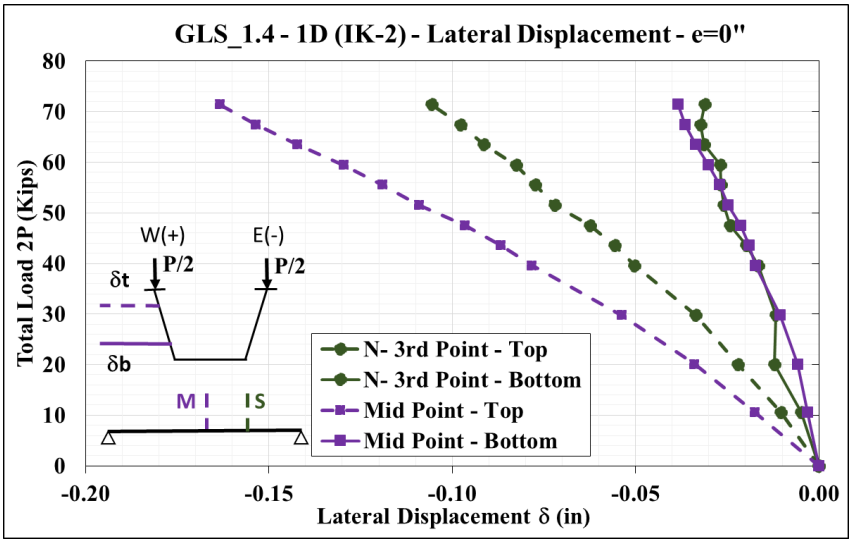

Figure C-32 – Total Load - Lateral Displacement - GLS_1.4

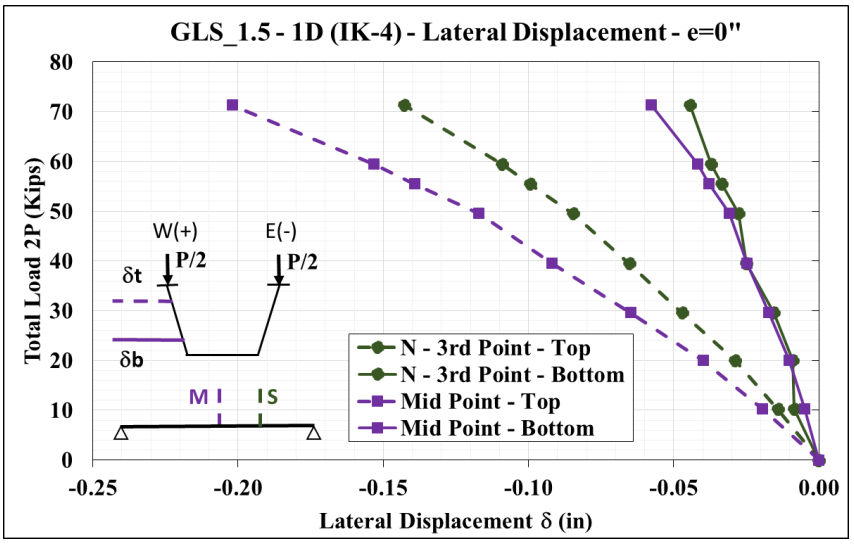

Figure C-33 – Total Load - Lateral Displacement - GLS_1.5

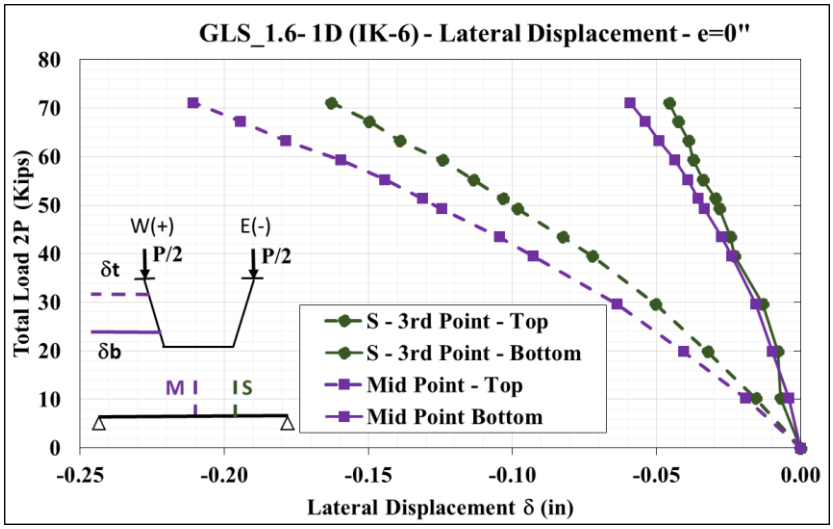

Figure C-34 – Total Load - Lateral Displacement - GLS_1.6

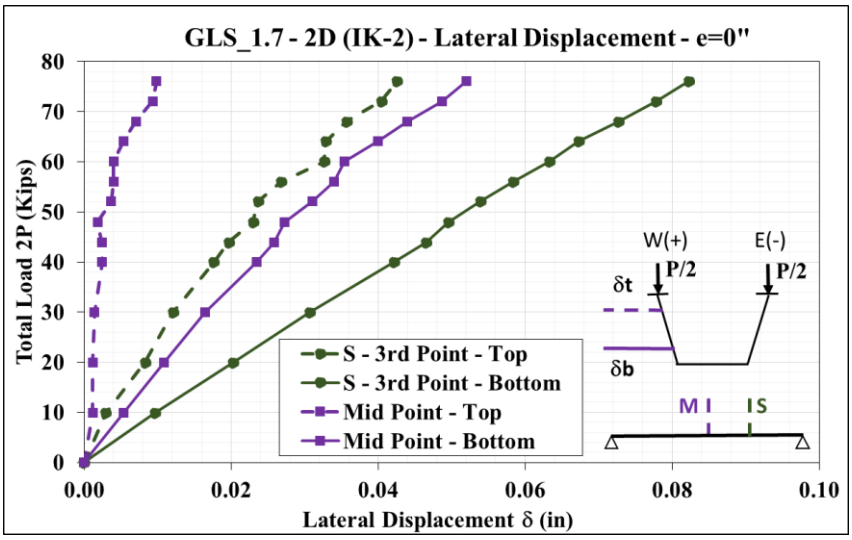

Figure C-35 – Total Load - Lateral Displacement - GLS_1.7

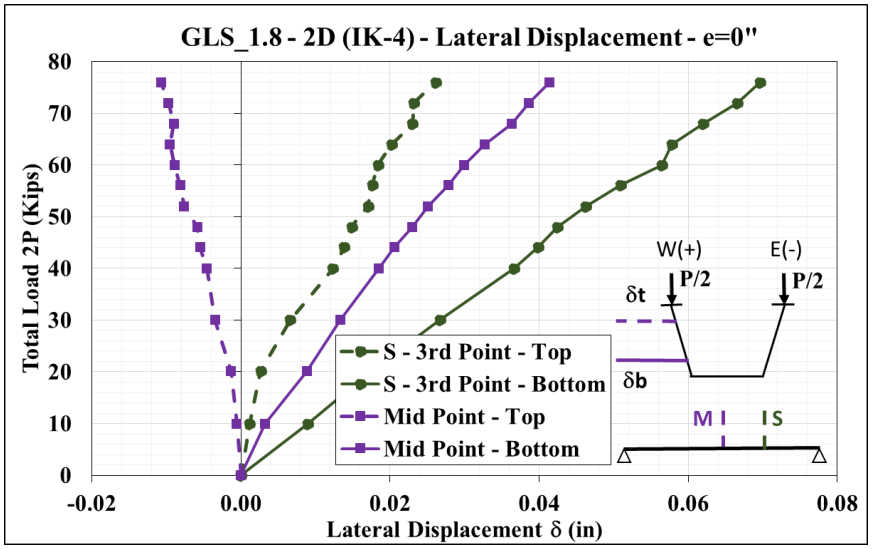

Figure C-36 – Total Load - Lateral Displacement - GLS_1.8

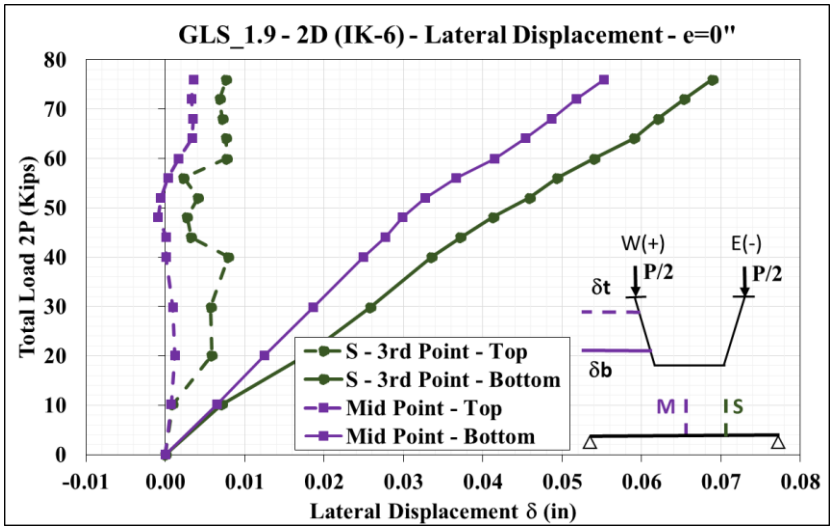

Figure C-37 – Total Load - Lateral Displacement - GLS_1.9

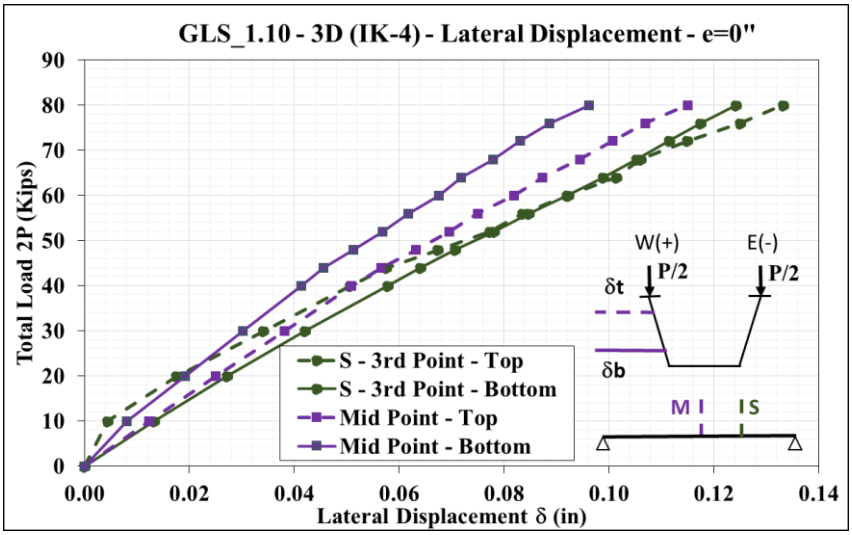

Figure C-38 – Total Load - Lateral Displacement - GLS_1.10

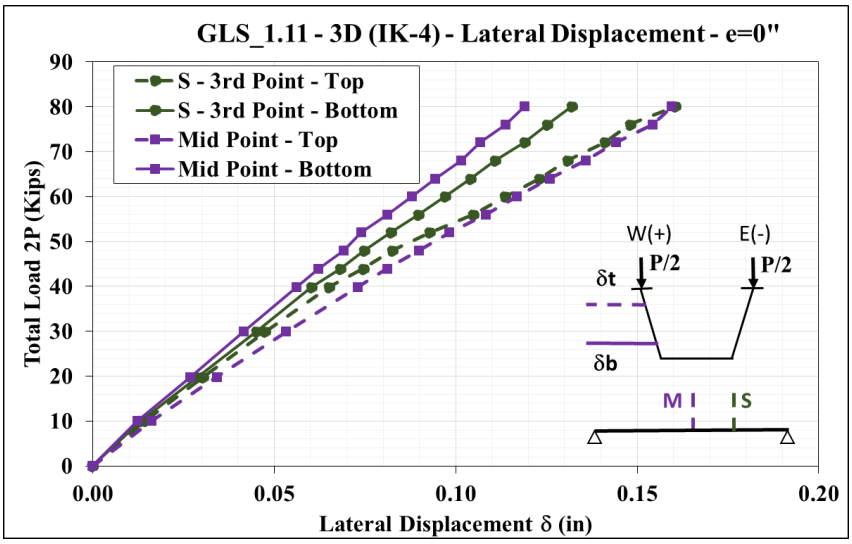

Figure C-39 – Total Load - Lateral Displacement - GLS_1.11

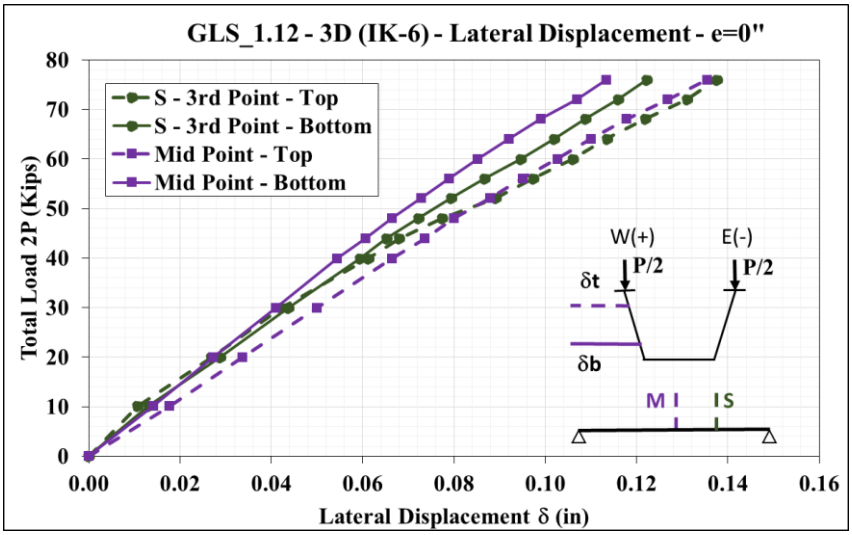

Figure C-40 – Total Load - Lateral Displacement - GLS_1.12

C.2.2 Tub #1 (Baseline Tub Girder) – Bracing Forces

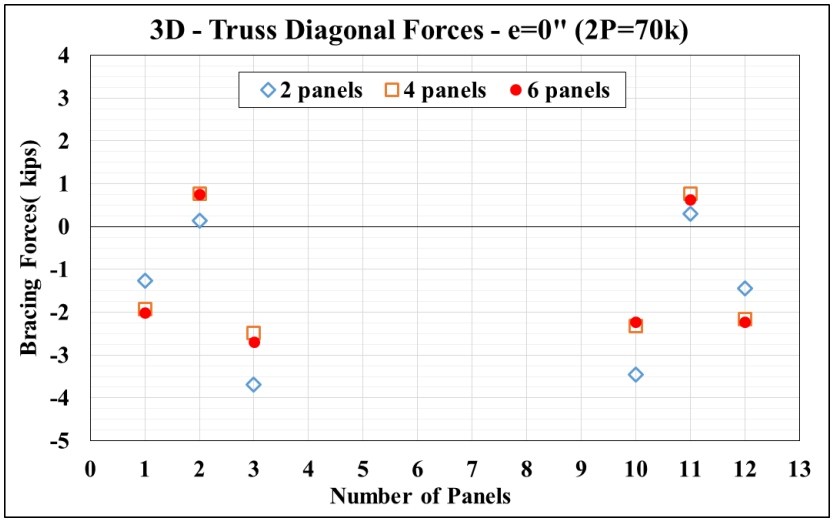

Figure C-41 – Top Lateral Bracing Diagonal Forces – 3 Truss Diagonals per End

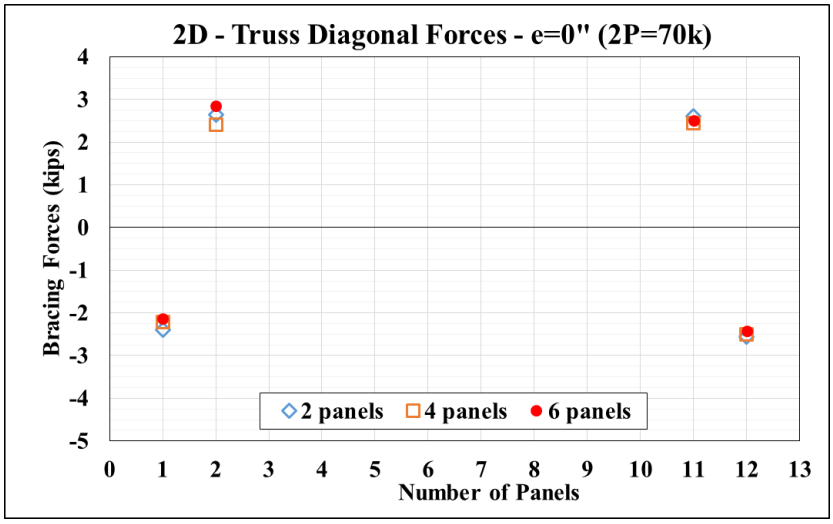

Figure C-42 – Top Lateral Bracing Diagonal Forces – 2 Truss Diagonals per End

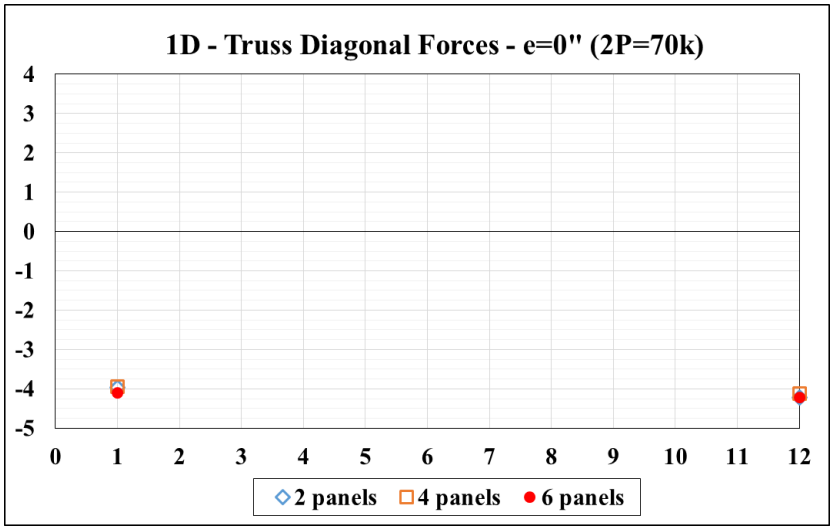

Figure C-43 – Top Lateral Bracing Diagonal Forces -1 Truss Diagonals per End

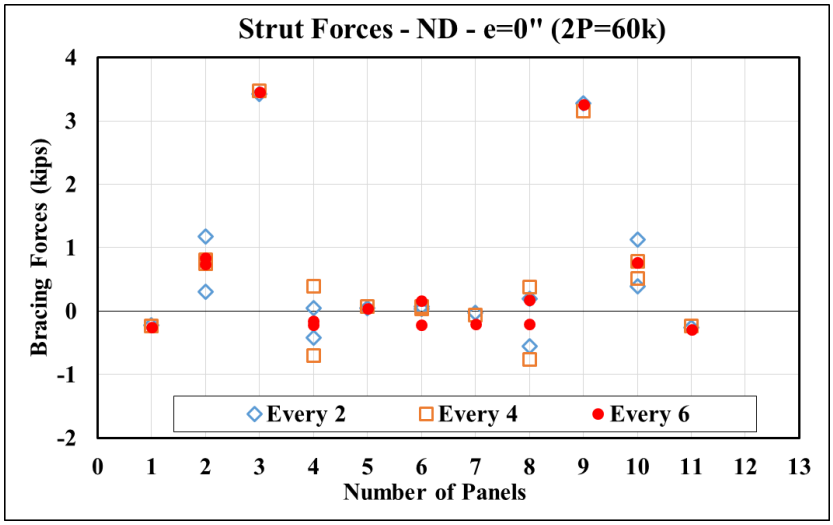

Figure C-44 – Strut Forces - 0 Truss Diagonals per End

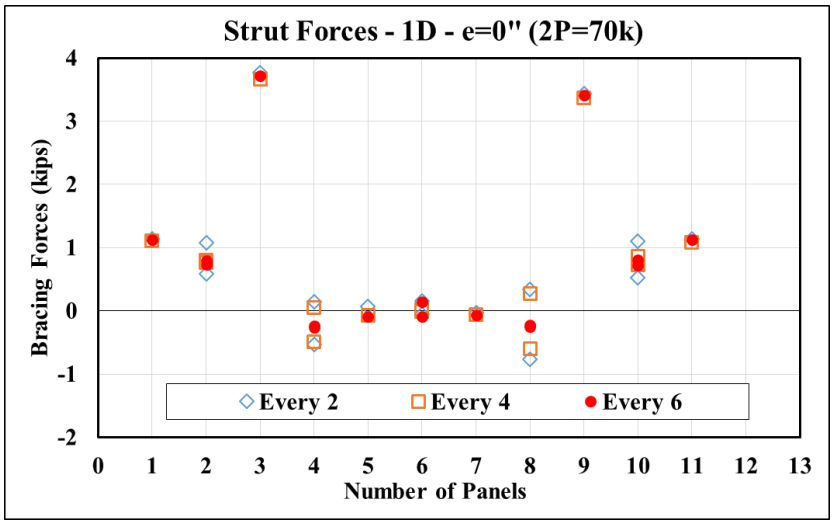

Figure C-45 – Strut Forces - 1 Truss Diagonals per End

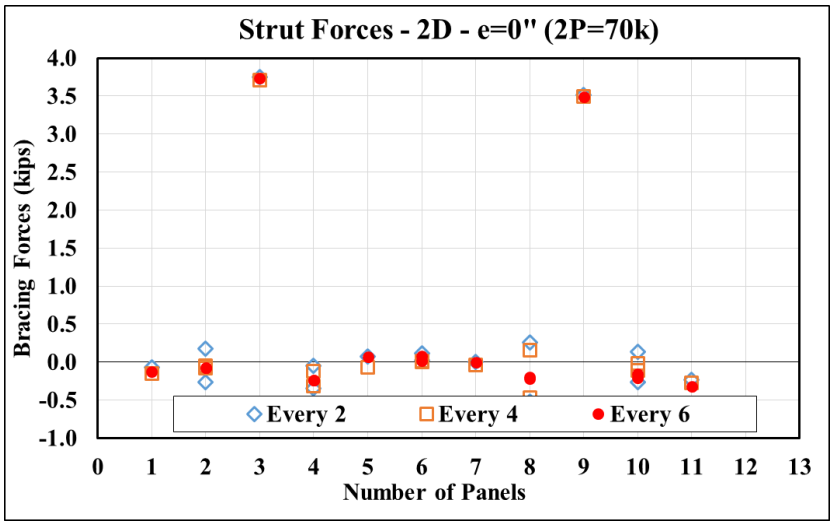

Figure C-46 – Strut Forces - 2 Truss Diagonals per End

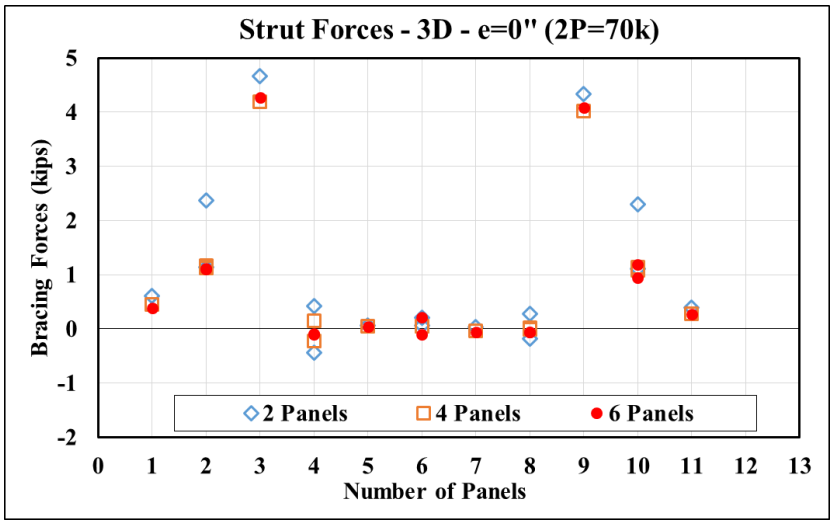

Figure C-47 – Strut Forces - 3 Truss Diagonals per End

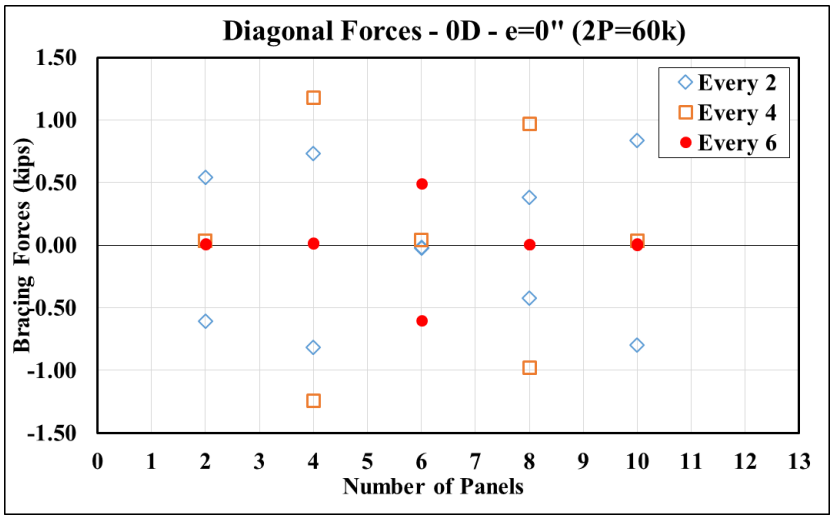

Figure C-48 – K-frame Diagonal Forces - 0 Truss Diagonals per End

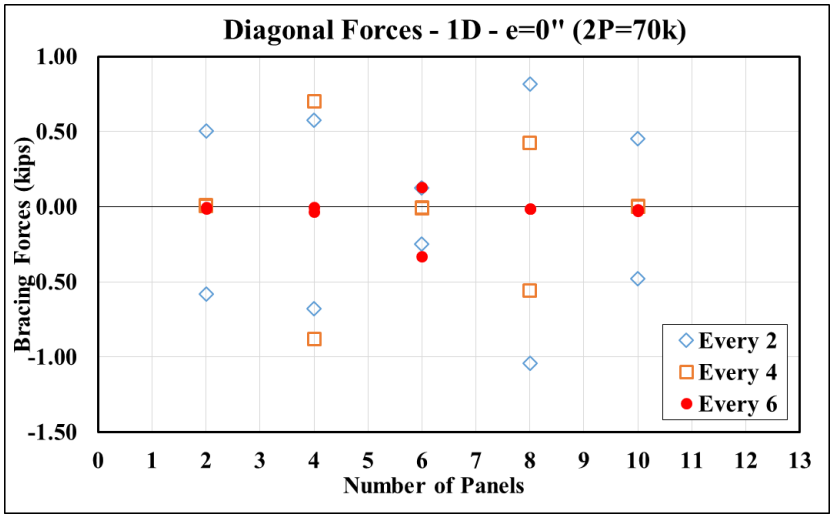

Figure C-49 – K-frame Diagonal Forces - 1 Truss Diagonals per End

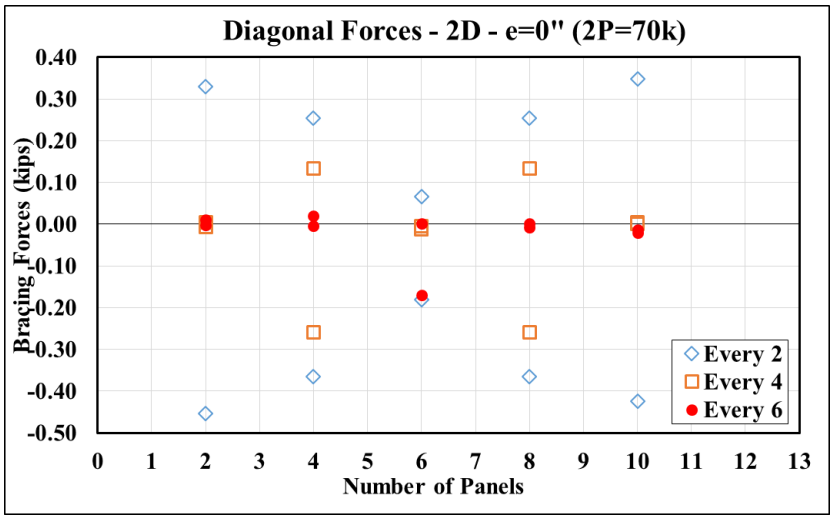

Figure C-50 – K-frame Diagonal Forces - 2 Truss Diagonals per End

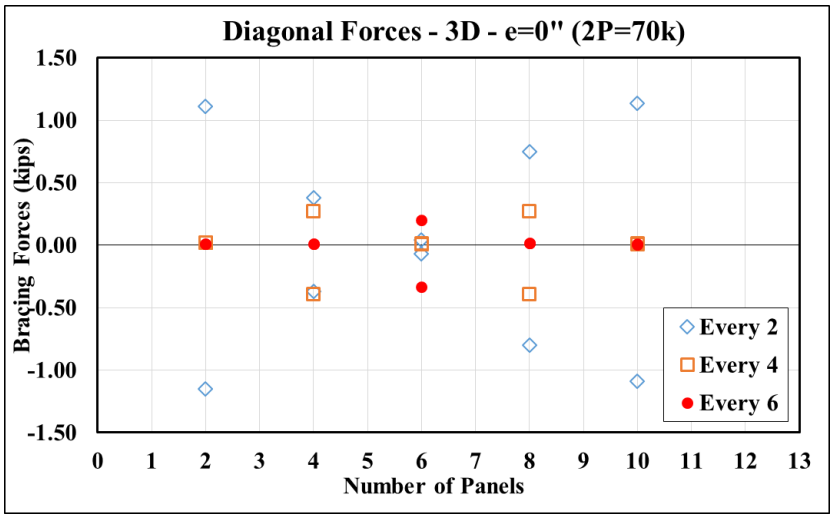

Figure C-51 – K-frame Diagonal Forces - 3 Truss Diagonals per End

C.2.3 Tub #2 (Flange Offset Tub Girder) – Load-Deflection Response

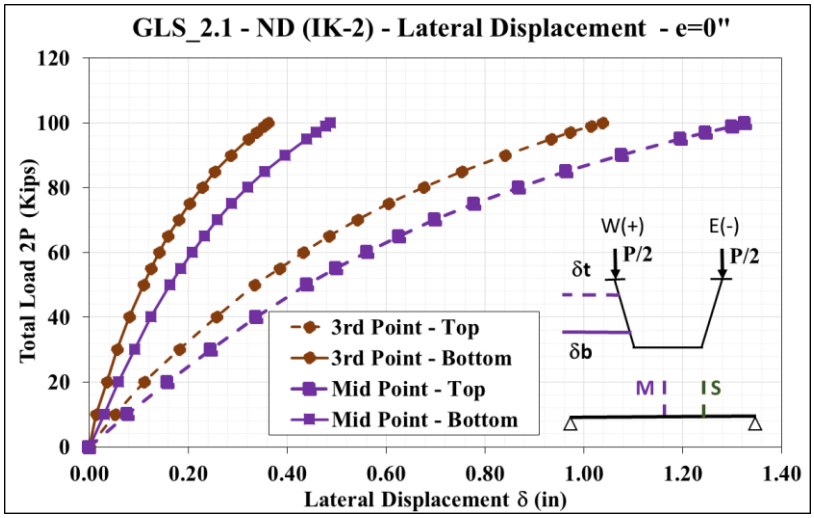

Figure C-52 – Total Load - Lateral Displacement - GLS_2.1

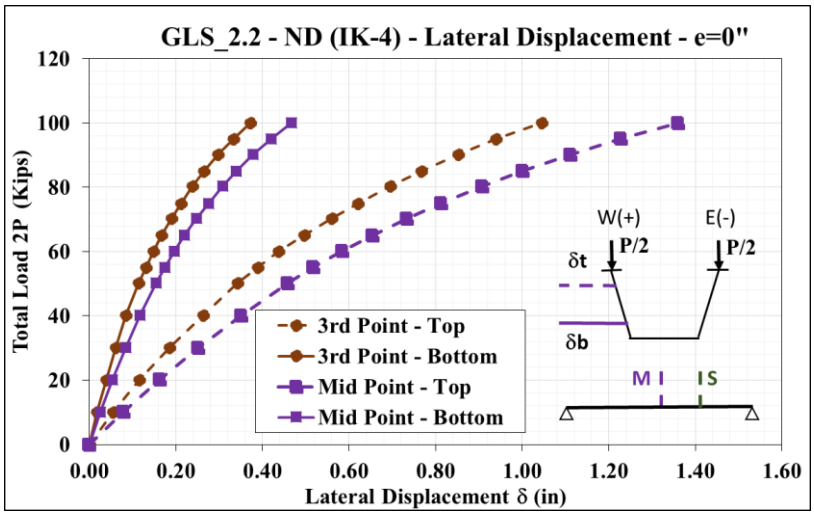

Figure C-53 – Total Load - Lateral Displacement - GLS_2.2

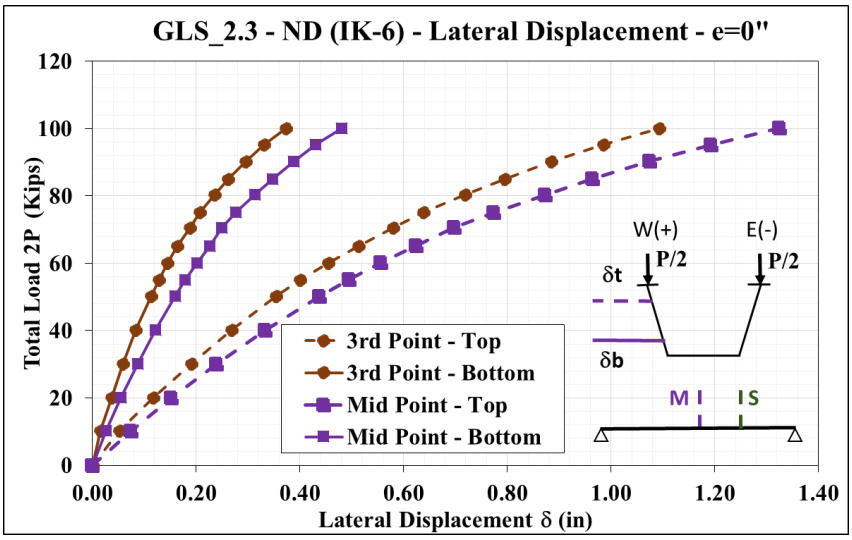

Figure C-54 – Total Load - Lateral Displacement - GLS_2.3

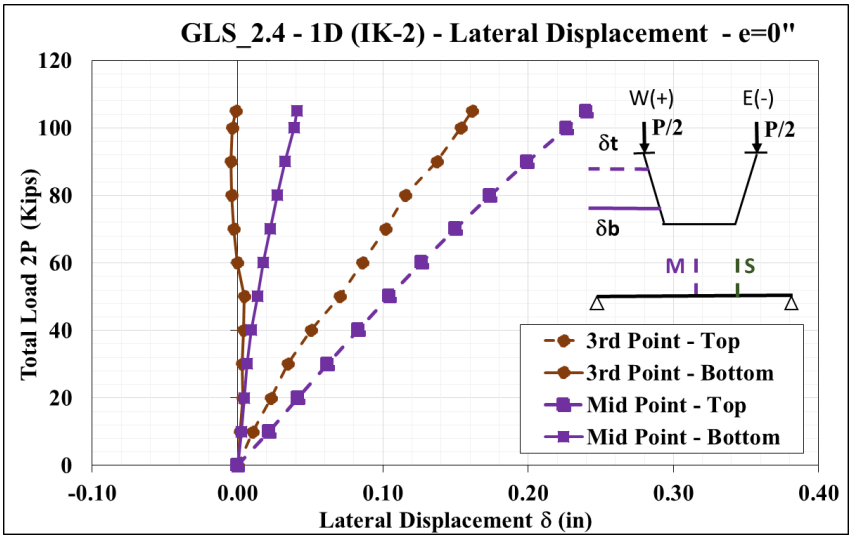

Figure C-55 – Total Load - Lateral Displacement - GLS_2.4

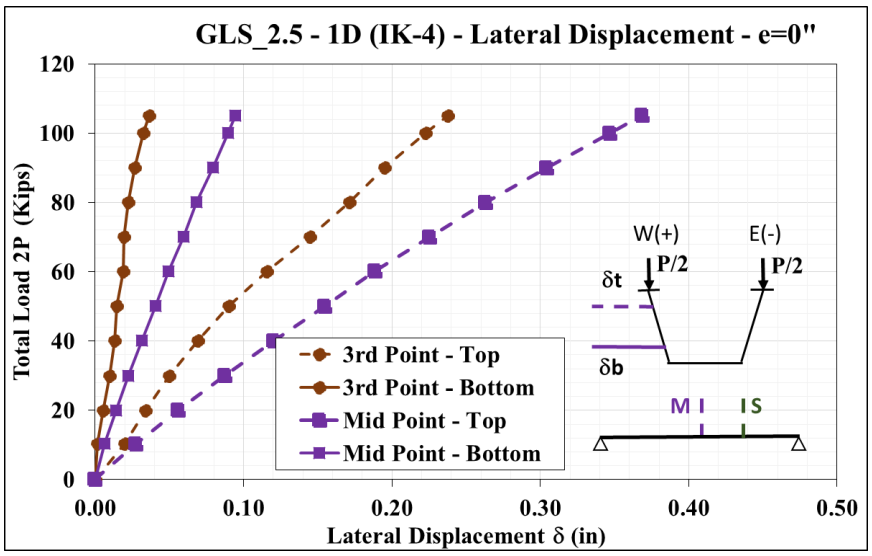

Figure C-56 – Total Load - Lateral Displacement - GLS_2.5

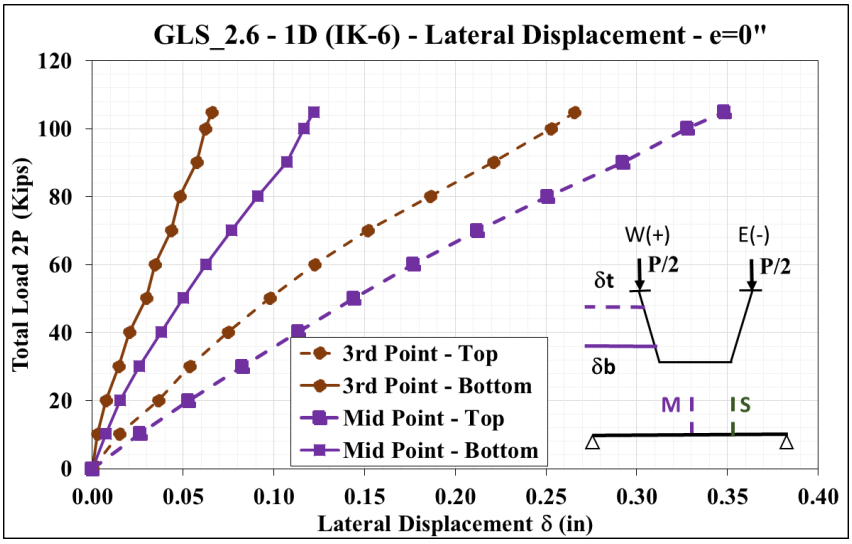

Figure C-57 – Total Load - Lateral Displacement - GLS_2.6

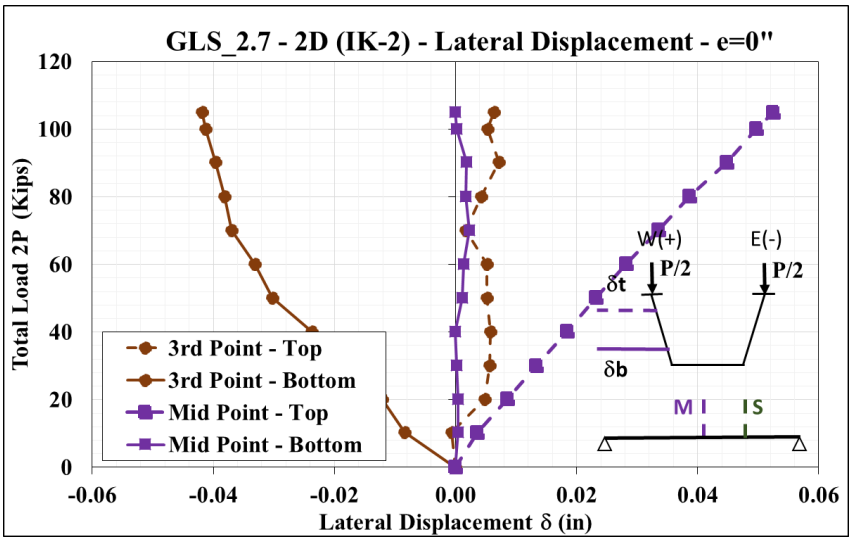

Figure C-58 – Total Load - Lateral Displacement - GLS_2.7

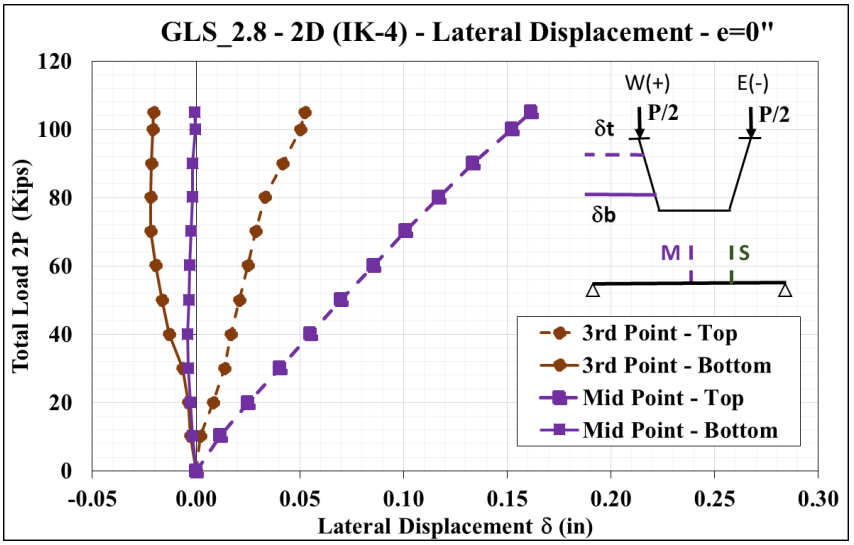

Figure C-59 – Total Load - Lateral Displacement - GLS_2.8

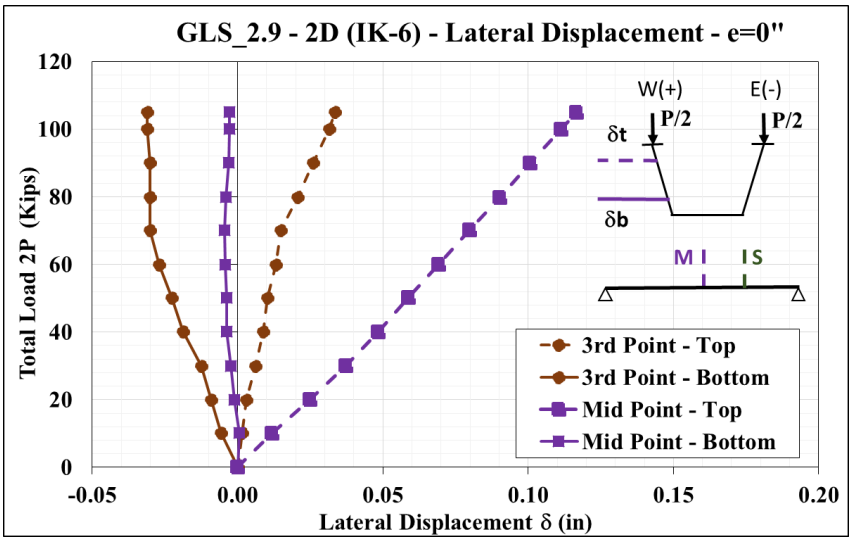

Figure C-60 – Total Load - Lateral Displacement - GLS_2.9

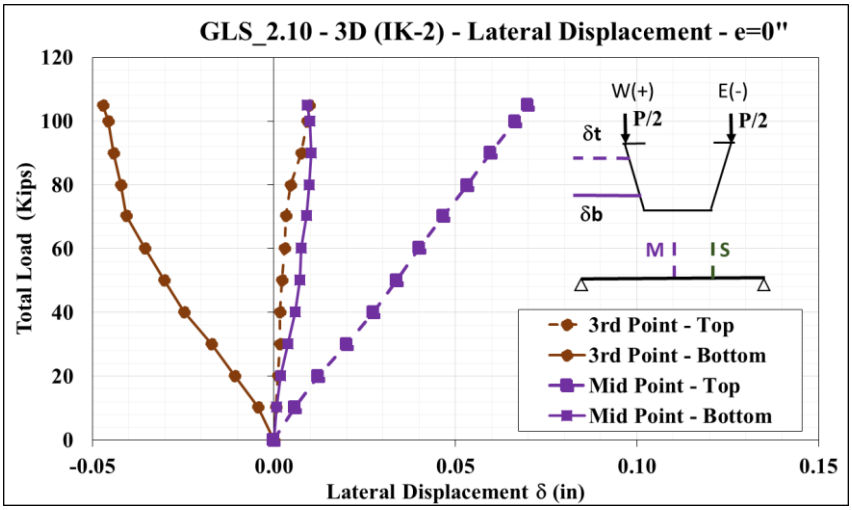

Figure C-61 – Total Load - Lateral Displacement - GLS_2.10

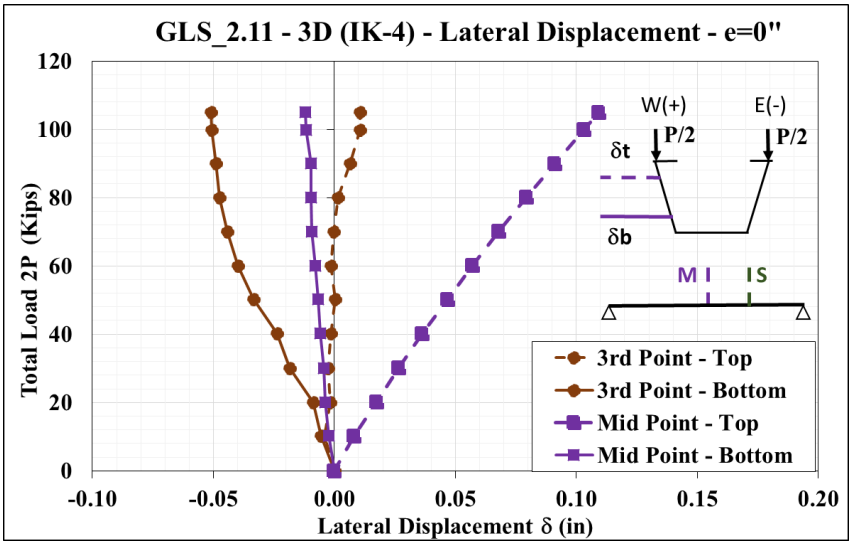

Figure C-62 – Total Load - Lateral Displacement - GLS_2.11

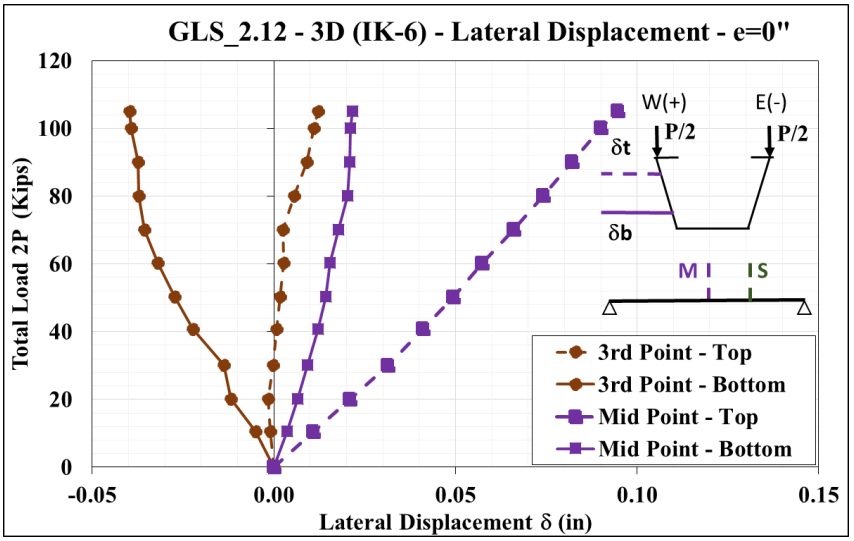

Figure C-63 – Total Load - Lateral Displacement - GLS_2.12

C.2.4 Tub #2 (Flange Offset Tub Girder) – Bracing Forces

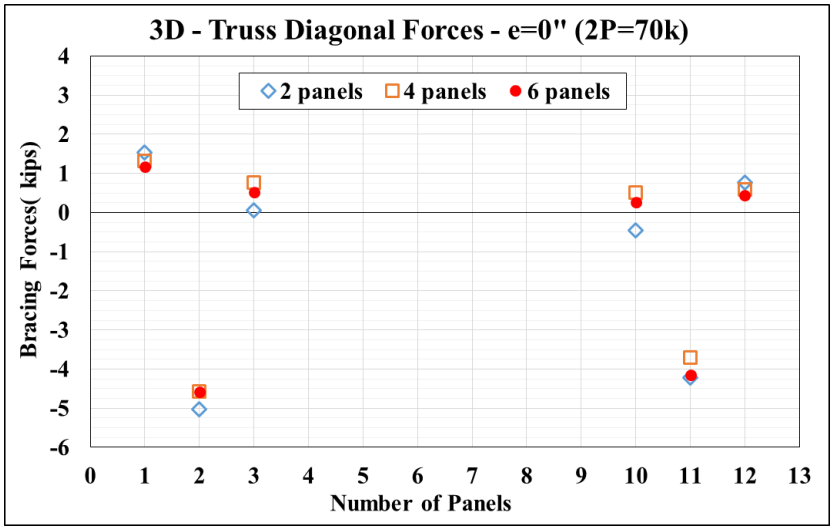

Figure C-64 – Top Lateral Bracing Diagonal Forces – 3 Truss Diagonals per End

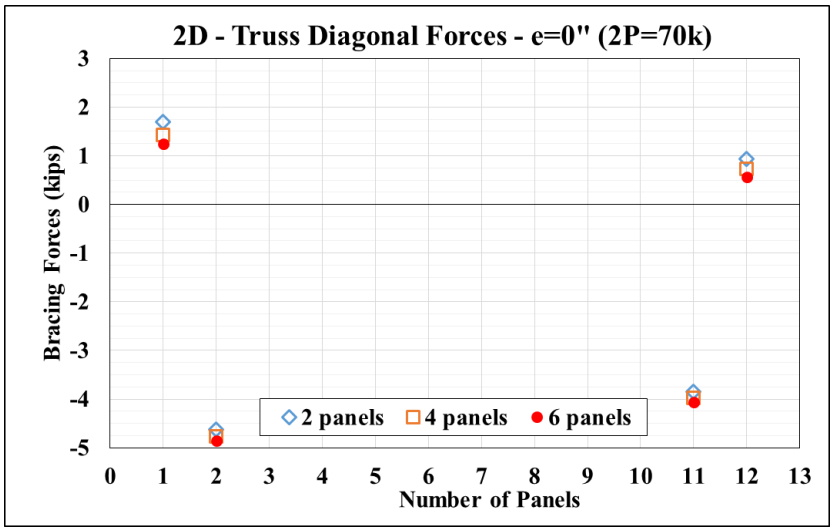

Figure C-65 – Top Lateral Bracing Diagonal Forces – 2 Truss Diagonals per End

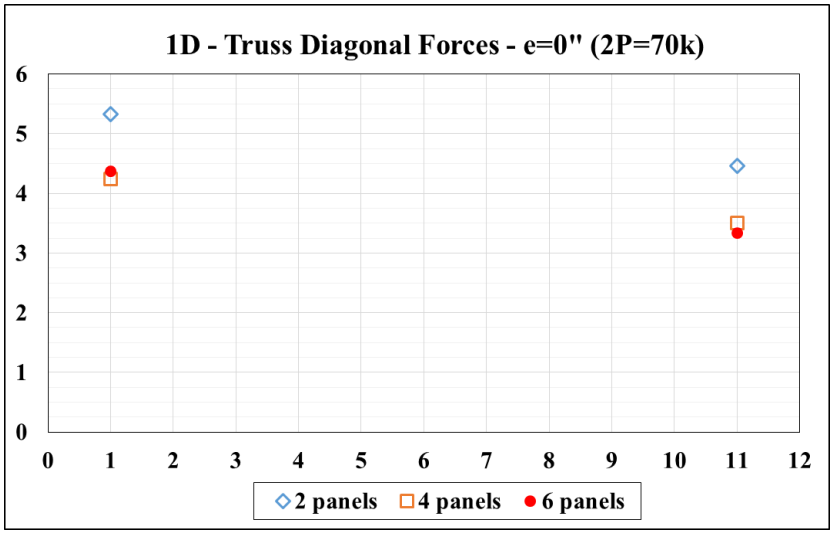

Figure C-66 – Top Lateral Bracing Diagonal Forces -1 Truss Diagonals per End

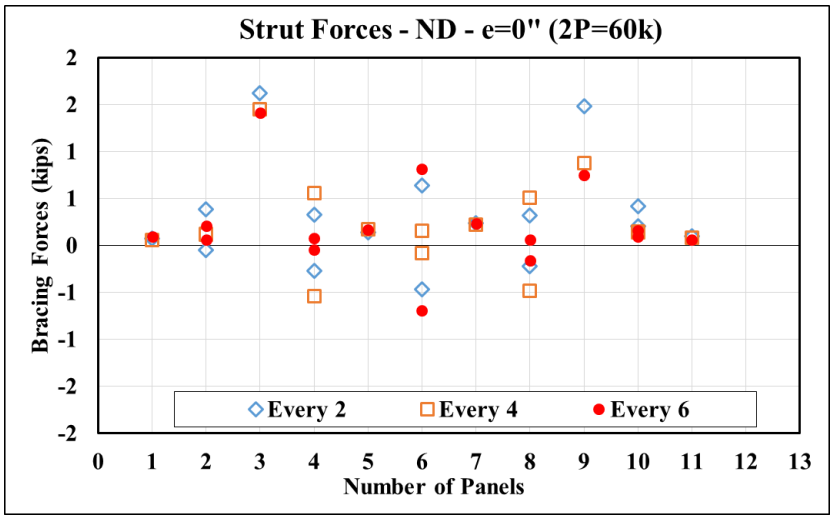

Figure C-67 – Strut Forces - 0 Truss Diagonals per End

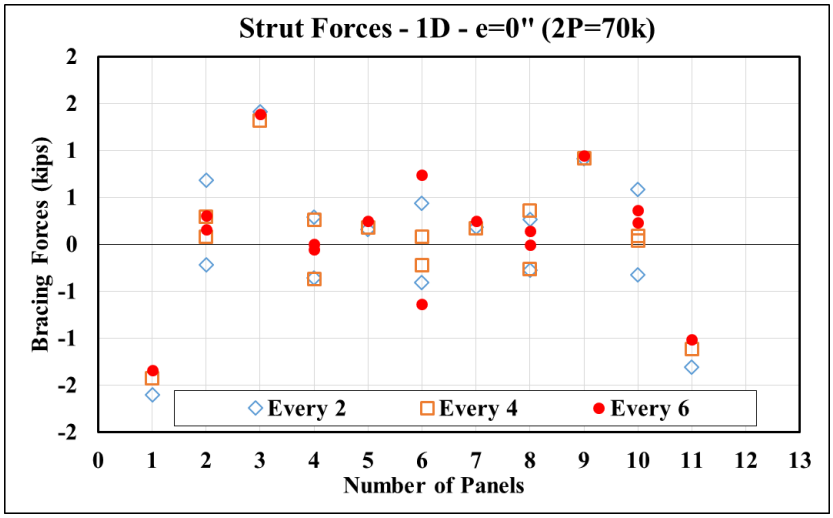

Figure C-68 – Strut Forces - 1 Truss Diagonals per End

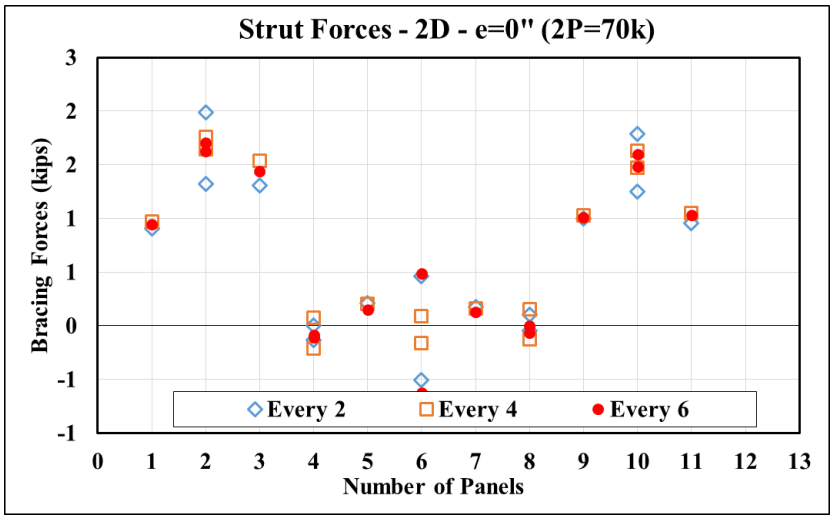

Figure C-69 – Strut Forces - 2 Truss Diagonals per End

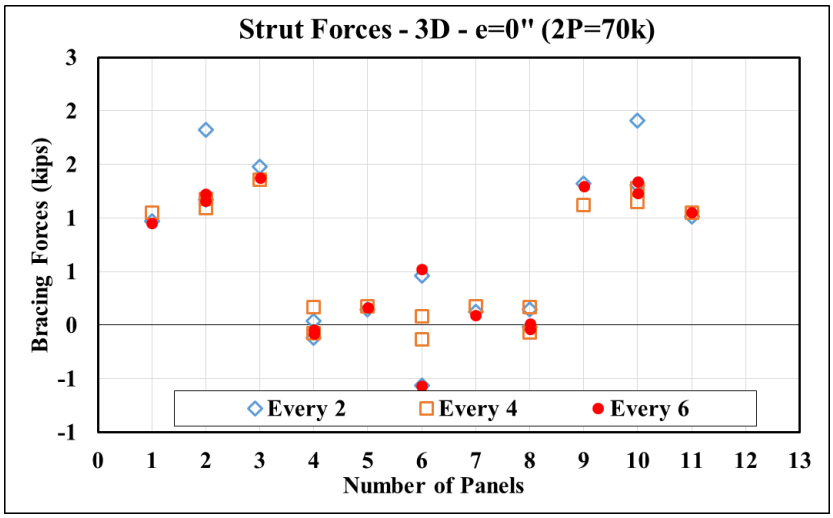

Figure C-70 – Strut Forces - 3 Truss Diagonals per End

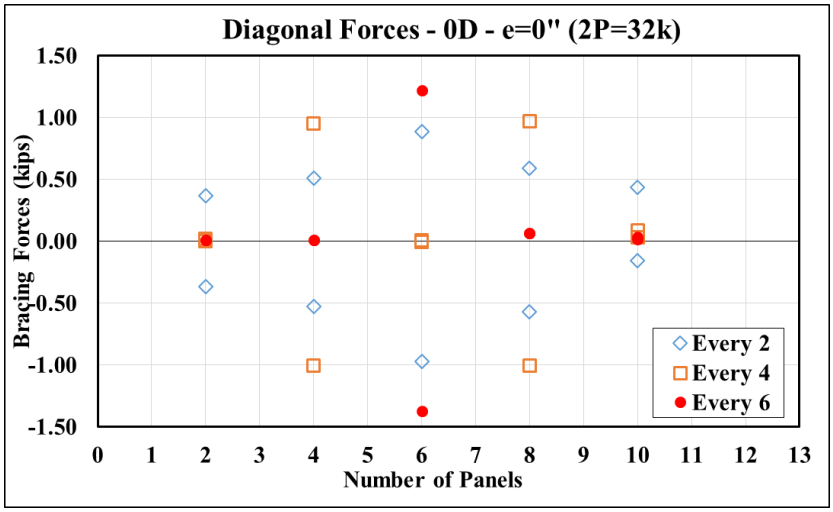

Figure C-71 – K-frame Diagonal Forces - 0 Truss Diagonals per End

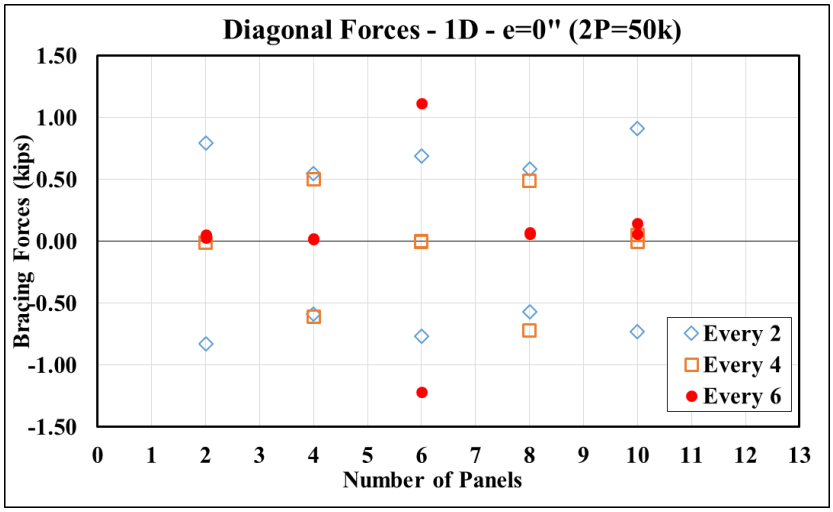

Figure C-72 – K-frame Diagonal Forces - 1 Truss Diagonals per End

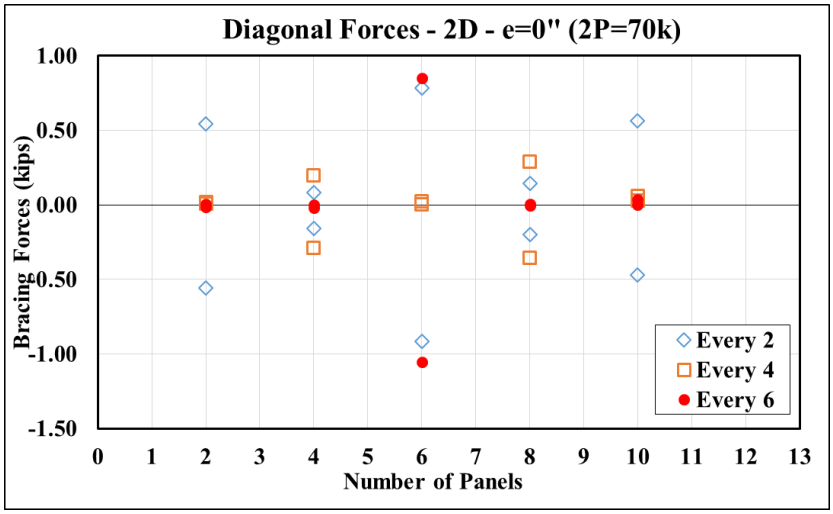

Figure C-73 – K-frame Diagonal Forces - 2 Truss Diagonals per End

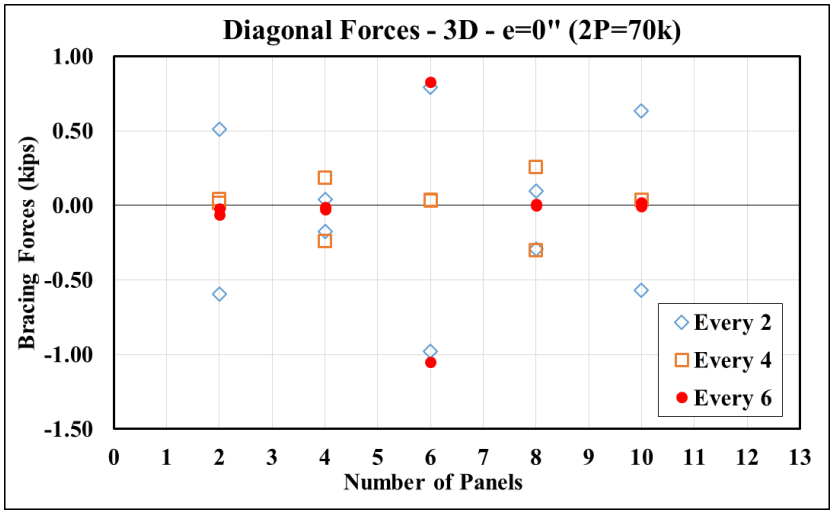

Figure C-74 – K-frame Diagonal Forces - 3 Truss Diagonals per End

C.2.5 Tub #3 (Flatter Web Tub Girder) – Load-Deflection Response

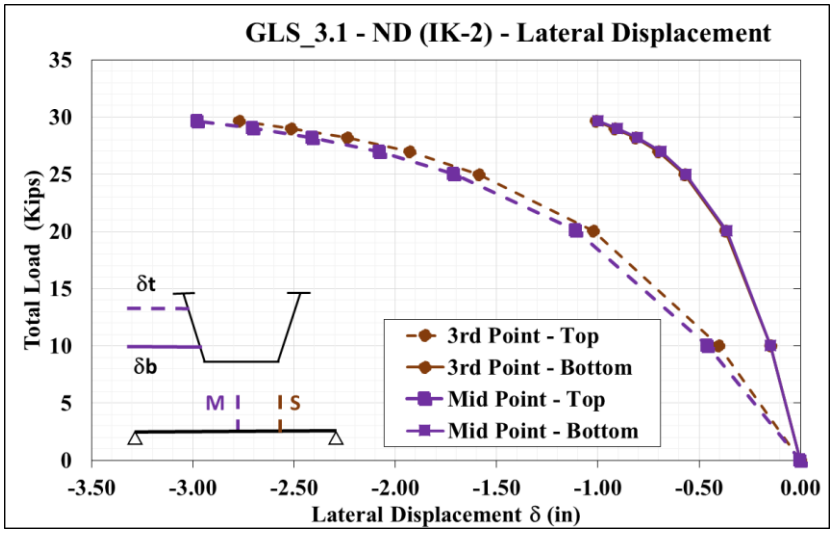

Figure C-75 – Total Load - Lateral Displacement - GLS_3.1

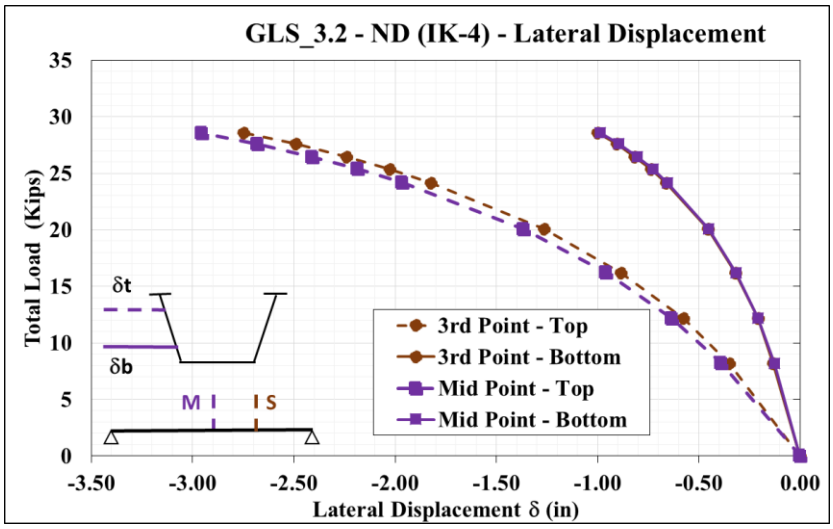

Figure C-76 – Total Load - Lateral Displacement - GLS_3.2

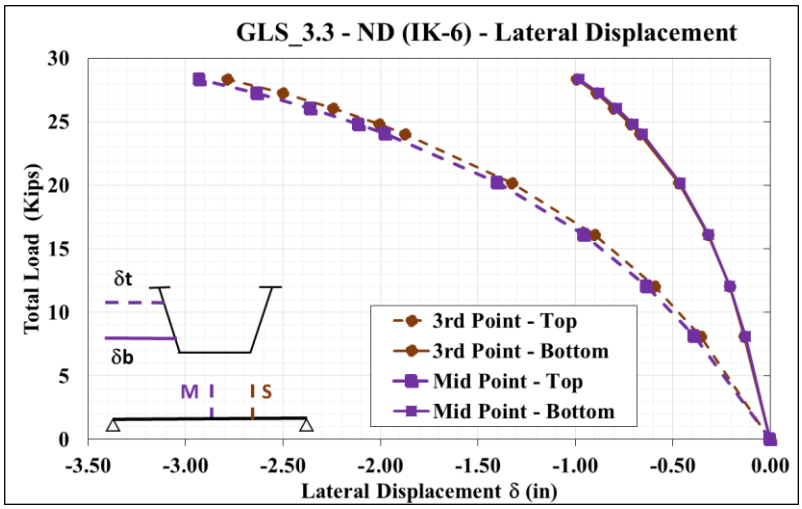

Figure C-77 – Total Load - Lateral Displacement - GLS_3.3

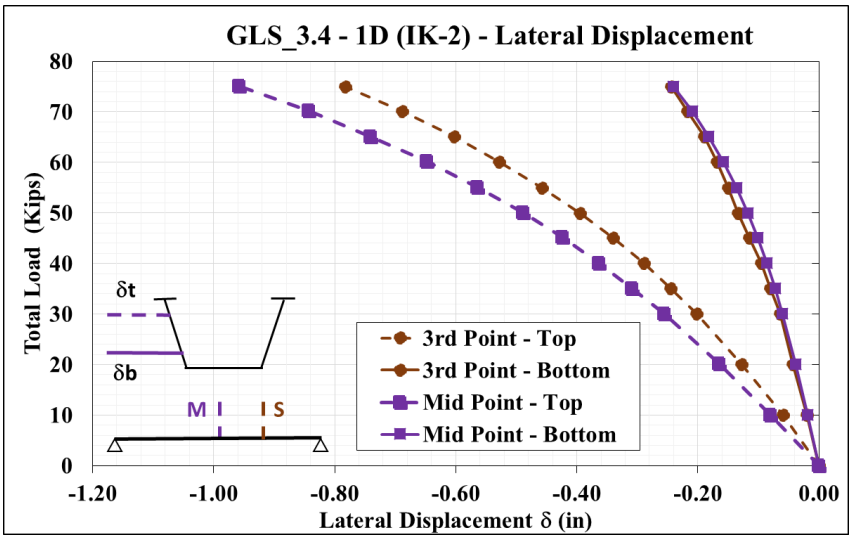

Figure C-78 – Total Load - Lateral Displacement - GLS_3.4

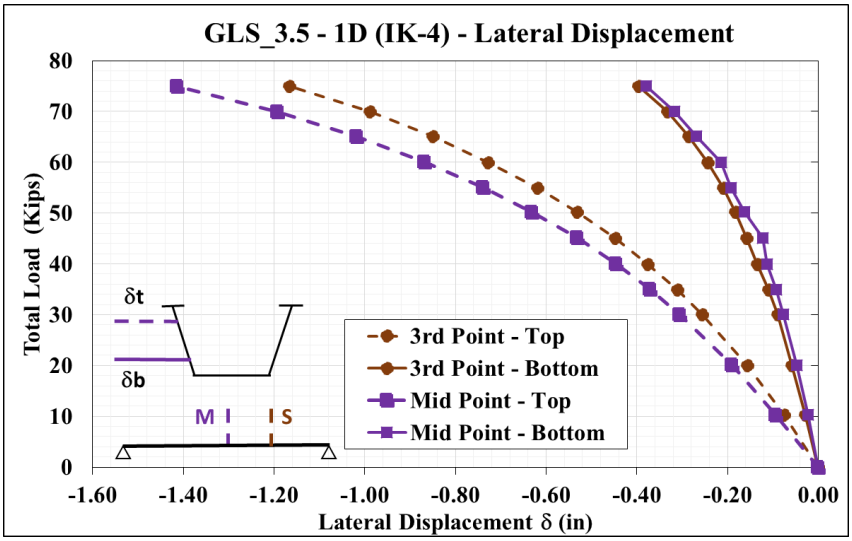

Figure C-79 – Total Load - Lateral Displacement - GLS_3.5

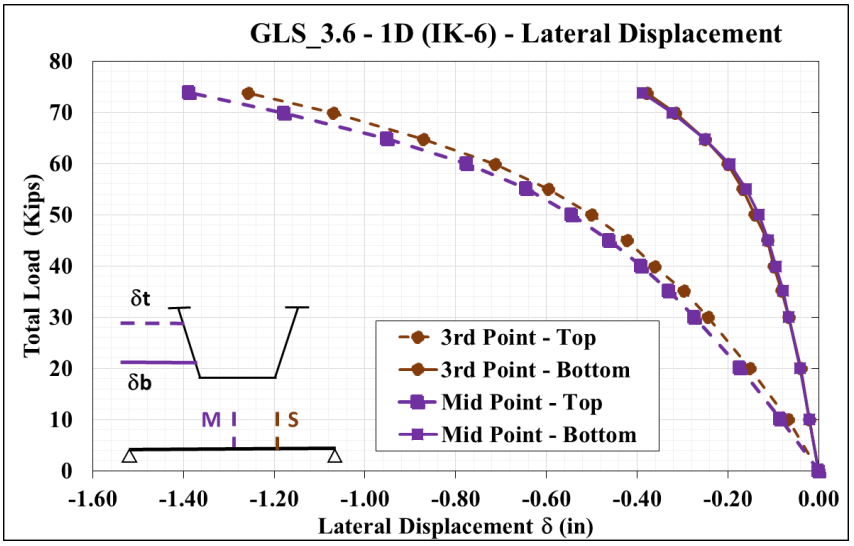

Figure C-80 – Total Load - Lateral Displacement - GLS_3.6

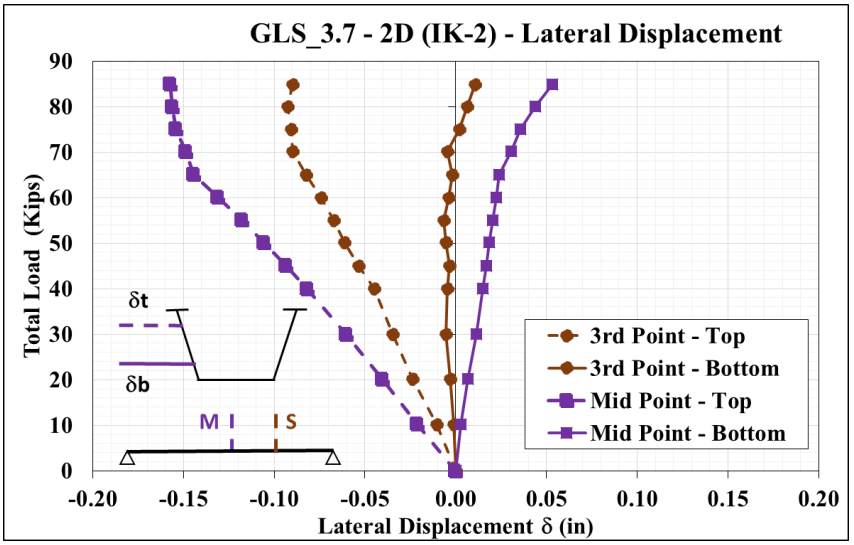

Figure C-81 – Total Load - Lateral Displacement - GLS_3.7

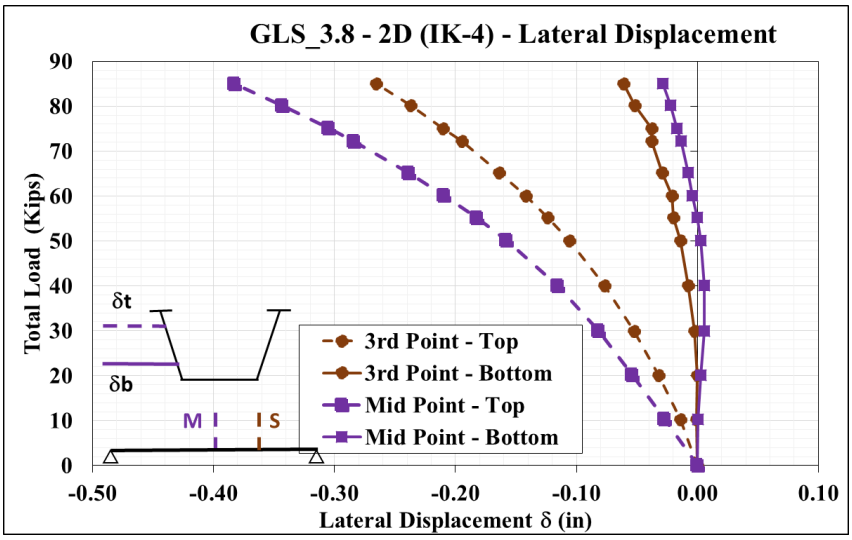

Figure C-82 – Total Load - Lateral Displacement - GLS_3.8

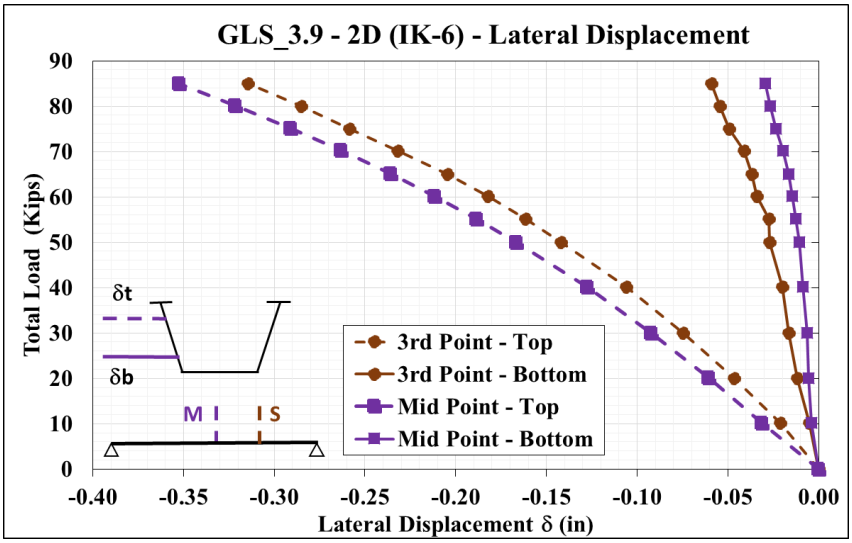

Figure C-83 – Total Load - Lateral Displacement - GLS_3.9

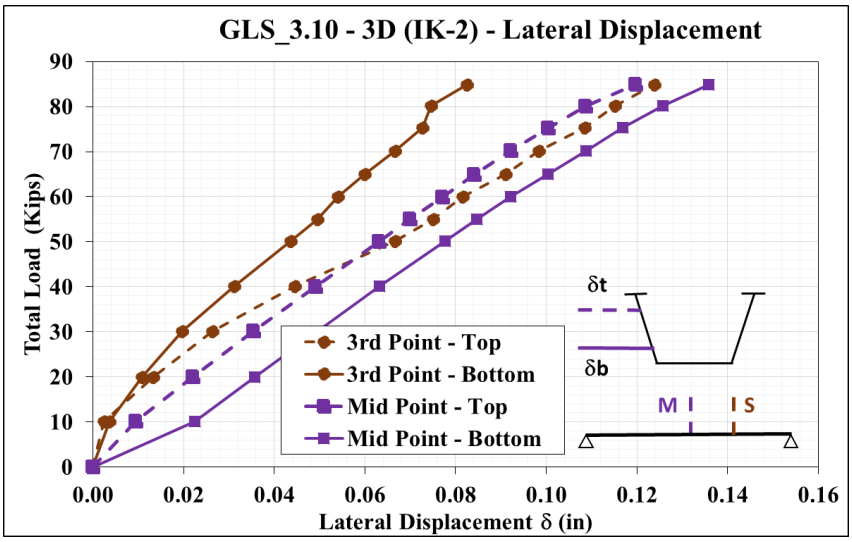

Figure C-84 – Total Load - Lateral Displacement - GLS_3.10

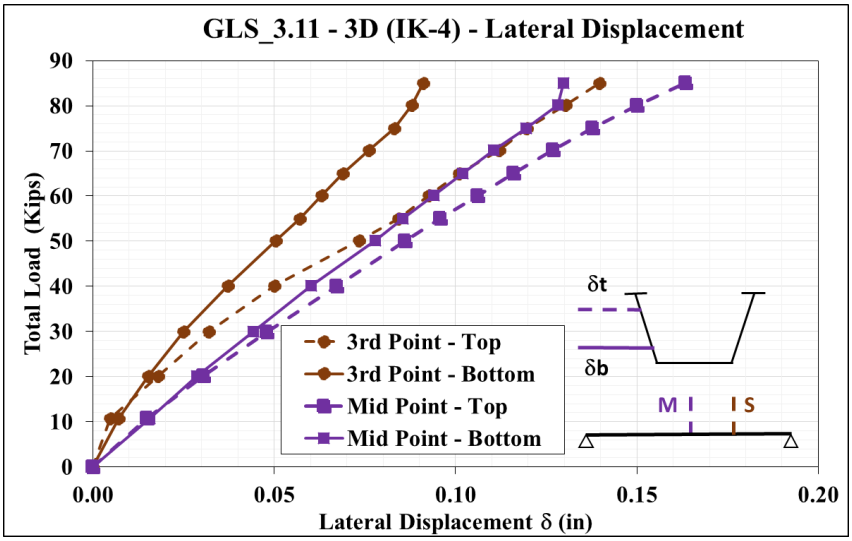

Figure C-85 – Total Load - Lateral Displacement - GLS_3.11

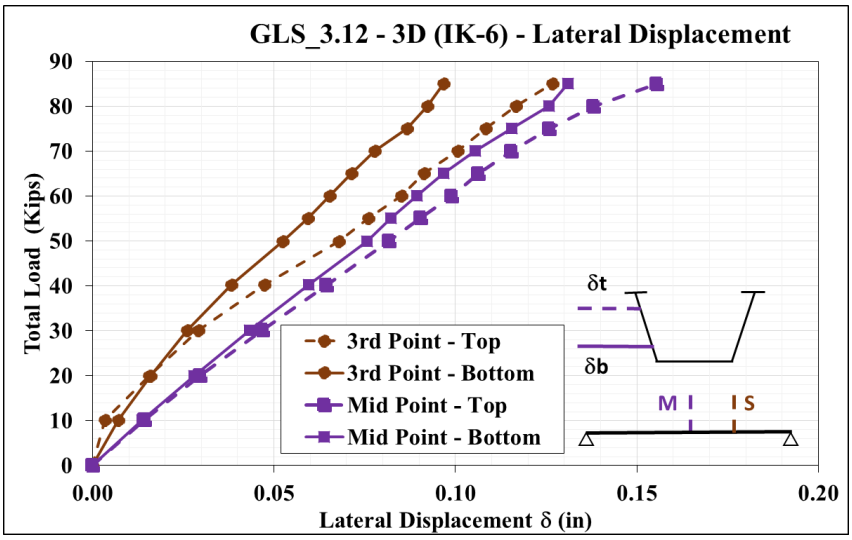

Figure C-86 – Total Load - Lateral Displacement - GLS_3.12

C.2.6 Tub #3 (Flatter Web Tub Girder) – Bracing Forces

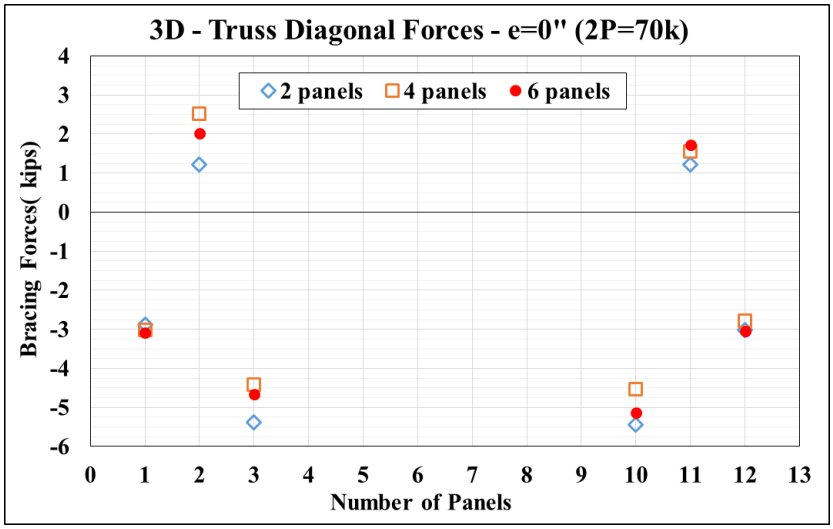

Figure C-87 – Top Lateral Bracing Diagonal Forces – 3 Truss Diagonals per End

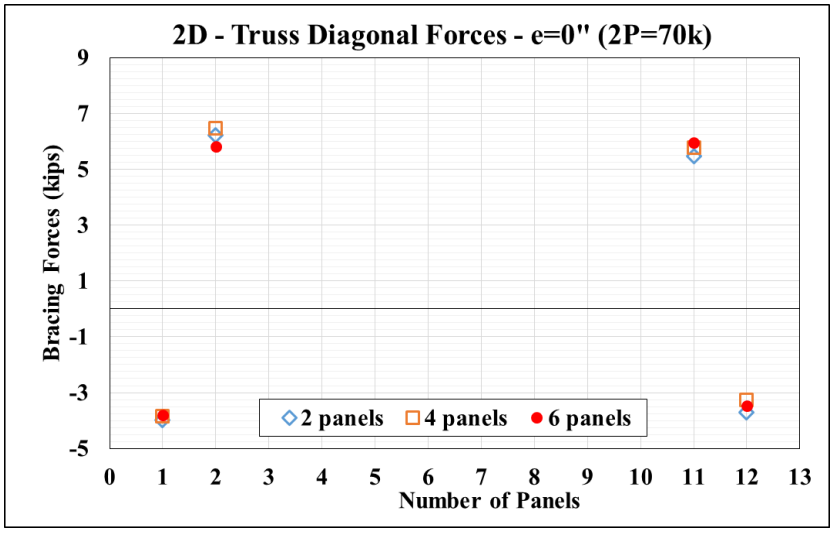

Figure C-88 – Top Lateral Bracing Diagonal Forces – 2 Truss Diagonals per End

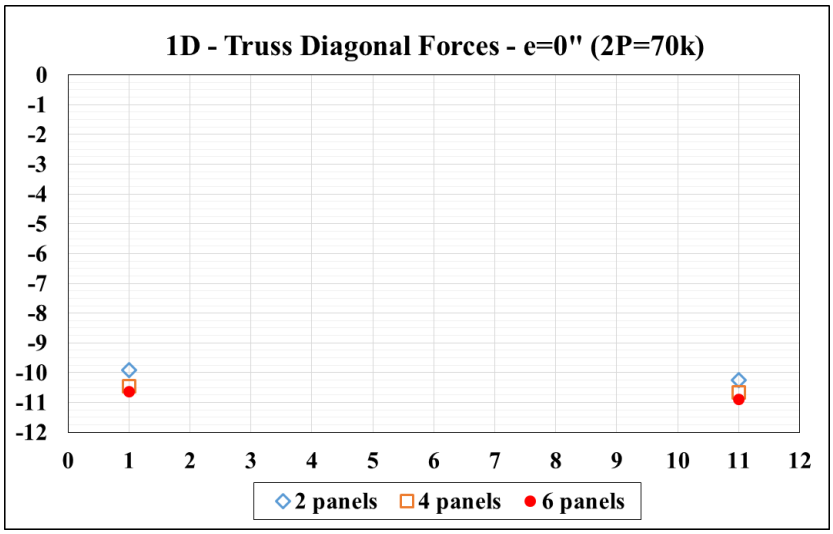

Figure C-89 – Top Lateral Bracing Diagonal Forces -1 Truss Diagonals per End

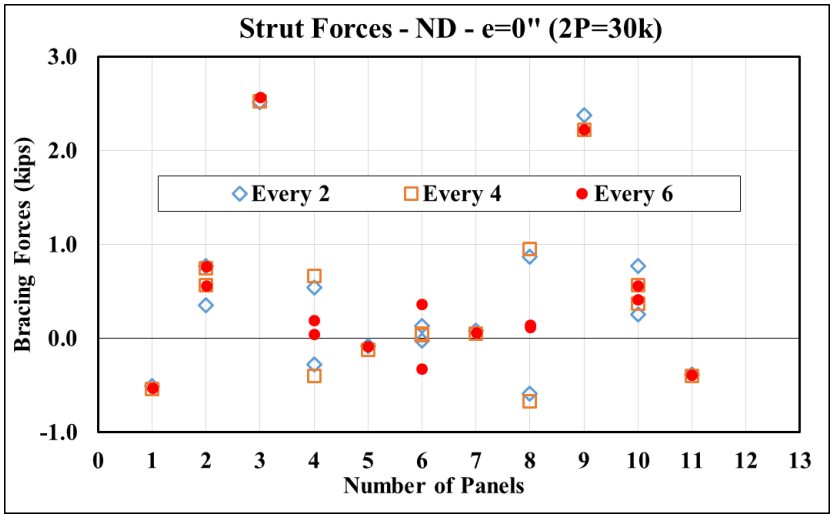

Figure C-90 – Strut Forces - 0 Truss Diagonals per End

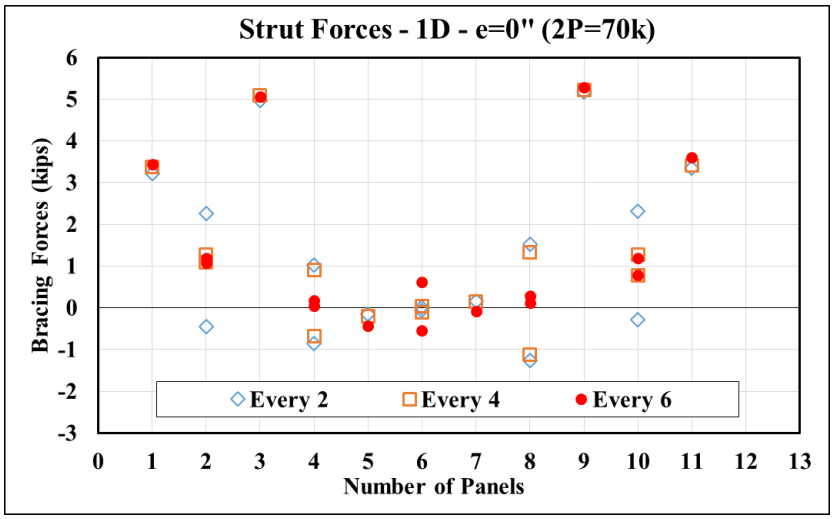

Figure C-91 – Strut Forces - 1 Truss Diagonals per End

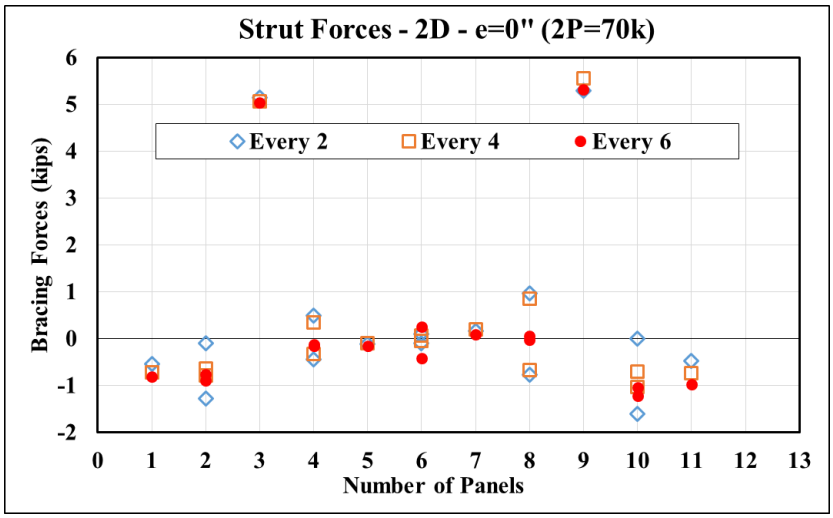

Figure C-92 – Strut Forces - 2 Truss Diagonals per End

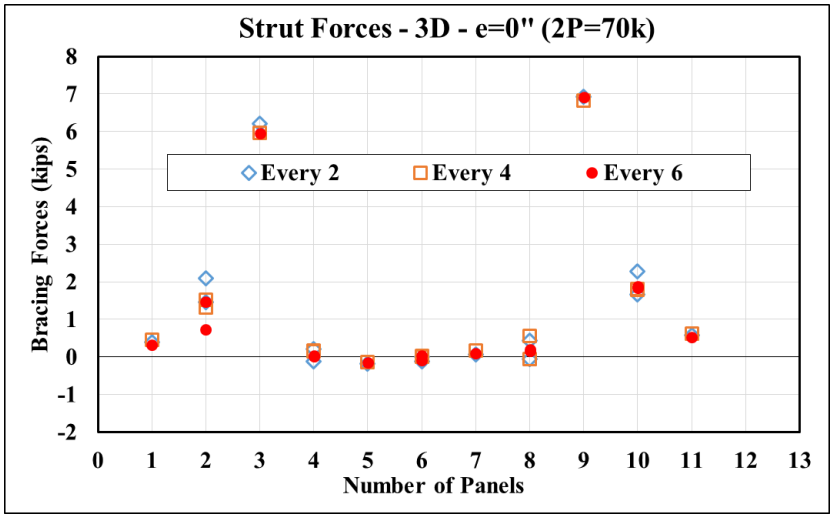

Figure C-93 – Strut Forces - 3 Truss Diagonals per End

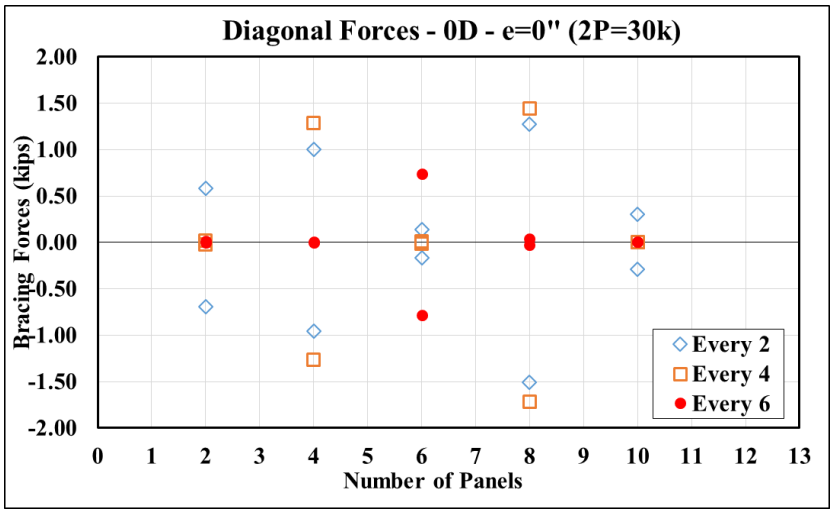

Figure C-94 – K-frame Diagonal Forces - 0 Truss Diagonals per End

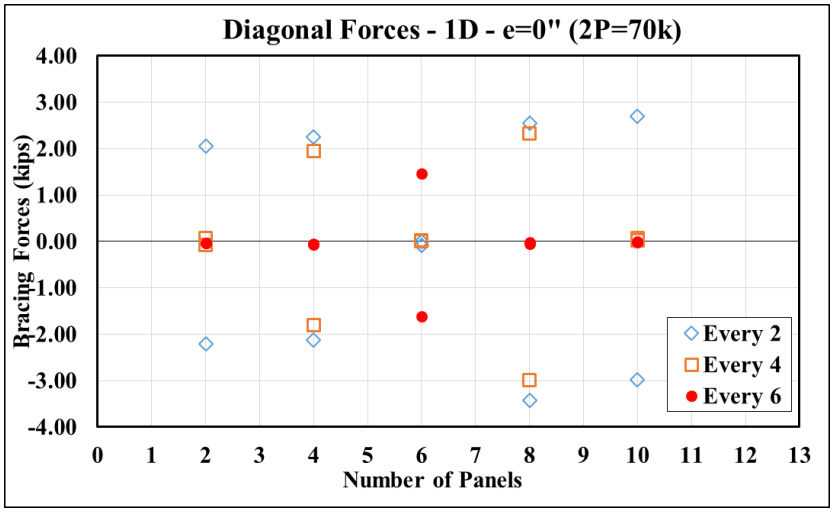

Figure C-95 – K-frame Diagonal Forces - 1 Truss Diagonals per End

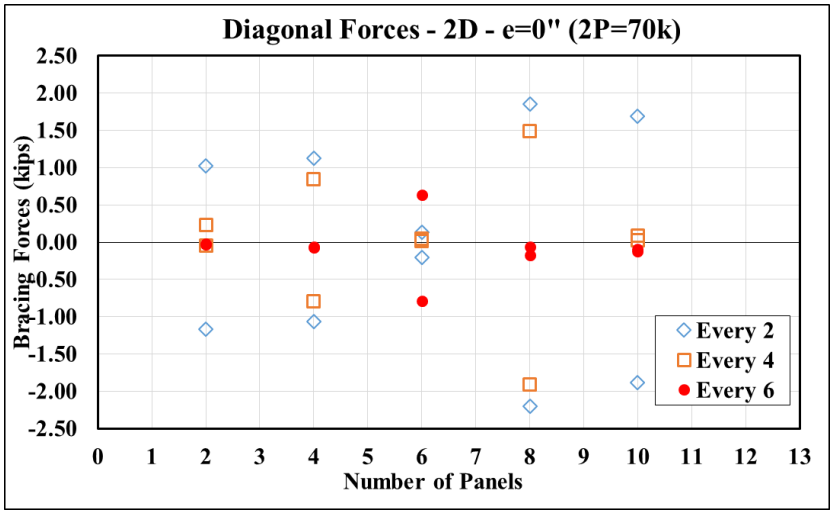

Figure C-96 – K-frame Diagonal Forces - 2 Truss Diagonals per End

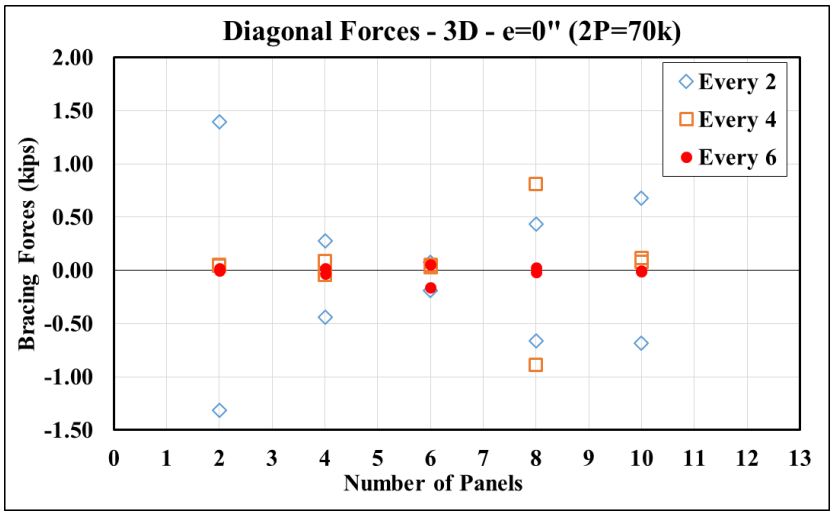

Figure C-97 – K-frame Diagonal Forces - 3 Truss Diagonals per End

C.3 Bending plus Torsion Experimental Results

C.3.1 Tub #1 (Baseline Tub Girder) – Load-Deflection Response

Table C-3 – Bending plus Torsion Test Results – Tub #1

Test Code	Eccentricity (in)	Number of Diagonals	K-Frame Location
GLS_1.13	8	0	2-Panel
GLS_1.14	8	0	4-Panel
GLS_1.15	8	0	6-Panel
GLS_1.16	8	1	2-Panel
GLS_1.17	8	1	4-Panel
GLS_1.18	8	1	6-Panel
GLS_1.19	8	2	2-Panel
GLS_1.20	8	2	4-Panel
GLS_1.21	8	2	6-Panel
GLS_1.22	8	3	2-Panel
GLS_1.23	8	3	4-Panel
GLS_1.24	8	3	6-Panel
GLS_1.25	16	0	2-Panel
GLS_1.26	16	0	4-Panel
GLS_1.27	16	0	6-Panel
GLS_1.28	16	1	2-Panel
GLS_1.29	16	1	4-Panel
GLS_1.30	16	1	6-Panel
GLS_1.31	16	2	2-Panel
GLS_1.32	16	2	4-Panel
GLS_1.33	16	2	6-Panel
GLS_1.34	16	3	2-Panel
GLS_1.35	16	3	4-Panel
GLS_1.36	16	3	6-Panel

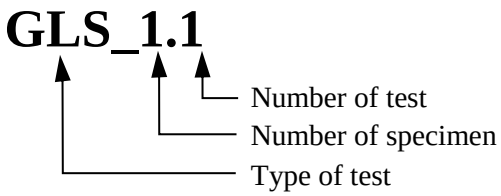

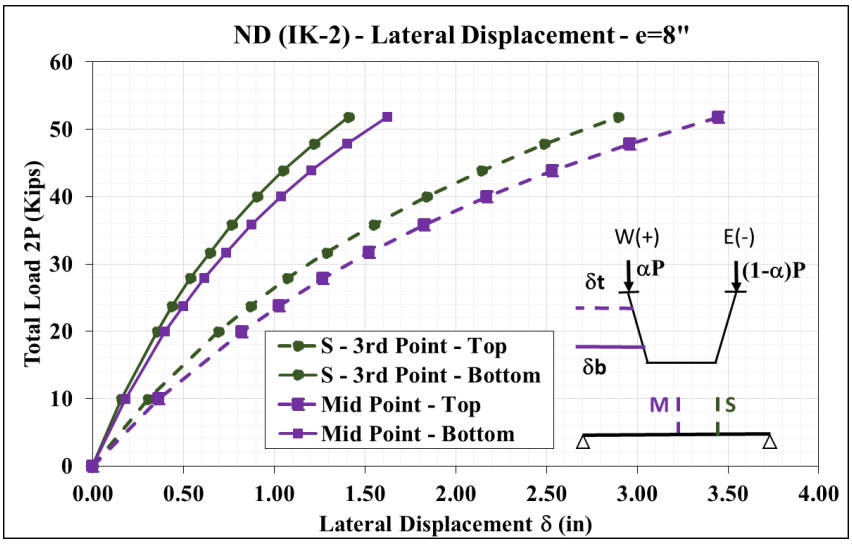

Figure C-98 – Total Load - Lateral Displacement - GLS_1.13

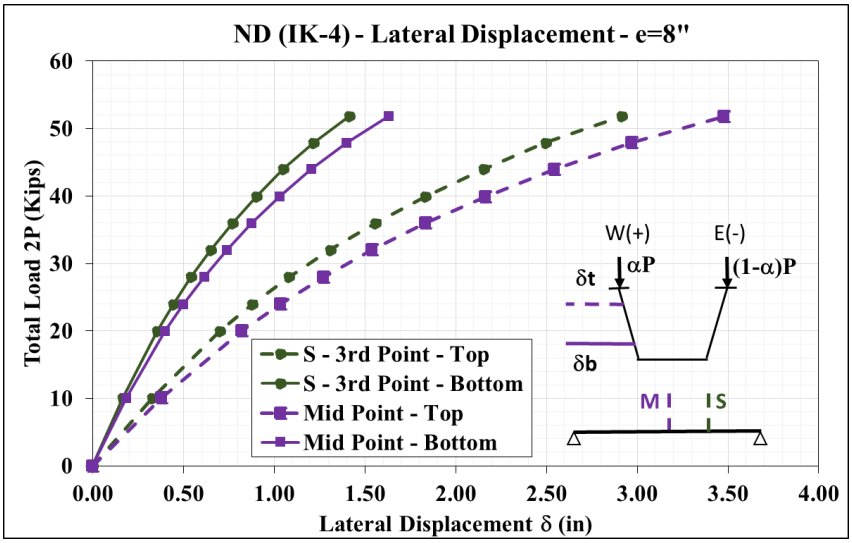

Figure C-99 – Total Load - Lateral Displacement - GLS_1.14

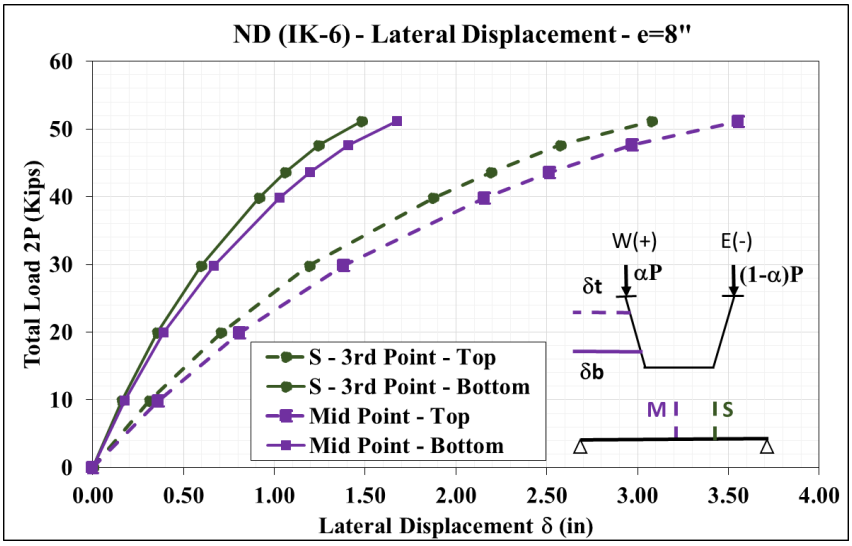

Figure C-100 – Total Load - Lateral Displacement - GLS_1.15

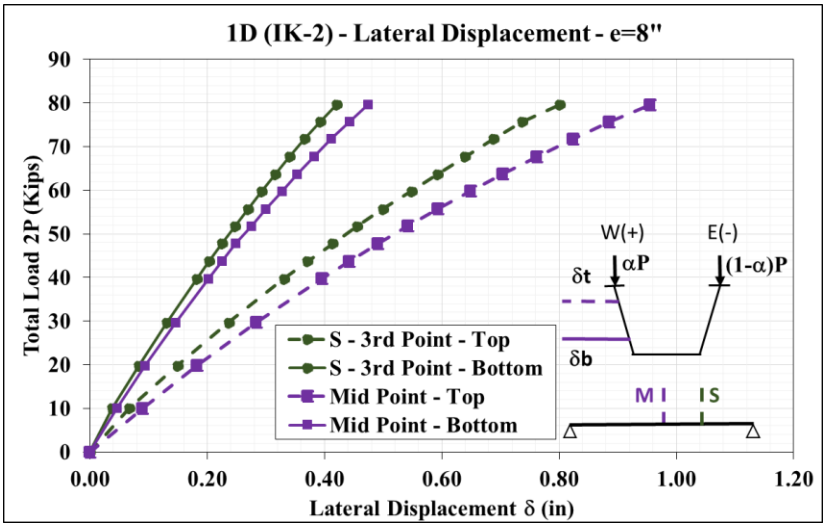

Figure C-101 – Total Load - Lateral Displacement - GLS_1.16

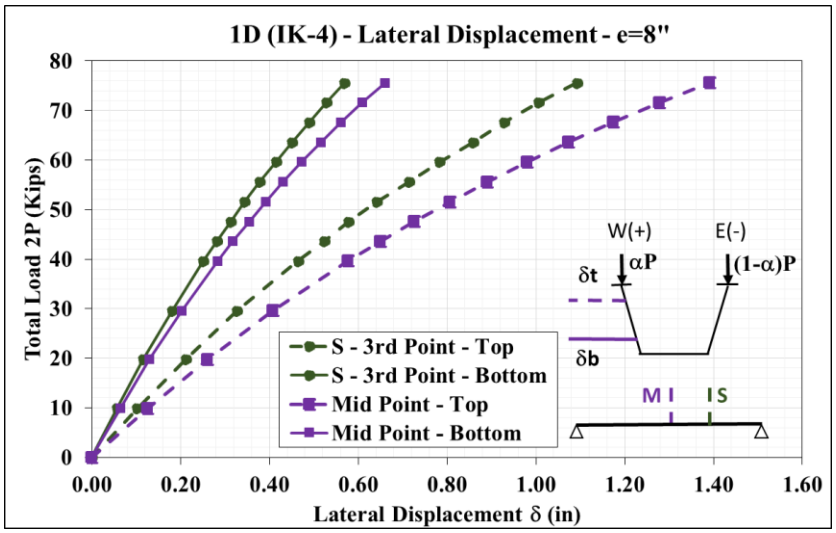

Figure C-102 – Total Load - Lateral Displacement - GLS_1.17

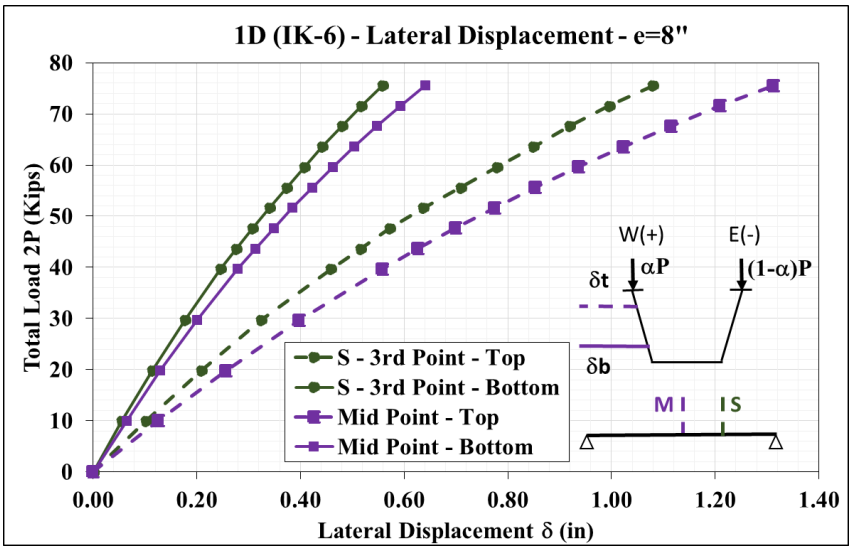

Figure C-103 – Total Load - Lateral Displacement - GLS_1.18

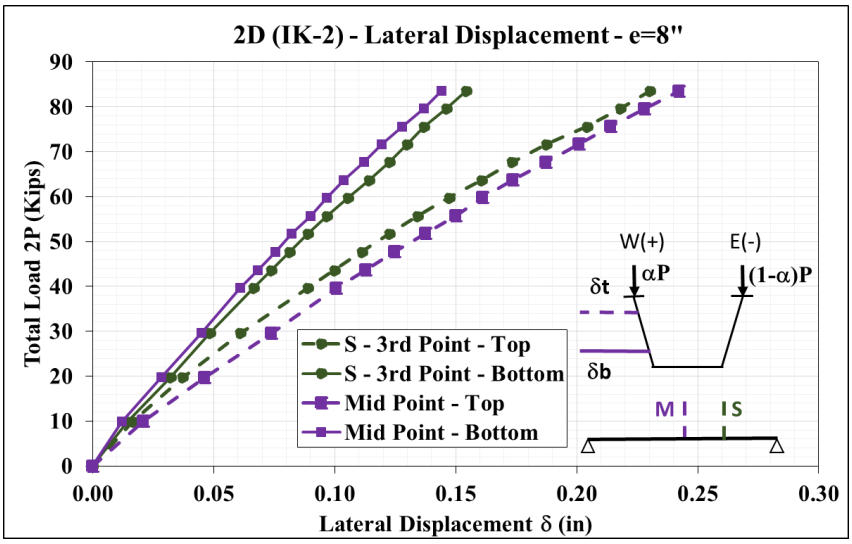

Figure C-104 – Total Load - Lateral Displacement - GLS_1.19

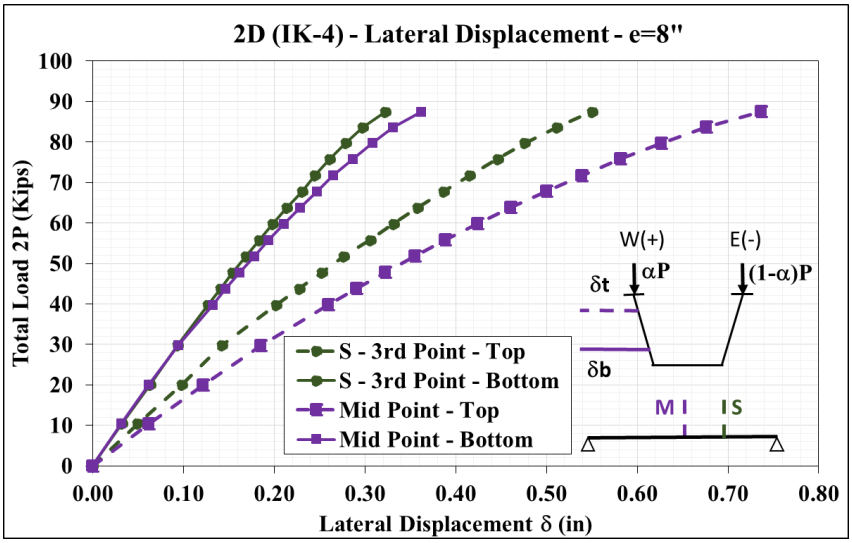

Figure C-105 – Total Load - Lateral Displacement - GLS_1.20

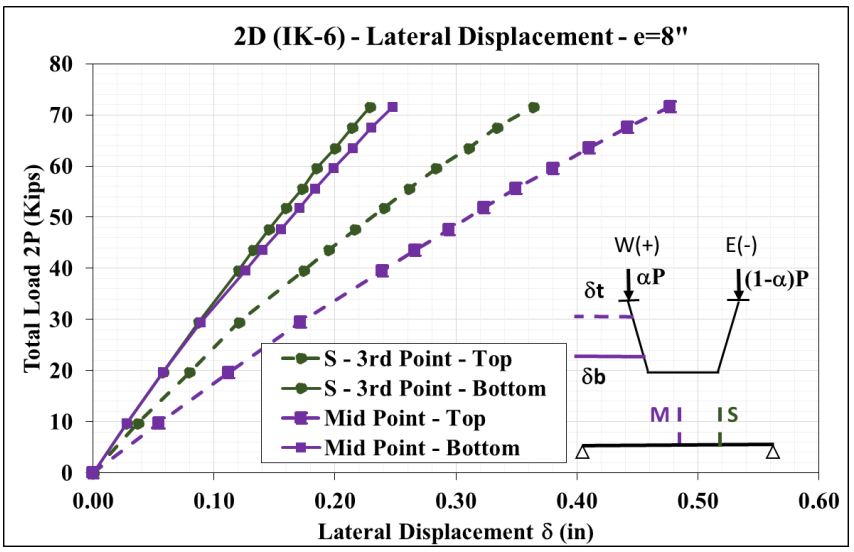

Figure C-106 – Total Load - Lateral Displacement - GLS_1.21

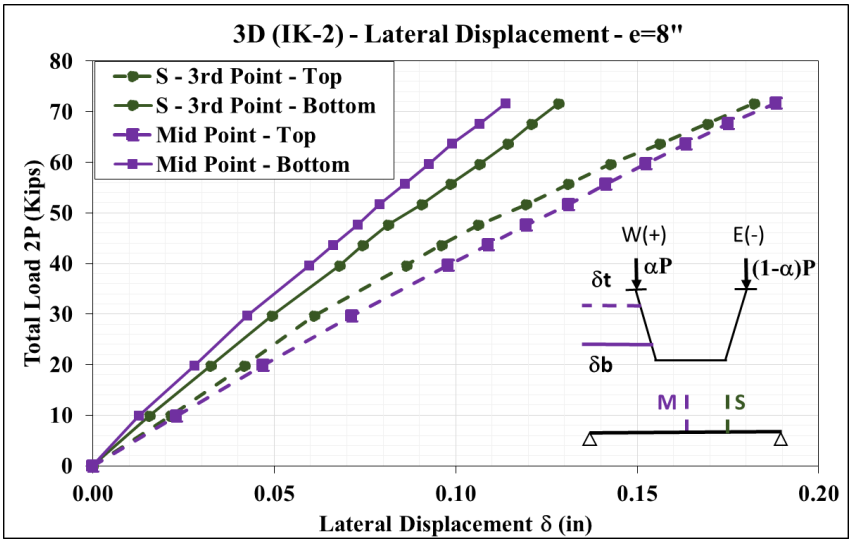

Figure C-107 – Total Load - Lateral Displacement - GLS_1.22

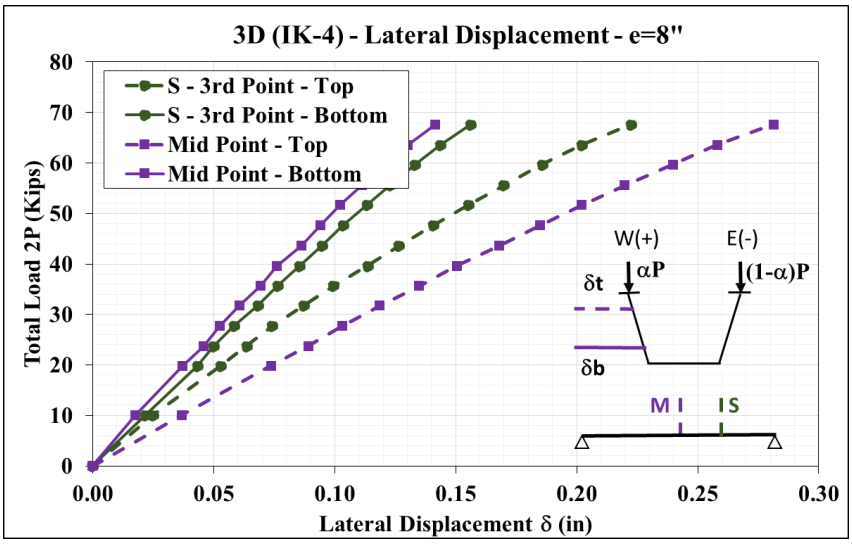

Figure C-108 – Total Load - Lateral Displacement - GLS_1.23

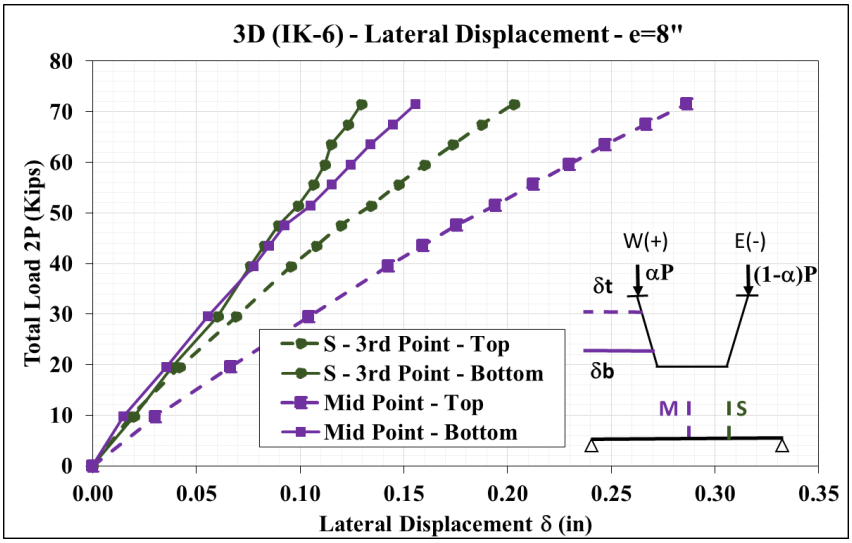

Figure C-109 – Total Load - Lateral Displacement - GLS_1.24

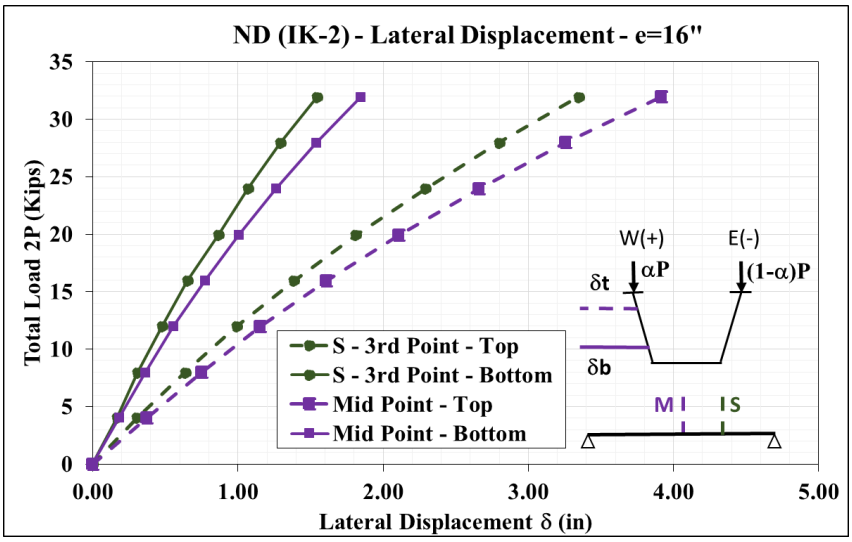

Figure C-110 – Total Load - Lateral Displacement - GLS_1.25

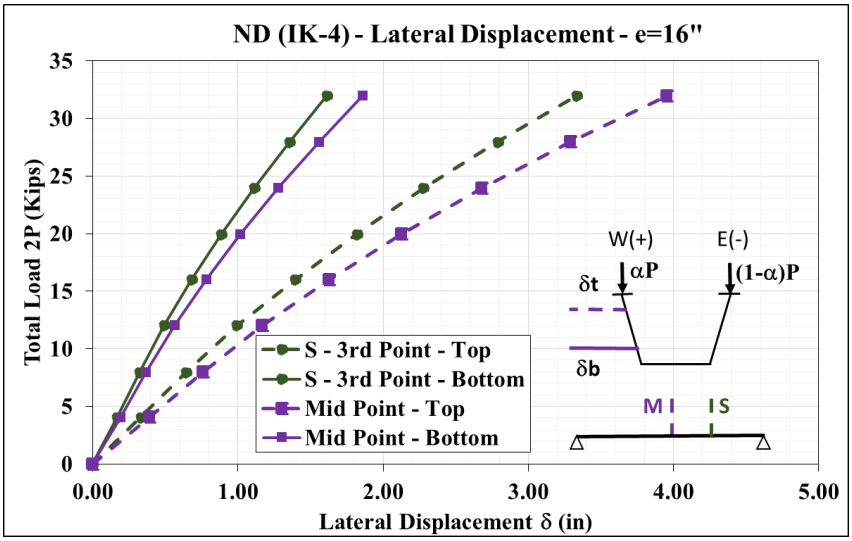

Figure C-111 – Total Load - Lateral Displacement - GLS_1.26

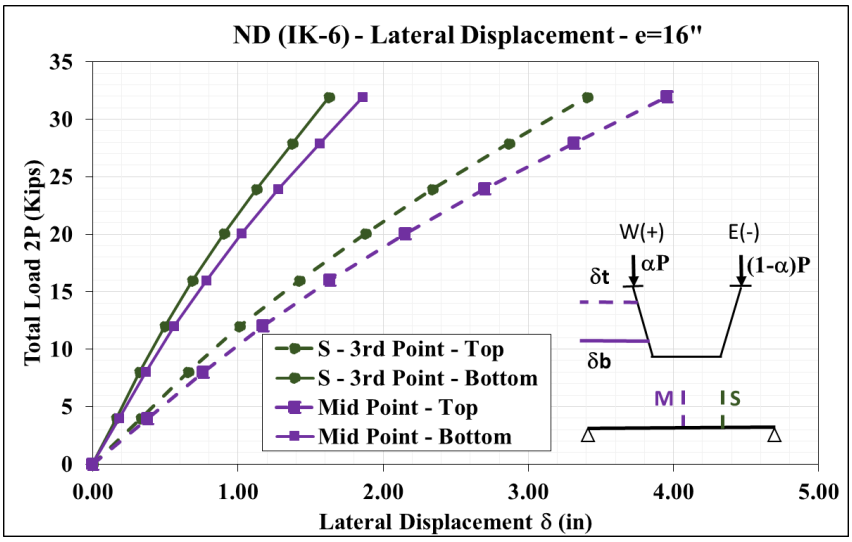

Figure C-112 – Total Load - Lateral Displacement - GLS_1.27

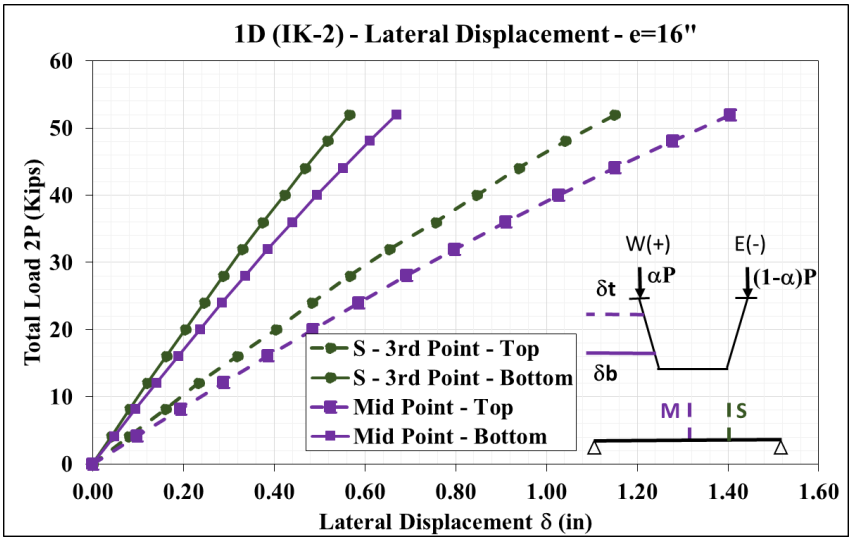

Figure C-113 – Total Load - Lateral Displacement - GLS_1.28

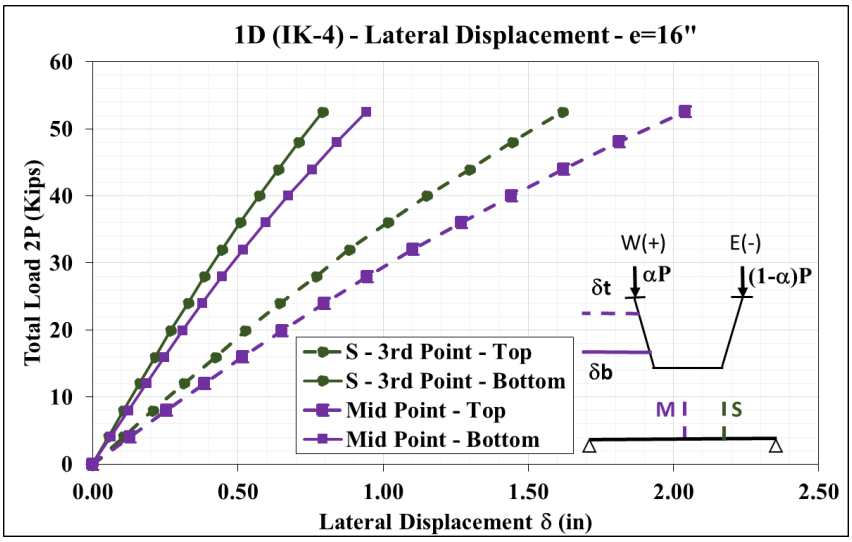

Figure C-114 – Total Load - Lateral Displacement - GLS_1.29

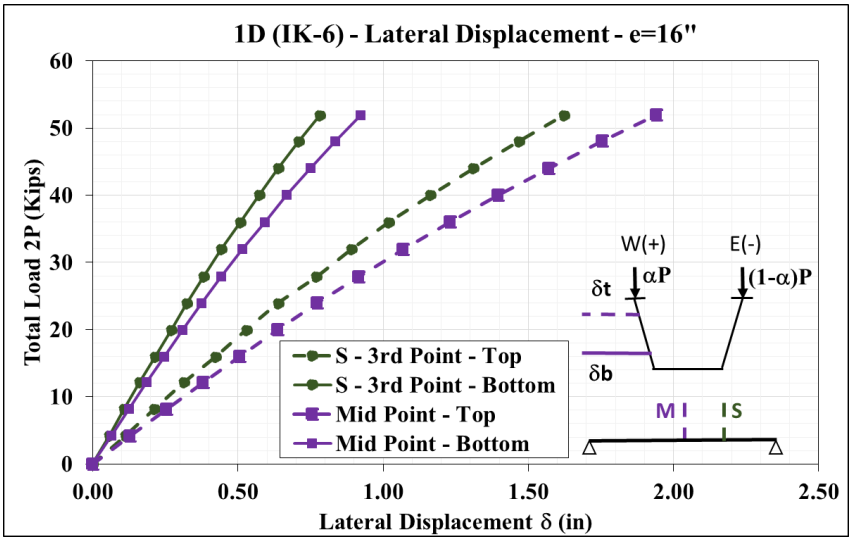

Figure C-115 – Total Load - Lateral Displacement - GLS_1.30

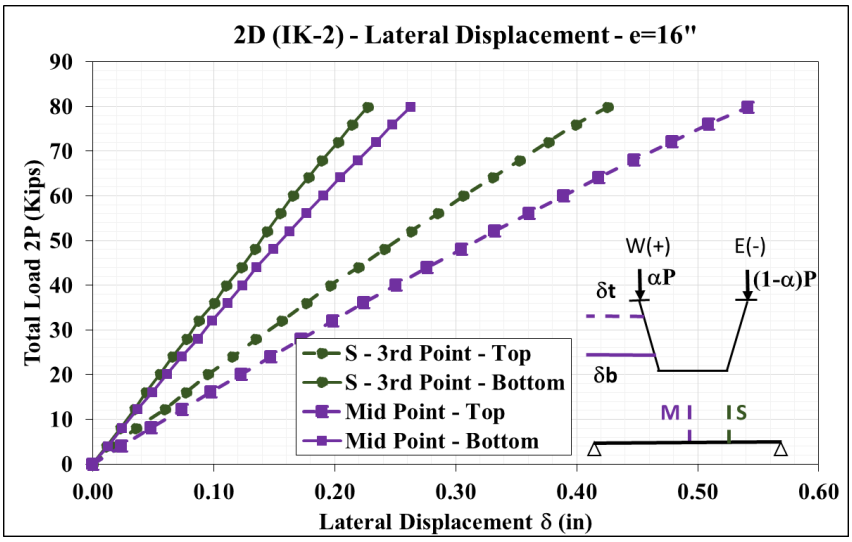

Figure C-116 – Total Load - Lateral Displacement - GLS_1.31

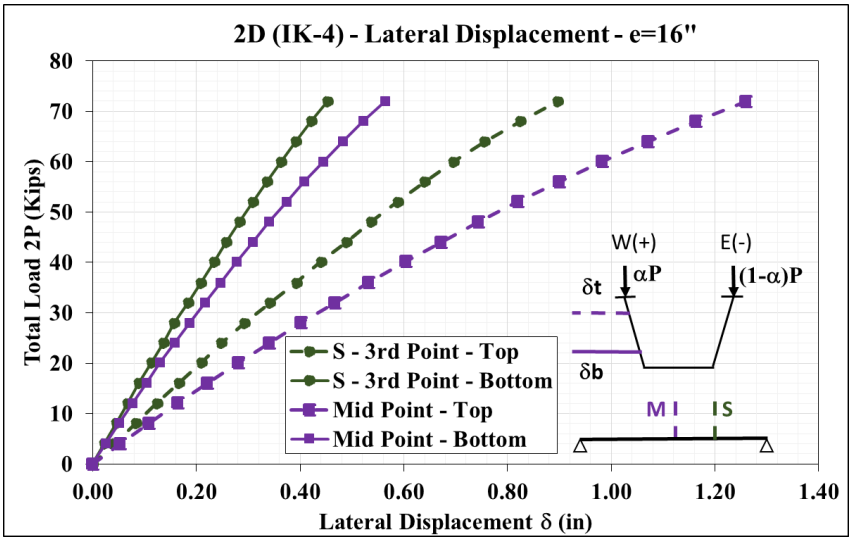

Figure C-117 – Total Load - Lateral Displacement - GLS_1.32

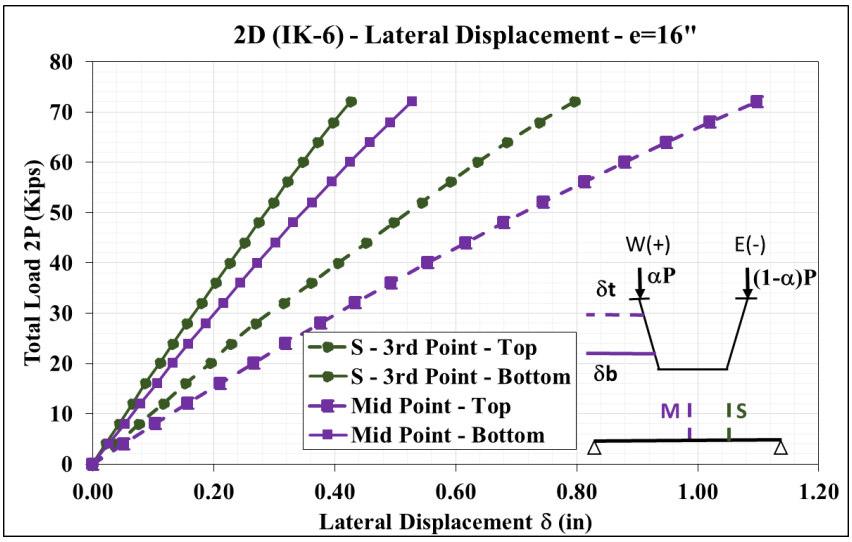

Figure C-118 – Total Load - Lateral Displacement - GLS_1.33

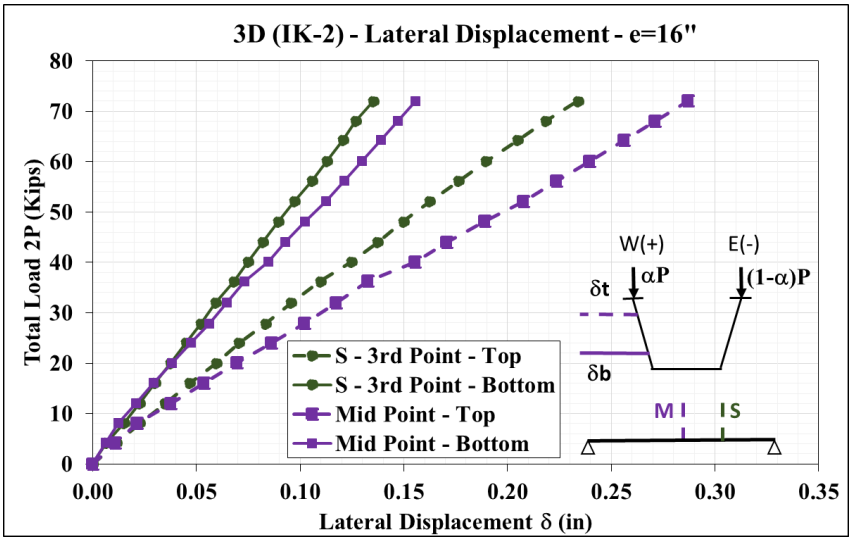

Figure C-119 – Total Load - Lateral Displacement - GLS_1.34

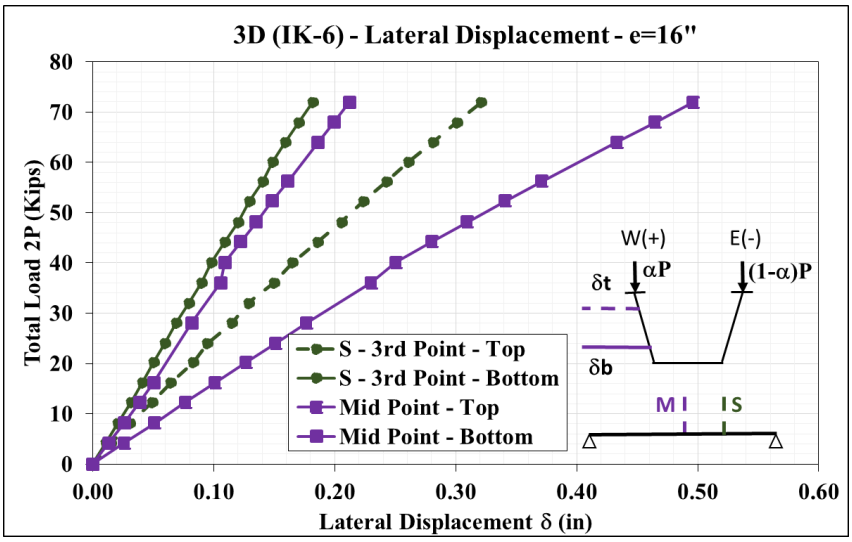

Figure C-120 – Total Load - Lateral Displacement - GLS_1.35

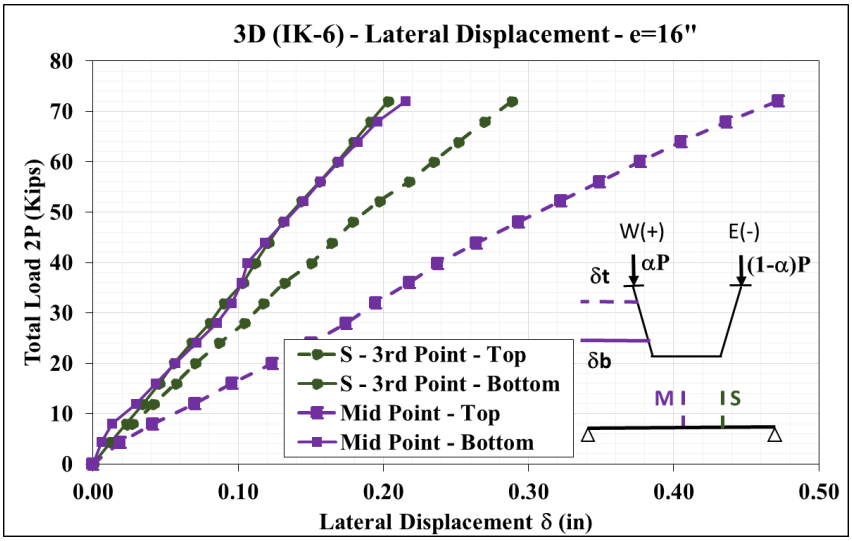

Figure C-121 – Total Load - Lateral Displacement - GLS_1.36

C.3.2 Tub #1 (Baseline Tub Girder) – Bracing Forces

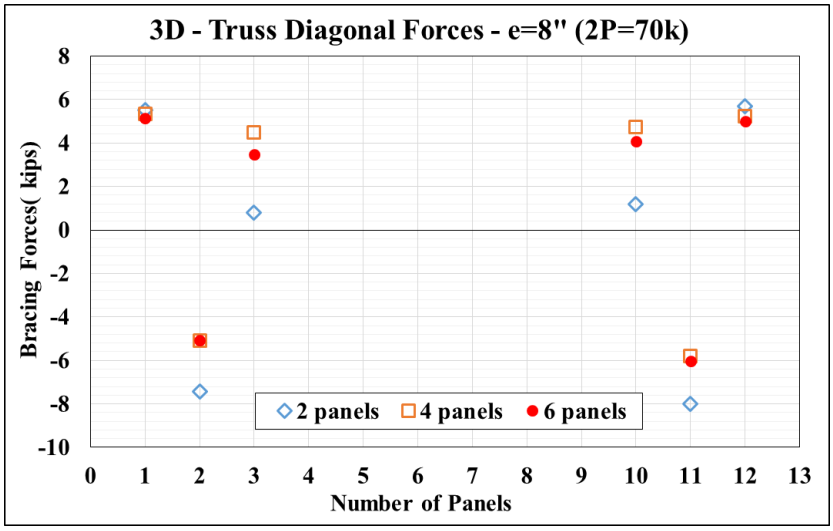

Figure C-122 – Top Lateral Bracing Diagonal Forces – 3 Truss Diagonals per End – e=8in

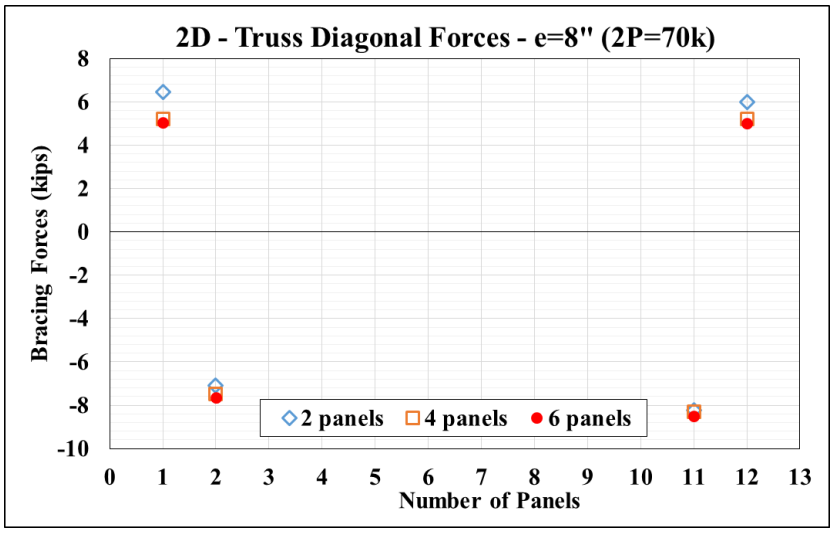

Figure C-123 – Top Lateral Bracing Diagonal Forces – 2 Truss Diagonals per End – e=8in

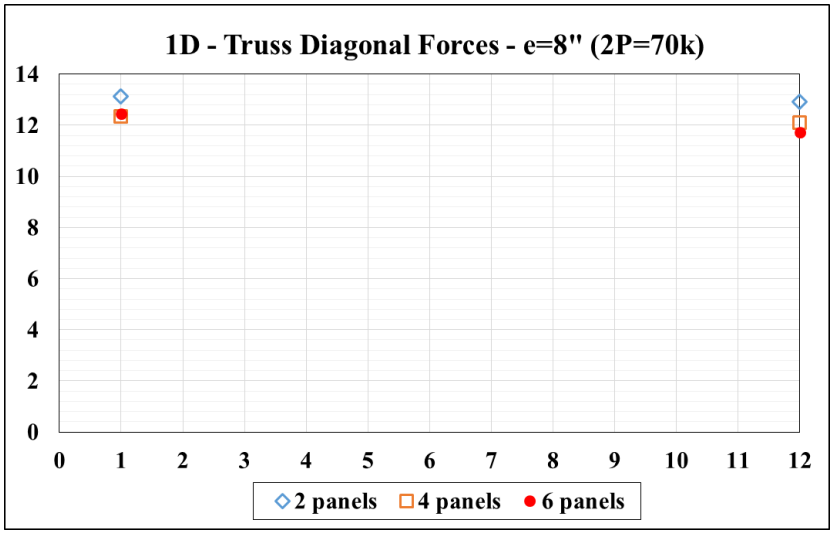

Figure C-124 – Top Lateral Bracing Diagonal Forces -1 Truss Diagonals per End – e=8in

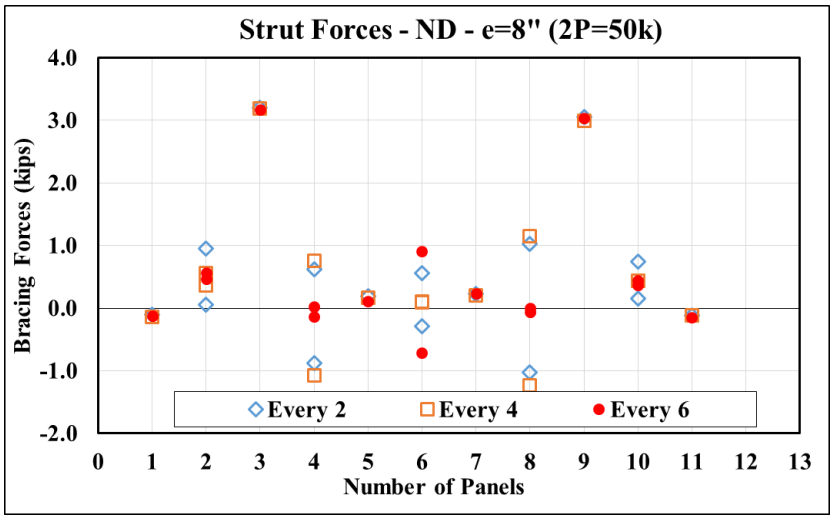

Figure C-125 – Strut Forces - 0 Truss Diagonals per End – e=8in

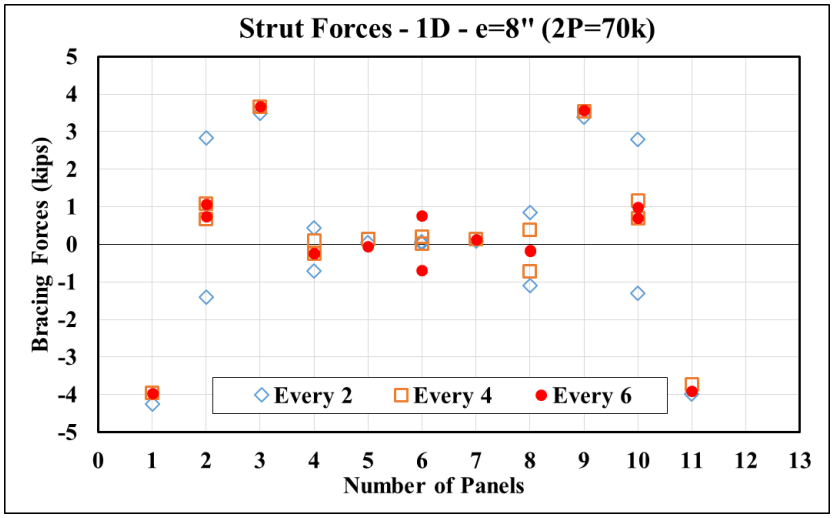

Figure C-126 – Strut Forces - 1 Truss Diagonals per End – e=8in

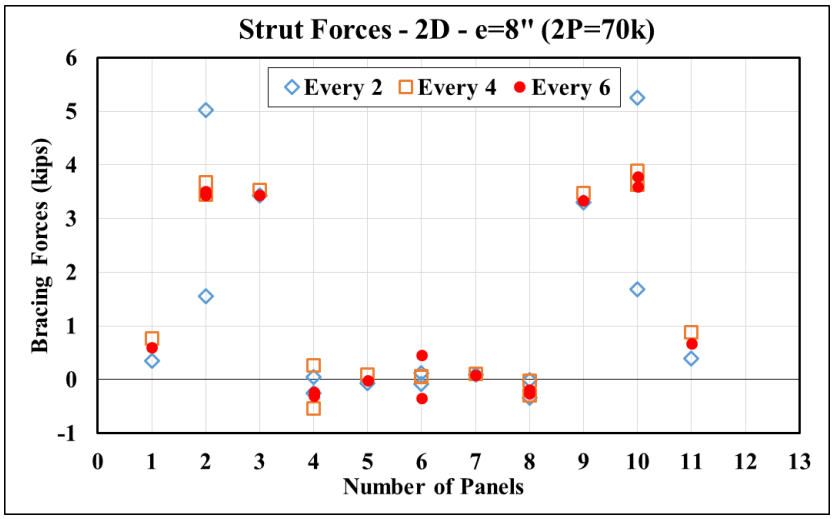

Figure C-127 – Strut Forces - 2 Truss Diagonals per End – e=8in

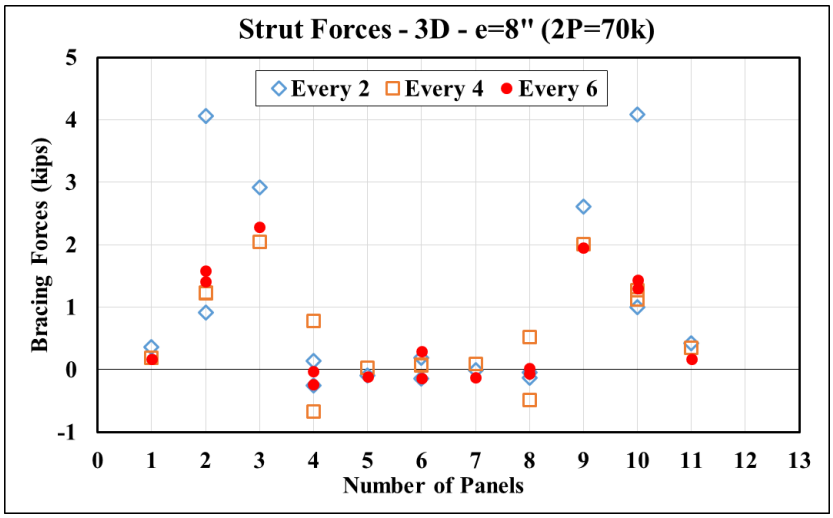

Figure C-128 – Strut Forces - 3 Truss Diagonals per End – e=8in

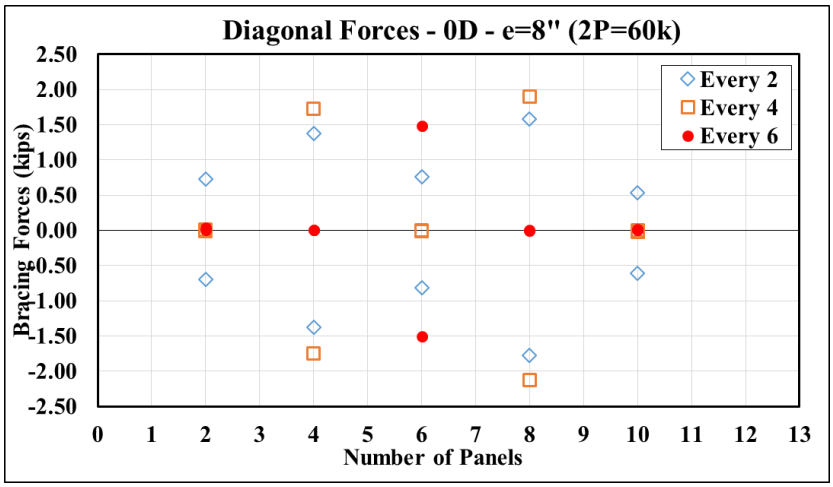

Figure C-129 – K-frame Diagonal Forces - 0 Truss Diagonals per End – e=8in

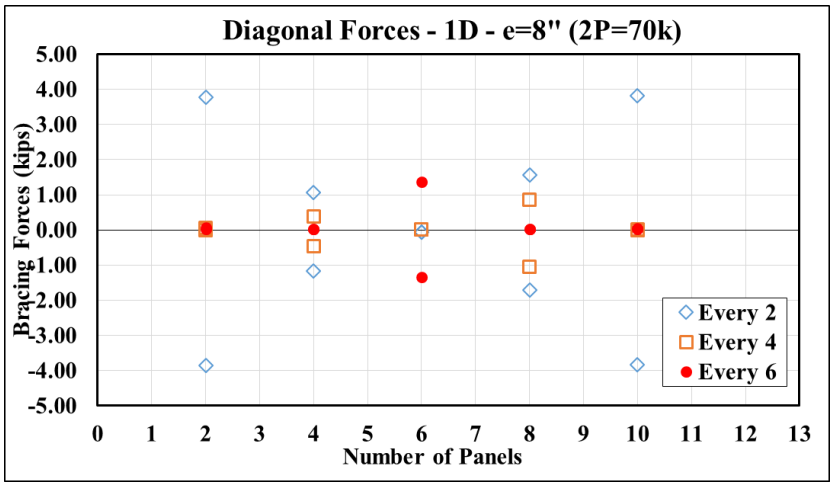

Figure C-130 – K-frame Diagonal Forces - 1 Truss Diagonals per End – e=8in

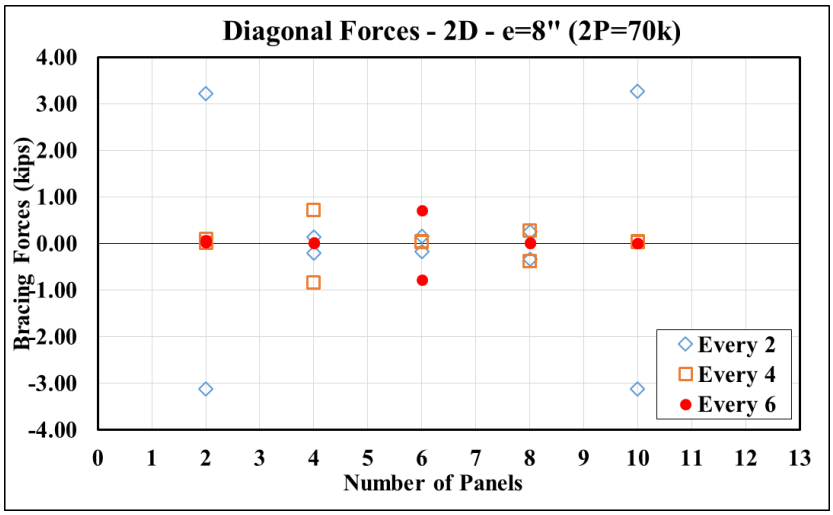

Figure C-131 – K-frame Diagonal Forces - 2 Truss Diagonals per End – e=8in

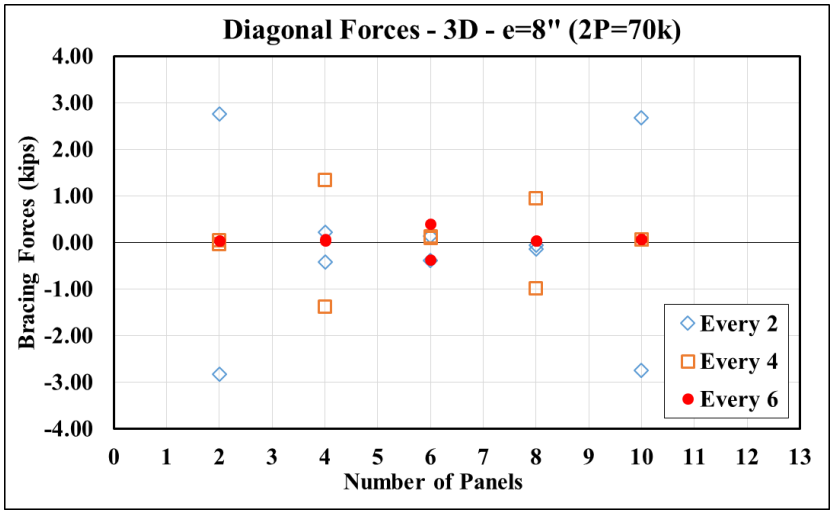

Figure C-132 – K-frame Diagonal Forces - 3 Truss Diagonals per End – e=8in

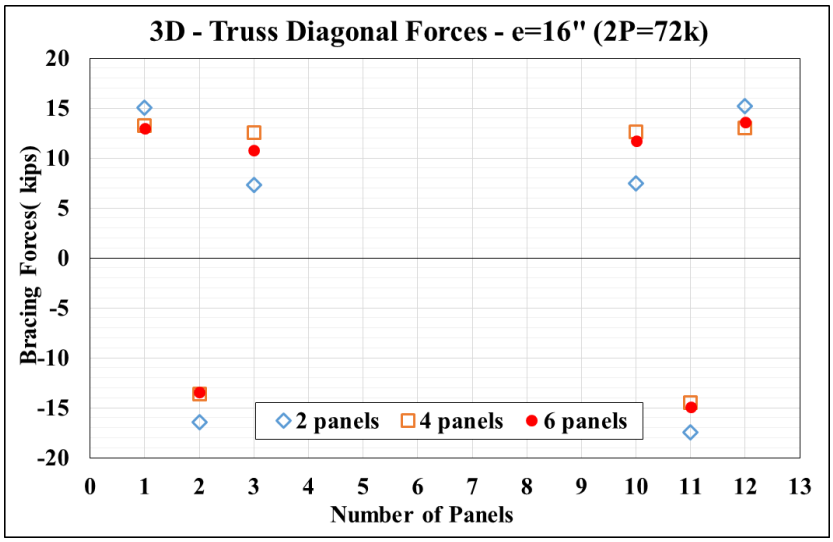

Figure C-133 – Top Lateral Bracing Diagonal Forces – 3 Truss Diagonals per End – e=16in

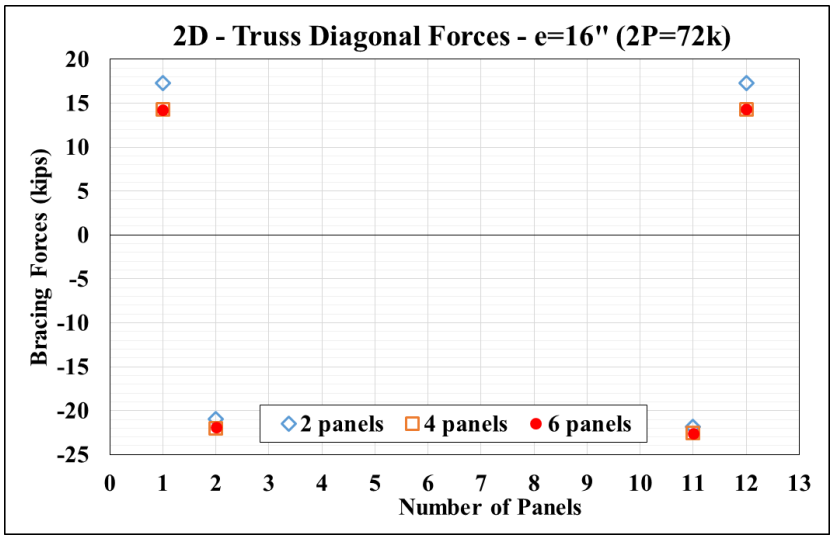

Figure C-134 – Top Lateral Bracing Diagonal Forces – 2 Truss Diagonals per End – e=16in

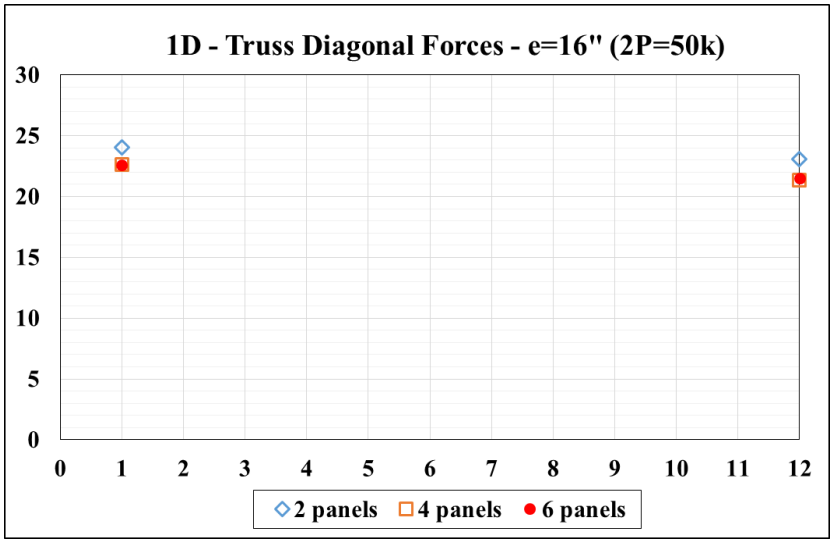

Figure C-135 – Top Lateral Bracing Diagonal Forces -1 Truss Diagonals per End – e=16in

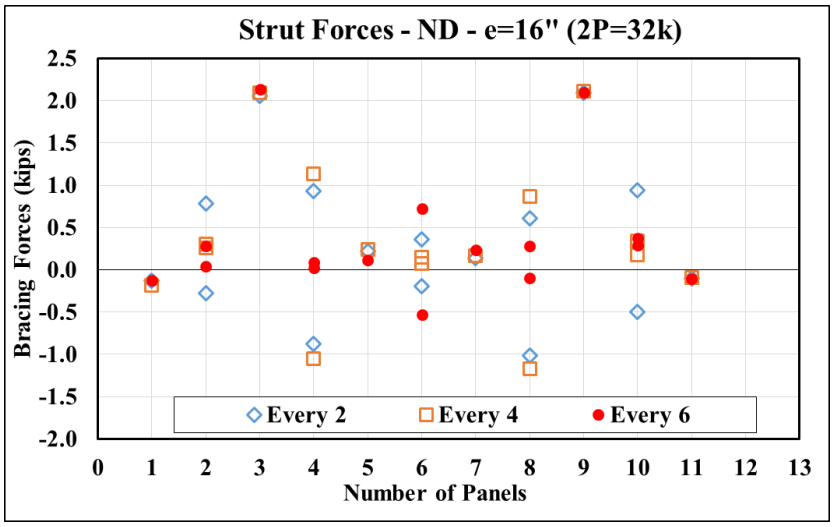

Figure C-136 – Strut Forces - 0 Truss Diagonals per End – e=16in

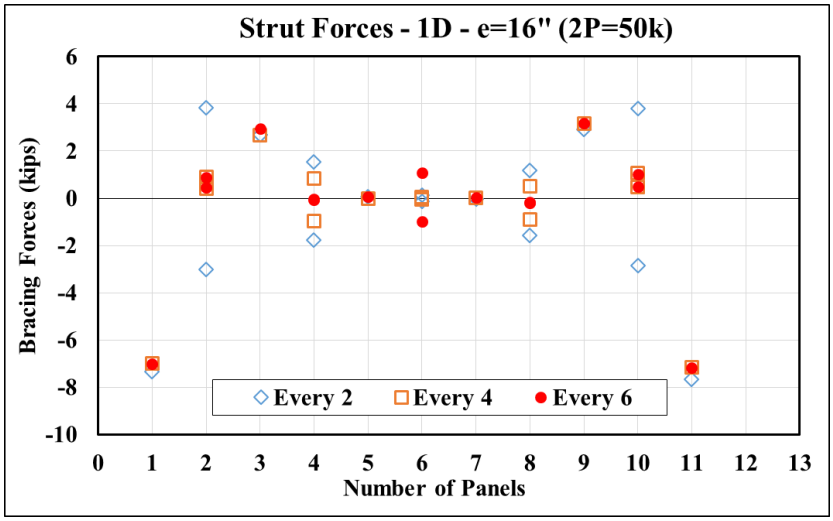

Figure C-137 – Strut Forces - 1 Truss Diagonals per End – e=16in

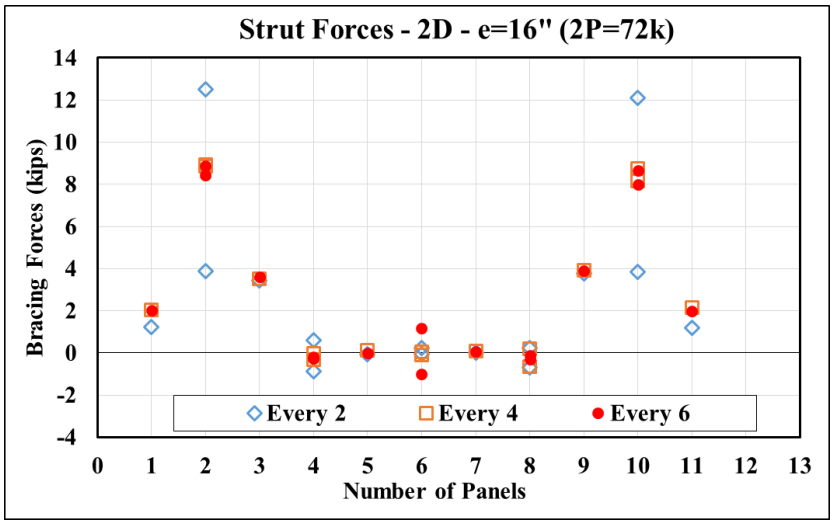

Figure C-138 – Strut Forces - 2 Truss Diagonals per End – e=16in

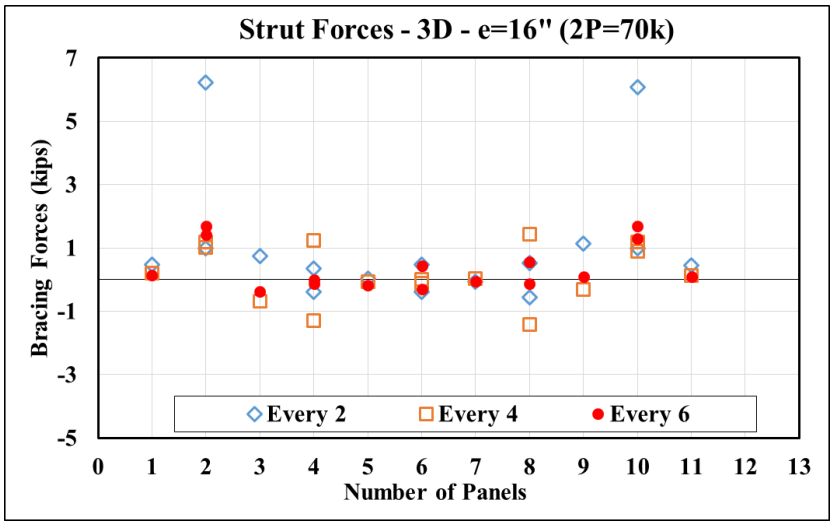

Figure C-139 – Strut Forces - 3 Truss Diagonals per End – e=16in

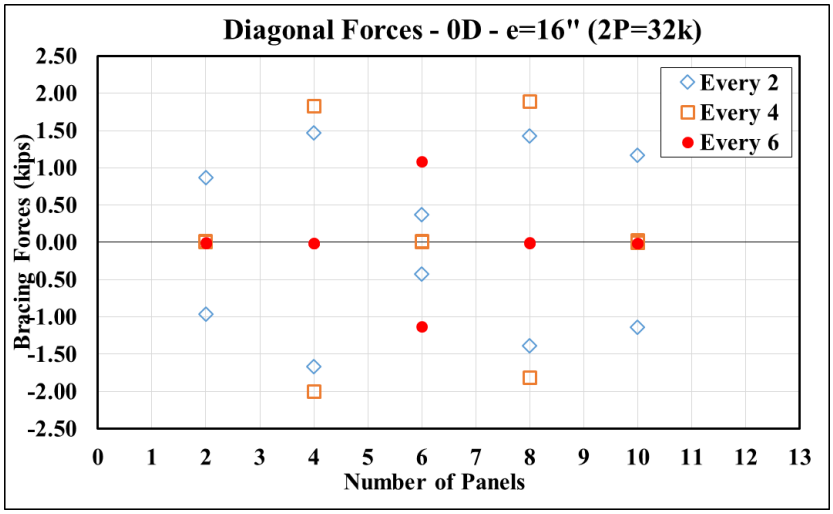

Figure C-140 – K-frame Diagonal Forces - 0 Truss Diagonals per End – e=16in

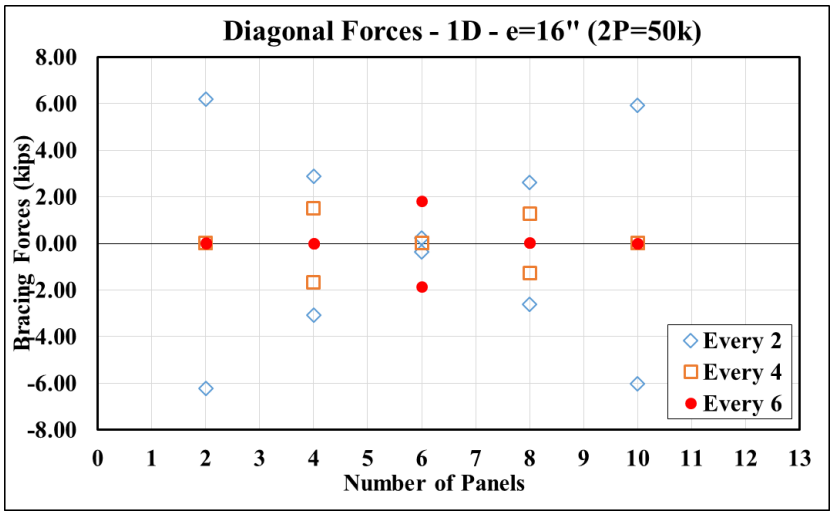

Figure C-141 – K-frame Diagonal Forces - 1 Truss Diagonals per End – e=16in

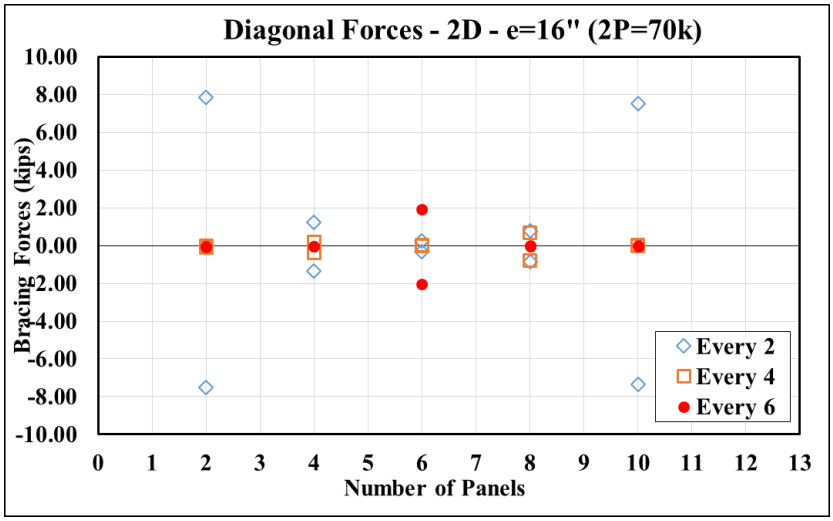

Figure C-142 – K-frame Diagonal Forces - 2 Truss Diagonals per End – e=16in

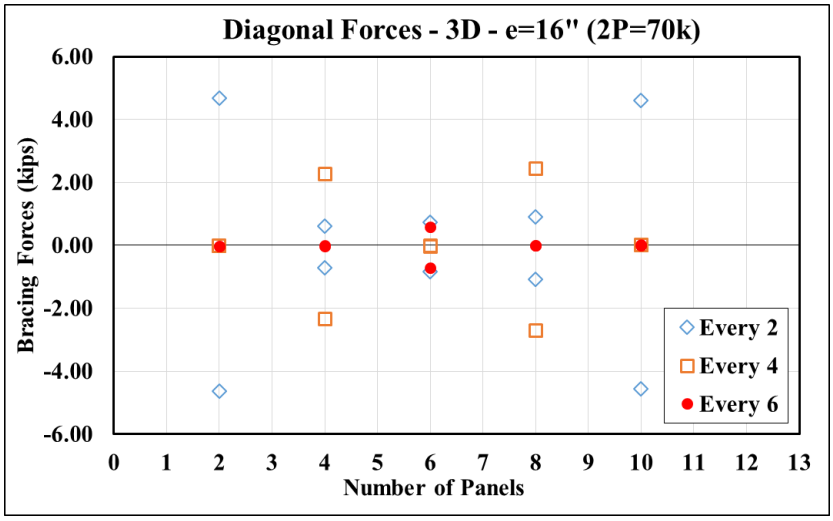

Figure C-143 – K-frame Diagonal Forces - 3 Truss Diagonals per End – e=16in

C.3.3 Tub #2 (Top Flange Offset Tub Girder) – Load-Deflection Response

Table C-4 – Bending plus Torsion Test Results – Tub #2

Test Code	Eccentricity (in)	Number of Diagonals	K-Frame Location
GLS_2.13	8	0	2-Panel
GLS_2.14	8	0	4-Panel
GLS_2.15	8	0	6-Panel
GLS_2.16	8	1	2-Panel
GLS_2.17	8	1	4-Panel
GLS_2.18	8	1	6-Panel
GLS_2.19	8	2	2-Panel
GLS_2.20	8	2	4-Panel
GLS_2.21	8	2	6-Panel
GLS_2.22	8	3	2-Panel
GLS_2.23	8	3	4-Panel
GLS_2.24	8	3	6-Panel
GLS_2.25	16	0	2-Panel
GLS_2.26	16	0	4-Panel
GLS_2.27	16	0	6-Panel
GLS_2.28	16	1	2-Panel
GLS_2.29	16	1	4-Panel
GLS_2.30	16	1	6-Panel
GLS_2.31	16	2	2-Panel
GLS_2.32	16	2	4-Panel
GLS_2.33	16	2	6-Panel
GLS_2.34	16	3	2-Panel
GLS_2.35	16	3	4-Panel
GLS_2.36	16	3	6-Panel

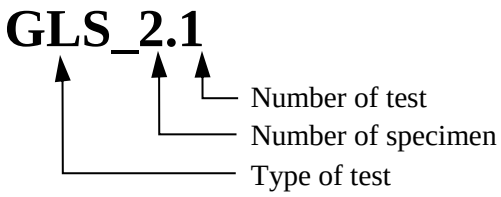

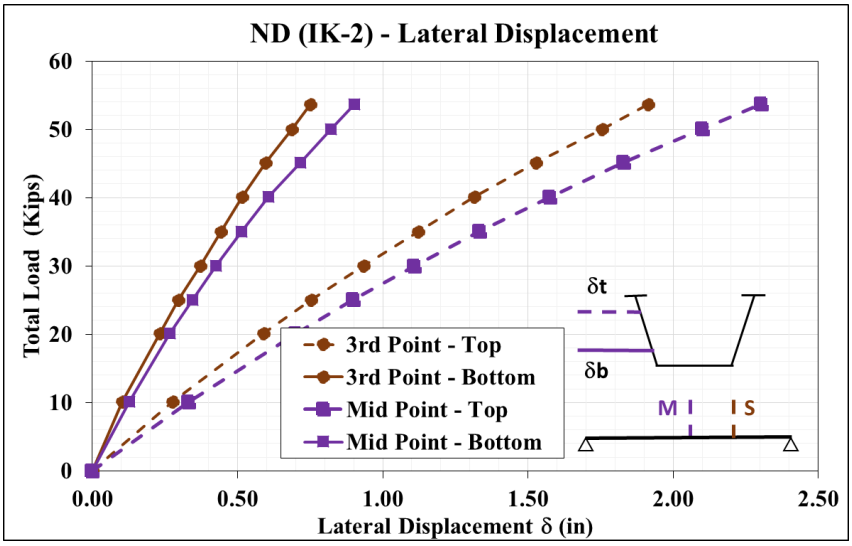

Figure C-144 – Total Load - Lateral Displacement - GLS_2.13

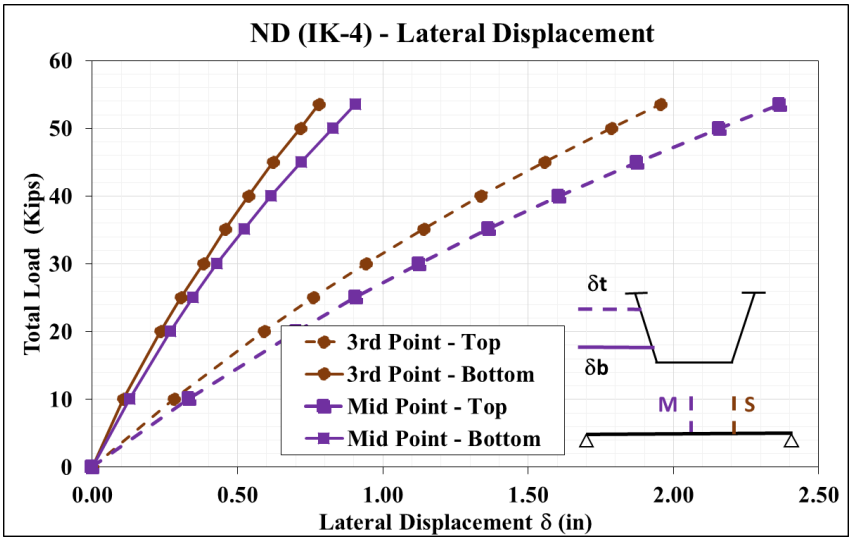

Figure C-145 – Total Load - Lateral Displacement - GLS_2.14

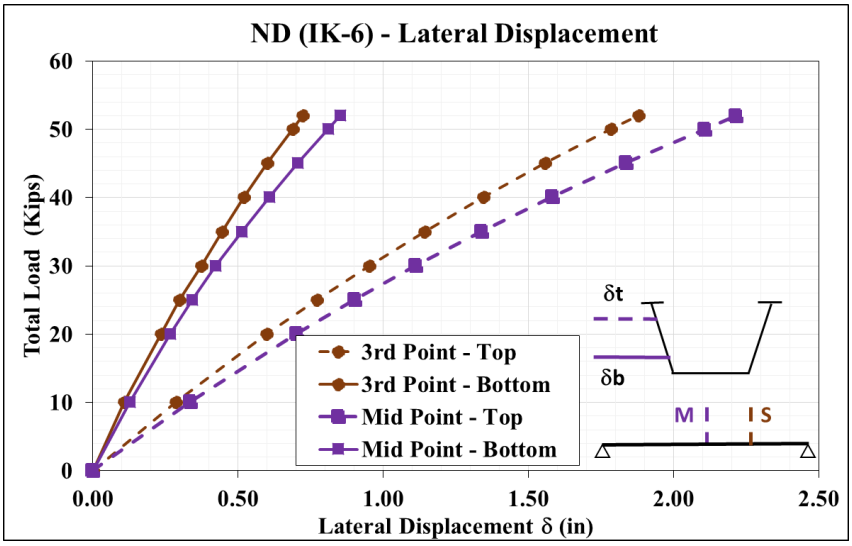

Figure C-146 – Total Load - Lateral Displacement - GLS_2.15

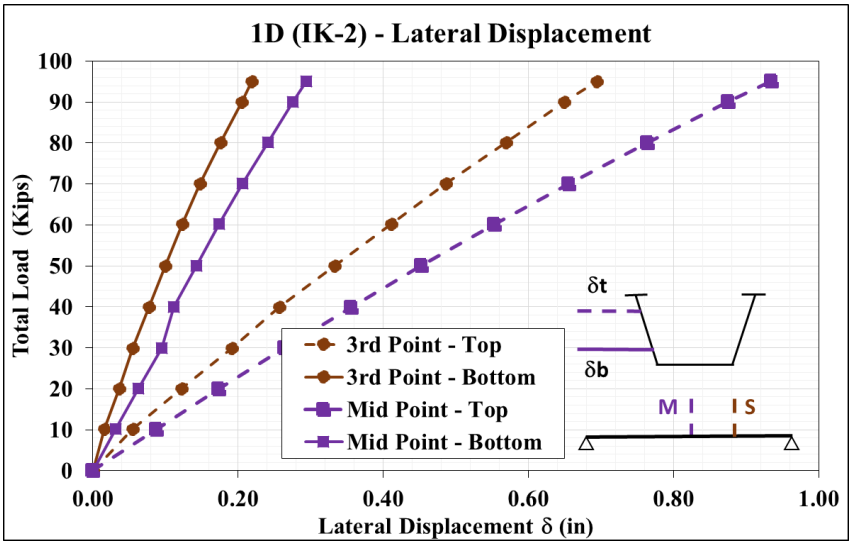

Figure C-147 – Total Load - Lateral Displacement - GLS_2.16

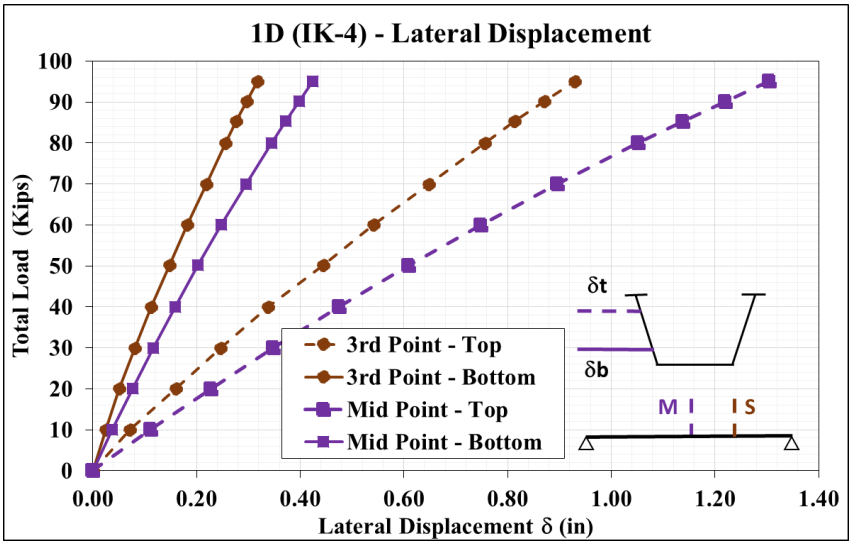

Figure C-148 – Total Load - Lateral Displacement - GLS_2.17

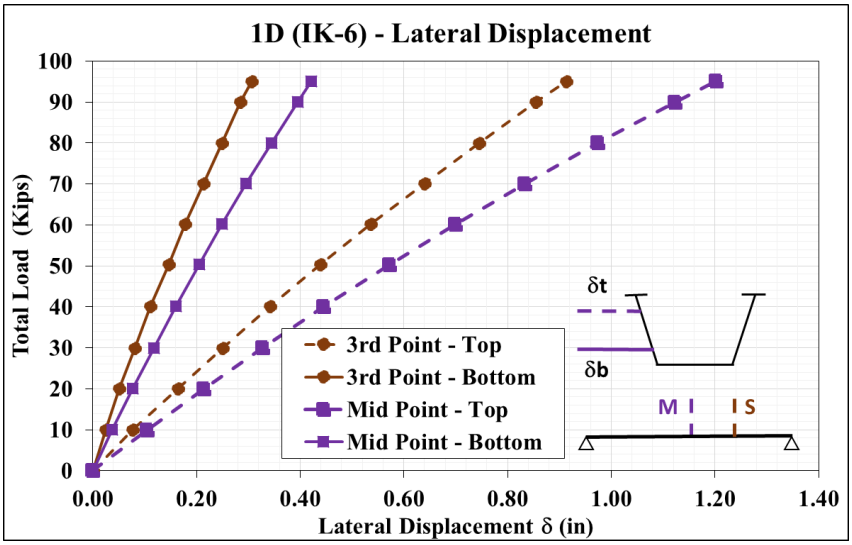

Figure C-149 – Total Load - Lateral Displacement - GLS_2.18

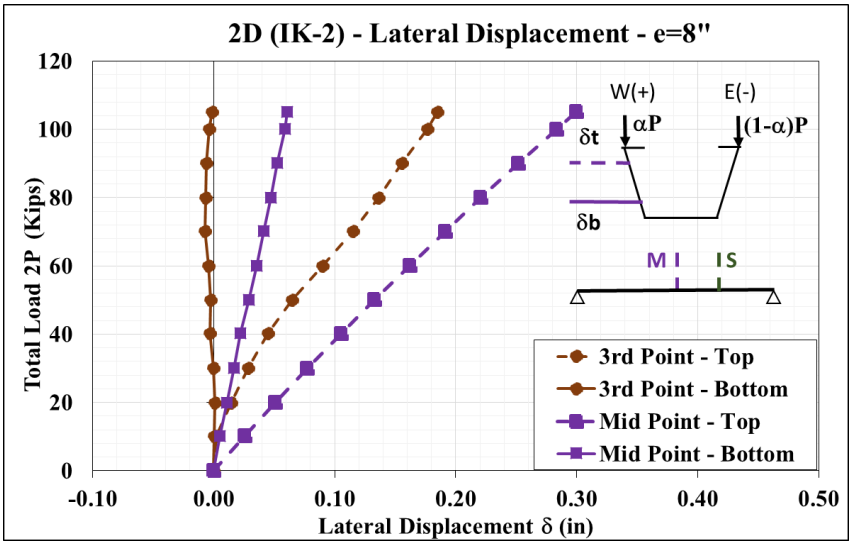

Figure C-150 – Total Load - Lateral Displacement - GLS_2.19

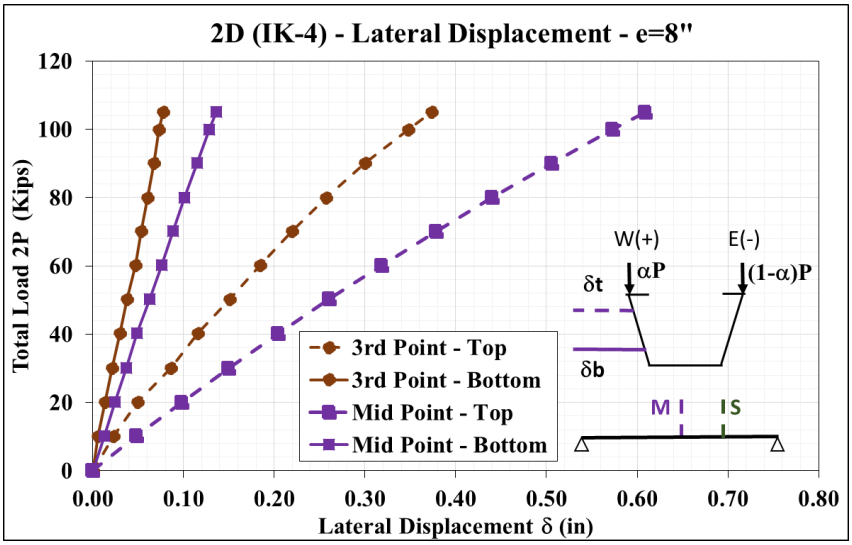

Figure C-151 – Total Load - Lateral Displacement - GLS_2.20

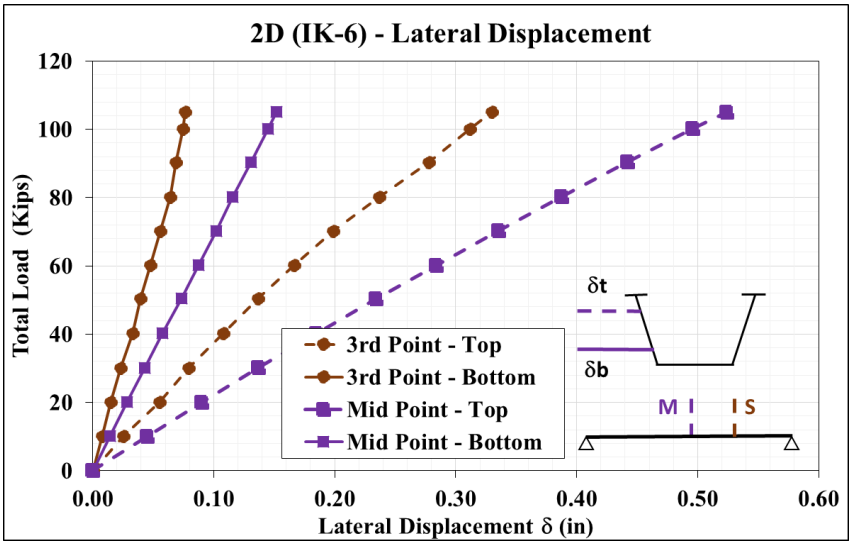

Figure C-152 – Total Load - Lateral Displacement - GLS_2.21

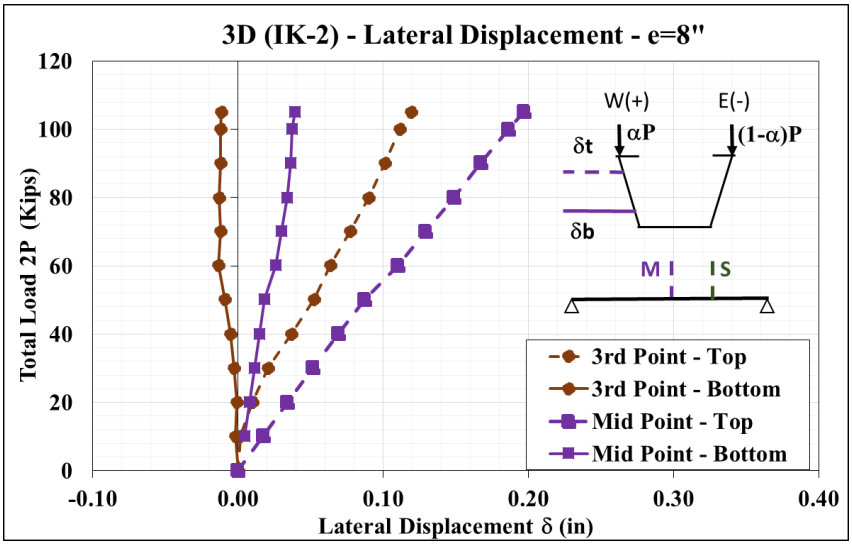

Figure C-153 – Total Load - Lateral Displacement - GLS_2.22

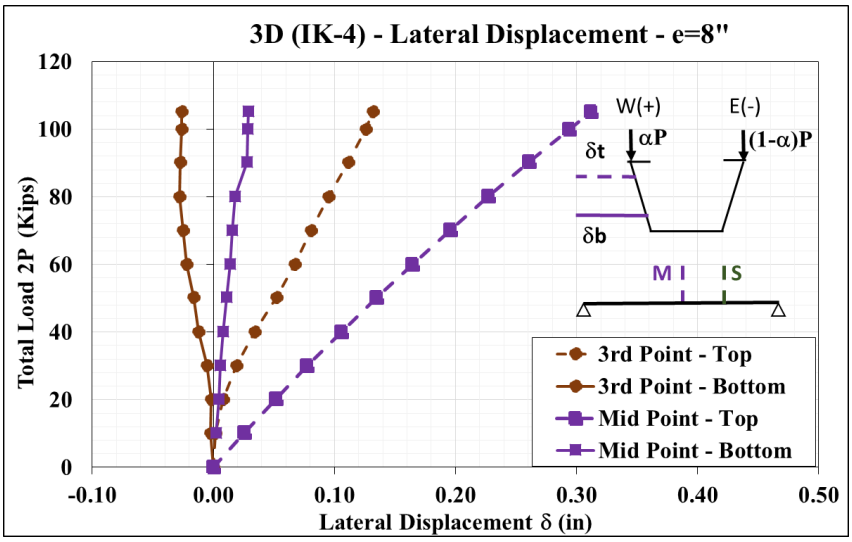

Figure C-154 – Total Load - Lateral Displacement - GLS_2.23

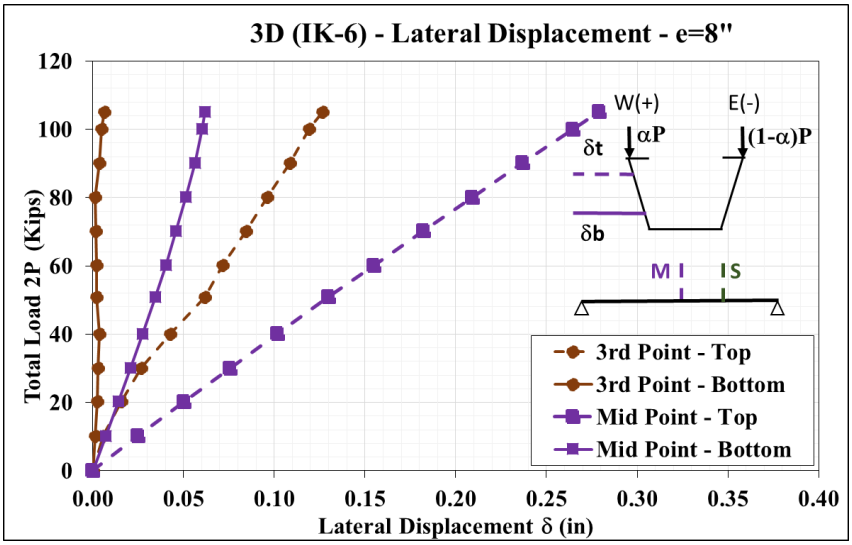

Figure C-155 – Total Load - Lateral Displacement - GLS_2.24

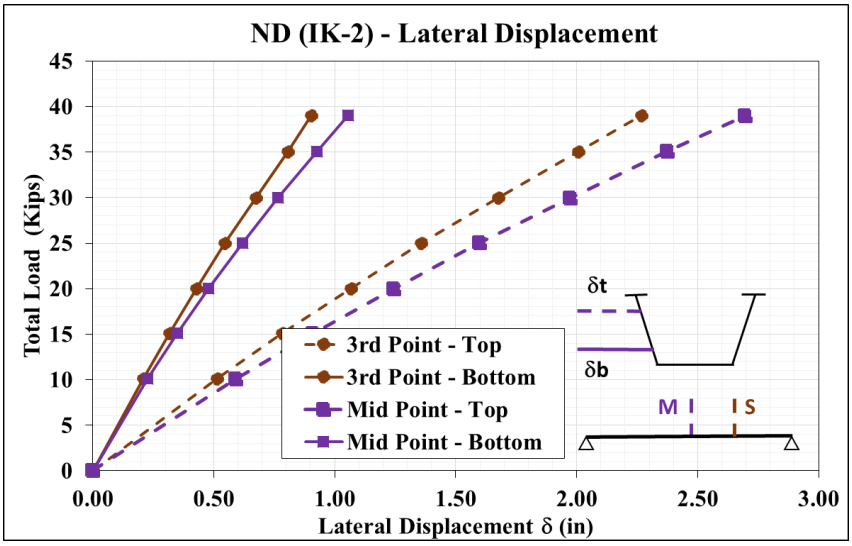

Figure C-156 – Total Load - Lateral Displacement - GLS_2.25

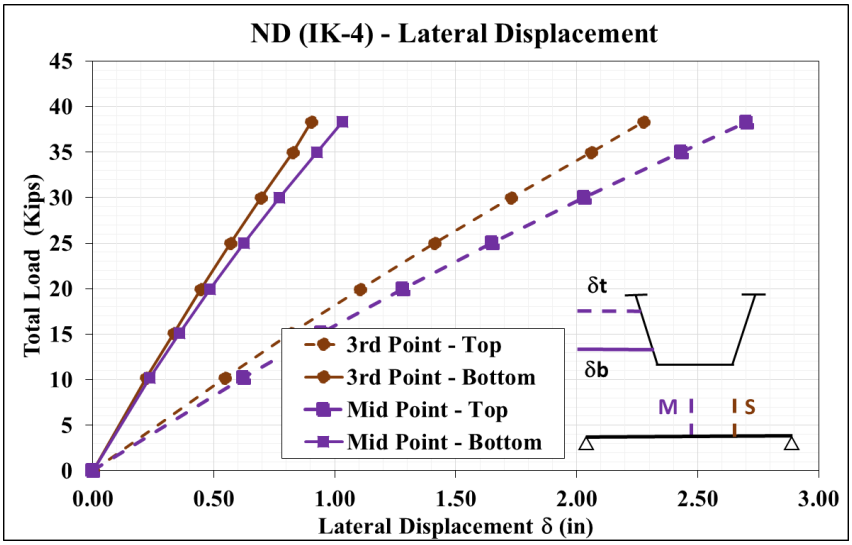

Figure C-157 – Total Load - Lateral Displacement - GLS_2.26

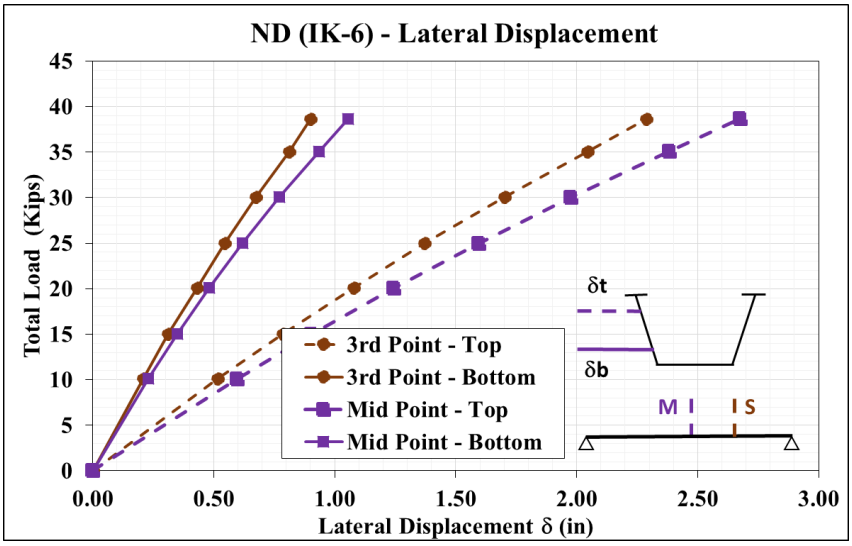

Figure C-158 – Total Load - Lateral Displacement - GLS_2.27

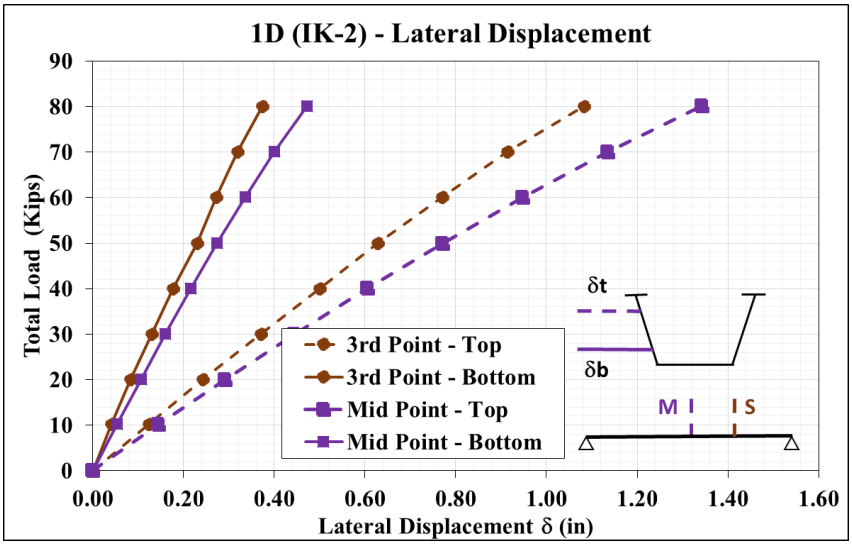

Figure C-159 – Total Load - Lateral Displacement - GLS_2.28

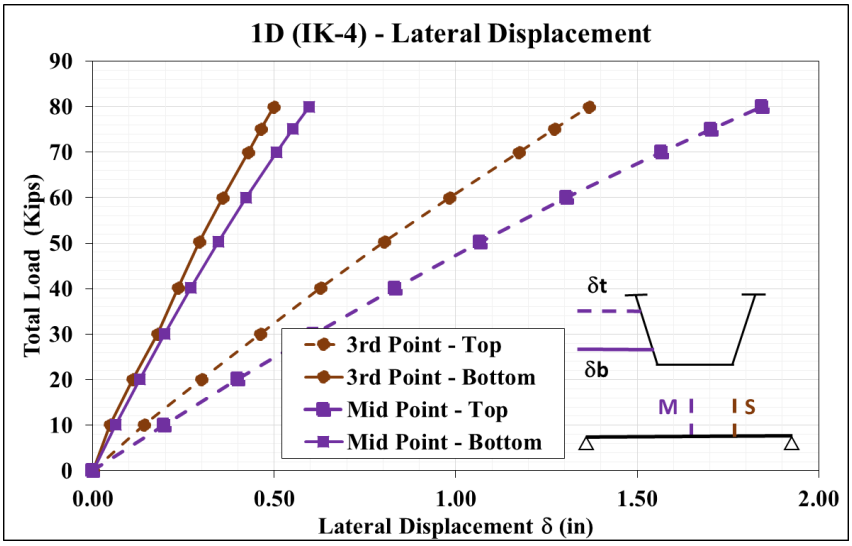

Figure C-160 – Total Load - Lateral Displacement - GLS_2.29

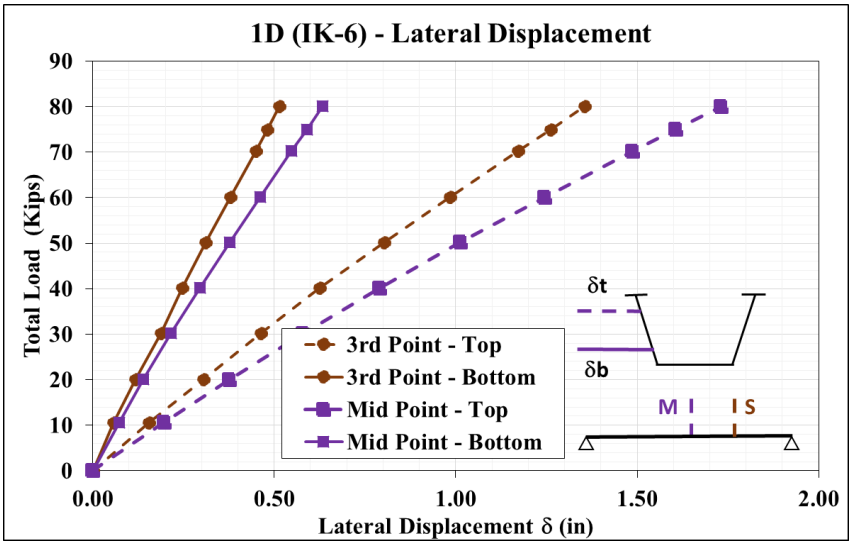

Figure C-161 – Total Load - Lateral Displacement - GLS_2.30

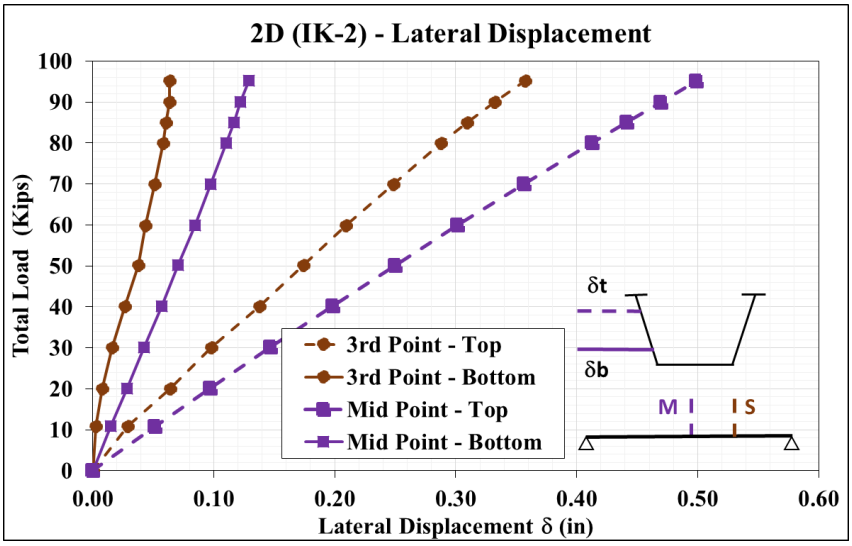

Figure C-162 – Total Load - Lateral Displacement - GLS_2.31

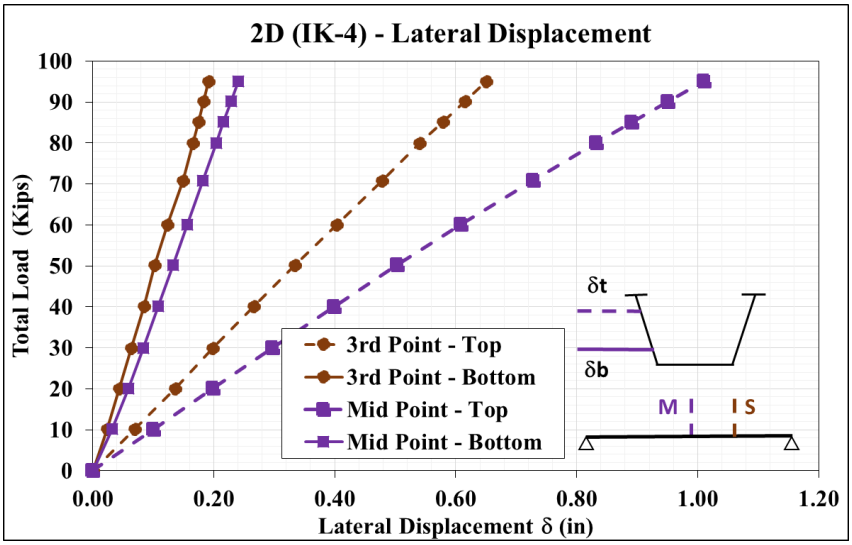

Figure C-163 – Total Load - Lateral Displacement - GLS_2.32

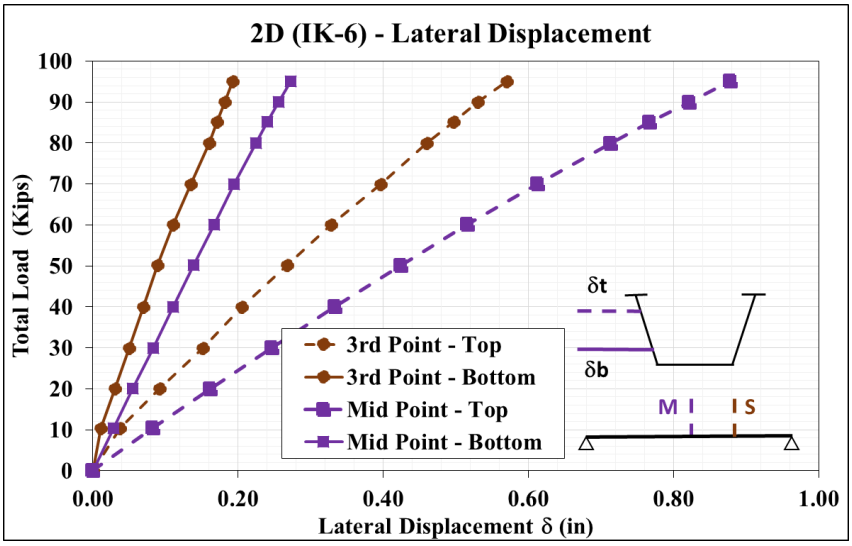

Figure C-164 – Total Load - Lateral Displacement - GLS_2.33

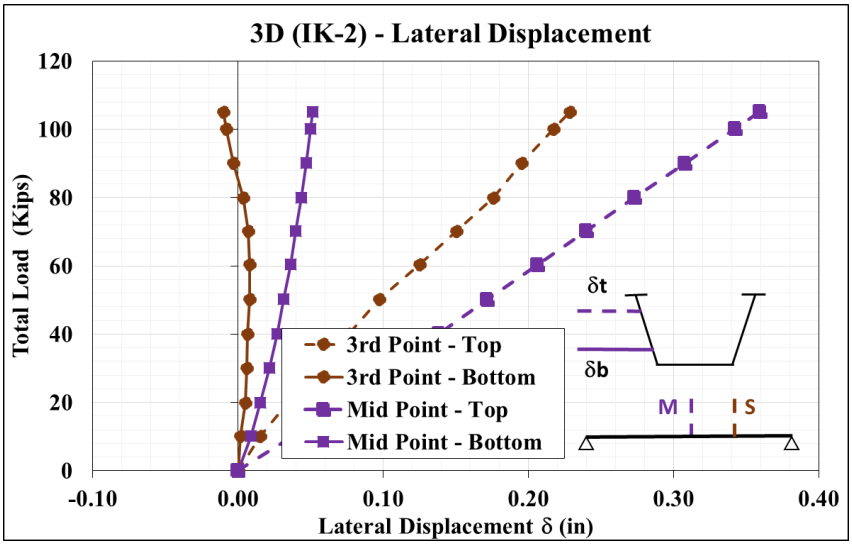

Figure C-165 – Total Load - Lateral Displacement - GLS_2.34

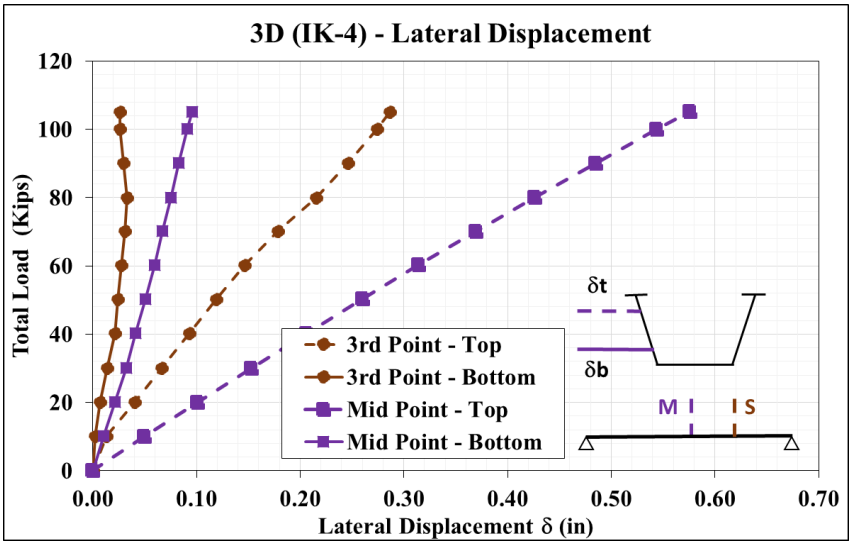

Figure C-166 – Total Load - Lateral Displacement - GLS_2.35

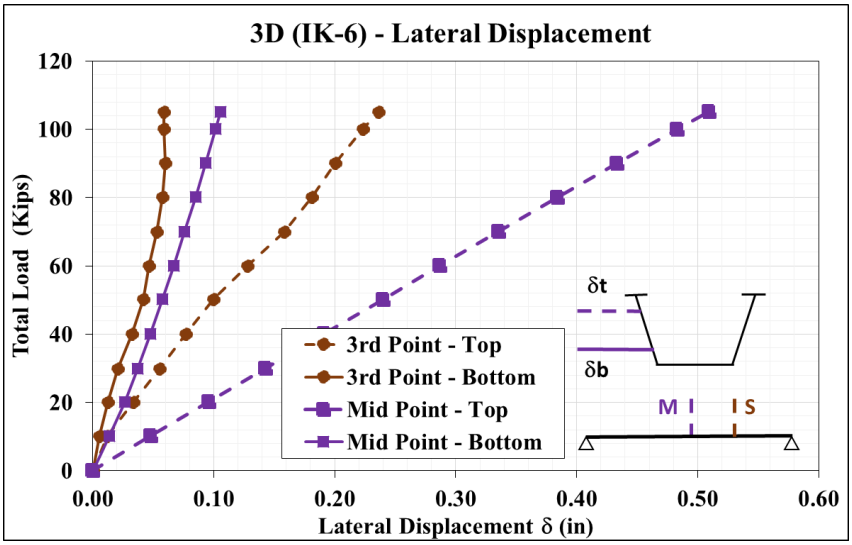

Figure C-167 – Total Load - Lateral Displacement - GLS_2.36

C.3.4 Tub #2 (Top Flange Offset Tub Girder) – Bracing Forces

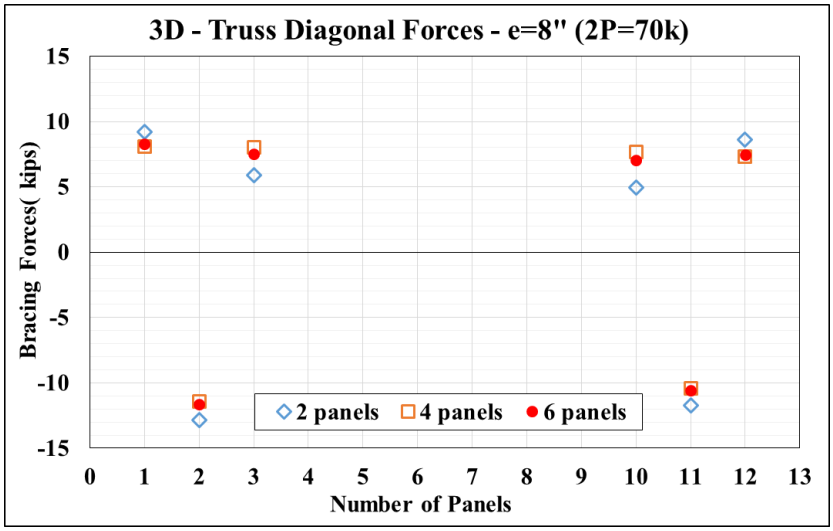

Figure C-168 – Top Lateral Bracing Diagonal Forces – 3 Truss Diagonals per End – e=8in

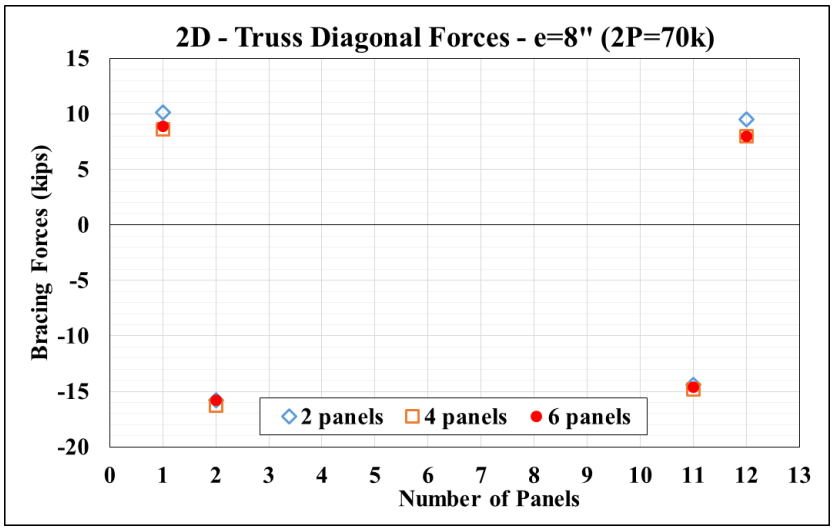

Figure C-169 – Top Lateral Bracing Diagonal Forces – 2 Truss Diagonals per End – e=8in

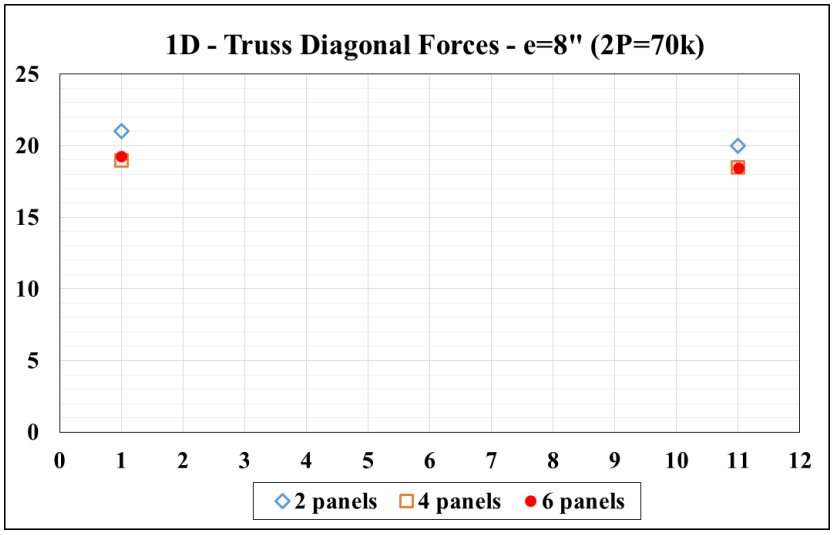

Figure C-170 – Top Lateral Bracing Diagonal Forces -1 Truss Diagonals per End – e=8in

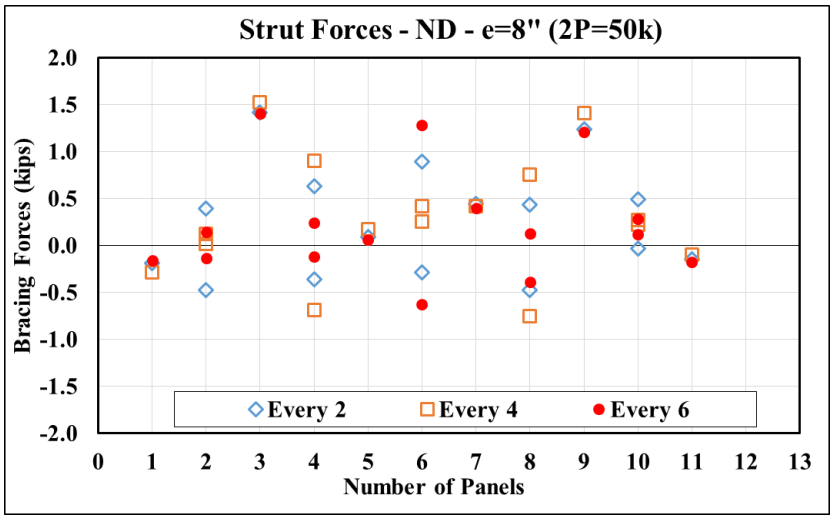

Figure C-171 – Strut Forces - 0 Truss Diagonals per End – e=8in

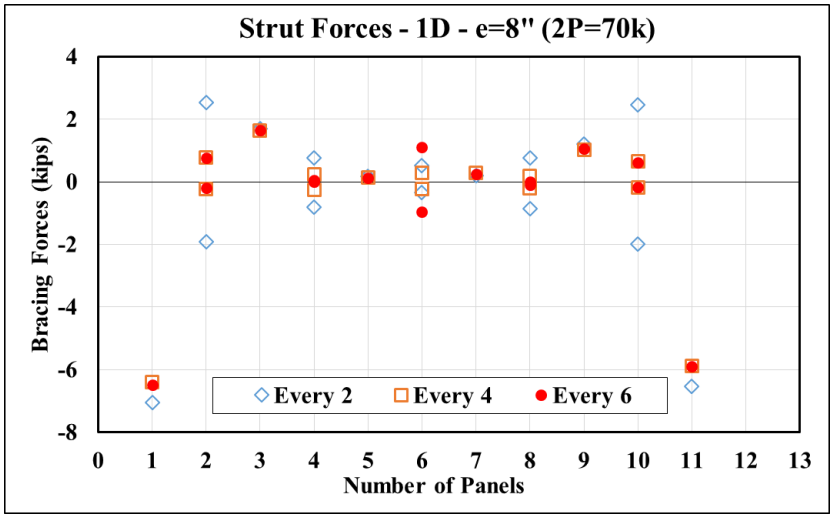

Figure C-172 – Strut Forces - 1 Truss Diagonals per End – e=8in

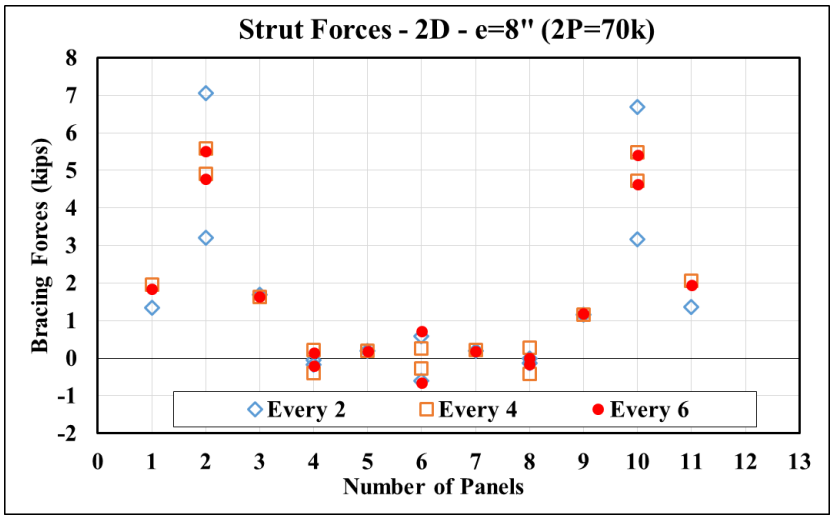

Figure C-173 – Strut Forces - 2 Truss Diagonals per End – e=8in

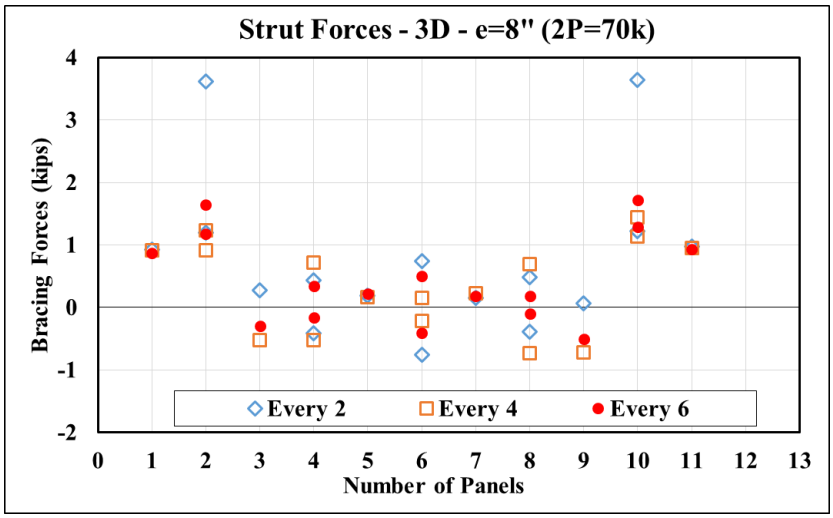

Figure C-174 – Strut Forces - 3 Truss Diagonals per End – e=8in

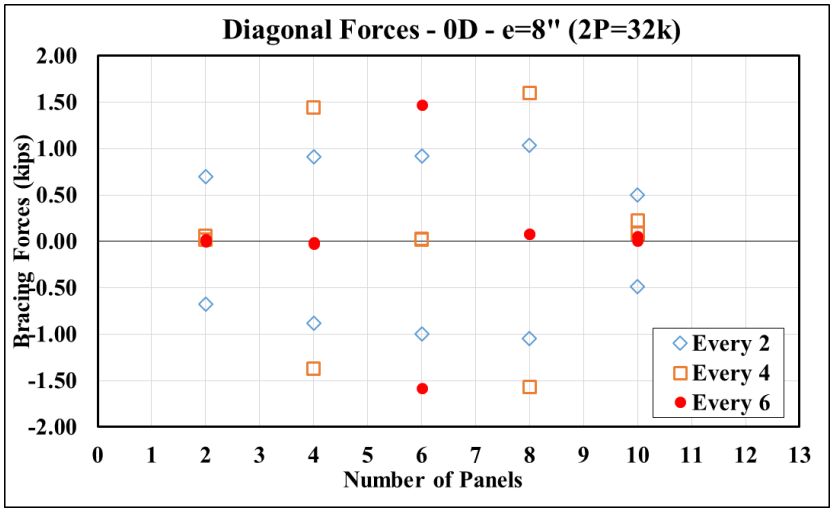

Figure C-175 – K-frame Diagonal Forces - 0 Truss Diagonals per End – e=8in

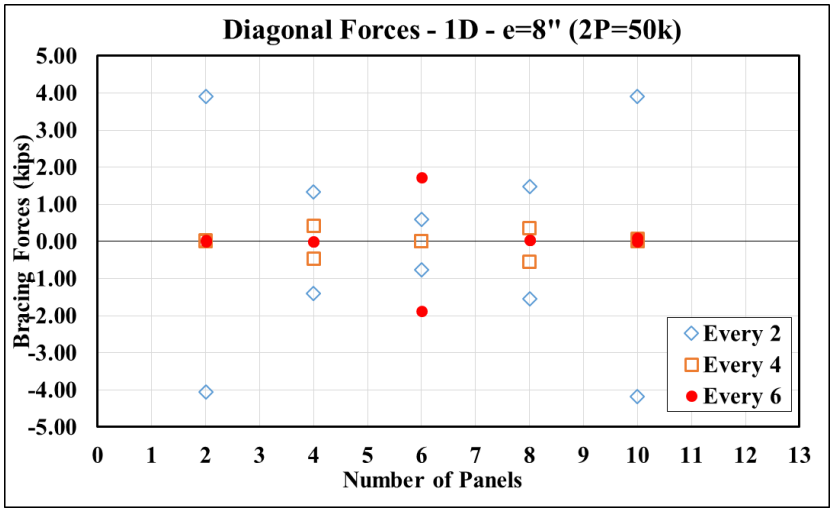

Figure C-176 – K-frame Diagonal Forces - 1 Truss Diagonals per End – e=8in

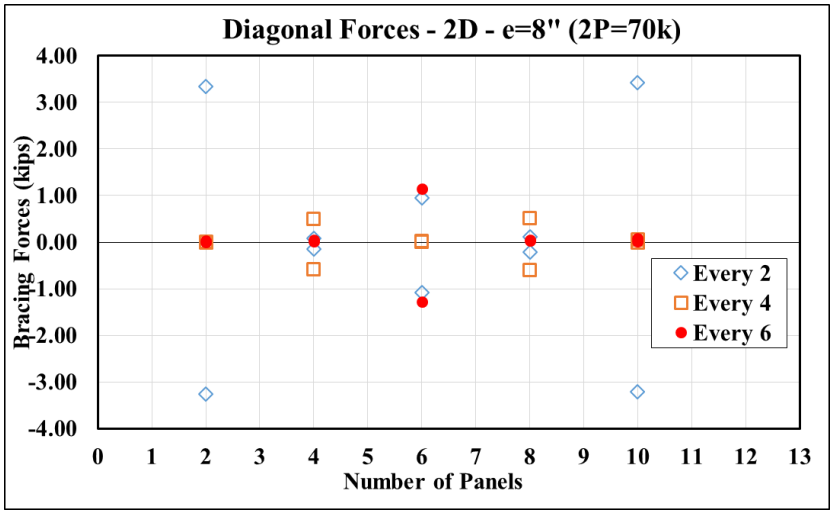

Figure C-177 – K-frame Diagonal Forces - 2 Truss Diagonals per End – e=8in

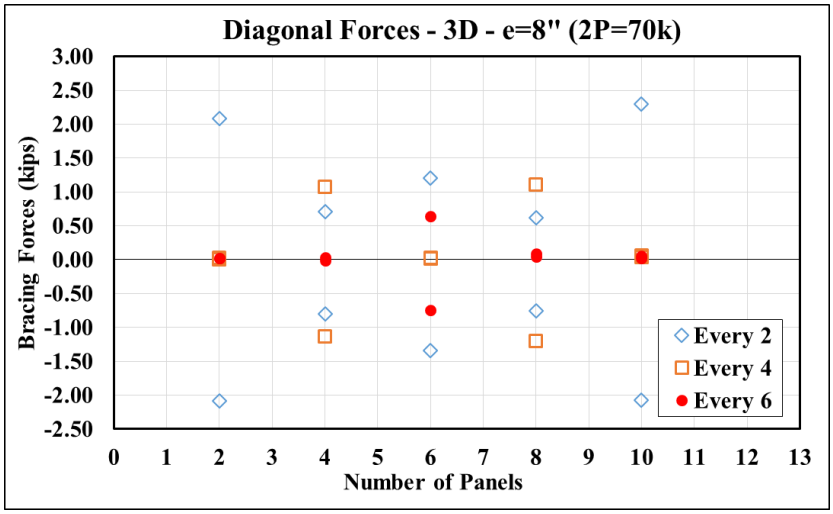

Figure C-178 – K-frame Diagonal Forces - 3 Truss Diagonals per End – e=8in

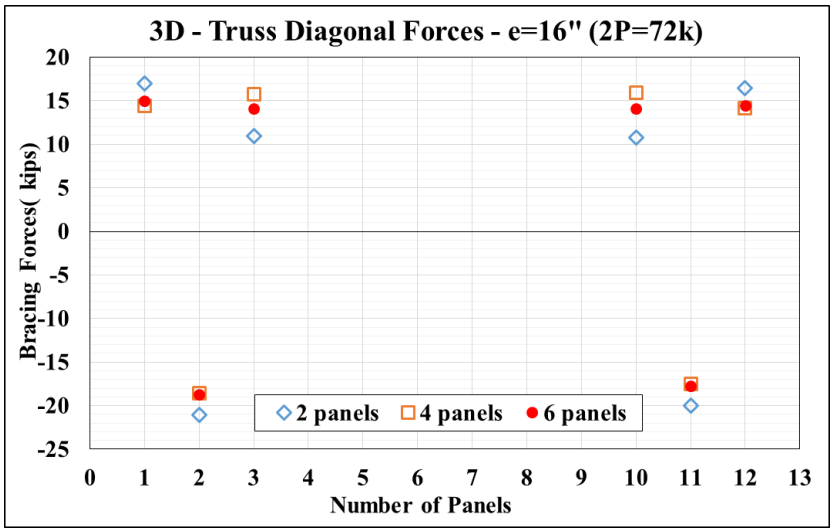

Figure C-179 – Top Lateral Bracing Diagonal Forces – 3 Truss Diagonals per End – e=16in

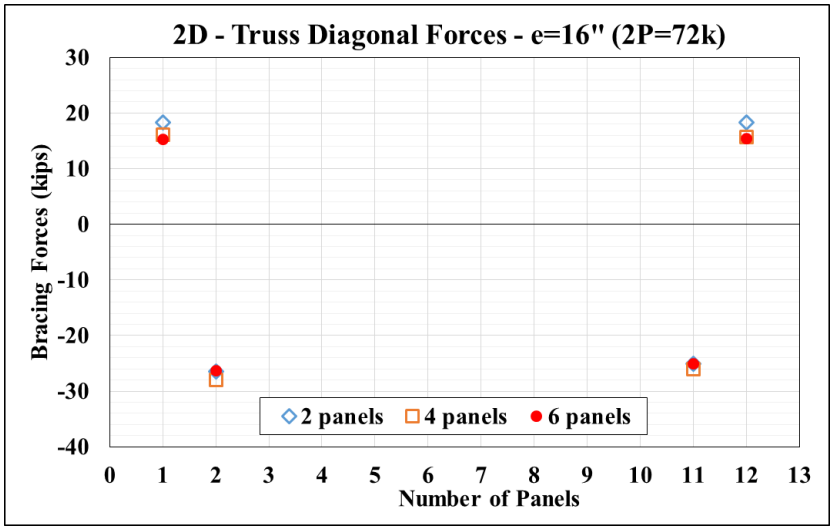

Figure C-180 – Top Lateral Bracing Diagonal Forces – 2 Truss Diagonals per End – e=16in

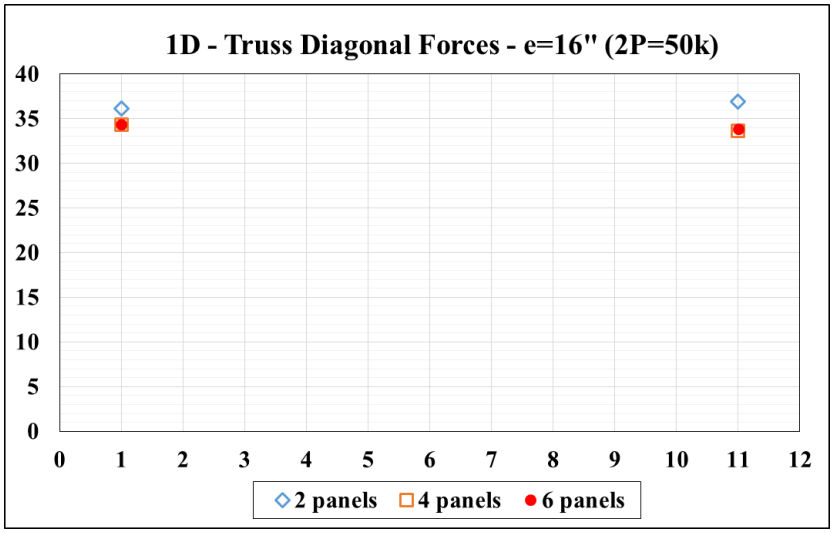

Figure C-181 – Top Lateral Bracing Diagonal Forces -1 Truss Diagonals per End – e=16in

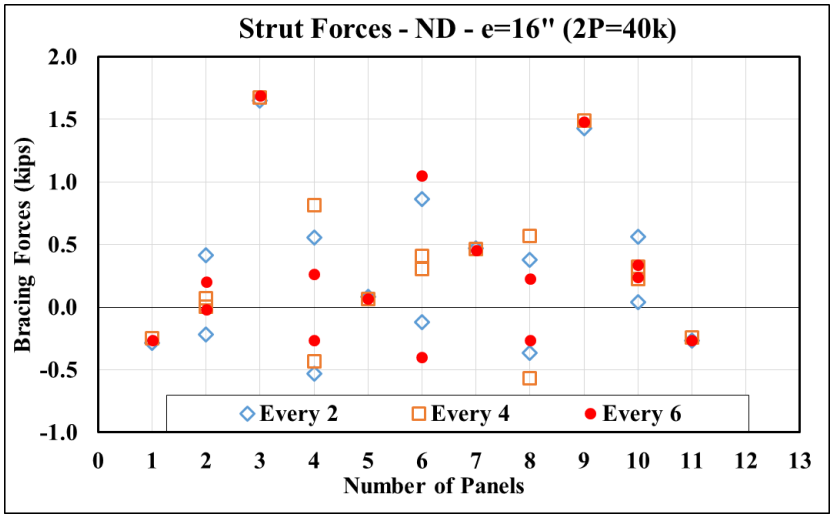

Figure C-182 – Strut Forces - 0 Truss Diagonals per End – e=16in

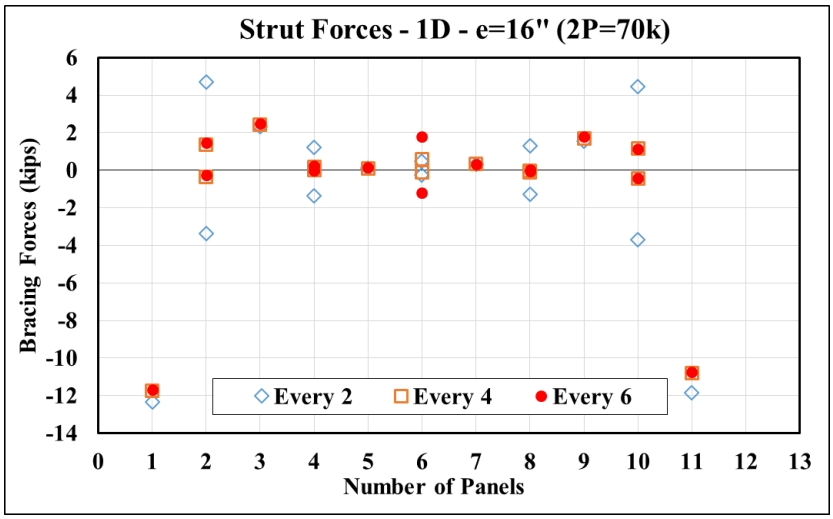

Figure C-183 – Strut Forces - 1 Truss Diagonals per End – e=16in

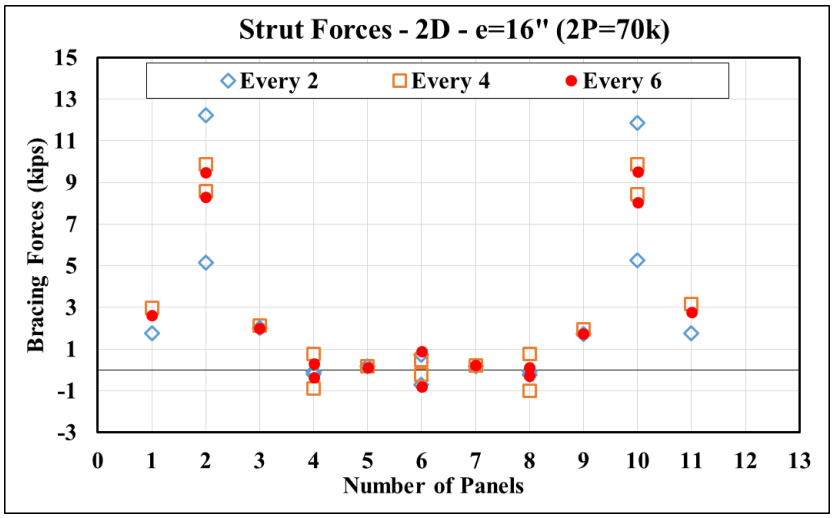

Figure C-184 – Strut Forces - 2 Truss Diagonals per End – e=16in

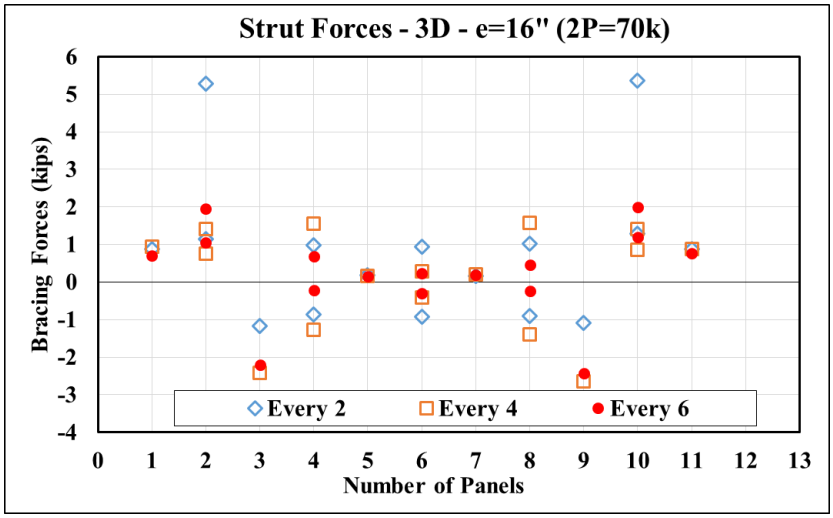

Figure C-185 – Strut Forces - 3 Truss Diagonals per End – e=16in

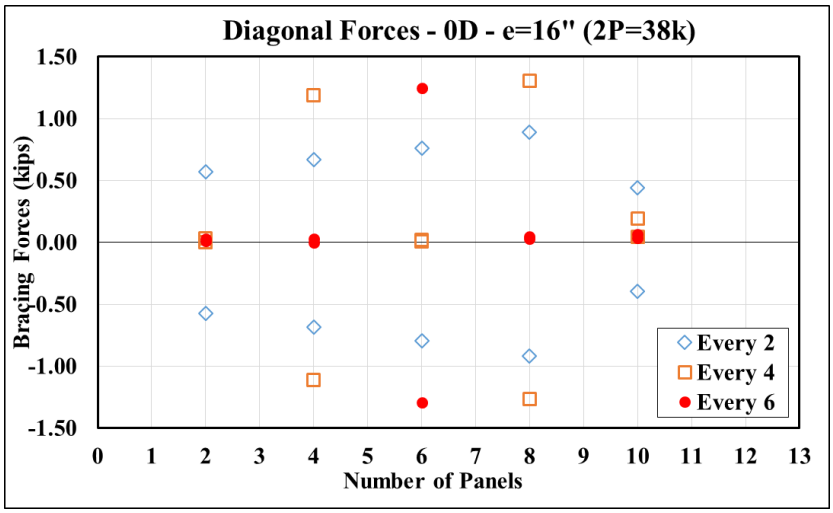

Figure C-186 – K-frame Diagonal Forces - 0 Truss Diagonals per End – e=16in

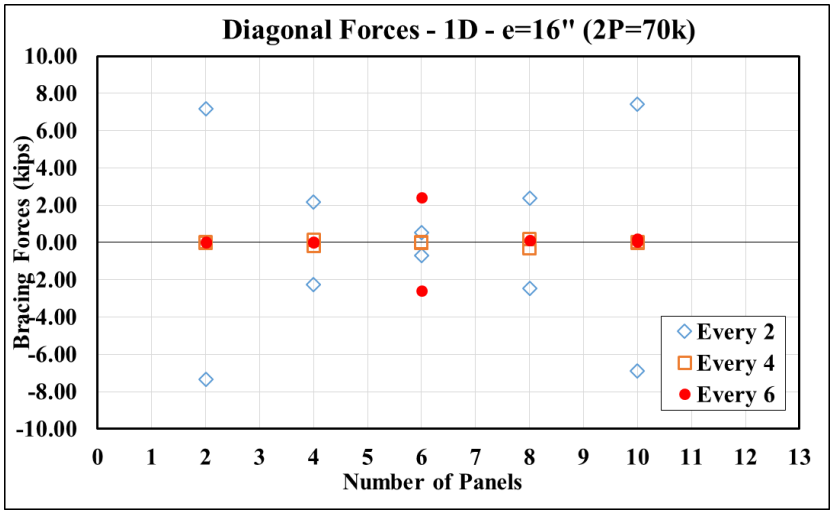

Figure C-187 – K-frame Diagonal Forces - 1 Truss Diagonals per End – e=16in

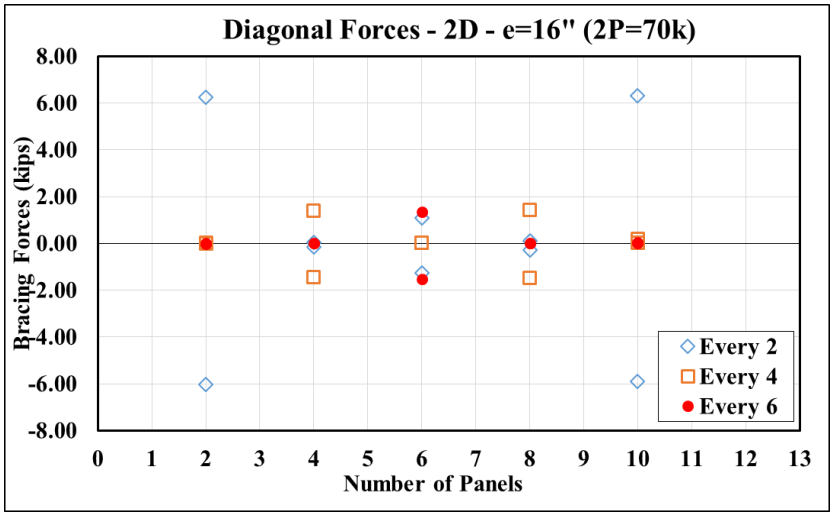

Figure C-188 – K-frame Diagonal Forces - 2 Truss Diagonals per End – e=16in

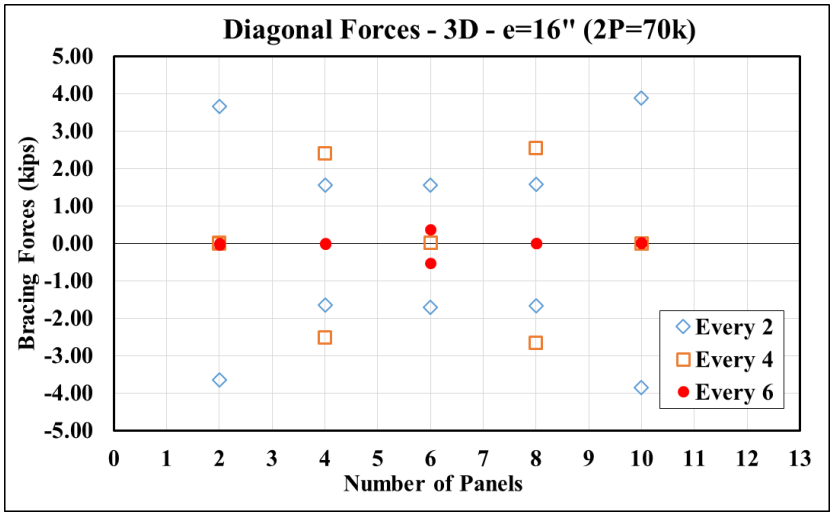

Figure C-189 – K-frame Diagonal Forces - 3 Truss Diagonals per End – e=16in

C.3.5 Tub #3 (Flatter Web Tub Girder) – Load-Deflection Response

Table C-5 – Bending plus Torsion Test Results – Tub #3

Test Code	Eccentricity (in)	Number of Diagonals	K-Frame Location
GLS_3.13	8	0	2-Panel
GLS_3.14	8	0	4-Panel
GLS_3.15	8	0	6-Panel
GLS_3.16	8	1	2-Panel
GLS_3.17	8	1	4-Panel
GLS_3.18	8	1	6-Panel
GLS_3.19	8	2	2-Panel
GLS_3.20	8	2	4-Panel
GLS_3.21	8	2	6-Panel
GLS_3.22	8	3	2-Panel
GLS_3.23	8	3	4-Panel
GLS_3.24	8	3	6-Panel
GLS_3.25	16	0	2-Panel
GLS_3.26	16	0	4-Panel
GLS_3.27	16	0	6-Panel
GLS_3.28	16	1	2-Panel
GLS_3.29	16	1	4-Panel
GLS_3.30	16	1	6-Panel
GLS_3.31	16	2	2-Panel
GLS_3.32	16	2	4-Panel
GLS_3.33	16	2	6-Panel
GLS_3.34	16	3	2-Panel
GLS_3.35	16	3	4-Panel
GLS_3.36	16	3	6-Panel

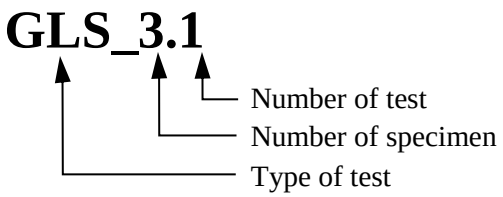

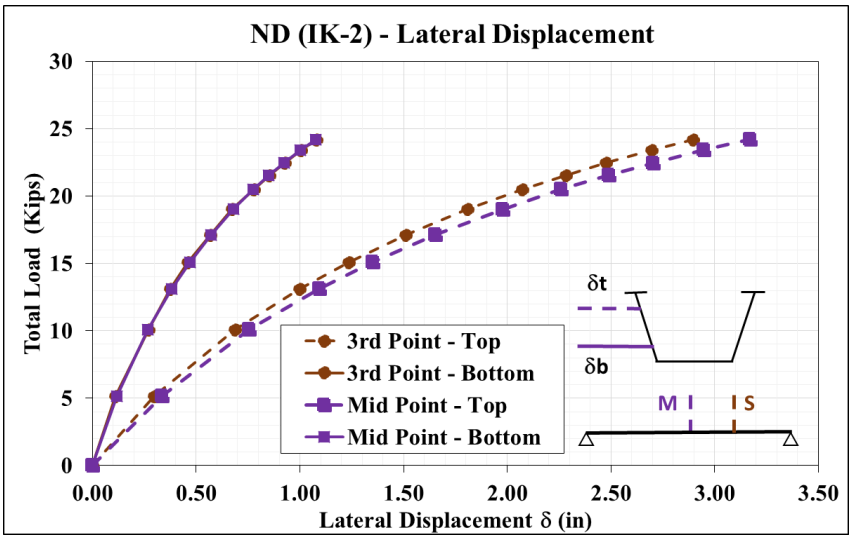

Figure C-190 – Total Load - Lateral Displacement - GLS_3.13

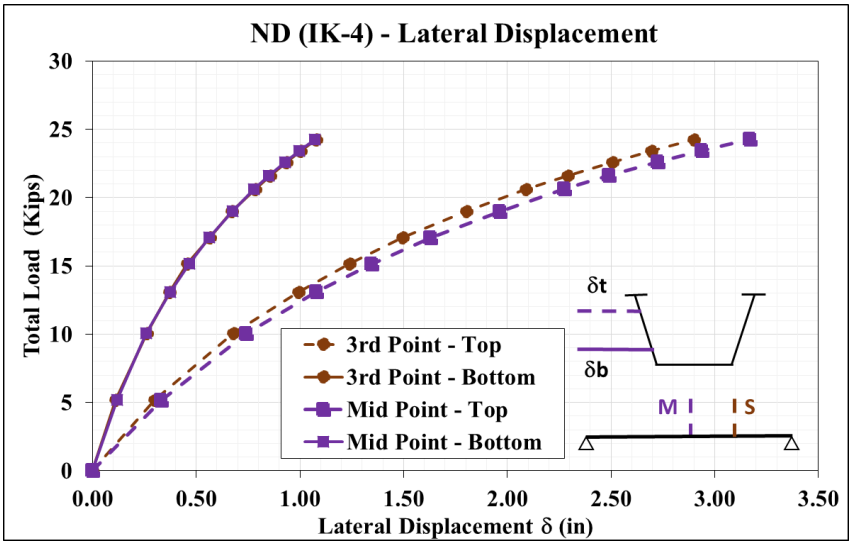

Figure C-191 – Total Load - Lateral Displacement - GLS_3.14

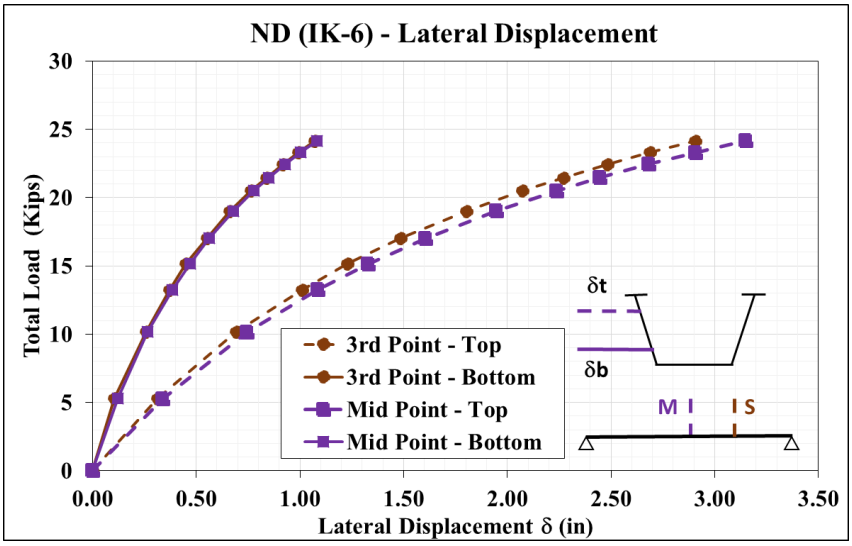

Figure C-192 – Total Load - Lateral Displacement - GLS_3.15

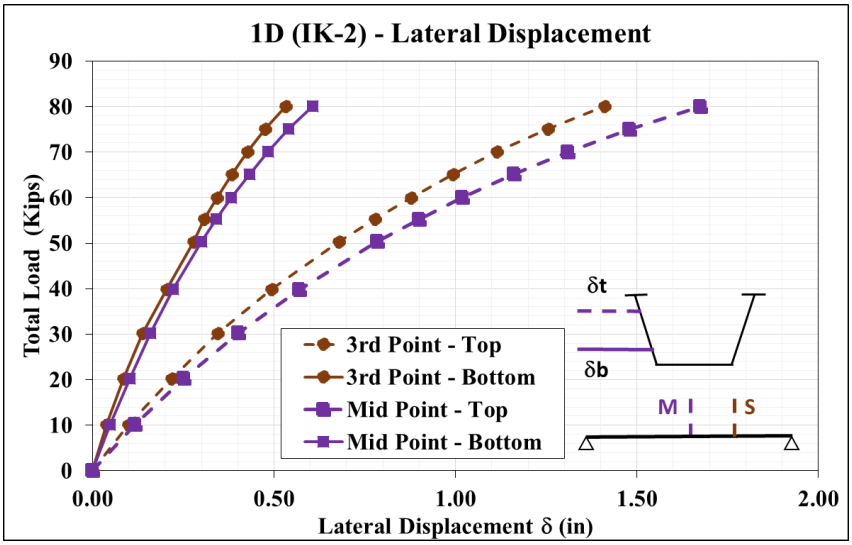

Figure C-193 – Total Load - Lateral Displacement - GLS_3.16

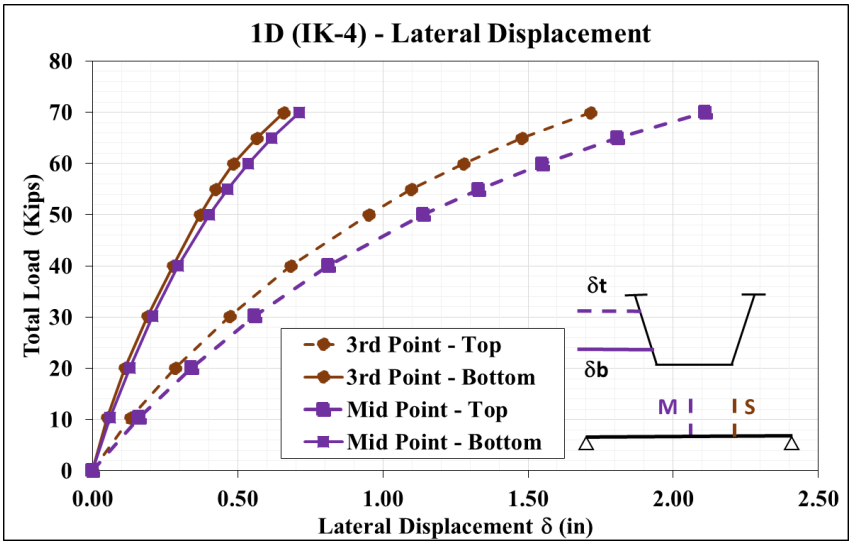

Figure C-194 – Total Load - Lateral Displacement - GLS_3.17

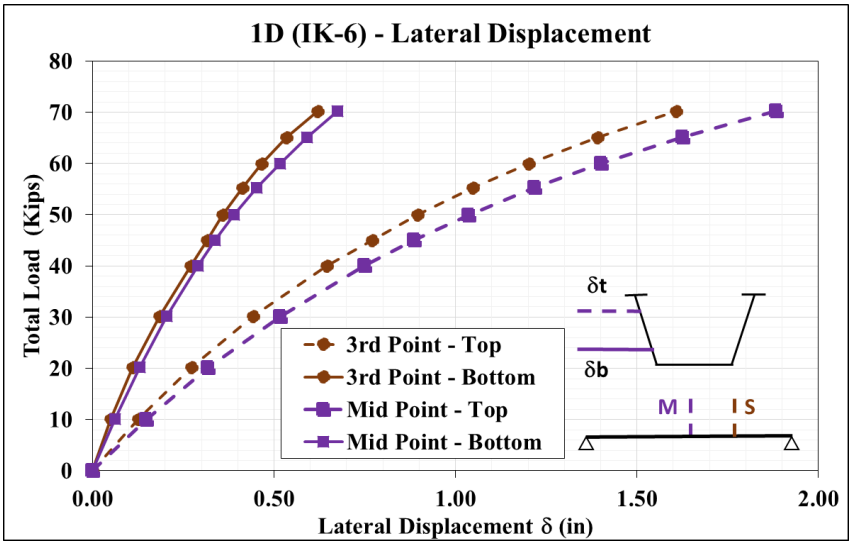

Figure C-195 – Total Load - Lateral Displacement - GLS_3.18

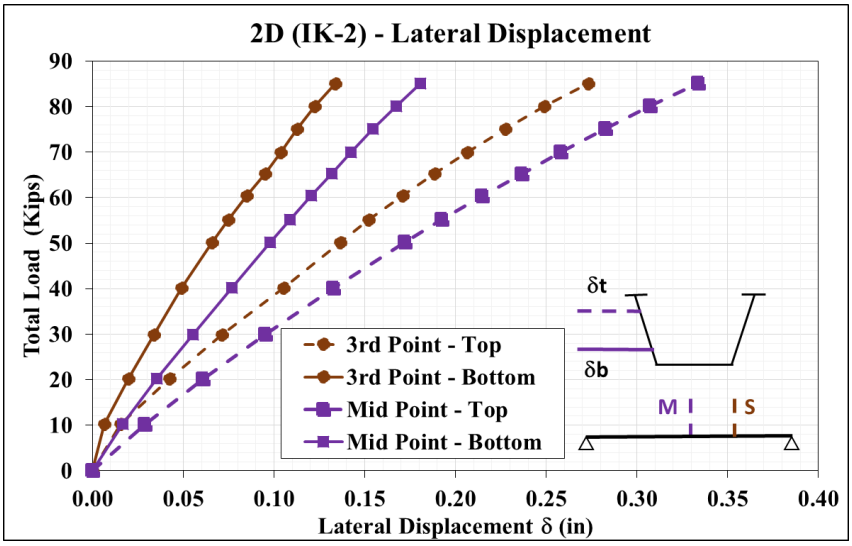

Figure C-196 – Total Load - Lateral Displacement - GLS_3.19

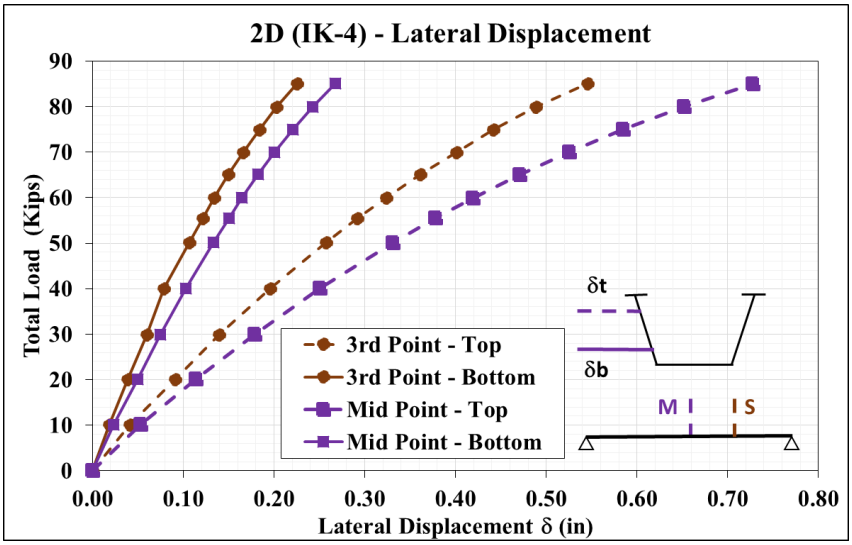

Figure C-197 – Total Load - Lateral Displacement - GLS_3.20

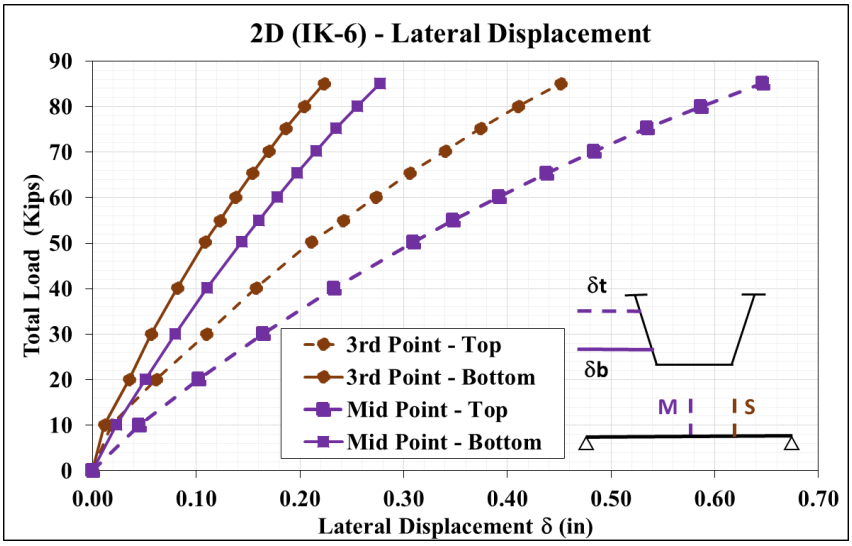

Figure C-198 – Total Load - Lateral Displacement - GLS_3.21

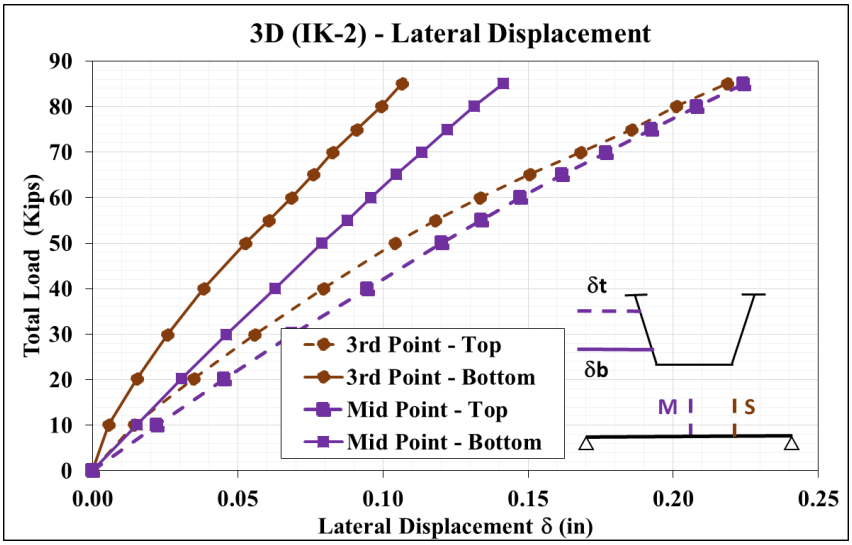

Figure C-199 – Total Load - Lateral Displacement - GLS_3.22

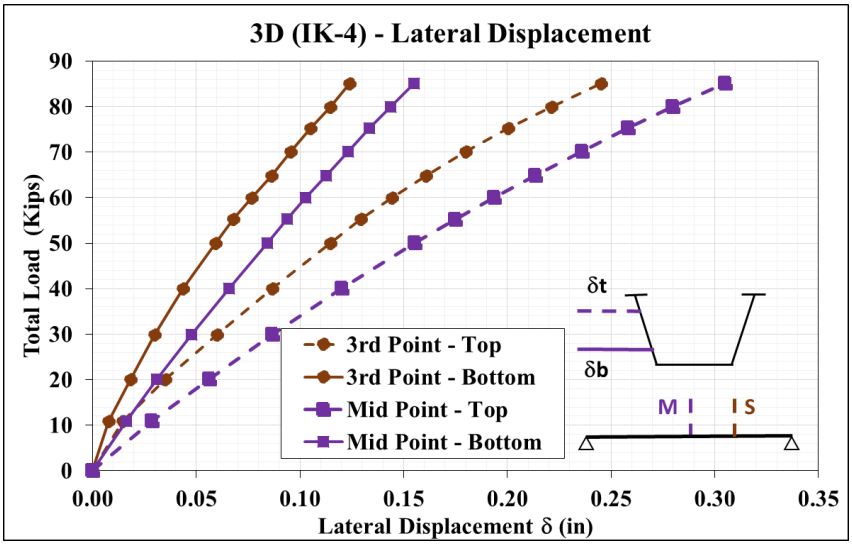

Figure C-200 – Total Load - Lateral Displacement - GLS_3.23

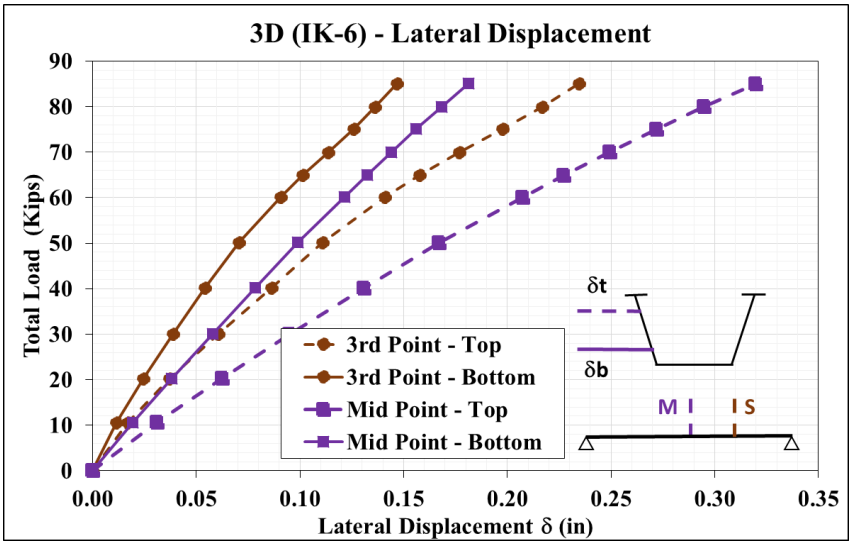

Figure C-201 – Total Load - Lateral Displacement - GLS_3.24

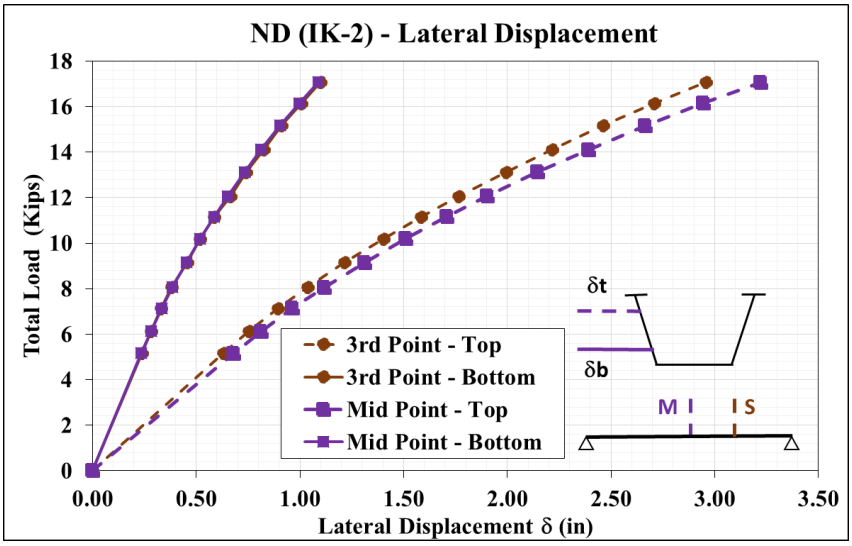

Figure C-202 – Total Load - Lateral Displacement - GLS_3.25

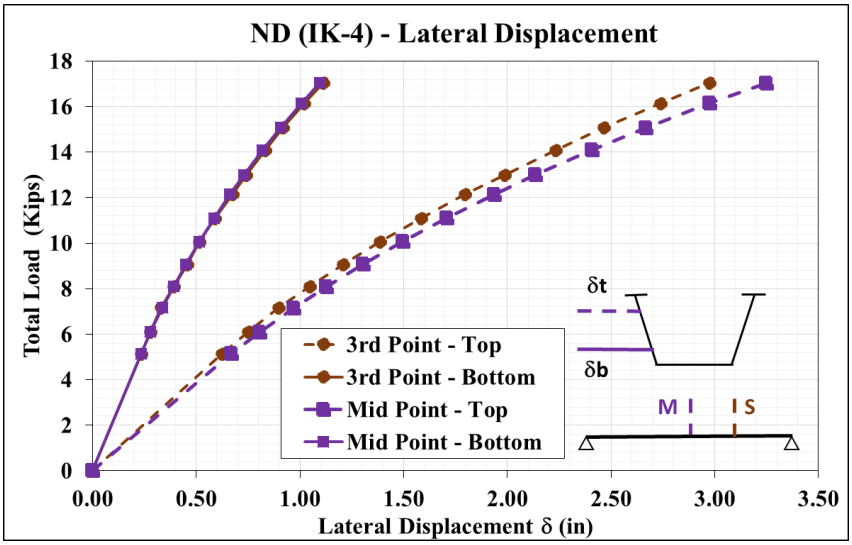

Figure C-203 – Total Load - Lateral Displacement - GLS_3.26

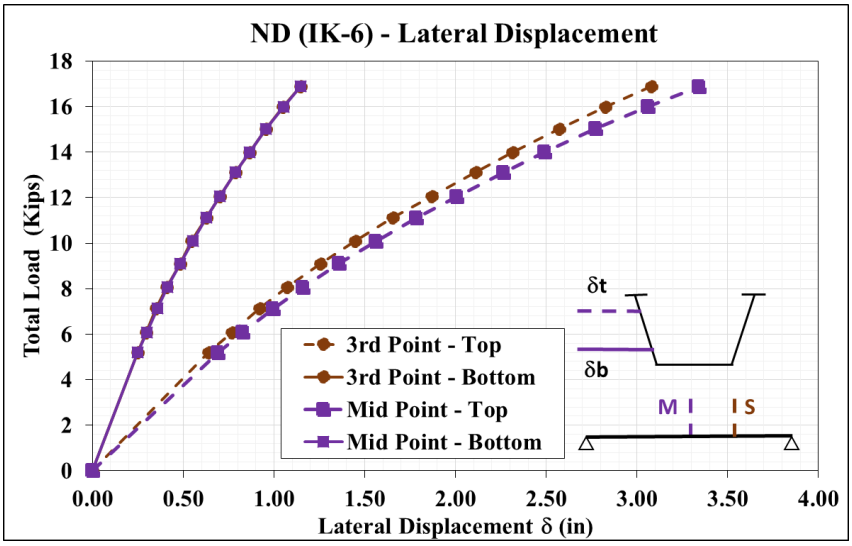

Figure C-204 – Total Load - Lateral Displacement - GLS_3.27

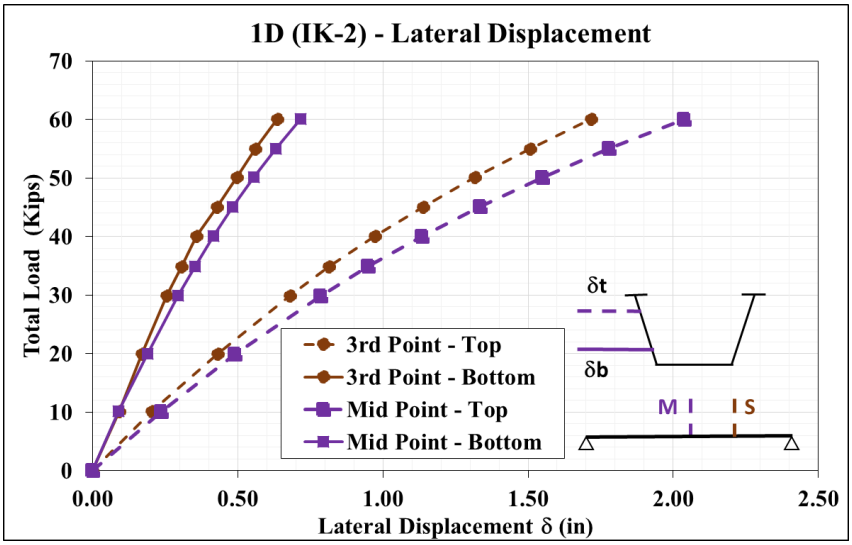

Figure C-205 – Total Load - Lateral Displacement - GLS_3.28

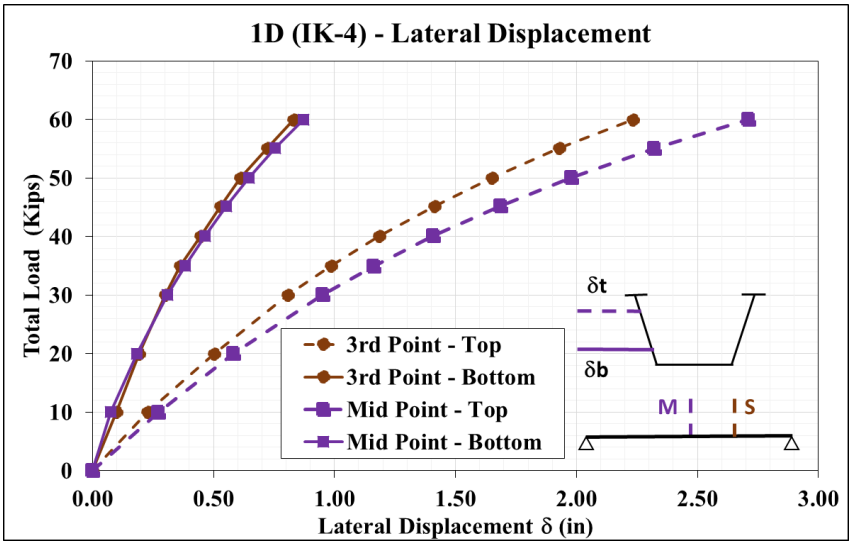

Figure C-206 – Total Load - Lateral Displacement - GLS_3.29

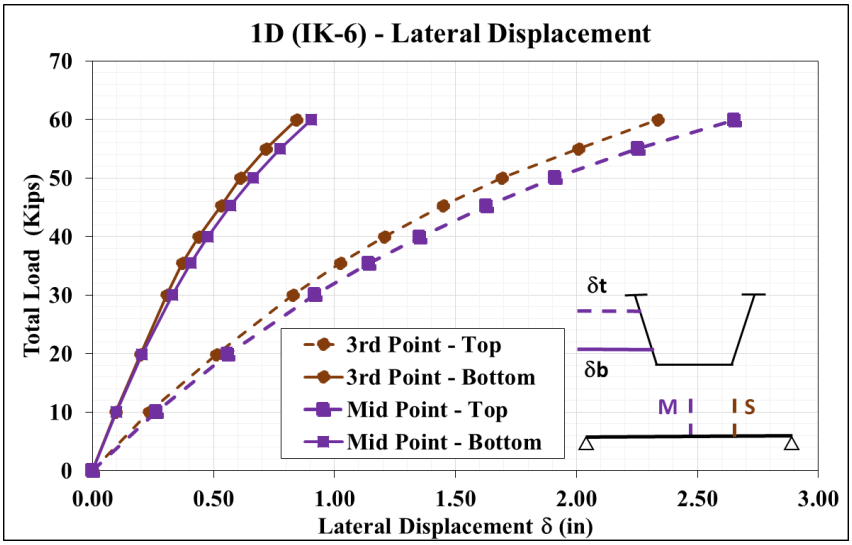

Figure C-207 – Total Load - Lateral Displacement - GLS_3.30

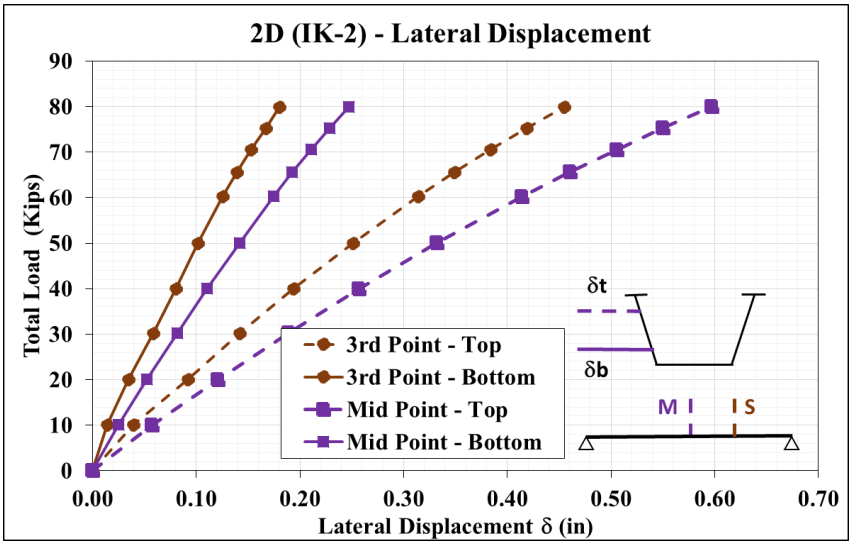

Figure C-208 – Total Load - Lateral Displacement - GLS_3.31

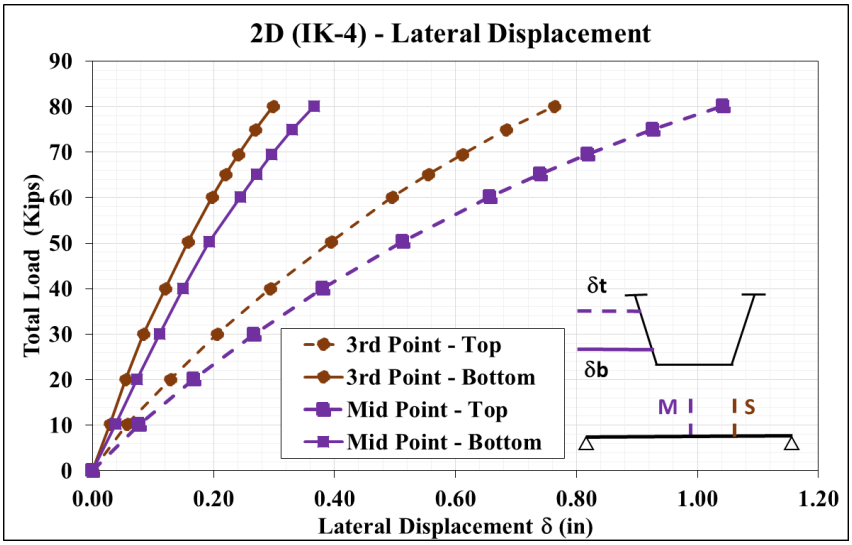

Figure C-209 – Total Load - Lateral Displacement - GLS_3.32

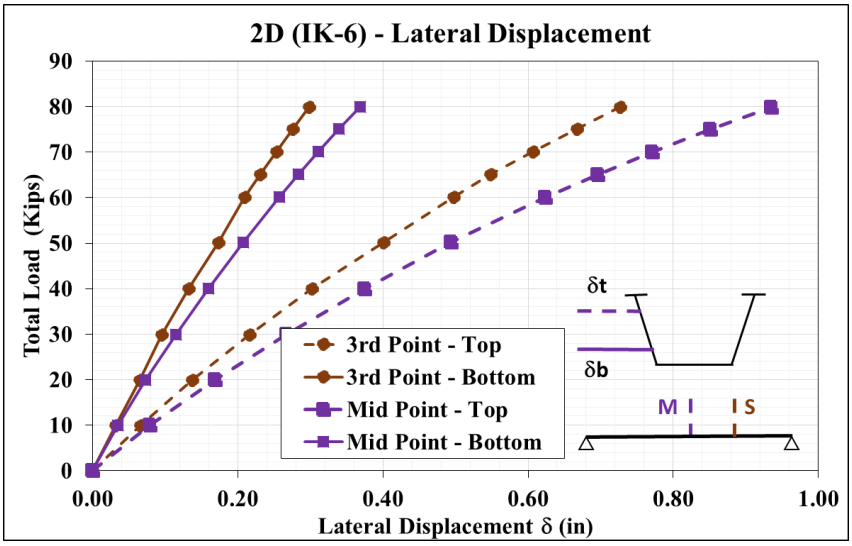

Figure C-210 – Total Load - Lateral Displacement - GLS_3.33

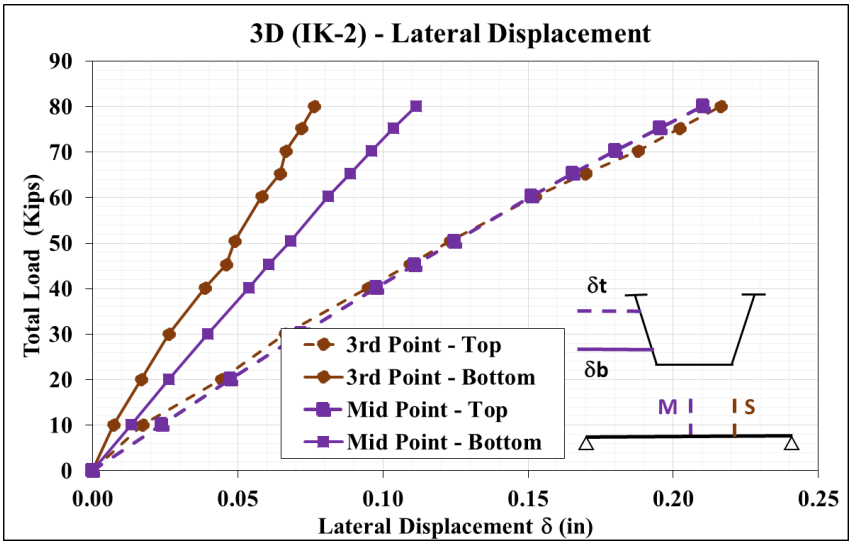

Figure C-211 – Total Load - Lateral Displacement - GLS_3.34

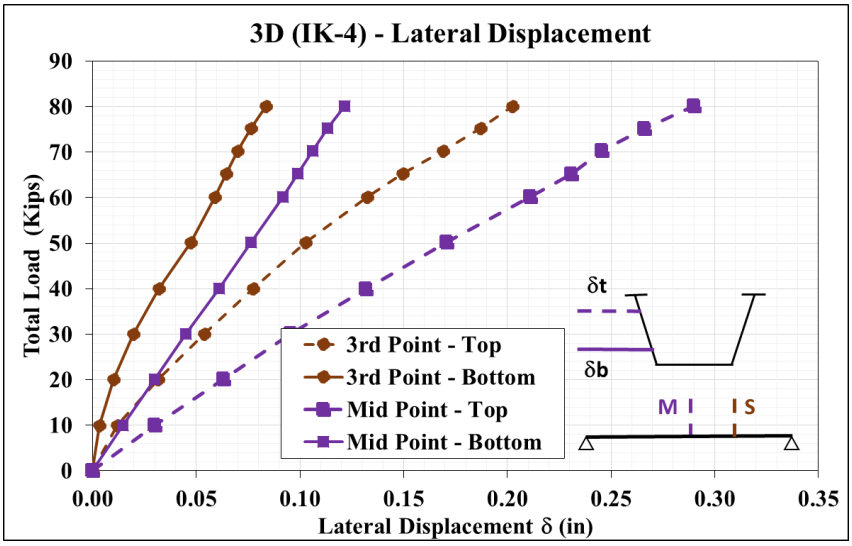

Figure C-212 – Total Load - Lateral Displacement - GLS_3.35

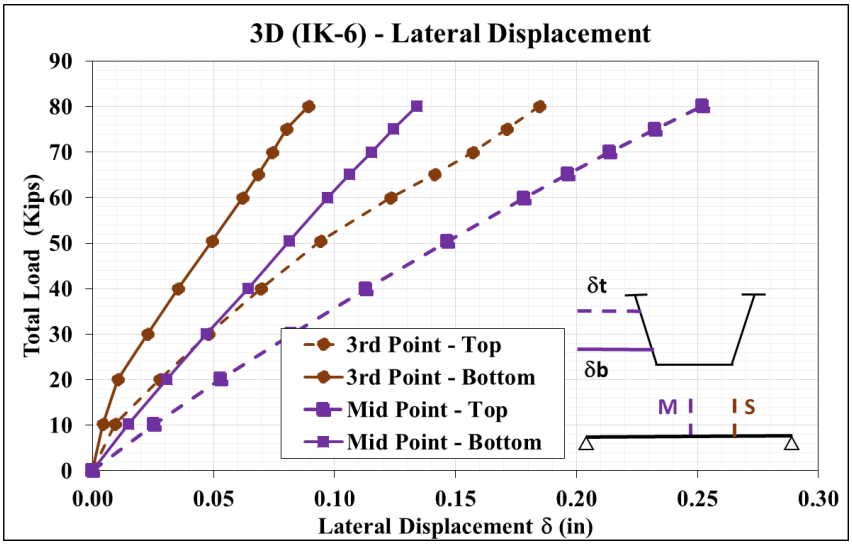

Figure C-213 – Total Load - Lateral Displacement - GLS_3.36

C.3.6 Tub #3 (Flatter Web Tub Girder) – Bracing Forces

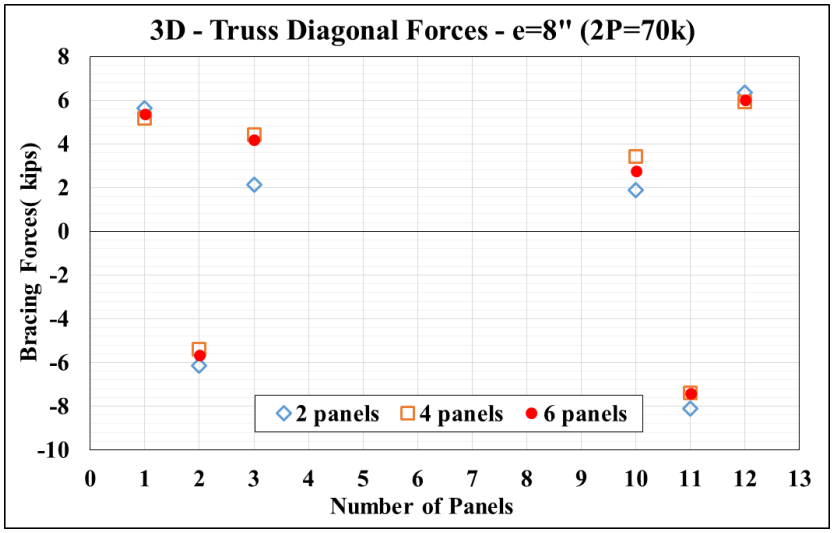

Figure C-214 – Top Lateral Bracing Diagonal Forces – 3 Truss Diagonals per End – e=8in

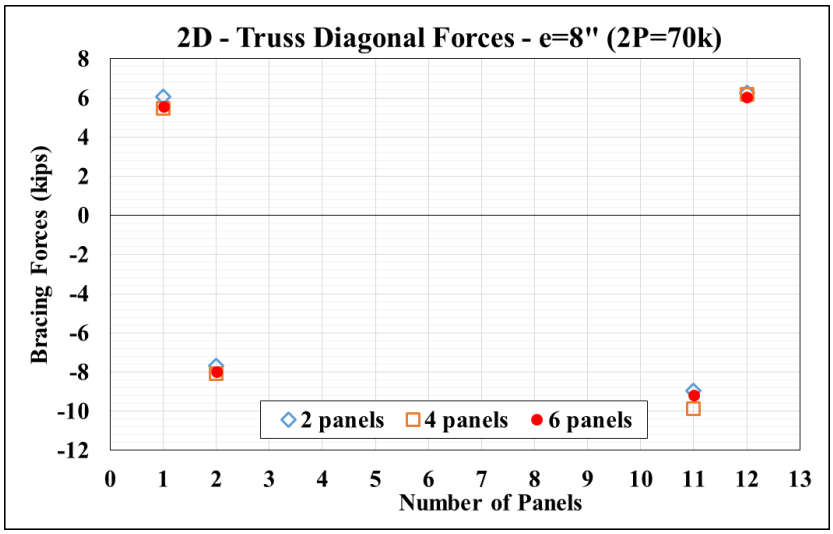

Figure C-215 – Top Lateral Bracing Diagonal Forces – 2 Truss Diagonals per End – e=8in

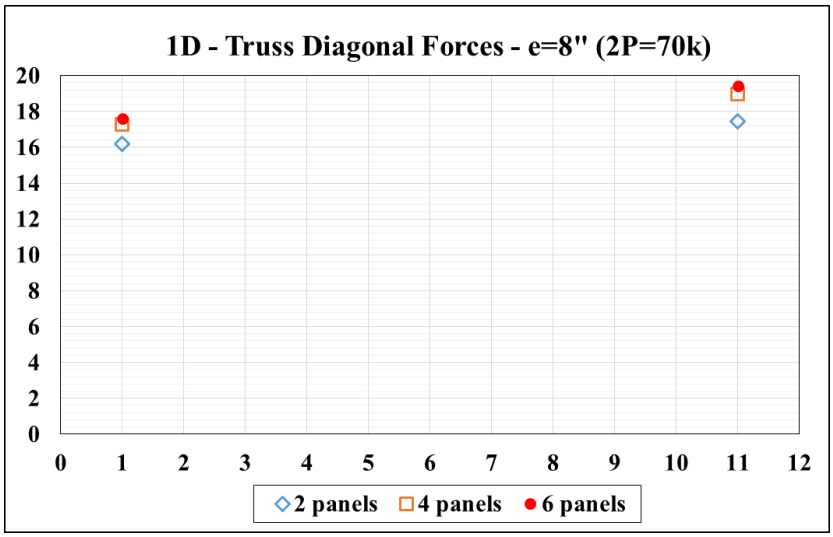

Figure C-216 – Top Lateral Bracing Diagonal Forces -1 Truss Diagonals per End – e=8in

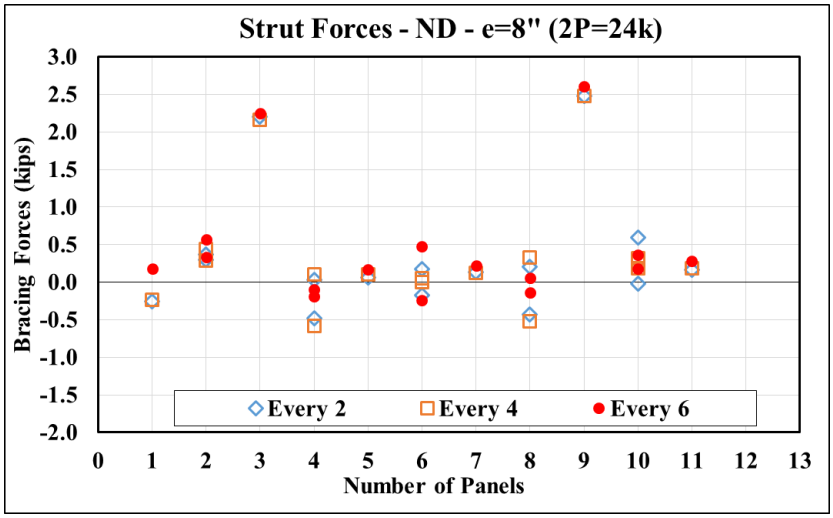

Figure C-217 – Strut Forces - 0 Truss Diagonals per End – e=8in

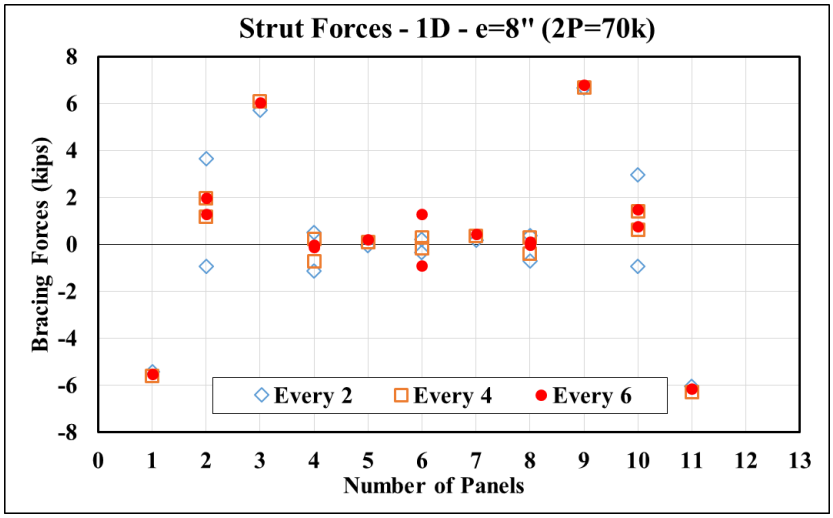

Figure C-218 – Strut Forces - 1 Truss Diagonals per End – e=8in

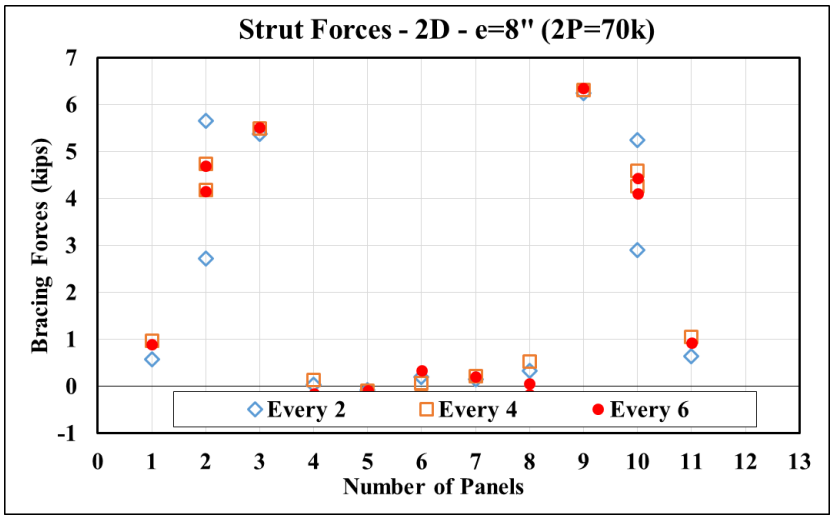

Figure C-219 – Strut Forces - 2 Truss Diagonals per End – e=8in

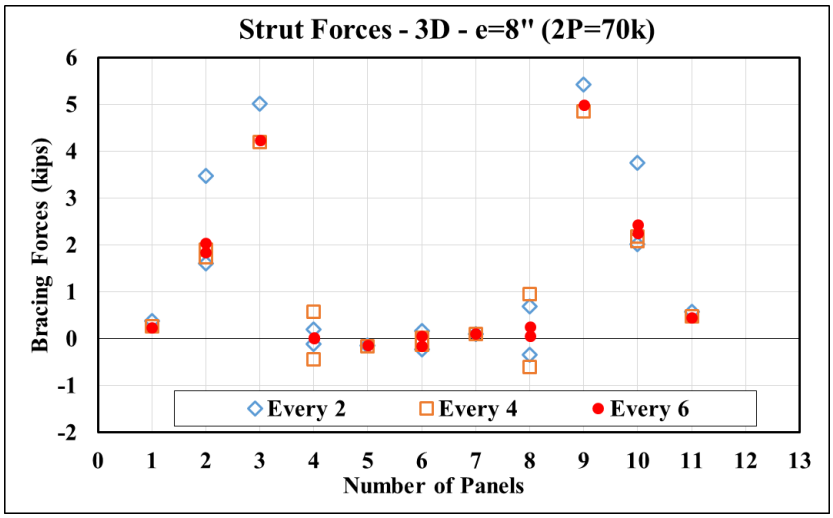

Figure C-220 – Strut Forces - 3 Truss Diagonals per End – e=8in

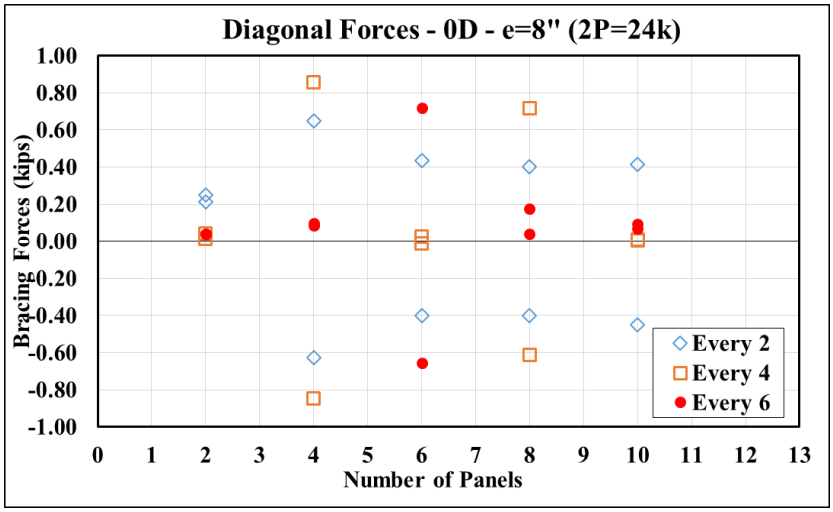

Figure C-221 – K-frame Diagonal Forces - 0 Truss Diagonals per End – e=8in

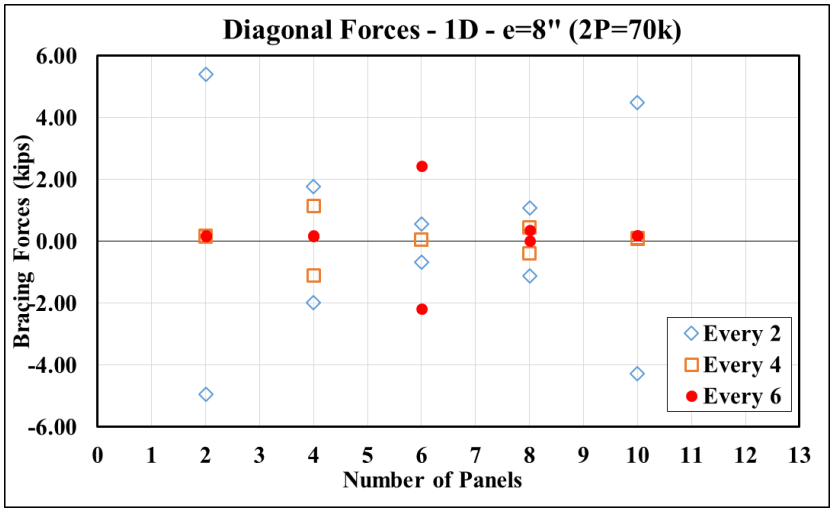

Figure C-222 – K-frame Diagonal Forces - 1 Truss Diagonals per End – e=8in

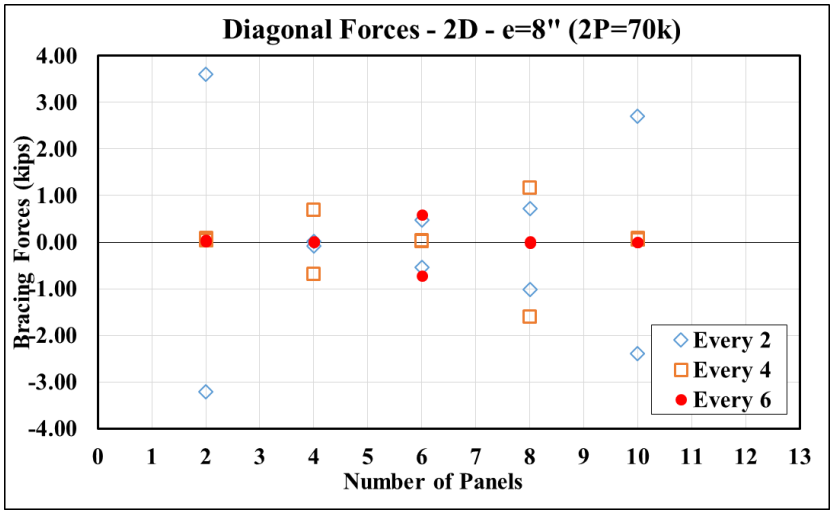

Figure C-223 – K-frame Diagonal Forces - 2 Truss Diagonals per End – e=8in

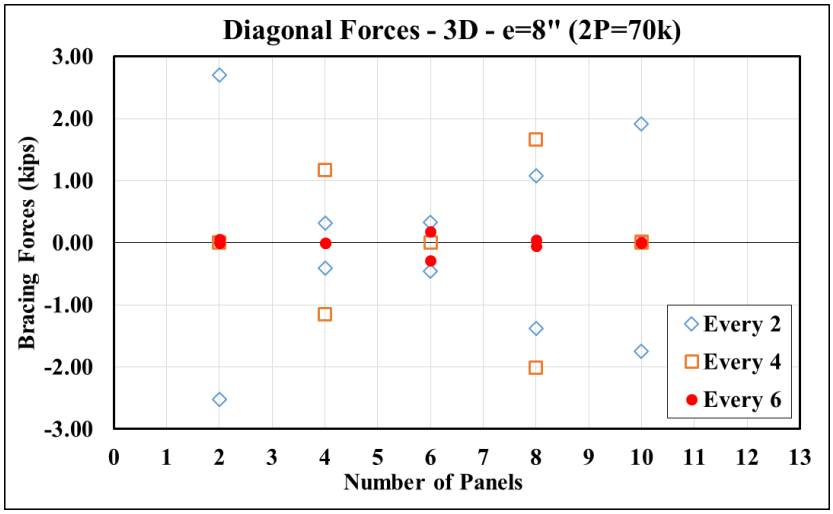

Figure C-224 – K-frame Diagonal Forces - 3 Truss Diagonals per End – e=8in

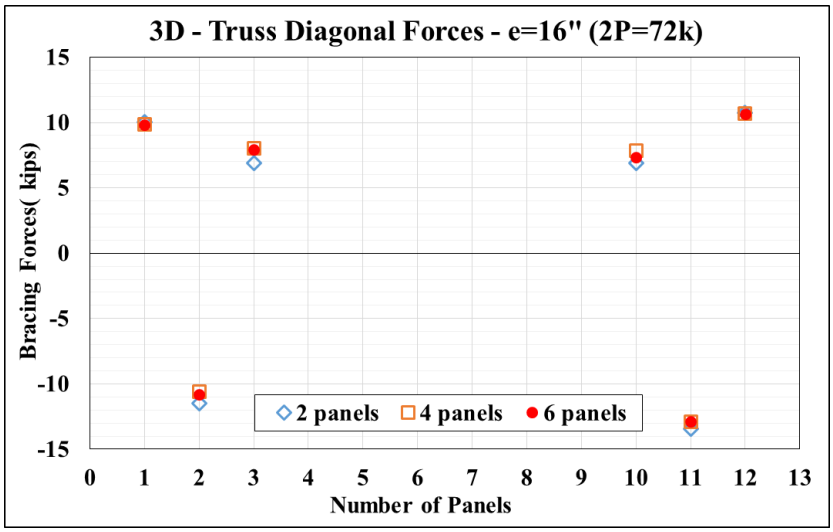

Figure C-225 – Top Lateral Bracing Diagonal Forces – 3 Truss Diagonals per End – e=16in

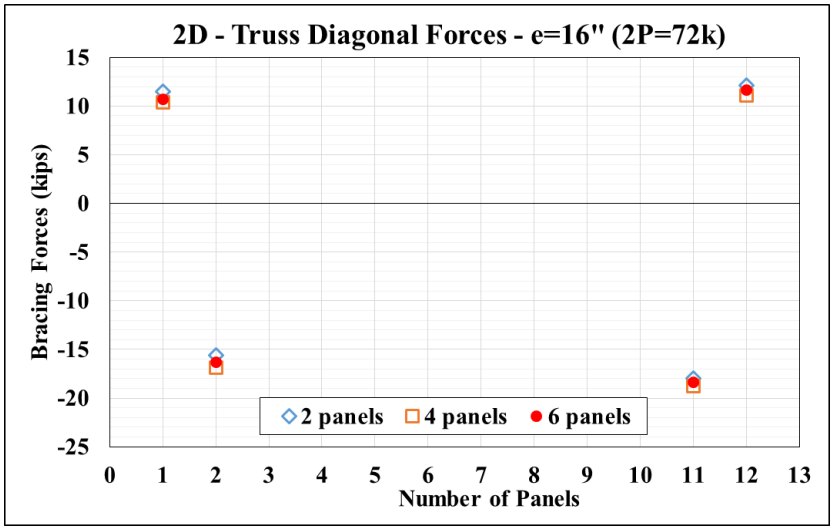

Figure C-226 – Top Lateral Bracing Diagonal Forces – 2 Truss Diagonals per End – e=16in

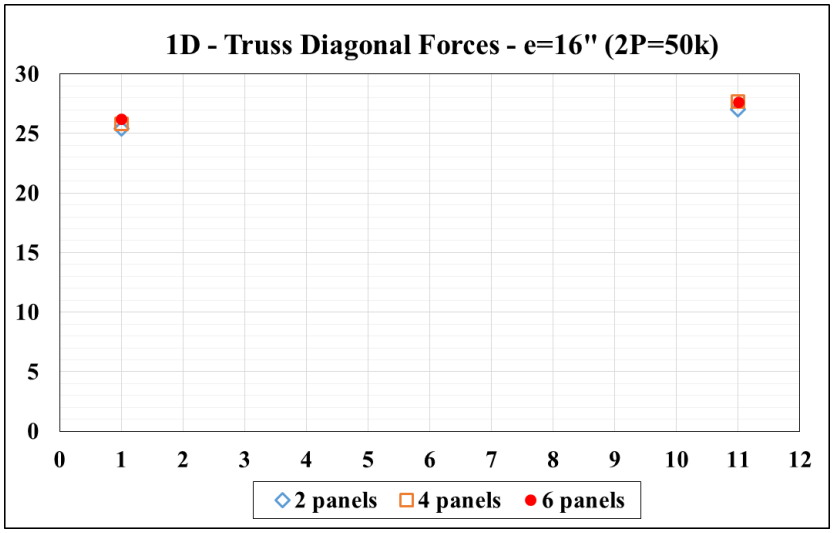

Figure C-227 – Top Lateral Bracing Diagonal Forces -1 Truss Diagonals per End – e=16in

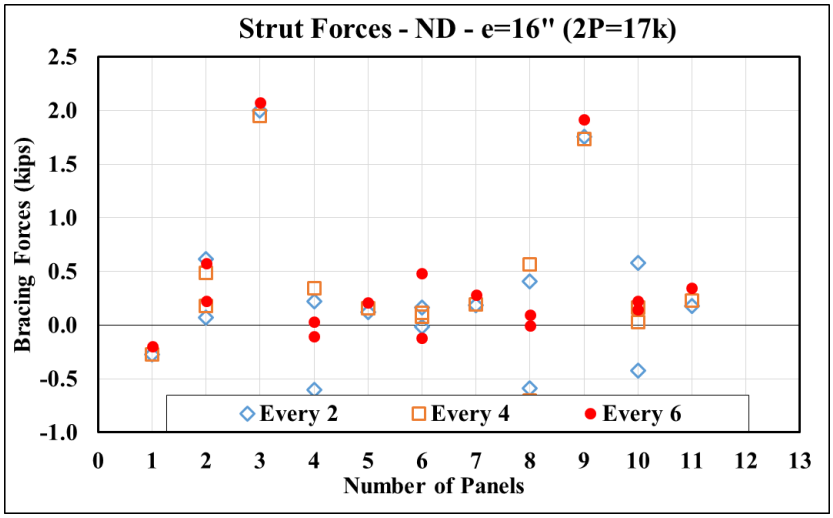

Figure C-228 – Strut Forces - 0 Truss Diagonals per End – e=16in

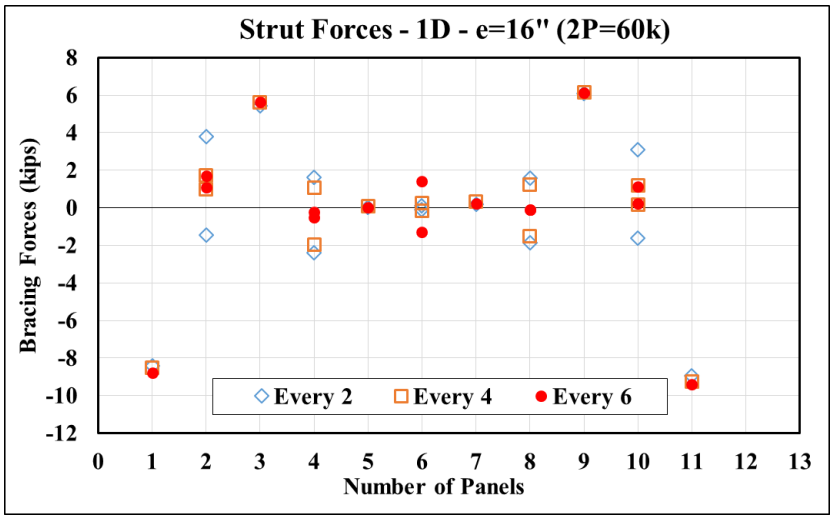

Figure C-229 – Strut Forces - 1 Truss Diagonals per End – e=16in

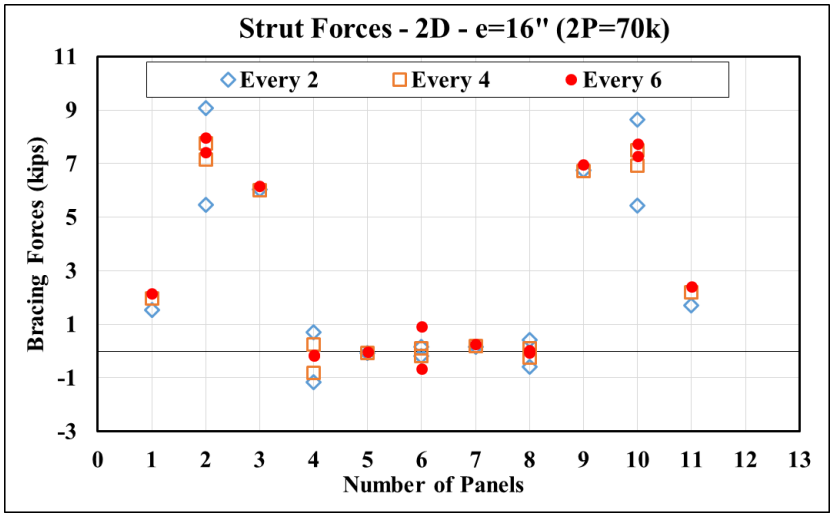

Figure C-230 – Strut Forces - 2 Truss Diagonals per End – e=16in

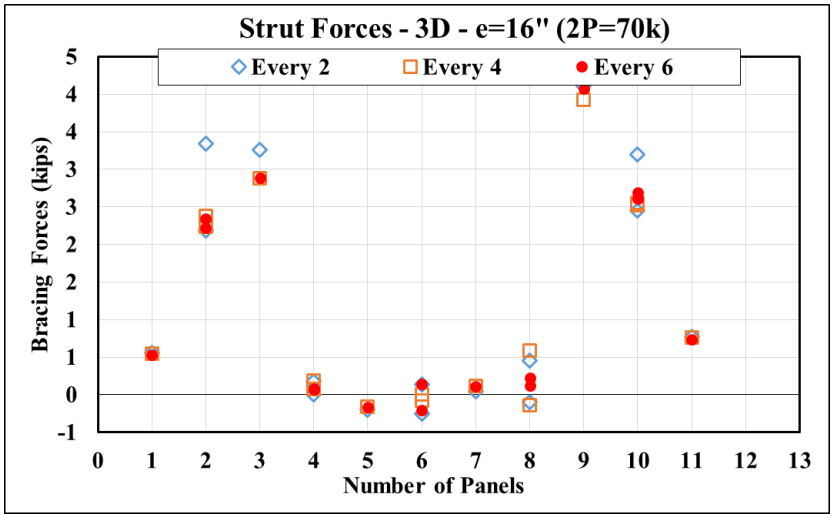

Figure C-231 – Strut Forces - 3 Truss Diagonals per End – e=16in

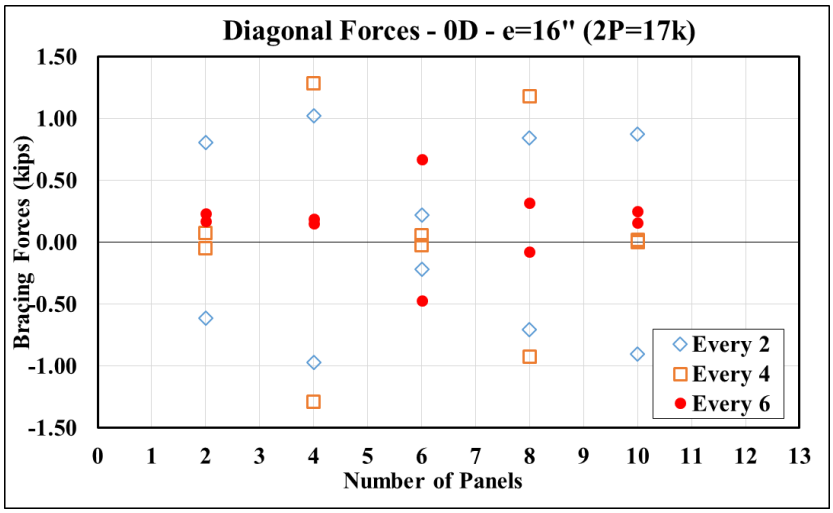

Figure C-232 – K-frame Diagonal Forces - 0 Truss Diagonals per End – e=16in

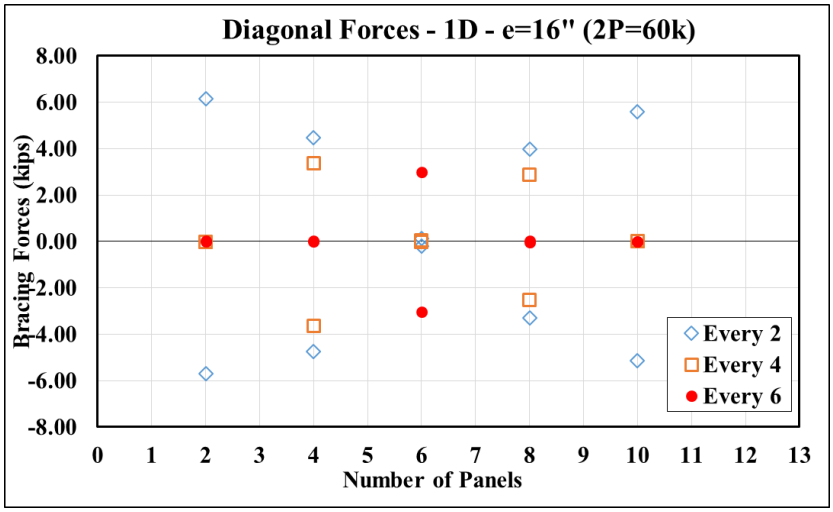

Figure C-233 – K-frame Diagonal Forces - 1 Truss Diagonals per End – e=16in

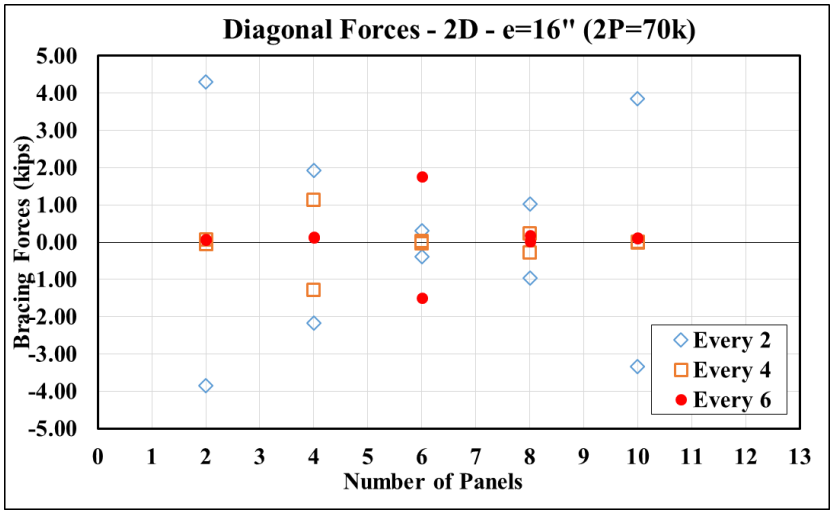

Figure C-234 – K-frame Diagonal Forces - 2 Truss Diagonals per End – e=16in

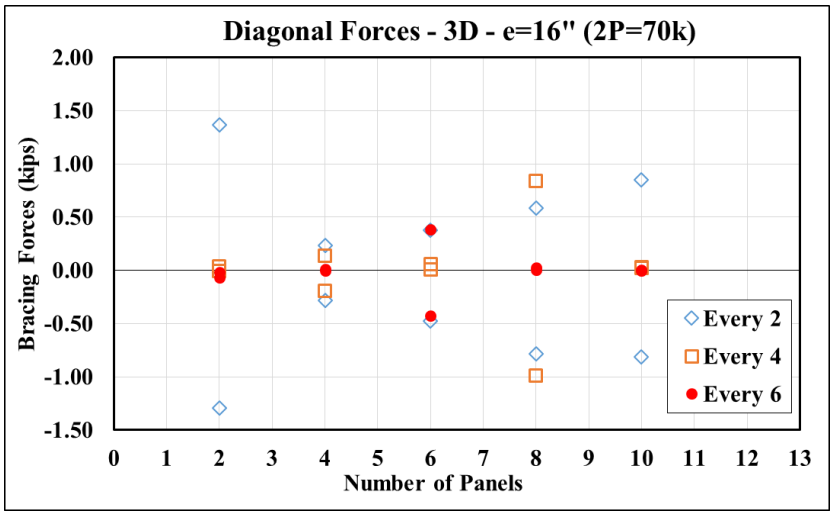

Figure C-235- K-frame Diagonal Forces - 3 Truss Diagonals per End – e=16in

Appendix D. Finite Element Analyses Results

D.1 Experiment vs. FEA

D.1.1 Load-Deflection Response

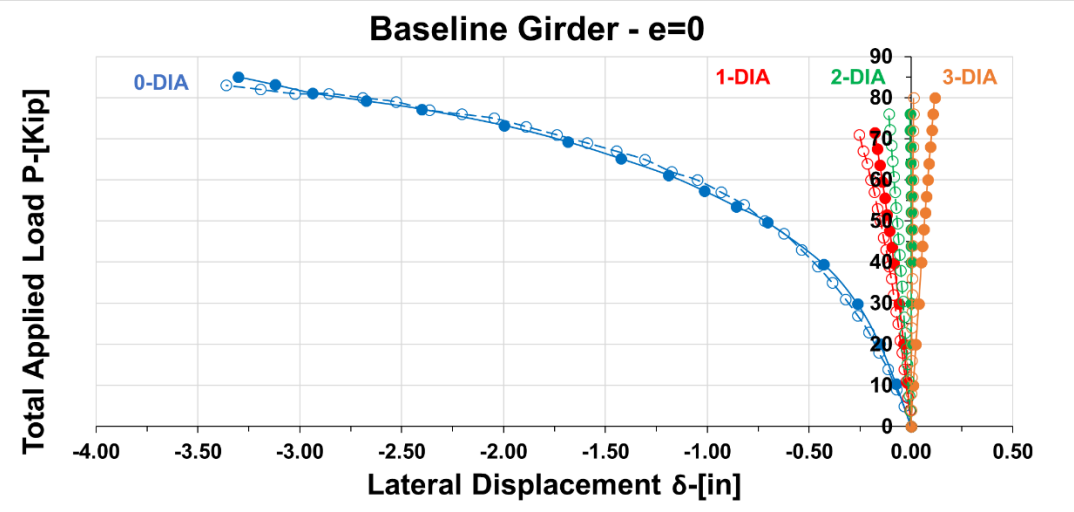

Figure D-1 – Load vs Lateral Displacement – Baseline – Concentric – Various TLB

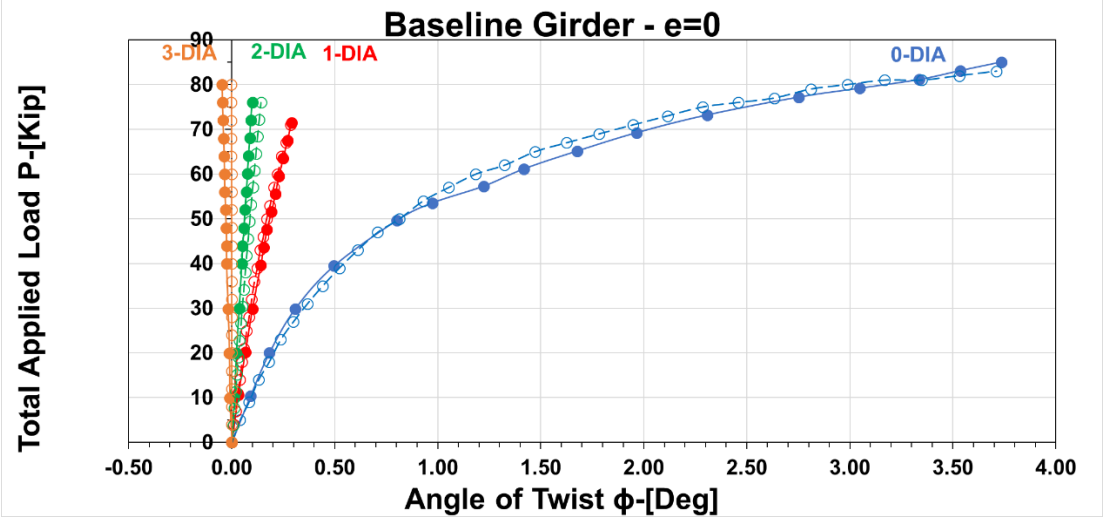

Figure D-2 – Load vs Angle of Twist – Baseline – Concentric – Various TLB

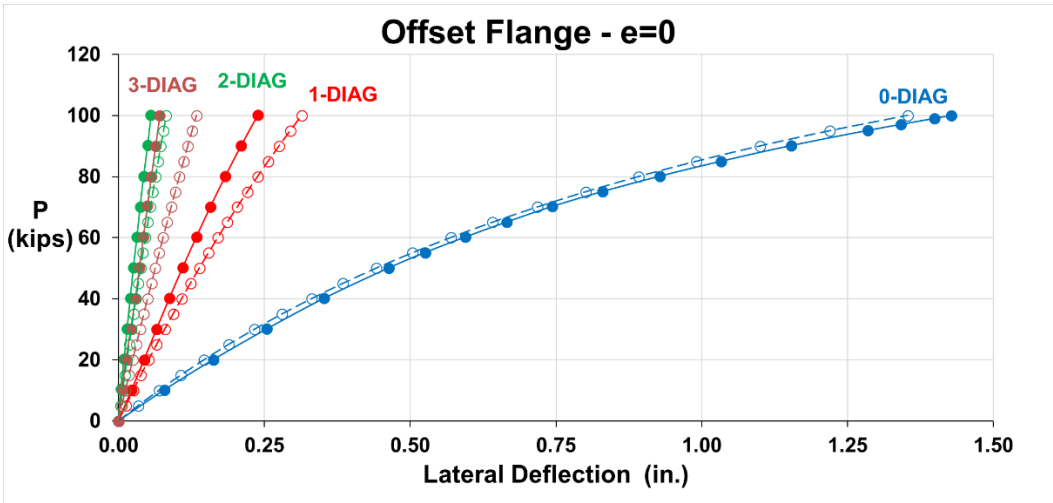

Figure D-3 – Load vs Lateral Displacement – Offset Flange – Concentric – Various TLB

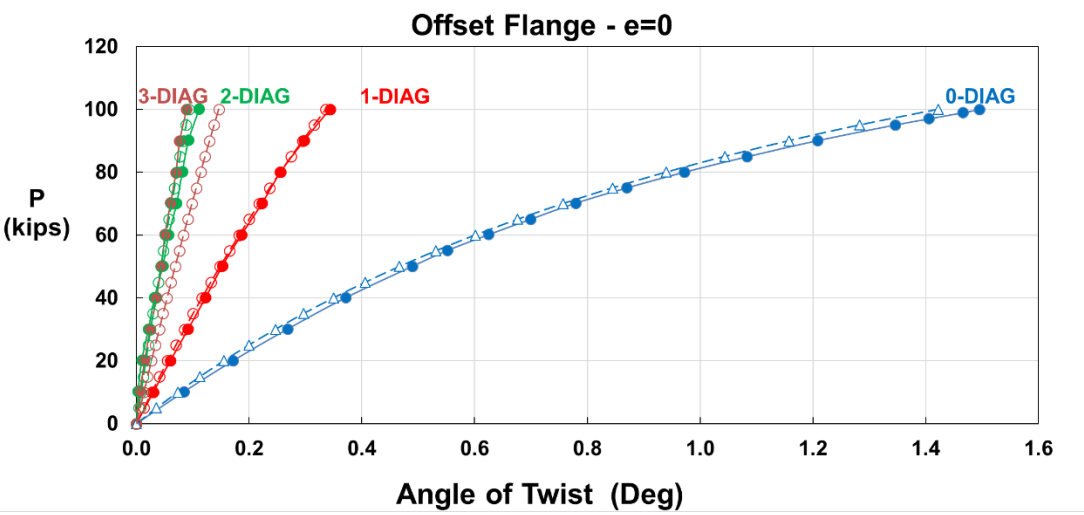

Figure D-4 – Load vs Angle of Twist – Offset Flange – Concentric – Various TLB

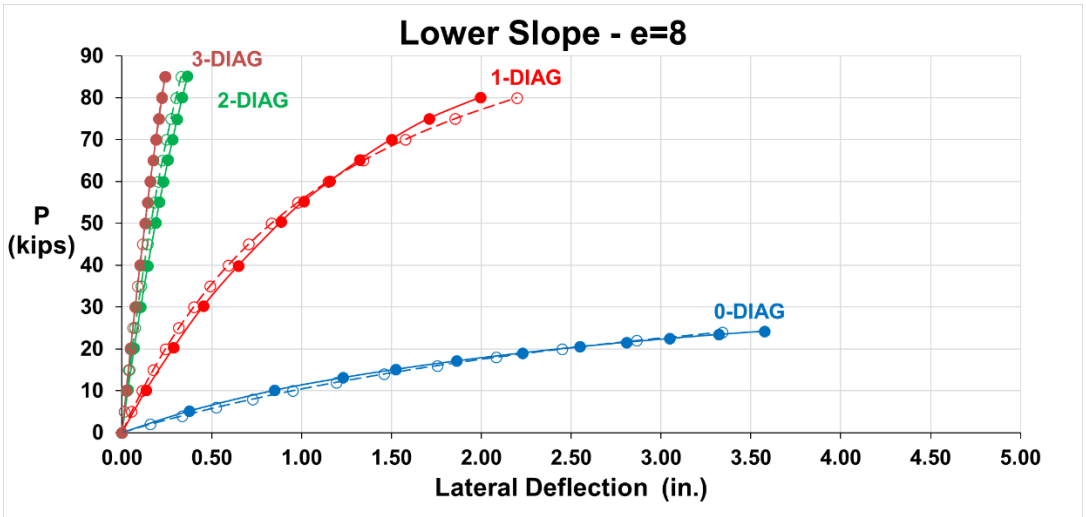

Figure D-5 – Load vs Lateral Displacement – Lower Slope – e=8 – Various TLB

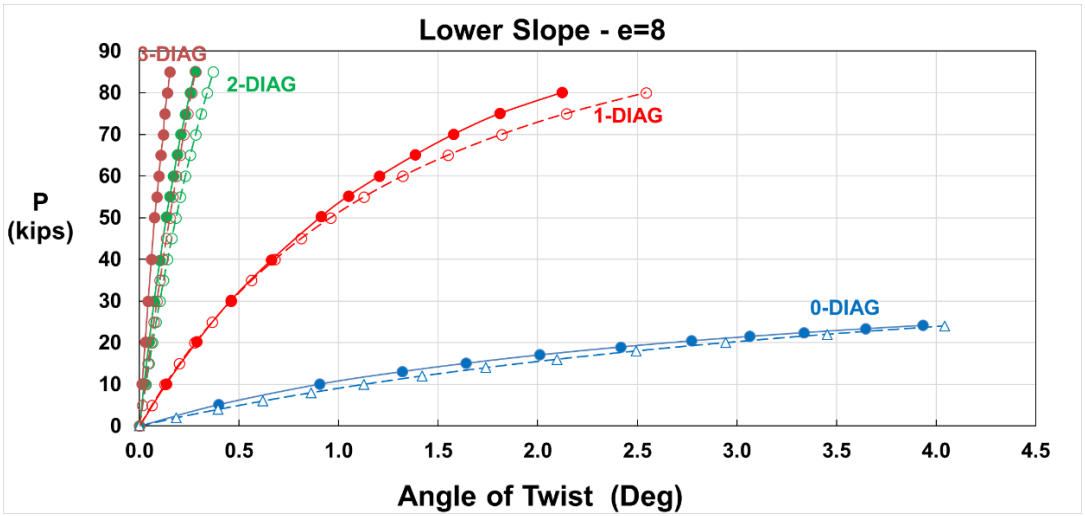

Figure D-6 – Load vs Angle of Twist – Lower Slope – e=8 – Various TLB

D.1.2 Load-Deflection Response with Eccentricity

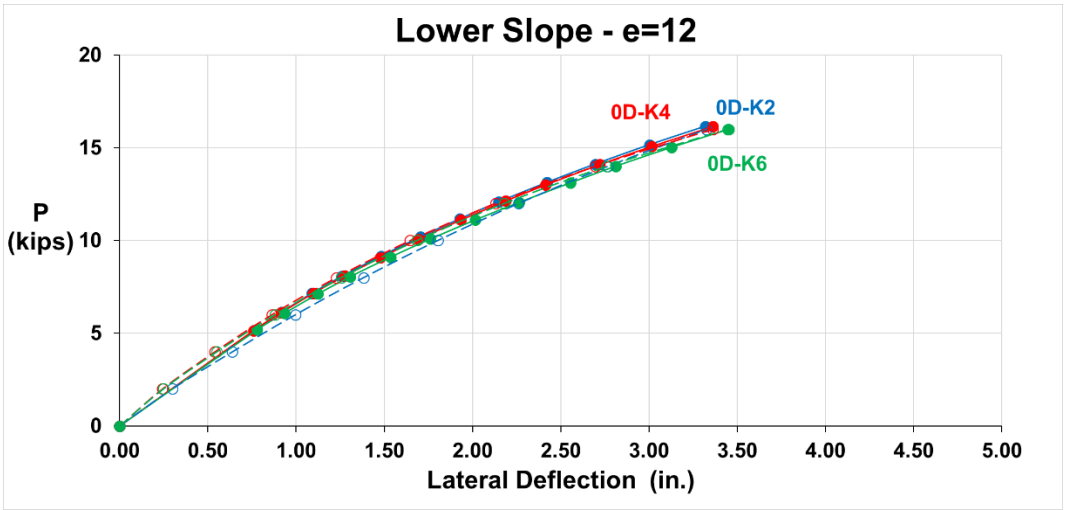

Figure D-7 – Load vs Lateral Displacement – Lower Slope – e=12 – Various Internal K

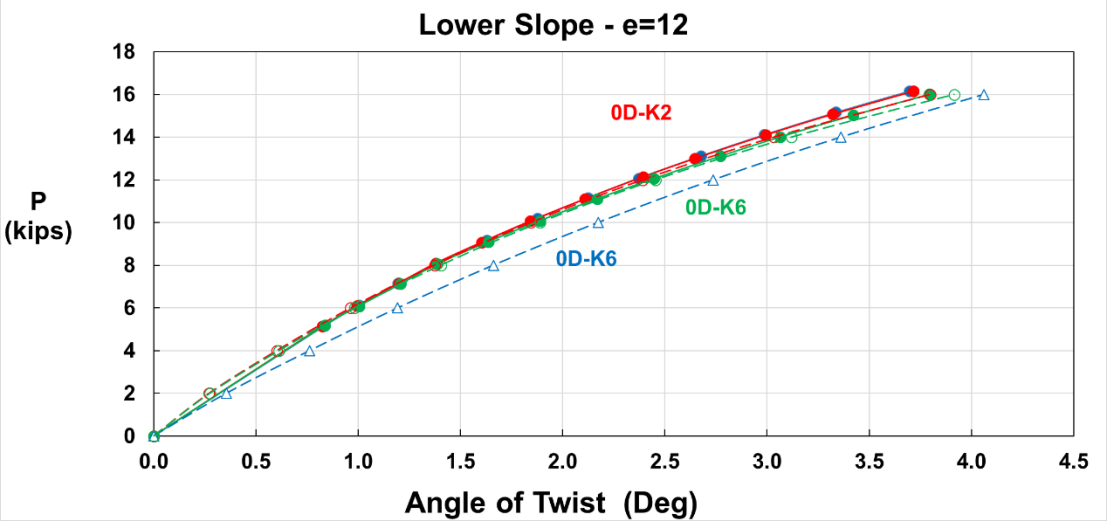

Figure D-8 – Load vs Angle of Twist – Lower Slope – e=12 – Various Internal K

D.1.3 Load-Brace Force Response

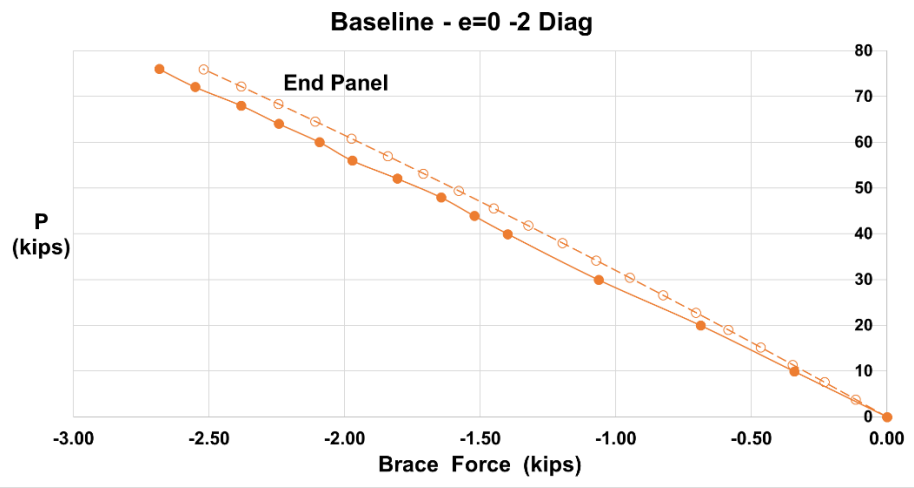

Figure D-9 – Load vs Lateral Brace Force – Baseline – e=0 – 2 Diagonals

D.1.4 Brace Force @ Different Load Level

Filled Marker- Exp; Open Marker - FEA

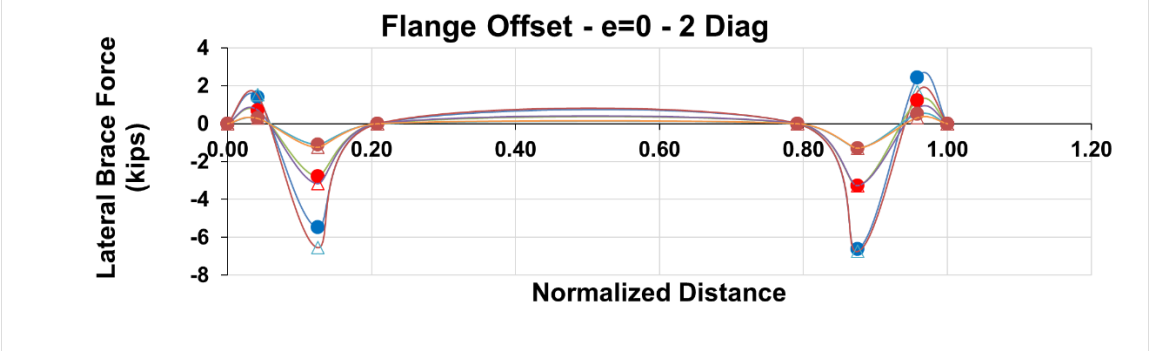

Figure D-10 –Lateral Brace Force @ Various P– Flange Offset – e=0 – 2 Diagonals

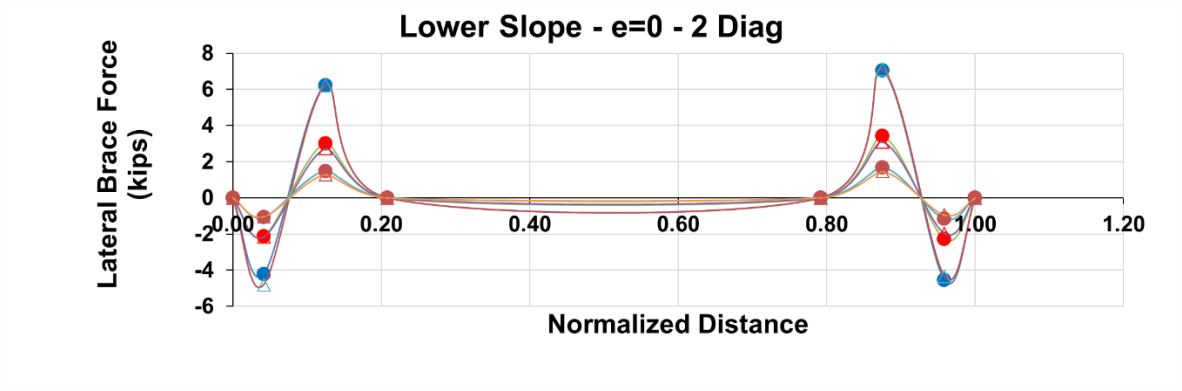

Figure D-11 –Lateral Brace Force @ Various P– Flatter Slope – e=0 – 2 Diagonals

D.2 Improved Bracing Detail-Parametric Study

D.2.1 Resized Prototype Girder Dimension

Table D-1 – Prototype Girders - Plate Dimensions - 1-Span

						Straight				Curved (Recalculated)			
	L/D		Span	Panels		Top Flange		Bottom Fl.	Web	Top Flange		Bottom Fl	Web
	(Theo.)	(Real)	(ft)	Length (ft)	QTY(ea)	tf (in)	bt(in)	tb (in)	tw (in)	tf (in)	bt(in)	tb (in)	tw (in)
T90	20	22	168.00	10.50	16.00	1.50	18	1.00	0.75	2.00	20	2.00	0.8125
	25	26	192.00	12.00	16.00	1.75	18	1.50	0.813	2.00	30	1.50	0.8125
	30	29	216.00	13.50	16.00	2.50	20	2.00	0.813	2.88	30	2.00	0.8125
T36	20	20	60.00	6.00	10.00	0.75	12	0.75	0.5	0.75	12	0.75	0.5000
	25	24	72.00	7.20	10.00	0.75	15	0.75	0.5	0.75	15	0.75	0.5000
	30	30	90.00	9.00	10.00	1.00	15	1.00	0.625	1.00	15	1.00	0.6250
	35	35	105.00	10.50	10.00	1.50	15	1.00	0.625	1.50	15	1.00	0.6250

Table D-2 – Prototype Girders - Plate Dimensions - 2-Span

	L/D (Theo.)	L/D (Real)	Span (ft)	Panels Length (ft)	Panels QTY(ea)	Straight Top Flange tf (in)	Straight Top Flange bt(in)	Straight Bottom Fl. tb (in)	Straight Web tw (in)	Curved (Recalculated) Top Flange tf (in)	Curved (Recalculated) Top Flange bt(in)	Curved (Recalculated) Bottom Fl tb (in)	Curved (Recalculated) Web tw (in)
T90	25	26	192.00	12.00	16.00	1.75	18	1.50	0.813	2.50	20	1.50	0.813
						2.00	20	2.00	0.813	2.00	20	2.00	0.813
	30	29	216.00	13.50	16.00	2.50	20	2.00	0.813	3.00	30	2.00	0.813
						2.88	30	2.00	0.813	2.88	30	2.00	0.813
	35	35	264.00	16.50	16.00	3.00	20	2.50	0.813	4.50	30	2.50	0.813
						3.50	30	2.50	0.813	3.50	30	2.50	0.813
	40	40	300.00	18.75	16.00	3.00	30	2.50	0.813	4.50	30	2.50	0.813
						3.75	30	2.75	0.813	3.75	30	2.75	0.813
T36	25	24	72.00	7.20	10.00	0.75	15	0.75	0.500	0.75	15	0.75	0.500
						1.00	15	1.00	0.500	1.00	15	1.00	0.500
	30	30	90.00	9.00	10.00	1.00	15	1.00	0.625	1.00	15	1.00	0.625
						1.50	15	1.25	0.625	1.50	15	1.25	0.625
	35	35	105.00	10.50	10.00	1.50	15	1.00	0.625	2.00	15	1.00	0.625
						2.00	15	1.50	0.625	2.00	15	1.50	0.625
	40	40	120.00	12.00	10.00	1.75	15	1.00	0.625	2.50	15	1.00	0.625
						2.75	15	1.50	0.625	2.75	15	1.5	0.625

Negative Momet Region
Positive Mometn region

D.2.2 Result Summary with Partial Length Top Lateral Bracing

Table D-3 – Summary of Results – Partial Top Lateral Bracing

						Normalized Displacement				Normalized Twist			
Section	**Radius**	**L/D**	**System**	**δmax (in)**	**βmax (deg)**	**1L**	**0.6L**	**0.5L**	**0.4L**	**1L**	**0.6L**	**0.5L**	**0.4L**
T36	Straight	20	1S	0.72	1.00	0.10	0.25	0.28	0.37	0.13	0.23	0.27	0.34
		25	1S	0.86	1.00	0.12	0.27	0.35	0.47	0.51	0.64	0.69	0.79
		30	1S	1.08	1.00	0.14	0.34	0.43	0.60	0.28	0.49	0.52	0.77
		35	1S	1.26	1.00	0.16	0.42	0.55	0.82	0.33	0.67	0.85	1.19
		25	2S	0.86	1.00	0.09	0.23	0.30	0.42	0.15	0.28	0.34	0.39
		30	2S	1.08	1.00	0.11	0.28	0.37	0.53	0.23	0.39	0.45	0.63
		35	2S	1.26	1.00	0.13	0.35	0.48	0.71	0.27	0.51	0.67	0.97
		40	2S	1.44	1.00	0.16	0.46	0.65	1.00	0.38	0.77	1.04	1.57
	2500ft	20	1S	0.72	1.00	0.13	0.26	0.32	0.42	0.13	0.23	0.27	0.35
		25	1S	0.86	1.00	0.17	0.33	0.41	0.55	0.23	0.36	0.43	0.58
		30	1S	1.08	1.00	0.24	0.46	0.60	0.83	0.32	0.57	0.71	0.96
		35	1S	1.26	1.00	0.36	0.68	0.91	1.36	0.44	0.87	1.10	1.74
		25	2S	0.86	1.00	0.14	0.29	0.37	0.50	0.18	0.30	0.36	0.50
		30	2S	1.08	1.00	0.22	0.41	0.53	0.72	0.25	0.46	0.59	0.79
		35	2S	1.26	1.00	0.19	0.39	0.53	0.77	0.29	0.54	0.71	1.00
		40	2S	1.44	1.00	0.43	0.76	1.03	1.50	0.47	0.91	1.26	1.92
T90	Straight	20	1S	2.02	1.00	0.03	-	0.40	1.06	0.06	-	0.36	0.97
		25	1S	2.30	1.00	0.06	-	0.51	1.55	0.07	-	0.59	1.61
		30	1S	2.59	1.00	0.06	-	0.58	1.98	0.10	-	0.71	2.24
		25	2S	2.30	1.00	0.04	-	0.34	0.83	0.07	-	0.42	0.95
		30	2S	2.59	1.00	0.05	-	0.44	0.99	0.08	-	0.51	1.10
		35	2S	3.17	1.00	0.07	-	0.81	2.33	0.13	-	1.10	3.08
		40	2S	3.60	1.00	0.08	-	0.88	3.35	0.17	-	1.30	4.35
		35	3S	3.17	1.00	0.05	-	0.61	1.20	0.10	-	0.85	1.64
	2500ft	20	1S	2.02	1.00	0.15	-	0.58	1.16	0.09	-	0.46	0.99
		25	1S	2.30	1.00	0.18	-	0.67	1.41	0.14	-	0.62	1.33
		30	1S	2.59	1.00	0.25	-	1.03	2.33	0.19	-	1.03	2.48
		25	2S	2.30	1.00	0.23	-	0.84	1.63	0.10	-	0.85	1.45
		30	2S	2.59	1.00	0.27	-	0.78	1.46	0.14	-	0.69	1.41
		35	2S	3.17	1.00	0.49	0.87	1.47	-	0.27	0.71	1.48	-
		40	2S	3.60	1.00	0.8	1.40	2.72	-	0.47	1.43	3.31	-

D.2.3 Prototype Girder TUB36

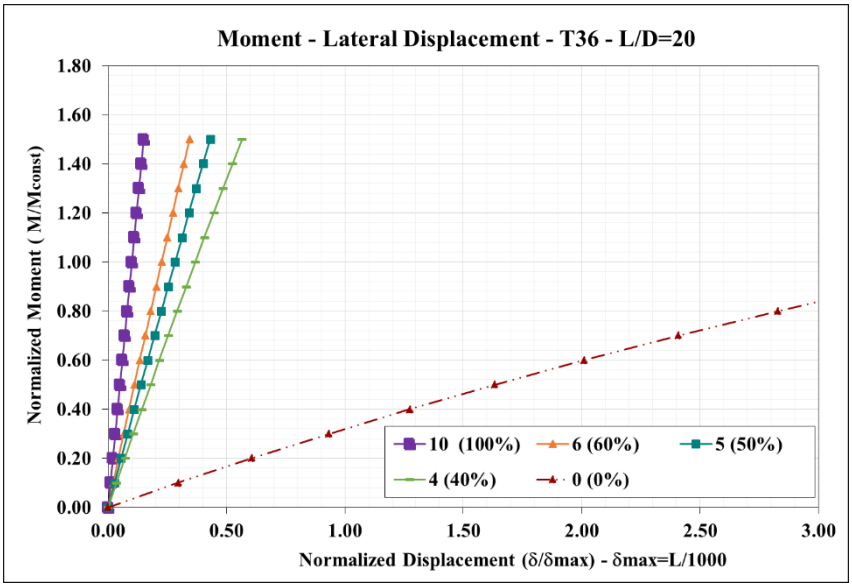

Figure D-12 – Moment vs Lateral Displacement - L/D=20 - 1S

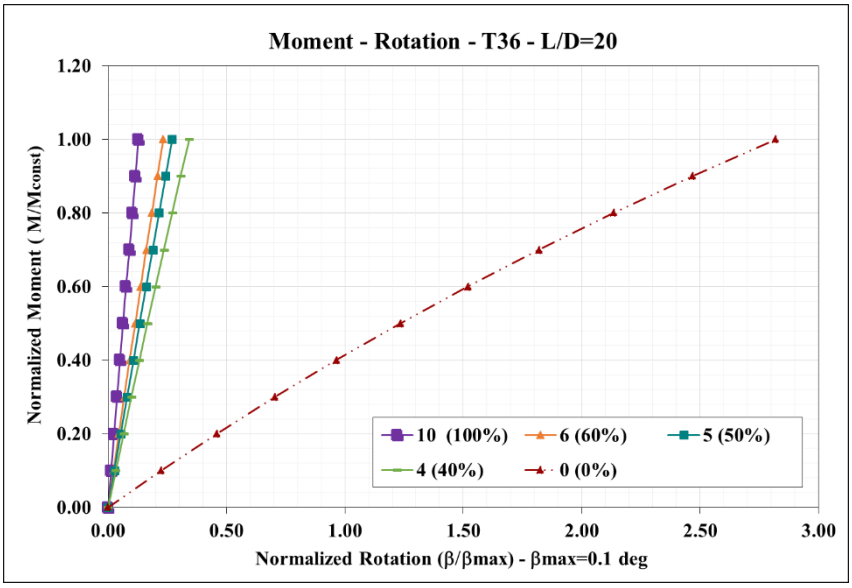

Figure D-13 – Moment vs Twist Angle - L/D=20 - 1S

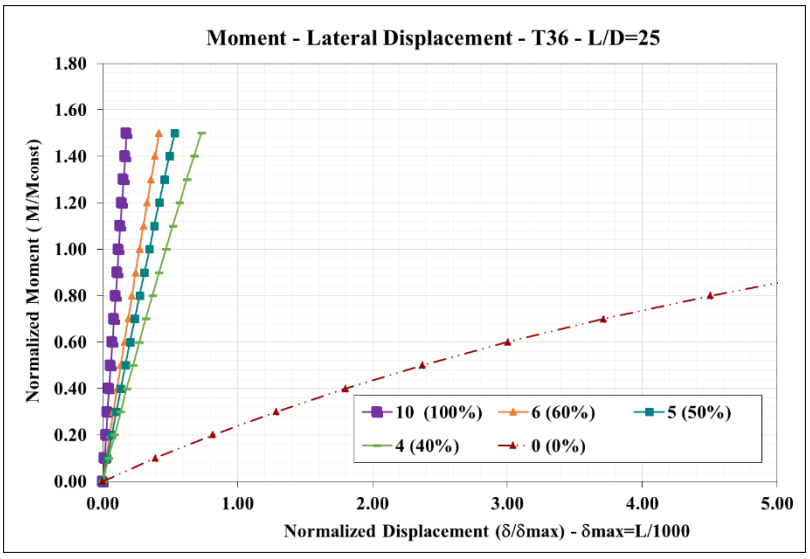

Figure D-14 – Moment vs Lateral Displacement - L/D=25 - 1S

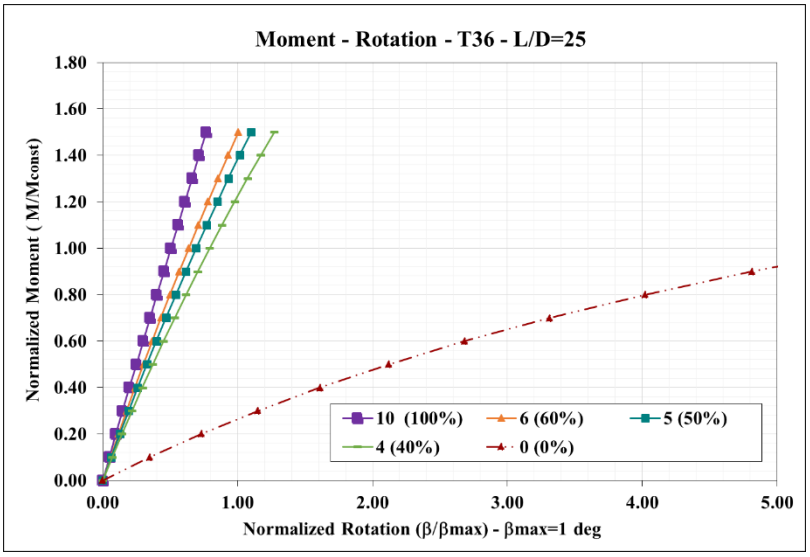

Figure D-15 – Moment vs Twist Angle - L/D=25 - 1S

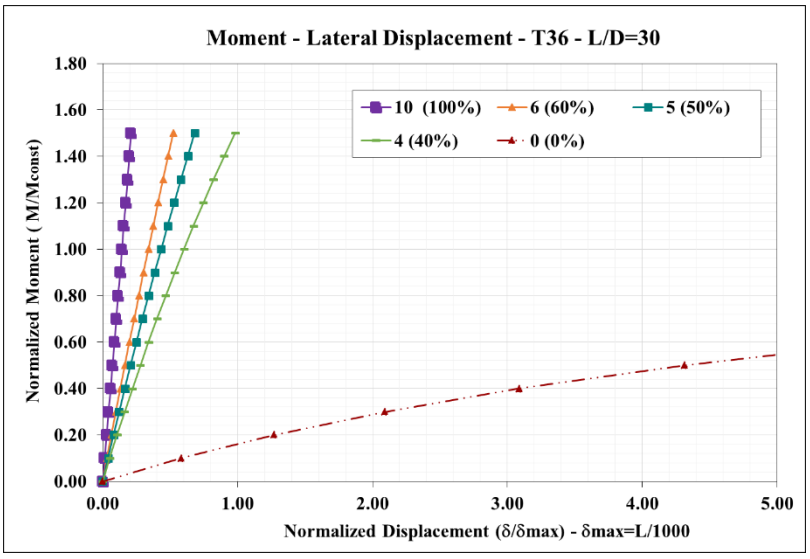

Figure D-16 – Moment vs Lateral Displacement - L/D=30 - 1S

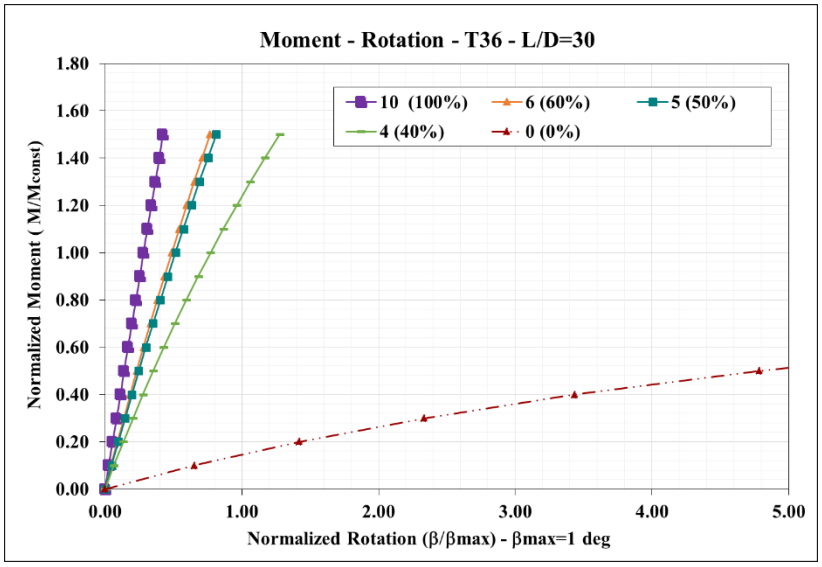

Figure D-17 – Moment vs Twist Angle - L/D=30 - 1S

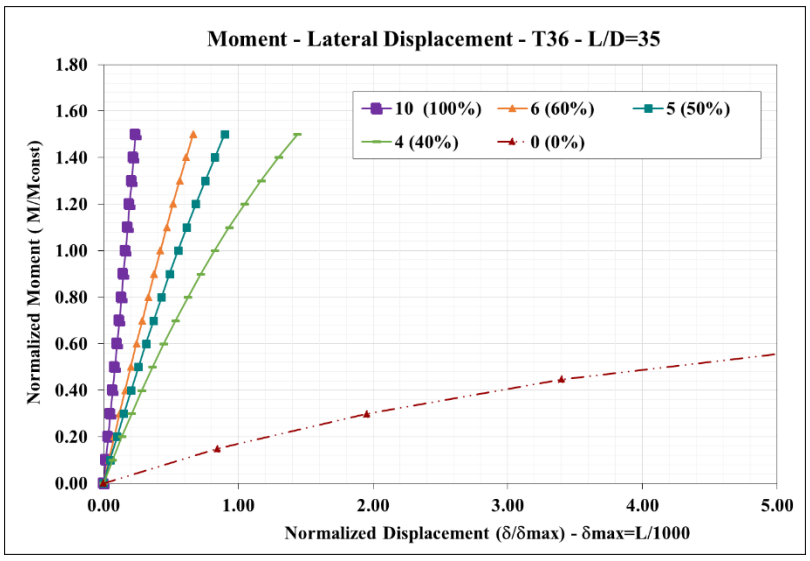

Figure D-18 – Moment vs Lateral Displacement - L/D=35 - 1S

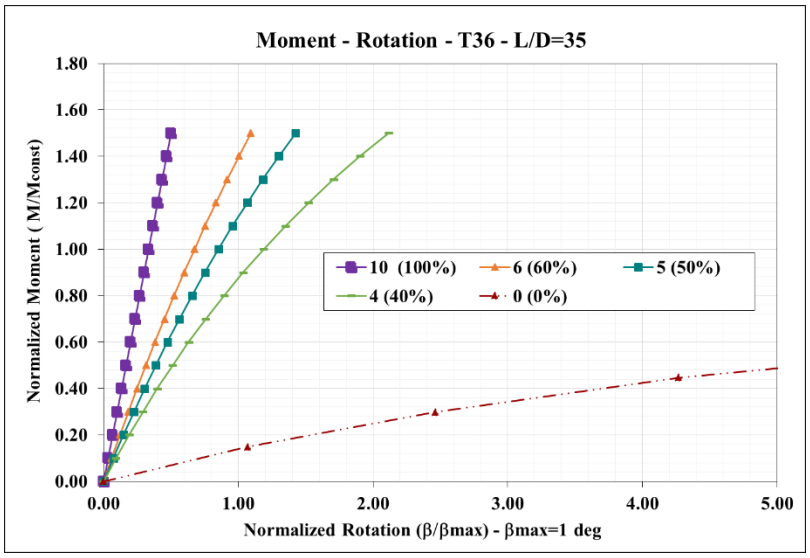

Figure D-19 – Moment vs Twist Angle - L/D=35 - 1S

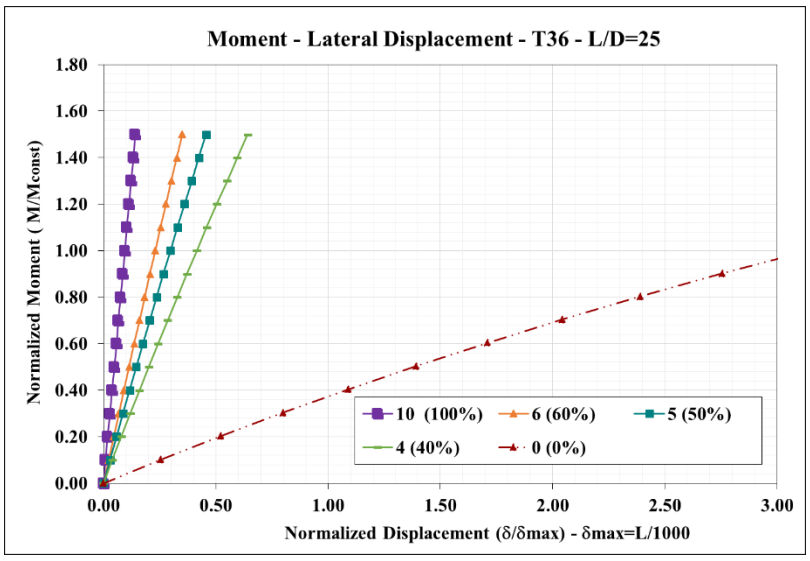

Figure D-20 – Moment vs Lateral Displacement - L/D=25 - 2S

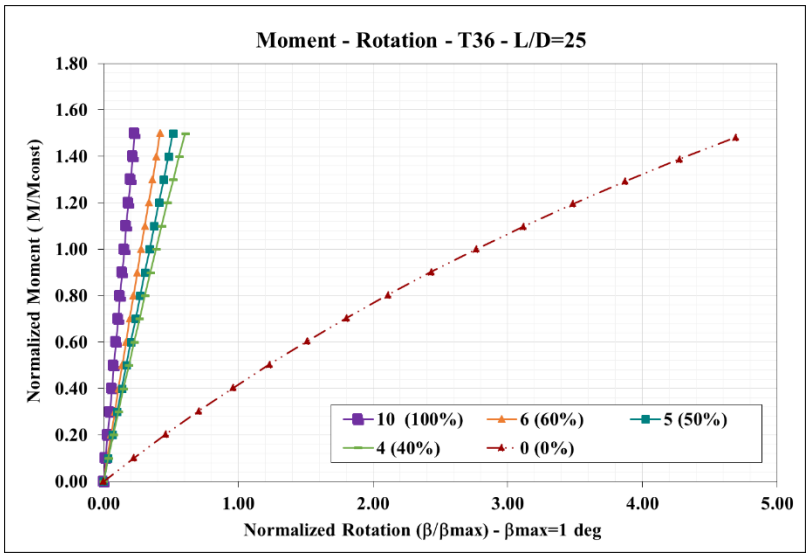

Figure D-21 – Moment vs Twist Angle - L/D=25 - 2S

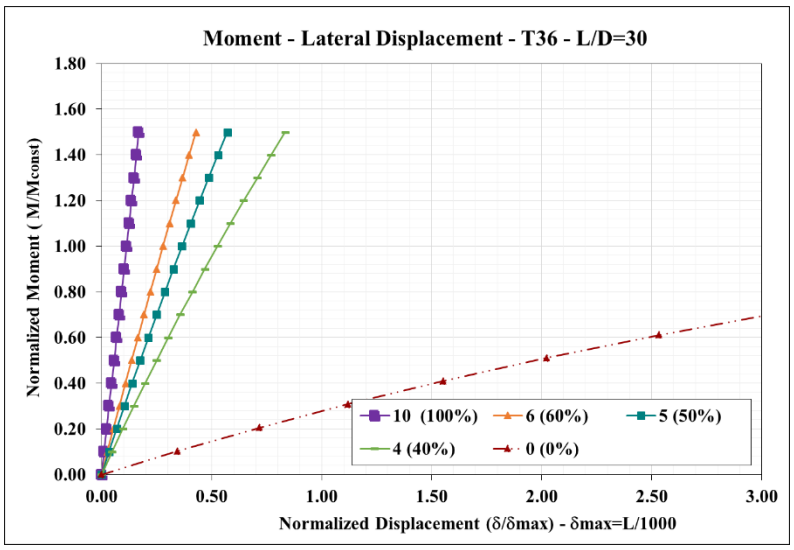

Figure D-22 – Moment vs Lateral Displacement - L/D=30 - 2S

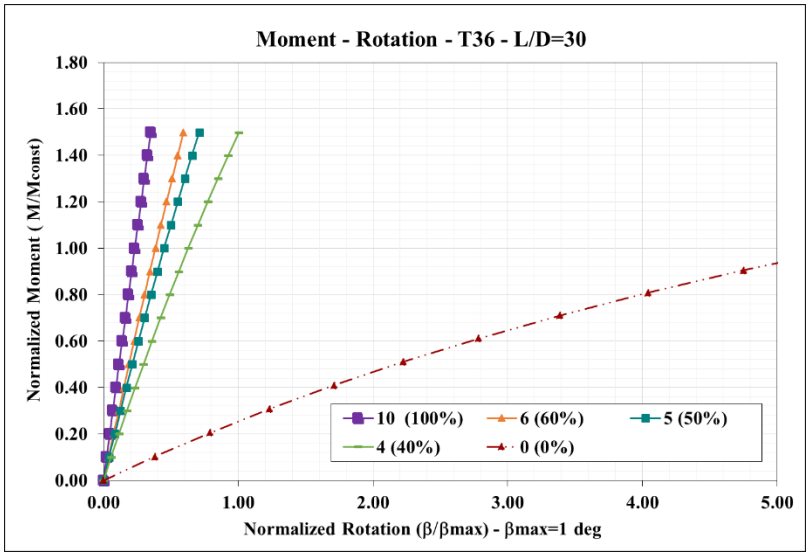

Figure D-23 – Moment vs Twist Angle - L/D=30 - 2S

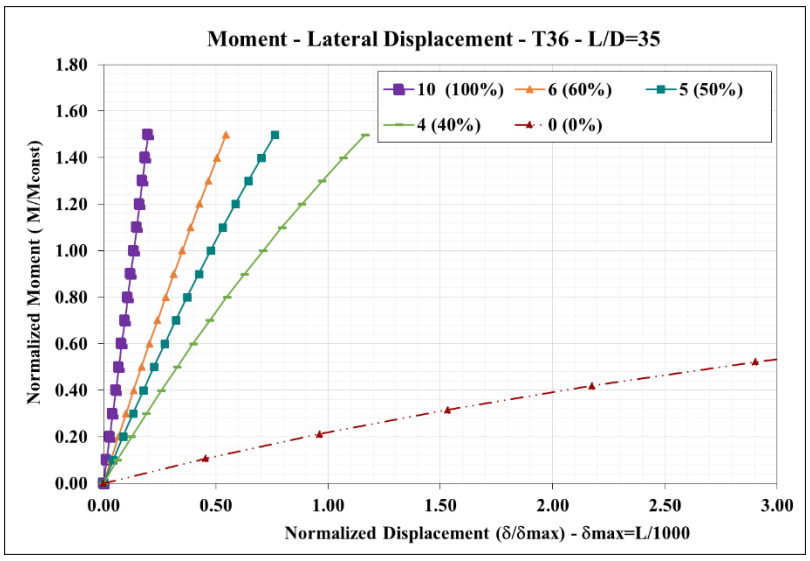

Figure D-24 – Moment vs Lateral Displacement - L/D=35 - 2S

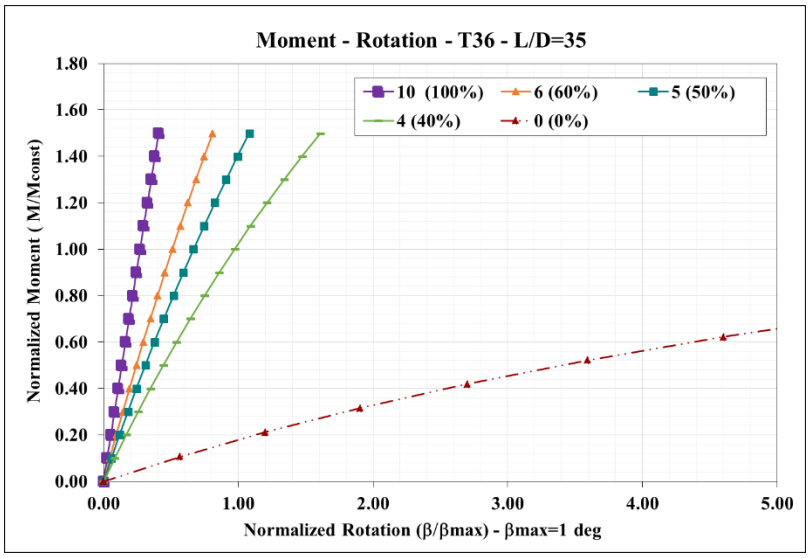

Figure D-25 – Moment vs Twist Angle - L/D=35 - 2S

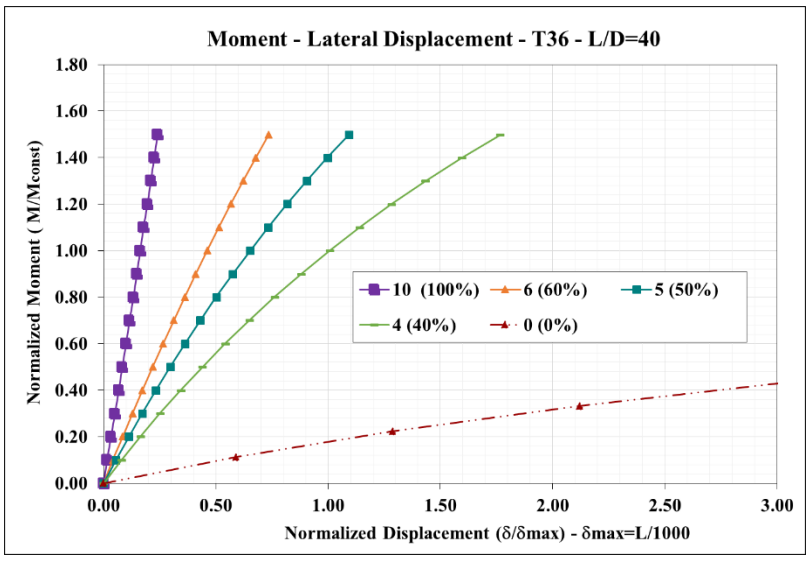

Figure D-26 – Moment vs Lateral Displacement - L/D=40 - 2S

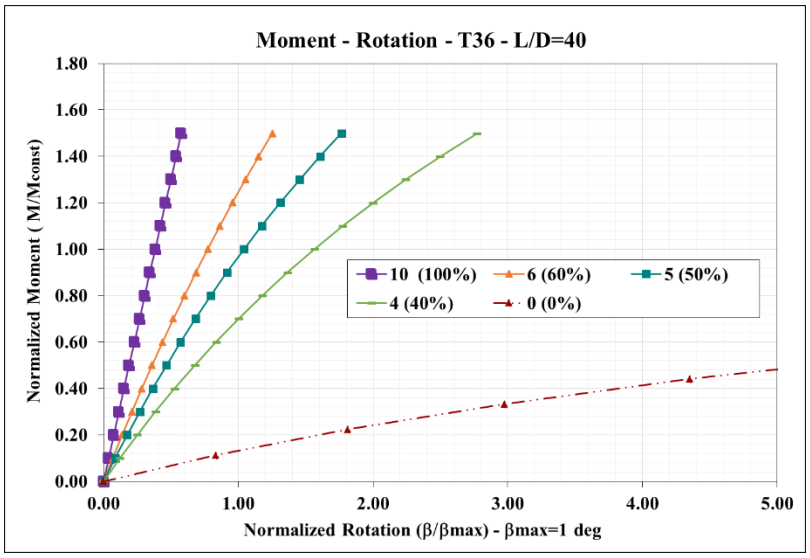

Figure D-27 – Moment vs Twist Angle - L/D=40 - 2S

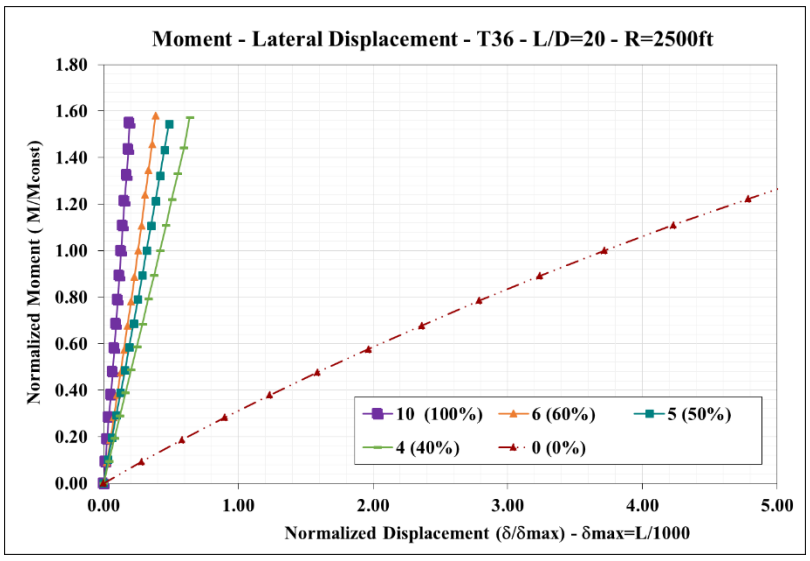

Figure D-28 – Moment vs Lateral Displacement - L/D=20 - 1S - R=2500ft

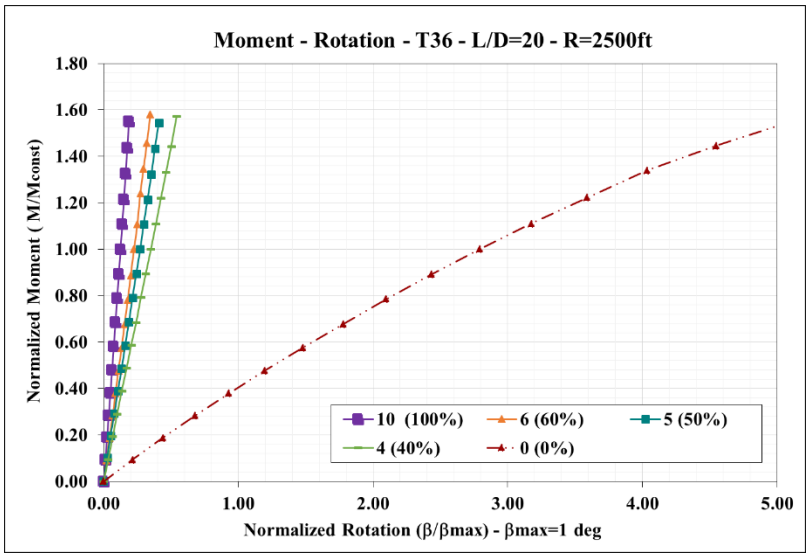

Figure D-29 – Moment vs Twist Angle - L/D=20 - 1S - R=2500ft

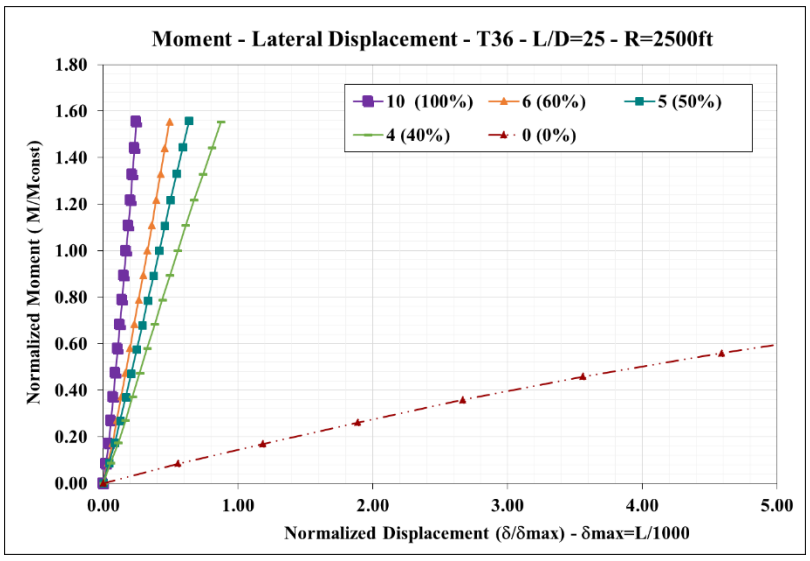

Figure D-30 – Moment vs Lateral Displacement - L/D=25 - 1S - R=2500ft

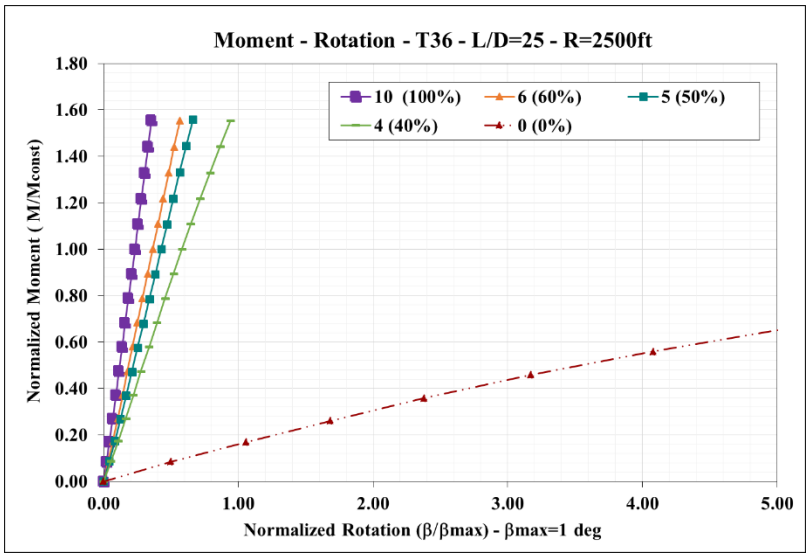

Figure D-31 – Moment vs Twist Angle - L/D=25 - 1S - R=2500ft

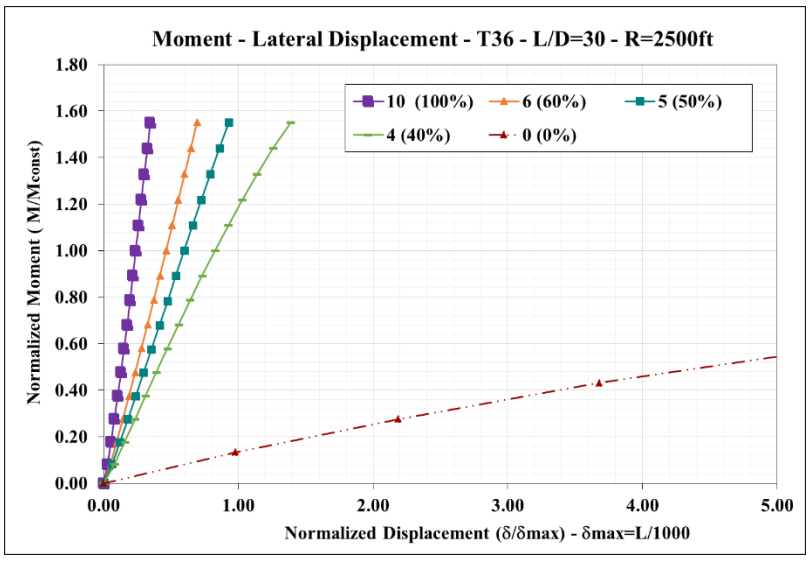

Figure D-32 – Moment vs Lateral Displacement - L/D=30 - 1S - R=2500ft

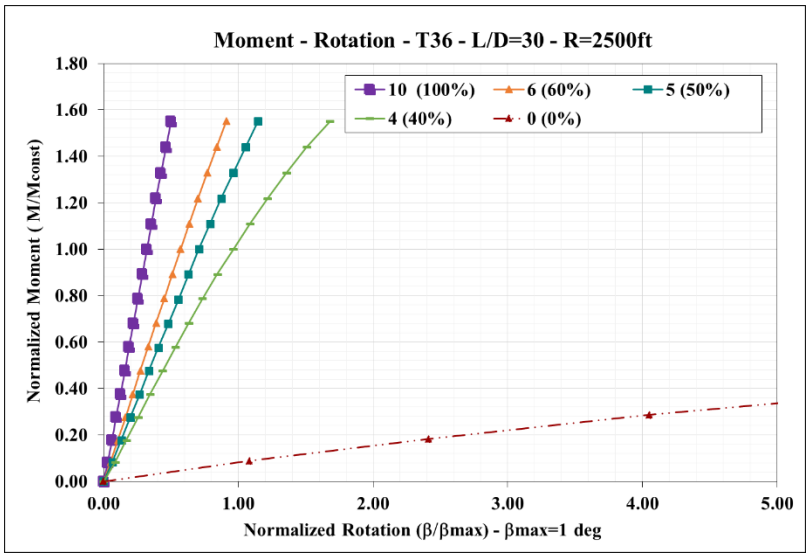

Figure D-33 – Moment vs Twist Angle - L/D=30 - 1S - R=2500ft

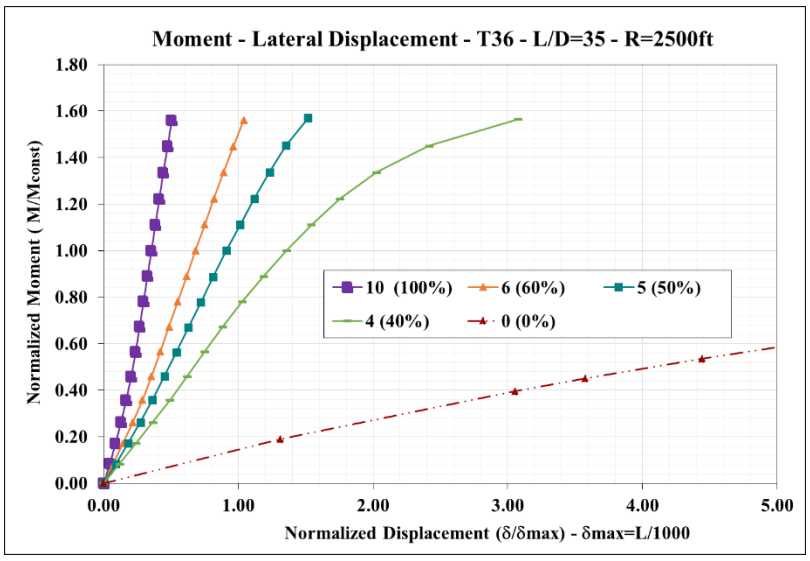

Figure D-34 – Moment vs Lateral Displacement - L/D=35 - 1S - R=2500ft

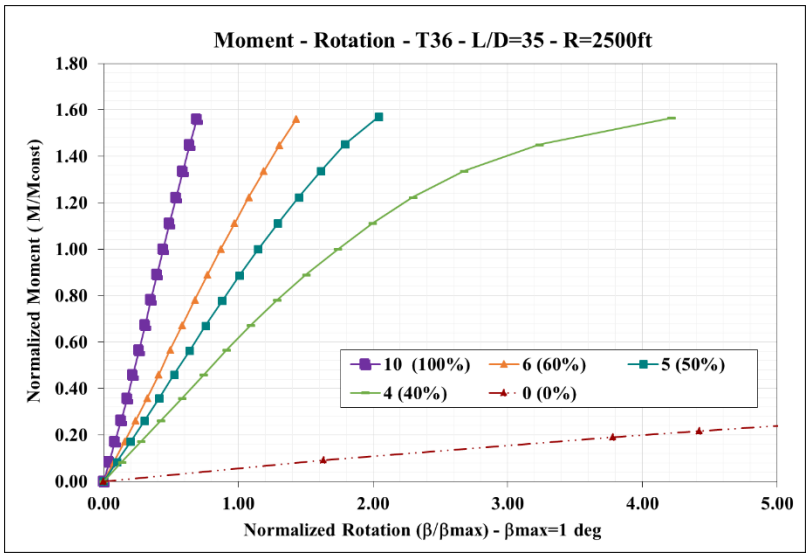

Figure D-35 – Moment vs Twist Angle - L/D=35 - 1S - R=2500ft

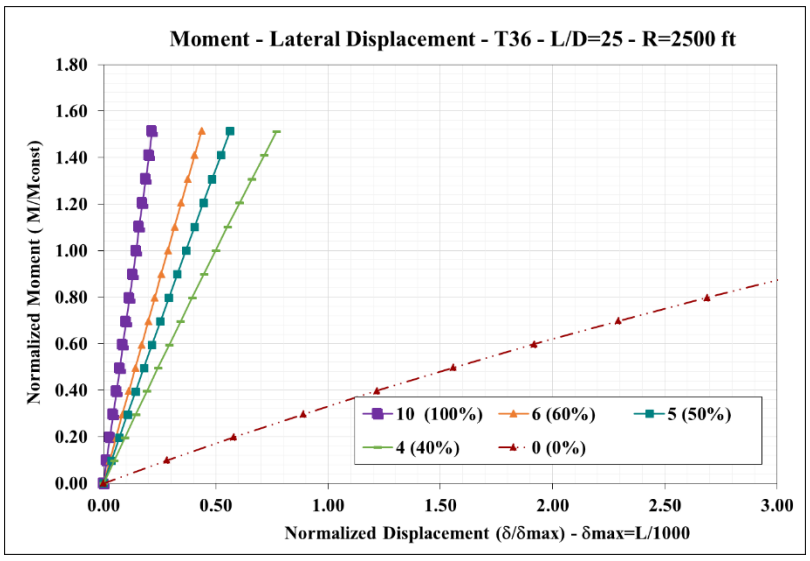

Figure D-36 – Moment vs Lateral Displacement - L/D=25 - 2S - R=2500ft

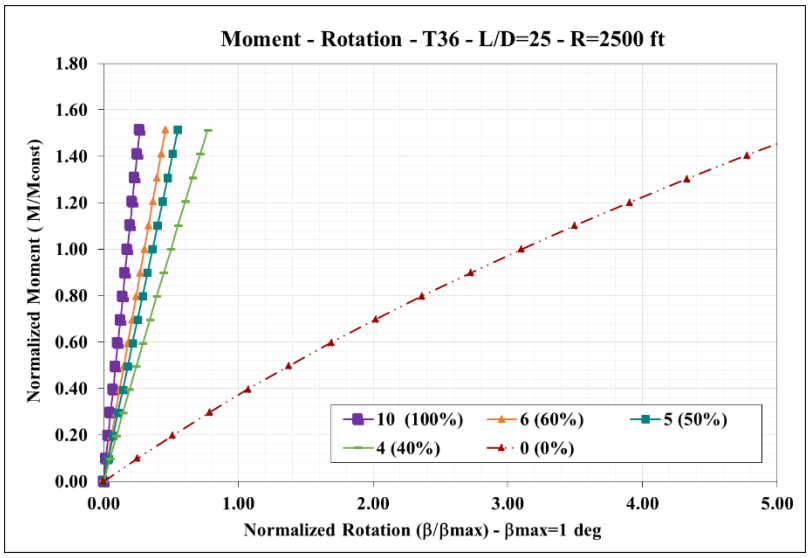

Figure D-37 – Moment vs Twist Angle - L/D=25 - 2S - R=2500ft

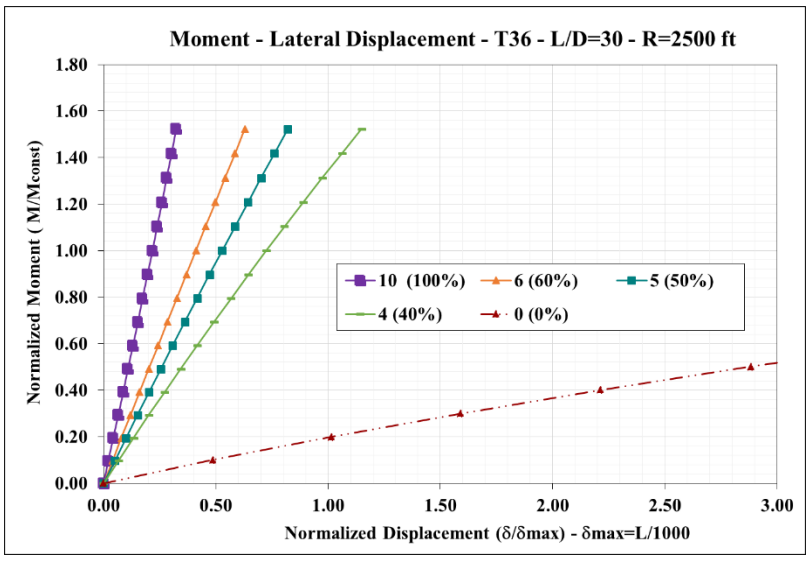

Figure D-38 – Moment vs Lateral Displacement - L/D=30 - 2S - R=2500ft

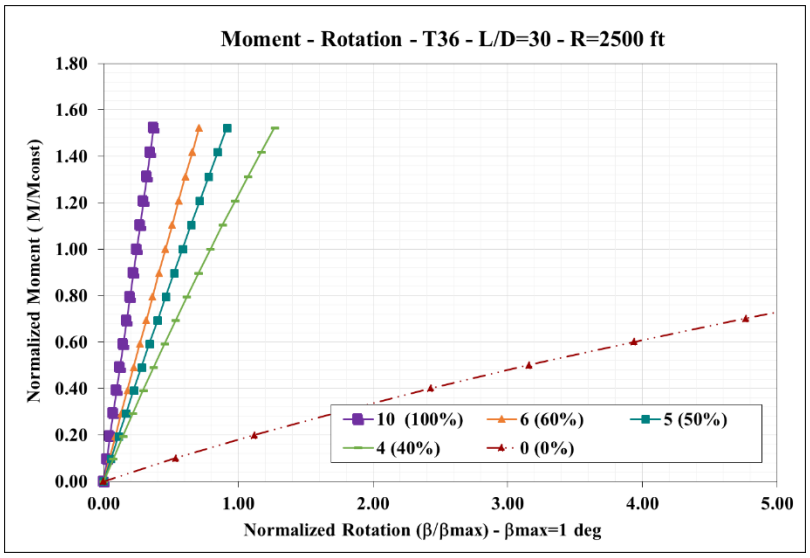

Figure D-39 – Moment vs Twist Angle - L/D=30 - 2S - R=2500ft

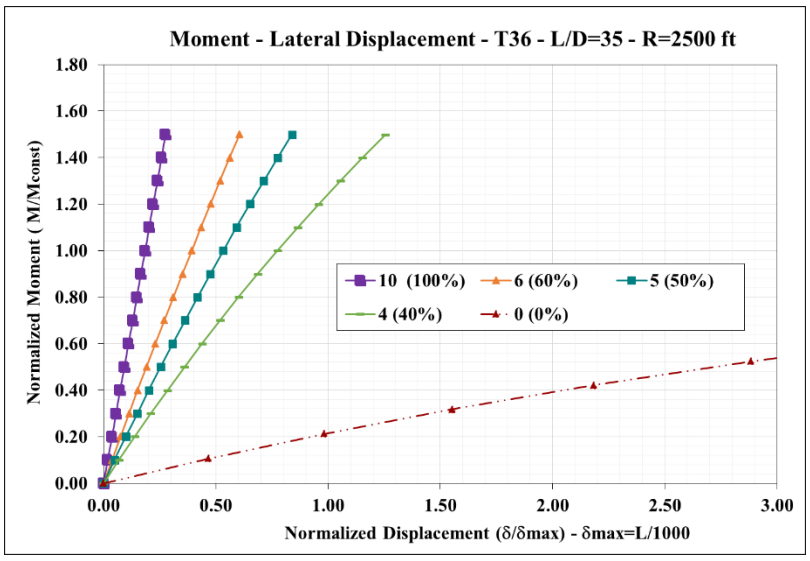

Figure D-40 – Moment vs Lateral Displacement - L/D=35 - 2S - R=2500ft

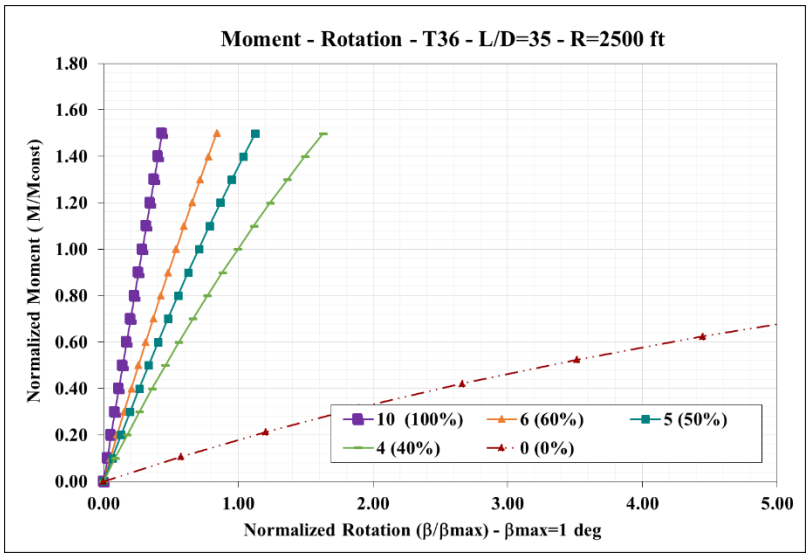

Figure D-41 – Moment vs Twist Angle - L/D=35 - 2S - R=2500ft

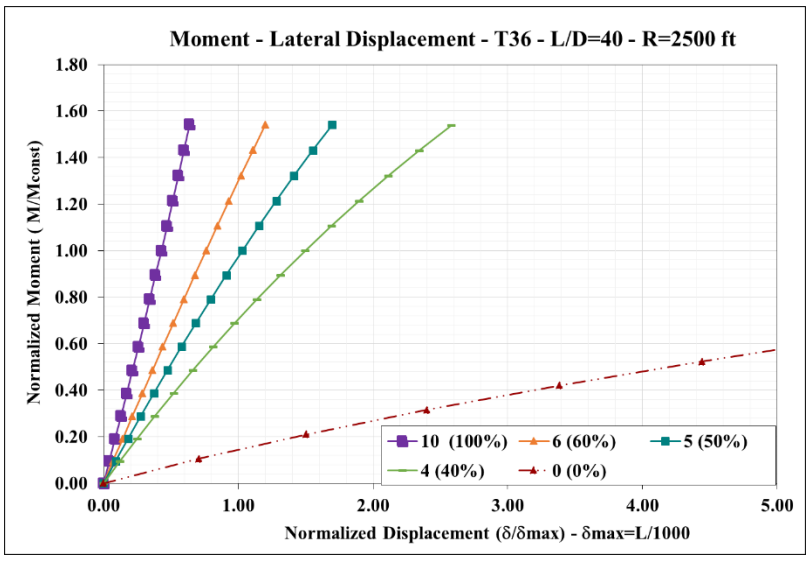

Figure D-42 – Moment vs Lateral Displacement - L/D=40 - 2S - R=2500ft

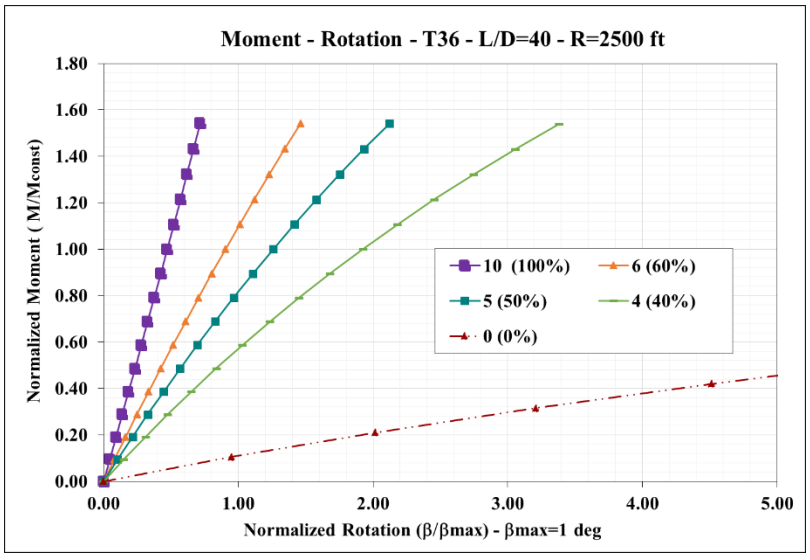

Figure D-43 – Moment vs Twist Angle - L/D=40 - 2S - R=2500ft

D.2.4 Prototype Girder TUB90

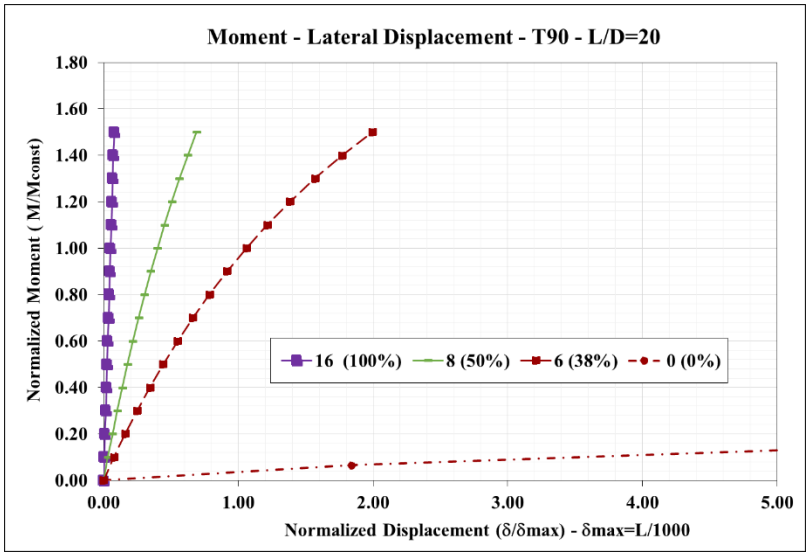

Figure D-44 – Moment vs Lateral Displacement - L/D=20 - 1S

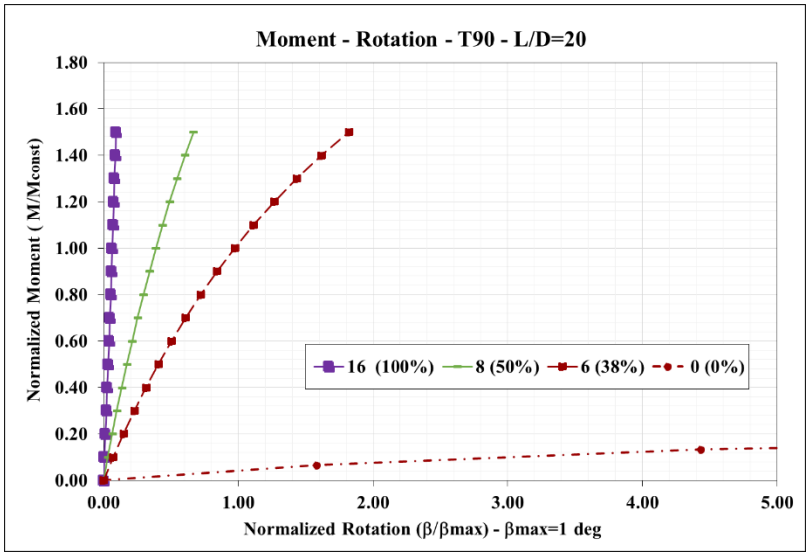

Figure D-45 – Moment vs Twist Angle - L/D=20 - 1S

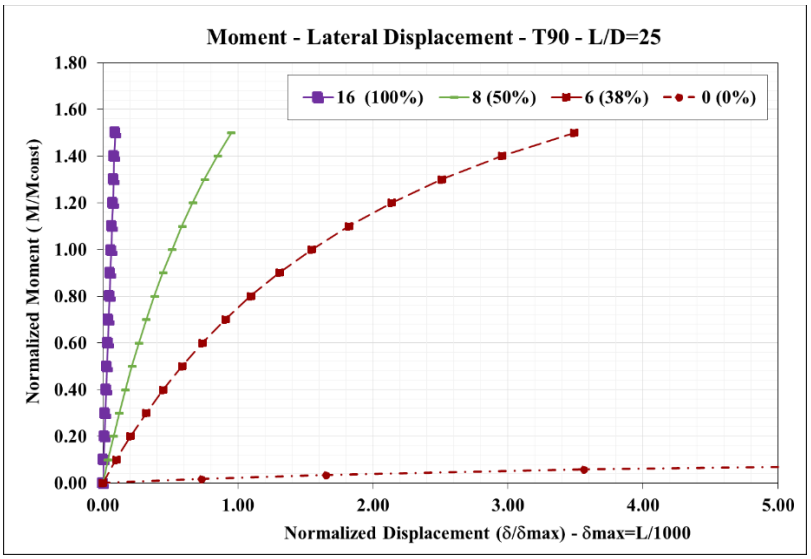

Figure D-46 – Moment vs Lateral Displacement - L/D=25 - 1S

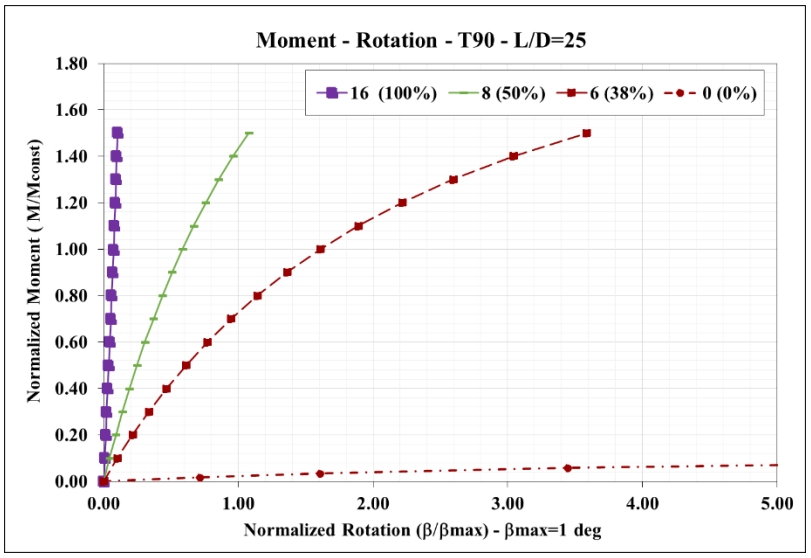

Figure D-47 – Moment vs Twist Angle - L/D=25 - 1S

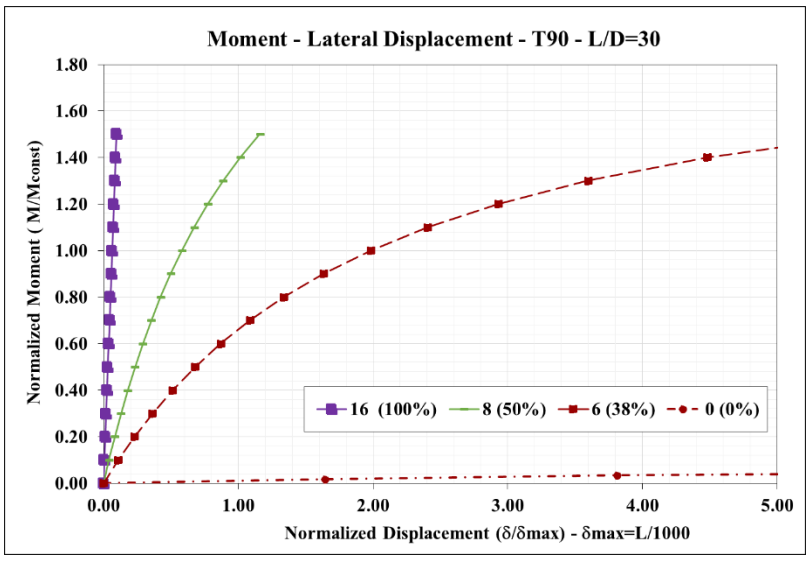

Figure D-48 – Moment vs Lateral Displacement - L/D=30 - 1S

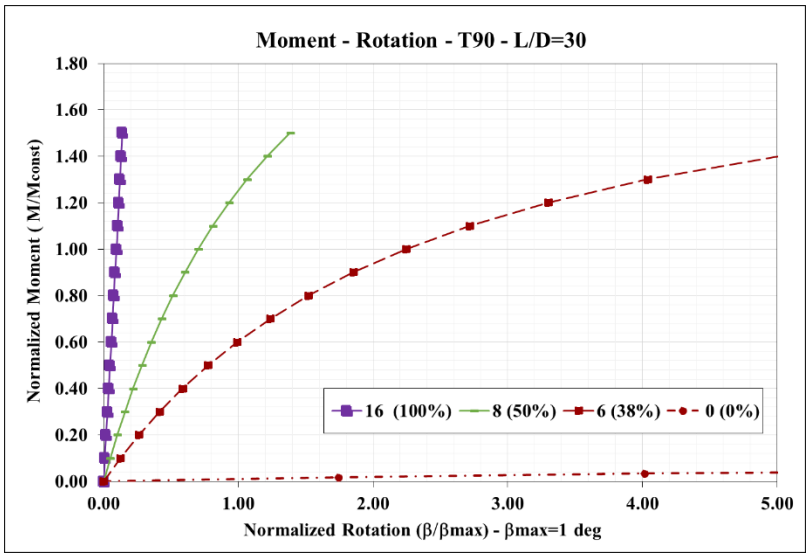

Figure D-49 – Moment vs Twist Angle - L/D=30 - 1S

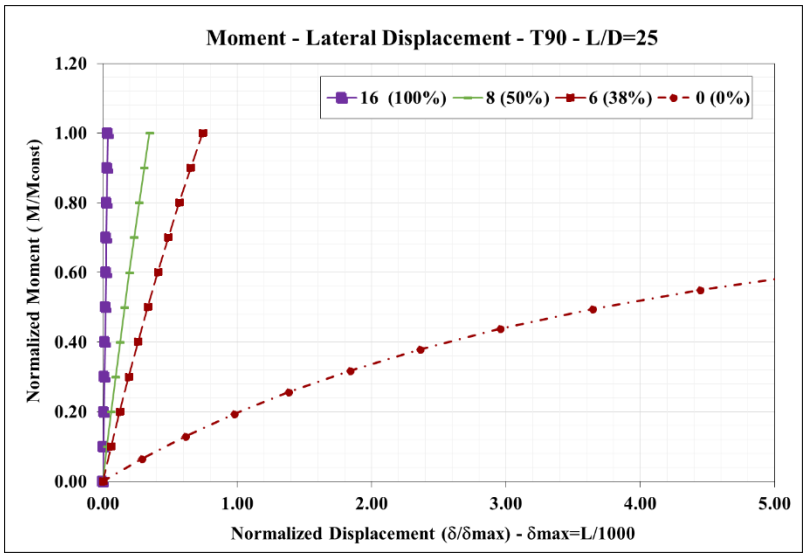

Figure D-50 – Moment vs Lateral Displacement - L/D=25 - 2S

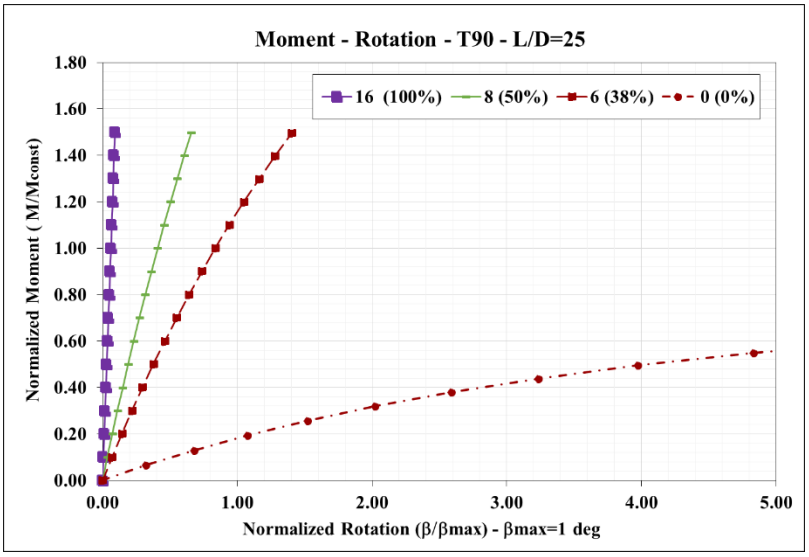

Figure D-51 – Moment vs Twist Angle - L/D=25 - 2S

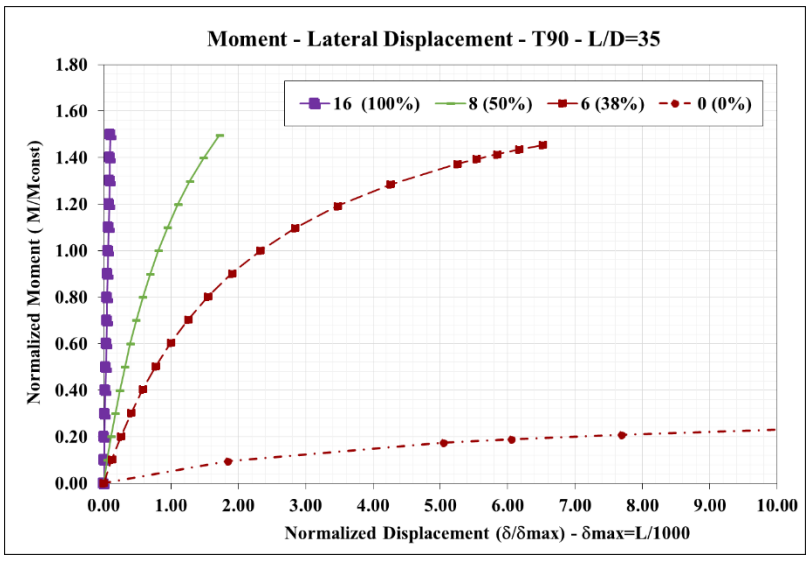

Figure D-52 – Moment vs Lateral Displacement - L/D=35 - 2S

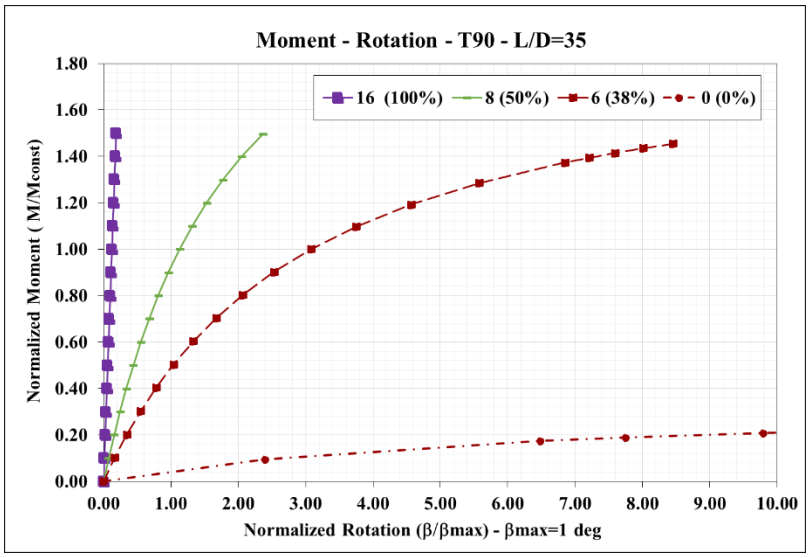

Figure D-53 – Moment vs Twist Angle - L/D=35 - 2S

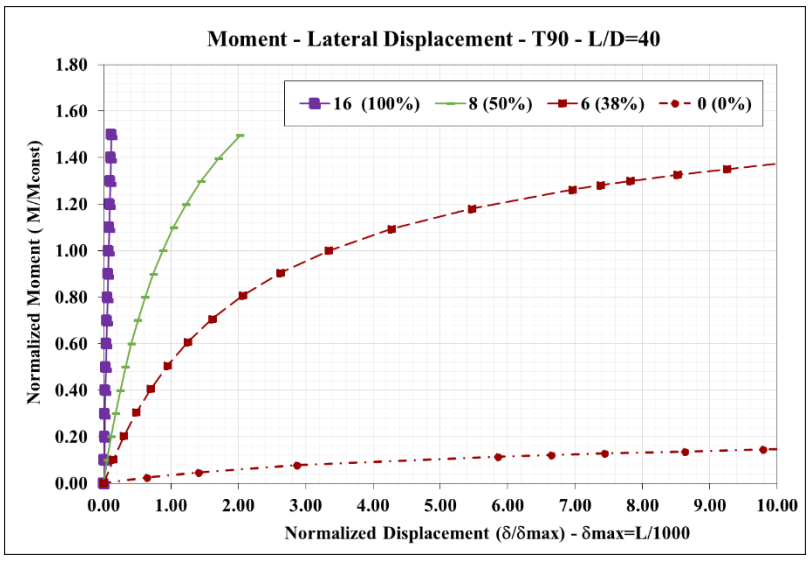

Figure D-54 – Moment vs Lateral Displacement - L/D=40 - 2S

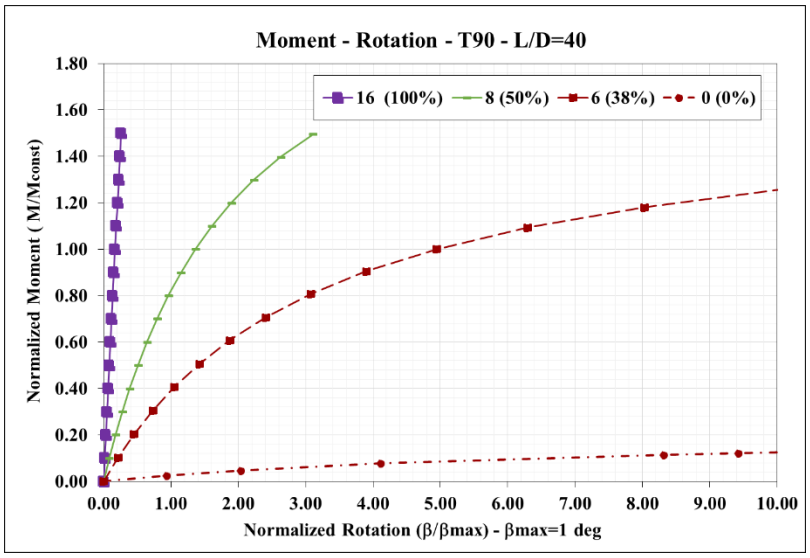

Figure D-55 – Moment vs Twist Angle - L/D=40 - 2S

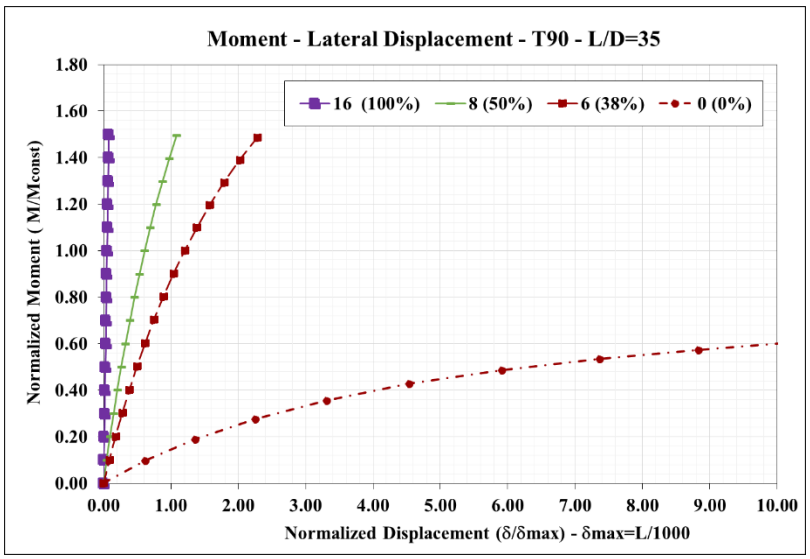

Figure D-56 – Moment vs Lateral Displacement - L/D=30-35 - 3S

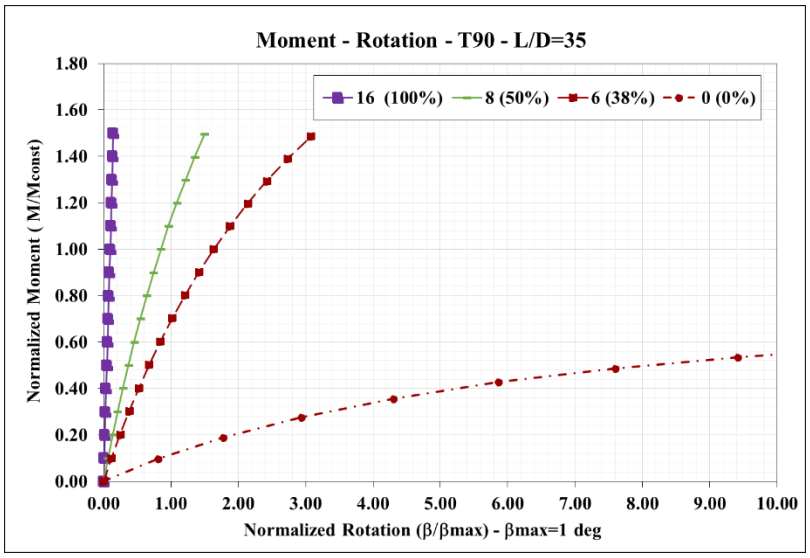

Figure D-57 – Moment vs Twist Angle - L/D=30-35 - 3S

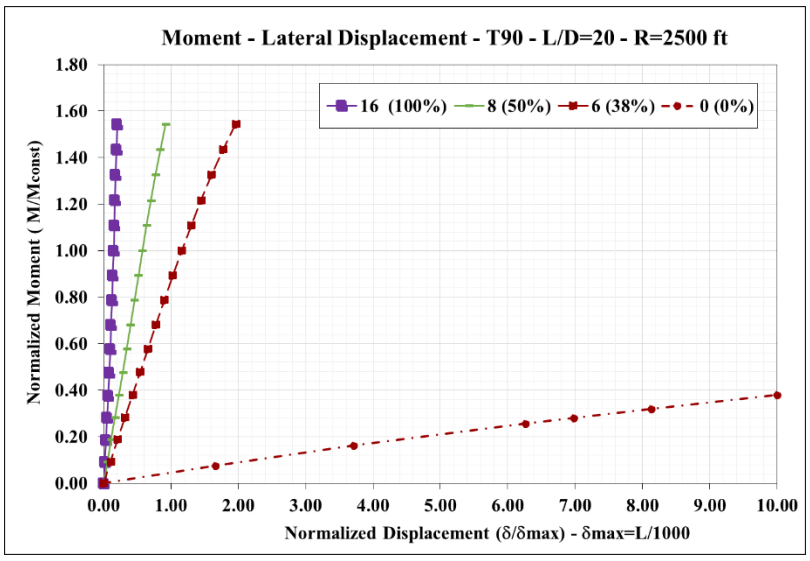

Figure D-58 – Moment vs Lateral Displacement - L/D=20 - 1S - R=2500ft

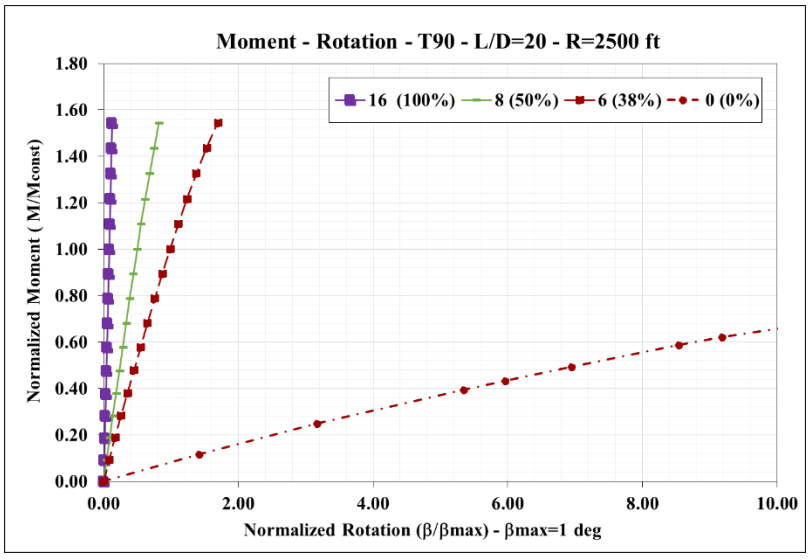

Figure D-59 – Moment vs Twist Angle - L/D=20 - 1S - R=2500ft

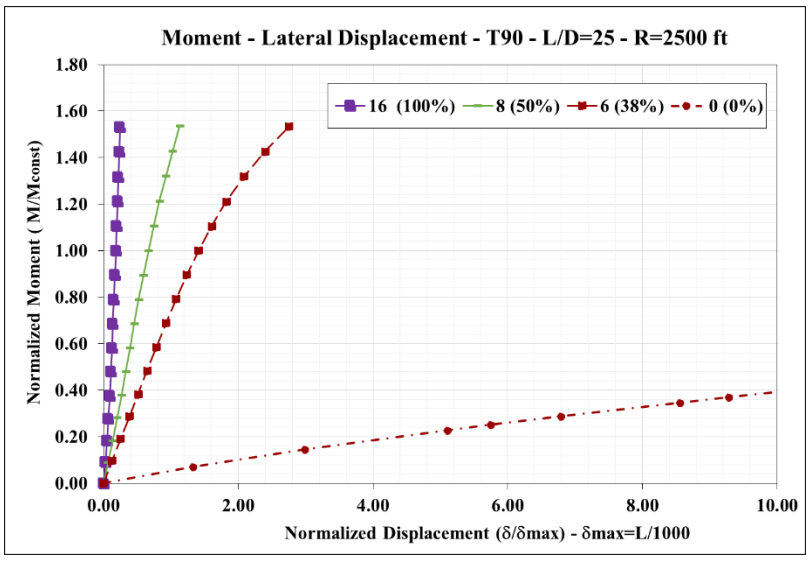

Figure D-60 – Moment vs Lateral Displacement - L/D=25 - 1S - R=2500ft

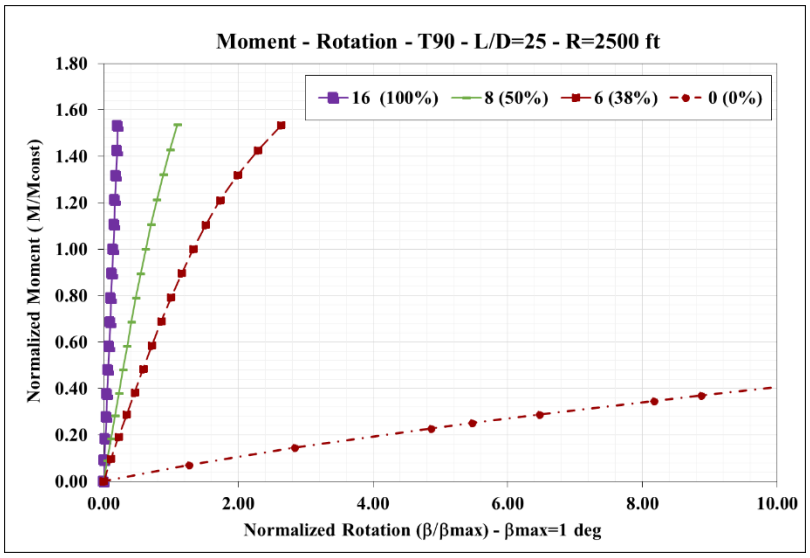

Figure D-61 – Moment vs Twist Angle - L/D=25 - 1S - R=2500ft

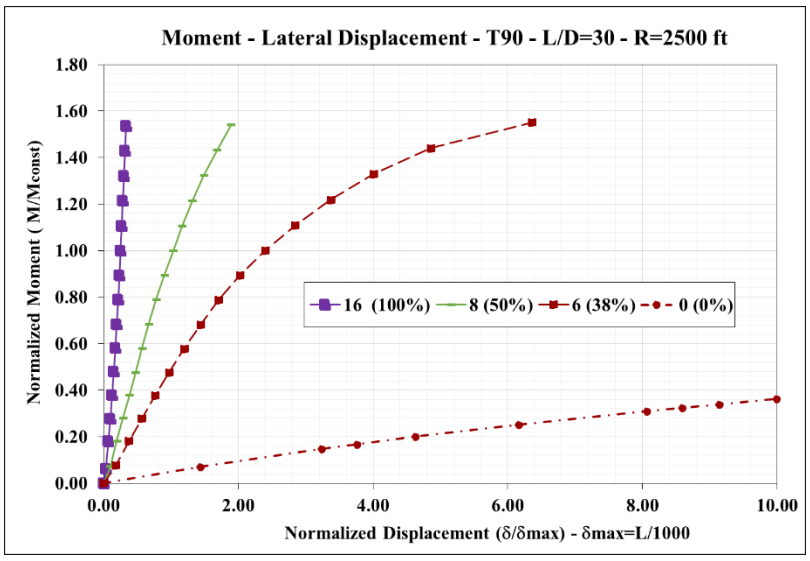

Figure D-62 – Moment vs Lateral Displacement - L/D=30 - 1S - R=2500ft

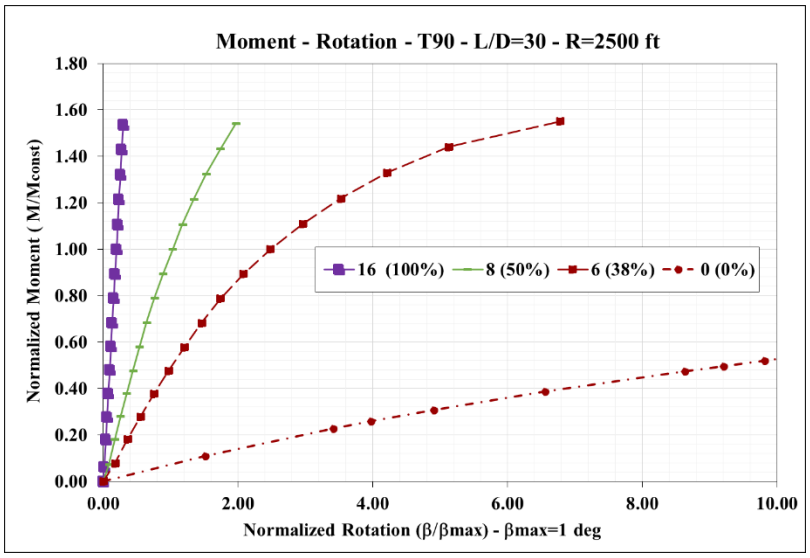

Figure D-63 – Moment vs Twist Angle - L/D=30 - 1S - R=2500ft

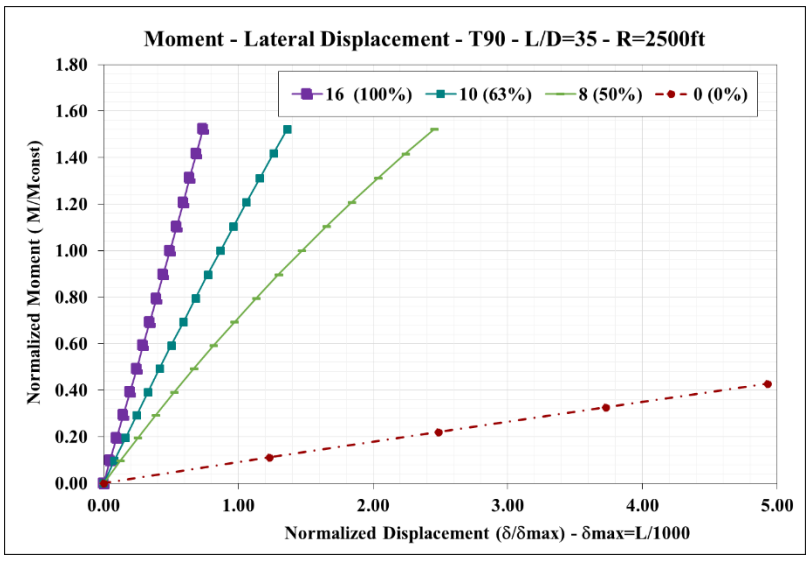

Figure D-64 – Moment vs Lateral Displacement - L/D=35 - 2S - R=2500ft

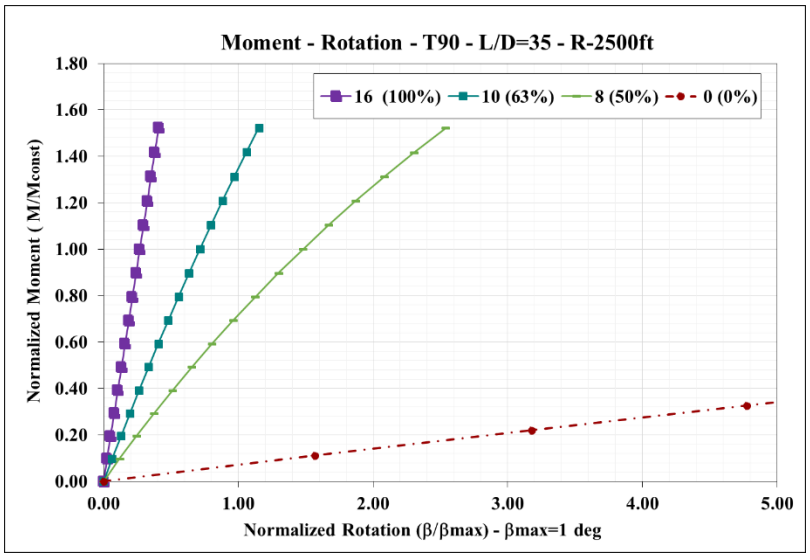

Figure D-65 – Moment vs Twist Angle - L/D=35 - 2S - R=2500ft

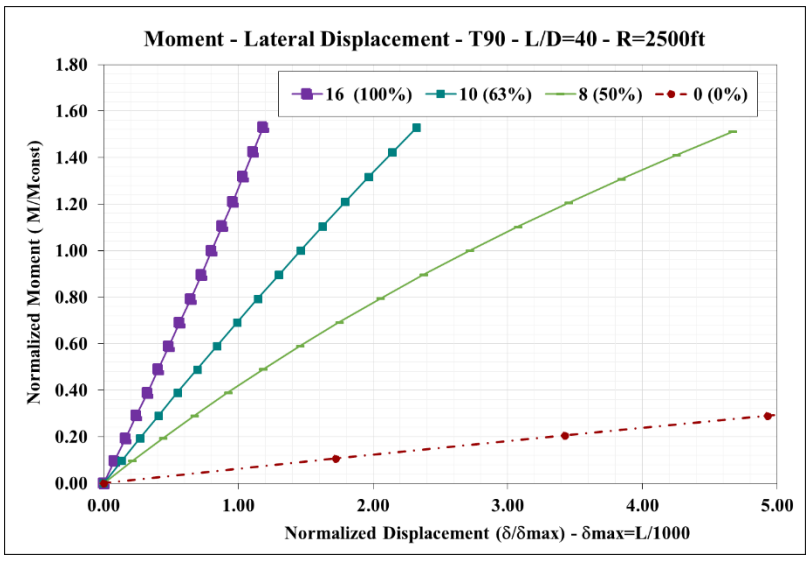

Figure D-66 – Moment vs Lateral Displacement - L/D=40 - 2S - R=2500ft

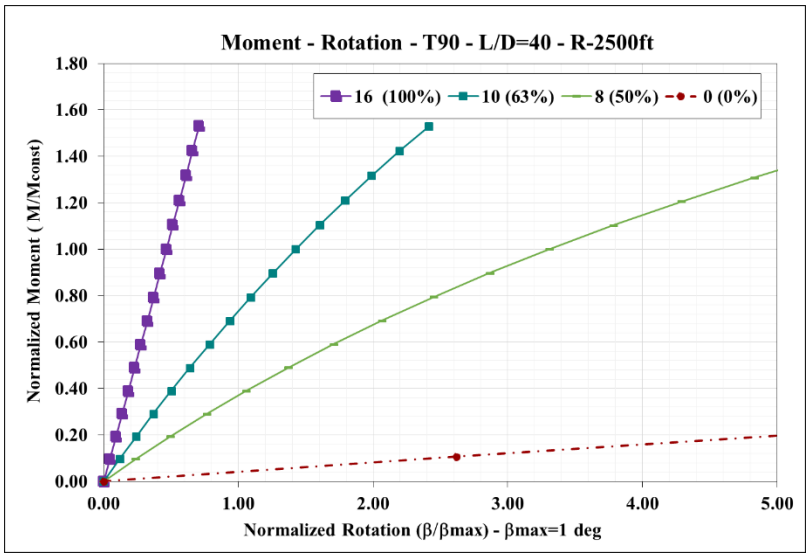

Figure D-67 – Moment vs Twist Angle - L/D=40 - 2S - R=2500ft

D.3 Flange Offset Detail-Parametric Study

D.3.1 Straight TUB36 L/D=30

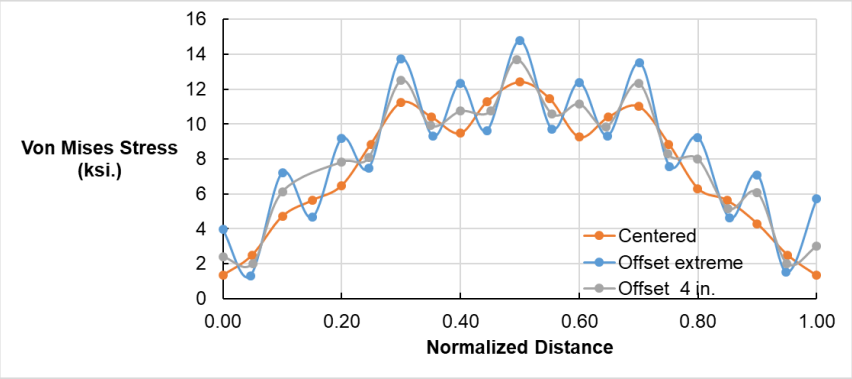

Figure D-68 – Stress of Top Flange Inner Edge - L/D=30- Various Flange Offset

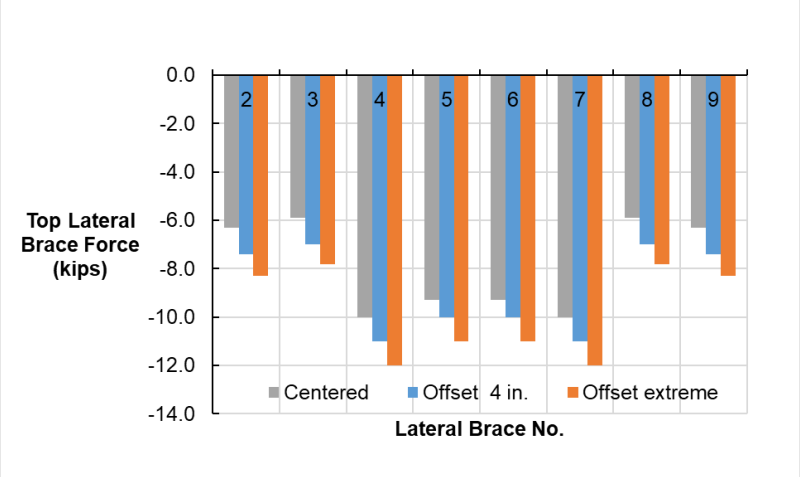

Figure D-69 – Top Lateral Truss Force - L/D=30- Various Flange Offset

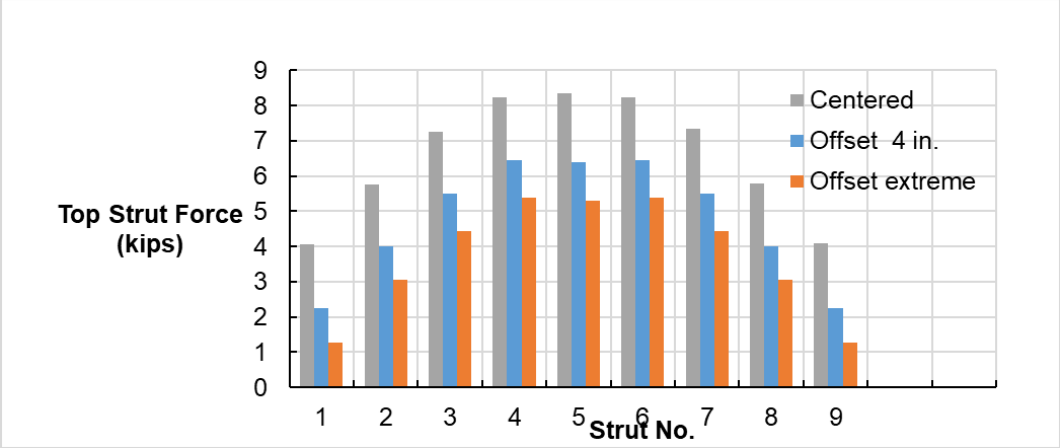

Figure D-70 – Top Strut Force - L/D=30- Various Flange Offset

D.3.2 Curved TUB90 L/D=24 R=800 ft.

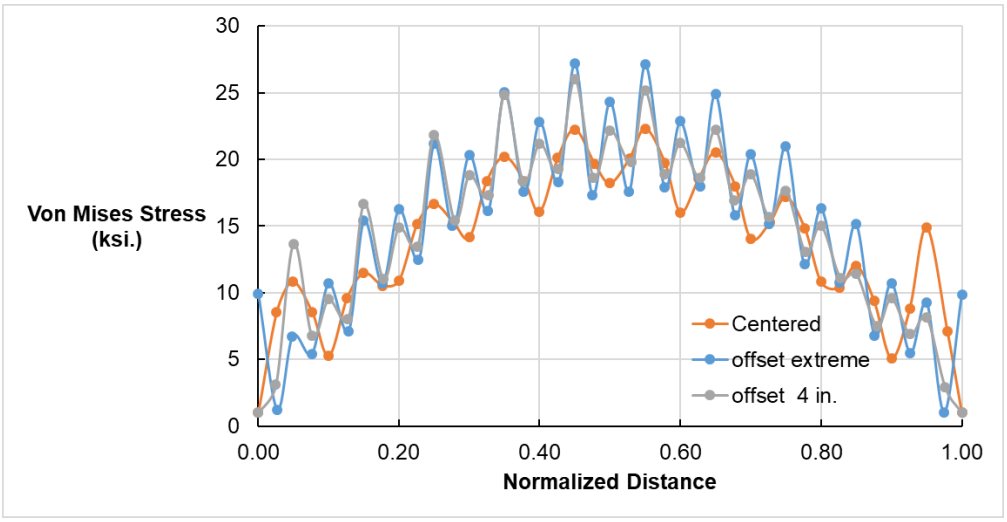

Figure D-71 – Stress of Top Flange Inner Edge -R=800 - L/D=24- Various Flange Offset

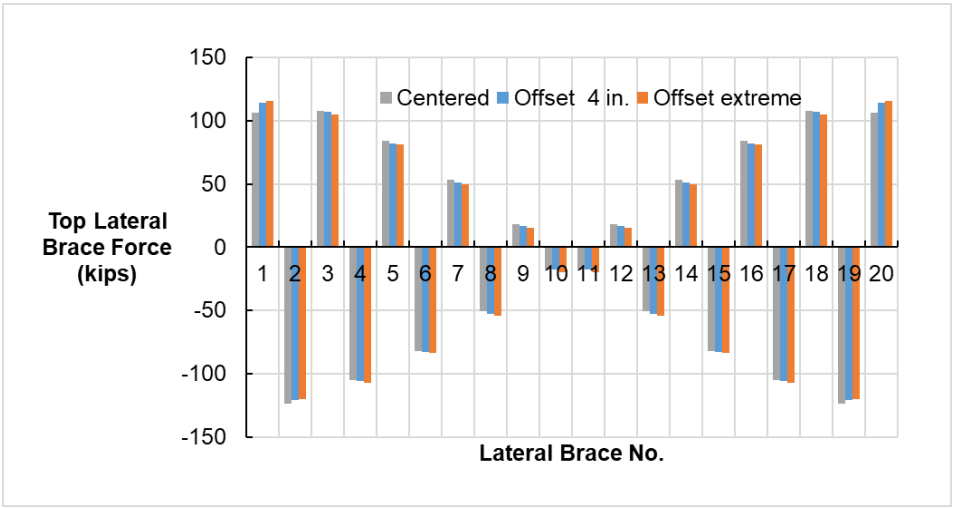

Figure D-72 – Top Lateral Truss Force - R=800 - L/D=24 - Various Flange Offset

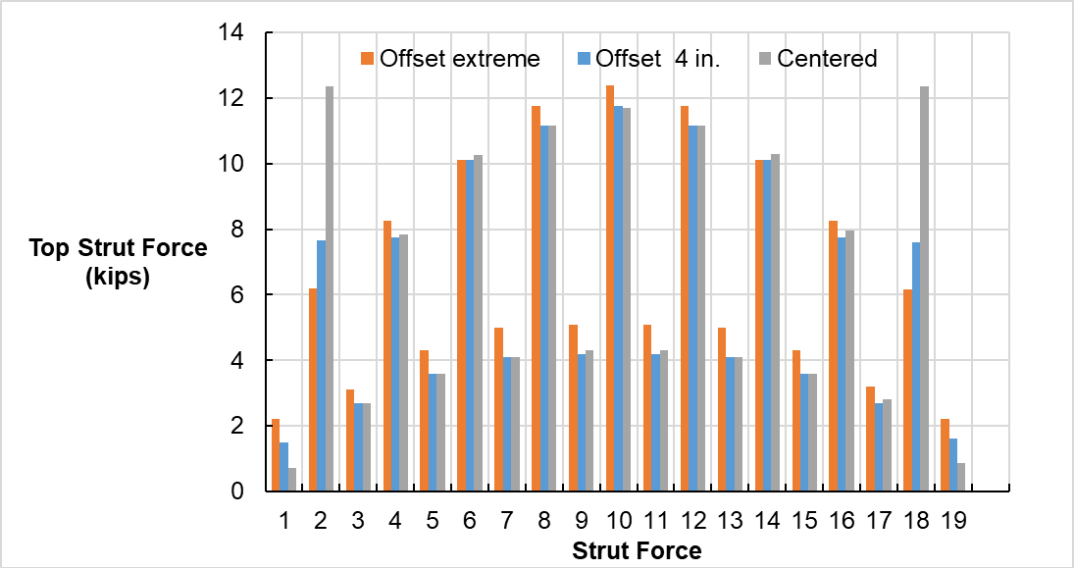

Figure D-73 – Top Strut Force - R=800 - L/D=24 - Various Flange Offset

D.4 Lower Slope Parametric Study

D.4.1 Straight TUB36 L/D=24

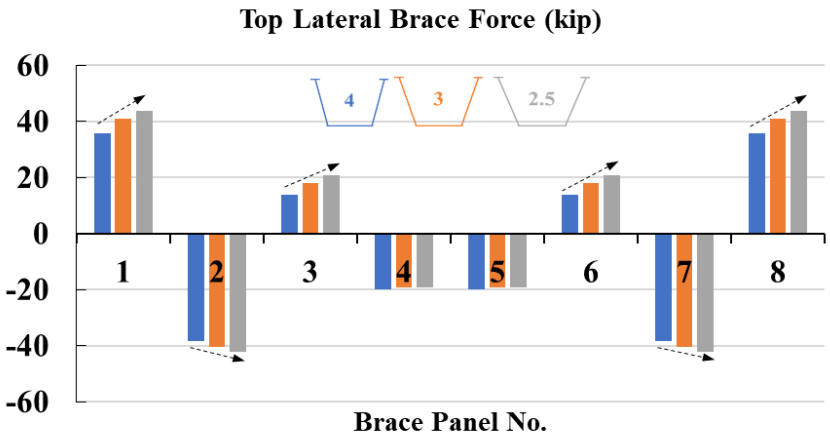

Figure D-74 – Top Lateral Truss Force - L/D=24 – Various Web Slopes

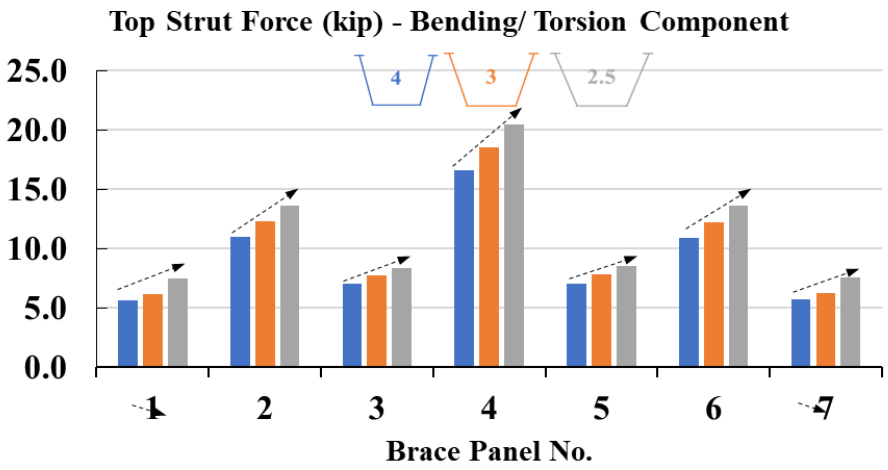

Figure D-75 – Top Strut Force - L/D=24 – Various Web Slopes

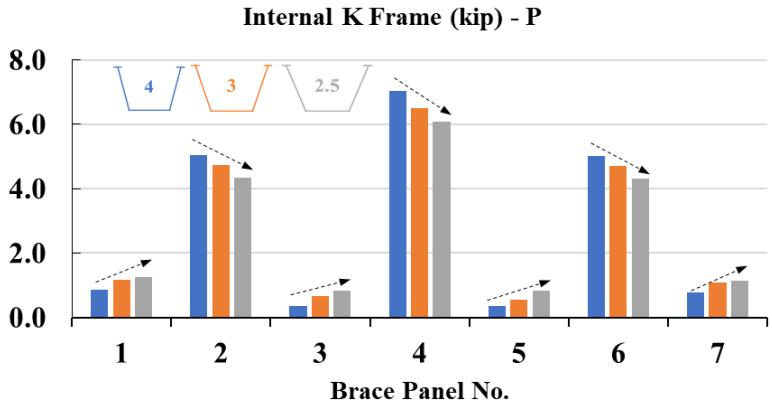

Figure D-76 – Force on one K-Diagonal - L/D=24 – Various Web Slopes

4 Girder with Various Web Slopes

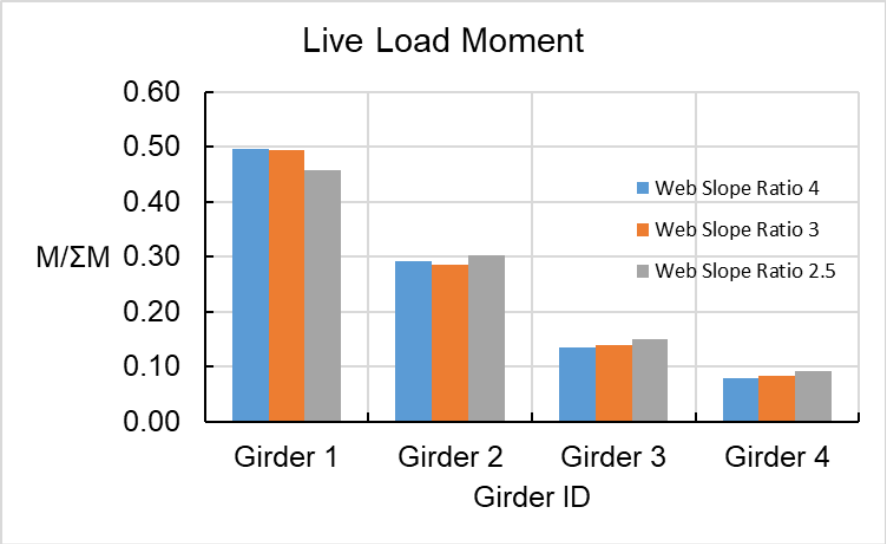

Figure D-77 – Live Load Moment Distribution - L/D=24 – Various Web Slopes

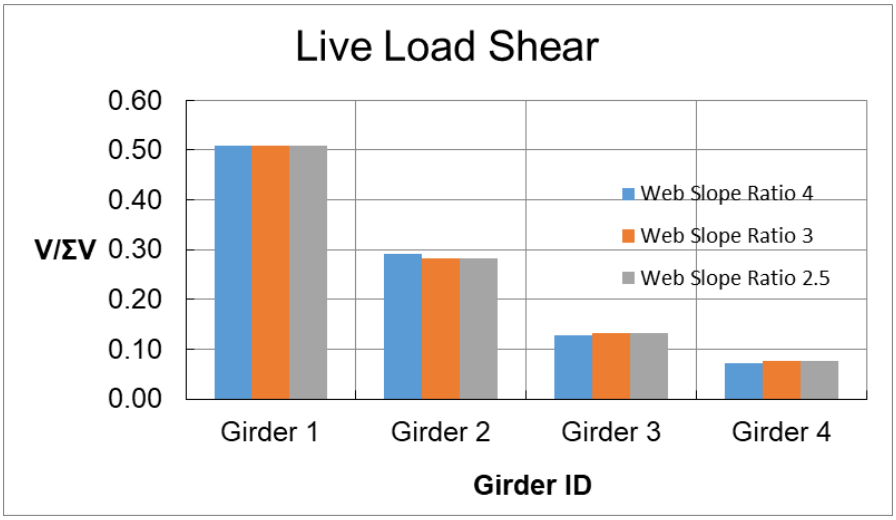

Figure D-78 – Live Load Shear Distribution - L/D=24 – Various Web Slopes

D.4.2 Straight TUB90 L/D=25

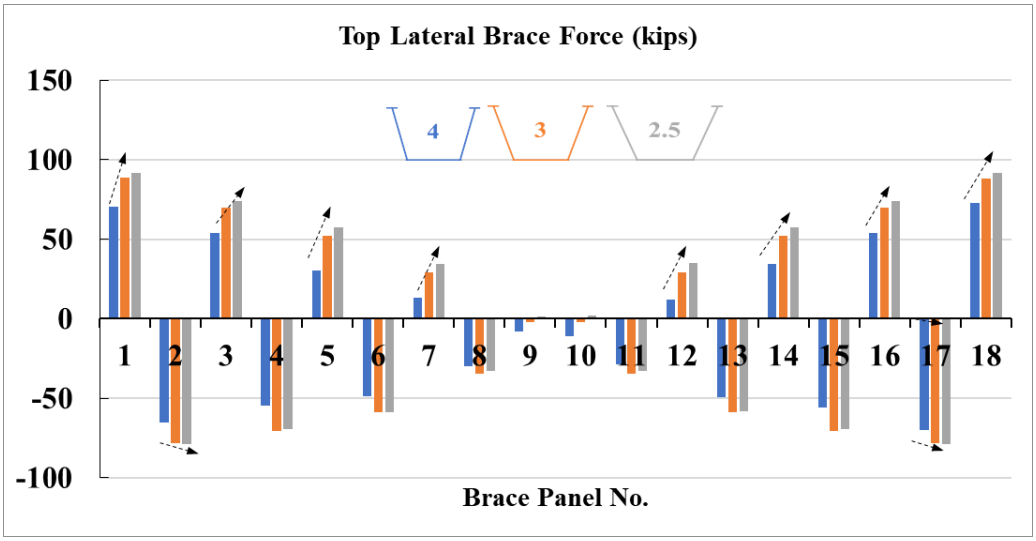

Figure D-79 – Top Lateral Truss Force - L/D=25 – Various Web Slopes

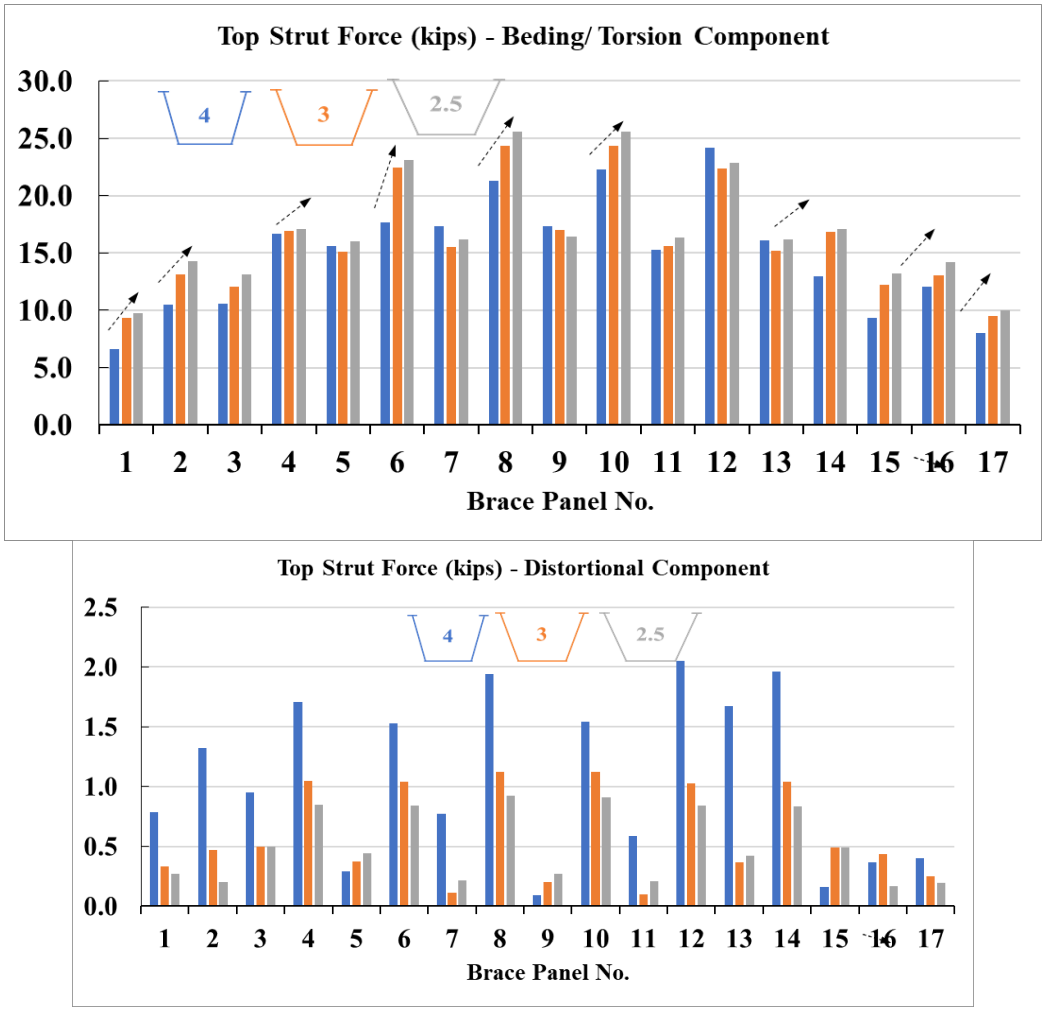

Figure D-80 – Top Strut Force - L/D=25 – Various Web Slopes

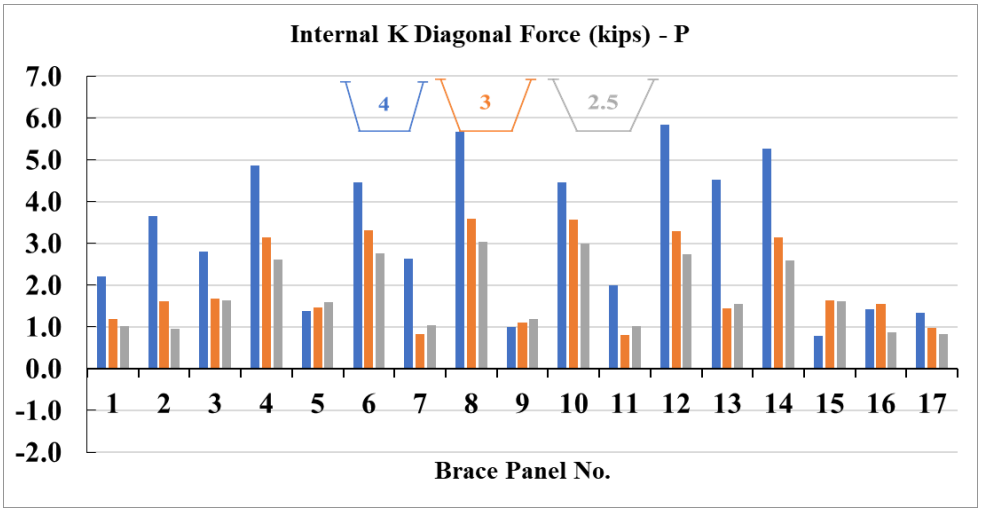

Figure D-81 – Force on one K-Diagonal - L/D=25 – Various Web Slopes

4 Girder with Various Web Slopes

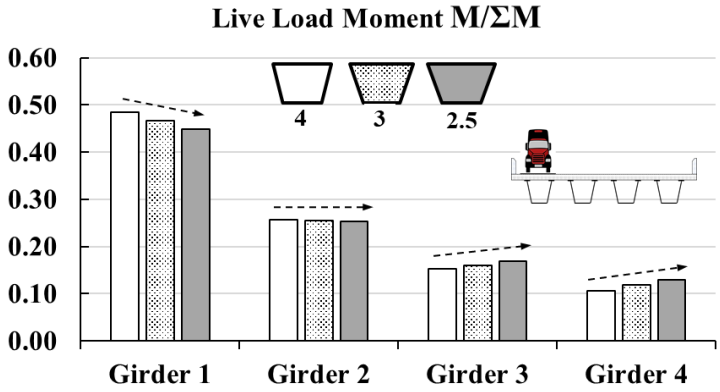

Figure D-82 – Live Load Moment Distribution - L/D=25 – Various Web Slopes

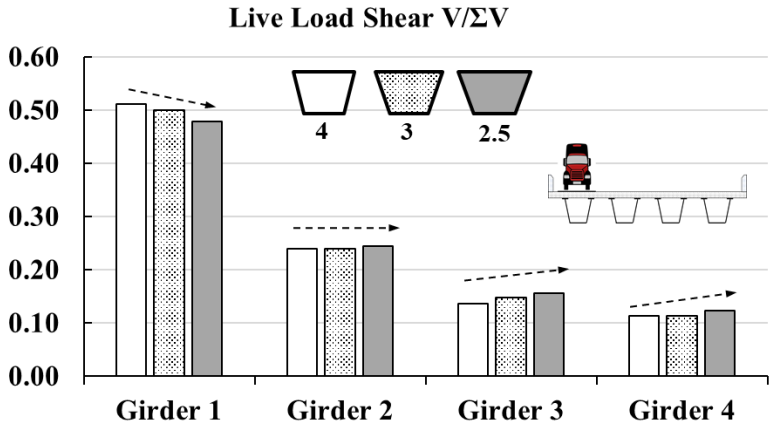

Figure D-83 – Live Load Shear Distribution - L/D=25 – Various Web Slopes

Appendix E. Design Example: Partial Top Lateral Bracing

Consider a simply supported horizontally curved steel tub girder with a radius of curvature equal to R=2500ft. that is subjected to vertical loads due to concrete deck construction. The girder spans 224ft. and is made up of 16 panels; each one of length equal to 14ft. K-frames are placed every panel point. The cross-sectional dimensions and properties for the bracing members are presented in Figure E-1.

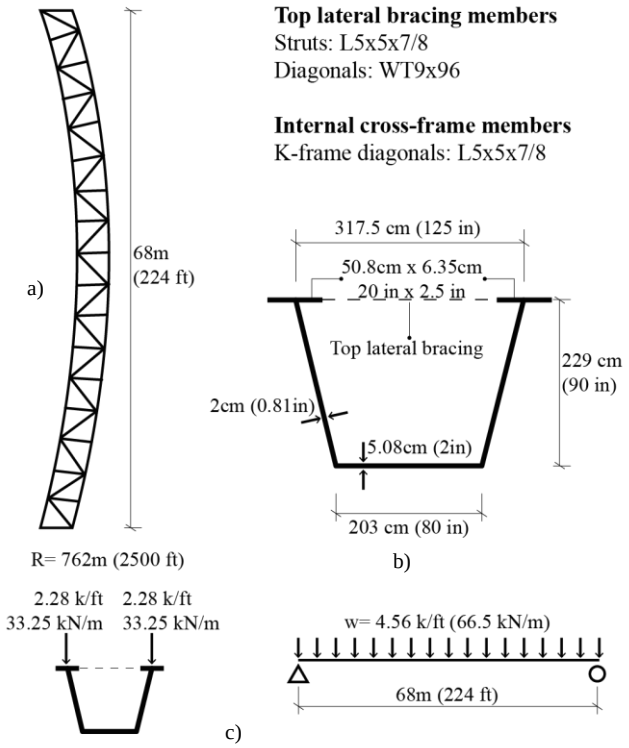

Figure E-1 – Tub Girder Example Features: a) Plan View. b) Cross-Sectional Properties, c) Applied Load

This example steel tub girder is subjected to uniformly distributed vertical loads due to the weight of the concrete poured at once. The weight of the concrete was calculated considering a 9in. thick deck, and two equal overhangs of 6.25ft. for a total concrete deck effective width equal to 23ft. A vertical distributed load equal to 4.56 k/ft. is assumed to consider the weight of the concrete deck, stay-in-place forms, tub girder self-weight, bracings, and construction life loads. This vertical load is equally distributed between the two top flanges since no eccentric load is considered in this example (no bracket loads for simplicity). Figure E-2 shows the corresponding bending moment and torsional diagrams of the example tub girder under the previously mentioned loads. The torsional demands have been calculated with the M/R method developed by Tung and Fountain 1970.

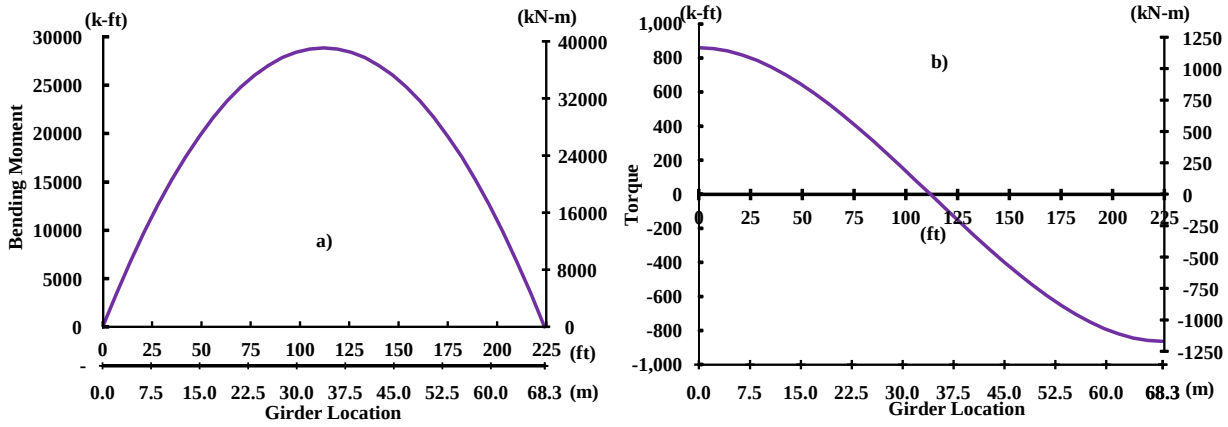

Figure E-2 – Demands on Example Girder: a) Bending Moment Diagram, b) Torque Diagram

E.1 Lateral Bending Stresses in Top Flange

First, the lateral bending stresses on the top flange are checked. Equation 6-1 gives the lateral component of the vertical applied loads on each top flange:

$$F_{lat} = \frac{1}{2}\Delta V_v \tan\theta_{web} = \frac{1}{2} * 4.56\frac{k}{ft} * 0.25 = 0.047\frac{k}{in}$$

Since no bracket loads are considered in this example, the lateral load $F_{h\_bracket}$=0. Next, the uniformly distributed lateral load produced by the curvature of the girder in one top flange is calculated:

$$F_{curv} = \frac{M}{Rh} = \frac{14300\,k-ft}{2500ft * 7.5ft} = 0.06\frac{k}{in}$$

Thus, the uniformly distributed lateral load acting on one top flange is equal to:

$$F_l = F_{lat} + \frac{1}{2}F_{h\_bracket} + \frac{1}{2}F_{curv} = 0.047\frac{k}{in} + 0 + 0.06\frac{k}{in} = 0.11\frac{k}{in}$$

The different stiffness values required to calculate the effective stiffness of the top flange β_{effe} are calculated with Equations from 6-6 to 6-9:

$$\beta_{top} = \frac{384EI_{top}}{{L_b}^3} = \frac{384 * 29000ksi * 1667in^4}{1344^3in^3} = 7.7\frac{k}{in}$$

$$\beta_{bottom} = \frac{384EI_{bottom}}{L^3} = \frac{384 * 29000ksi * 85333in^4}{2688^3in^3} = 48.9\frac{k}{in}$$

$$\beta_{dia} = \frac{EA_{dia}}{L_{dia}}(\cos\gamma)^2 = \frac{29000ksi * 8in^2}{98.5in}\left(\frac{40}{98.5}\right)^2 = 388.6\frac{k}{in}$$

$$\beta_{strut} = \frac{EA_{strut}}{0.5L_{strut}} = \frac{29000ksi * 8in^2}{0.5 * 125in} = 3713\frac{k}{in}$$

Now the effective stiffness of one top flange is equal to:

$$\beta_{effe} = 7.7 + \left[\frac{1}{1/(0.5 * 48.9) + 1/388.6 + 1/3713}\right] = 30.5\frac{k}{in}$$

Thus, the estimated lateral displacement of one top flange (δ_{lat}) due to a distributed lateral load F_l along the unbraced length L_b is equal to:

$$\delta_{lat} = \frac{F_l L_b}{\beta_{effe}} = \frac{0.11\frac{k}{in} * 1344in}{30.5\frac{k}{in}} = 4.8in$$

A FEA of the example girder was performed using the modeling assumptions described in the parametric study presented herein. According to the FEA, a maximum lateral displacement of the top flange at midspan equal to 9cm (3.6in) was obtained. Thus, the methodology presented herein overestimated about 30% the lateral displacement of the top flange. This over estimation can be attributed to the fact that in order to calculate the effective stiffness of the top flange β_{effe}, the contribution of only one K-frame at midspan was considered. Additionally, the uniformly distributed lateral load F_{curv} produced by the girder curvature was calculated with the maximum moment at midspan and assumed constant along the unbraced length. These two assumptions add more flexibility and higher demands in the top flange when calculating the lateral displacement.

Subsequently, the equivalent uniformly distributed lateral load F_{l_equi} to generate a maximum lateral displacement δ_{lat} in one top flange without any type of bracing contribution is obtained with Equation 6-12:

$$F_{l\_equi} = \frac{384EI_{top}}{{L_b}^4}\delta_{lat} = \frac{384 * 29000ksi * 1667in^4}{1344^4in^4}4.8in = 0.027\frac{k}{in}$$

The maximum moment of the unbraced top flange is calculated with Equation 6-2:

$$M_{l\_1} = \frac{F_{l\_equi}{L_b}^2}{12} = \frac{0.027\frac{k}{in} * 1344^2in^2}{12} = 340\ k - ft$$

The section modulus of one top flange is equal to:

$$S_{lat} = \frac{tf_{top} * {bf_{top}}^2}{6} = \frac{2.5in * 20^2in^2}{6} = 167in^3$$

Then, the maximum lateral bending stress in the top flange, which is located at the transition zones, is obtained.

$$\sigma_{lat} = \frac{340\ k-ft * 12}{167 in^3} = 24.5 ksi\ in\ compression$$

In order to obtain the maximum compression stress in the top flanges, the longitudinal stress due to positive bending of the tub girder has to be added. Since the maximum lateral bending stress σ_{lat} was found at the transition point, the bending stress of the girder at that point is calculated as well. The bending moment at the transition zones (end of forth panel) M_{bend} is equal to 21450 k-ft. while the section modulus of the steel tub girder $S_{tub\_top} = 12511 in^3$. Thus, the stress in the top flange σ_{bend} due to bending is equal to:

$$\sigma_{bend} = \frac{21450\ \text{k} - \text{ft} * 12}{12511 in^3} = 20.5 ksi\ in\ compression$$

Hence, the estimated total stress in the top flange at the transition zone σ_{total} is equal to:

$$\sigma_{total} = \sigma_{lat} + \sigma_{bend} = 24.5 + 20.5 = 45.10 ksi\ in\ compression$$

According to the FEA of the example girder, a maximum Von Misses stress of 39ksi was observed at the transition zones. Thus, the methodology presented herein overestimated the maximum compression stresses in top flanges about 16%.

E.2 Top Lateral Bracing Forces

Since the most critical bracing forces have been observed at the transition zones, this example shows the calculation of the axial forces of the truss diagonal and the K-frame strut in the transition zones. First, the shear flow q is calculated with Equation 6-14. For this example, the torsional demand T is equal to 592k-ft, from Figure E-2. Also, the enclosed area Ao is equal to 9020 in². Then, the shear flow is equal to:

$$q = \frac{T}{2A_o} = \frac{592\text{k} - \text{ft} * 12}{2 * 9020\ \text{in}^2} = 0.39 \frac{k}{in}$$

Next, the truss diagonal force component due to torsional moments D_{EPM} is calculated with Equation 6-15:

$$D_{EPM} = -\frac{qb}{\sin \alpha} = -\frac{0.39 \frac{k}{in} * 125 in}{\sin 36.70} = 82.4\ kips$$

Next, the axial force component due to bending is calculated with Equation 6-18:

$$K_1 = \frac{d}{A_d} + \left(\frac{b}{A_s} + \frac{s^3}{2{b_f}^3 t_f}\right) \sin^2 \alpha$$

$$K_1 = \frac{209.4in}{28.10in^2} + \left(\frac{125in}{8in^2} + \frac{168^3in^3}{2 * 20^3in^3 * 2.5in}\right)\sin^2 36.7$$

$$K_1 = 55.4\frac{1}{in}$$

$$D_{BEND} = -\frac{4 * f_{xtop}\, s\, \cos\alpha}{K_1} = -\frac{4 * 17.98ksi * 168in * \cos 36.7}{55.4\frac{1}{in}}$$

$$D_{BEND} = -172kips$$

Lastly, the force in the truss diagonal at transition zone is estimated with Equation 6-23:

$$D_{TOTAL} = D_{EPM} + D_{BEND} = -82.4 - 172 = -254kip$$

During the FEA of the example girder, the axial force of the truss diagonals at the transition zones was equal to -210kips. The methodology presented here overestimated the force of the truss diagonals at transition zones in about 20%. When calculating the truss diagonal forces in the girder with partial top lateral bracing provided along the entire length of the girder, the axial force in the truss diagonal previously analyzed was equal to -125 kips. Thus, after removing 50% of truss diagonals, the axial force in the diagonals at transition zones increased about 1.7 times.

E.3 Internal K-Frame Bracing Forces

The K-frame bracing forces at the transition zones are calculated since they are the most critical. The strut axial forces induced by the top lateral diagonals are calculated with Equation 6-16, Equation 6-19, Equation 6-21 and Equation 6-22 (minus half the lateral load distributed along $L_b/2$):

$$S_{EPM} = qb = 0.39\frac{k}{in} * 125in = 49.3kips$$

$$S_{BEND} = \frac{1}{2}D_{BEND}\sin\alpha = 0.5 * 172kips * \sin 36.7 = 51.5kips$$

$$S_{LAT} = F_{lat}s = 0.047\frac{k}{in} * 168in = 8kips$$

$$S_{TOTAL} = S_{EPM} + S_{BEND} + S_{LAT} - (F_l - F_{lat})(\,L_b/2)$$

$$S_{TOTAL}=49.3+51.5+8-(0.11-0.047)*1344/2$$

$$S_{TOTAL} = 66kips$$

Next, the distortional loads in the struts are calculated considering no K-frame between the transition zones:

$$S_{KF} = \pm \frac{(8.5 * 168in)(80in)}{4 * 9020 \text{ in}^2}\left(0 - \frac{21450 \text{ k} - \text{ft}}{2500ft}\right) = \pm 26kips$$

Thus the axial forces in the two parts of the strut at the transition zone are equal to:

$$S_1 = 66 + 26 = 409kN\ (92kips)$$

$$S_2 = 66 - 26 = 177kN\ (40kips)$$

The axial forces S_1 and S_2 obtained in the FEA of the girder were 95.8kips and 41.85kips. Thus, the axial forces in the K-frame struts at the transition zone are underestimated about 5%.

Additionally, the distortional loads induced in the K-frame diagonals are calculated:

$$D_{KF} = \pm \frac{s_K L_{DK}}{2A_o}\left(\frac{M}{R} - \frac{a}{b}ew\right) = \pm \frac{(8.5 * 168in)(98.4in)}{2 * 9020 \text{ in}^2}\left(\frac{21450 \text{ k} - \text{ft}}{2500ft}\right)$$

$$D_{1,2} = D_{KF} = \pm 67$$

The diagonal forces D_1 and D_2 from the finite-element analysis were 69.6kips and -63.48kips. The variation in axial forces in K-frame diagonals at the transition zone was about 5%.